

**THE INFLUENCE OF TOPOGRAPHICALLY COMPLEX SLOPES ON  
DEEPWATER PROCESSES AND STRATIGRAPHIC ARCHITECTURE**

Hannah Louise Brooks

Submitted in accordance with the requirements for the degree of

Doctor of Philosophy

The University of Leeds

School of Earth and Environment

July 2017

This copy has been supplied on the understanding that it is copyright material and that no quotation from the thesis may be published without proper acknowledgement

© 2017 The University of Leeds and Hannah Louise Brooks

The right of Hannah Louise Brooks to be identified as Author of this work has been asserted by her in accordance with the Copyright, Designs and Patents Act 1988.

The candidate confirms that the work submitted is her own, except where work which has formed part of jointly-authored publications has been included. The contribution of the candidate and the other authors to this work is explicitly indicated below. The candidate confirms that appropriate credit has been given within the thesis where reference has been made to the work of others.

The work in Chapter 4 is accepted for publication in *Sedimentology* as follows:

**Hannah L. Brooks, David M. Hodgson, Rufus L. Brunt, Jeff Peakall, and Stephen S. Flint (2017) Exhumed lateral margins and increasing flow confinement of a submarine landslide complex, *Sedimentology*.**

As the primary author, I was responsible for field data collection, analysis and interpretation, and writing of the manuscript. The contribution of the other authors was limited to discussion on the data and editorial suggestions.

The work in Chapter 5 was accepted for publication in *GSA Bulletin* pending minor revisions. The reviewer's suggestions have been incorporated into the version in Chapter 5.

**Hannah L. Brooks , David M. Hodgson, Rufus L. Brunt , Jeff Peakall , Menno Hofstra, Stephen S. Flint (2017) Deepwater channel-lobe transition zone dynamics- processes and depositional architecture, an example from the Karoo basin, South Africa, *GSA Bulletin*.**

As the primary author, I was responsible for field data collection, analysis and interpretation, and writing of the manuscript. The contribution of the other authors was limited to discussion on the data and editorial suggestions.

The work in Chapter 6 of the thesis is under review for publication in *Geosphere* as follows:

**Hannah L. Brooks, David M. Hodgson, Rufus L. Brunt , Jeff Peakall , Miquel Poyatos Moré, Stephen S. Flint (2017) Disconnected submarine lobes, and their role in the evolution of a stepped slope over multiple sea-level cycles**

As the primary author, I was responsible for field data collection, analysis and interpretation, and writing of the manuscript. The contribution of the other authors was limited to discussion on the data and editorial suggestions.

## ACKNOWLEDGEMENTS

Firstly I would like to thank my supervisors Dave Hodgson, Jeff Peakall, Steve Flint and Rufus Brunt. I am immensely grateful for all of support and guidance you have given over the years. I really appreciate all the time and effort you have invested in me and my work that has vastly improved me as a researcher and as a wine connoisseur.

I am also grateful to the sponsors of the SLOPE 4 project (Anadarko, BHP Billiton, BP, ConocoPhillips, ENGIE, Maersk Oil, Murphy, Nexen, Petrobras, Premier Oil, Shell, Statoil, Total, VNG Norge and Woodside) for providing the funds that have made this project possible and for the input given by those who attended sponsors meetings.

Thank you to past and present Stratigraphy Group members for their help, support, guidance and drinking stamina that has got me through the highs and lows of the past 4 years: Luz Gomis, Miquel Poyatos Moré, Yvonne Sychala, Menno Hofstra, Janet Richardson, Andrea Ortiz-Karpf, Sarah Cobain, Dan Bell, Riccardo Teloni, Marcello Gugliotta, Emma Morris, Chris Stevenson, Bonita Barret-Crosdil, Grace Cosgrove and Aurelia Privat. Thanks also to Cathy Burns, Michelle Shiers, Catherine Russell and Dan Collins for being there especially over the last few months. Thank you Rachel Harding and Billy Head, without you we would never have finished the SLOPE report. Thank you to all of my field assistants, those mentioned above as well as Colleen Kurcinka, Geoff Reith and Lewis Burden for coping with some seriously challenging outcrops, situations and heat. I have had so many amazing adventures with you all over these years that I will never forget!

Thank you to the people of Laingsburg and Prince Albert for their help, and to the farmers in the area who allowed me on to their land, and occasionally rescued me from rivers. Thank you to Annalie Theron and DeVille Wickens for logistic support.

Thank you to my family for all the encouragement you have given me, to Mum and Peter for unceasing support and never doubting I could do this, to Sophie for having no idea what I do but always being proud of me regardless and to Dad, Jo, Harry and James for a retreat to the ocean or just a BBQ in the garden.

Finally, to William. I couldn't have got to this point without you. It has been your continual love and support, which has kept me motivated over the past 7 years, thank you for everything. There is too much to say here, but you are my rock... and I believe I have won our bet and you owe me a holiday!

## ABSTRACT

Topographically complex slope to basin floor profiles are increasingly recognised in modern seafloor, seismic reflection and outcrop datasets, and range from simple slope profiles, through stepped slopes with high gradient ramps linking low gradient steps, to slopes with 3D enclosed minibasins linked by tortuous corridors. This study investigates a range of slope to basin floor topographic configurations with multi-scale (mm to 100 km) variability, using regionally extensive exposures from the Permian slope to basin floor deposits in the Laingsburg depocentre, Karoo Basin, South Africa. Over 400 outcrop logs, totalling 14 km in thickness, combined with a large database from earlier Stratigraphy Group studies, are used to assess the influence of dynamic seabed relief on turbidity current processes and depositional patterns across a range of scales, and their transfer into the stratigraphic record.

Degradation plays a large role in shaping submarine slopes. The formation and evolution of a submarine slide complex is investigated, including time transgressive lateral margins of basal shear surfaces/zones and varying confined of remobilized and turbidite infill.

The base of slope is a key area of gradient change. Here, the spatial and temporal variations of a channel-lobe transition zone (CLTZ) are documented, including how topographic influence on turbidity currents varies and evolves, causing CLTZ expansion/contraction and migration. In addition, how these topographically complex areas are transferred into the stratigraphic record, as single surfaces and volumes of rock, is discussed.

Areas of dynamic and fixed topography have been recognised as having long-term effects, leading to the evolution of a stepped slope profile. In the Laingsburg depocentre stepped slope topography initiated before major clastic input and increased temporally, gradually outpacing sediment supply. The effects of slope orientation and gradient change on flow processes and stratigraphic architecture are presented as a range of intraslope lobe deposits and bypass dominated zones.

## Contents

ACKNOWLEDGEMENTS.....	ii
ABSTRACT .....	iii
LIST OF TABLES .....	xii
LIST OF FIGURES .....	xiii
<b>1 Introduction.....</b>	<b>1</b>
<b>1.1 Background and rationale.....</b>	<b>1</b>
<b>1.2 Aims and research questions .....</b>	<b>2</b>
<b>1.3 Thesis outline.....</b>	<b>8</b>
<b>2 Slope to basin floor topography .....</b>	<b>11</b>
<b>Topographic impact on flow processes, products, and stratigraphic architecture .....</b>	<b>11</b>
<b>2.1 Introduction.....</b>	<b>11</b>
<b>2.2 Experimental studies.....</b>	<b>13</b>
2.2.1 <i>Downflow gradient changes- Hydraulic jump .....</i>	13
2.2.2 <i>Lateral slopes and downflow obstacles- Reflection, deflection and flow                   decoupling.....</i>	18
2.2.3 <i>Summary.....</i>	23
<b>2.3 Exhumed studies .....</b>	<b>23</b>
2.3.1 <i>Downslope obstacles and gradient change .....</i>	23
2.3.2 <i>Lateral slope and obstacles .....</i>	31
2.3.3 <i>Categorising confinement.....</i>	32
2.3.4 <i>Mass flow deposit relief.....</i>	34

2.3.5	<i>Summary</i> .....	37
<b>2.4</b>	<b>Modern seafloor studies</b> .....	<b>38</b>
2.4.1	<i>Downslope gradient change</i> .....	38
2.4.2	<i>Submarine slide erosional and depositional relief</i> .....	46
2.4.3	<i>Summary</i> .....	49
<b>2.5</b>	<b>Reflection seismic studies</b> .....	<b>49</b>
2.5.1	<i>Downslope changes in gradient and confinement</i> .....	49
2.5.2	<i>Submarine slide topography</i> .....	57
2.5.3	<i>Summary</i> .....	62
<b>2.6</b>	<b>Summary</b> .....	<b>63</b>
<b>3</b>	<b>Regional setting, methodology and dataset</b> .....	<b>65</b>
<b>3.1</b>	<b>Geological background- regional setting</b> .....	<b>65</b>
<b>3.2</b>	<b>Study area- Laingsburg depocentre</b> .....	<b>70</b>
3.2.1	<i>Prince Albert Formation</i> .....	72
3.2.2	<i>Whitehill Formation</i> .....	72
3.2.3	<i>Collingham Formation</i> .....	72
3.2.4	<i>Vischkuil Formation</i> .....	73
3.2.5	<i>Laingsburg Formation</i> .....	74
3.2.6	<i>Fort Brown Formation</i> .....	76
<b>3.3</b>	<b>Methodology and dataset</b> .....	<b>76</b>
3.3.1	<i>SLOPE, SLOPE 2, SLOPE 3 and LOBE project databases</i> .....	76
3.3.2	<i>Fieldwork- This study</i> .....	77

3.3.3	<i>Isopach and palaeogeographic maps- This study</i> .....	80
3.3.4	<i>Datacube and surface maps – SLOPE 4 collaboration</i> .....	81
<b>3.4</b>	<b>Facies framework</b> .....	<b>81</b>
3.4.1	<i>Bedded</i> .....	84
3.4.2	<i>Sandstone and siltstone thin beds</i> .....	86
3.4.3	<i>Sandstones</i> .....	90
3.4.4	<i>Mass transport</i> .....	96
3.4.5	<i>Other</i> .....	98
4	Exhumed lateral margins and increasing infill confinement of a submarine slide complex	104
4.1	Introduction .....	104
4.2	Geological background.....	106
4.2.1	Karoo Basin and stratigraphy .....	106
4.2.2	Study location .....	108
4.3	Methodology.....	109
4.4	Facies associations .....	109
4.5	Stratigraphic subdivision and correlation .....	115
4.5.1	Sequence of erosion and deposition .....	117
4.6	Discussion.....	124
4.6.1	Evolutionary model.....	124
4.6.2	Evolution of surfaces .....	128
4.6.3	Confinement styles.....	132



4.6.4	Source slope.....	137
4.6.5	Sedimentation rates vs. degradation rates.....	138
4.7	Conclusions.....	140
<b>5</b>	<b>Deepwater channel-lobe transition zone dynamics.....</b>	<b>143</b>
<b>5.1</b>	<b>Introduction.....</b>	<b>143</b>
<b>5.2</b>	<b>Terminology.....</b>	<b>144</b>
<b>5.3</b>	<b>Geological background and location of study.....</b>	<b>144</b>
<b>5.4</b>	<b>Methodology.....</b>	<b>150</b>
<b>5.5</b>	<b>Facies groups.....</b>	<b>150</b>
<b>5.6</b>	<b>Architectural elements.....</b>	<b>155</b>
<b>5.7</b>	<b>Correlation panels.....</b>	<b>156</b>
5.7.1	<i>Unit D/E.....</i>	161
5.7.2	<i>Subunit E1.....</i>	162
5.7.3	<i>Subunit E2.....</i>	162
5.7.4	<i>Subunit E3.....</i>	162
<b>5.8</b>	<b>Slagtersfontein detailed section.....</b>	<b>164</b>
5.8.1	<i>Section 1.....</i>	168
5.8.2	<i>Section 2.....</i>	168
5.8.3	<i>Section 3.....</i>	169
5.8.4	<i>Section 4.....</i>	170
5.8.5	<i>Section 5.....</i>	171
<b>5.9</b>	<b>Architecture of an exhumed CLTZ.....</b>	<b>171</b>

5.9.1	<i>Erosional elements</i> .....	172
5.9.2	<i>Depositional elements</i> .....	172
<b>5.10</b>	<b>Discussion</b> .....	<b>173</b>
5.10.1	<i>Evolution of slope profile</i> .....	173
5.10.2	<i>Spatial variability and evolution of the CLTZ</i> .....	176
5.10.3	<i>Comparison to other CLTZs</i> .....	180
5.10.4	<i>A generic model for CLTZ stratigraphic architecture</i> .....	183
<b>5.11</b>	<b>Conclusions</b> .....	<b>186</b>
<b>6</b>	<b>Disconnected submarine lobes, and their role in the evolution of a stepped slope over multiple sea-level cycles</b> .....	<b>188</b>
6.1	Introduction .....	188
6.2	Geology of the Karoo Basin.....	190
6.2.1	The Laingsburg and Fort Brown Formations .....	192
6.3	Methodology.....	193
6.4	Results.....	193
6.4.1	Structureless sandstone .....	197
6.4.2	Structured sandstone .....	198
6.4.3	Hybrid beds.....	199
6.4.4	Thin bedded siltstone and sandstone .....	199
6.4.5	Chaotic Facies .....	200
6.4.6	Regional mudstone.....	200
6.5	Environments of deposition.....	201

6.6	Unit A/B, B/C and D/E thickness and facies distribution.....	203
6.7	Discussion .....	208
6.7.1	Units A/B, B/C and D/E.....	208
6.7.2	Thickness and facies distribution of Units C, D, E and F .....	212
6.7.3	Slope to basin floor evolution: Units C-F .....	220
6.7.4	Early basin floor topography development and evolution .....	221
6.7.5	Topographic evolution of a stepped slope profile .....	225
6.8	Conclusions.....	230
7	Discussion and Conclusions .....	234
7.1	Introduction.....	234
7.2	How does orientation and gradient of slope to basin floor topography influence sediment gravity flow processes and resultant stratigraphic architecture?.....	234
7.2.1	Frontal slope- gradient decrease and reversal .....	236
7.2.2	Frontal slope- gradient increase .....	241
7.2.3	Lateral and oblique-lateral slopes.....	242
7.3	How does topographic influence on turbidity currents vary and evolve? .....	245
7.3.1	Topography evolution over deposition of a single system .....	245
7.3.2	Topography evolution over deposition of multiple systems .....	246
7.4	How are topographically complex components transferred into the stratigraphic record?.....	252
7.4.1	Bypass dominated zones.....	253
7.4.2	Basal shear surfaces.....	254

7.4.3	Differential compaction.....	255
7.5	Subsurface applications and implication of study .....	255
7.5.1	Bypass dominated zones and up-dip pinch outs.....	255
7.5.2	Stepped slope evolution.....	258
7.5.3	Submarine slide complexes .....	259
7.6	Conclusions .....	261
7.7	Recommendations for further research .....	264
7.7.1	What is the detailed sedimentological expression of the stepped slope topography in early basin floor Units A and B? .....	264
7.7.2	How does the sedimentological expression of slope to basin floor topography differ in passive vs active margins? .....	265
7.7.3	Integration with modern seafloor datasets, numerical and physical experiments.....	265
8	References.....	268
	<b>Appendix A.....</b>	<b>322</b>
	<b>Appendix A.1 .....</b>	<b>322</b>
	<b>Appendix A.2 .....</b>	<b>322</b>
	<b>Appendix B- Additional correlation panels.....</b>	<b>336</b>
	<b>Appendix B.1- Vrisgewaagd .....</b>	<b>337</b>
	<b>Appendix B.2- N1 Dome South .....</b>	<b>355</b>
	<b>Appendix B.3- Baviaans South .....</b>	<b>357</b>
	<b>Appendix B.4- Floriskraal North.....</b>	<b>359</b>

<b>Appendix B.4- Floriskraal South .....</b>	<b>360</b>
<b>Appendix C.....</b>	<b>361</b>
<b>Appendix C.1 .....</b>	<b>361</b>
<b>Appendix D .....</b>	<b>363</b>

## LIST OF TABLES

Table 2.1 <i>Comparison chart of the main sedimentological and stratigraphic characteristics of intraslope lobes and basin-floor lobes (from Spychala, 2016).</i> .....	25
Table 2.2 <i>Three tiers of mass-transport-deposit surface topography are defined at the Sierra Contreras, Tres Pasos Formation (Cretaceous), Southern Chile. The cause of the topography and the effect on overlying turbidite architecture are outlined (from Armitage et al., 2009).</i> .....	35
Table 2.3 <i>Example mechanisms for creating topography on the slope to basin floor.</i> .....	64
Table 3.1 <i>Representative chart of thickness data preparation for the creation of isopach maps in ArcGIS.</i> .....	80
Table 3.2 <i>Facies framework</i> .....	82
Table 3.3 <i>Bedded mudstone characteristics.</i> .....	84
Table 3.4 <i>Bedded siltstone characteristics.</i> .....	85
Table 3.5 <i>Siltstone dominated thin beds characteristics.</i> .....	86
Table 3.6 <i>Sandstone dominated thin beds characteristics.</i> .....	88
Table 3.7 <i>Structured sandstone characteristics.</i> .....	90
Table 3.8 <i>Scoured sandstone and siltstone characteristics.</i> .....	91
Table 3.9 <i>Sigmoidal bedform characteristics.</i> .....	92
Table 3.10 <i>Banded sandstone characteristics.</i> .....	94
Table 3.11 <i>Structureless sandstone characteristics.</i> .....	95
Table 3.12 <i>Chaotic deposit characteristics.</i> .....	96
Table 3.13 <i>Remobilized deposit characteristics.</i> .....	97
Table 3.14 <i>Mudclast conglomerate characteristics.</i> .....	98
Table 3.15 <i>Hybrid bed characteristics.</i> .....	100
Table 3.16 <i>Clastic injectite characteristics.</i> .....	102
Table 5.1 <i>Table of facies groups for Chapter 5.</i> .....	152

Table 5.2 CLTZ lengths from modern sea-floor datasets (modified from Wynn et al., 2002). .....	180
Table 5.3 Key characteristics of CLTZ model with examples from other outcrop and modern seafloor studies. ....	185
Table 6.1 Example mechanisms for creating topography on the slope to basin floor and applicability to the Laingsburg depocentre stepped slope formation. ....	227

## LIST OF FIGURES

Figure 1.1 A) Models of simple and topographically complex slope profiles. (B) Examples of intraslope “perched apron”, Einstein-Fuji slope Eastern Gulf of Mexico, Seismic attribute map (From Sylvester et al., 2012). (C) Intraslope “ponded apron” from the Brazos-Trinity intraslope basins, Gulf of Mexico (From Prather et al., 2017). (D) Examples of slope gradient variations (From Posamentier and Walker, 2006). ....	3
Figure 1.2- Key results from data chapters 4, 5 and 6, colour coded in relation to each research question. Beige relates to question 1, green to question 2 and blue to question 3. ....	4
Figure 2.1 Schematic diagram showing the key features of a hydraulic jump (from Sumner et al., 2013). ....	13
Figure 2.2 Experiment of 1-phase suspension flow that produced a scour just before the jump and mainly plane bed laminations at and down slope of the jump (from Postma et al., 2009). ....	14
Figure 2.3 A. Plot of theoretical relations between the Froude number of the incoming flow ( $Fr_1$ ), $h_2/h_1$ -ratio and energy loss ( $\Delta H/h_1$ ). B. Depending on the balance between upstream forces related to the incoming flow velocity and the downstream forces depending on flow depth, hydraulic jumps occur at a slope break (normal jump, kinematic energy = potential energy), downstream of a slope break (flushed jump, kinematic > potential), or upstream of the slope break (submerged jump, kinematic < potential) (from Cartigny, 2012). ....	15

- Figure 2.4 (top) Graphs showing time ( $t$ ) versus flow velocity ( $u$ ) and distance ( $x$ ) versus flow velocity ( $u$ ) and the different terminology used to describe unsteady and non-uniform flow behaviour. (bottom) Diagram illustrating variance in flow behaviour depending on the type of gradient change. At the base-of-slope a decrease in slope is expected and therefore diverging and depletive flow behaviour. Abrupt decreases in gradient, are often associated with flow expansion as divergent flow behaviour will result from the gradient and confinement changes in this region (from Kneller, 1995). ..... 17
- Figure 2.5 Schematic diagram of a train of downslope asymmetrical cyclic steps (flow from left to right), beneath a turbidity current (Cartigny, 2012)..... 17
- Figure 2.6 The effect of internal Froude number ( $Fr_i$ ) on the behaviour of flows downstream of topography (from Kneller and Buckee, 2000). ..... 19
- Figure 2.7 Schematic illustration of the joint effects of the dividing streamline, the Froude number and the degree of confinement ( $h/z$ ) (from Kneller and McCaffrey 1999). ..... 20
- Figure 2.8 The three types of internal bores defined by Rottman and Simpson (1989) (From Kneller and Buckee, 2000). ..... 21
- Figure 2.9 Depositional model for turbidity currents obstructed by a lateral slope that are (a) slow and highly depositional or (b) fast and capable of erosion and/or bypass of sediment, and (c) and (d) their resulting cross-stream deposit thickness trends. SLFR= sediment load fallout rate, from Amy et al., 2004. .... 22
- Figure 2.10 (A) Block diagram showing the key recognition criteria of intraslope lobes. Stacking patterns are aggradational to slightly compensational; onlap combined with injection onto mudprone slope; highly amalgamated zone in the lobe complex axis; subtle confinement leads to fringes that show aggradation stacking; high degree of confinement leads to preservation of beds with evidence of flow direction, erosional based beds and abrupt facies changes; climbing ripple lamination is the dominant facies of the lobe off-axis; incision by low-aspect-ratio channel that originate in the same unit as the intraslope lobes; more lobe deposits can be found down-dip of basin-floor or on steps basinward of the slope. (B) Simplified logs of typical thicknesses and stacking pattern from lobe axis to lobe fringe (downdip and laterally) in intraslope lobes that are



*observed over a few kilometres. Position of schematic logs are from fringe (1) to axis (4) (from Spychala et al., 2015).*.....24

**Figure 2.11 Schematic illustration of the distribution of Unit D (Fort Brown Fm., Karoo Basin, South Africa) depositional environments at (A) Early (B) Late stages from synthesis of field data. (C) A schematic long profile of the D3 channel system (dashed line) in relation to the mean regional palaeoslope (solid line) (from Brunt et al., 2013a).** .....25

**Figure 2.12 Block diagram showing how channel architecture and reservoir style is related to palaeobathymetry. This study focuses on weakly confined channel systems (from Moody et al., 2012).** .....26

**Figure 2.13 Main characteristics of submarine channels, channel-lobe transitions and lobe deposits as originally described by Mutti and Normark (1987). With: 1a = erosional channel; 1b = depositional channel; 1c = 'zone of roughness'; 1d = lobate relief; 2a = beds truncating against channel margin; 2b = beds converging against channel edge; 2c = bedding irregularity resulting from scours and large-scale bedforms; 2d = even-parallel bedding; 3a = clast-supported conglomerates; 3b = mud-supported conglomerates; 3c = thin-bedded overbank deposits; 3d+e = coarse-grained, internally stratified sandstone facies; 3f = complete and base-missing Bouma sequences; 4a = deep and relative narrow scours locally associated with stone clasts; 4b = armoured mudstone clasts; 4c = mud-draped scours; 4d = broad scours, locally associated with mudstone clasts; 4e = tabular scours invariably associated with mudstone rip-up clasts from underlying substratum; 4f = nests of mudstone clasts commonly showing inverse grading and 'take-off' attitude of individual clasts; 5a = slump units; 5b = impact features (redrawn from Mutti and Normark, 1987).** .....27

**Figure 2.14 Conceptual depositional model of deep-marine fan systems, illustrating relationships between lobe and channel transitions in a slope-to-basin setting. (A) Detached fan systems. (B) Attached fan systems. Modified after Mutti (1985) and Mutti and Normark (1987) (from Fugelli and Olsen, 2005).** .....28

**Figure 2.15 Four temporal and spatial domains, Build, Cut, Fill, Spill, characterize the principle phases of submarine channel-lobe deposition recorded by migration of the channel-lobe transition over a channel site. These domains relate variable confinement to the probable facies recording**

*deposition from a region within a series of related flows and their contribution to channel, wedge and lobe sedimentary bodies. This diagram shows the build, cut, fill, and spill phases through the evolution of a single-story channel (from Gardner et al., 2003). ..... 29*

**Figure 2.16** *A) Cartoon diagram in Wheeler space to illustrate the progressive-confinement model along the axis of a deep-water system during a cycle of waxing-to-waning sediment supply. The illustration emphasizes that the composite erosional surface is time transgressive. Note that during slope degradation frontal lobes form ahead of an evolving channel–levee system that lengthens down dip and up dip. The basal sandstone will be younger into the basin until a maximum regressive surface is formed. B) Three-dimensional Wheeler space cartoon with two strike sections that emphasize the challenge of identification of key regressive surfaces away from the axis on the slope and basin floor due to diachroneity of lithological contacts (from Hodgson et al., 2016). ..... 30*

**Figure 2.17** *Submarine basin-floor lobes interaction with topographic features (i) low amounts of aggradation on the slope compared to the basin- abrupt pinch-out against structure; (ii) moderate amount of aggradation on the slope compared to the basin- aggradation onlap with draping muds; (iii) low-gradient slope and high aggradation rates- facies transition and remobilization; and (iv) unconfined- downlap (from Spychala et al., 2017a). ..... 32*

**Figure 2.18** *Schematic plan view of lobe stacking patterns. (A) Compensational stacking; (B) Aggradational stacking; (C) Progradational stacking; (D) Retrogradational stacking. Dashed blue line indicates the locus of deposition of the next lobe (from Spychala, 2016). ..... 34*

**Figure 2.19** *Idealized transect of Casaglia-Monte della Colonna (CMC), (from the middle Miocene Marnoso-arenacea Formation of the Northern Apennines) parallel to the SW-NE direction of slide movement, showing the external geometry and internal distribution of structures. The sketch outlines three segments (a,b,c), which have been identified on the basis of the body geometry and the type and distribution of structures (from Lucentre and Pini, 2003). ..... 35*

**Figure 2.20** *Conceptual diagram of the MTD surface-topography hierarchy developed for the Sierra Contreras, Tres Pasos Formation (Cretaceous), Southern Chile. Each of the three tiers is shown, outlining the scale and the effect on subsequent turbidite beds. Although the tiers are successively separated by an order of magnitude in size, there is range within the hierarchy with*

<i>respect to the topographic dimensions, facilitating a more flexible comparison of MTDs (from Armitage et al., 2009).</i> .....	36
<b>Figure 2.21 (upper) Shaded swath bathymetry of the Rhone Deep Sea Neo-fan. (lower) Morpho-acoustic interpretation of the same dataset showing the independent nature of the Neo-channel mouth and a large scour field developed downdip of a slope break (from Bonnel et al., 2005).</b> ...	40
<b>Figure 2.22(a) Typical cross section through low efficiency submarine fan system with an attached lobe, and a high efficiency system with a detached lobe. (b) Summary of spatial distribution of erosional features and deposition bedforms within a CLTZ (from Wynn et al., 2002a).</b> .....	41
<b>Figure 2.23 Morphology and dimensions of four isolated and amalgamated scour types documented along the north east Atlantic margin (from Macdonald et al., 2011a).</b> .....	42
<b>Figure 2.24 Morphology and dimensions of erosional features in CLTZs (from Wynn et al., 2002a).</b> .....	42
<b>Figure 2.25 A) Map of the Moroccan Turbidite System showing the pathway of Bed 5 through the Agadir Canyon, into the Agadir Basin, through the Madeira Channel System, and ultimately spreading across the Madeira Abyssal Plain (adapted from Stevenson et al., 2014a). Shallow sediment cores taken across the system are marked as white circles, with those detailed in this study highlighted in yellow. Base-of-slope and basin-floor bypass zones are highlighted as red areas. B) Schematic core transect of Bed 5 along its pathway from the Agadir Canyon to the Madeira Abyssal Plain (from Stevenson et al., 2015).</b> .....	44
<b>Figure 2.26 Cartoon summarising the three main types of flow behaviour and resultant depositional architectures across the Maderia Channel System. In plan-view arrows indicate flow direction and size of arrow represents flow velocity, darker shaded areas indicate areas of deposition whereas lighter areas represent non-deposition. In cross section arrows indicate zones of deposition (from Stevenson et al., 2013).</b> .....	45
<b>Figure 2.27 Comparison of shapes and area of failures studies within the COSTA project (from Canals et al., 2004).</b> .....	47
<b>Figure 2.28 Three dimensional map of slope offshore Norway showing the geomorphology of the Storegaa slide, from <a href="http://www.offshore-technology.com/projects/ormen-lange-field/ormen-lange-field8.html">http://www.offshore-technology.com/projects/ormen-lange-field/ormen-lange-field8.html</a>.</b> .....	48

Figure 2.29 <i>Shaded relief image of Ana Slide, Ana Slide covers 6 km<sup>2</sup> and is located on the eastern Balearic flank of Eivissa Channel (from Lafuerza et al., 2012).</i> .....	48
Figure 2.30 <i>Ternary diagram modified from Meckel et al. (2000), and Booth et al. (2002), showing slope type end-member and key processes controlling graded to above-grade slope transition (from Prather, 2003).</i> .....	50
Figure 2.31 <i>Idealised ponded depositional sequence (I-VI) and idealised bypass deposition sequence (VII-XI) (from Prather, 2000).</i> .....	51
Figure 2.32 <i>Schematic diagrams illustrating the importance of the areal extent of sediment gravity flows relative to the areas of receiving depressions. (A) Silled sub-basin in which sand-transporting flows are small in volume relative to the scale of the receiving space. (B) Silled sub-basin in which sand-transporting flows are large in volume relative to the scale of the receiving space. The diagram shows spill to the next sub-basin downslope with associated incision and bypass in the upper sub-basin. (C) Connected tortuous corridor in which sand-transporting flows are small in volume relative to the potential flow path. A possible example is shown in figure 8 of Demyttenaere et al. (2000). (D) Connected tortuous corridor in which sand-transporting flows are large in volume relative to the potential flow path (from Smith, 2004a).</i> .....	52
Figure 2.33 <i>Seismic section showing the stepped topography with numerous ramps and flats along the middle Angolan continental slope (from Hay, 2012).</i> .....	53
Figure 2.34 <i>Conceptual model for depositional evolution along a stepped-slope profile (modified from O'Byrne et al., 2004). Predicted slope evolution describes depositional and erosional response of turbidity currents to progressive slope build-up and associated accommodation reduction (from Hay, 2012).</i> .....	54
Figure 2.35 <i>Sketch illustrating the structural controls on depositional systems on shelf, slope, and base-of-slope systems affected by gravity-driven tectonics. Terrestrial fluvial-delta systems in orange, sand-rich facies in yellow, deep-water fans in pale yellow, slope muds in grey, salt structures in pink. Note the complex and tortuous paths taken by slope channels around salt structures and folds. Sands can also pond in intraslope basins until the basin is filled and then channels continue down the topographic slope. Typical scale of 150 km (93 mi), modified from Mayall et al., 2010.</i> .....	55

**Figure 2.36 Summary figure showing the range of channel responses to growth-related seabed bathymetry. The vertical axis goes from small structures to large structures orientated at a high angle to regional dip. The horizontal axis goes from structural growth, which predates channel development and/or low erosion of channels, through offset stacking due to growing structures to channels cutting through growing structures. Examples described in the text are plotted on this matrix. The direction of flow is shown by blue arrows except in the middle lower seismic line, where flow would be into the page (from Mayall et al., 2010). .....56**

**Figure 2.37 Illustration of styles of accommodation associated with mass-transport deposits (from Kneller et al., 2016). .....58**

**Figure 2.38 Downdip changes in the morphology of a slide in the Magdalena Fan, Offshore Columbia. View between the northern downdip anticline and the updip anticline. V-Z seismic cross sections showing that the height and slope of the lateral walls of C1 decrease downdip and highlighting changes in the slope of the lateral margins which are sometimes related to changes in the substrate units (modified from Ortiz-Karpf, 2016). .....59**

**Figure 2.39 Composite mass transport deposit (MTD) (elements lettered A to H) and interpreted stratigraphy of updip ponded deposits (I), (A) with seismic data and (B) without seismic data. The truncation onlap sequences and sediment tilting suggest that the MTD was moving downslope slowly after emplacement. Upper slope, Nile Cone. Seismic data courtesy of BG Scale division is 100 ms two-way travel time (TWTT). trunc. = stratigraphic truncation (from Kneller et al., 2016). .....60**

**Figure 2.40 Schematic depiction of the two main types of submarine landslides according to their frontal emplacement: (a) Frontally emergent landslide. Note that the material ramps out the basal shear surface onto the seabed and is free to travel considerable distances over the undeformed slope position. (b) Frontally confined landslide. The mass is buttressed against the frontal ramp and does not abandon the original basal shear surface (from Frey-Martinez et al., 2006). .....61**

**Figure 2.41 Schematic illustration of the factors (slope angle, depth BSS, and slope length) controlling the height of the CoG (centre of gravity) above the frontal ramp and thus the frontal emplacement style of subaqueous landslides (yellow: confined; red: emergent). These controlling**

*factors are interchangeable, so that steeper slopes, shallower excavation or longer slopes all produce more emphasis on frontal thrusting and emergence (from Moernaut and De Batist, 2011).* ..... 62

Figure 3.1 *Reconstruction of SW Gondwana and the Karoo basin during the Late Palaeozoic. The high-standing Precambrian basement (from Scheffler et. al., 2003, 2006).* ..... 65

Figure 3.2 *Geological map of the Western Cape Province, South Africa (modified from Flint et al., 2011).* ..... 66

Figure 3.3 *Graphic summary of the generalised Cape-Karoo stratigraphy (from Linol and de Wit, 2016)* ..... 67

Figure 3.4 *Interpreted structural palaeogeography of the Karoo Basin at Ecca Group time. Modified from de Wit and Ransome (1992), Hällich (1992) and van Lente (2004).* ..... 68

Figure 3.5 *Model for the evolution of the Cape and Karoo basins. Each tectonic episode consisted of uplift, local fault-controlled subsidence and large scale regional subsidence with only minor brittle deformation. The principal episodes of basin formation were (A–D) Saldanian orogeny and Cape basin, (E–F) regional uplift and early Karoo basin (Dwyka–Ecca–lower Beaufort), and (G–H) Cape strike-slip orogeny and late Karoo basin (upper Beaufort–Stormberg). Dynamic topography was determined by first-order crustal faults and vertical motion of basement blocks due to mantle flow. Major subsidence in the Ordovician, Devonian and Permian is attributed to lithospheric deflection which suggests that mantle flow was coupled to palaeo-Pacific subduction. Red box indicates Permian phase relevant to this study (modified from Tankard et al., 2009).* ..... 69

Figure 3.6 *A lithostratigraphy of Western Cape. B Stratigraphy of Laingsburg depocentre (from Flint et al., 2011).* ..... 71

Figure 3.7 *Schematic section showing sequence stratigraphic division of Laingsburg and Fort Brown formations. Sand-rich Sub-unit sequence tract and overlying transgressive-highstand systems tract mudstones represent a sequence, groups of these and overlying inter-unit transgressive-highstand sequence set mudstones represent composite sequences, groups of composite*

<i>sequences and thicker interunit transgressive-highstand composite sequence mudstones represent composite sequence sets (Flint et al., 2011).</i> .....	74
Figure 3.8 <i>Location of logged sections new and revisited/ relogged in this study colour coded by chapter in which dataset is used. Grid references in Appendix A.</i> .....	78
Figure 3.9 <i>Location of roads, tracks, rivers and farms within the Laingsburg depocentre.</i> .....	79
Figure 3.10 <i>Representative chart of thickness data preparation for the creation of isopach maps in ArcGIS.</i> .....	80
Figure 3.11 <i>Well exposed individual thin beds are seen to be very laterally continuous (right). More normally, the mudstones break up into small pencil shaped shards due to a well-developed fracture network (left).</i> .....	84
Figure 3.12 <i>Thinly laminated siltstone beds.</i> .....	85
Figure 3.13 <i>Unit E, distal external levee - Allemansdrift farm (Left). Unit E lobe fringe- Slagtersfontein Farm (Right).</i> .....	86
Figure 3.14 <i>Unit D external levee, Krantz, GPS for scale (left) and Unit D External levee, C-D Ridge, pencil for scale (right).</i> .....	88
Figure 3.15 <i>Planar laminated sandstone (left) and rippled external levee at Grootkloof (right).</i> .....	90
Figure 3.16 <i>Varying scale scour surfaces – Slagtersfontein farm.</i> .....	91
Figure 3.17 <i>Sigmoidal bedforms in sandstone beds, Sub-unit E2, external levee, Heuningberg south limb (left) and Unit D, lower proximal external levee, CD Ridge - near to the Bav 1A wellsite (right).</i> .....	92
Figure 3.18 <i>Lobe axis banded sandstone from the Wilgehout River locality.</i> .....	94
Figure 3.19 <i>Photograph of structureless sandstone in Unit B, at Skeiding. Interpreted to be a channel complex (left) and a Close up photograph of structureless sandstone from Unit C2, near Baviaans farm, Interpreted to be part of a channel axis deposit (right).</i> .....	95
Figure 3.20 <i>Mud rich debrite with sandstone pseudo nodules (left) and Sand rich debrite within the C1 lobe exposed at Zoutkloof (right).</i> .....	96
Figure 3.21 <i>Folded deposits present at Vrisgewaagd farm and Skerwerkraal farm.</i> .....	97
Figure 3.22 <i>Rip-up conglomerate (left) and base of bed mudclasts (right).</i> .....	98

- Figure 3.23 *Hybrid beds- Slagtersfontein farm (top and bottom left), Allemansdrift farm (top and bottom right).* ..... 100
- Figure 3.24 *Clastic injectite complex beneath, and probably sourced from Unit E at Leeugat, northern limb of the Floriskraal syncline (left) and Close up of dykes below Unit E at Leeugat (right).*..... 102
- Figure 4.1 *Example of a submarine landslide confined by a basal shear surface including lateral margins from a 3D seismic volume of upper to mid slope deposits, Magdalena Fan, Caribbean Sea, offshore Colombia. (A) Variance extraction map of submarine slide. (B) Seismic cross sections through submarine slide highlighting the erosional basal shear surface and depositional relief at the top of the initial remobilized/ mass transport deposit (MTD) fill, showing the widening and shallowing of the basal shear surface down-dip (adapted from Ortiz-Karpf et al., 2017).* ..... 105
- Figure 4.2 *(A) Image of southwestern Karoo Basin showing Tanqua and Laingsburg depocentres outlined and study area enlarged. (B) Enlargement of outcrop section showing data points and outcrop location. Sections east and west of the zones of no exposure/ tectonic deformation show in place strata unaffected by large-scale erosion surfaces. (C) (Left) Stratigraphic column of Late Carboniferous, Permian and Early Triassic deposits in the Laingsburg depocentre. Blue dashed box indicates units involved in this study. (Right) Logged section of strata outside of outcrop, showing in place deposit, unaffected by large-scale erosion. Lower logged units correspond to the Whitehill, Collingham and Vischkuil formations. Upper units of thick remobilized sandstone and bedded turbidites may correspond to the Vischkuil/ Laingsburg Formations or the equivalent formations to the East.* ..... 108
- Figure 4.3 *(A) Logs and correlation of units across outcrop. Colours indicate facies associations, red lines show observed and interpreted surfaces. Numbers indicate package divisions. Log of Surface 2 infill (Packages 4 and 5) shown in figure 4.9. (B) Photopanel of outcrop with overlay of logged sections, facies associations and erosional surfaces. Panel and logs shown in more detail in Appendix B.1.* ..... 110



**Figure 4.4 Representative photographs depicting facies associations present throughout the outcrop.**

**(A) Iron-rich mudstone, Prince Albert Formation. (B) Organic rich mudstone, Whitehill Formation, notebook shown 20 cm long. (C) Iron cemented sandstone turbidite beds. (D) Matjiesfontein chert, marker bed, lens cap 7 cm in diameter. (E) Interbedded sandstone/ siltstone turbidites and ash deposits (marked as A), notebook 20 cm long. (F) Interbedded turbidites and chert layers, notebook 20 cm long. (G) Sharp topped sandstone and siltstone beds, upper turbidite marker package. (H) Sandstone to siltstone graded turbidite beds. (I) Thin-bedded turbidites. (J) Planar and climbing ripple laminated turbidite. (K) Iron-rich ripple laminated turbidite. (L) Thick debrite. (M) Section of debrite with mm- cm scale mudstone clast in distinctive blue mud-rich matrix, pencil for scale. (N) Folded interbedded sandstone and siltstone turbidites, geologist for scale. (O) Folded and slumped sandstone beds, white dashed lines indicates fold of beds, geologist for scale. (P) Base of folded sandstone bed. ....111**

**Figure 4.5 Sketches illustrating stratigraphic evolution, divided into 7 key stages. (P1) Deposition of lower Ecca group, folded and chaotic strata and megaclasts. (S1) Formation of surface 1, (P2) overlain by folded, chaotic deposits and clasts. (P3) Deposition of onlapping and infilling turbidites and chaotic strata. (S2) Formation of surface 2. (P4) Infill of surface by chaotic deposits. (P5) Deposition of onlapping and infilling turbidites and folded strata. Palaeocurrents from ripple, groove, flute and scout marks. Note formation and filling of surfaces may have been instantaneous. ....116**

**Figure 4.6 Photograph of lower stratigraphy, Collingham Fm. with Matjiesfontein chert bed, decreasing upwards in ash and chert with a transitional boundary to overlying silt-rich turbidites. A sharp, slightly erosive boundary marks the deposition of chaotic and remobilized strata. ....117**

**Figure 4.7 Key architectural characteristics across outcrop. (A) Lower stratigraphy (Package 1) cut by Surface 1, which passes from a sharp, stepped surface to intense zone of sheared mudrock laterally (detailed photo shown in figure 4.8A), overlain by onlapping turbidites and chaotic deposits (Package 3), cut by Surface 2, overlain by chaotic deposits and megaclast (Package 4) and further overlain by onlapping graded turbidites, chaotic packages and upper turbidite package datum (Package 5). (B) Collingham clast (Package 2) overlain by onlapping but rotated turbidites (Package 3), cut by Surface 2 and overlain by debrites and further onlapping turbidites**

*(Package 4). (C) Debrite and slumps (Package 2) overlain by megaclasts (Package 2) and debrites (Package 3), cut by Surface 2 overlain by debrites (Package 4) and onlapping, graded turbidites (Package 5). Facies association colour key shown on figure 4.3. .... 118*

**Figure 4.8 Photos basal shear zone (Surface 1) and slumped sandstone-rich turbidites and surface 2.**

*(A) Section of basal shear zone with foiled fabric, contorted strata, sheath folds and white lines showing numerous small scale faults. (B) Stepped section of surface 2 cutting folded and dewatered sandstone turbidites (Package 3). Overlying turbidites onlap surface (Package 5). (C) Erosional surface eroding slumped sandstone (Package 3) overlain by Collingham clast (Package 4). (D) Stepped surface 2 with onlapping turbidites (Package 5) from opposing sides of topography. (E) Scour present on top of erosional surface with coarse lag of medium sandstone and mudclasts. (F) Scour on top of erosional surface mantled with mudstone clasts. .... 119*

**Figure 4.9 Logged section through Package 4 and Package 5. Base of log is Surface 2. Location of log**

*shown on figure 4.3 and 4.7C. Chaotic deposits of Package 4 are overlain by thick graded turbidite beds which transition upwards into thinner sharp topped beds with intervening layers of chaotic and folded deposits that are laterally extensive over the outcrop. Top 12 m of log are used as upper datum for figure 4.3. Key for facies association on figure 4.3. .... 123*

**Figure 4.10 Sketches illustrating depositional and erosional evolution over the outcrop and the**

*surrounding area, with sequential panels simplified from figure 4.3. (P1i) Deposition of lower Ecca Group stratigraphy towards the east. (P1ii) Unconfined remobilized deposition. (S1 and P2) Erosion by basal shear surface 1 and remobilized infill towards the north. (P3i) partially confined turbidite infill, with overlying chaotic deposits. (P3ii) Partially remobilized intraslope lobe complex. (S2 and P4) Erosion by basal shear surface 2 and chaotic infill. (P4i) Fully confined turbidite and chaotic infill of surface 2. (P5ii) Overspill of confining topography and unconfined turbidite deposition. .... 125*

**Figure 4.11 Post deposition failure of surfaces. Including tilting of onlapping strata and failure away**

*from lateral margins and headwall. Both Surface 1 and 2 basal shear surfaces display a variation when eroding into coarser sediment (sharp/ stepped) or finer material (chaotic zone of shear). Dashed brackets numbered 1-3 refer to slide complex subdivisions (Stage 1, 2 and 3), discussed in text and shown in figure 4.12. .... 130*

**Figure 4.12** *Three key stages of outcrop evolution. Stage 1- deposition of frontally emergent remobilized deposits with onlapping turbidity currents, with basal shear surface located up-dip of the outcrop exposure in this study. Stage 2- Formation of basal shear surface 1, with initial remobilized deposits either frontally confined with frontal ramp creating down-dip topography or frontally emergent and creating a mounded topographic barrier down-dip. Subsequent infilling turbidites are partially confined. Stage 3- Formation of basal shear surface 2 with initial remobilized deposits either frontally confined with frontal ramp creating down-dip topography or frontally emergent and creating a mounded topographic barrier down-dip. Subsequent turbidite and remobilized infill transitions stratigraphically from fully confined to unconfined.* 134

**Figure 4.13** *(A) Simplified dip section of Stage 1, 2 and 3 basal shear surfaces and subsequent deposits, showing possible scenario to create strike section documented in this study. (B) Evolution of turbidite confinement from Stages 1-3 showing transition from unconfined turbidites, to partially confined and fully confined with each subsequent failure. Dip section shows how increasing slope gradient and mounding of deposits down-dip could create increased turbidite confinement whilst initial remobilized deposits remain frontally emergent with decreasing run-out distance.* .....135

**Figure 4.14** *Sketch of shelf and slope systems indicating how interplay of sediment supply rate and rate of slope degradation can vary the infill of submarine slide basal shear surfaces. Slides in areas of high sediment supply can cause the capture and rerouting of sediment pathways, and become quickly infilled and overspilled. In locations distal to sediment supply, slides can remain underfilled with degradation rate outpacing sedimentation rate. In intermediary areas periods of high and low sediment supply mean that on average sediment supply is roughly equal to degradation rate.* .....139

**Figure 5.1** *(A) Location of the study area within southwestern Africa. Black box indicates location of map B. (B) Regional geological map of the Western Cape. The study area is located in the Laingsburg depocentre, where Ecca Group stratigraphy is exposed, north of the Swartberg branch of the Cape Fold Belt (Modified from Flint et al., 2011).* .....145

**Figure 5.2 (A) Stratigraphic column showing the Permian Eccca Group deposits in the Laingsburg depocentre, southwestern Karoo Basin. This stratigraphy represents margin progradation from deepwater basin plain deposits (Vischkuil and Laingsburg formations), through submarine slope (Fort Brown Formation) and continues to shallow water (Waterford Formation). Blue box indicates detailed section shown in B. (B) Submarine slope system Unit D/E and Unit E of the Fort Brown Fm., the focus of this study (modified from van der Merwe et al., 2014). ..... 146**

**Figure 5.3. (A) Location of the study area relative to Laingsburg town. Dashed lines indicate the location of outcrop belts. White shading indicates the exposure of Fort Brown and Laingsburg formations. Locations marked Roggekraal, Zoutkloof and Geelbek are the study areas related to the corresponding up-dip deposits of Unit E (Spychala et al., 2015). (B) Enlarged area shows the four sections of regional panels involved in this study and the key Slagtersfontein location. The northern panel 1, contains 64 logs, the central northern panel 2, contains 67 logs, the central southern panel 3, contains 39 logs, and the southern panel 4 contains 30 logs. The highest concentration of data is in the Slagtersfontein study area on panel 2. Locally the top of Unit E3 along panel 3 is lost to modern erosion by a tributary of the Gamka River. Aerial photographs are from NASA Visible Earth (National Aeronautics and Space Administration, <http://visibleearth.nasa.gov/>; regional scale) and Chief Directorate: National Geo-spatial Information, South Africa (<http://www.ngi.gov.za/>; Laingsburg depocentre). (C) Google Earth image of Slagtersfontein study area showing laterally continuous Unit D and abrupt thickening of Unit E down-dip. Tops and bases of units are mapped by walking surfaces and tracking with GPS..... 148**

**Figure 5.4 Regional dip correlation panel along the Baviaans South outcrop belt with data from previous studies (van der Merwe et al., 2014; Spychala et al., 2015), showing the D-E interunit mudstone, Unit D/E, Unit E, and the E-F interunit mudstone Interpretations of architectural elements show the down-dip transition in Unit E from slope channels, through intraslope lobes, channel-levee systems and channel-lobe transition zone, to basin-floor fans. Datum used is top Unit B, an underlying basin-floor fan (shown in Fig. 5.2A). Map highlights the location of outcrop belt within Figure 5.3, with the red line denoting the location of this dip section and black dashed lines showing other exposed sections. .... 149**

- Figure 5.5 Representative photographs of sedimentary facies. (A) Structureless sandstone; (B) Structured sandstone, dashed white lines indicate sheared climbing ripple laminations; (C) Mudstone clast conglomerate; (D) Scoured siltstone and sandstone, dashed red lines indicate erosional surfaces; (E) Hybrid beds, dashed white line indicates division between lower sandstone turbidite and upper debrite; (F) Interbedded sandstone and siltstone; (G) Remobilised deposits; (H) Hemipelagic mudstone. Scales: logging pole with 10 cm divisions, camera lens 7 cm in diameter. ....151**
- Figure 5.6 Regional correlation panels of Unit D/E and subunits E2 and E3. Panels positioned north (top) to south (base). Southern panel (panel 4) shown on Figure 5.7 with facies associations, consisting of E3 with two small outcrops of Unit E2, in the up-dip area. Relative spatial positions shown in fence diagram (Fig. 5.8). More detailed panel of Slagtersfontein CLTZ shown in detailed panels (Figs 5.10 and 5.11). Rose diagrams show palaeocurrent directions from ripples, grooves and flutes throughout all units. ....157**
- Figure 5.7 Regional correlation panels showing facies associations of Unit D/E and subunits E2 and E3. For Unit divisions of panels A, B and C see Figure 5.6. For logs and more detailed panels, see Appendix B.2-5. ....158**
- Figure 5.8 Fence diagram showing 3D architecture and facies associations of Units D/E, E2 and E3. For geographic positions of outcrop belts see Figure 5.3B. For unit divisions see Figure 5.6. For key see Figure 5.7.....159**
- Figure 5.9 Combined thickness isopach maps and gross depositional environment reconstructions for (A) Unit D/E, (B) Subunit E2 and (C) Subunit E3. Contours indicate thickness of unit in metres, contour spacing at 2 m for D/E, 1 m for E2 and 5 m for E3. Black circles indicate locations of data from logged sections shown on panels (Figs 5.6 and 5.7), red circles indicate data from logs presented in Appendix A and B2-5. White arrows indicate average palaeocurrent direction. Geographic area covered is the same as that shown in Figure 5.3B, presented in palinspastically restored positions Mapped thickness distributions were created by fitting a surface to thickness values extracted from the logged sections. The surfacing operation was conducted in ArcGIS using the simple kriging tool within the Geostatistical Wizard (<http://resources.arcgis.com/en/home/>). Output maps are extended to the extremities of the**

*input data by the surfacing algorithm, which creates rectangular maps that may extend beyond the edge of the input data. Additional modifications were made to subunit E3 surfaces to account for minimum values of the down-dip logged sections along panel 3. Channel and lobe boundaries are not precise locations and are interpreted from thickness trends and palaeocurrent directions. Palaeogeographic maps are based on the distribution of sedimentary facies and architectural elements. .... 160*

**Figure 5.10** *Slagtersfontein detailed section, location shown on figure 5.6, 5.7 and 5.8. Up-dip area of Slagtersfontein panel, divided into sections 1-3 for description purposes. Deposits transition from levee (section 1) to sediment bypass dominated zone (sections 2 and 3), figure 5.11 continues down-dip showing sections 4 and 5. (A) Simplified panel section across whole Slagtersfontein study area, highlighting the focus of this figure. Colours indicate subunits E2 and E3 separated by the E2-E3 intra-unit mudstone. (B) Panel showing logged sections of E2 and E3, datumed on Top Unit D. For larger regional panel 2, see figures 5.7 and 5.8. Logs and log key are in Appendix B2-5. (C) Schematic sketch of key features in subunits E2 and E3 across section, showing down-dip changes in thickness, facies and sedimentary structures. .... 165*

**Figure 5.11** *Down-dip area of Slagtersfontein panel, continuing from Figure 5.10, divided into sections 4-5 for description purposes. Deposits transition from thin, dewatered, scoured and reworked sandstone (section 4) to abruptly thickening lobe deposits (section 5). (A) Simplified panel section across whole Slagtersfontein study area, highlighting the focus of this figure. Colours indicate sub-units E2 and E3 separated by the E2-E3 intra-unit mudstone. (B) Panel showing logged sections of E2 and E3, and localised deposition of Unit D/E. Datum for panel is Top Unit D. (C) Schematic sketch of key features in subunits E2 and E3 showing down-dip changes in thickness, facies and sedimentary structures. T1- T4 refer to sequence of deposition shown in Figure 5.15. For key see Figure 5.10. .... 166*

**Figure 5.12** *Representative photographs of Unit E3 over sections 2 to 5 of the Slagtersfontein CLTZ. (A) Basal spill-over fringe deposits and aggradational sandstone bed. (B) Composite erosional surfaces, aggradational sandstone bed with scoured top and overlying siltstone and lag deposits. (C) Rippled thin sandstone beds. (D) Discontinuous lenticular sandstone beds cut by erosional surfaces and draped by lags. (E) Highly dewatered sandstone beds with erosional surfaces*

*throughout. (F) Megaflute scour at top of unit, eroding dewatered sandstone. (G) Thin eroded sandstone bed, constituting the entire coarse component of E3. (H) Thick amalgamated sandstone beds and sand-rich hybrid beds of E3 proximal lobes. (I) Discontinuous lenticular sandstone beds, cut by erosional surfaces and draped by lags, at the base of E3 lobe deposits. (J) Sand-rich hybrid bed. Scales: logging pole with 10 cm divisions, notebook 15 cm in length. ....167*

**Figure 5.13** *(A) Location of section shown in B and C within the CLTZ. Colours indicate subunits E2 and E3 separated by the E2-E3 intra-unit mudstone. (B) Outline of beds over outcrop and coloured with facies association scheme. Abbreviations: Sc. st. and sd.- Scoured siltstone and sandstone, Int. st. & sd.- Interbedded siltstone and sandstone, Lag- Bypass lag, St-less sand- Structureless sandstone, Int. st. & sd.- Interbedded siltstone and sandstone, E2-E3 st.- E2- E3 intra-unit mudstone, Int. silt.- Interbedded siltstone, SOF- Spill-over fringe, D-E silt- Unit D-E inter-unit mudstone. (B) Sections logged at mm scale over 20 m outcrop distance, showing bed scale changes in subunits E2 and E3 within the CLTZ. This key area shows features consistent with a fluctuation of high and low energy deposits throughout E3, with a layering of medium sandstone, low energy thin-beds, composite erosional surface with mudclast lags, thick aggradational beds, and further erosional surface and lag deposits which decrease upwards. For whole Slagtersfontein section see Figures 5.10 and 5.11. ....169*

**Figure 5.14** *Summary figure of overall stepped-slope profile architecture and related deposits of Unit E. Flows were fed through entrenched slope channels to intraslope lobes, and channel levee systems, to the CLTZ and basin-floor lobes. Logs show typical section through key areas. Logs from outside of the study area modified from van der Merwe et al., 2014. ....175*

**Figure 5.15** *Sketch of interpreted variations in the CLTZ over the Slagtersfontein section shown in Figures 5.10 and 5.11. T1-T4 show the minimum extent of progressive expansions and contractions of the CLTZ. T1 shows the initial location of bypass and deposition dominated areas with initial deposition of structured sandstone with a minimum thickness of a few metres. T2 shows the eastward movement or extension of the bypass dominated channel-lobe transition zone, with erosion of initial lobe deposits and focus of deposition shifted down-dip. T3 shows the westward movement or contraction of the bypass zone and backfilling of the system, with build-up of sand-rich proximal lobe deposits over bypass surfaces. T4 shows the final stage of CLTZ*

*extension or easterly movement, indicated by efficient sediment bypass in the up-dip area, a large erosional surface cutting into the lobes and a widespread megaflood surface which expands down-dip of this area. .... 177*

**Figure 5.16 (A) Plan view of a CLTZ, highlighting the key depositional features and their spatial distribution modified from Wynn et al. (2002). Note area of mixed depositional and erosional features, area of reworked and scoured lobe and axial- and off-axis proximal lobe deposits. Diagram in Wheeler space illustrates movement of a CLTZ over 6 time periods A-F, with (B) showing a plan view outline for each time period and (C) illustrating resultant build-up of deposits and potential erosion over a dip-section (X-X') and a distal strike-section. (D) A further strike-section through a more proximal area of the CLTZ, illustrating deposition and potential erosion. This diagram highlights the composite nature of deposits and erosional surfaces throughout CLTZs and the dynamic expansions, contractions and shifting of the zone that they represent. Overall preservation potential is variable but low, with shifting of the zone often decimating evidence of previous positions. The dark black lines represent periods of migration of the CLTZ. Grey draping units represent a hiatus in sand deposition and may include silt-rich lateral or frontal lobe fringe. .... 182**

**Figure 6.1 Examples of slope and basin floor topography and resultant deposits. (A) Simple slope profile with single break-in-slope changing from bypass dominated channel-levee system to depositional dominated basin floor lobes, with potential for channel-lobe transition zone (CLTZ) development at base-of-slope. (B) Stepped-slope profile with higher gradient ramps linking lower gradient steps. Formation of entrenched channel/channel levee systems on ramps and intraslope/ basin floor lobes on steps, with potential for CLTZ development at breaks-of-slope. (C) Topographically complex slope, encompassing varying magnitudes of topography. Development of several ramps within entrenched channel/channel levee systems, including a step on the basin floor. Intraslope and basin-floor lobe development on lower gradient steps. Formation of tortuous corridor controlled by slope topography, and minibasin where 3D closure occurs. Topography on slopes is generally of much greater magnitude than on the basin floor. .... 190**



Figure 6.2 (A) Map of Africa and geological map of SW Africa with location of Laingsburg depocentre.

(B) Enlarged section of Laingsburg depocentre showing location of outcrop belts along post depositional fold limbs. Black dashed lines highlight the regional scale correlation panels. (C) Stratigraphic column of Ecca group stratigraphy, highlighting Laingsburg and Fort Brown submarine fan Units A, B, C, D, E and F as well as discontinuous smaller fan units A/B, B/C and D/E. ....191

Figure 6.3 Representative photographs depicting facies associations present throughout the outcrop.

(A) Thick structureless amalgamated sandstone. (B) Base of structureless sandstone bed showing grooves and tool marks. (C) Elongated mudstone clasts present near the base of a structureless sandstone bed, lens cap 7 cm in diameter. (D) Laminated and graded tops of structured sandstone beds. (E) Planar/ ripple laminated very fine sandstone- siltstone beds. (F) Climbing ripple laminated sandstone bed, with mudclasts draping laminations and forming a layer at the base of the bed, lens cap 7 cm in diameter. (G) Dewatered banded sandstone. (H) Ripple laminated sandstone, pencil 7 cm in length. (I) 10-30 cm beds with bi-partite bed structure, lower division of fine sandstone and thinner upper division of poorly sorted sandstone and siltstone with mm-cm mudstone clasts and organic matter. (j) Interbedded 10-15 cm sandstone beds and thinner siltstone beds. (K) Interbedded sandstone and siltstone with deformation. (L) Interbedded cm thick siltstone beds, overlain by thicker structured sandstone beds. (L) Tightly folded sandstone and siltstone thin beds, notebook 15 cm in length. (N) Debrite with mm-cm scale mudclasts and organic fragments. (O) 10s of m thick regional mudstone packages separating larger and smaller fan units, car for scale marked by dashed box. ....194

Figure 6.4 Core examples of Unit B/C demonstrating key features and range of structures recognised,

including: sharp base and top of units; clastic injectites surrounding unit; mudclast layers throughout unit and mudclast conglomerates; ripple laminated sandstone and siltstone; planar laminated sandstone and siltstone; dewatering structures and small scale scouring. Blue arrows indicate top and base of units. ....195

Figure 6.5 Core examples of Unit A/B demonstrating key features and range of structures recognised,

including: sharp base and top of units; mudclast layers throughout unit; ripple laminated

*sandstone and siltstone; planar laminated sandstone and siltstone; dewatering structures and small scale scouring. Colour and hue modified from original to accentuate structures..... 196*

**Figure 6.6 Range of discontinuous beds within A/B, B/C and D/E. (A) Basal scour with draped infilling sandstone and siltstone. (B) Erosional surface cutting 1-2 m within unit truncating strata, with onlap of overlying beds. (C) Onlap of basal beds onto topography created by regional mudstone. (D) Downlap of basal beds onto regional mudstone. (E) Erosion surface within unit cutting down to base. Infilling beds onlap, and then drape over surface. .... 197**

**Figure 6.7 Key architectural elements recognised in Units A/B, B/C and D/E. Sketch of 3D lobe shows divisions of sub-environments, with scale demonstrating general thickness of smaller and larger fan units. Lobe axis, lobe off-axis, lobe fringe and proximal lobe panels show representative section from Units A/B, B/C and D/E. Blue indicates interpretation as clastic injectite (Cobain et al., 2015). .... 203**

**Figure 6.8 Thickness (left) and facies (right) maps of Units A/B, B/C and D/E. Thickness maps show isopach thickness in metres. Facies maps represent gross depositional environment for the time interval. A/B and B/C deposits are restricted to up-dip of the Faberskraal-Geelbek area. A/B deposits are thickest, most sand-rich and axial in the Baviaans and Heuningberg areas, with bypass dominated proximal lobe scours/distributary channels present in the Baviaans area. Deposits decrease in thickness and sand content to off-axis facies to the east and west. Lobe fringe deposits and pinch-outs are a combination of sand- and silt-rich in Geelbek and Heuningberg. B/C deposits are thickest, most sand-rich and axial in the Baviaans area. Deposits decrease in thickness and sand content to off-axis and fringe facies to gradually to the north and more abruptly to the east and west. Pinchouts are sand-rich at the lateral east and west margins and silt rich to the north. Unit D/E is present discontinuously in (a) Heuningberg, with thick axial deposits abruptly thinning and pinching out west, south and east, (B) in Geelbek, present locally as a single debrite bed, and (c) in Floriskraal, present in a southeast-northwest transect decreasing in thickness abruptly to the east and west (Slagtersfontein) with sand-rich pinch out, to the south with a silt rich pinch out, and more gradually to the north (N1 Dome) with a silt and debrite-rich pinch out. .... 208**

- Figure 6.9 *Thickness and facies maps of smaller fan units overlain on 3D box models demonstrating controlling basin floor and slope topography. ....210*
- Figure 6.10 *Shelf, slope and basin floor profile during deposition of larger and smaller fan units. Lower sea-level during deposition of larger units, exposes shelf and activates canyons in upper slope connecting sediment pathways down the slope. Comparatively lower sea-level during deposition of smaller units reduces/cuts off main sediment input. ....211*
- Figure 6.11 *Thickness and facies maps of Units C and D. Thickness is shown as isopachs with units in metres. Facies maps represent gross depositional environments for the given time intervals. Based on studies by, Sixsmith et al., 2004; Di Celma et al., 2011; Hodgson et al., 2011; Brunt et al., 2013 a; Morris et al., 2014a, b; van der Merwe et al., 2014; Morris et al., 2016. ....214*
- Figure 6.12 *Thickness and facies maps of ‘sand-attached’ units C and D overlain on 3D box models demonstrating controlling slope to basin floor topography. Based on studies by, Sixsmith et al., 2004; Di Celma et al., 2011; Hodgson et al., 2011; Brunt et al., 2013 a; Morris et al., 2014a, b; van der Merwe et al., 2014; Morris et al., 2016. ....215*
- Figure 6.13 *Thickness and facies maps of Units E and F. Thickness is shown as isopachs with units in metres. Facies maps represent gross depositional environments for the given time intervals. Based on studies by, Figueiredo et al., 2010; 2013; van der Merwe et al., 2014; Spsychala et al., 2015; Chapter 5. ....218*
- Figure 6.14 *Thickness and facies maps of ‘sand-detached’ units E and F overlain on 3D box models demonstrating controlling slope to basin floor topography. Based on studies by, Figueiredo et al., 2010; 2013; van der Merwe et al., 2014; Spsychala et al., 2015; Chapter 5. ....219*
- Figure 6.15 *Schematic section showing sequence stratigraphic division of Laingsburg and Fort Brown formations. Sand-rich Sub-unit sequence tract and overlying transgressive-highstand systems tract mudstones represent a sequence. Groups of these and the overlying inter-unit transgressive-highstand sequence set mudstones represent composite sequences. Groups of composite sequences and thicker interunit transgressive-highstand composite sequence mudstones represent composite sequence sets. A/B, B/C and D/E are deposited at the start of each composite sequence set (Flint et al., 2011). ....220*

- Figure 6.16 *Dip-section through central line of Laingsburg depocentre showing thickness of Vischkuil, Laingsburg and Fort Brown formations. The section demonstrates system scale compensational stacking between units as well as the prevalence of two separate areas of increased deposition with an intervening area of thinning, exacerbated by differential compaction. .... 223*
- Figure 6.17 (A) *Lobe updip, downdip and lateral pinchouts of smaller and larger units colour coded into stratigraphic packages. Grey shaded area indicates the region of sustained topographic influence throughout deposition of all units. (B) Thickness maps of the combined Collingham and Vischkuil formations, Unit A and Unit B. Overlay shows area of sustained topographic influence. .... 224*
- Figure 6.18 *Graph showing comparison of sedimentation and deformation rates throughout the deposition of the Laingsburg and Fort Brown formations. Phase 1 includes Units A, A/B and B; overall sedimentation rate outpaces deformation rate, with units A/B deposited onto a more deformed slope. Phase 2 includes Units B/C, C and D; overall sedimentation rate was roughly equal to deformation rate, periodically healing and overspilling slope topography in time of increased sedimentation. Phase 3 includes Units D/E, E and F; overall sedimentation rate was outpaced by deformation rate. Sedimentation rate was only sufficiently high during the later stage Sub-units E3 and F3 to equal deformation rate. .... 228*
- Figure 7.1 *Models of a simple slope profile, a stepped slope profile, a degraded slope profile and slope profile with mini-basin and tortuous corridors and a combined model showing a topographically complex slope. .... 235*
- Figure 7.2 *Types of intraslope lobe. Partially confined lobes in intraslope steps. Confined to unconfined lobes in submarine slides and 'disconnected' intraslope lobes with multiple input points. .... 238*
- Figure 7.3 *Variations across the base of slope in Sub-unit E3 (Chapter 5) from a levee-lobe transition zone (top) to a channel-lobe transition zone. .... 240*
- Figure 7.4 (A) *cross sections and (B) plan view of CLTZ, modified from Wynn et al. (2002a). .... 241*
- Figure 7.5 *Outcrop examples of the effect of lateral slopes on sedimentology and stratigraphic architecture of slope to basin floor systems at varying scales. (A) High gradient lateral margins of*

- submarine slide basal shear surfaces can contribute to complete ponding of later flows as well as cause remobilization down-slope into the centre of the basal shear surface. (B) The style of onlap of intraslope and basin floor lobes can be controlled by lateral slopes, varying from abrupt onlap against high gradient slopes to downlap in unconfined settings (from Spychala et al., 2017a). (C) The stacking of multiple lobe complexes through successive depositional systems can be influenced by active uplift of a lateral basin margin. ....244*
- Figure 7.6** *Variation in turbidity current confinement overlying varying morphologies of basal shear surface and initial remobilized infill, with stacking example from Chapter 4 and two other scenarios of decreased slope uplift and a longer slope. ....248*
- Figure 7.7** *Graph showing comparison of sedimentation and deformation rates throughout the deposition of the Laingsburg and Fort Brown formation (more detail given in figure 6.18), further extended to show a scenario where deformation continues to outpace sedimentation. ....250*
- Figure 7.8 (Top)** *Variations in sedimentation vs. deformation rate if deformation were to increase/decrease in magnitude, and (bottom) if no long-term clastic shut off were to occur. 251*
- Figure 7.9** *Example of CLTZ preservation as a single surface (from Hodgson et al., 2016) and as a volume of rock (Chapter 5). ....253*
- Figure 7.10** *Kyrre Formation, Måløy Slope, Norway- In this seismic section an area of high amplitude reflectors has been recognised, which well data has shown to be sand rich, lying down-dip of a fold structure with no apparent sand, suggesting that sand was bypassed over the structure (from Jackson et al., 2008). ....257*
- Figure 7. 11** *Bypass related erosional surfaces and deposits can be visible as sharp negative spikes in gamma ray logs. Recognition of these spikes can distinguish between bypass surfaces and distal lobe fringe fines. In a basinal context these bypass surfaces are key conduits between up-dip and down-dip coarse deposits. Logs modified from Stevenson et al. (2015). ....258*
- Figure 7.12** *Core, Gamma Ray and Neutron Porosity logs of Unit A/B. ....259*
- Figure 7.13** *Overlay of simplified panel from Chapter 4 onto example of submarine slide from Magdelana fan, offshore Colombia (from Ortiz-Karpf, 2016). ....260*
- Figure 7.14** *When deformation rate is constant and sedimentation rate gradually decreases simple slope profiles can evolve into stepped slope profiles and then slopes with minibasins and*

*tortuous corridors. Slope degradation can occur associated with all slope types but slope failures may increase in frequency and magnitude as relative slope deformation increases. .... 263*

# 1 Introduction

## 1.1 Background and rationale

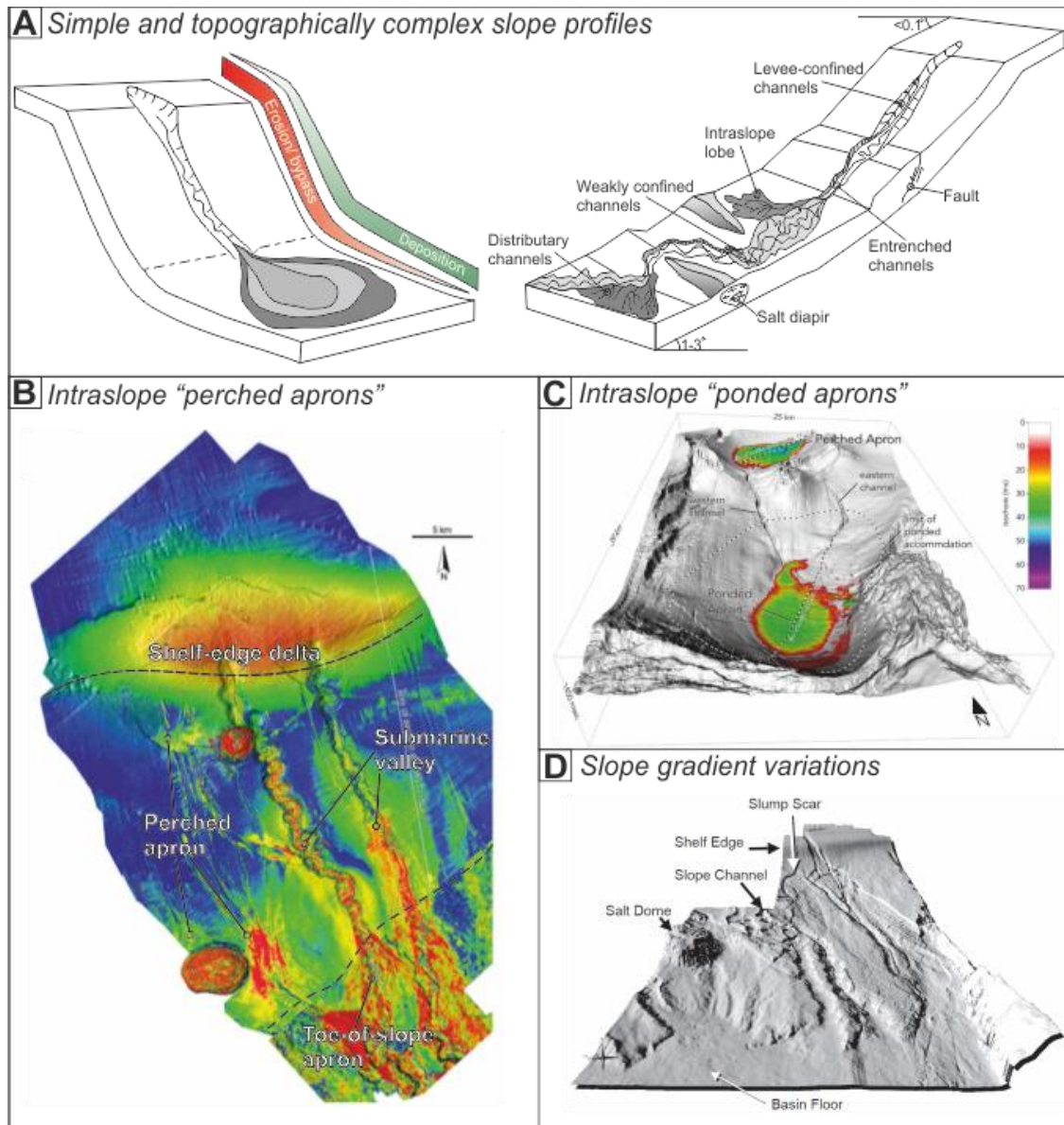
Deepwater siliciclastic systems are fed by sediment gravity flows, and form some of the largest depositional systems on the planet. Sediment is transported from the continental shelf, down through the continental slope to the deep-ocean basin floor. Significant volumes of sediment can be deposited on submarine slopes (e.g. Booth et al., 2003; Prather, 2003; Steffens et al., 2003; Mayall et al., 2010; Talling et al., 2012; Talling, 2014). Sediment gravity flows consist of turbidity currents, as well as slides, slumps and debris flows (mass flows), which form remobilized deposits or mass transport deposits (MTDs) that stack to form mass transport complexes (MTCs). MTC sediment is sourced from failure of the continental shelf and submarine landslides. Sediment gravity currents and submarine landslides present significant hazards for underwater infrastructure and have the potential to create tsunamigenic waves (Barley, 1999; Piper et al., 1999; Masson et al., 2006; Hsu et al., 2008; Romero-Otero, 2009; Talling, 2014). Moreover, the deposits of ancient deepwater systems within the subsurface represent significant hydrocarbon reservoirs and are targets for oil and gas exploration (Weimer and Pettingill, 2007).

Early submarine fan models showed the continental slope as a simple area, dominated by bypass processes feeding sediment to the basin floor, which was dominated by depositional processes (Normark, 1970, 1978; Walker, 1978; Stow et al., 1985; Reading and Richards, 1994). Recent studies, however, show that topographical complexity within slope environments is the norm (Fig. 1.1), even in passive margin settings, where such complexities have a fundamental influence on sediment gravity flow behaviour, and influence sediment dispersal patterns and consequently geometry, architecture and facies of sedimentary bodies (e.g. van Andel and Komar, 1964; Pickering and Hiscott, 1985; Simpson, 1997; Hodgson and Haughton, 2004; Amy et al., 2007; Covault and Romans, 2009; Moody et al., 2012).

## **1.2 Aims and research questions**

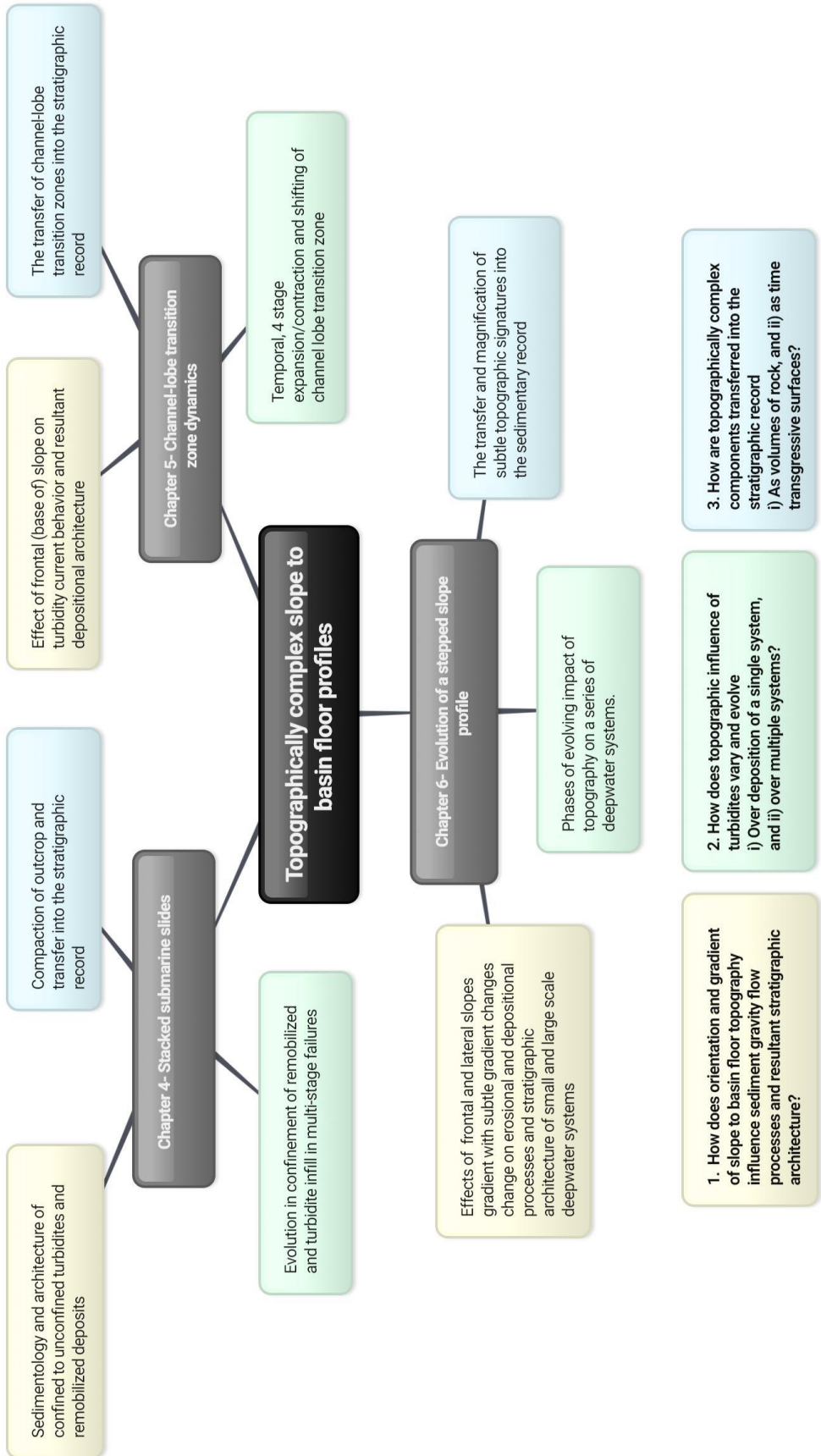
The effect of varying origins, morphology and scales of slope and basin floor topography on stratigraphic architecture of deepwater successions is poorly understood. The principal aim of this thesis is to understand the effects that complex but subtle slope and basin floor topography have on sediment gravity flow processes and resultant depositional architecture. This will enhance our understanding of deepwater system evolution, as well as helping to bridge the gap between the small scale experimental studies assessing dynamics of single flows and the large scale studies of slope and basin floor architecture using seismic reflection and modern seafloor datasets. This study will also add to our knowledge of the Karoo Basin succession in the Laingsburg depocentre along with additional SLOPE 4 projects. Previous studies undertaken as part of the SLOPE project have investigated the regional and localised aspects of stratigraphic architecture of the Laingsburg depocentre, which have been utilized in this study to investigate the influence of varying scales of topography.





**Figure 1.1** A) Models of simple and topographically complex slope profiles. (B) Examples of intraslope "perched apron", Einstein-Fuji slope Eastern Gulf of Mexico, Seismic attribute map (From Sylvester et al., 2012). (C) Intraslope "ponded apron" from the Brazos-Trinity intraslope basins, Gulf of Mexico (From Prather et al., 2017). (D) Examples of slope gradient variations (From Posamentier and Walker, 2006).

In this context, the thesis is focussed around key research questions that span data chapters 4-6 (Fig. 1.2). These are outlined in detail as follows, and will be returned to at the end of the thesis (Chapter 7):



**Figure 1.2-** Key results from data chapters 4, 5 and 6, colour coded in relation to each research question. Beige relates to question 1, green to question 2 and blue to question 3.

**Question 1:** *How does the orientation and gradient of slope to basin floor topography influence sediment gravity flow processes and resultant stratigraphic architecture?*

*Rationale:* Gradient variations and topographic obstacles along deep water slope and basin floor profiles have been documented to have significant impact on gravity flow behaviour, with consequent effect on sedimentary facies (e.g. Baines, 1984; Kneller and McCaffrey, 1991; Edwards et al., 1994; Haughton, 1994; Smith, 2004a; Hodgson and Haughton 2004; Stevenson et al., 2013; Spychala et al., 2017a) and depositional architecture (e.g. Prather, 2003; Deptuck et al., 2012; Mayall et al., 2010; Hay, 2012; Prather et al., 2012a, b; Moody et al., 2012; Wynn et al., 2012). The distribution, length scales and orientations of gradient variations can range widely, creating topographically complex slope to basin floor systems.

Many experimental and numerical studies have been undertaken with the aim of understanding the effects of gradient and confinement changes and obstacles on turbidity current processes, which can result in the reflection, deflection or decoupling of flows (e.g. Baines, 1984; Lawrence, 1986; Edwards et al., 1994; Meiburg and Kneller, 2009; Nasr-Azadani and Meiburg 2014; Wang et al., 2017). However, relating these process changes to deposits in the sedimentary record and scaling these processes to bed, package or system scale can be challenging (e.g. Pickering and Hiscott, 1985; Marjanac, 1990; Kneller and McCaffrey, 1991; Edwards et al., 1994; Haughton, 1994; Smith, 2004a; Jackson and Johnson, 2009). The effects of slope gradient on flow processes is more notable in situations where gradient change is of higher magnitude (e.g. Pickering and Hilton, 1998; Sinclair, 2000; Sinclair and Tomasso, 2002; Hodgson and Haughton, 2004; Marini et al., 2015) but more difficult to constrain where gradient change is subtle ( $<1^\circ$ ) (e.g. Smith, 2004b; Stevenson et al., 2013; Spychala et al., 2017a).

Key areas of topographic variability within slope to basin floor profiles include: slope failure, forming a concave basal shear surface, which can capture sediment routing systems, or pond deposits (e.g. Alves and Cartwright, 2010; Ortiz-Karpf et al., 2015; Kneller et al., 2016; Fallgatter et al., 2017; Qin et al., 2017); the resultant remobilized deposits, which can deflect/reflect flows and pond deposits within the rugose top surface (Armitage et al., 2009; Jackson and Johnson, 2009; Ortiz-Karpf et al., 2015; Kneller et al., 2016; Sobiesiak et al., 2016; Fallgatter et al., 2017); intraslope basins or flats (Prather et al., 2003), forming intraslope accommodation, with the potential to pond deposits, forming intraslope lobes (e.g. Steffens et al., 2003; Deptuck et al., 2012; Prather et al., 2012a,b; Spychala et al., 2015) or weakly

confined channel systems (e.g. Beaubouef and Friedman, 2000; Pirmez et al., 2000; Deptuck et al., 2012; Moody et al., 2012); intraslope variations in gradient and orientation (e.g. Hay, 2012), which can lead to increased/ decreased flow velocity, and deflection of flows, resulting in changes in system architecture, e.g. tortuous corridors (e.g. Steffens et al., 2003; Smith et al., 2004a; Burgreen and Graham, 2014); the base-of-slope, where a reduction in gradient and/or flow confinement can cause flows to undergo hydraulic jumps, transitioning from super- to sub-critical flow conditions (Mutti and Normark, 1987, 1991; Weirich, 1989; Kostic and Parker, 2006; Sumner et al., 2013) with the potential to create a sediment bypass dominated channel-lobe transition zone (e.g. Wynn et al., 2002a; Hofstra et al., 2015; Pemberton et al., 2016); and, lateral basin margins or lateral intrabasinal slopes, which can affect basin-floor depositional systems by deflecting flows (e.g. Kneller et al., 1991; Sinclair, 1994; Kneller, 1995; Amy et al., 2004; Gamberi et al., 2014; Sychala et al., 2017b) with the potential to cause onlap geometries in lobes (e.g. Smith and Joseph, 2004; Bersezio et al., 2009; Marini et al., 2015). Intraslope and basinal gradient changes can be related to dynamic substrate i.e. mud and salt diapirism, active faulting, and folding (Jackson et al., 2008).

The studies presented in this thesis investigate relatively subtle gradient changes (<1° to a few degrees) within a range of depositional settings across a slope to basin floor setting in the Laingsburg depocentre, allowing for analysis and discussion of the effects of frontal, lateral and oblique orientated gradient increases and decreases on deepwater stratigraphy.

**Question 2:** *How does topographic influence on turbidity currents vary and evolve*

*i) During deposition of a single system, and ii) during multiple successive systems?*

*Rationale:* The effect of topography on turbidite systems will inevitably depend of the scale and orientation of the topography as discussed in the rationale to Question 1, but also with variability in flow dynamics, both of which will vary temporally. Topographic variation will occur due to both active deformation of the slope (e.g. Barton, 2012; Deptuck et al., 2012; Hay, 2012; Prather et al., 2012a, b) and the modifications each flow will make as it erodes and deposits (e.g. Normark et al., 1979, 2009; Pickering and Corregidor, 2005; Dakin et al., 2013; Ortiz-Karpp et al., 2015; Sychala et al., 2015), therefore each individual flow will be interacting with a unique bathymetric configuration. Variability in flow dynamics will result from intrinsic and extrinsic controls. Extrinsic controls determine the initial thickness and volume of flows,

the sediment concentration and grain size distribution, and intrinsic factors are of influence throughout the flow pathway, causing flows to deposit or erode, and increase or decrease sediment concentration, flow velocity, stratification etc. (Kneller and McCaffrey, 1999; Kneller and Buckee, 2000). Therefore, each incoming flow is unique and the resultant effect of the same topography on flow processes will vary. Within the deposition of an individual system subsequent flows have the potential to increase (e.g. erode entrenched channel systems) or decrease topographical complexity (e.g. healing of intraslope accommodation), in an attempt to form a slope to basin floor profile that is at equilibrium (Pirmez, 2000; Prather, 2003).

Slope topography is likely to change more dramatically over the deposition of multiple systems. At this longer time scale, an actively deforming seabed has the potential to significantly alter the configuration of the slope and basin floor systems (e.g. Stewart and Clark, 1999; Lopez-Mir et al., 2014). Moreover, erosional or depositional relief of the preceding system or multiple stacked systems may be apparent on the seabed (e.g. Jackson and Johnson, 2005; Pickering and Corregidor, 2005; Sychala et al., 2015; Ortiz-Karpf et al., 2015) or result in topography generated by differential compaction (Færseth and Lien, 2002; Koša, 2007). Therefore, the ability of flows to heal topography and reach an equilibrium profile can be outpaced, be equal to, or be surpassed by formation of new topography at the onset of each depositional system.

Basins undergoing frequent episodic sediment input have been demonstrated to form more ponded and healed basin successions, which can often be associated with more numerous hydrocarbon reservoir and seal pairs (Prather, 2000, 2003). Sixty nine percent of producing deepwater hydrocarbon reservoirs occur in slope accommodation (Prather et al., 2009), with seventy five percent of global Tertiary deepwater reservoirs deposited across stepped slope profiles (O'Byrne et al., 2004). Through understanding how the effects of topography change throughout deepwater system evolution, generic models can be established, to predict changes in system architecture and to aid the interpretation of lower resolution datasets. Therefore, understanding the dynamics of these systems and being able to predict stratigraphic architecture is crucial for hydrocarbon exploration.

**Question 3:** *How are topographically complex components transferred into the stratigraphic record i) as surfaces, and ii) as stratigraphic successions?*

*Rationale:* The transfer of deepwater systems into the stratigraphic record can be complicated, especially in topographically complex areas where flow processes can be highly variable. Individual surfaces or beds can represent a large range of time scales. Therefore, it is important to consider the location of an outcrop within a system, whether the setting is overall aggradational or degradational, and the flow processes that formed the strata, when interpreting resultant deposits in order to delineate the preservation potential. Modern seafloor datasets afford a single timeslice of a system showing a geomorphic palimpsest (e.g. Wynn et al., 2002a), but if a surface is not actively aggrading or is later eroded it will not be preserved in the stratigraphic record. Distinguishing between stratigraphic surfaces that are time transgressive and composite, and geomorphic surfaces that are rarely preserved in the rock record can be challenging (e.g. Strong and Paola, 2009; Sylvester et al., 2011; Holbrook and Bhattacharya, 2012; Blum et al., 2013; Hodgson et al., 2016). This distinction between physiographic snapshot and stratigraphic transfer is important in understanding the preservation potential of all systems.

Moreover the stratigraphic record does not simply show surfaces and rock volumes as they were at initial deposition. Dewatering, compaction and deformation takes place, possibly through multiple cycles. Compaction has a significant impact on volumes of sediment, especially in lithologically variable successions, where differential compaction can greatly impact the resultant preserved geometry (e.g. Alves, 2010). This can occur after the entire succession is deposited, or when systems are still active, resulting in topographic highs and lows, and compensational stacking of sand-rich elements.

Therefore, in order to draw conclusions about original depositional topography from the rock record it is important to understand (i) how preserved sediments encapsulate formational processes, and (ii) what changes sediments undergo from deposition to exhumation.

### **1.3 Thesis outline**

This thesis includes three manuscripts that have been accepted or submitted for publication in international peer-reviewed journals (Chapters 4-6).

**Chapter 2:** *Topography of slope to basin floor profiles.* This chapter summarizes the current understanding of topographic influence on stratigraphic architecture from experimental and exhumed, modern and seismic studies.

**Chapter 3:** *Regional setting and methodology.* This chapter introduces the geological background and regional setting of the Laingsburg depocentre, Karoo Basin, South Africa. It discusses the methods used in this study and provides an illustrated summary of the sedimentary facies.

**Chapter 4:** *Exhumed lateral margins and increasing infill confinement of a submarine slide complex.* In review for publication in *Sedimentology*. This chapter documents three exhumed, stacked submarine landslides including two superimposed basal shear surfaces and their subsequent infills exposed in an outcrop at the distal end of the Laingsburg depocentre.

**Chapter 5:** *Deepwater channel-lobe transition zone dynamics: processes and depositional architecture.* Accepted for publication in *GSA Bulletin*. This chapter documents the erosional and depositional elements of a channel-lobe transition zone, along with the spatial and temporal evolution and transfer into the stratigraphic record. A dynamic model for CLTZ evolution is presented.

**Chapter 6:** *Disconnected submarine lobes, and their role in the evolution of a stepped slope over multiple sea-level cycles.* This chapter documents the topographic controls and formation of thin units A/B, B/C and D/E which form a unique type of intraslope, and basin floor lobe. These units are utilised along with previous studies from the larger units to establish evolution of the entire Laingsburg depocentre over the numerous deepwater systems of the Laingsburg and Fort Brown formations. To be submitted to *Geosphere* in summer 2017.

**Chapter 7:** This chapter provides an extended discussion that addresses the key research questions presented in Chapter 1. Findings from research presented in chapters 3-6 are collated and synthesised to answer these research questions. This chapter also includes the conclusions and wider implications of the research. Finally, possible future research foci are proposed.





## 2 Slope to basin floor topography

### Topographic impact on flow processes, products, and stratigraphic architecture

#### 2.1 Introduction

The research in this thesis investigates the stratigraphic record of interactions between sediment gravity flows and depositional or erosional seabed relief at a range of scales and morphological configurations. Therefore, presented here is a review of the literature that have investigated and interpreted these interactions, using experimental, outcrop, modern and subsurface datasets. Each of these approaches to studying topographical effects on gravity currents varies in scale and detail giving different insights into this phenomenon.

Changes in the gradient and orientation of seabed topography impacts sediment gravity flow behaviour, and can cause turbidity currents i) to deflect and reflect off intrabasinal slopes, ii) to pond within confined lows, and iii) to decelerate or accelerate flows (Kneller and McCaffrey, 1999). Reflection and deflection of turbidity currents off topography was first suggested by van Andel and Komar (1969), and subsequently these processes have been documented in a variety of systems. The flow of turbidity currents into regions of bathymetric complexity leads to spatial variations in flow character that can affect the suspended load fall out rate, and therefore sedimentary facies (Kneller, 1995, 1999; Amy et al., 2004). The variation of the flow at bathymetric perturbations can be characterised by the Froude number (1) (Baines, 1984; Armi, 1986). The Froude number (1) is related to flow velocity (U), flow height (h) and the reduced gravity ( $g'$ ), where the gravity constant (g) is influenced by the density difference between the flow mixture ( $\rho_{mix}$ ) and the ambient fluid ( $\rho$ ).

$$Fr = \frac{U}{\sqrt{g'h}}; g' = \frac{\rho_{mix} - \rho}{\rho} g \left[ \frac{m}{s^2} \right] \quad (1) \text{ (From Postma et al., 2009)}$$

The transition from supercritical conditions ( $Fr > 1$ ) to subcritical conditions ( $Fr < 1$ ) result in flow expansion and the formation of a standing wave (Baines, 1984; Armi, 1986). Low  $Fr'$  numbers result in flow decoupling, which results in a lower high-density flow that travels around the topographic barrier and an upper low density flow which moves over and away from the barrier (e.g. Kneller and McCaffrey, 1999; Nasr-Azadani and Meiburg, 2014).

Turbidity currents and other sediment gravity flows in deepwater systems do not flow onto completely flat surfaces, but onto areas with topographical complexities (e.g. Normark, 1985; Apps et al., 1994). The continental slope is recorded as topographically complex, but even in

basin plain settings turbidity currents may encounter isolated topography in the form of seamounts or basement highs (Rothwell et al., 1992; Ricci-Lucchi and Camerlenghi, 1993), be ponded against basin-bounding slopes (e.g., van Andel and Komar, 1969; Rothwell et al., 1998), and / or interact with the relief formed by previous deposits.

Breaks-in-slope can cause differential deposition, such as that related with the base-of-slope area. This can be related to a hydraulic jump within sediment gravity flows (e.g. Weirich, 1988). Preferential deposition of sediment has been shown to occur downstream of slope breaks, as well as upstream of humps, caused by the deceleration in flow velocity and decreased sediment capacity (Kubo, 2003). Bathymetric perturbation can cause acceleration of flow and consequently increased erosion (Gee et al., 2001).

Lateral slopes can cause confinement and deflection of turbidity currents (Kneller and McCaffrey, 1999; Kneller and Buckee, 2000). Overall, confinement can be classified as weak, moderate or high (Sinclair, 2000; Haughton, 2000; Sinclair and Tomasso, 2002; Amy et al., 2004, 2007; Hodgson and Haughton, 2004), which impacts the depositional architecture (Pickering and Hilton, 1998; Sinclair, 2000; Haughton, 2000; Sinclair and Tomasso, 2002; Amy et al., 2004, 2007; Hodgson and Haughton, 2004; Smith and Joseph, 2004; Aas et al., 2010; Etienne, 2012; Etienne et al., 2012; Pr lat and Hodgson, 2013; Burgreen and Graham, 2014; Yang and Kim, 2014; Marini et al., 2015).

Slope topography can be related to the difference between slope morphology and an idealised equilibrium profile (Pirmez et al., 2000; Kneller, 2003) as: above grade, with well-developed ponded accommodation; above grade, with stepped profiles; and graded, without significant topography (Prather, 2003).

Current knowledge of topographical effects on sediment gravity flows and subsequent deposits are discussed below separated into experimental (section 2.2), outcrop (section 2.3), modern (section 2.4) and seismic reflection (section 2.5) datasets, which each give a unique perspective on the subject.

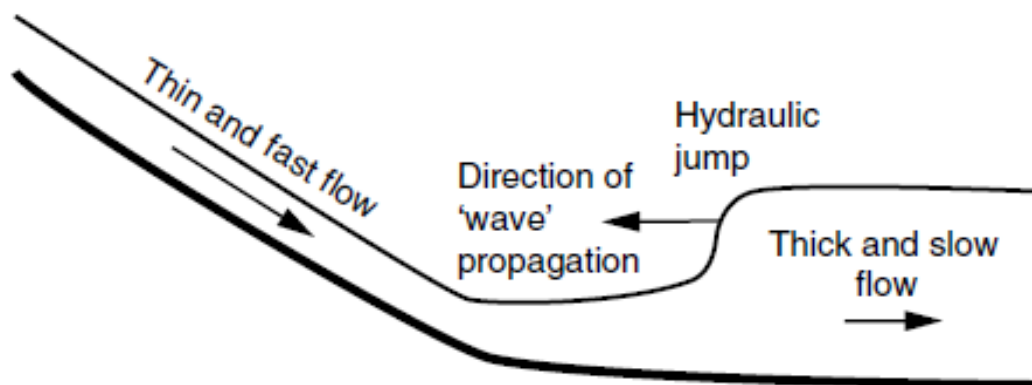
## 2.2 Experimental studies

Experimental modelling has added greatly to the knowledge of flow processes and flow topographic interaction. Experimental studies using flume tank modelling of flows have shown that introducing a gradient change or obstacle into a stratified flow causes upstream disturbances, as well as altering the flow properties and the dynamics of the flow as it travels downstream.

### 2.2.1 Downflow gradient changes- Hydraulic jump

Hydraulic jumps can occur in both turbidity currents and debris flows (Wierich, 1989) and this process has been invoked in many seafloor processes. During a hydraulic jump there is an abrupt change in flow velocity and density of a submarine density flow, as the flow increases in thickness and rapidly decreases in velocity.

Hydraulic jumps occur in the transition between supercritical and subcritical flow conditions. Supercritical and subcritical flows in subaerial flows are quantified in terms of their Froude number ( $Fr$ ) (1).



**Figure 2.1** Schematic diagram showing the key features of a hydraulic jump (from Sumner et al., 2013).

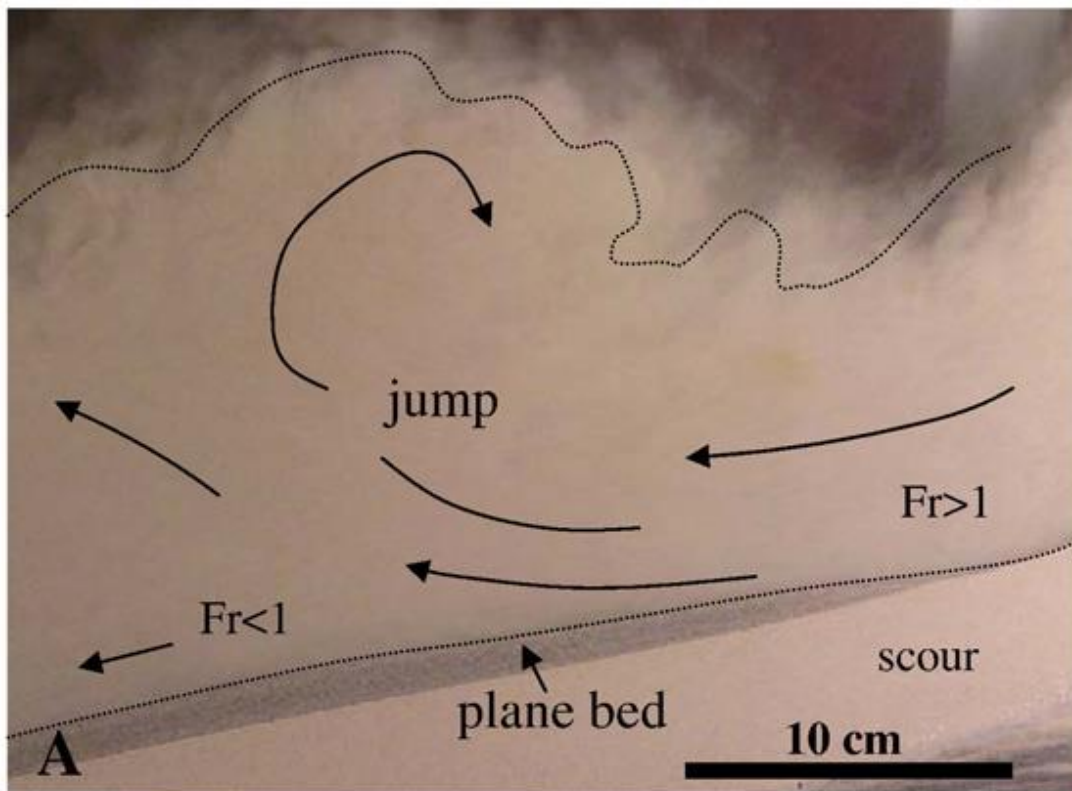
The Froude number is dimensionless and compares ( $U$ ) the depth averaged velocity to the speed the wave would propagate along its surface ( $g$ =acceleration due to gravity,  $h$ =thickness of flow). For a supercritical flow  $Fr > 1$  and for a subcritical flow  $Fr < 1$ , when  $Fr = 1$  hydraulic jump occurs (Fig. 2.1) (Sumner et al., 2013). When a flow is supercritical inertial forces are greater than gravitational forces, the flow is travelling at a greater velocity than a surface wave could propagate. This leads to a relatively thin and fast flow, which exerts higher shear stress on the bed. When a flow is subcritical, the opposite is true, gravitational forces are greater than inertial forces, and the flow is travelling at a lower velocity than a surface wave would

propagate. When the flow velocity and the velocity of the surface wave are equal, this is where hydraulic jump occurs (Kostic and Parker, 2006; Sumner et al., 2013).

For density currents the densiometric Froude number is used, this modifies the equation to account for gravity.

$$Fr = \frac{U}{\sqrt{g'h}} \quad (1) \text{ (From Postma et al., 2009)}$$

Waltham (2004) showed for the above equation that the hydraulic jump does not always occur when  $Fr = \text{unity}$ . This is due to density currents having a highly non-uniform vertical velocity and stratified profile, and therefore suggested that it might be more accurate to use a different characteristic of flow velocity.



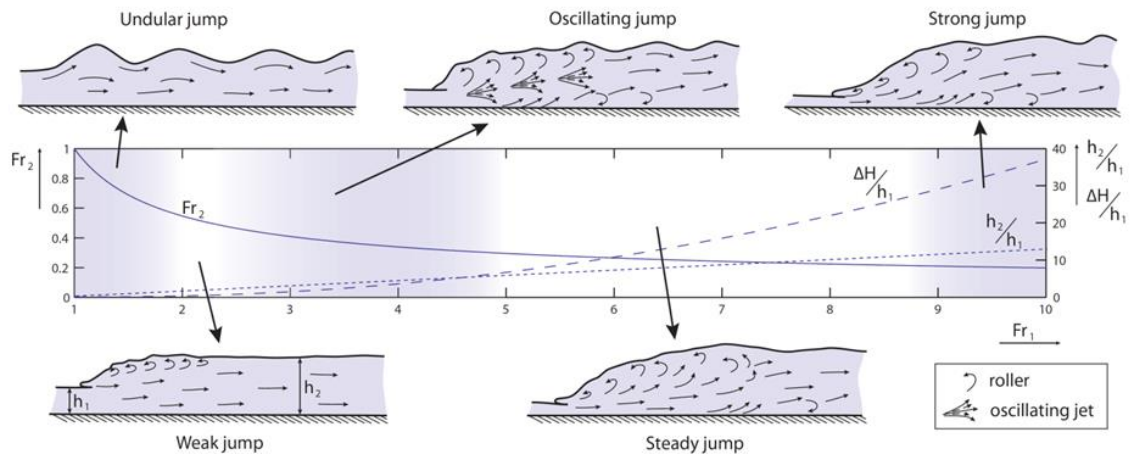
**Figure 2.2** Experiment of 1-phase suspension flow that produced a scour just before the jump and mainly plane bed laminations at and down slope of the jump (from Postma et al., 2009).

To study hydraulic jumps many researchers have used flume tank experimentation to replicate the transition from supercritical to subcritical flow (Fig. 2.2). This has allowed detailed study of the changes in flow dynamics over this transition. Although they show similar features there are different types of hydraulic jump that can be recognised experimentally. The type of jump is a factor of both the Froude number of the incoming flow and the energy lost over the

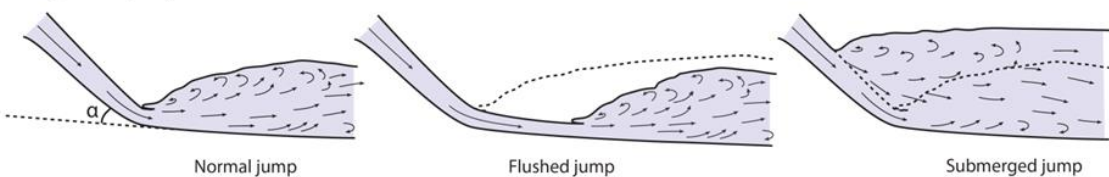
hydraulic jump. A theoretical relationship has also been shown between the outgoing Froude number ( $Fr_2$ ), the dimensionless energy loss expressed in metres of water column ( $\Delta H/h_1$ ), and the ratio of conjugated depths ( $h_2/h_1$ ) as a function of the incoming Froude number ( $Fr_1$ ) (Fig. 2.3) (Cartigny, 2012).

Previous theoretical and experimental studies have suggested that on average hydraulic jump causes flow thickness to double and flow velocity to halve (Komar, 1971), although more

#### A. Hydraulic jump strenght and type



#### B. Hydraulic jump location



**Figure 2.3** A. Plot of theoretical relations between the Froude number of the incoming flow ( $Fr_1$ ),  $h_2/h_1$ -ratio and energy loss ( $\Delta H/h_1$ ). B. Depending on the balance between upstream forces related to the incoming flow velocity and the downstream forces depending on flow depth, hydraulic jumps occur at a slope break (normal jump, kinematic energy = potential energy), downstream of a slope break (flushed jump, kinematic > potential), or upstream of the slope break (submerged jump, kinematic < potential) (from Cartigny, 2012).

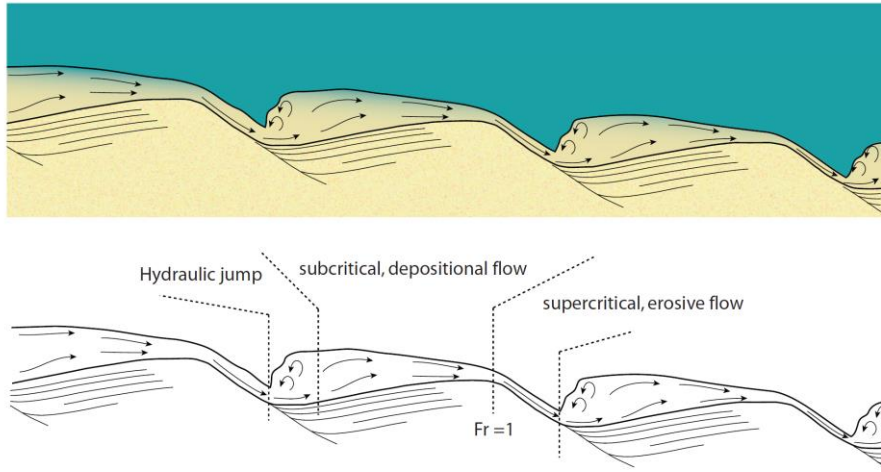
recent studies show that this would only be true if the average flow has a Froude number  $>2$  immediately prior to the hydraulic jump (Sumner et al., 2013). This is unlikely as in unconfined settings over steep non-cohesive slopes  $Fr$  is generally not much higher than critical value (Sumner et al, 2013). Komar (1971) also suggested, evidenced from theoretical and experimental modelling, that a submerged hydraulic jump can cover a distance of 1 kilometre or less. But this distance varies greatly with the magnitude of the break in slope, flow velocity, composition and other flow dynamics. Larger magnitude breaks in slope will result in a greater reduction in flow velocity, which will in turn increase the likelihood of flow scouring (Lee et al., 2002). Classical estimates for the occurrence of hydraulic jump (Komar, 1971) only apply to layer averaged flows. More recent studies by Macdonald et al. (2011a), Sumner et al. (2013)

and Dorrell et al. (2016) indicate the presence of a 'scattered field of hydraulic jumps' where multiple hydraulic jumps occur in a widespread zone rather than a single large jump.

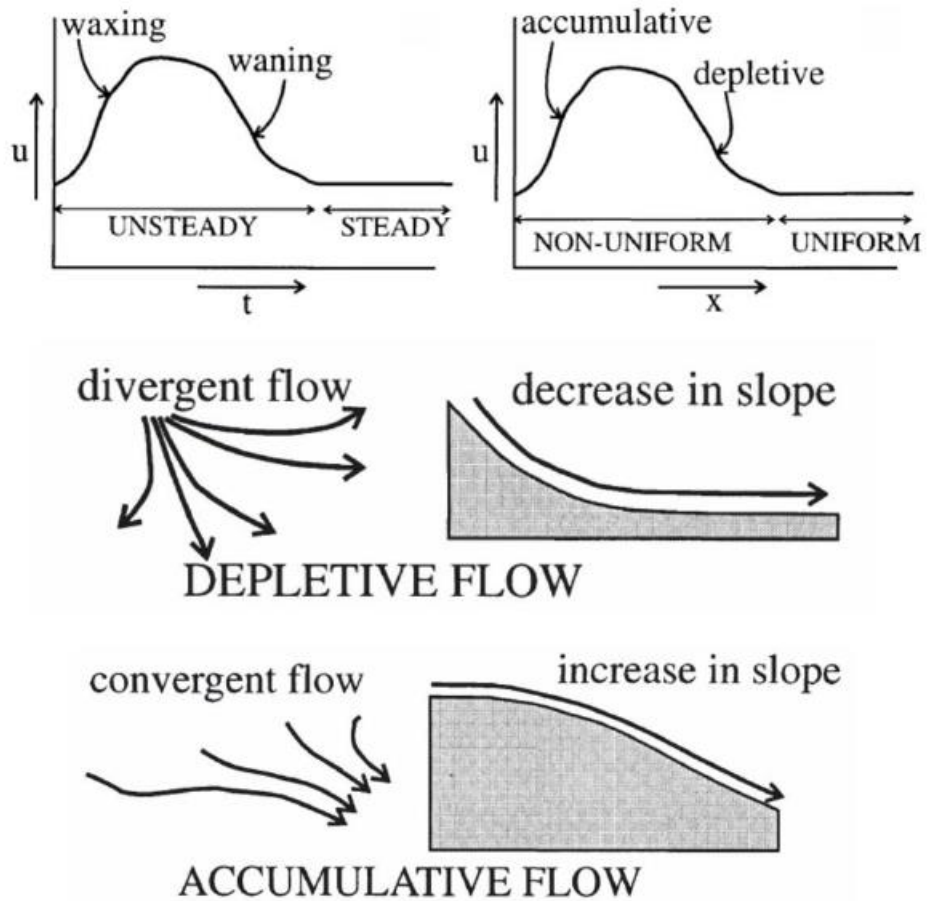
The formation of hydraulic jumps and the erosion of deep-water scours have long been linked (Mutti and Normark, 1987). Physical and numerical modelling of hydraulic jumps has reproduced the scour formation (Kostic and Parker, 2006) as well as cyclic step formation (Taki and Parker, 2005; Kostic, 2011). As the Froude number increases supercritical flows on mobile beds form a typical sequence of bedforms: antidunes, breaking antidunes, chutes-and-pools and cyclic steps (Cartigny, 2012).

Antidunes are features where the bedform is in phase with the surface wave and can show upstream or downstream migration (Middleton, 1965; Hand, 1969, 1974; Winterwerp et al., 1992; Alexander et al., 2001; Cartigny et al., 2014; Postma and Cartigny, 2014). As new antidunes at the downstream end are formed, those at the upstream end are eroded away, and as Froude number increases antidune amplitude also increases (Cartigny et al., 2014). Subaerial observations suggest this increase occurs until the wave height over wavelength exceeds 0.14, at this point breaking surface waves occur, leading to the formation of breaking antidunes, causing cyclic destruction and regeneration of antidunes (Kennedy, 1961). Chutes-and-pools form where abrupt transitions from shallow to deep bed morphology are related to transitions from subcritical to supercritical flow (Schminke et al., 1973; Alexander et al., 2001; Cartigny, 2012).

Cyclic steps are trains of upstream-migrating steps bounded upstream and downstream by hydraulic jumps, these can form from instability caused by Froude supercritical flows passing over an erodible substrate (Cartigny, 2011; Lang and Winsemann, 2013; Covault et al., 2014; Postma and Cartigny, 2014; Postma et al., 2014) (Fig. 2.4). The concept of cyclic steps has been used to interpret chains of scours (Cartigny et al., 2014; Postma and Cartigny, 2014), in this case, hydraulic jumps are in phase with the topography and the flow depths are thought to be the same magnitude as the scour depths, in contrast to hydraulic jumps associated with flow spreading (Fildani et al., 2006). 'Non-uniform' flow behaviour (velocity changes over distance) is predicted at slope changes, where a decrease in slope can result in depletive and divergent flow (Kneller and Branney, 1995). Fluctuations in flow velocity over time are classified as 'unsteady' (Fig. 2.5), where waxing flows occur when velocity increases over time and waning when velocity decreases (Kneller and Branney, 1995).



**Figure 2.5** Schematic diagram of a train of downslope asymmetrical cyclic steps (flow from left to right), beneath a turbidity current (Cartigny, 2012).



**Figure 2.4** (top) Graphs showing time ( $t$ ) versus flow velocity ( $u$ ) and distance ( $x$ ) versus flow velocity ( $u$ ) and the different terminology used to describe unsteady and non-uniform flow behaviour. (bottom) Diagram illustrating variance in flow behaviour depending on the type of gradient change. At the base-of-slope a decrease in slope is expected and therefore diverging and depletive flow behaviour. Abrupt decreases in gradient, are often associated with flow expansion as divergent flow behaviour will result from the gradient and confinement changes in this region (from Kneller, 1995).

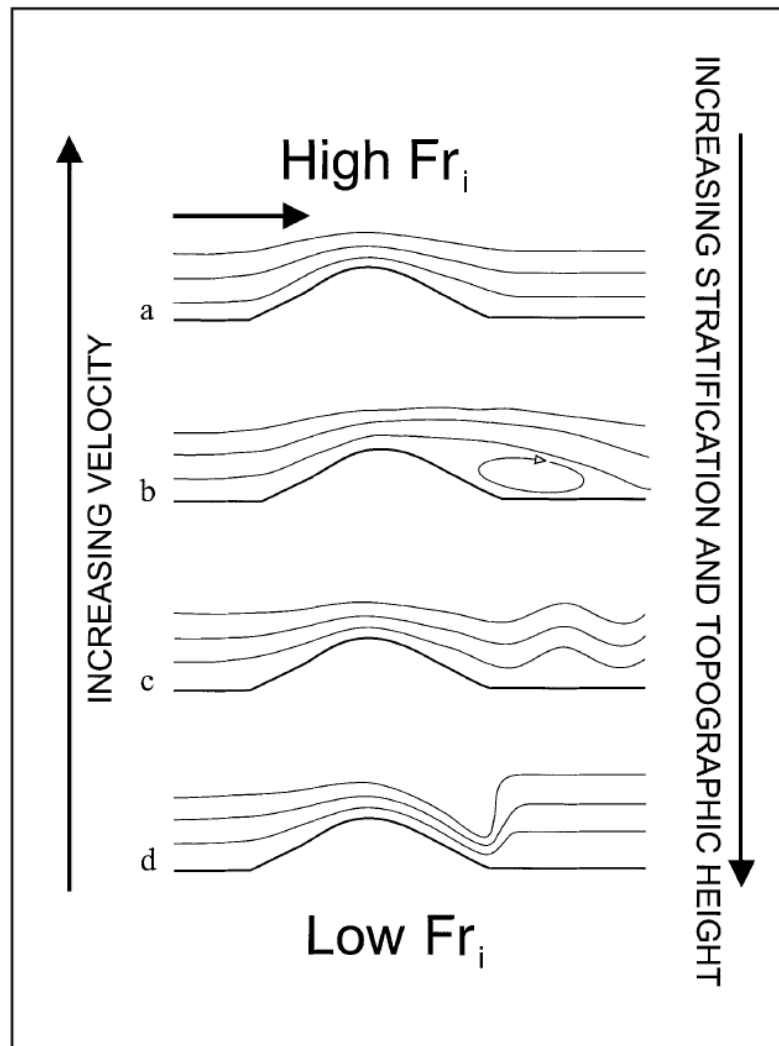
### 2.2.2 *Lateral slopes and downflow obstacles- Reflection, deflection and flow decoupling*

Flow overspilling, reflection and deflection are dependent on flow properties and the height, geometry and orientation of topographic highs (Kneller and McCaffrey, 1999). Key flow properties include flow thickness, duration and acceleration, grain-size of the transported sediment and density stratification. A relationship has been noted between the Froude number ( $Fr$ ) (1) of a flow and the relationship between obstacle height and flow thickness (Kneller and McCaffrey, 1999; Kneller and Buckee, 2000). Experimental studies can give insight into the effect of obstacles on flow capacity (Alexander and Morris, 1994; Lane-Serff et al., 1995; Morris et al., 1998; Kneller and McCaffrey, 1999).

For the same obstacle height, higher energy flows have a greater capacity whilst passing over obstacles. For flows with the same capacity, an obstacle height can be determined beyond which the entire flow will be blocked, causing reflection and deflection of the flow (Baines and Davies, 1980; Lawrence, 1987). Therefore, three main subdivisions of topographic control can be recognised: (i) when the obstacle height is significantly less than flow thickness, a change in Froude number may occur causing the flow to undergo hydraulic jump from super- to sub-critical flow conditions; (ii) when obstacle height and flow height are similar ( $< 2 \times$  obstacle height, Alexander and Morris, 1994), the upper portion of the flow may breach the obstacle with the lower portion reflected and deflected; and (iii) when obstacle height greatly exceeds flow thickness ( $> 2 \times$  flow thickness, Alexander and Morris, 1994) reflection and deflection of the entire flow will occur, and possibly a hydraulic jump will form (Edwards, 1993; Pantin and Leeder, 1987; Kneller and Buckee, 2000).

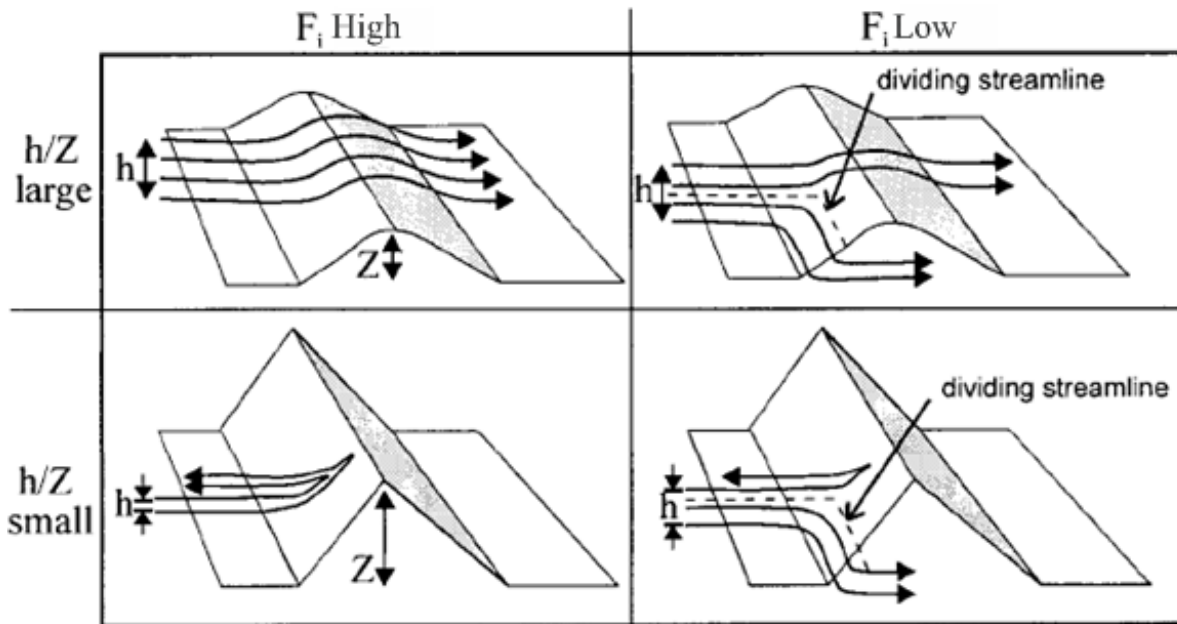
Even small obstacles will greatly effect flow dynamics. If the obstacle height is not sufficient to deflect lower denser portions of flow, the flow will still decelerate and rapidly deposit sediments, while upper portions of flow continue down-dip. Kneller and Buckee (2000) describe four types of downflow effect on an obstacle (Fig. 2.5) based on the relationship between Froude number ( $Fr$ ) (1), the velocity and stratification of the flow. With obstacle height increase relative to flow height, flow stratification increases and Froude number increase hydraulic jump are more likely to occur on the lee side of an obstacle (Fig. 2.6).





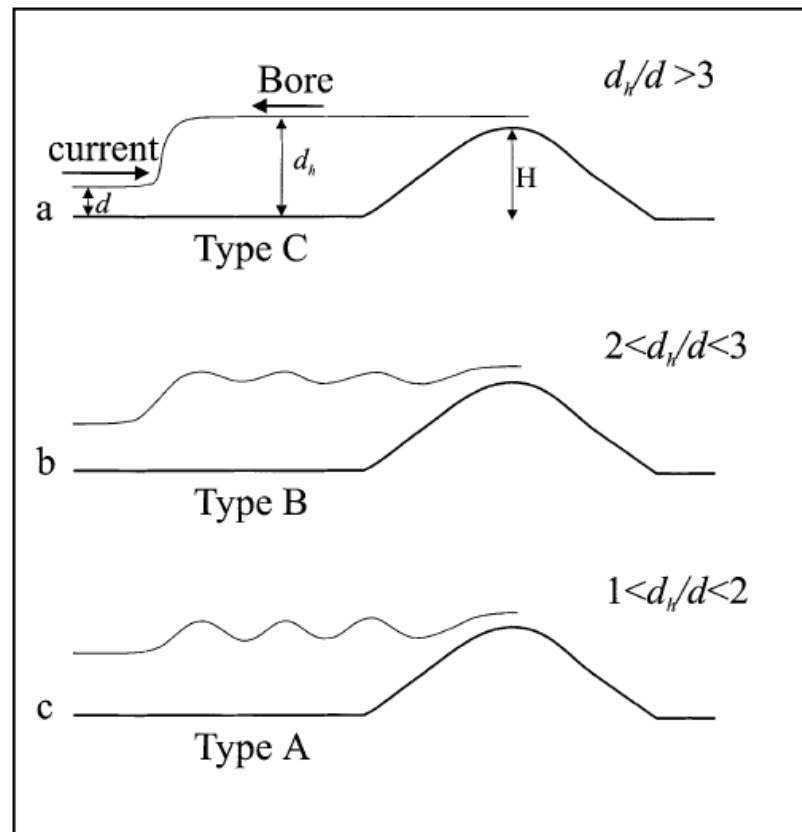
**Figure 2.6** The effect of internal Froude number ( $Fr_i$ ) on the behaviour of flows downstream of topography (from Kneller and Buckee, 2000).

As discussed above, when moving over an obstacle, stratified layers within a flow act independently, but this is subject to the Froude number ( $Fr$ ) (1). When the Froude number is high, the flow tends to act as a unity, with the entire flow overtopping topography or reflected/deflected (Fig. 2.7). For low Froude numbers there is a critical plane within the flow (dividing streamline, Baines, 1995), above which the flow and sediment particles can move up and over the obstacle, whereas in the denser lower regions of the flow, below the dividing streamline, the flow has insufficient energy to surmount topography, and is deflected around it (Fig. 2.7).



**Figure 2.7** Schematic illustration of the joint effects of the dividing streamline, the Froude number and the degree of confinement ( $h/z$ ) (from Kneller and McCaffrey 1999).

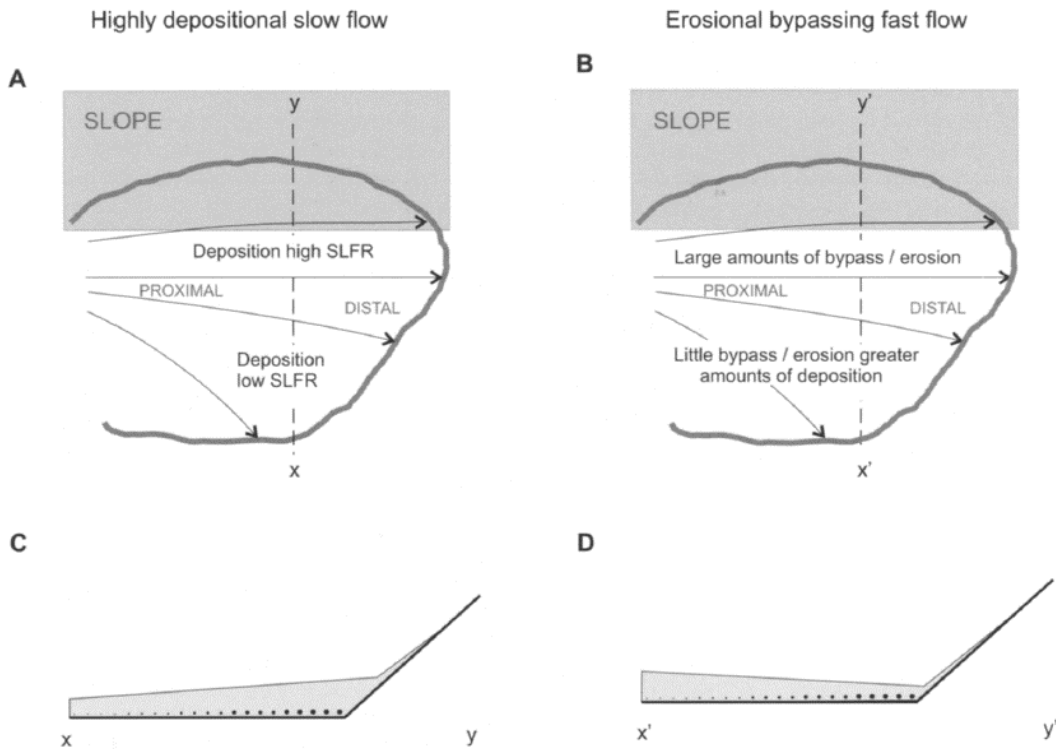
When a flow obstacle is much larger than flow height the flow will run up and increase in height. For density-stratified flows, the maximum run up height is dependent on velocity and density profiles and can be highly variable (Kneller and Buckee, 2000). When a flow is fully confined a disturbance is generated upstream of the obstacle, consisting of an internal bore. An internal bore is an abrupt downstream increase in flow thickness and an associate decrease in flow velocity, which can migrate upstream (Rottman and Simpson, 1989; Edwards, 1993; Kneller and Buckee, 2000).



**Figure 2.8** The three types of internal bores defined by Rottman and Simpson (1989) (From Kneller and Buckee, 2000).

Kneller and Buckee (2000) differentiate types of bore (Fig. 2.8) based on the relationship between the height of the bore and the flow height. The weakest bore (Type A, fig. 2.8) is characterised by a group of internal solitary waves. The strongest bore (Type C, fig. 2.8) is generated by erosion at the head of the turbidity current, producing higher stratification through increased entrainment of ambient fluid. With an intermediary type (Type B, fig. 2.8) (Kneller and Buckee, 2000).

Flows will inevitably experience a decrease in competence and capacity associated with interaction with obstacles. Therefore, a marked localised increase in sedimentation is likely to occur (Alexander and Morris, 1994; Kneller, 1995; Kneller and McCaffrey, 1995), which may migrate upstream in steady currents (Kneller and Buckee, 2000). This increased deposition may also occur in the lee of the obstacle in association with a downstream hydraulic jump (Kneller and Buckee, 2000).



**Figure 2.9** Depositional model for turbidity currents obstructed by a lateral slope that are (a) slow and highly depositional or (b) fast and capable of erosion and/or bypass of sediment, and (c) and (d) their resulting cross-stream deposit thickness trends. SLFR= sediment load fallout rate, from Amy et al., 2004.

Three-dimensional models based on flume and numerical experiments have attempted to recreate turbidite thickness patterns where obstructed by lateral slopes (Kneller et al., 1991; Kneller, 1995; McCaffrey and Kneller, 2001; Amy et al., 2004). In the experimental currents obstructed by a lateral slope, flow velocity non-uniformity patterns consist of streamlines that are parallel close to the slope but diverge at positions away from the slope (Amy et al., 2004) (Fig. 2.9). In this pattern, flow is more depletive far from the slope than near to the slope and therefore higher suspended-load fallout rates and thicker deposits should be expected far from the slope beneath the most depletive portion of the flow (Amy et al., 2004). However, this is converse to the thinning-away-from-slope pattern of some experimental datasets (Amy et al., 2004), where maximum sediment thickness was attributed to sediment deposited on the slope transforming into a higher concentration flow and coming to rest at the base-of-slope (McCaffrey and Kneller, 2001). Therefore, an interpretation of deposit thickness based on flow velocity non-uniformity alone (e.g. Kneller 1995; Kneller and McCaffrey, 1999) cannot explain these experimental depositional patterns. To explain this using flow concentration a non-uniform mechanism is required where a current is weakly depletive close to the slope but is highly depletive far from the slope and thus maintains relatively high concentrations and high sediment load fallout rate close to the slope in medial and distal settings (Amy et al., 2004).

This pattern of flow concentration non-uniformity could arise if there were lower rates of deposition and/or entrainment in proximal regions close to the slope (Amy et al., 2004).

### 2.2.3 *Summary*

Physical experiments can give help create models for the behaviour of particulate gravity currents interacting with topography, and give some indication of the range and spatial distribution of the depositional facies they create. Despite this they are often challenging to directly compare with observed facies at outcrop, with physical experiments unable to replicate the scale and stacking of flows in the 'real world'. Therefore finding from these studies can be used to general transport and depositional processes but are problematic to apply above the bed/ package scale.

## 2.3 **Exhumed studies**

Outcrop studies show a wide range of sedimentological and stratigraphic variations in deposits on slope to basin floor profiles which can be used to interpret variations in palaeotopography. Outcrop studies allow mm scale analysis of sediments as well as 2D and some 3D constraint of systems.

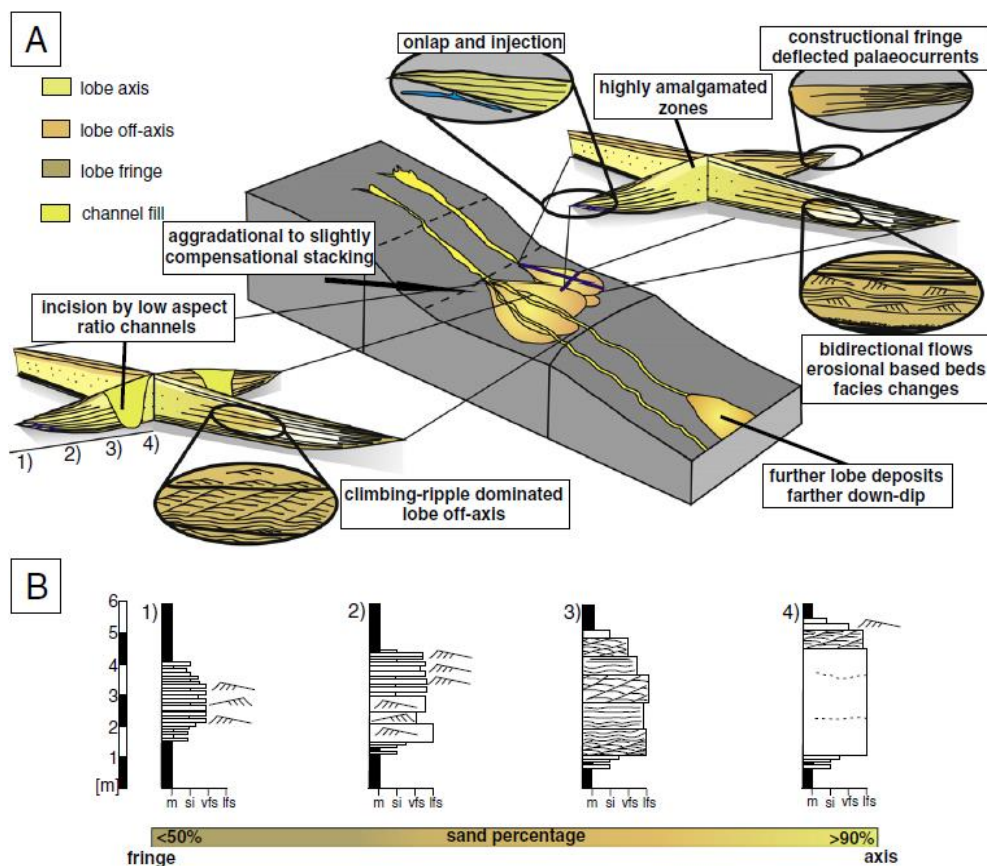
### 2.3.1 *Downslope obstacles and gradient change*

Breaks in slope, either within the slope, at the regional base of slope or within the basin floor are commonly associated with changes in flow properties and therefore have been recognised at outcrop from facies and architecture variations (Pickering and Hiscott, 1985; Simpson, 1997; Hodgson and Haughton, 2004; Amy et al., 2007; Covault and Romans, 2009; Moody et al., 2012; Sychala et al., 2015; Sychala et al., 2017a). Higher gradient settings are generally characterized by channel-levee systems (e.g. Posamentier, 2003; Posamentier and Kolla, 2003; Kane et al., 2007; Wynn et al., 2007; Di Celma et al., 2011; Hodgson et al., 2011). Unconfined, lower gradient environments are dominated by lobe deposition (e.g. Shanmugam and Moiola, 1991; Shanmugam et al., 1995; Bouma et al., 2000; Johnson et al., 2001; Hodgson et al., 2006; Pr lat et al., 2009; Flint et al., 2011; Sychala et al., 2015). In topographically complex systems this relationship can become more complicated.

#### 2.3.1.1 *Intraslope*

Intraslope lobe deposits are rarely documented in outcrop (Plink-Bj rklund and Steel, 2002; Sinclair and Tomasso, 2002; Beaubouef et al., 2007; Figueiredo et al., 2010; Bernhardt et al., 2012; van der Merwe et al., 2014; Sychala et al., 2015; Jones et al., 2017). Key criteria for the

recognition for intraslope lobes at outcrop were established by Spychala et al. (2015) (Fig. 2.10) and include, aggradational to slightly compensational lobe stacking patterns; onlap onto mud dominated slope deposits; highly amalgamated lobe axes; aggradational fringes and later incision by low-aspect-ratio channels within the same depositional sequence. Intraslope lobes generally have a lower aspect ratio (due to confinement) and higher sand content than basin floor lobes (Table 2.1). Intraslope lobes can be characterised as weakly confined, often associated with a reduction in slope gradient, or partially to fully confined where a down-dip topographic barrier causes the ponding of the lower portion or the complete flow. This can lead to grain-size breaks and sorting within a system, with concentration of coarse sediments in topographic lows, and fine sediments in topographic highs (Babonneau et al., 2004), as well as evidence of erosion or bypass across topographic highs (Burgess et al., 2000).

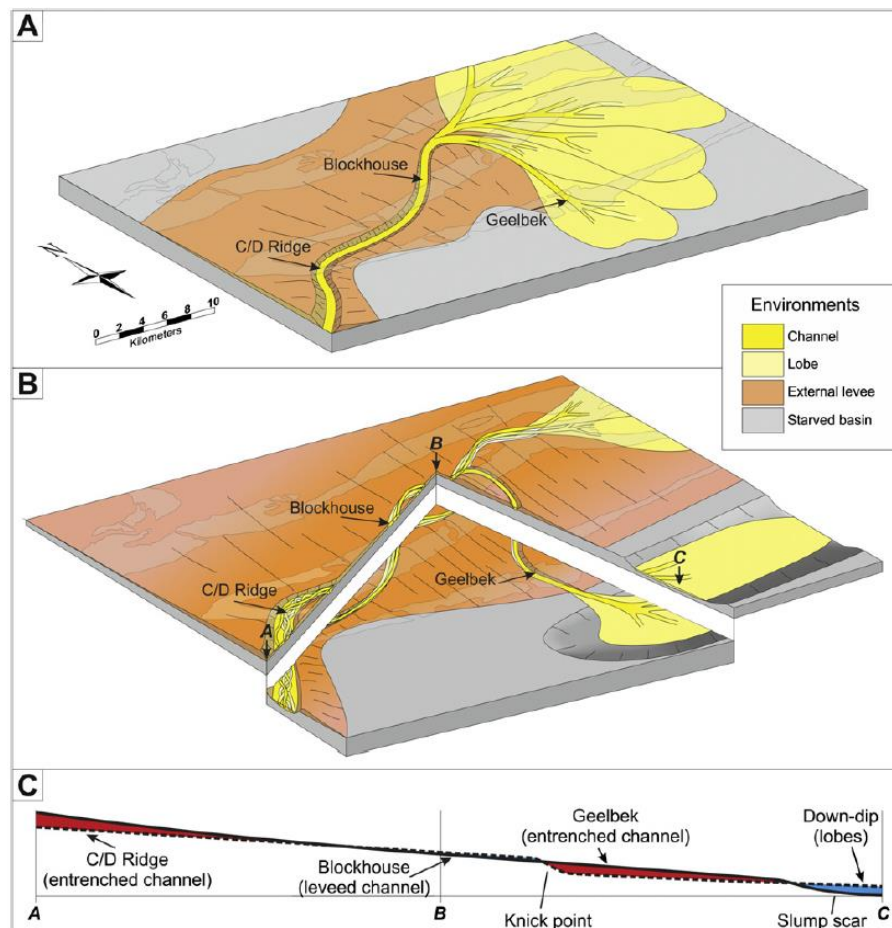


**Figure 2.10** (A) Block diagram showing the key recognition criteria of intraslope lobes. Stacking patterns are aggradational to slightly compensational; onlap combined with injection onto mudprone slope; highly amalgamated zone in the lobe complex axis; subtle confinement leads to fringes that show aggradation stacking; high degree of confinement leads to preservation of beds with evidence of flow direction, erosional based beds and abrupt facies changes; climbing ripple lamination is the dominant facies of the lobe off-axis; incision by low-aspect-ratio channel that originate in the same unit as the intraslope lobes; more lobe deposits can be found down-dip of basin-floor or on steps basinward of the slope. (B) Simplified logs of typical thicknesses and stacking pattern from lobe axis to lobe fringe (down-dip and laterally) in intraslope lobes that are observed over a few kilometres. Position of schematic logs are from fringe (1) to axis (4) (from Spychala et al., 2015).

	Intraslope lobes	Basin-floor lobes
Depositional setting	Slope	Basin floor/ terminal end of system
Degree of confinement	Weak to high	Unconfined to weak
Stacking patterns	Aggradational to slightly compensational	Compensational
Aspect ratio	Low	High
Sand percentage	Average: 70% (>90% lobe axis; 50% lobe fringe)	Average: 60% (>80% lobe axis; <40% lobe fringe)
Sediment features	Immature sandstones, moderate sorting, micas and mud chips abundant, sediment features reflect highly variable flow patterns, paucity of hybrid beds, depleted of fine grained sediments	Relative mature sandstones, fair to good sorting, abundance of hybrid beds in lobe fringe positions, fines concentrated in lobe fringe deposits, rich on mud clast and carbonaceous material in banded facies

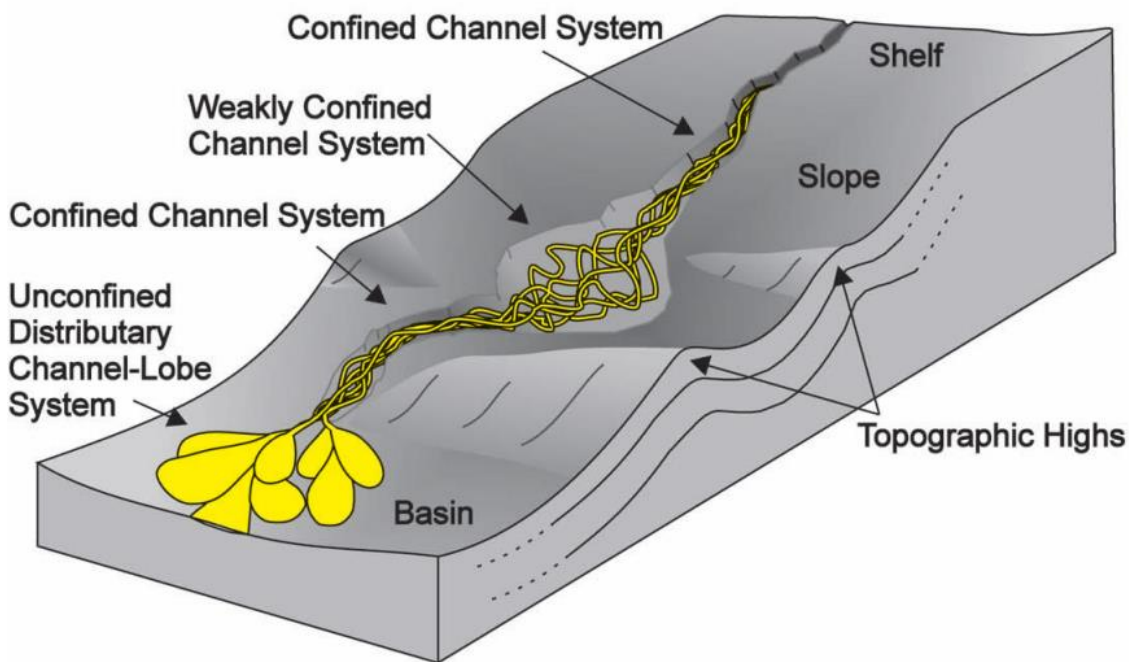
**Table 2.1** Comparison chart of the main sedimentological and stratigraphic characteristics of intraslope lobes and basin-floor lobes (from Spychala, 2016).

Confinement and gradient change along the slope profile can change channel-levee system dynamics. Leading to variations in channel entrenchment across the slope (Fig. 2.11) as a new base-level is established and the slope attempts to grade to equilibrium (Brunt et al., 2013a).



**Figure 2.11** Schematic illustration of the distribution of Unit D (Fort Brown Fm., Karoo Basin, South Africa) depositional environments at (A) Early (B) Late stages from synthesis of field data. (C) A schematic long profile of the D3 channel system (dashed line) in relation to the mean regional palaeoslope (solid line) (from Brunt et al., 2013a).

Moreover, variations in channel-levee system confinement can lead to changes in the width of channel-belts. Weakly confined channel systems are highly distributive channels that form in low relief minibasins (Fig. 2.12). Channels diverge in the up-dip part of the minibasin and converge down-dip (Moody et al., 2012).



**Figure 2.12** Block diagram showing how channel architecture and reservoir style is related to palaeobathymetry. This study focuses on weakly confined channel systems (from Moody et al., 2012).

### 2.3.1.2 Base-of-slope

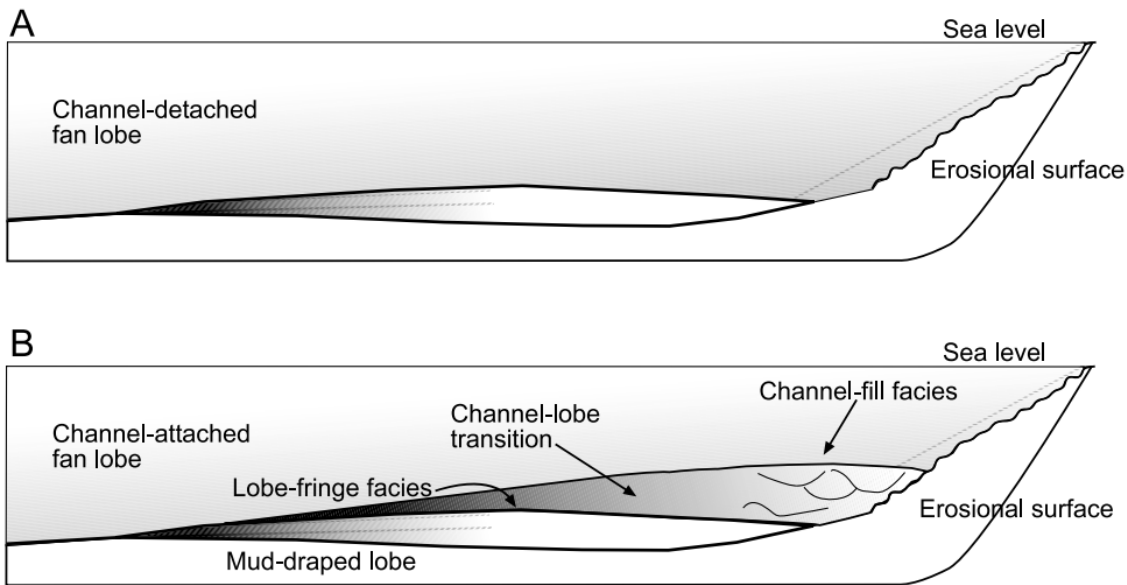
The intervening area between slope channel-levee complexes and basin-floor lobes is characterised by abrupt decreases in gradient and confinement and lateral expansion of flows, often associated with hydraulic jumps from supercritical to subcritical flow conditions (section 2.2.1) (Mutti and Normark, 1987, 1991; Weirich, 1989; Kostic and Parker, 2006; Sumner et al., 2013). This base-of-slope is associated with the development of channel-lobe transition zones (e.g. Gardner et al., 2003; Hodgson et al., 2006; Brunt et al., 2013a; van der Merwe et al., 2014). This transition can occur at a single point, or form a spatial geographic zone, with a variety of bedforms recognized in outcrop datasets (Mutti, 1977; Mutti and Normark, 1987, 1991; Wynn et al., 2002a; Ito et al., 2014; Hofstra et al., 2015; Pemberton et al., 2016). First characterised by Mutti and Normark (1987) (Fig. 2.13) CLTZs were recognised in outcrop datasets as areas consisting of both depositional and erosive elements that create a complex zone.



	CHANNELS	TRANSITION	LOBES
MORPHOLOGICAL EXPRESSION	CHANNELS 1a 1b	ROUGHNESS 1c	LOBE 1d
BEDDING PATTERN (Outcrop scale)	2a 2b	2c	2d
DEPOSITIONAL FEATURES	3a 3b 3c	3d 3e	3f
EROSIONAL FEATURES and OUT-SIZE MUDSTONE CLAST	4a 4b	4c 4d	4e 4f
CHAOTIC UNIT	5a	5b	
OTHER FEATURES	SHALLOW WATER TRACE FOSSILS LOCALLY COMMON		COMPENSATION CYCLES

**Figure 2.13** Main characteristics of submarine channels, channel-lobe transitions and lobe deposits as originally described by Mutti and Normark (1987). With: 1a = erosional channel; 1b = depositional channel; 1c = 'zone of roughness'; 1d = lobate relief; 2a = beds truncating against channel margin; 2b = beds converging against channel edge; 2c = bedding irregularity resulting from scours and large-scale bedforms; 2d = even-parallel bedding; 3a = clast-supported conglomerates; 3b = mud-supported conglomerates; 3c = thin-bedded overbank deposits; 3d+e = coarse-grained, internally stratified sandstone facies; 3f = complete and base-missing Bouma sequences; 4a = deep and relative narrow scours locally associated with stone clasts; 4b = armoured mudstone clasts; 4c = mud-draped scours; 4d = broad scours, locally associated with mudstone clasts; 4e = tabular scours invariably associated with mudstone rip-up clasts from underlying substratum; 4f = nests of mudstone clasts commonly showing inverse grading and 'take-off' attitude of individual clasts; 5a = slump units; 5b = impact features (redrawn from Mutti and Normark, 1987).

Mutti and Normark (1987) made the distinction between CLTZs created by dominantly coarse sandy turbidity currents and turbidity currents containing a substantial mud component. Because the efficiency of dominantly sand-rich flow is significantly less, it results in rapid deposition after leaving the channel mouth. This results in typical wedge-shaped deposits and includes a region of intense scouring. When flows contain a mud-component, scouring of the seafloor will be generally less intense, deposition will not be very significant and most sediment will bypass and will be deposited further basin-inwards, forming detached lobes. Two stratigraphic end member CLTZ types have been identified (Fig. 2.14), sand-attached systems and sand-detached systems (*sensu* Mutti and Normark 1987, 1991).



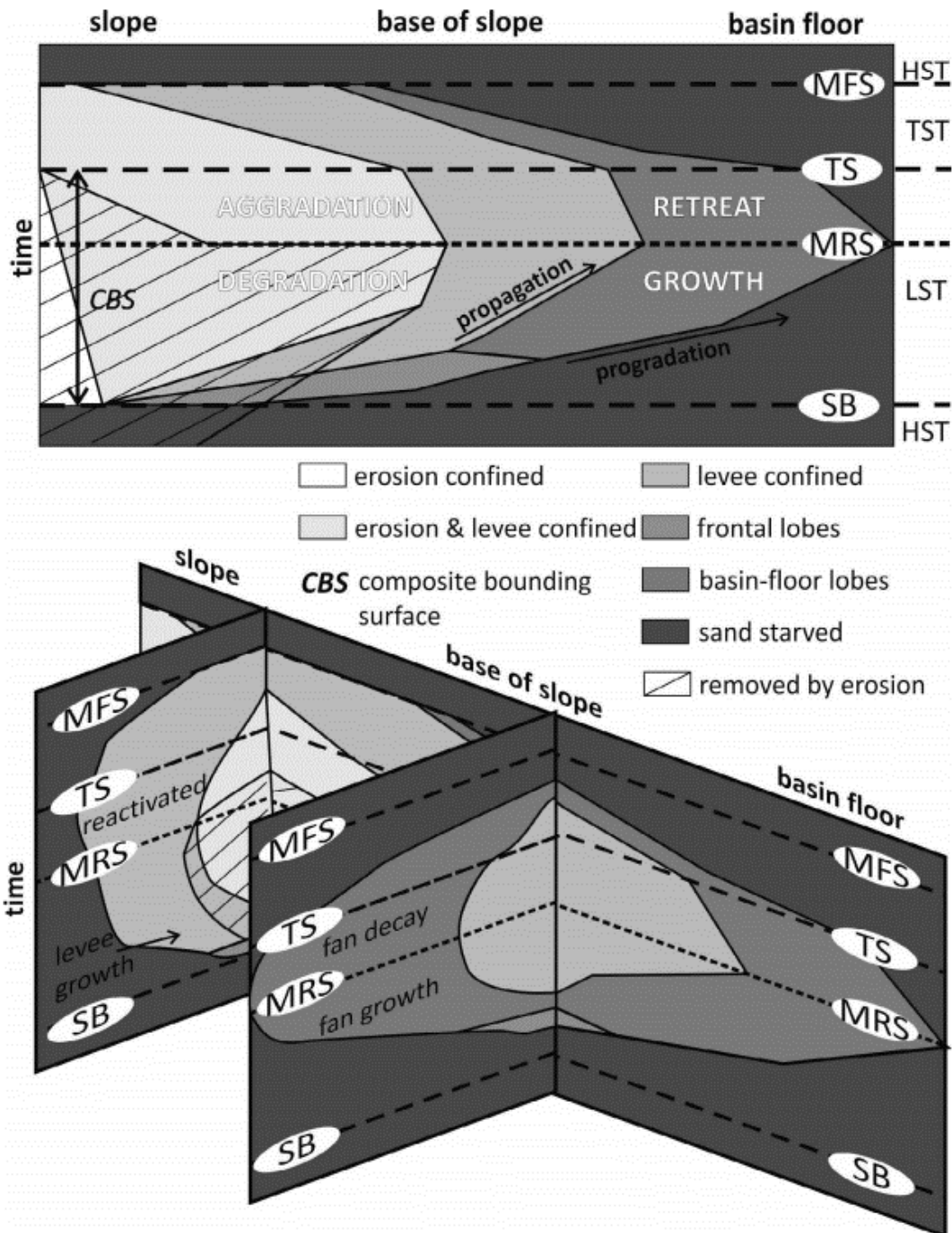
**Figure 2.14** Conceptual depositional model of deep-marine fan systems, illustrating relationships between lobe and channel transitions in a slope-to-basin setting. (A) Detached fan systems. (B) Attached fan systems. Modified after Mutti (1985) and Mutti and Normark (1987) (from Fugelli and Olsen, 2005).

Other outcrop studies have noted the changes in flow characteristics (Ito, 1998), the presence of composite erosional surfaces and scour-fills of various dimensions (Mutti and Normark, 1987; Ito et al., 2014; Hofstra et al., 2015; Pemberton et al., 2016), coarse sediment lags (Ito et al., 2014), and sediment waves (Vicente Bravo and Robles, 1995; Ito et al., 2014; Pemberton et al., 2016). Although these studies are limited in spatial extent with location within the CLTZ unknown and no direct link to up- and down-dip genetically related deposits.

CLTZs are complex areas with a complicated transfer into the sedimentary record the transition can be preserved in a single stratigraphic horizon, showing down-dip transition from channel-levee to lobes (e.g. Elliott, 2000; Gardner et al., 2003) or as a vertical succession of channel elements that transition upwards into lobes or vice versa (Fig. 2.15) (e.g. Gardner et al., 2003; Pemberton et al., 2016), which records the transition of the CLTZ across the depositional sign through time. Overall outcrop record of the bypass dominated CLTZs recorded in experimental (section 2.2.1) and modern seafloor (section 2.4.1) is extremely limited with only individual features record e.g. scours (e.g. Hofstra et al., 2015; Pemberton et al., 2016) and no studies showing the complete downslope transition from channel-levee through bypass dominated CLTZ to lobes in a single stratigraphic horizon.



elements of CLTZ are rare as they were either never preserved or later eroded, therefore an outcrop showing the overall dip profile through a bypass dominated CLTZ would be unique.

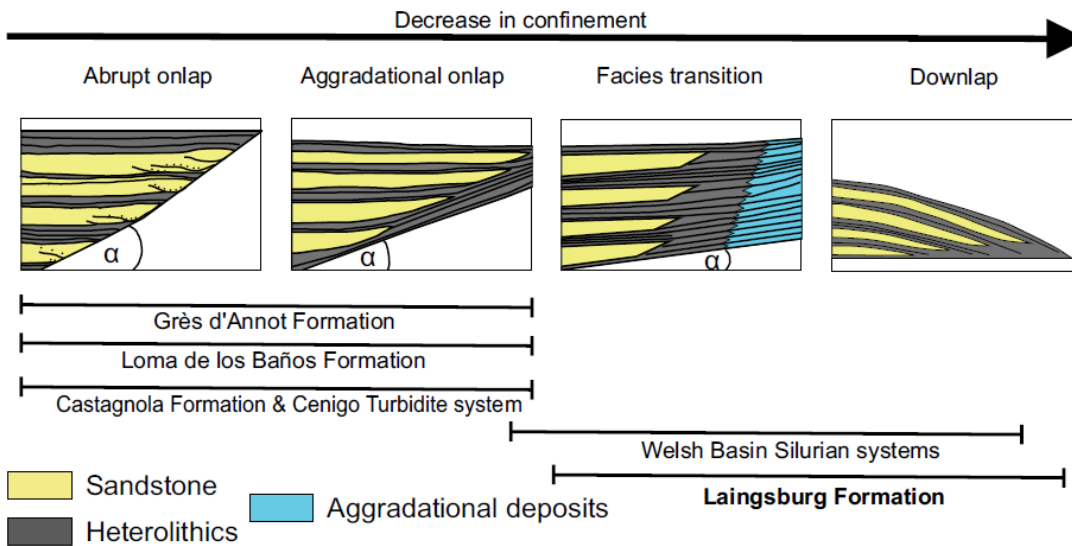


**Figure 2.16** A) Cartoon diagram in Wheeler space to illustrate the progressive-confinement model along the axis of a deep-water system during a cycle of waxing-to-waning sediment supply. The illustration emphasizes that the composite erosional surface is time transgressive. Note that during slope degradation frontal lobes form ahead of an evolving channel–levee system that lengthens down dip and up dip. The basal sandstone will be younger into the basin until a maximum regressive surface is formed. B) Three-dimensional Wheeler space cartoon with two strike sections that emphasize the challenge of identification of key regressive surfaces away from the axis on the slope and basin floor due to diachroneity of lithological contacts (from Hodgson et al., 2016).

### 2.3.2 *Lateral slope and obstacles*

Primary data of the effect of lateral slope and obstacles on flow from experiment datasets is discussed in section (2.2.2), some similar features have been recorded in outcrop datasets. At a bed scale, the sedimentary record of lateral slopes and obstacles can include the vertical repetition of sequences (van Andel and Komar, 1969; Kneller and McCaffrey, 1999); variation of palaeocurrent directions (Pickering and Hiscott, 1985; Marjanac, 1990; Kneller et al., 1991; Edwards, 1993; Sychala et al., 2015); oscillatory ripples (Ricci-Lucchi and Valmori, 1980; Marjanac, 1990) and abrupt reversals in grading (Pickering and Hiscott, 1985). These features have been interpreted to show reflection of the turbidity current from topography at a lateral slope or basin margin (Amy et al., 2005; Kneller and Buckee, 2000).

At a package or system scale, variation in flow dynamics and gradient of slope can cause various reactions by turbidity currents (shown by experimental datasets, discussed in section 2.2.2.) this is expressed in outcrop by a wide variety of lobe onlap configurations (Fig. 2.17) (e.g. Smith and Joseph, 2004; Bersezio et al., 2009; Marini et al., 2015; Sychala et al., 2017a). Smith and Joseph (2004) illustrated a continuum of onlap configurations from abrupt to aggradational onlap as a function of coeval aggradation on the bounding slope and the basin-floor. They inferred that abrupt onlap occurred with high slope angles, when little or no coeval sediments are deposited on the slope. Aggradational onlaps occur when aggradation rates on the slope are high associated with a progressive facies change towards the lateral slope (Smith and Joseph, 2004). Smith (2004b) and Sychala et al. (2017a) illustrated low-gradient lateral bounding slope scenarios to explain thick intervals of thin-bedded aggradational 'lobe fringe' deposits, in belts several kilometres wide, adjacent to basin-floor lobe complexes. These observations are generally in line with those observed in experimental datasets, with the height on the obstacle and flow dynamics controlling the amount of the flow that is reflected (section 2.2.2). Unlike the experimental datasets (section 2.2.2), outcrop studies consider the dynamic nature of most topography therefore taking into consideration when the topography formed pre- or syn-depositionally.



**Figure 2.17** Submarine basin-floor lobes interaction with topographic features (i) low amounts of aggradation on the slope compared to the basin- abrupt pinch-out against structure; (ii) moderate amount of aggradation on the slope compared to the basin- aggradation onlap with draping muds; (iii) low-gradient slope and high aggradation rates- facies transition and remobilization; and (iv) unconfined-downlap (from Spychala et al., 2017a).

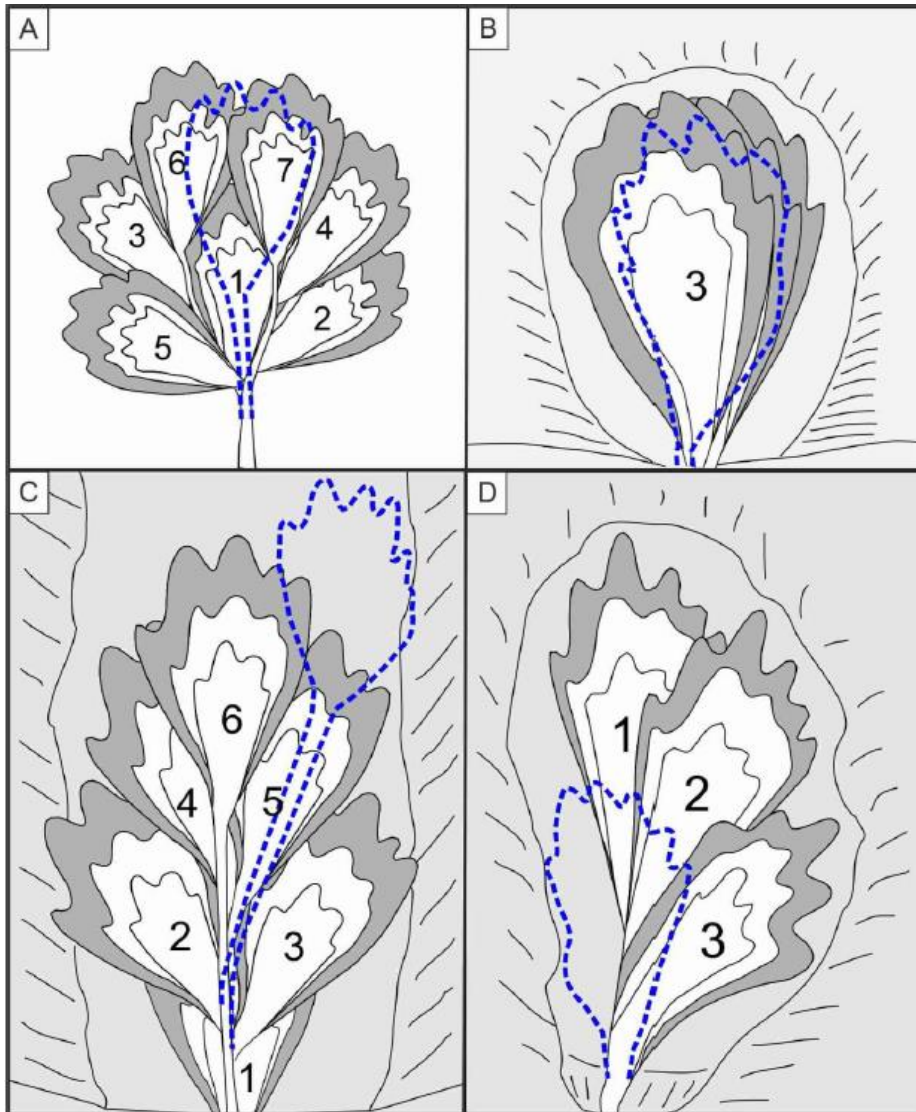
### 2.3.3 Categorising confinement

Unlike experimental datasets that generally examine the effect of a single topographic variation, outcrop datasets examine ‘real world’ scenarios which can show a variety of topographical influence on many scales. The angle of confining slopes as well as the amount of down-dip and lateral confinement can be used to characterise basins at outcrop (Pickering and Hilton, 1998; Sinclair, 2000; Haughton, 2000; Sinclair and Tomasso, 2002, Amy et al., 2004, 2007; Hodgson and Haughton, 2004; Smith and Joseph, 2004; Aas et al., 2010; Etienne, 2012; Etienne et al., 2012; Yang and Kim, 2014; Marini et al., 2015). Highly confined basins are more commonly recognised at outcrop as they display more obvious stratigraphic features. Outcropping basins with high to moderate confinement include: The Gres d’Annot Format, lateral palaeoslope values are reported between 4° and 10° (Amy et al., 2007; Salles et al., 2014); The Laga Formation; 6 to 8° (Marini et al., 2015); Castagnola Formation; 10 to 12° (northern margin) and 4° (southern margin) (Felletti, 2002; Southern et al., 2015; Marini et al., 2016); and the Cengio Turbidite systems; 5 to 10° (Bersezio et al., 2009; Felletti and Bersezio, 2010). Syn-depositional remobilization is associated with all of these basins indicating lateral slope instability (Spychala et al., 2017a). When basins are highly confined in all directions thick mudstone caps can form, suggestive of flow ponding, and sandstones showing evidence of flow reversals during deposition (as discussed above), e.g. the Ordovician Cloridorme Formation (Hiscott and Picketing, 1984; Picketing and Hiscott, 1985); the Contessa megabed

(Ricci-Lucchi and Valmori, 1980); and the Eocene of Middle Dalmatia (Marjanac, 1987, 1988, 1990).

Moderately confined basins with slope gradients  $<5-1^\circ$  include: the Akitio trench slope basin, (Bailleul et al., 2007); the Ross Sandstone (Pyles, 2008; Pyles and Jennette, 2009); and the Hikuwai sandstone and Mapiri Formation (Burgreen and Graham, 2014). Weakly confined basins include the Welsh Basin Silurian sandstone systems, namely the Mynydd Bach, Aberystwyth, Cwmystwyth and Pysgotwr formations (Smith, 1987a,b; Wilson et al., 1992; Smith, 2004b) and Unit A of the Laingsburg Formation, Karoo basin, South Africa (Spychala et al., 2017a). Lateral slopes within these basins are estimated to be  $< 1^\circ$ , likely fluctuating between  $0.05-0.3^\circ$  in the Laingsburg Formation (Spychala et al., 2017a). General recognition criteria for intraslope lobes was established by Smith (2004b), and includes palaeoflow parallel to the strike of the palaeoslope, and lateral replacement of sand-prone lobe complexes by thin-bedded turbidites.

This degree of confinement will affect the stacking of lobe complexes, both intraslope and basin-floor (Fig. 2.18). In unconfined settings, compensational stacking of lobes and lobe complexes is observed (Fig. 2.18a) (Straub, 2009), controlled by the avulsion of feeder-channels to redirect to a new topographic low after the creation of sufficient depositional relief in a lobe complex (Prélat and Hodgson, 2013). Aggradational stacking (Fig. 2.18b) occurs where flows are confined and therefore avulsion is not possible (Burgreen and Graham, 2014). Progradational stacking (Fig. 2.18c) is associated with basin configurations that limit lateral migration, when tectonics increases basin-floor gradient and when sedimentation rates rapidly increase (Macdonald et al., 2011b; Grundvåg et al., 2014; Picot et al., 2016). Progradational stacking is considered more common in proximal and base-of-slope settings where there is less accommodation. Retrogradational stacking (Fig. 2.18d) can be the result of decreased sediment supply at the end of a depositional cycle (e.g. at the end of a LST) when sediment is trapped on the shelf e.g. the Peira Cava Basin, France (Amy et al., 2007).

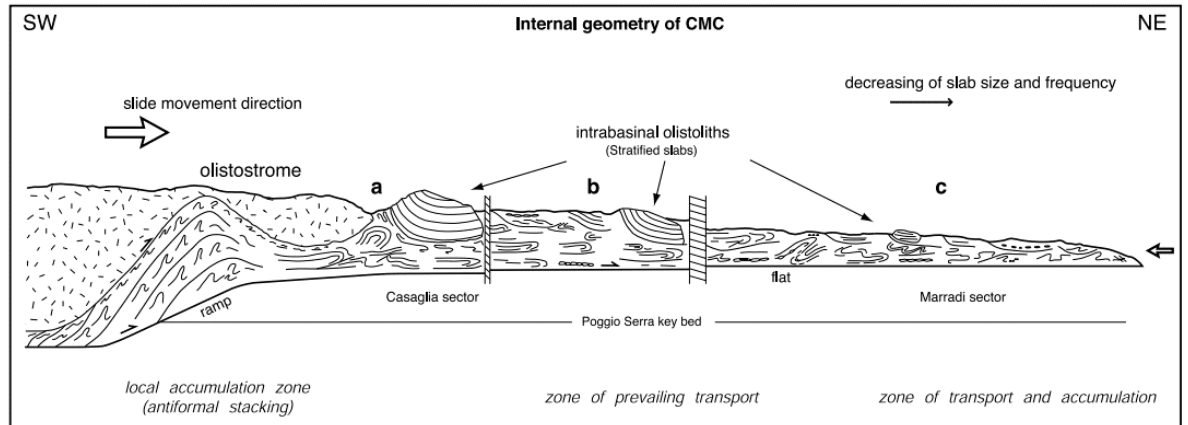


**Figure 2.18** Schematic plan view of lobe stacking patterns. (A) Compensational stacking; (B) Aggradational stacking; (C) Progradational stacking; (D) Retrogradational stacking. Dashed blue line indicates the locus of deposition of the next lobe (from Spychala, 2016).

#### 2.3.4 Mass flow deposit relief

Mass transport deposits include debris flow, slump, and slide deposits (Moscardelli and Wood, 2008), and can comprise a large proportion (locally, >50%) of slopes and basin floor successions (Posamentier and Walker, 2006). The erosion and evacuation of slope regions, as well as the deposition of the evacuated material, can create significant and complex topography (Kneller et al., 2016). The evacuated basal shear surface of a slide is rarely recognised at outcrop (e.g. Lucente and Pini, 2003; Shultz et al., 2005; van der Merwe et al., 2009; Dakin et al., 2013), but can act as any seafloor depression and cause subsequent remobilized and turbidity current deposits to onlap and pond within. Frontal ramps can form during failure, creating partial down-dip confinement (Fig. 2.19) (Lucente and Pini, 2003).





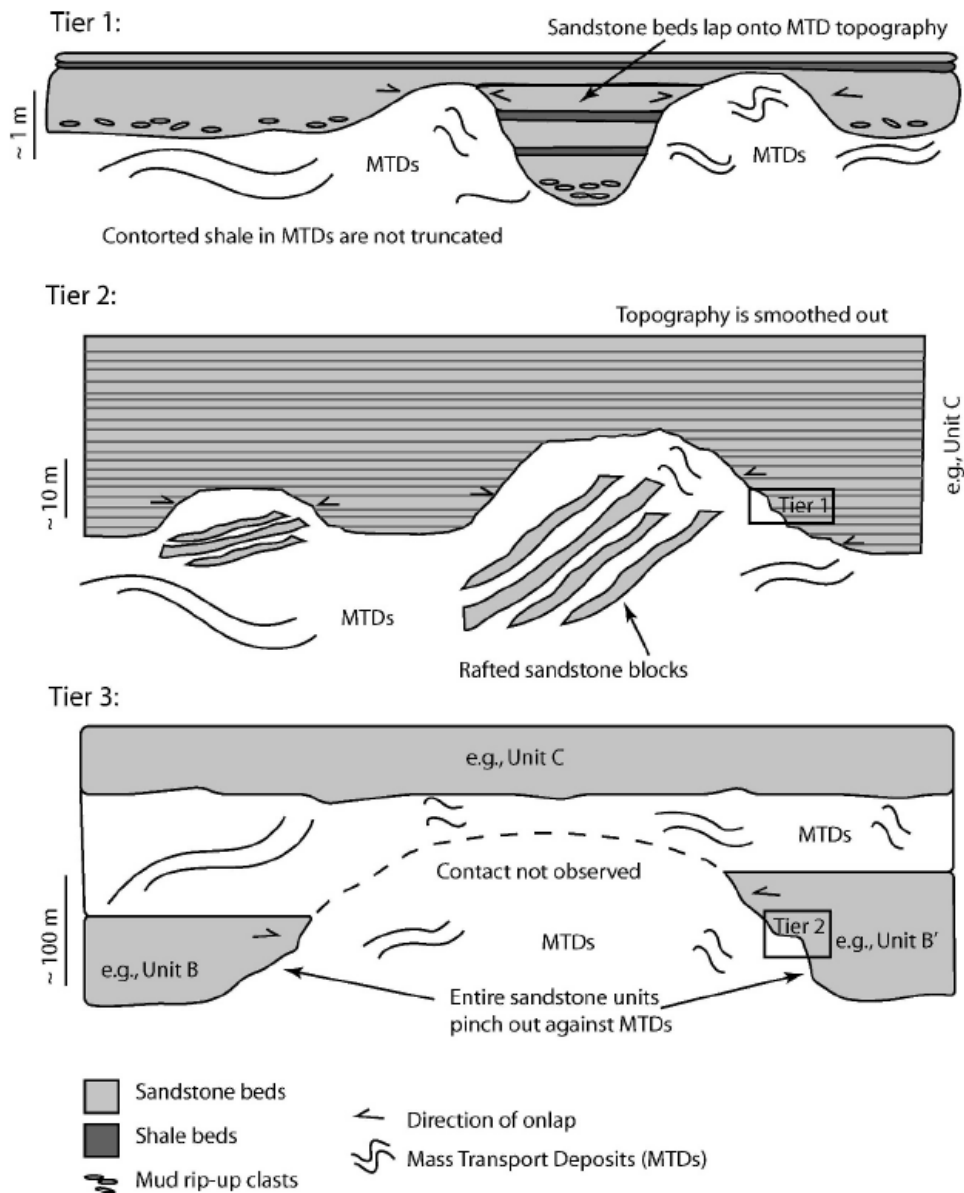
**Figure 2.19** Idealized transect of Casaglia-Monte della Colonna (CMC), (from the middle Miocene Marnoso-arenacea Formation of the Northern Apennines) parallel to the SW-NE direction of slide movement, showing the external geometry and internal distribution of structures. The sketch outlines three segments (a,b,c), which have been identified on the basis of the body geometry and the type and distribution of structures (from Lucentre and Pini, 2003).

The topography on the top surface of mass-transport deposits can be defined as: very localized (a few metres wavelength and amplitude); localized (a few tens of metres wavelength, a few metres to ~ 10 m amplitude); and sub-regional (kilometres in wavelength, tens of metres in amplitude) (Dykstra et al., 2011). This topography can cause “ponding” or partial confinement of turbidites immediately above the mass-transport deposits (Dykstra et al., 2011).

Armitage et al. (2009) divided mass transport topography into Tiers (1-3) based on the amount of relief created (Table 2.2; Fig. 2.20).

Horizontal (x) axis of MTD surface topography	Vertical (y) axis of MTD surface topography	Topographic development	Effect on sandstone architecture
<b>Tier 1:</b> Meters to several meters.	Meters to several meters.	Locally irregular nature of the MTD top surface formed as a result of cohesive freezing. May include an element of loading from overlying sandstone.	Creates pods of sandstone on the surface of the MTD, which may enhance foundering. Individual sedimentation units may fill this scale of topography. Sandstone is locally ponded.
<b>Tier 2:</b> 10 m to several tens of meters.	Meters to several tens of meters.	Rafted sandstone blocks.	Basal sections of the sandstone unit lap onto the MTD surface topography. Laterally partitions significant quantities of sandstone (compartmentalizes unit).
<b>Tier 3:</b> 100 m to several hundreds of meters.	100 m to several hundreds of meters.	Individual MTD (or oversized block).	Partitions entire sandstone conduits. Defines units at the outcrop scale. Entire units pinch out against MTD surface topography.

**Table 2.2** Three tiers of mass-transport-deposit surface topography are defined at the Sierra Contreras, Tres Pasos Formation (Cretaceous), Southern Chile. The cause of the topography and the effect on overlying turbidite architecture are outlined (from Armitage et al., 2009).



**Figure 2.20** Conceptual diagram of the MTD surface-topography hierarchy developed for the Sierra Contreras, Tres Pasos Formation (Cretaceous), Southern Chile. Each of the three tiers is shown, outlining the scale and the effect on subsequent turbidite beds. Although the tiers are successively separated by an order of magnitude in size, there is range within the hierarchy with respect to the topographic dimensions, facilitating a more flexible comparison of MTDs (from Armitage et al., 2009).

Many outcrop examples demonstrate this ability of large-volume debrites to locally (and possibly more regionally) control the topography of submarine slope (Dykstra et al., 2006; Posamentier and Walker, 2006; Walker, 2008). Jackson and Johnson (2009) record relatively minor outcrop relief (minimum of 5 m, compacted) developed at the top of a debrite that influenced the local routing of subsequent gravity flows and the stratal architecture of related deposits. Other examples include the Ainsa Basin (Eocene), northern Spain (Pickering and Corregidor, 2005) and the Delaware Basin (Permian), USA (Amerman et al., 2011). In these examples, mud-rich debrites are associated with relief of up to 35 m along their upper surfaces

causing younger turbidites to onlap. Surface relief can result from original depositional topography (either from catastrophic emplacement or creep), differential compaction (Alves, 2010), or a combination of these. Due to this differential compaction and creep in some cases, with large amounts of relief, this influence by the underlying feature can persist into the overlying stratigraphy for hundreds of metres of section (e.g., Walker, 2008). Turbidites can be fully ponded within topographic lows, or just partially confined with no true three dimensional closure of confining topography. The amount of control depends on the relationship between the scale of topography and magnitude of the turbidity currents. This topography can dramatically affect grain-size distribution, types and abundances of sedimentary structures, and grading of beds in the turbidite successions (e.g., Walker, 2008; Dykstra et al., 2011).

Studies of exhumed systems (e.g. Martinson and Bakken, 1990; Lucente and Pini, 2003; Pickering and Corregidor, 2005; Spörli and Rowland, 2007; Callot et al., 2008) and rare examples in core (e.g. Eggenhuisen et al., 2010) provide crucial information on process interaction and temporal/spatial evolution of deposits. However, because of the large scale of basal shear surfaces (kms in width, hundreds of metres in depth) recognising these features at outcrop is challenging, even with good palaeogeographical constraint (Lucente and Pini, 2003; Shultz et al., 2005). In particular, an exhumed lateral margin of a basal shear surface has never previously been documented and large-scale (10s m deep) basal erosion has rarely been shown (e.g. Lucente and Pini, 2003; Shultz et al., 2005; van der Merwe et al., 2009). Therefore previous outcrop studies often show numerous examples of depositional relief and the influence on subsequent flows but very little on erosional relief (discussed further in sections 2.4.2 and 2.5.5).

### *2.3.5 Summary*

Exhumed studies can give significant detail on spatial and temporal variation in erosion and sedimentation across slope to basin floor profiles and allow interpretation of palaeotopography. Unlike experimental datasets they do not allow for direct observations of flows, with flow dynamics, instead, interpreted from the geological record. Therefore strata only represents flow dynamics during deposition or erosion, and therefore the sedimentary record is bias towards these processes, with bypass dominated areas poorly understood. Previous outcrop studies on topographically complex areas are often limited in spatial or stratal extent, generally examining a single area effect by one type of topography (lateral or frontal, gradient increase or decrease) or a narrow range of stratigraphy.

## 2.4 Modern seafloor studies

The effect of slope and basin-floor topography on flow dynamics has also been noted in modern seafloor datasets, including, changes in slope and basin floor gradient as well as the formation of submarine slides. Modern seafloor datasets allows analysis of large scale, undeformed areas that are still active and therefore are unbiased towards deposited and strongly erosional flows that create stratigraphic records.

### 2.4.1 Downslope gradient change

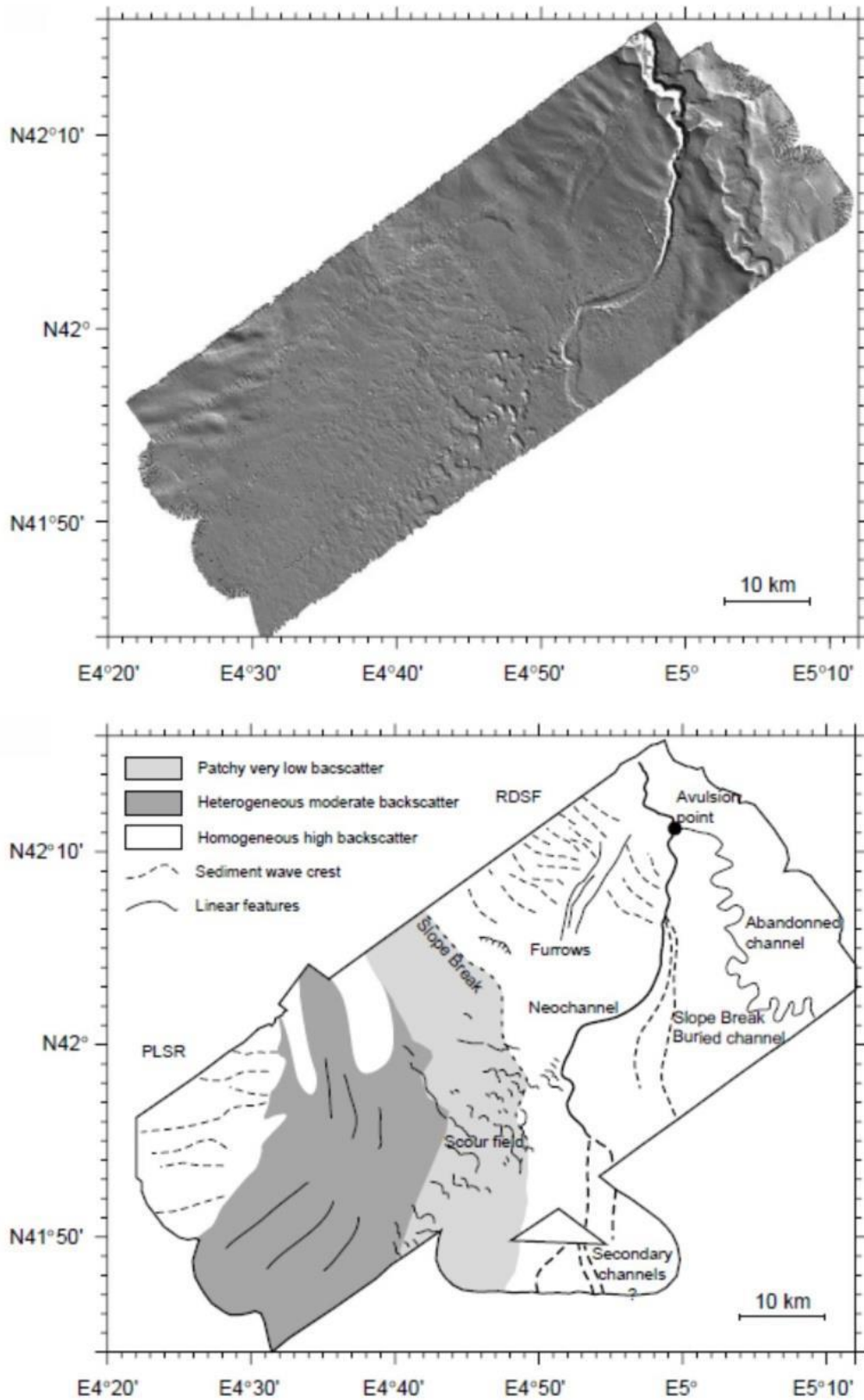
Channel-lobe transition zones (CLTZs) have been interpreted from outcrop studies, but are often limited in spatial extent due to outcrop limitations. CLTZs have been recognised in many modern seafloor datasets (Fig. 2.21) (e.g. Piper and Sayoye, 1993; Palanques et al., 1995; Morris et al., 1998; Wynn et al., 2002a; Habgood et al., 2003; Bonnel et al., 2005), allowing an assemblage of erosional and depositional bedforms to be identified (e.g. Palanques et al., 1995; Wynn et al., 2002a; Bonnel et al., 2005). As in outcrop datasets, CLTZs can be categorised as attached or detached, with the latter including a spatial geographic zone dominated by bypass (Fig. 2.22) (Mutti and Normark, 1987; Wynn et al., 2002a).

The only generic model of CLTZs is presented by Wynn et al. (2002a) (Fig. 2.22), which is based on bathymetric and acoustic backscatter expression in recent systems. The system is divided into a more proximal erosion dominated area, including various scour forms, and a more distal deposition dominated area, with sediment waves as reworked deposits (Wynn et al., 2002a). Despite this segregation, as a whole the zone is interpreted as sediment bypass dominated (*sensu* Stevenson et al., 2015), where the majority of the sediment reaching the CLTZ is deposited further into the basin. The deposits that tend to be in the CLTZ area are relatively coarse-grained, patchily distributed and extensively reworked (Wynn et al., 2002a).

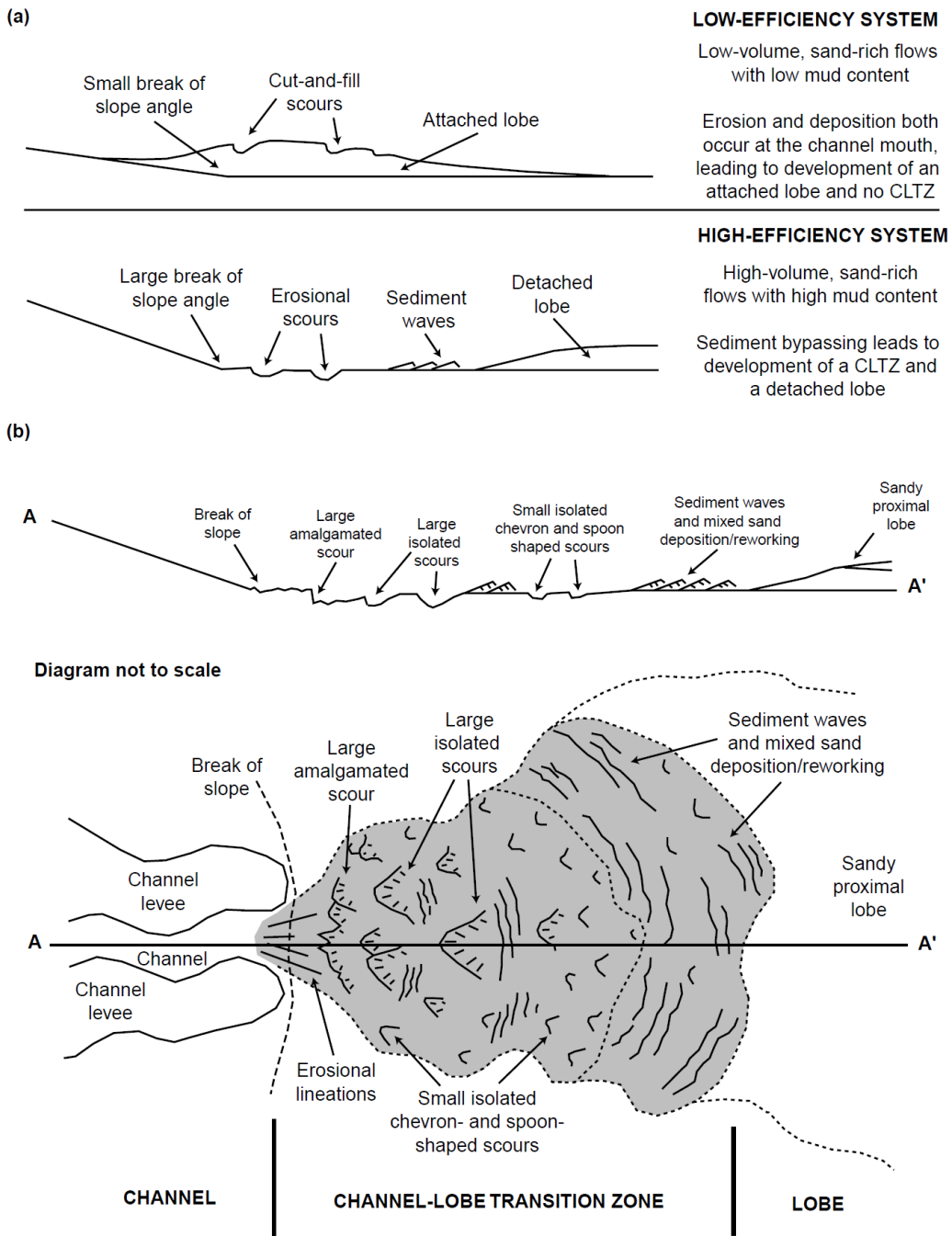
The erosional zone is dominated by scour features (Wynn et al., 2002a), these can take many forms with several distinct scour morphologies documented. Macdonald *et al.*, (2011a) describe 4 scour types that were documented in the modern environment along the northeast Atlantic margin (Figure 2.23): 1) *Spoon-shaped*, these scours have a regular elliptical morphology in planform, are elongate downstream and have a low width: length ratio, also documented in the Valencia channel-mouth (Palanques et al., 1995); 2) *Heel-shaped scours*, these scours have outward flaring limbs and are wider than they are long; 3) *Crescentic scours*, these scours are similar to heel shaped but with positive relief between the limbs, broadly lunate shape, and are generally as wide or wider than they are long — these have also been

recognised from the canyon-fan transition off West Portugal (Wynn et al., 2002a) (Fig. 2.24) and the Valencia channel mouth (Palanques et al., 1995); and 4) *Oval scours*, these are elliptical and elongated across the slope.


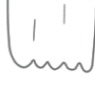





Individual scours can overlap and interact to form scour fields, where scours coalesce into larger more composite features. These areas can be several km's across (Wynn et al., 2002a). In many cases it is possible to identify the individual scours from erosional remnants of the scour, irregular topography, hummocks or elongated positive relief (Macdonald et al., 2011a).



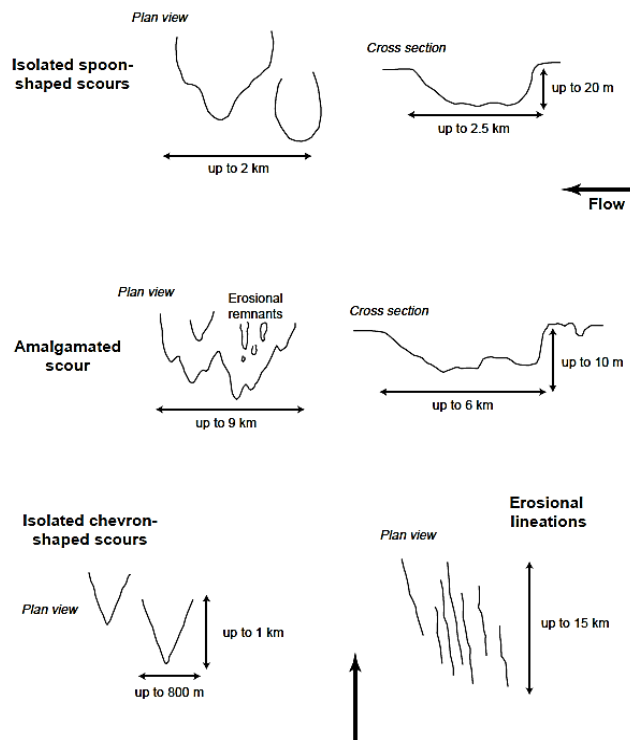
**Figure 2.21** (upper) Shaded swath bathymetry of the Rhone Deep Sea Neo-fan. (lower) Morpho-acoustic interpretation of the same dataset showing the independent nature of the Neo-channel mouth and a large scour field developed downdip of a slope break (from Bonnel et al., 2005).



**Figure 2.22(a)** Typical cross section through low efficiency submarine fan system with an attached lobe, and a high efficiency system with a detached lobe. (b) Summary of spatial distribution of erosional features and deposition bedforms within a CLTZ (from Wynn et al., 2002a).

SCOUR TYPE	PLAN VIEW (not to scale)		ISOLATED SCOUR MAX. DIMENSIONS (m)		
	Isolated	Amalgamated	Length	Width	Depth
SPOON			600	225	20
HEEL			350	890	30
CRESCCENTIC			1000	1000	14
OVAL			-	3170	48

**Figure 2.23** Morphology and dimensions of four isolated and amalgamated scour types documented along the north east Atlantic margin (from Macdonald et al., 2011a).



**Figure 2.24** Morphology and dimensions of erosional features in CLTZs (from Wynn et al., 2002a).

Despite significant research into these features, still little is known about the processes that form deep-water scours. It is evident from modern and ancient examples that there is a wide



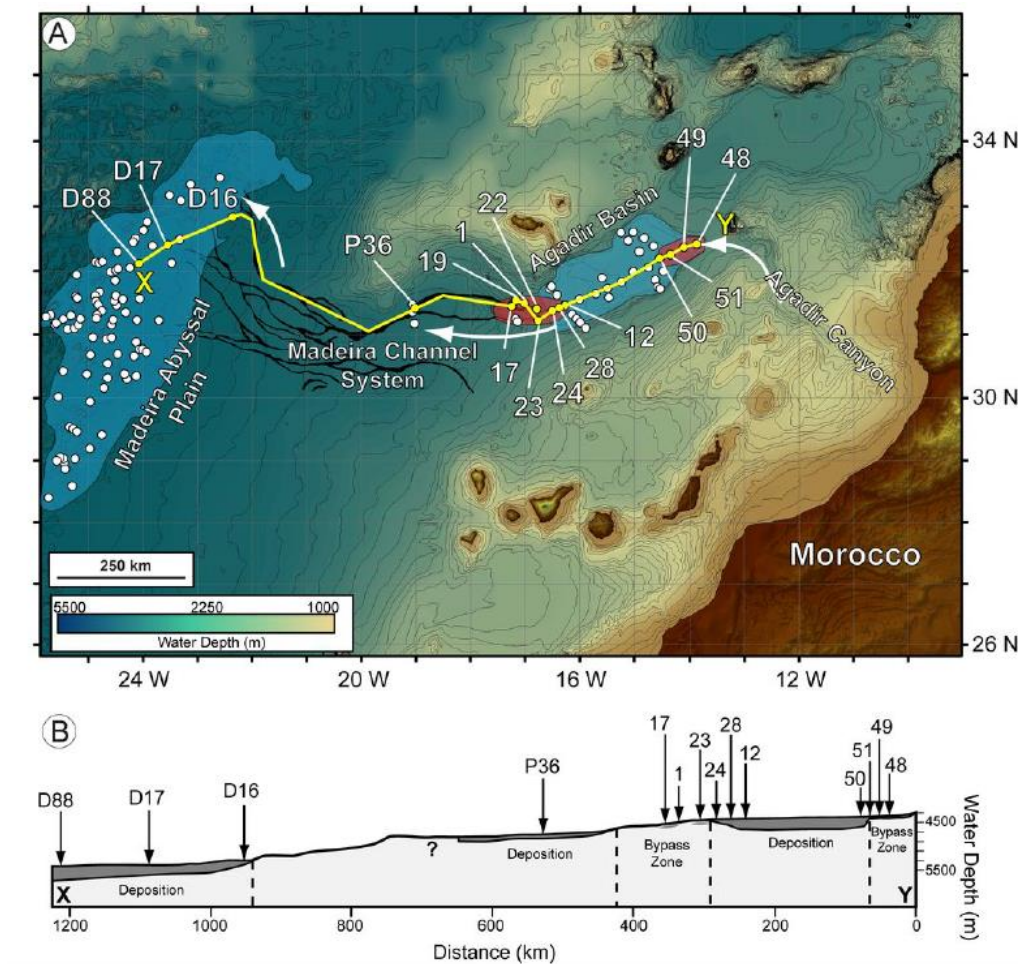
variation in shape and size, and scours in comparable environments can look very different, as can scours in the same system. The reasons for this are unknown. Studies have speculated that a complex interplay of substrate character (e.g. sand/mud ratio, consolidation rate), seafloor morphology (e.g. slope angle, degree of channelisation), flow character (e.g. volume, velocity, density) and flow frequency are important factors contributing to scour morphology and dimensions (Macdonald, 2010). While the development of isolated scours into extensive amalgamated surfaces is clear, the initial genesis of the isolated scours is difficult to assess. Some scours suggest complex formation processes. For example successive cut-and-fill cycles spanning 10's of thousands of years have been recognised within single scours (Macdonald et al., 2011a). The abandonment and infilling of scours can be caused by either allogenic or autogenic factors. Allogenic factors include a shutdown of an entire system, for example during a sea level highstand, or other factors, which reduce sediment supply to the system. Autogenic factors include debrite infills caused by failures of channel/ canyon margins or migration of the channel thalweg (Macdonald, 2010). Moreover, individual scour processes are independent of one another; a scour can be infilled whilst an adjacent scour actively eroded (Macdonald et al., 2011a). There have been several proposed explanations for this including: lateral migration of the primary zone of erosion; formation of hydraulic jump; or interactions between the flow and topography causing spatial variations in bed shear stress (Macdonald et al., 2011a).

Depositional elements within CLTZs include sediment waves, sediment mounds/lag and reworked coarse deposits (Wynn et al., 2002a, b). Sediment waves are depositional bedforms located within the central and distal sections of CLTZs (Fig. 2.22) with wavelengths of 1-2 km, wave heights of 4 m and crest lengths of maximum 4 km, aligned orthogonal to the main flow direction (Normark and Piper, 1991; Wynn and Stow, 2002; Wynn et al., 2002b; Klauke et al., 2004; Ercilla et al., 2008). These features consist of a coarse sand-gravel composition (Piper et al., 1985; Kidd et al., 1998; Migeon et al., 2001; Wynn et al., 2002b). Sediment mounds and lag deposits are features up to 40 m long and 1.5 m high, comprise coarse material, generally pebbly sand and gravel, and are located immediately down-dip of scours (Wynn et al., 2002a). Reworked coarse deposits are located more distally in a CLTZ, and generally form features parallel to current direction (Fig. 2.23) (Wynn et al., 2002a). Modern expression of the CLTZ is mostly limited by the resolution of sonar and shallow seismic datasets (Wynn et al., 2002a) therefore sub-metre scale features have not been described.

CLTZs form with decreases in seafloor gradient that coincide with decreased confinement. Increases in seafloor gradient have also been studied in detail in modern systems including

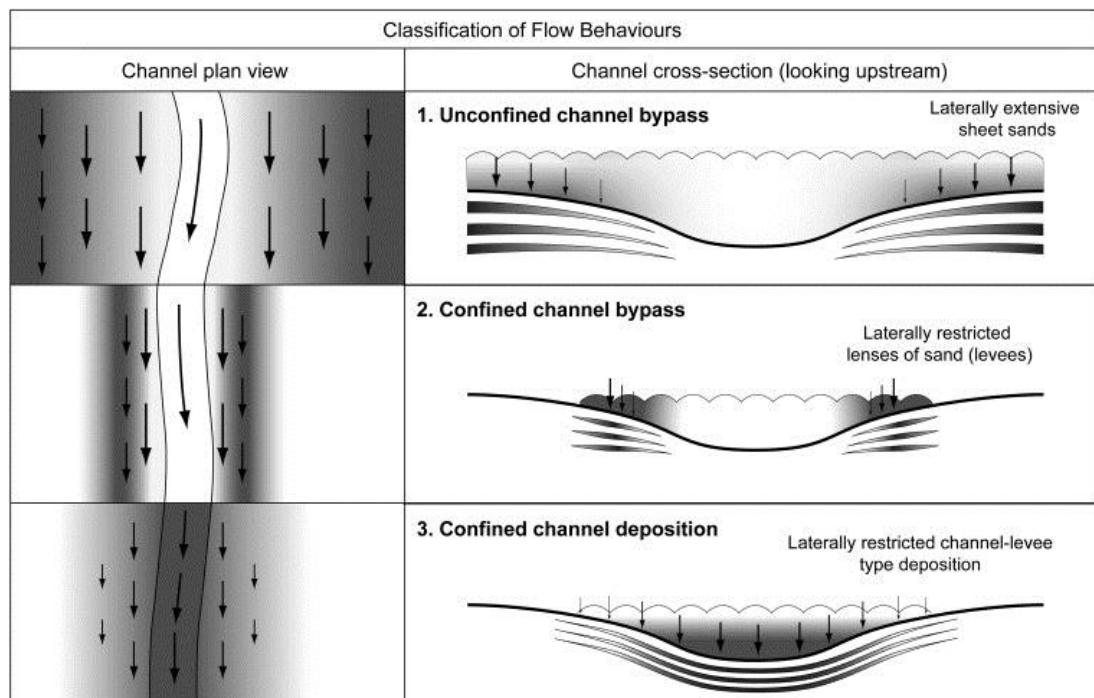
rechannelization on the basin-floor (Stevenson et al., 2013). Increases in slope or basin floor gradient can lead to an increase in flow bypass. The establishment of an optimum slope gradient and flow conditions can lead to flow travelling in a state of equilibrium.

The Moroccan Agadir basin, modern seafloor datasets show a zone of base of slope bypass/CLTZ, near to the mouth of Agadir Canyon, consisting of frequent erosional scours overlain by fine-grained sands/mud and thin gravel lags, as well as a basin floor bypass zone where flows pass from the Agadir Basin ( $0.02^\circ$ ) to the high aspect ratio Madeira Channel System ( $0.06^\circ$ ) (Fig. 2.25) (Stevenson et al., 2013). This planform view of modern systems allows anatomical links to be made between up-dip and down-dip sands, with cores allowing detailed sedimentology to augment basin scale data (Stevenson et al., 2013).



**Figure 2.25** A) Map of the Moroccan Turbidite System showing the pathway of Bed 5 through the Agadir Canyon, into the Agadir Basin, through the Madeira Channel System, and ultimately spreading across the Madeira Abyssal Plain (adapted from Stevenson et al., 2014a). Shallow sediment cores taken across the system are marked as white circles, with those detailed in this study highlighted in yellow. Base-of-slope and basin-floor bypass zones are highlighted as red areas. B) Schematic core transect of Bed 5 along its pathway from the Agadir Canyon to the Madeira Abyssal Plain (from Stevenson et al., 2015).

Bypass-dominated channels described from shallow seismic profiles (Fig. 2.24) (e.g. Agadir Basin, Stevenson et al., 2013) show acceleration of turbidity currents with an increase in slope gradient from  $<0.02^\circ$  to  $>0.06^\circ$ , therefore intensifying ambient mixing at the head and reducing mixing in the body of the flow. Flows can become autosuspended, whereby there is no deposition or entrainment of sediment. For this to occur, flows must be powerful enough to suspend the entire sediment load, but not powerful enough to erode underlying substrate (Sequeiros et al., 2009). Stevenson et al. (2013) describes three main flow behaviours and depositional architectures across the Maderia Channel System (Fig. 2.26).



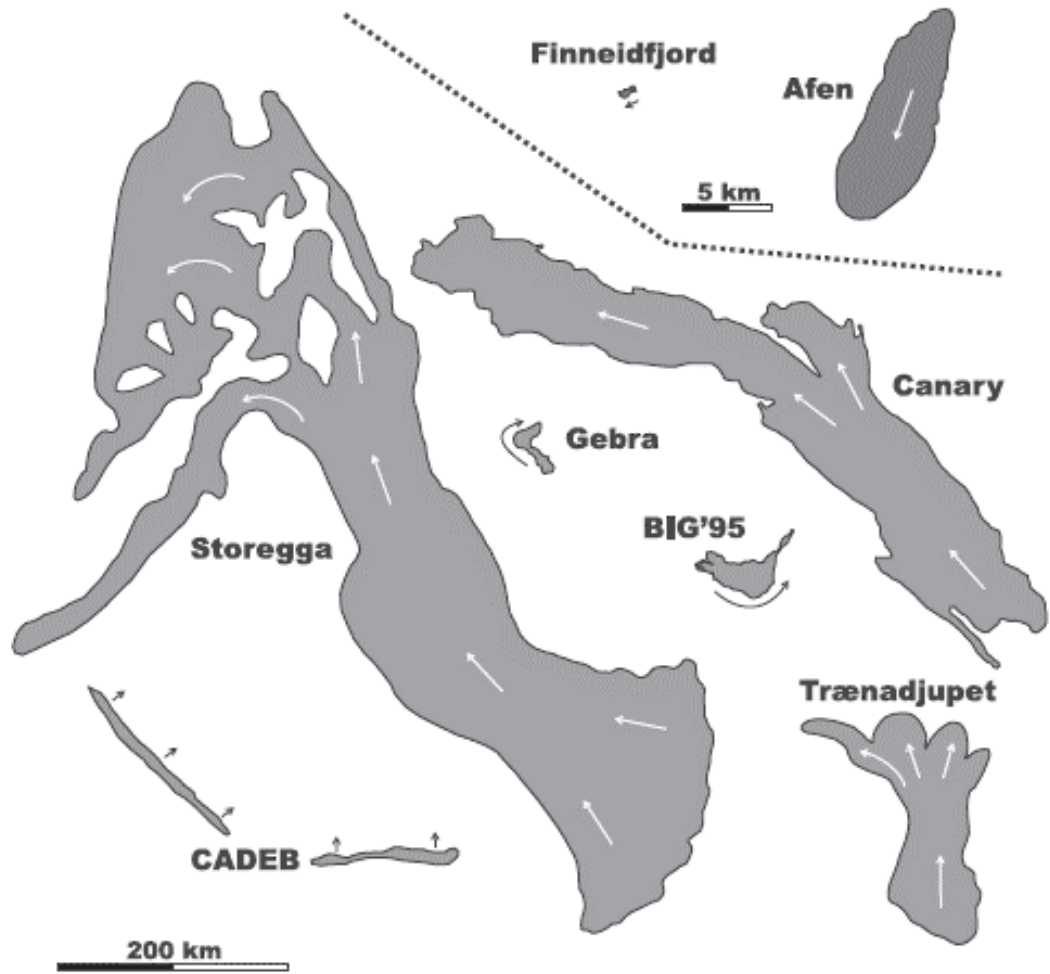
**Figure 2.26** Cartoon summarising the three main types of flow behaviour and resultant depositional architectures across the Maderia Channel System. In plan-view arrows indicate flow direction and size of arrow represents flow velocity, darker shaded areas indicate areas of deposition whereas lighter areas represent non-deposition. In cross section arrows indicate zones of deposition (from Stevenson et al., 2013).

In confined channel bypass (*sensu* Stevenson et al., 2013) (Fig. 2.26), thinner flows are confined in the channel, so a higher proportion of sediment is bypassed downslope, with only the uppermost areas of flow overspilling the channel or undergoing flow stripping, forming lenses of ripple cross laminated sand. This is displayed as composite erosion surfaces in many systems (e.g. Hubbard et al., 2014). Confined channel deposits (*sensu* Stevenson et al., 2013) (Fig. 2.26) occur where there is decrease in gradient or not enough acceleration for flows to bypass, forming thicker ripple cross laminated sand in the channel axis and finer grained marginal sediment (Stevenson et al., 2013). In unconfined channel bypass (*sensu* Stevenson et al., 2013) (Fig. 2.26), flow spreading is extensive with flows large in volume relative to the

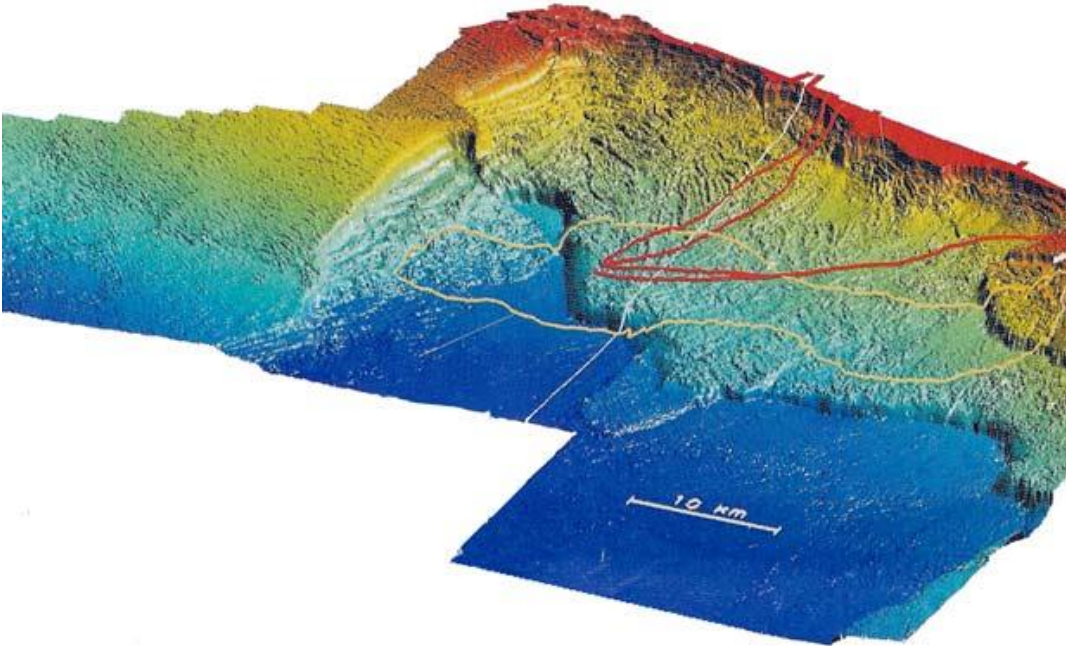
channel size; deposits in the Maderia system related to this process are extensive ripple cross-laminated sands. The decrease in flow confinement impacts the upper more dilute section of the turbidity current, with the coarser sediment confined in the channel and bypassed downslope (Stevenson et al., 2013). A decrease in gradient will cause unconfined channel deposition, with shallowing of gradient decelerating both the confined and unconfined flows (Stevenson et al., 2013).

#### *2.4.2 Submarine slide erosional and depositional relief*

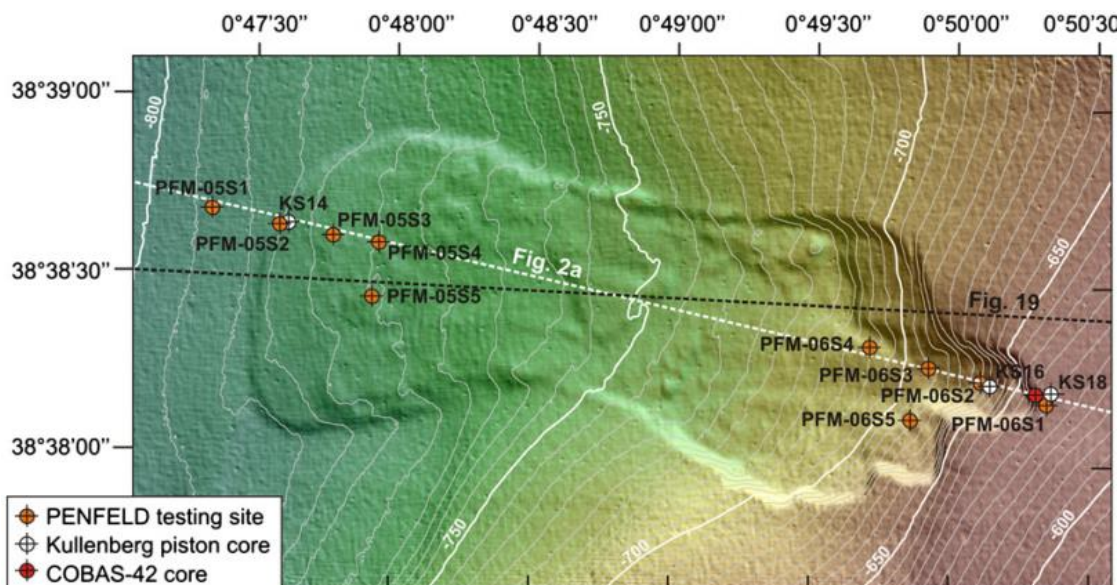
Recent improvements in seabed (e.g. swath bathymetry) and sub-surface mapping techniques (high-resolution 3D seismic imaging) have revealed a wealth of slide scars and a diversity of related deposits on many of the world's continental margins (e.g. Vanneste et al., 2006; Morcardelli and Wood, 2015). Modern studies demonstrate the geometry and scale of basal shear surfaces to submarine landslides as well as the run out and character of resultant deposits, including the Storegga slide (Haflidason et al., 2004; Solheim et al., 2005), the Hinlopen slide (Vanneste et al., 2006), further slides offshore Norway (Baeten et al., 2013; Laberg et al., 2014), various slides across the US continental slope (McAdoo et al., 2000), and slides on submarine island flanks in the Canary Islands (e.g. Gee et al., 2001; Urgeles et al., 2001; Masson et al., 2002; Hürmann et al., 2004; Hunt et al., 2013; León et al., 2017). Many of these failures involved thousands of km<sup>2</sup> of substrate (Fig. 2.27), and their formation represents an important mechanism for transferring sediment down the continental slope (Krastel et al., 2016). Modern seafloor datasets are more continuous and shown substantially larger areas that outcrop this can allow the recognition of both the slide area of failure (basal shear surface) and the resultant deposits (Figs 2.27, 2.28 and 2.29).



**Figure 2.27** Comparison of shapes and area of failures studies within the COSTA project (from Canals et al., 2004).



**Figure 2.28** Three dimensional map of slope offshore Norway showing the geomorphology of the Storegaa slide, from <http://www.offshore-technology.com/projects/ormen-lange-field/ormen-lange-field8.html>.



**Figure 2.29** Shaded relief image of Ana Slide, Ana Slide covers 6 km<sup>2</sup> and is located on the eastern Balearic flank of Eivissa Channel (from Lafuerza et al., 2012).

This large amount of modern seafloor data demonstrates the various locations, orientations, sizes and morphologies of submarine slides and their resultant deposits, therefore indicating the types and amount of relief created by slide scars (Figs 2.27, 2.28 and 2.29). In order to understand the impact that this topography has on resultant remobilized and turbidity flows, reflection seismic datasets are required.

### 2.4.3 Summary

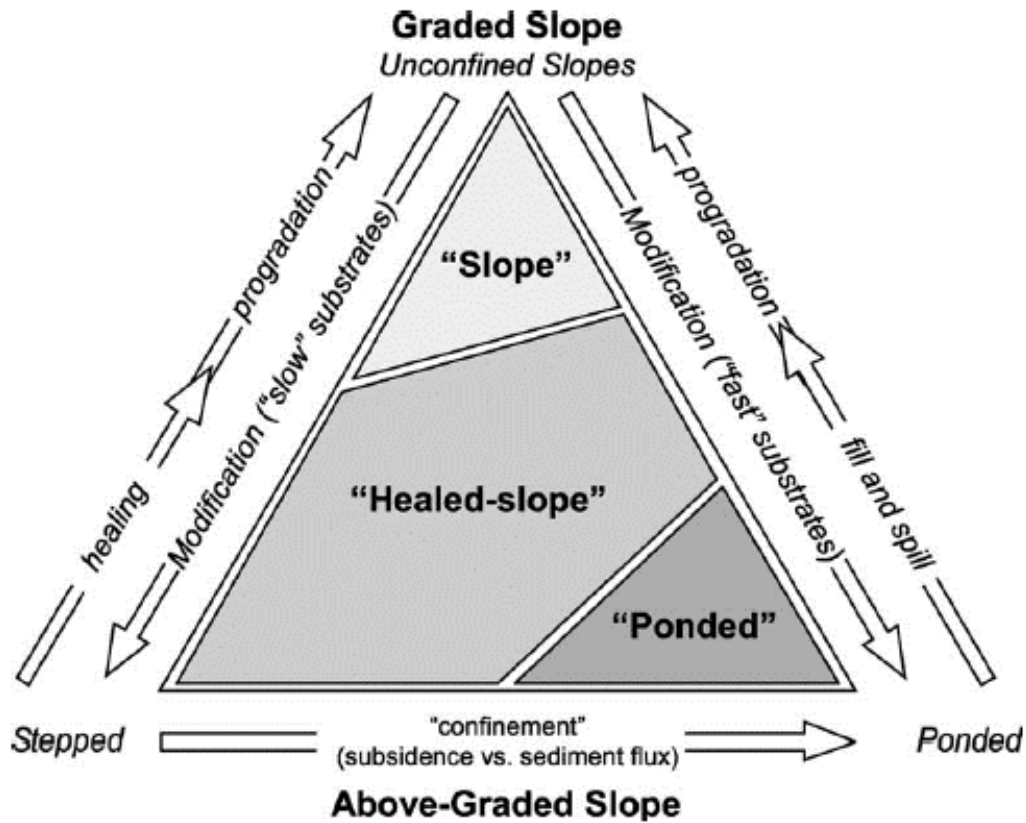
Modern datasets have the potential to show far larger and more continuous areas of the seafloor compared to outcrop datasets. Moreover studies of the modern seafloor are unbiased towards deposition/ erosion and allow far greater understanding of bypass processes, which are often overlooked in stratigraphic record. Despite this they are limited in resolution generally allowing only regional scale study where not cored. Moreover they only display a single snapshot in time and do not show the temporal evolution that this is possible in outcrop and seismic datasets.

## 2.5 Reflection seismic studies

Reflection seismic datasets allow analysis of spatially large areas covering 10's to 100's of kilometres from the shelf, through slope and basin floor areas. Moreover they can cover 100's of metres of stratigraphy and therefore allow significant knowledge of temporal variations. Despite this the resolution of seismic datasets allows only large scale analysis of depositional packages

### 2.5.1 Downslope changes in gradient and confinement

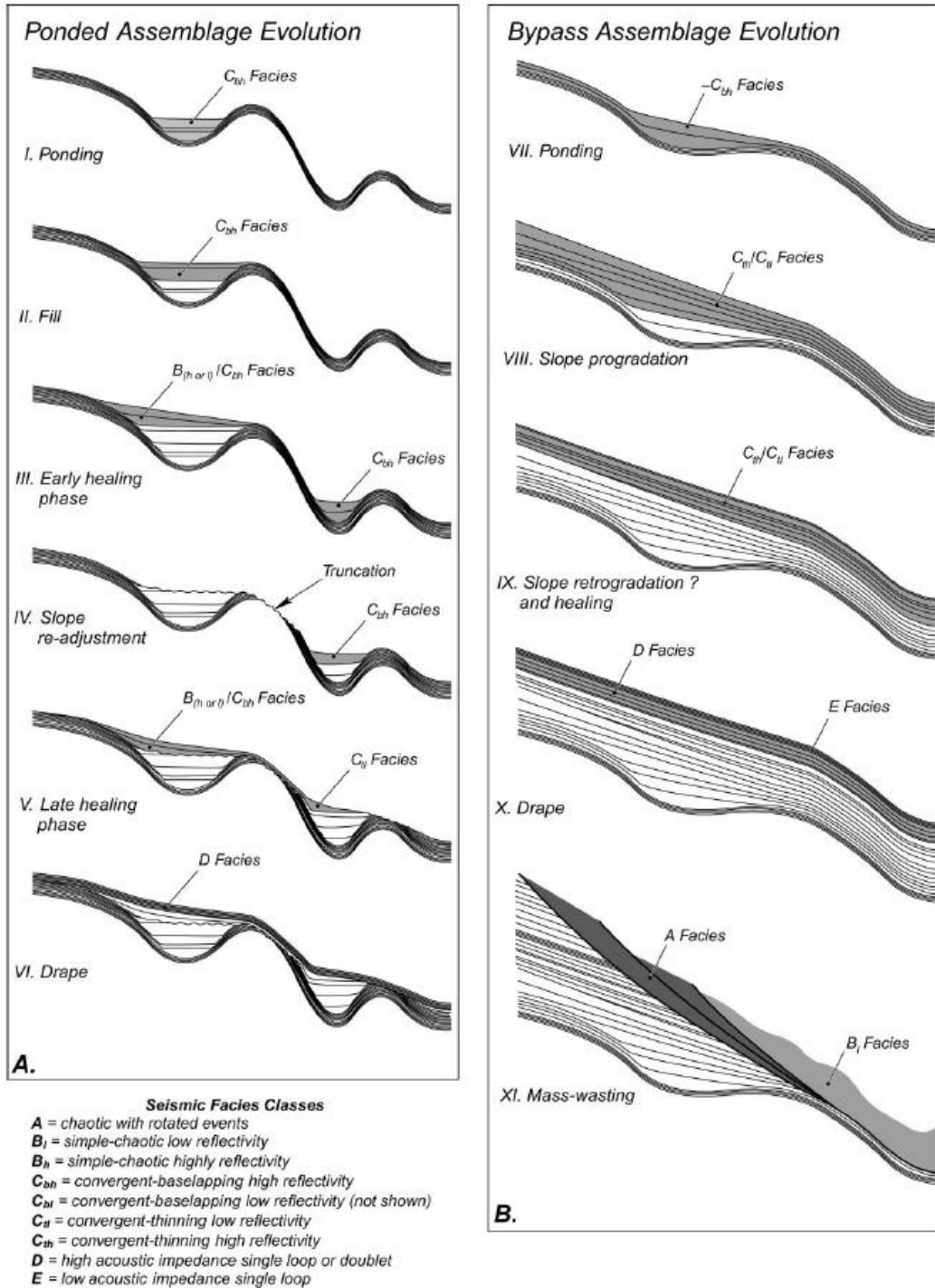
Changes in gradient impact the behaviour of a sediment gravity flows, which directly controls the dispersal patterns of sand and the character of the deposits. In subsurface reflection seismic datasets, research has demonstrated that slope bathymetry has a key influence on reservoir quality, architecture and distribution (Prather, 2000, 2003; Booth et al., 2003; Gamberi and Rovere, 2011; Bohn et al., 2012; Prather et al., 2012). Due to the large scale of seismic datasets, bathymetrically complex slopes are categorised by variation in the overall slope profile (Fig. 2.30), and give a 3D and basin wide perspective on topographic confinement (e.g. sections 2.3.1, 2.3.2 and 2.3.3) often unavailable in outcrop studies. Prather (2003) characterise slopes as: above grade slopes with well-developed ponded accommodation with large amounts of mid- to upper-slope healed-slope accommodation (e.g. Gulf of Mexico); above grade slopes with stepped profiles, that lack well-developed ponded accommodation (e.g. Niger delta slope, Lower Congo, NW Borneo; and graded slopes without significant topography (e.g. eastern Gulf of Mexico). The angle of confining slopes interpreted from seismic datasets can be more subtle and complex than those identified from outcrop (e.g. Gervais et al., 2006; Heiniö and Davies, 2007; Hanquiez et al., 2010; Prather et al., 2012a).



**Figure 2.30** Ternary diagram modified from Meckel et al. (2000), and Booth et al. (2002), showing slope type end-member and key processes controlling graded to above-grade slope transition (from Prather, 2003).

Accommodation on the submarine slope is the gap between the sediment surface (the background slope surface) and the equilibrium profile (the slope profile of no net erosion or deposition) (Pirmez et al., 2000; Kneller, 2003). The gradient of the equilibrium profile responds to changes in the volume and composition of turbidity currents, and the position of base level (Pirmez et al., 2000; Prather, 2003).



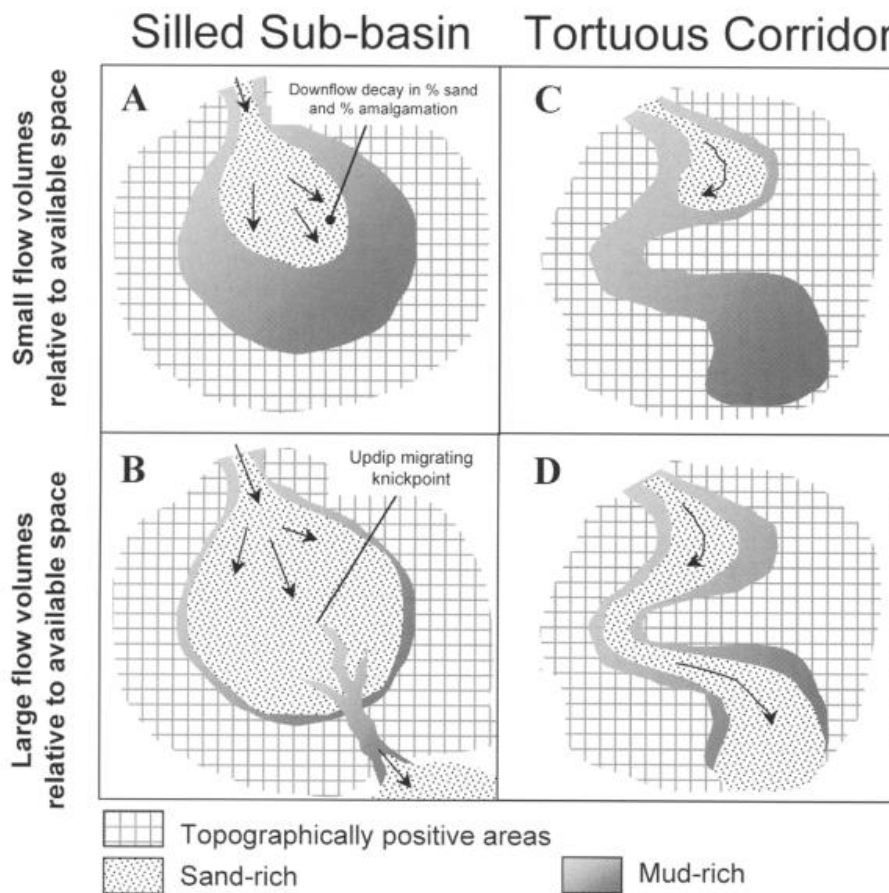


**Figure 2.31** Idealised ponded depositional sequence (I-VI) and idealised bypass deposition sequence (VII-XI) (from Prather, 2000).

Ponded accommodation occurs with 3D closure of topographic lows (Fig. 2.31) (Prather et al., 1998; Prather, 2000) that forms within intraslope basins as the result of localized withdrawal of mobile substrates (i.e. salt or shale; Prather, 2003). Healed slope accommodation (Fig. 2.31) is the space between the top of ponded accommodation and below a 3D convex surface fit to

the rugose seafloor topography. Healed slope accommodation is more common and volumetrically greater than ponded accommodation in many slopes (Steffens et al., 2003).

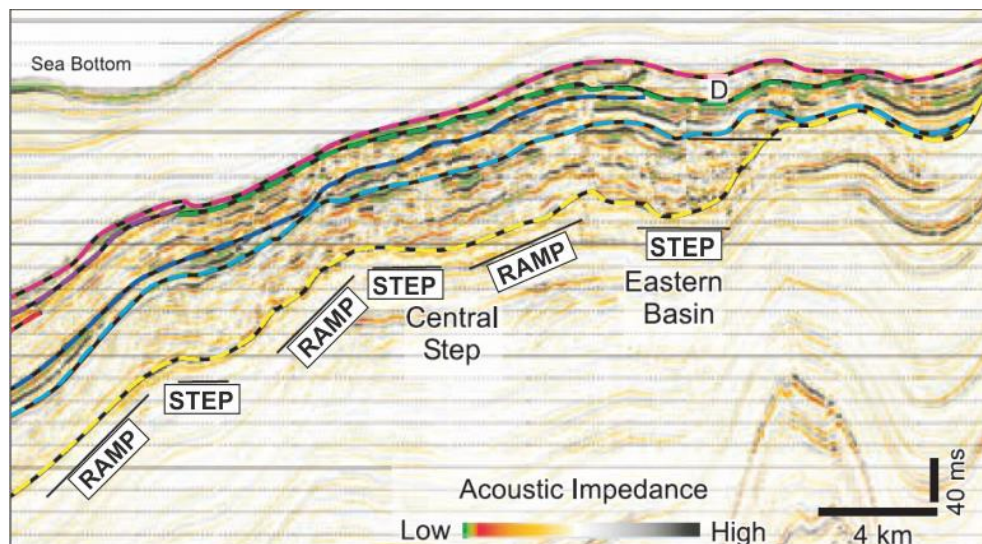
Smith (2004a) classified three broad classes of complex slope topography (Fig. 2.32): (1) Silled sub-basins (i.e. closed depressions), most commonly documented from in salt-withdrawal minibasins of the Plio-Pleistocene Gulf of Mexico slope (Diegel et al., 1995; Liu and Bryant, 2000); (2) Partially silled basins with lateral escape paths, e.g. the Chumash Fracture Zone (Normark et al., 1984) and the physiography present on the Brunei slope (Demyttenaere et al., 2000); (3) Tectonically induced bounding slopes that guide, but do not block, flow paths, which can vary from highly tortuous to close to linear and commonly exhibit segments of lower ('steps') and higher (between 'steps') gradients (e.g. Hay, 2012).



**Figure 2.32** Schematic diagrams illustrating the importance of the areal extent of sediment gravity flows relative to the areas of receiving depressions. (A) Silled sub-basin in which sand-transporting flows are small in volume relative to the scale of the receiving space. (B) Silled sub-basin in which sand-transporting flows are large in volume relative to the scale of the receiving space. The diagram shows spill to the next sub-basin downslope with associated incision and bypass in the upper sub-basin. (C) Connected tortuous corridor in which sand-transporting flows are small in volume relative to the potential flow path. A possible example is shown in figure 8 of Demyttenaere et al. (2000). (D) Connected tortuous corridor in which sand-transporting flows are large in volume relative to the potential flow path (from Smith, 2004a).

Systems can therefore be classified into two end members silled sub-basins and tortuous corridors (Fig. 2.32). In the cascade of silled sub-basins model, topographic barriers between sub-basins are effective in blocking at least the basal sand-rich portions of flows until fill is achieved (Smith, 2004a). When substantial portions of flows to travel beyond the former barrier, flow will accelerate on the steep slope downdip of the barrier, and lead to downcutting and successive flows cut back into the fill of the updip sub-basin (Smith, 2004a) also known as up-dip migrating knickpoints (Pirmez et al., 2000).

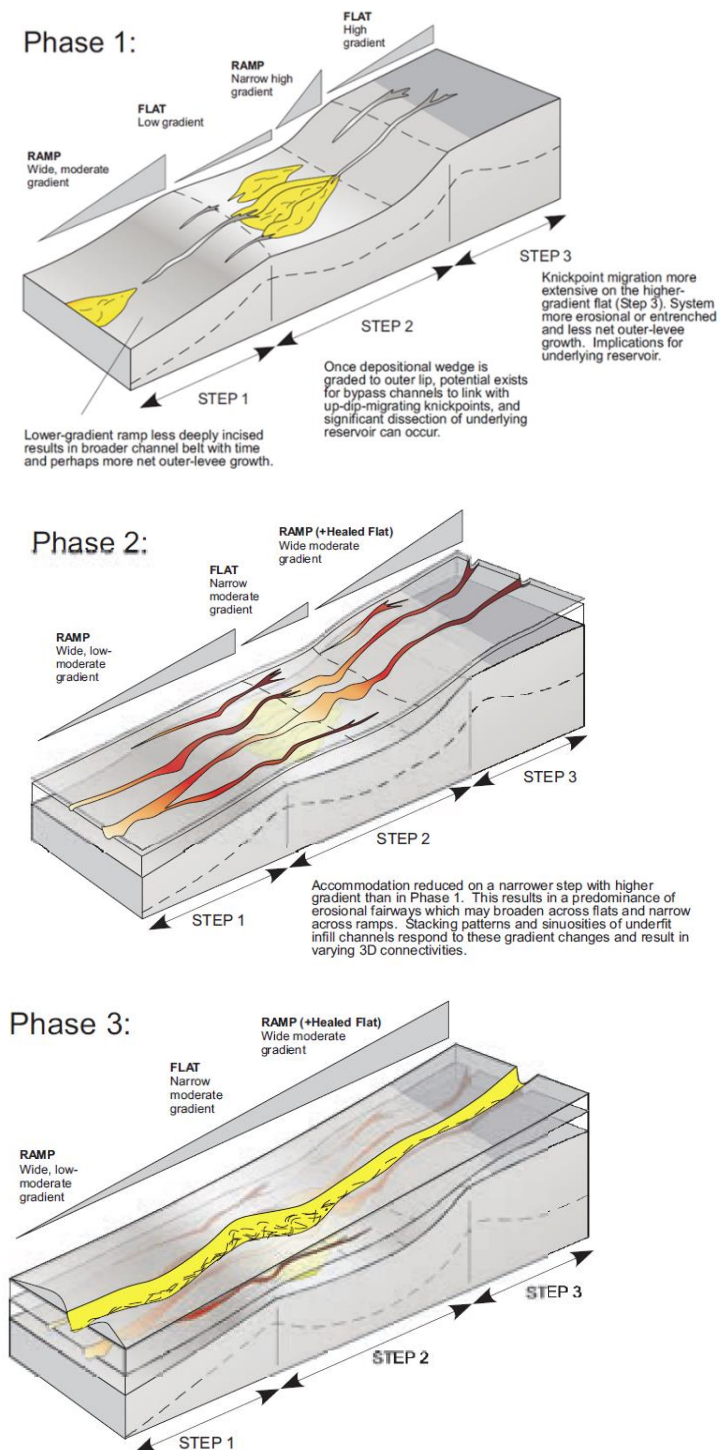
Slopes with less extreme topographic controls include stepped slope profiles. Stepped slope profiles are classified as above grade slopes that exhibit subtle changes in depositional gradient that result in low gradient steps that are linked by high gradient ramps. Above-grade slopes are low relief systems that lack the 3D closure of ponded mini-basins (Meckel et al., 2002) and are characterised by complicated, connected flow pathways with varying depositional gradients that are marked by alternating sections of erosion and bypass (Fig. 2.33) (O'Byrne et al., 2004; Smith, 2004; Hay, 2012). Step flats are areas of net accumulation and have a low or negative gradient, and are essentially toe of slope settings. Entry or exit ramps are zones of net sediment bypass, which will have a higher gradient (O'Byrne et al., 2004). Stepped slope profiles are dominated by healed-accommodation. The shape of this accommodation varies but it is generally strike-orientated curvilinear elongated ellipsoids on mud-prone stepped-slope profiles (Prather, 2003).



**Figure 2.33** Seismic section showing the stepped topography with numerous ramps and flats along the middle Angolan continental slope (from Hay, 2012).

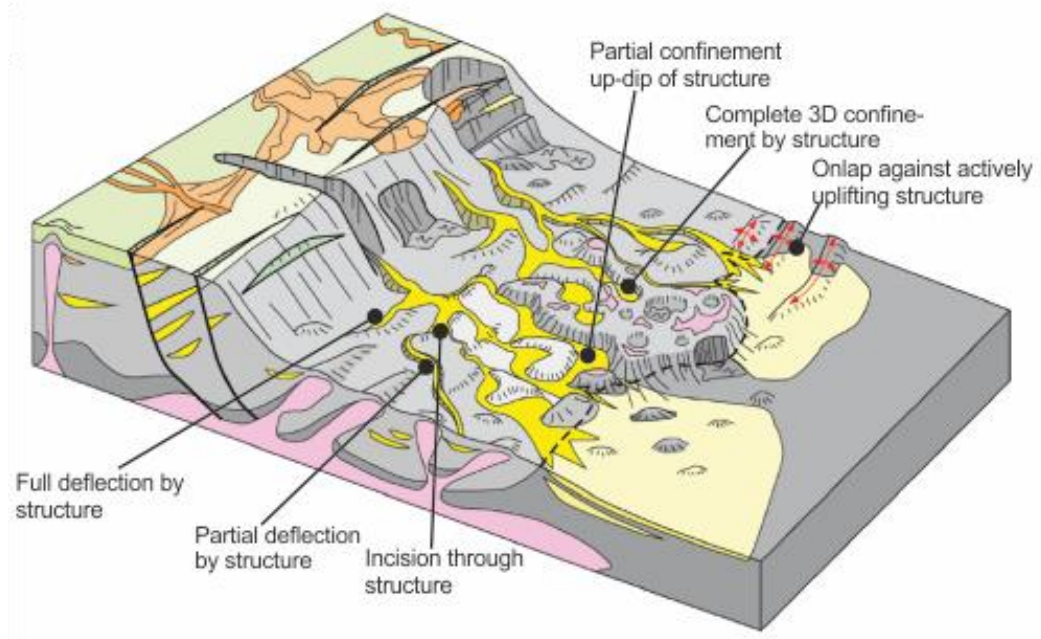
An example from offshore Angola (Fig. 2.33) from Hay (2012) demonstrates the evolution of stepped slope profiles through healing from a slope with distinct areas of net deposition and

net bypass (Fig. 2.34), lessening gradient changes, creating broader zones of erosion and finally creating a through-going bypassing channel system as the slope reaches equilibrium (Fig 2.34).



**Figure 2.34** Conceptual model for depositional evolution along a stepped-slope profile (modified from O'Byrne et al., 2004). Predicted slope evolution describes depositional and erosional response of turbidity currents to progressive slope build-up and associated accommodation reduction (from Hay, 2012).

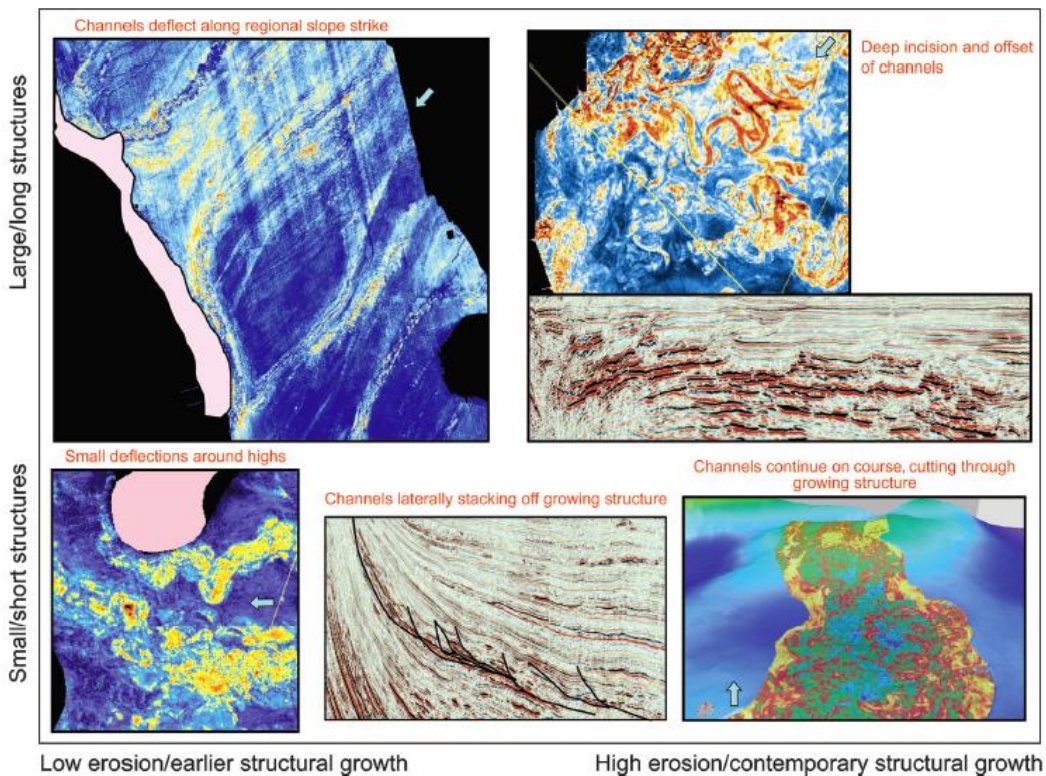
If unobstructed, a slope will grade to equilibrium (Pirmez, 2000; Prather, 2003), but an important consideration in all of these settings is the rate/amount of structural growth *versus* the nature and rate of sediment supply and deposition or timing (Jackson et al., 2008; Mayall et al., 2010). For example, where structural growth is rapid compared to sediment supply, basinward transported sediments may be deflected or completely trapped on the slope (Jackson et al., 2008). In contrast, where structural growth is slow in comparison to sediment supply, any topographic variations associated with these structures may be smoothed-out, resulting in only minor or no re-routing and/or trapping of sediments (Jackson et al., 2008). Exceptions to this may be on steep slopes, where erosion at the base of out-of-grade channels with a constant supply of sediment may result in these systems incising into and cross-cutting even the most rapidly growing structures (e.g. Badalini et al., 2000; Pirmez et al., 2000; Heiniö and Davies, 2007).



**Figure 2.35** Sketch illustrating the structural controls on depositional systems on shelf, slope, and base-of-slope systems affected by gravity-driven tectonics. Terrestrial fluvial-delta systems in orange, sand-rich facies in yellow, deep-water fans in pale yellow, slope muds in grey, salt structures in pink. Note the complex and tortuous paths taken by slope channels around salt structures and folds. Sands can also pond in intraslope basins until the basin is filled and then channels continue down the topographic slope. Typical scale of 150 km (93 mi), modified from Mayall et al., 2010.

Clark and Cartwright (2009) reported four end-member channel interactions with structures (folds/faults) in the deep-water Nile Delta, including: deflection of channels to fold tips; diversion of channels by folds; confinement of channels between two parallel folds, and blocking of channels by folds (Fig. 2.35). The influence of flow dynamics and height of topography at individual flow scale has been discussed above (section 2.2.2). At a system scale Mayall et al. (2010) demonstrates that a more complex interplay of characteristics can

influence channel response to topography (Fig. 2.34), including: the size, shape, and orientation of the structure on the depositional slope; the timing and rate of structural growth compared to channel initiation and development (e.g., Morley, 2009); and the erosional power of the channel complex systems/ variation in substrate resistance to erosion (e.g., Mitchell, 2006) (Fig. 2.36). Where structures are large (e.g. diapir, salt wall or large fault) and located parallel or oblique to slope strike, channels make major diversions to continue downslope (Huyghe et al., 2004) (Fig. 2.35).



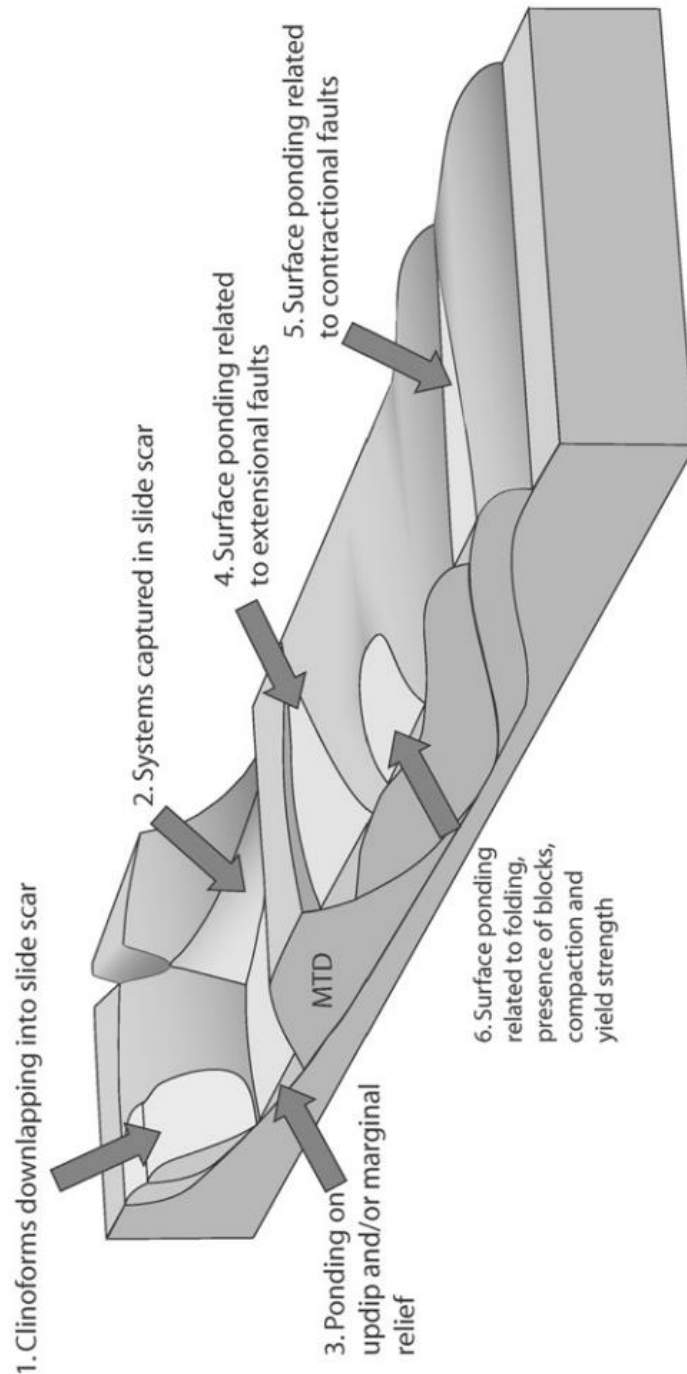
**Figure 2.36** Summary figure showing the range of channel responses to growth-related seabed bathymetry. The vertical axis goes from small structures to large structures orientated at a high angle to regional dip. The horizontal axis goes from structural growth, which predates channel development and/or low erosion of channels, through offset stacking due to growing structures to channels cutting through growing structures. Examples described in the text are plotted on this matrix. The direction of flow is shown by blue arrows except in the middle lower seismic line, where flow would be into the page (from Mayall et al., 2010).

Where a channel system traverses a part of an undeformed slope that later exhibits growth of topography a range of channel responses can be recognized depending on the rate of structural growth and the erosive power of the flows crossing the growing structure (Fig. 2.36) (Mayall et al., 2010). Where the rate of growth of the structure is greater than the ability of a channel to erode through it, channel complex systems are deflected. When channels form prior to or at the onset of deformation the channel can appear to cut through the growing structure when the downcutting rate keeps pace with the structural growth. When structural

deformation is ongoing the erosive power of flows has been shown to be a major factor in determining channel incision across topography, with channel shear stress and flow velocity partly determining whether a channel erosion can keep pace with deformation (Jolly et al., 2017). Detailed study by Jolly et al. (2017) shows that submarine channels in the Niger Delta can keep pace with structural uplift rates of up to 70 m in 1.7 m.y., and that channel entrenchment upstream of growing structures plays a major role in driving this process. When topography creates 3D topographic closure the 'fill-and-spill' model for silled sub-basins (Fig. 2.32) can be applied (Smith, 2004a).

### *2.5.2 Submarine slide topography*

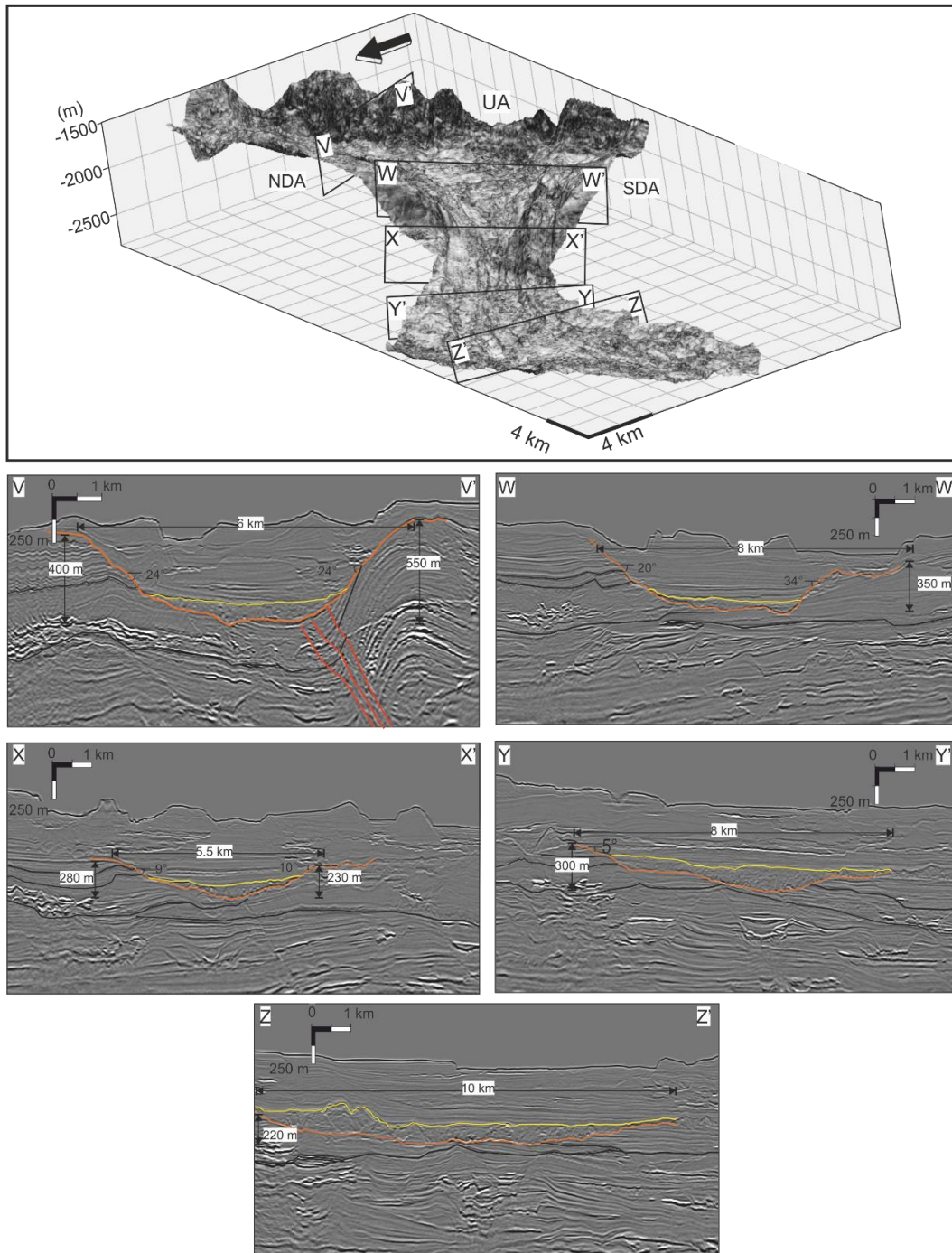
The predominance of mass wasting processes in most continental margins around the world makes MTCs a potentially important element of any deepwater stratigraphic succession (Moscardelli and Wood, 2007). In addition, their influence in the shaping of seafloor bathymetry and continental margin architecture is well documented (Frey-Martinez et al., 2005; Moscardelli et al., 2006; Moscardelli and Wood, 2008; Ortiz-Karpf et al., 2015), as they have the capacity to extensively resculpt seafloor topography on the continental slope and rise. Therefore, reservoir distribution and geometry on the slope and rise are often significantly affected (Gamboa et al., 2010; Omosanya and Alves, 2013; Alves et al., 2014). Turbidity currents may be captured within slide scars and on the trailing edges, margins, and rugose upper surface of MTDs, developed when the MTD comes to rest or from later creep or compaction (Fig. 2.37) (Alves et al., 2014).; McGilvery et al., 2004; Moscardelli et al., 2006; Armitage et al., 2009; Jackson and Johnson, 2009; Alves, 2010; Olafiranye et al., 2013; Kneller et al., 2015, 2016).



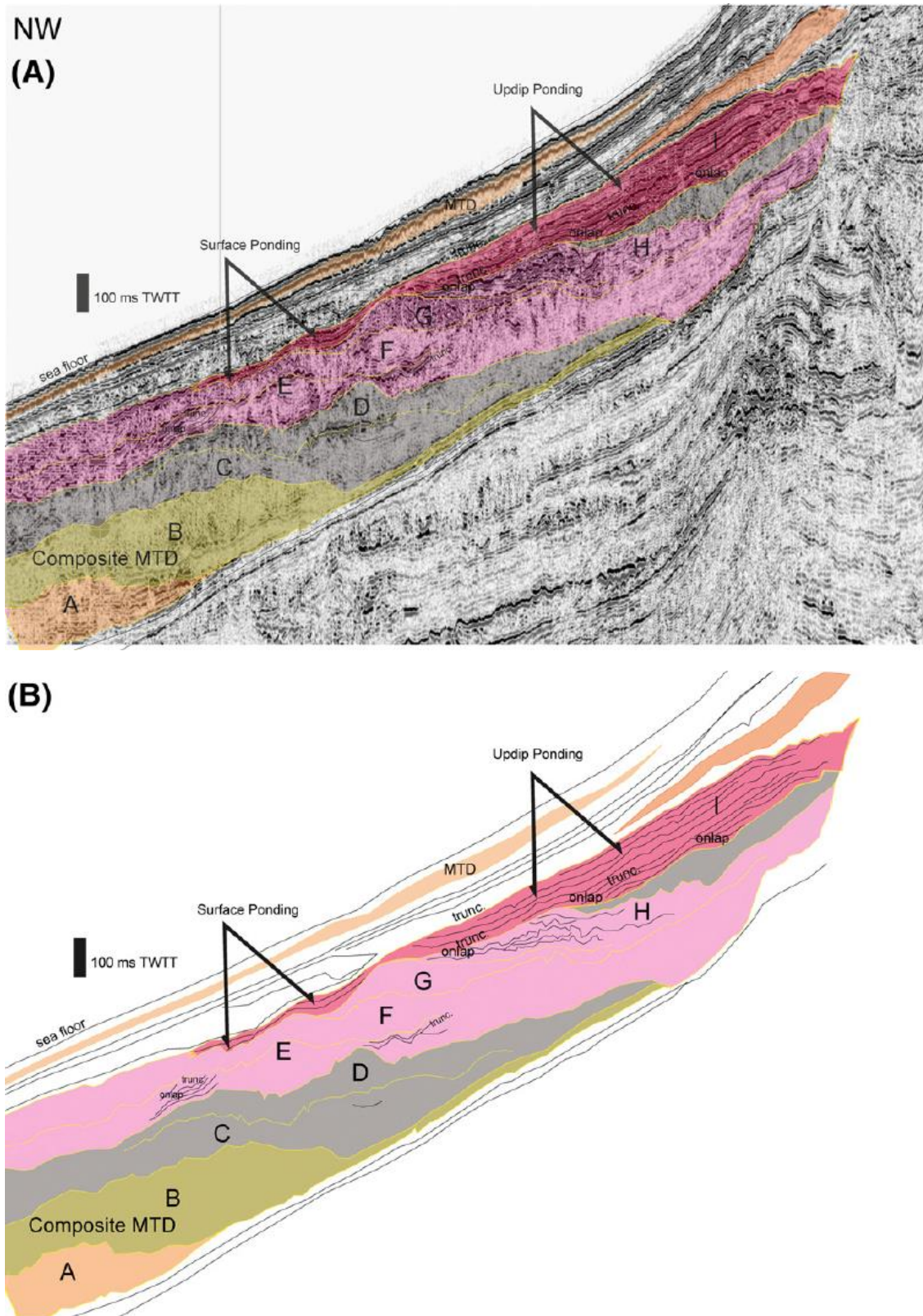
**Figure 2.37** Illustration of styles of accommodation associated with mass-transport deposits (from Kneller et al., 2016).

The assistance of 3D seismic datasets which can map both the surface morphology across strike (Fig. 2.38) and down-dip (Fig. 2.39) and allow recognition of large scale basal shear surface morphology (Fig. 2.38), as well as stages of infill and evolution. Therefore situations in which basal shear surfaces and MTDs pond or redirect flows can be predicted at large scale (Fig. 3.38 and 3.39), but bed and package scale complexities within slide scars remain unknown.



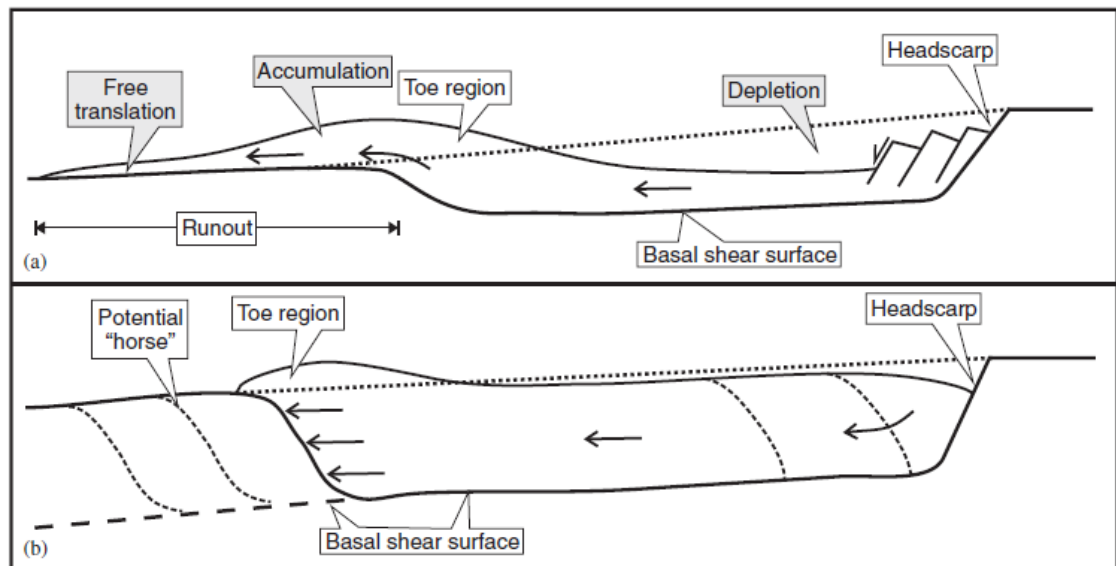


**Figure 2.38** Downdip changes in the morphology of a slide in the Magdalena Fan, Offshore Columbia. View between the northern downdip anticline and the updip anticline. V-Z seismic cross sections showing that the height and slope of the lateral walls of C1 decrease downdip and highlighting changes in the slope of the lateral margins which are sometimes related to changes in the substrate units (modified from Ortiz-Karpf, 2016).



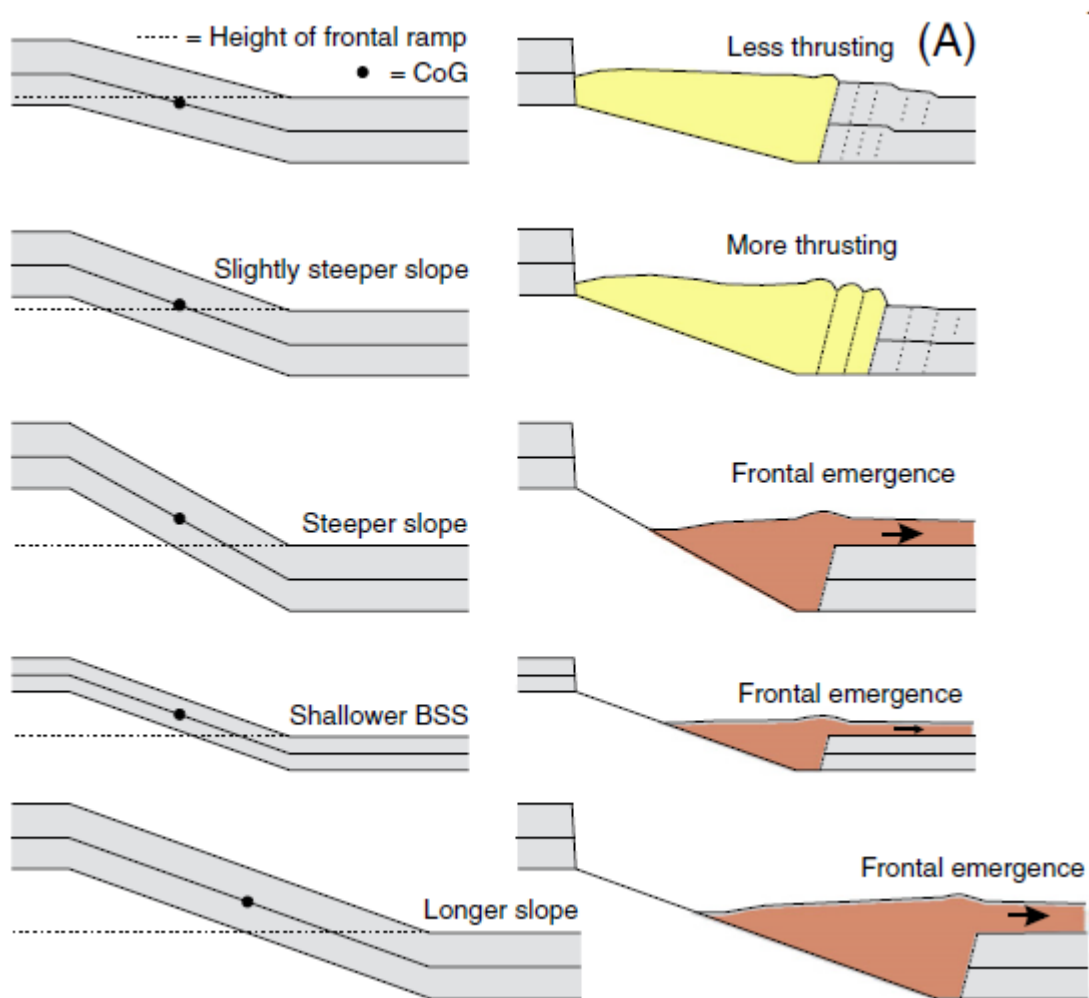
**Figure 2.39** Composite mass transport deposit (MTD) (elements lettered A to H) and interpreted stratigraphy of updip ponded deposits (I), (A) with seismic data and (B) without seismic data. The truncation onlap sequences and sediment tilting suggest that the MTD was moving downslope slowly after emplacement. Upper slope, Nile Cone. Seismic data courtesy of BG Scale division is 100 ms two-way travel time (TWTT). trunc. = stratigraphic truncation (from Kneller et al., 2016).

Variations in flow confinement can occur at m-to 10's of metre scale above relief on upper surfaces of remobilized units (Armitage et al., 2009; Jackson and Johnson, 2009; Kneller et al., 2016) (as shown in section 2.3.5). Flow confinement can also occur at a larger scale (10's-100 m), above basal shear surfaces when a large frontal ramp is formed during the erosion and/or as a result of remobilized deposits forming a topographical barrier down-dip (Frey-Martinez et al., 2006; Moernaut and De Batist, 2011; Jackson and Johnson, 2009; Kneller et al., 2016) (as shown in section 2.4.2). Previous models have classified the remobilized infill above a basal shear surface into two end member scenarios: *frontally emergent* where deposits have outrun the slide scar surface on the seabed, or *frontally confined* where topography downslope results in the ponding of remobilized deposits within slide scar accommodation restricting outflow onto the seabed (Fig. 2.40) (Frey-Martinez et al., 2006; Moernaut and De Batist, 2011).



**Figure 2.40** Schematic depiction of the two main types of submarine landslides according to their frontal emplacement: (a) *Frontally emergent* landslide. Note that the material ramps out the basal shear surface onto the seabed and is free to travel considerable distances over the undeformed slope position. (b) *Frontally confined* landslide. The mass is buttressed against the frontal ramp and does not abandon the original basal shear surface (from Frey-Martinez et al., 2006).

Factors determining the confinement style of slides are the shape of the slope profile (controlling the headscarp height, depth of incision and location of frontal ramp), the gradient of the slope (controlling the length of the slope section and the height drop of the slide scar) and the geotechnical properties of the substrate (Fig. 2.41) (e.g. Moernaut and De Batist, 2011).



**Figure 2.41** Schematic illustration of the factors (slope angle, depth BSS, and slope length) controlling the height of the CoG (centre of gravity) above the frontal ramp and thus the frontal emplacement style of subaqueous landslides (yellow: confined; red: emergent). These controlling factors are interchangeable, so that steeper slopes, shallower excavation or longer slopes all produce more emphasis on frontal thrusting and emergence (from Moernaut and De Batist, 2011).

Slide-scars may also capture down-slope drainage in the form of submarine channel-levee systems. The channel system may be entirely contained within the slide scar or rerouted (Winker and Booth, 2000; Loncke et al., 2009; Kertznus, 2009).

### 2.5.3 Summary

Overall reflection seismic datasets are highly useful in furthering understanding of topography of slope to basin floor profiles, allowing large scale analysis and temporal evolution to be documented. Despite this they significant lack resolution compared to outcrop and therefore more broadly classify topographical complexity in slope profiles and often miss more subtle markers of topographic variation. Moreover the detailed sedimentology and facies of these

studies is completely unknown when lacking well logs, and challenging to extrapolate in topographically complex areas where cored.

## 2.6 Summary

Overall experimental datasets allow insight into the flow conditions throughout the flow pathway as well as during the depositional and erosional phases, and greatly add to the understanding of flow dynamics in general and how they change in response to topography. Despite this they do not fully represent 'real world' topographical changes and flow conditions, and are challenging to scale up. Outcrop datasets provide the most detailed studies of 'real world' deposits, allowing mm scale observations and correlation of units over areas of topographical complexity. Outcrop studies provide 2D and sometimes 3D exposures allowing some spatial constraint on systems as well as knowledge of the temporal evolution, although outcrops are generally limited in spatial extent and have gaps in data and have undergone some degree of deformation, all of which must be considered. Modern datasets are undeformed and allow more spatially continuous data to be collected over large areas of slopes and basin floor, but are generally limited to a single snapshot in time and therefore do not show system evolution and have limited resolution. Seismic reflection datasets also allow more spatially continuous and large scale analysis and unlike modern datasets study of temporal evolution of slope to basin floor systems is possible. Despite this, seismic reflection studies are also limited in resolution of data, with sediments often having undergone significant deformation.

To link the small scale experimental knowledge with the large scale understanding of spatial and temporal evolution of slope to basin floor systems from modern and seismic datasets requires knowledge gained using outcrop studies. To bridge this sufficiently, outcrop exposure would have to span 'seismic scale' areas (10's- 100's of kilometres) and expose continuous sections of stratigraphic units (100's of metres of section), showing a range of topographic influence (lateral/ frontal gradient increases/decreases) at varying scales, which is uniquely possible in the Laingsburg depocentre, Karoo basin, South Africa.

The key methods for creating topography on the slope to basin floor are outlined in table 2.3.

Table 2. 3 Example mechanisms for creating topography on the slope to basin floor.

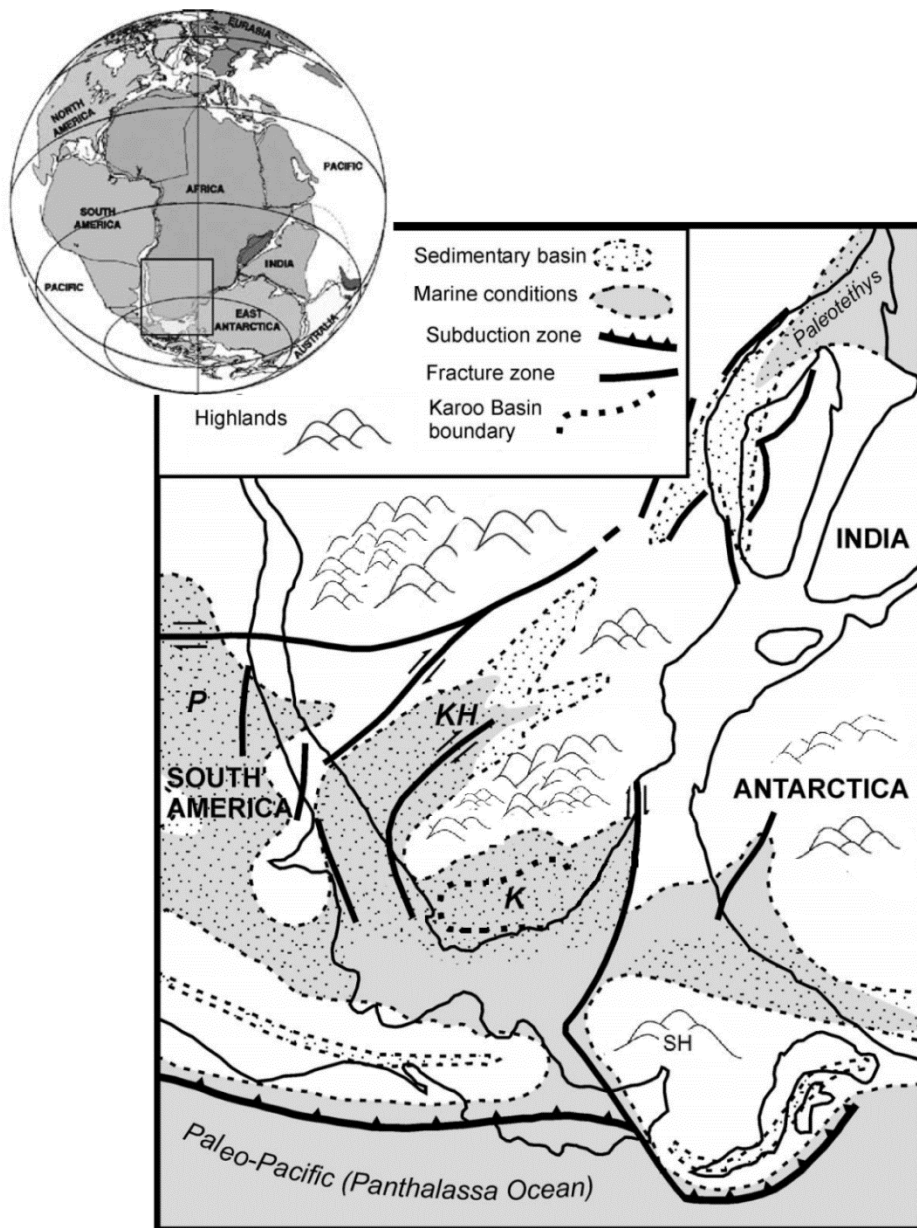
<b>Method of creating topography</b>	<b>Description</b>	<b>Timescale over which stratigraphy is affected*</b>	<b>Height of topography created</b>	<b>Local/regional</b>	<b>Static/dynamic</b>	<b>Example</b>
Erosional and depositional relief	Erosion or deposition by single or multiple flows, e.g. scours and canyons or lobes and MTCs	Short to mid	cm to 100s of m	Local	Static	Prélat et al., 2009; Gamberi and Rovere, 2011; Kneller et al. 2016
Mobile substrate	Salt and shale diapirs and walls and associated withdrawal mini-basins	Mid to long	m to 100s of m	Local/regional	Dynamic	Prather et al., 1998; Mayall et al., 2006; Clark and Cartwright, 2009; Barton, 2012; Deptuck et al., 2012; Hay, 2012; Prather et al., 2012a, b; Doughty-Jones et al., 2017.
Tectonic structures	Small scale to regional scale faulting and folding, including gravity-driven structures	Short to long	cm to 100s of m	Local/regional	Static/dynamic	Hodgson and Haughton, 2004; Jackson et al., 2008; Mayall et al., 2010; Burgeen and Graham, 2014
Inherited relief	Residual topography from underlying basement or stratigraphy	Short to mid	m to 100s of m	Local/regional	Static	Adeogba et al., 2005; Olafiranye et al., 2013
Differential compaction	Accentuation of underlying topography through variably compacting substrate	Short to long	m to 10s of m	Local	Dynamic	Posamentier, 2003; Koša, 2007
Regional uplift and subduction	Uniform or differential uplift or subduction over sub-basins or basins	Mid to long	10s of m to 100s of m	Regional	Static/dynamic	Barton and Wood, 1984; Leeder and Gawthorpe, 1987

\* Short= Instantaneous to < my, mid= millions of years to 10s of million years, long= 10s of million years to 100s of million years.

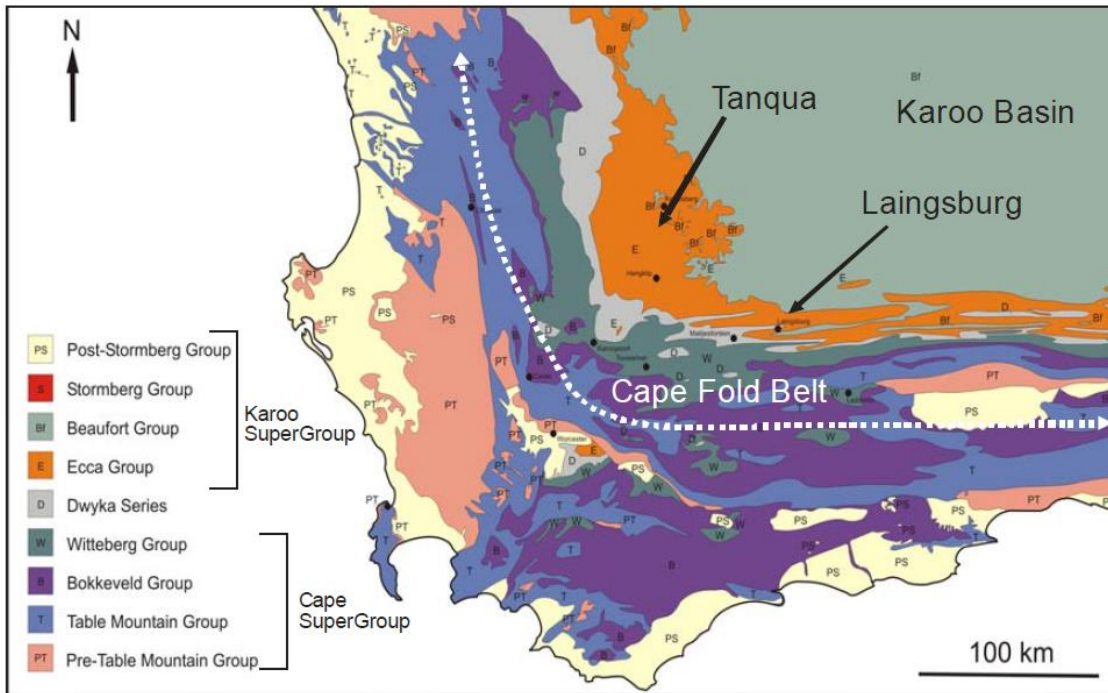
### 3 Regional setting, methodology and dataset

#### 3.1 Geological background- regional setting

The Palaeozoic to early Mesozoic tectonostratigraphic development of southern Africa relates to western Gondwanan evolution (Fig. 3.1). From the Early Ordovician to Early Jurassic, two sedimentary mega-successions separated by a major unconformity were deposited in two laterally offset major sedimentary basins in southern Africa. These are the Cape and Karoo Supergroups (Figs 3.2 and 3.3) (Visser, 1997; Tankard et al., 2009, 2012).



**Figure 3.1** Reconstruction of SW Gondwana and the Karoo basin during the Late Palaeozoic. The high-standing Precambrian basement (from Scheffler et. al., 2003, 2006).



**Figure 3.2** Geological map of the Western Cape Province, South Africa (modified from Flint et al., 2011).

The Cape Supergroup (Figs 3.2 and 3.3) comprises 8000 m of shallow marine, deltaic and fluvial deposits that thicken towards the south into an east-west trending depo-axis (Rust, 1973; Turner, 1999) and spans from the Early Ordovician to Early Carboniferous (Veevers et al., 1994). Sediments of this mega-succession were derived from a cratonic source to the north (Tankard et al., 1982). The Karoo supergroup (Figs 3.2 and 3.3) comprises of 5500 m of deep marine to fluvial deposits that span from Late Carboniferous to Triassic (Figs 3.2 and 3.3). The Late Carboniferous to early Permian period (300 - 280 Ma) was marked regionally by large scale subsidence, producing a series of interconnected basins (Visser and Praekelt, 1996).



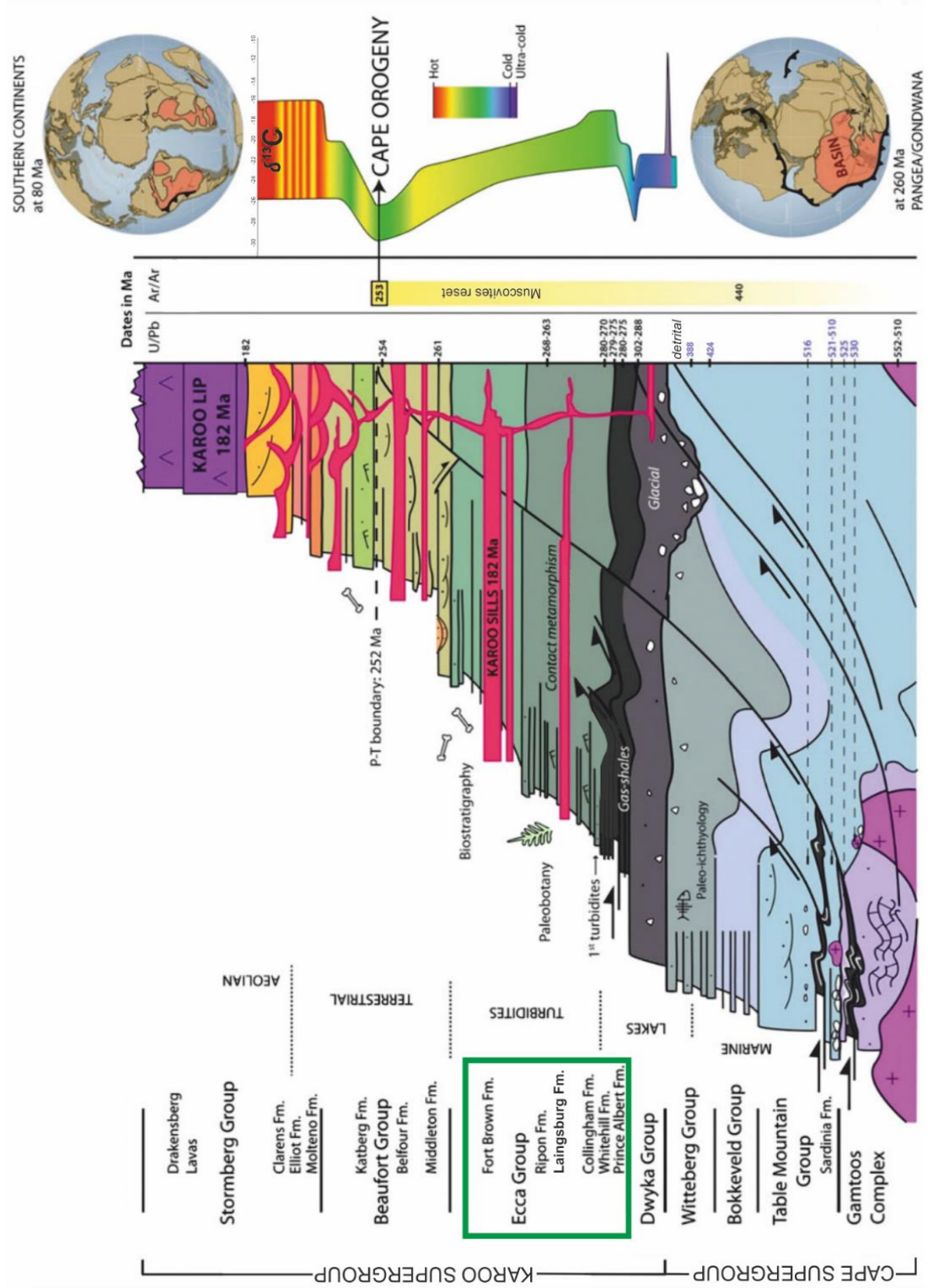
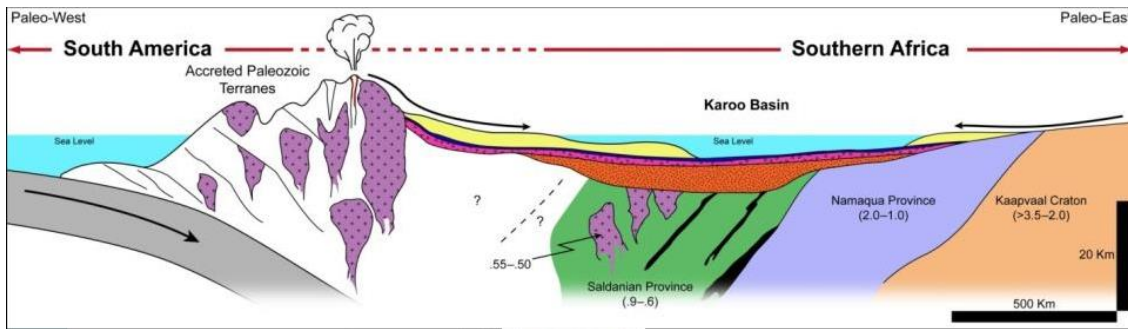


Figure 3.3 Graphic summary of the generalised Cape-Karoo stratigraphy (from Linol and de Wit, 2016)

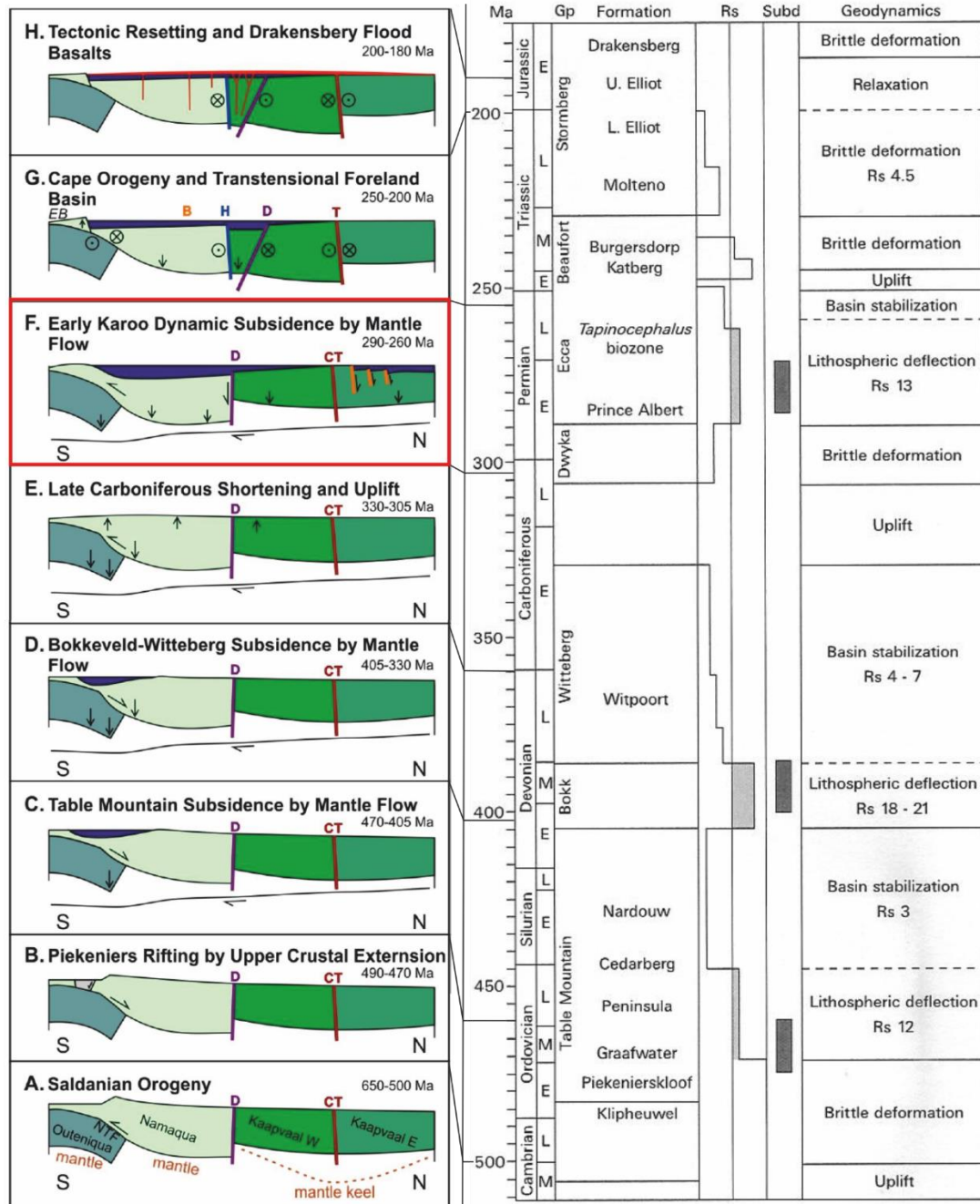


**Figure 3.4** Interpreted structural palaeogeography of the Karoo Basin at Ecca Group time. Modified from de Wit and Ransome (1992), Hålbich (1992) and van Lente (2004).

The Sierra Australis-Colorado basins (Argentina), the Karoo-Falklands basin and the Beacon Basin, Antarctica developed as extensional back-arc basins, related to oblique subduction of the palaeo-Pacific plate under western Gondwana (Visser and Praekelt, 1996). During this time strongly diachronous Dwyka Formation (and equivalent) glacial systems were dominant across most of southern Gondwana. Northward subduction of the Panthalassan (palaeo-Pacific Ocean) plate beneath the Gondwana plate led to the formation of a magmatic arc and retro-arc fold-thrust belt (Veevers et al., 1994; Visser and Praekelt, 1996).

Previous authors have considered that the Karoo Basin formed as a retroarc foreland basin with the present-day fold-thrust belt (Cape Fold Belt) lying along the southern margin (Fig. 3.4) (De Wit and Ransome, 1992; Cole, 1992; Visser and Praekelt, 1996; Visser, 1997; Catuneanu et al. 1998; Catuneanu, 2004). However, provenance analyses (Johnson et al., 1991; Andersson et al., 2004; van Lente, 2004) with more recent radiometric dating (Blewett and Phillips, 2016) and tectonostratigraphic analyses (Tankard et al., 2009, 2012) indicate that the Cape Fold Belt (CFB) is Triassic in age.

Tankard et al. (2009) interpreted Karoo Basin subsidence during Ecca time as a result of dynamic subsidence by mantle flow, complicated by the vertical detachment of basement blocks (Fig. 3.5), with subsidence not driven by asymmetric crustal loading. There are no direct microfaunal indicators for palaeobathymetry for the turbidite succession but a simple estimate of the uncompacted thickness of the succession (Fig. 3.3) from basin floor fans to first deltaic deposits implies an approximate water depth of 1200-1800 m.



**Figure 3.5** Model for the evolution of the Cape and Karoo basins. Each tectonic episode consisted of uplift, local fault-controlled subsidence and large scale regional subsidence with only minor brittle deformation. The principal episodes of basin formation were (A–D) Saldanian orogeny and Cape basin, (E–F) regional uplift and early Karoo basin (Dwyka–Ecca–lower Beaufort), and (G–H) Cape strike-slip orogeny and late Karoo basin (upper Beaufort–Stormberg). Dynamic topography was determined by first-order crustal faults and vertical motion of basement blocks due to mantle flow. Major subsidence in the Ordovician, Devonian and Permian is attributed to lithospheric deflection which suggests that mantle flow was coupled to palaeo-Pacific subduction. Red box indicates Permian phase relevant to this study (modified from Tankard et al., 2009).

### 3.2 Study area- Laingsburg depocentre

#### Ecce Group

The Ecce Group is divided into seven formations that record a basin-fill succession from anoxic mudstones through to deltaic sandstones (Figs 3.3 and 3.6). The lower two formations (Prince Albert and Whitehill formations) were deposited in a single continuous basin across the southern Karoo (Visser, 1993; Johnson, 1991; King, 2005). The upper five formations (Collingham, Vischkuil, Laingsburg, Fort Brown and Waterford formations) are unique to the Laingsburg depocentre, but have a stratigraphic equivalent in both the Tanqua and Grahamstown depocentres.

The Vischkuil to Waterford formations form an 1800 m thick progradational succession from basin-floor deposits (Vischkuil and Laingsburg formations; Sixsmith et al., 2004; van der Merwe et al., 2010), channelized submarine slope (Fort Brown Fm.; Hodgson et al., 2011; Di Celma et al., 2011; Flint et al., 2011) to shelf-edge and shelf deltas (Waterford Fm.; Jones et al., 2015; Poyatos-Moré et al., 2016). Regional palaeoflow is towards the NE and E throughout the succession with the entry point to the SW (van der Merwe et al., 2014). Around the town of Prince Albert the distal reaches interact with the Ripon Formation, a deep-water system derived from the east (Kingsley, 1981; Visser, 1993). The Ripon deposits are distinctive at outcrop due to their coarser (medium sandstone) grain size (Kingsley, 1981; Visser, 1993).

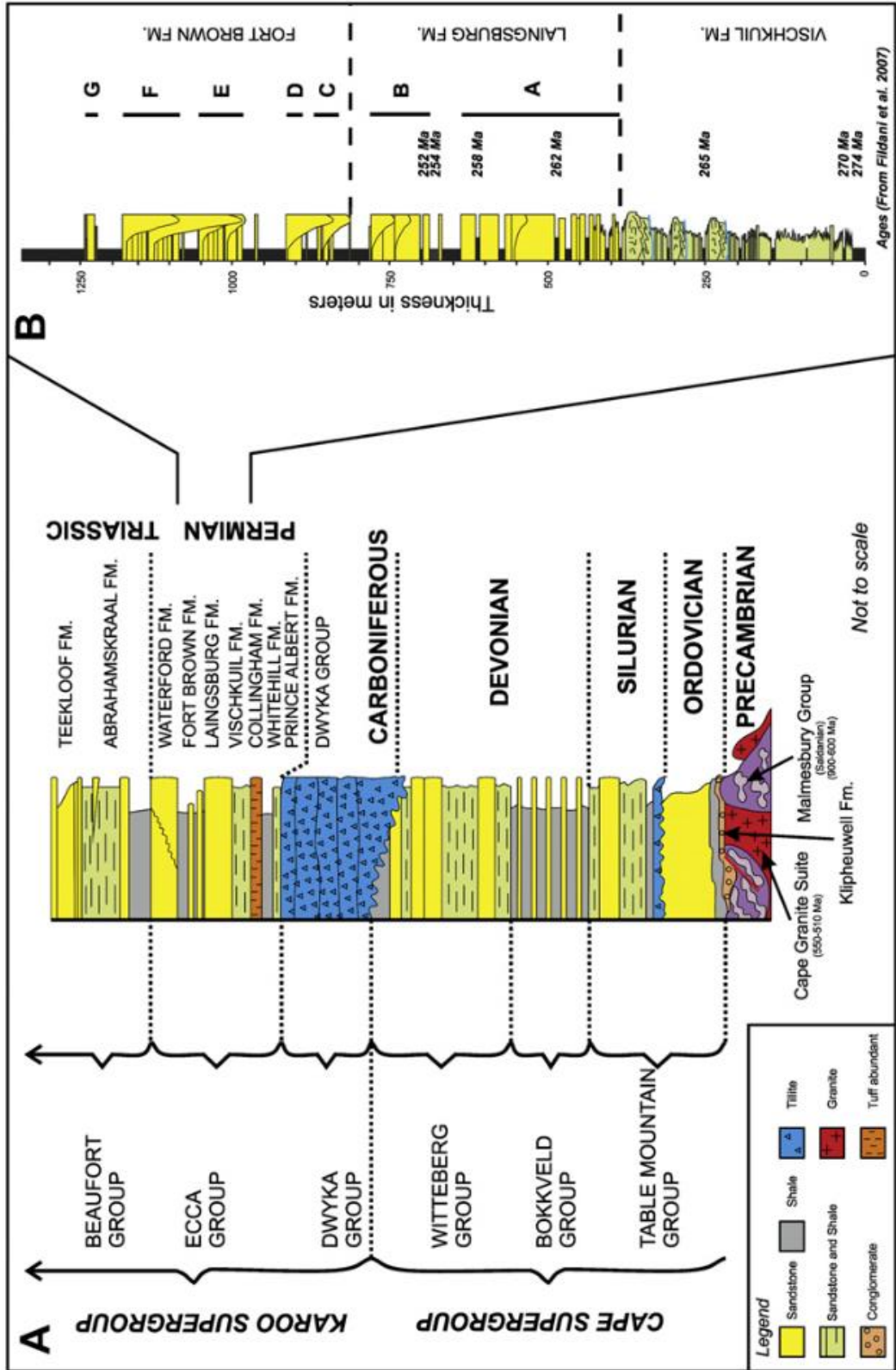


Figure 3.6 A lithostratigraphy of Western Cape. B Stratigraphy of Laingsburg depocentre (from Flint et al., 2011).

### 3.2.1 *Prince Albert Formation*

The Prince Albert Formation is a dark grey - black carbonaceous shale, with some graded silty layers, the formation is of Artinskian to Middle Kungurian age (Visser, 1992) and reaches a thickness of 165 m in the Laingsburg area, but thins out northwards and eastwards (Visser, 1991). The sharp contact between the Prince Albert Formation and the Dwyka Group records a rapid glacial retreat (Visser, 1996; Isbell et al., 2008). Four phases of deposition have been recorded: the lower part is dominated by mudstone containing dropstones and other ice-rafted detritus; the middle part is dominated by mudstone and isolated mud-rich turbidite deposits; and the uppermost unit is dominated by shale, containing phosphatic nodules and is only present in the Laingsburg depocentre (Visser and Loock, 1978; Visser, 1991). Marine faunas including palaeoniscoid fish, lamellibranchs, radiolaria, foraminifera, sponge spicules, and coprolites, have been recorded in the Prince Albert Formation and in the base of the Whitehill Fm. (McLachlan and Anderson, 1973, 1975; Johnson et al., 1997).

### 3.2.2 *Whitehill Formation*

The Lower Permian Whitehill Formation covered much of southern Gondwana about  $280 \pm 2.1$  Ma (Faure and Cole, 1999; Smithard et al., 2015) and consists of carbonaceous shale, which weathers white, with chert bands and lenses. The environment of deposition remains unresolved for the Whitehill Formation, with most researchers proposing a predominantly marine environment (e.g. Teichert, 1974; Kensley, 1975; Oelofsen and Araujo, 1987; Christie, 1990; Visser, 1992, 1994), and others suggesting a non-marine, brackish water body with no connection to the ocean (Cole and McLachlan, 1991; Veevers et al., 1994; Pickford, 1995). Its distinctive white-weathering means it is often visible on satellite imagery and therefore makes an excellent marker horizon across the entire basin. The thickness of the formation remains relatively consistent across the basin, at 35-45 m, with the lower contact of the formation sharp and well-defined, and biostratigraphy suggesting synchronous deposition over the Karoo Basin (Johnson et al., 1997).

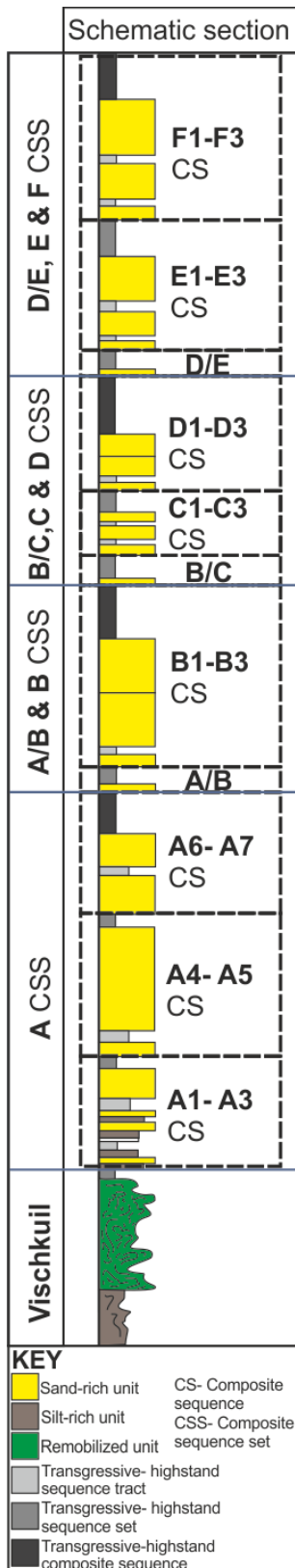
### 3.2.3 *Collingham Formation*

The Collingham Formation sharply overlies the Whitehill Formation and is characterised by siltstone and fine sandstone beds intercalated with yellow-brown tuffs. It attains a thickness of almost 80 m west of Laingsburg (Viljoen, 1994). Tuff layers within the Collingham Formation range in thickness from 1 - 20 cm but are commonly < 5 cm thick, sharp based and are infrequently reworked in their upper portions (Viljoen, 1994). They show no tractional structures and are interpreted to have been deposited from suspension (Wickens, 1994). Glass

shards are infrequently preserved in these tuffs (McLachlan and Jonker, 1990; Viljoen, 1994). The ash fall beds in the Collingham Formation have a dacitic chemistry and have been interpreted as being derived from the Choyoi igneous complex of Patagonia (Viljoen, 1994). This activity is known to have climaxed between 275-250 Ma. They are commonly colour banded which suggest some reworking of the yellow-brown ash. Significant trace fossils assemblages have been recorded including arthropod and gastropod trackways, and fish trails (Anderson, 1974). Three members of the Collingham Formation are recorded: the basal Zoutekloof Member; the central Buffels River Member; and the uppermost Wilgehout River Member, which occurs only in the Laingsburg area (Viljoen, 1994). The Collingham Formation thins substantially to the east beyond Prince Albert (Viljoen, 1994). The Zoutekloof and central Buffels River members are separated by a regionally persistent marker bed called the Matjiesfontein chert, which is uniformly thick (0.46 – 0.48 m) over at least 5000 km<sup>2</sup>. It shows an upward transition from parallel lamination, through rare ripple cross lamination to a convolute-laminated top and in places exhibits weak normal grading and amalgamation. It is interpreted as a subaqueous reworked/resedimented ash (Viljoen, 1994) that was deposited across an essentially flat basin floor.

#### 3.2.4 *Vischkuil Formation*

The Vischkuil Formation comprises predominantly mudstone and siltstone and attains a thickness of 270 metres thick in the Laingsburg area (Wickens, 1994; van der Merwe et al., 2009). The lower Vischkuil Formation shows no syn-sedimentary deformation and exhibits palaeocurrent indicators to the NW. Regionally persistent hemipelagic claystone units have been interpreted as containing the basinal equivalents of shelfal maximum flooding surfaces (van der Merwe et al., 2009). The interpreted lowstand systems tract comprises an increased volume of fine-grained sandstone in normally graded silt-prone turbidite beds and is overlain by another hemipelagic claystone drape (van der Merwe et al., 2009). The upper Vischkuil Formation was derived from the southwest and includes three 20-45 m thick debrites, with matrix supported fine-grained sandstone clasts up to 80 cm in diameter, which can be mapped over 3000 km<sup>2</sup> (van der Merwe et al., 2009). In each case, the emplacement of a debris flow resulted in widespread deformation of 3-10 m of silt-prone turbidite substrate. Van der Merwe et al. (2010) interpreted the base of each slide/debrite package as a sequence boundary and the overlying sandstone prone section as a lowstand systems tract. The six sequences of the Vischkuil Formation are grouped into two composite sequences (van der Merwe et al., 2010). Sequences V1 and V2 form the lower composite sequence. The composite sequence boundary



for the upper composite sequence is interpreted at the base of sequence V3 where the major polarity shift in palaeocurrent directions is recorded. The high degree of organization in the stratigraphy, the simple sequence isopachs and the regional extent of correlation markers (Van der Merwe, 2009; Van der Merwe et al., 2010) all indicate a well-modulated cyclicity of sand supply to the basin plain, with a gradual increase in sand volume over time. Sequence 6 is overlain sharply by the 300 m thick sandstone dominated Unit A of the Laingsburg Formation. The shift from northwestward flowing turbidity currents to an eastward prograding deepwater to shelf system represents establishment of a long term feeder system from the southwest (van der Merwe, 2010). The Vischkuil Formation is aerially restricted to the Laingsburg sub-basin and is likely equivalent to part of the Tieberg Formation in the Tanqua depocentre.

### 3.2.5 Laingsburg Formation

The Laingsburg Formation consists of Units A, A/B and B. Unit A is sub-divided into seven sandstone-dominated packages 15 - 100 m thick (A1-A7), separated regionally by hemipelagic claystone and thin-bedded siltstone packages 1 - 15 m thick (Sixsmith, 2000). Unit A is dominated by tabular sandstone beds arranged in 5 - 15 m thick thinning- or thickening-upward packages that are interpreted as submarine lobe deposits (Sixsmith et al., 2004). Sixsmith (2000) and Sixsmith et al. (2004) interpreted each regional sandstone-dominated package (A1-A7) to represent the lowstand systems tract to a depositional sequence, with the overlying fine-grained hemipelagic claystone and heterolithic package as the associated transgressive and highstand systems tract (Fig. 3.7). On a regional scale, the fine-grained units of Unit A tend to maintain the same sedimentary characteristics, grain size and overall thicknesses over tens of km

**Figure 3.7** Schematic section showing sequence stratigraphic division of Laingsburg and Fort Brown formations. Sand-rich Sub-unit sequence tract and overlying transgressive-highstand systems tract mudstones represent a sequence, groups of these and overlying inter-unit transgressive-highstand sequence set mudstones represent composite sequences, groups of composite sequences and thicker interunit transgressive-highstand composite sequence mudstones represent composite sequence sets (Flint et al., 2011).



while sandstone-dominated LST packages vary in character over shorter distances (Sixsmith, 2000). More recent work has concentrated on the relative thicknesses and character of the fine-grained packages bounding the sequences, but also the stacking patterns of the sandy packages and their map pattern distributions. The fine-grained units between A3 and A4 and between A5 and A6 are the finest grained and the thickest (average thickness of 10 m) found within Unit A (Sixsmith, 2000). Also, the lower three sequences (A1-A3) show a basinward-stepping or progradational stacking pattern followed by a backstep (A4), an abrupt basinward step followed by aggradation (A5 and A6) with a final backstepping trend in A7 (Sixsmith, 2000).

On the basis of stratal stacking patterns, Flint et al. (2011) grouped A1-A3 into a lowstand sequence set, and with the A3-A4 claystone forming a lower Unit A composite sequence (Fig. 3.7). The claystone between A3 and A4 is more widespread and thicker than the claystone between A4 and A5. A4 and A5 are therefore grouped into a second lowstand sequence set, and form a middle A composite sequence with the A5-A6 claystone (Fig. 3.7). Similarly A6 and A7 are interpreted as a lowstand sequence set, with the overlying claystone representing the transgressive to highstand sequence set (Fig. 3.7). These together represent the upper Unit A composite sequence. Unit A and the overlying the A/B claystone are therefore interpreted as a composite sequence set (Neal and Abreu, 2009; Flint et al., 2011).

Grecula (2000) documented a NE thinning of Unit B from 225 to 50 m over 20 km and divided Unit B into a 'lower' and 'upper' B unit based on a widespread and abrupt upward transition from thick-bedded sandstone packages to ripple laminated thin-bedded deposits. Additional work has permitted further division based on regionally mapped internal mudstones and abrupt sedimentary facies changes into Subunits B1, B2 and B3 (Fig. 3.7), where B1 and B2 represent lower Unit B and B3 is the upper Unit B of Grecula et al. (2003). Depositional architectures are broadly divided into four categories: erosional channel-fills; weakly confined channel-fills; leveed channels; and lobes (Brunt et al., 2013b). The three regionally mapped Unit B sequences (B1, B2 and B3) stack into a composite sequence (Fig. 3.7) (Flint et al., 2011). Together with the underlying A/B unit and 10 m of claystone between A/B and B, the A/B-B succession is interpreted as two composite sequences with the composite sequence set boundary at the base of the A/B unit (Fig. 3.8). Flint et al. (2011) speculated that if preserved/exposed up depositional dip (or farther along depositional strike) the A/B unit would thicken into a fully developed composite sequence and that only the most distal section is exposed.

### 3.2.6 Fort Brown Formation

The Fort Brown Formation consists of submarine slope to basin floor fan units B/C, C, D, E, and F (Fig. 3.7). Regional mapping and correlation of Units C to F have demonstrated an architectural change from sand-attached (Units C and D) to sand-detached channel-lobe transition zones (Units E and F) (*sensu* Mutti, 1985) (van der Merwe et al., 2014). The recognition of intraslope lobes in Units D/E, E and F (Figueiredo et al., 2010; Spychala et al., 2015), as well as tracts of coarse sediment bypass (van der Merwe et al., 2014) supports the presence of a stepped slope profile at the time of E and F deposition (van der Merwe et al., 2014). The mapping of successive slope-to-basin-floor systems in the Laingsburg depocentre indicates the presence of a lateral, broadly E-W orientated basin margin to the south of the Laingsburg area (van der Merwe et al., 2014). In the east of the Laingsburg depocentre, the Vischkuil and Laingsburg formations thin and pinch out, along with the sand-rich component of the Fort Brown Formation.

Each sand-rich unit of the Fort Brown Formation is interpreted as a lowstand systems tract (LST; e.g. E1, E2, and E3) with a related transgressive/highstand systems tract mudstone which is ~1-8 m thick between each LST (Fig. 3.7) (Figueiredo et al., 2010, 2013), which form a depositional sequence (Flint et al., 2011). A series of depositional sequences (e.g. D, E and F) and the related overlying hemipelagic mudstone representing the transgressive/highstand sequence set, together form a lowstand sequence set (Flint et al., 2011). A series of lowstand sequence sets, along with overlying hemipelagic mudstone representing the transgressive/highstand composite sequence, create a composite sequence set. The Fort Brown Formation has been divided into 2 composite sequence sets, with the first comprising of Units B/C, C and D, and the second including Units D/E, E and F (Fig. 3.7) (Flint et al., 2011).

## 3.3 Methodology and dataset

In order to fully address the research questions proposed in Chapter 1, this study examines all Units in the Laingsburg and Fort Brown formations, as well as more detailed studies on Unit E and on the less extensive, smaller Units A/B, B/C and D/E for the first time in detail (Fig. 3.7).

### 3.3.1 SLOPE, SLOPE 2, SLOPE 3 and LOBE project databases

Detailed mapping and correlation of all units utilizes regional correlation work undertaken in previous studies across the Laingsburg depocentre (Appendix D.1-D.7) (Grecula et al., 2003; Hodgson, 2009; Pr elat et al., 2009; Di Celma et al., 2010; Figueiredo et al., 2010, 2013; Flint et

al., 2011; Hodgson et al., 2011; Kane and Hodgson, 2011; Brunt et al., 2013a, b; Morris et al., 2014a,b; van der Merwe et al., 2014; Spsychala et al., 2015, 2017a,b).

Previous work in the Laingsburg depocentre includes sedimentary facies patterns and architectural descriptions recorded in seven regional scale (60–90 km long) depositional dip-parallel correlation panels. From south to north, these are Floriskraal South, Floriskraal North, Baviaans South, N1 Dome South, Baviaans North, Faberskraal South, Faberskraal North) (Appendix D.1-D.7). The database includes more than 1000 measured sections that were correlated by walking out key surfaces and units (typically the mudstones between each sand-prone unit). The correlation panels follow the west-east-trending limbs of the main post-depositional folds, and careful tracing of markers around the closures of these folds provides high confidence correlation between fold limbs.

### 3.3.2 *Fieldwork- This study*

This study included the collection of over 400 measured sections, totalling 14 km in thickness (Fig. 3.8; Appendix A) and the revisiting and relogging of over 250 others throughout the Laingsburg depocentre (Figs 3.8 and 3.9). These were logged at mm-cm scale to create detailed panel sections, over 10s of kilometres in dip and strike section. Logged sections document the lithology, grain size, sedimentary structures and stratal boundaries. The correlation framework was established by walking stratigraphic surfaces between sections, with the aid of regional mudstone units for long distance correlations. Correlation panels are augmented by helicopter, unmanned aerial photography and other photopanel. Logged sections are used to create isopach and palaeogeographic maps (Section 3.3.3). The Chapter 4 dataset contains 20 logged sections (Fig. 3.8; Appendix A). The Chapter 5 dataset contains 311 logged sections (Fig. 3.8; Appendix A) new and revisited (partially re-logged). Lastly, the Chapter 6 dataset contains 341 logged sections (Fig. 3.8; Appendix A) new and revisited. Locations of farms, roads and rivers are shown in figure 3.9.

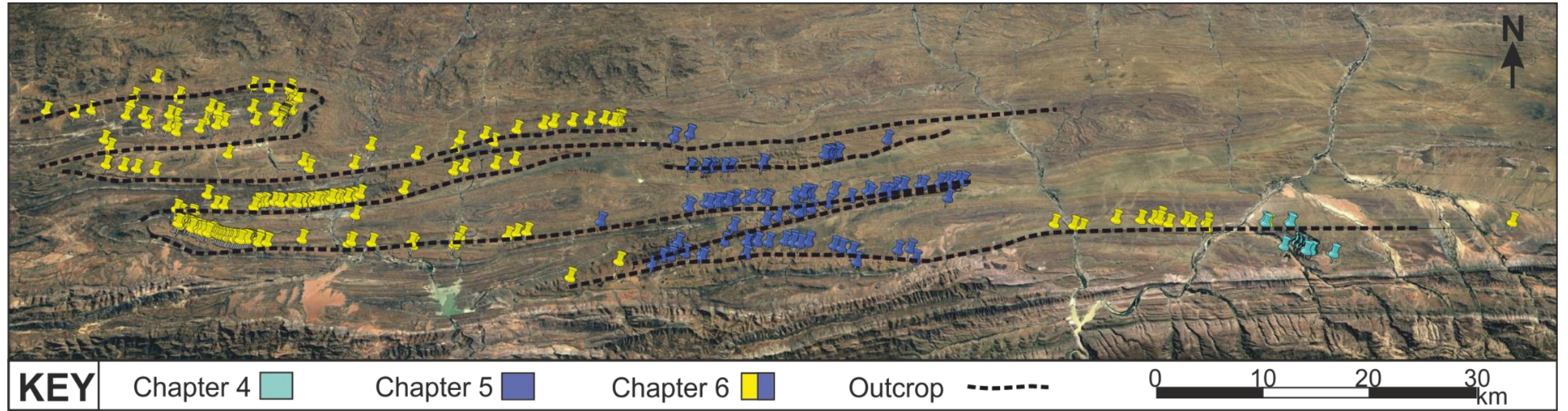


Figure 3.8 Location of logged sections new and revisited/ relogged in this study colour coded by chapter in which dataset is used. Grid references in Appendix A.

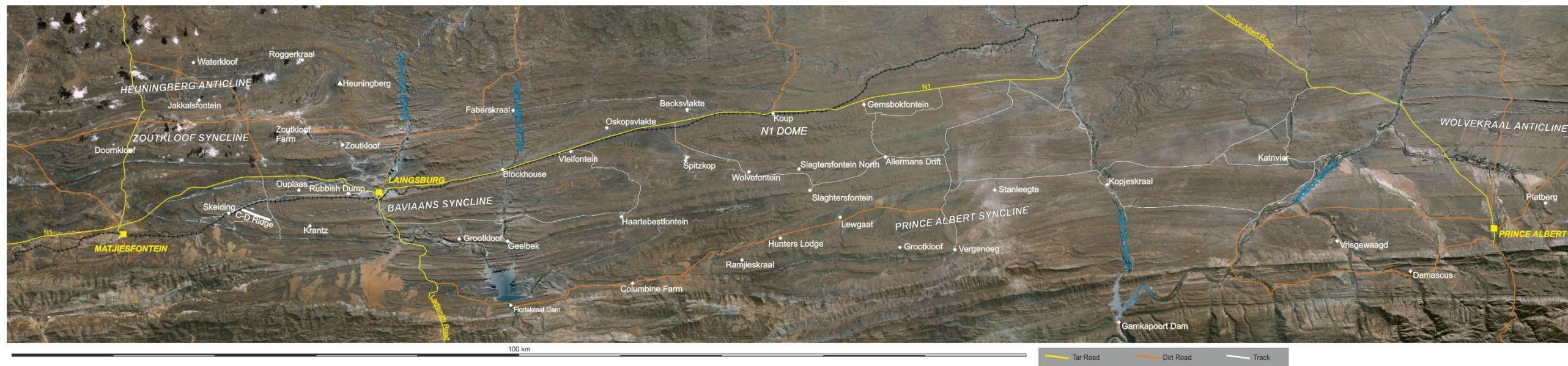


Figure 3.9 Location of roads, tracks, rivers and farms within the Laingsburg depocentre.

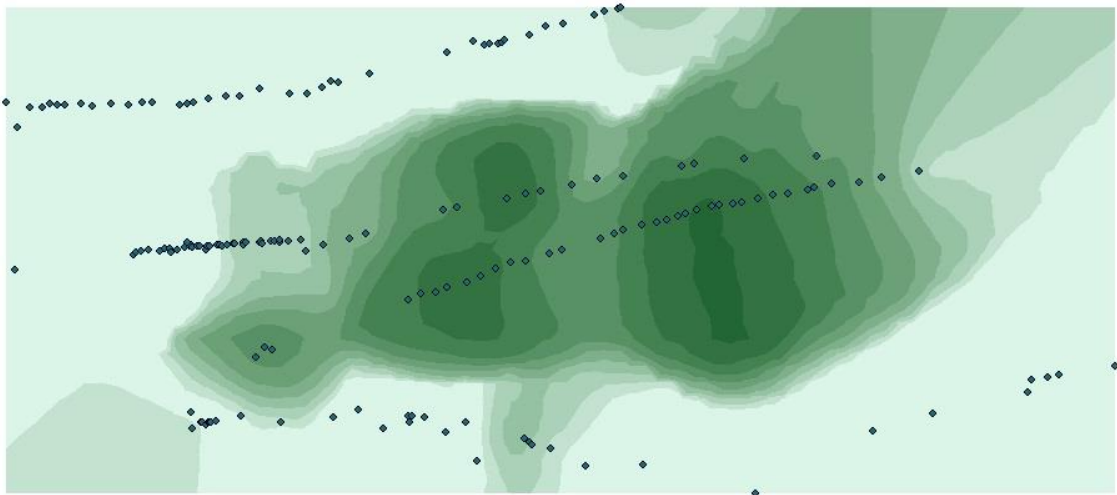
### 3.3.3 Isopach and palaeogeographic maps- This study

Thickness distributions were created by fitting a surface to thickness values from logged sections. Input data were collected and prepared in Excel (Table 3.1).

Obect ID	Log_code	X_Base	Y_Base	Y_BaseStretch17.2	DE_Total	E2_Total	E3_Total
1	WFN201410	521025	6331025	6331728.432	0	1.45	4
2	WFN20132	521359	6330383	6330976.008	0	1.5	4.6
3	WFN20144	521730	6330901	6331583.104	0	1.4	3.8
4	WFN20146	522090	6330877	6331554.976	0	1.2	4.9
5	WFN20149	522313	6330984	6331680.38	0	0.8	2.2
6	WFN20149	522571	6330965	6331658.112	0	1.05	3.5
7	WFN20132	522767	6330960	6331652.252	0	1.1	4.45

**Table 3.1** Representative chart of thickness data preparation for the creation of isopach maps in ArcGIS.

The surface operation was conducted in ArcGIS using the simple kriging tool within the Geostatistical Wizard (<http://resources.arcgis.com/en/home/>). Maps are extended beyond the extremities of the input data by the surfacing algorithm, with unrealistic values removed. An example of an output is shown in figure 3.10.



**Figure 3.10** Representative chart of thickness data preparation for the creation of isopach maps in ArcGIS.

Palaeogeographic maps were created by using panels to reconstruct broad depositional environment for a given interval and overlaying this with isopach contours modified in CorelDraw. Data have been used from previous studies in the Karoo (Grecula et al., 2003; Figueiredo et al., 2010, 2013; Di Celma et al., 2011; Flint et al., 2011; van der Merwe et al., 2014; Spychala et al., 2015, 2017a,b) with some palaeogeographic maps modified from van der Merwe et al. (2014). Restored palaeocurrent data presented on maps were collected from ripple lamination and tool marks.

### 3.3.4 *Datacube and surface maps – SLOPE 4 collaboration*

The datacube was collated by Dr Rachel Harding at Manchester University and utilises outcrop logs collected in all 4 phases of the SLOPE project, which were used to create two Schlumberger Petrel 2015 projects in order to visualize complete basin floor-to-slope-to-shelf systems of the Laingsburg depocentre interactively in 3D. My contribution to this project was supplying field datasets and panels as well as verification of correlations and surfaces. The main focus of the Laingsburg datacube is the outcrop sedimentary logs and correlations of the submarine slope deposits of the Fort Brown Formation, (Units C-G) from SLOPE Phase 3 (Flint et al., 2011) plus the Waterford Formation upper slope to deltaic section (Waterford Clinothems WfC1-8; Jones et al., 2013, 2015; Poyatos-Moré et al., 2016). The structural framework of the Fort Brown Fm. covers 2265 km<sup>2</sup> (Data: Appendix C). Surface maps (tops and bases) of the main sand prone units/subunits have been constructed, along with a map for Top Vischkuil Fm. Thickness maps between these surfaces represent the thickness of sand prone units and inter unit claystones.

The Datacube was created in Petrel by importing composite logs consisting of the complete Whitehill to Waterford stratigraphy as wells, with the top Whitehill used as a basal datum. Tops and bases of key units were selected using the well top function, and additional data were used to interpret polylines to add datapoints between outcrop logs. Depth structure maps were created for each key surface using the 'make a surface' function and thickness maps were created between key surfaces. Post depositional tectonic shortening was corrected for by stretching 13% in the Y direction, according to a mean value for palinspastic restoration derived by Spikings et al. (2015).

## 3.4 **Facies framework**

The sedimentary facies of the Laingsburg and Fort Brown formations are described below (Tables 1.1-1.15), these have been recognised in this study and are based on previous studies undertaken in the Laingsburg depocentre (e.g. Grecula et al., 2003; Hodgson, 2009; Prélat et al., 2009; Di Celma et al., 2010; Figueiredo et al., 2010, 2013; Flint et al., 2011; Hodgson et al., 2011; Kane and Hodgson, 2011; Brunt et al., 2013a, b; Morris et al., 2014a, b). These facies are combined into architectural elements and environments of deposition in the following Chapters (4-6).

Table 3.2 *Facies framework*

<b>Classification</b>	<b>Facies</b>	<b>Process</b>	<b>Environment</b>
<b>Bedded</b>	Mudstone	Hemipelagic suspension fallout and very dilute turbidity currents	Condensed intervals, basin mudstones
	Siltstone	Distal run-out of turbidity currents	Condensed intervals, basin mudstones
	Siltstone and mudstone couplets	The mudstone drapes are deposits from the dilute tail ends of turbidite flows or represent periods of localised and/or regional shutdowns allowing pelagic sedimentation	Channel abandonment facies, basin mudstones
<b>Sandstone and siltstone thin beds</b>	Spill-over fringe	Deposition from numerous very dilute turbidity currents that are the result of flow-stripping in up-dip perched lobe deposits	Basin floor
	Silt prone	The bed thicknesses and the low sand volume suggest that deposition was by dilute distal turbidites. The bioturbated interval suggests either a longer time period between events or a change in oxygen and nutrient delivery	Distal levee; distal lobe
	Sand prone	Aggradational facies, with some erosion surfaces	Channel margin; proximal levee; frontal splay
	Scoured siltstone and sandstone	Erosion by numerous bypass dominated turbidity currents	Bypass dominated zone
<b>Sandstones</b>	Sigmoidal bedforms	Highly aggradational	Proximal external levee; frontal splay



	Structured	Medium-to-high density flows escaping confinement and deposited rapidly	Frontal lobe, crevasse splay, external levee.
	Banded	Late stage rapid deposition in channel axis	Proximal lobe
	Structureless	Tractional bedforms suppressed in highly depositional settings	Channel axis; lobe axis
<b>Remobilised</b>	Mudclast Conglomerate	The presence of the mud clasts indicate erosion higher in the channel profile. Mudclasts are deposited as a channel lag/drape. Locally, clasts show secondary injection features	Channel axis, lobe axis
	Debrite	Easily identified at outcrop by a high interstitial mud content, giving a grey colour and crumbly weathering texture. Often contains large quantities of organic fragments	Lobe fringe, channel axis
	Folded and Megaclasts	Slumps and slides remobilizing primary strata	Submarine slope to basin floor
<b>Other</b>	Hybrid Beds	Erosive flows entrain mudstone clasts and fine-grained sediment into the turbulent flow, suppressing turbulence, and producing high-concentration to pseudo-laminar flow conditions	Bypass dominated zone
	Injectite	Tractional bedforms suppressed in highly depositional settings	Channel axis; lobe axis

### 3.4.1 Bedded

#### 3.4.1.1 Bedded mudstone



**Figure 3.11** Well exposed individual thin beds are seen to be very laterally continuous (right). More normally, the mudstones break up into small pencil shaped shards due to a well-developed fracture network (left).

**Table 3.3** Bedded mudstone characteristics.

	Values and interpretation
<b>Depositional environment</b>	Submarine slope and basin floor
<b>Description</b>	Structureless siltstone and claystone, smooth to touch in core examples, black in colour (no bioturbation observed), concretionary nodules and concreted ash deposits are common, rare mm-thick bed of fine siltstone and very fine sandstone.
<b>Sedimentary structures</b>	Typically structureless. Little to no internal stratification seen at outcrop or core.
<b>Process interpretation</b>	Hemipelagic suspension fallout and very dilute turbidity currents.
<b>Bed thickness range</b>	From 1 cm to ~1 m.
<b>Net : Gross range</b>	0%
<b>Basal bounding surface</b>	Normally gradational, occasionally sharp bases.
<b>Upper bounding surface</b>	Sharp, occasionally erosional.
<b>Outcrop thickness</b>	Very variable. From 10s cm to 10s m. Inter-unit mudstones typically show a gradual thinning down dip.
<b>Outcrop width / geometry</b>	Very extensive. Inter-unit mudstones are mapped laterally and down-dip through the entire Laingsburg area. The thinner intra-unit mudstones show a similar lateral and down-dip continuity.
<b>Trace fossils and other features</b>	Hemipelagic mode of deposition ensures regional coverage of the mudstone deposits. Hence they are invaluable as correlation markers; this is particularly true of the mudstone markers used to divide Unit C.
<b>Example localities (Fig. 3.9)</b>	Interfan mudstones are ubiquitous. The intra-unit mudstones are well developed in Unit C, E and F (CD Ridge, N1).

## 3.4.1.2 Bedded siltstone



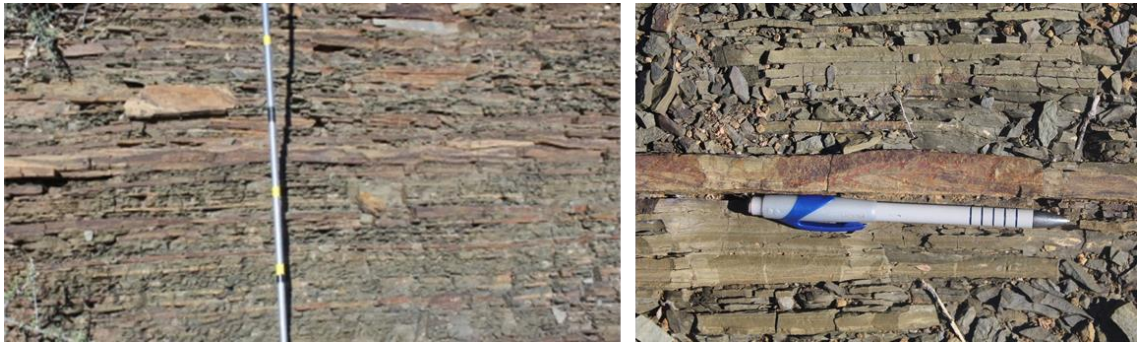
Figure 3.12 Thinly laminated siltstone beds.

Table 3.4 Bedded siltstone characteristics.

Feature	Values and interpretation
<b>Depositional environment</b>	Submarine slope and basin floor.
<b>Description</b>	In outcrop typically looks thinly laminated. Core shows 5-40 cm thick beds of fine, medium and coarse siltstone. 40% fine siltstone. Coarser siltstones tend to occur in mm-thick beds although beds 2-10 cm thick have been observed in places.
<b>Sedimentary structures</b>	Typically structureless. Little to no internal stratification seen at outcrop. Thin laminations of fine, medium and coarse siltstone observed in the cores.
<b>Process interpretation</b>	Settling of fine grained turbidites and suspension fallout (Bouma Td/Te division).
<b>Bed thickness range</b>	Very variable. From 1 cm to 1 m.
<b>Net : Gross range</b>	0%
<b>Basal bounding surface</b>	Normally gradational, occasionally sharp and rare erosional bases.
<b>Upper bounding surface</b>	Sharp, occasionally erosional.
<b>Outcrop thickness</b>	Very variable. From 10s of cm to 10s of m. Inter-unit mudstones typically show a gradual thinning down dip.
<b>Outcrop width / geometry</b>	Very extensive.
<b>Trace fossils and other features</b>	None.
<b>Example localities (Fig. 3.9)</b>	Units C, E and F (CD Ridge, Baviaans Farm and the N1 outcrop localities).

### 3.4.2 Sandstone and siltstone thin beds

#### 3.4.2.1 Siltstone dominated



**Figure 3.13** Unit E, distal external levee - Allemandsdrift farm (Left). Unit E lobe fringe- Slagtersfontein Farm (Right).

**Table 3.5** Siltstone dominated thin beds characteristics.

Feature	Values and interpretation
<b>Depositional environment</b>	Regions distal to sediment feeder system; such as distal overbank, distal levee (internal and external examples), channel margin, distal lobe, abandonment fill (slope valley) or basin floor
<b>Description</b>	Siltstone dominated (60%) thin beds of sandstone and siltstone packages 5-20 cm thick, individual beds are <1-5 cm thick. Can occur in 10's of km wide laterally extensive packages. Consist of very thin (<2 cm) beds and minor structureless, planar to ripple laminated sandstone beds, that are often graded and very uniform in thickness.
<b>Sedimentary structures</b>	Thinly interbedded very fine sandstone and siltstone beds. Many of the very fine sandstone beds are structureless, however, wavy laminae, rare current ripple lamination and planar (parallel) laminae are all present locally. The siltstone (coarse) is generally planar laminated. There are few erosion surfaces, some of which are associated with bed dip changes above. Some areas can be intensely bioturbated.
<b>Process interpretation</b>	The bed thicknesses and the low sand volume suggest that deposition was by dilute distal turbidites. The bioturbated interval suggests either a longer time period between events or a change in oxygen and nutrient delivery. Laterally extensive packages are interpreted as deposition from numerous very dilute turbidity currents that are the result of flow-stripping in up-dip perched lobe deposits. As flows traverse perched accommodation, the confining down-dip topography is partially surmounted by the uppermost, lower-density fraction of the turbidity currents.
<b>Bed thickness range</b>	Individual beds are typically <5-20 cm
<b>Net : Gross range</b>	10 - 30%
<b>Basal bounding surface</b>	Gradational

<b>Upper bounding surface</b>	Gradational
<b>Outcrop thickness</b>	Forms packages that range from 10 m to >100 m
<b>Outcrop width / geometry</b>	Facies unit can be traced for up to 10s km (e.g., Units C and D). Individual thin-beds may be traceable for up to 100 m
<b>Trace fossils and other features</b>	None
<b>Example localities (Fig. 3.9)</b>	Commonly forms uppermost channel fill in Unit's C and D, of the CD Ridge. Also found as part of external levee deposits in Units B, C and D e.g., CD Ridge, Geelbek, N1, Zoutkloof.

## 3.4.2.2 Sandstone dominated



**Figure 3.14** Unit D external levee, Krantz, GPS for scale (left) and Unit D External levee, C-D Ridge, pencil for scale (right).

**Table 3.6** Sandstone dominated thin beds characteristics.

Feature	Values and interpretation
<b>Depositional environment</b>	This facies is present in frontal splays, proximal internal levee, proximal external levee, lobe fringe and off-axis sub-environments.
<b>Description</b>	Thin beds of sandstone and siltstone packages are 5-20 cm thick, individual beds are <1-5 cm thick.
<b>Sedimentary structures</b>	Typically consist of thin alternating very fine/ fine sandstone beds and siltstones; occasionally the sandstones are gradational into silts suggesting development of Bouma C - D divisions. Sedimentary structures within the very fine sandstone beds include wavy laminae, current ripple laminae, planar laminae, multiple cosets of ripple lamination, climbing ripple lamination, stoss side preserved ripple laminae, and some are structureless. The coarse siltstone beds are generally planar laminated. Erosion surfaces and amalgamated contacts are observed.
<b>Process interpretation</b>	Evidence of a high rate of deposition. Aggradational facies, with some erosion surfaces. The higher the sand content, the closer to the channel.
<b>Bed thickness range</b>	Individual beds 2 - 15 cm.
<b>Net : Gross range</b>	40 - 65%.
<b>Basal bounding surface</b>	Mostly gradational from thick-bedded sandstones, or gradational from siltstone prone thin beds. Occasional sharp, non-erosive basal contact.
<b>Upper bounding surface</b>	Often gradational into silty thin-bedded heteroliths.
<b>Outcrop thickness</b>	Whole unit up to 150 m in thickness.
<b>Outcrop width / geometry</b>	Facies unit can be traced for up to 10s km laterally (e.g., Units C and D). Individual 5 cm scale thin-beds may be traceable for up to 250 m.

<b>Trace fossils and other features</b>	None
<b>Other remarks</b>	Associated with external levees, internal levees and frontal splay deposits.
<b>Example localities (Fig. 3.9)</b>	Lower part of Unit D at Geelbek, Zoutkloof and the CD Ridge. Upper and lateral fill of channel elements within CD Ridge, N1, Geelbek etc.

### 3.4.3 Sandstones

#### 3.4.3.1 Structured sandstone



Figure 3.15 Planar laminated sandstone (left) and rippled external levee at Grootkloof (right).

Table 3.7 Structured sandstone characteristics.

Feature	Values and interpretation
<b>Depositional environment</b>	Rapid deposition from expanding flows: Frontal lobe, crevasse splay, external levee. Sustained bedload traction, particularly within channels
<b>Description</b>	Very fine sandstone with an abundance of unidirectional current ripple laminae. Little silt or clay grade material present. Beds are 5-40 cm thick
<b>Sedimentary structures</b>	Well-developed ripples and climbing ripples are common. Upper surfaces commonly rippled where present. Lots of erosion surfaces, some soft-sedimentary deformation, but little bioturbation and few mudstone drapes. Erosion surfaces are associated with multidirectional current ripple laminae
<b>Process interpretation</b>	Medium-to-high density flows escaping confinement and deposited rapidly. Evidence of a high rate of deposition. Aggradational facies, with some erosion surfaces. The higher the sand content, the closer to the channel. The core shown is taken from the Unit C2 external levee
<b>Bed thickness range</b>	Beds are 5-70 cm thick
<b>Net : Gross range</b>	50-70%
<b>Basal bounding surface</b>	Sharp contact, this facies generally overlies thinly bedded sandstone and siltstone (cm scale beds)
<b>Upper bounding surface</b>	Normally gradational into rippled thin beds
<b>Outcrop thickness</b>	Range 5 - 200 cm Mostly 5 - 30 cm
<b>Outcrop width / geometry</b>	Individual beds continuous for >100 m
<b>Trace fossils and other features</b>	None
<b>Example localities (Fig. 3.9)</b>	Unit B: Skeiding, Doornkloof; Sub unit F2: Zoutkloof; Sub-unit C2: CD Ridge; Sub-unit C3: Baviaans farm



## 3.4.3.2 Scoured sandstone and siltstone



Figure 3.16 Varying scale scour surfaces – Slagtersfontein farm.

Table 3.8 Scoured sandstone and siltstone characteristics.

Feature	Values and interpretation
<b>Depositional environment</b>	Channel-lobe transition zone
<b>Description</b>	Thin-bedded siltstone with thin, lenticular and poorly sorted silty sandstone beds that overlie and are cut by erosional surfaces. Scours can be asymmetric down dip with steeper headwalls < 3- 15 m in length, 1-3 m in width and < 1 m in depth
<b>Sedimentary structures</b>	Soft sediment deformation
<b>Process interpretation</b>	Erosion by numerous bypass dominated turbidity currents
<b>Bed thickness range</b>	0.02-1.2 m
<b>Net : Gross range</b>	Variable
<b>Basal bounding surface</b>	Sharp or erosive, uneven
<b>Upper bounding surface</b>	Sharp and erosive, irregularly overlain by bypass lags or thinly laminated siltstone
<b>Outcrop thickness</b>	Amalgamated packages 3-4 m thick
<b>Outcrop width / geometry</b>	Occurring in areas up to kilometres in width and length
<b>Example localities (Fig. 3.9)</b>	Prevalent across the sediment bypass zone- Slagtersfontein- Unit E, Wolfefontein, Unit F

### 3.4.3.3 Sigmoidal bedforms

#### Field Images



**Figure 3.17** Sigmoidal bedforms in sandstone beds, Sub-unit E2, external levee, Heuningberg south limb (left) and Unit D, lower proximal external levee, CD Ridge - near to the Bav 1A wellsite (right).

**Table 3.9** Sigmoidal bedform characteristics.

Feature	Values and interpretation
<b>Depositional environment</b>	High density, high velocity flows escaping confinement and depositing rapidly, typically found in proximal external levee and frontal splay deposits.
<b>Description</b>	Predominantly a depositional facies, rich in very fine sandstone, erosion surfaces are rare. 80-90% of the facies is very fine sandstone to very coarse siltstone.
<b>Sedimentary structures</b>	Sigmoidal shaped bedforms dominate, in core they form convex up-concave up (through parallel) laminae. Other sedimentary structures include; current ripple laminae, planar laminae, low angle ripples, occasional locally developed cross bedding, stoss-side preserved ripple laminae, dm scale ripple laminae and climbing ripple laminae. Small scale erosional features cutting 2 - 10 cm and <50 cm in width. Component beds coarsen and thicken upward from siltstone to fine sandstone.
<b>Process interpretation</b>	Medium-to-high density flows escaping confinement and deposited rapidly. Evidence of a high rate of deposition. Aggradational facies, with some erosion surfaces. The higher the sand content, the closer to the channel. The core shown is taken from the Unit C2 external levee.
<b>Bed thickness range</b>	Individual beds are 2-30 cm thick.
<b>Net : Gross range</b>	50-70%
<b>Basal bounding surface</b>	Sharp contact, this facies generally overlies thinly bedded sandstone and siltstone (cm scale beds).
<b>Upper bounding surface</b>	The unit becomes finer grained and thinner bedded upwards.
<b>Outcrop thickness</b>	The unit can be <5-25 m thick.

<b>Outcrop width / geometry</b>	Facies unit can be traced for up to 10s km laterally (e.g., Units C and D). Individual 5 cm scale thin-beds may be traceable for up to 250 m.
<b>Trace fossils and other features</b>	None.
<b>Other remarks</b>	Facies is likely to have been deposited beneath long-lived flows. Erosional features develop under heads of flows, with tractional structures and silt deposition forming at the tail end of unconfined flows.
<b>Example localities (Fig. 3.9)</b>	Proximal D levee at the western edge of the CD Ridge, frontal splay deposit in Sub-unit C3; Baviaans farm and the CD Ridge, Unit B external levee on the south limb of the Baviaans syncline, external levee deposits in Sub-units E2 and F2.

## 3.4.3.4 Banded sandstone



**Figure 3.18** Lobe axis banded sandstone from the Wilgehout River locality.

**Table 3.10** Banded sandstone characteristics.

Feature	Values and interpretation
<b>Depositional environment</b>	Late stage bulk fill within channels (axis and off-axis deposits) and proximal areas of frontal lobes
<b>Description</b>	This facies occurs in discrete horizons within an overall massive fine grained sandstone unit (often occurs in sandstone beds that grade from fine sandstone-very fine sandstone). Many of the mud clast rich horizons of muddy sandstone – sandstone unit rich in mm-sized mud clasts
<b>Sedimentary structures</b>	Generally occurs in massive fine-grained sandstone. Some zones of minor bioturbation are recognised in this facies
<b>Process interpretation</b>	Typically occurs in the finer grained zones within the graded fine to very fine sandstone beds. These deposits are more cohesive due to the presence of small mud clasts buoyed towards the upper Ta division of turbidity flows
<b>Bed thickness range</b>	These horizons are typically 1-5 cm thick and are not common
<b>Net : Gross range</b>	50 - 75%
<b>Basal bounding surface</b>	Uneven, erosive base
<b>Upper bounding surface</b>	Usually overlain by sandstone, slightly scalloped contact observed in places
<b>Outcrop thickness</b>	Usually distinct horizons, only observed in core therefore outcrop thickness range is unknown
<b>Outcrop width / geometry</b>	Usually distinct horizons, only observed in core therefore outcrop width/geometry is unknown
<b>Trace fossils and other features</b>	None
<b>Example localities (Fig. 3.9)</b>	Channel axis and off-axis deposits in the CD Ridge

### 3.4.3.5 Structureless sandstone



**Figure 3.19** Photograph of structureless sandstone in Unit B, at Skeiding. Interpreted to be a channel complex (left) and a Close up photograph of structureless sandstone from Unit C2, near Baviaans farm, Interpreted to be part of a channel axis deposit (right).

**Table 3.11** Structureless sandstone characteristics.

Feature	Values and interpretation
<b>Depositional environment</b>	Fall in capacity of high concentration flows and rapid deposition. Late stage bulk fill within channels and proximal areas of frontal lobes
<b>Description</b>	Predominantly a depositional facies, rich in very fine sandstone and rare erosion surfaces. 80-90% of the facies is very fine sandstone-very coarse siltstone
<b>Sedimentary structures</b>	Normally appears massive. Occasional dewatering pipes and dishes. Widespread amalgamation along erosive surfaces
<b>Process interpretation</b>	Medium-to-high density flows escaping confinement and deposited rapidly. Evidence of a high rate of deposition. Aggradational facies, with some erosion surfaces. The higher the sand content, the closer to the channel. The core shown is taken from the Sub-unit C2 external levee
<b>Bed thickness range</b>	Variable <10 - 200 cm
<b>Net : Gross range</b>	95 - 100%
<b>Basal bounding surface</b>	Sharp based, often shows large degree of erosion
<b>Upper bounding surface</b>	Normally sharp, overlain by thin-bed heteroliths
<b>Outcrop thickness</b>	Variable <1 m to amalgamated sections of >30 m
<b>Outcrop width / geometry</b>	Axial infill of channel elements 100 – 400 m in width. Will have considerable down-dip extent
<b>Trace fossils and other features</b>	Thick amalgamated structureless sandstones may break up laterally (off-axis) into thick-bedded sandstones or thin bedded heteroliths
<b>Example localities (Fig. 3.9)</b>	Skeiding, Rubbish Dump, N1, Geelbek

### 3.4.4 Mass transport

#### 3.4.4.1 Chaotic



**Figure 3.20** Mud rich debrite with sandstone pseudo nodules (left) and Sand rich debrite within the C1 lobe exposed at Zoutkloof (right).

**Table 3.12** Chaotic deposit characteristics.

Feature	Values and interpretation
<b>Depositional environment</b>	Lobe fringe, channel axis
<b>Description</b>	Easily identified at outcrop by a high interstitial mud content, giving a grey colour and crumbly weathering texture. Often contains large quantities of organic fragments (fig. 3.20).
<b>Sedimentary structures</b>	Normally structureless.
<b>Process interpretation</b>	High density cohesive flows preserve the integrity of organic fragments. Occurrence at lobe fringe is probably due to reduced friction effects of debris flows riding over the top of de-watering sands deposited by precursor turbidity current (i.e., hybrid bed).
<b>Bed thickness range</b>	5 mm to several metres
<b>Net : Gross range</b>	Highly variable
<b>Basal bounding surface</b>	Sharp
<b>Upper bounding surface</b>	Sharp
<b>Outcrop thickness</b>	From 10s of cm to 10s of m, typically thickening down-dip.
<b>Outcrop width / geometry</b>	Variable: may be deposited in and limited by shape of containing scour / bed topography, or show lateral extents of many kilometres.
<b>Trace fossils and other features</b>	Significantly more common in the distal areas of each system. Absent from the CD Ridge boreholes. Plant fragments often make up a large proportion of the debrites; large fragments typically rise to the top of individual debrite beds.
<b>Example localities (Fig. 3.9)</b>	Unit C at Geelbek

## 3.4.4.2 Remobilized



Figure 3.21 *Folded deposits present at Vriesgewaagd farm and Skerwerkraal farm.*

Table 3.13 *Remobilized deposit characteristics.*

Feature	Values and interpretation
<b>Depositional environment</b>	Submarine slope to basin floor
<b>Description</b>	Clasts and megaclasts: blocks of intact remobilised strata, varying in sizes and degrees of disaggregation. Clasts vary in scale from small 10's cm scale. Fractured and disaggregated at edges with no ductile deformation features. Internal bedding is well preserved within clasts.
<b>Sedimentary structures</b>	Dewatering structures and syn-sedimentary faults.
<b>Process interpretation</b>	Folded strata are interpreted to form as slumps and slides remobilise primary bedding, undergoing ductile deformation. Clast and megaclasts are interpreted to form as cohesive material is remobilised as slides and undergo only brittle deformation.
<b>Bed thickness range</b>	cm - 10s of metres.
<b>Net : Gross range</b>	Very variable.
<b>Basal bounding surface</b>	Gradational to sharp.
<b>Upper bounding surface</b>	Gradational to sharp.
<b>Outcrop thickness</b>	Up to 10's of metres.
<b>Outcrop width / geometry</b>	Up to several kilometres.
<b>Trace fossils and other features</b>	None.
<b>Example localities (Fig. 3.9)</b>	Vriesgewaagd farm, Skerwerkraal Farm.

### 3.4.5 Other

#### 3.4.5.1 Mudclast conglomerate



Figure 3.22 Rip-up conglomerate (left) and base of bed mudclasts (right).

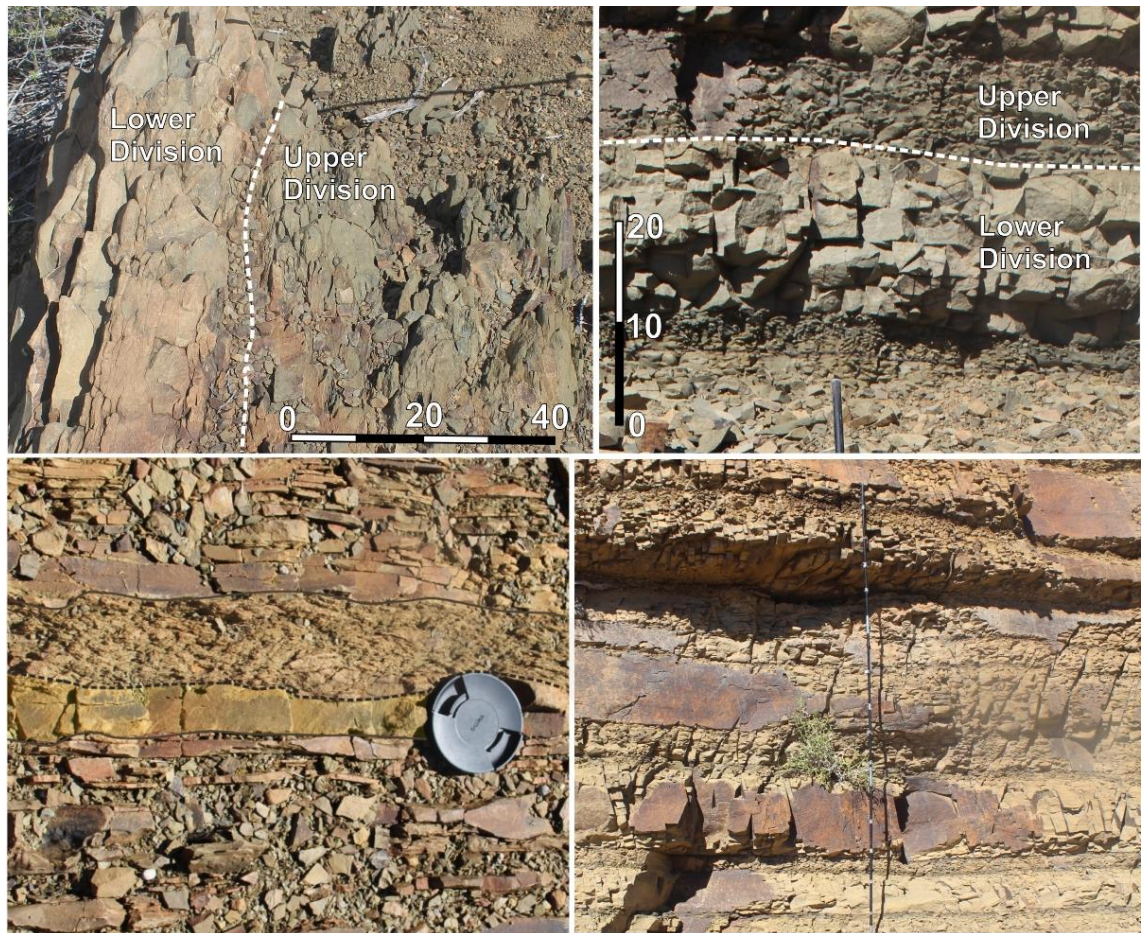
Table 3.14 Mudclast conglomerate characteristics.

Feature	Values and interpretation
Depositional environment	Mud clast mantled surfaces (MCMS) and mud clast conglomerate deposited and moved in traction beneath confined flows. Sand and finer-grained material is inferred to have been bypassed through the system. MCMS deposits are mostly associated with flows confined within channels
Description	Usually a matrix of massive fine sandstone. This facies is rich in mudstone (mudstone and siltstone) clasts averaging <1-4 cm in diameter, although some are up to 20 cm. The clast-rich zone is generally preserved at/near the base of sand beds as MCMS and/or mud clast conglomerate. Locally medium sandstone is present.
Sedimentary structures	Facies found draping erosionally cut surfaces. Consists of tightly packed mudstone clasts 1 - 2 cm in diameter. Clasts are normally well rounded. Also occurs in a continuum from high concentration clast supported conglomerates to matrix supported conglomerates. Clasts commonly well rounded and 1 - 15 cm in size
Process interpretation	The presence of the mud clasts indicate erosion higher in the channel profile. Mudclasts are deposited as a channel lag/drape. Locally, clasts show secondary injection features
Bed thickness range	Typically MCMS is just one or two clasts thick. Local accumulations in scoured depressions may be as thick as 5 – 10 cm
Net : Gross range	0 - 10%
Basal bounding surface	Lies above a sharp erosionally bounded surface. The erosional surface is normally planar with local topography related to the erodability of the underlying substrate
Upper bounding surface	Typically overlain by thin bedded bypass facies. Minimal thickness means easily lost to erosion
Outcrop thickness	Typically MCMS is just one or two clasts thick. Local accumulations in scoured depressions may be as thick as 5 - 10 cm
Outcrop width / geometry	Can be remarkably continuous, may drape the full erosional width of channels (50 - 400 m), except where incised by later erosional episodes.



Trace fossils and other features	None
Other remarks	Often very continuous layers. MCMS have proved useful for tracing channel bounding surfaces through areas of poor exposure
Example localities (Fig. 3.9)	Unit B Skeiding, CD Ridge. Baviaans North, and in Unit C2

## 3.4.5.2 Hybrid bed



**Figure 3.23** Hybrid beds- Slagtersfontein farm (top and bottom left), Allemansdrift farm (top and bottom right).

**Table 3.15** Hybrid bed characteristics.

Feature	Values and interpretation
Depositional environment	Silt-rich hybrid beds: lobe fringe settings. Sand-rich hybrid beds: proximal lobe settings downdip of areas of sediment bypass.
Description	<p>A bipartite bed structure. Lower division: weakly normally graded fine-grained sandstone (0.1 – 1 m thick), with some dewatering structures and rare planar lamination, and occasional mudstone clast layers (clasts 1- 10 cm a-axis). Upper division: poorly sorted very fine-grained sand and silt (0.1 - 1m thick), with dispersed sub-angular, elongate, mm-cm scale mudstone clasts and plant fragments. These occur as two types:</p> <ol style="list-style-type: none"> <li>1. thick and sand-rich, lower sandstone division (&gt;50 cm thick) with occasional mudstone clast layers, and poorly sorted upper division, which has a significant coarse (fine sand) component;</li> <li>2. thin and silt-rich, lower sandstone division (&lt;20 cm thick), and poorly sorted upper division, with a minor coarse (fine sand) component.</li> </ol>

Sedimentary structures	Dewatering structures
Process interpretation	Erosive flows entrain mudstone clasts and fine-grained sediment into the turbulent flow, suppressing turbulence, and producing high-concentration to pseudo-laminar flow conditions. The bipartite beds form through deposition of the lower division from a sand-rich turbidity current with the 'linked' poorly sorted upper division interpreted as deposition from a cogenetic debris flow. Sand-rich hybrid beds form down-dip of bypass dominated areas, highly erosive areas in axial settings.
Bed thickness range	0.2-1.5 m
Net : Gross range	30-70%
Basal bounding surface	Sharp, can be erosive
Upper bounding surface	Sharp
Outcrop thickness	Creates 10's of metre thick packages.
Outcrop width / geometry	Occurring in outcrop continuously for several kilometres.
Trace fossils and other features	None
Other remarks	Organic rich upper division.
Example localities (Fig. 3.9)	Hybrid beds rare across study area, present within Slagtersfontein proximal lobes, and Allemansdrift/Grootfontein lateral lobe fringes.

## 3.4.5.3 Clastic injectites



**Figure 3.24** *Clastic injectite complex beneath, and probably sourced from Unit E at Leeugat, northern limb of the Floriskraal syncline (left) and Close up of dykes below Unit E at Leeugat (right).*

**Table 3.16** *Clastic injectite characteristics.*

Feature	Values and interpretation
<b>Depositional environment</b>	Associated with sharp contacts of sandstone above slope mudstones. As the basal contacts of the 'units' of the Laingsburg/ Fort Brown Formations are typically sharper than upper contacts, clastic intrusion complexes are more common injecting down from beneath these Units. Regional mapping suggests that the potential for clastic injection is increased beneath channel/ lobe axes and beyond the pinch out of sand rich units (e.g., Unit C in the Hartbees area)
<b>Description</b>	Very clean pale coloured sandstones, occurring at vertical dykes cutting through stratigraphy and laterally extensive sills often exploiting bedding surfaces.
<b>Sedimentary structures</b>	Internally structureless. Bounding surfaces may show preserved patterns on fracture surfaces on dyke/sill walls, formed during the injection process (see Cobain et al., 2017)
<b>Process interpretation</b>	Injectites are a post-depositional feature caused by seismicity and / or overpressuring by rapid fluid migration into parent sands, rapid burial or instability of overlying sediments. Fluidized sand propagates through weaknesses (bedding planes and fractures) of surrounding siltstone
<b>Bed thickness range</b>	Sub-centimetre scale to 10s of metres
<b>Net : Gross range</b>	Normally 100%. May be lowered locally by the inclusion of ripped-up mudstone clasts
<b>Basal bounding surface</b>	Very sharp
<b>Upper bounding surface</b>	Very sharp
<b>Outcrop thickness</b>	Sub-centimetre scale to 10s of metres
<b>Outcrop width / geometry</b>	Highly variable. Dykes are typically 2-25 cm wide, with exceptional widths of several metres and penetrate downward by a few metres. However, dykes injecting downwards by 10s of metres are not

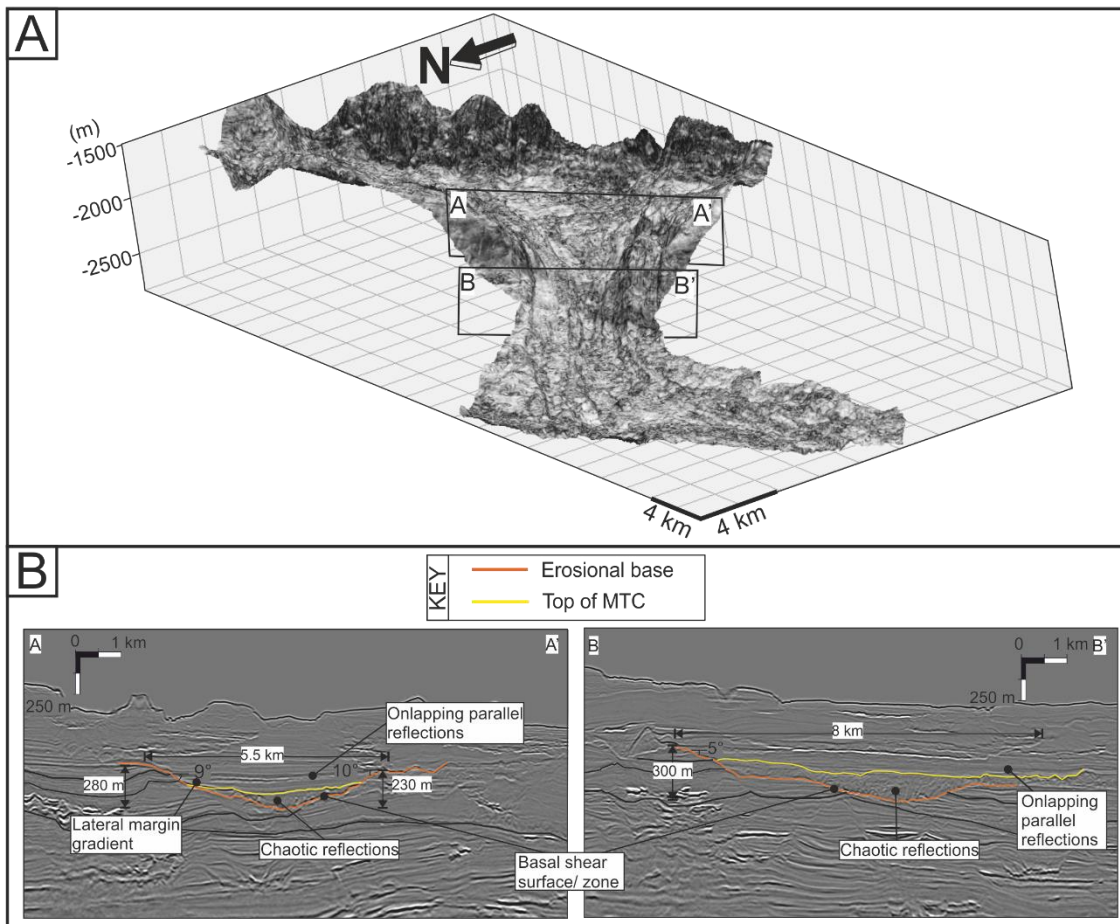
	<p>uncommon</p> <p>Sills range from a few centimetres up to a few metres in thickness. Sills may be remarkably laterally continuous: several sills in the range of 10-50 cm in thickness can be traced for more than 800 m beneath Unit B from the Skeiding axis to the nose of the Baviaans syncline</p>
<b>Trace fossils and other features</b>	None
<b>Other remarks</b>	None
<b>Example localities (Fig. 3.9)</b>	Common where there are channels: e.g., Skeiding, CD Ridge, Baviaans Farm area, Hunters Lodge, etc.

## 4 Exhumed lateral margins and increasing infill confinement of a submarine slide complex

### 4.1 Introduction

Submarine landslides degrade and reshape continental margins, and can cover areas of thousands of square kilometres (e.g. McAdoo et al., 2000; Frey-Martinez et al., 2005; Moscardelli et al., 2006; Moscardelli and Wood, 2008, 2015). Their catastrophic nature means they can destroy seabed infrastructure (Locat and Lee, 2002; Hoffman et al., 2004; Shipp et al., 2004; Masson et al., 2006) and have the potential to disrupt the overlying water column to form tsunamigenic waves (e.g. Pelinovsky and Poplavsky, 1996; Driscoll et al., 2000; Løvholt et al., 2005). The quasi-instantaneous modification of the seascape by these events leads to the rerouting, capture and ponding of subsequent flows (e.g. Alves and Cartwright, 2010; Ortiz-Karpf et al., 2015; Kneller et al., 2016; Fallgatter et al., 2017; Qin et al., 2017). Therefore, understanding the formation and infill of major submarine landslides is required to assess their geohazard potential, and the stratigraphic evolution of continental margins. However, submarine landslides on the modern seabed, and buried examples imaged in reflection seismic data, illustrate their wide range of scales, geometries, run out distances, and return periods (e.g. Bellaiche et al., 1986; Normark and Gutmacher, 1988; Normark, 1990; Gee et al., 2001; Masson et al., 2002; Hürmann et al., 2004; Haflidason et al., 2004; Solheim et al., 2005; Frey-Martinez et al., 2006; Jackson, 2011; Baeten et al., 2013; Hunt et al., 2013; Laberg et al., 2014; Alfaro and Holz, 2014; León et al., 2017).

Submarine landslides move down-slope across a basal shear surface (*sensu* Bull et al., 2009), also known as glide/failure/slip/basal shear planes (e.g. Alves, 2010; Masson et al., 2010; Baeten et al., 2014) or detachment/décollement surfaces (e.g. Vanneste et al., 2006). The basal shear surface develops due to progressive shear failure (Varnes, 1978; Bull et al., 2009), and extensive substrate entrainment leads to downslope increases in flow volume (bulking) (Prior et al., 1984; Gee et al., 2006; Dykstra et al., 2011; Joanne et al., 2013; Ortiz-Karpf et al., 2017a). Lateral margins are part of the basal shear surface, and typically form steep planar surfaces (e.g. Fig. 4.1) perpendicular or sub-parallel to the direction of net displacement (Frey-Martinez et al., 2006; Bull et al., 2009; Gamberi et al., 2011; Alves, 2015; Ortiz-Karpf et al., 2017a).



**Figure 4.1** Example of a submarine landslide confined by a basal shear surface including lateral margins from a 3D seismic volume of upper to mid slope deposits, Magdalena Fan, Caribbean Sea, offshore Colombia. (A) Variance extraction map of submarine slide. (B) Seismic cross sections through submarine slide highlighting the erosional basal shear surface and depositional relief at the top of the initial remobilized/ mass transport deposit (MTD) fill, showing the widening and shallowing of the basal shear surface down-dip (adapted from Ortiz-Karpf et al., 2017).

Basal shear surfaces can have a thickness forming a basal shear zone (*sensu* Alves and Lourenço, 2010), and can be modified by further failure events, creating complex and composite features, and differential compaction (Alves, 2010). Failed material found above and beyond the basal shear surface (Hampton et al., 1996; Frey-Martinez et al., 2005) is referred to as mass transport deposits (MTDs) in reflection seismic datasets, and include slides, slumps and debris flows (Varnes, 1958) and their spatial transitions (Martinsen, 1994). Slides can form as a single failure or as composite slide complex (e.g. Gee et al., 2006; Antobreh and Krastel, 2007; Li et al., 2017) with products of failure often treated as multiple separate events (MTDs) in seismic and outcrop datasets (e.g. Moscardelli et al., 2006; Ortiz-Karpf et al., 2017b; Sobiesiak et al., 2016). The erosional relief of the basal shear surface, and the depositional relief of the MTDs, impact subsequent sediment gravity flow behaviour (e.g. Kneller et al., 2016). Understanding of the evolution of submarine landslides and their impact of subsequent

flow processes is limited by the low vertical resolution and lithological calibration from modern and subsurface examples. Detailed information on the substrate lithology, the basal shear surface/zone, and the sedimentology and stratigraphic architecture of overlying strata can be provided by exhumed examples (e.g. Martinsen, 1989; Martinsen and Bakken, 1990; Lucente and Pini, 2003; Pickering and Corregidor, 2005; Spörli and Rowland, 2007; Callot et al., 2008; King et al., 2011). These examples permit the character and evolution of the basal shear surface (e.g. Alves and Lourenço, 2010; Dakin et al., 2013), and process interactions between subsequent flows and submarine landslide relief (e.g. Armitage et al., 2009; Jackson and Johnson, 2009; Ortiz-Karpf et al., 2015; Kneller et al., 2016; Sobiesiak et al., 2016; Fallgatter et al., 2017), to be investigated. However, exhumed submarine landslide systems of scales comparable to modern and subsurface examples are beyond the scale of most outcrops. For example, large-scale (10s m deep) basal erosion has rarely been demonstrated (e.g. Lucente and Pini, 2003; Shultz et al., 2005; van der Merwe et al., 2009; Dakin et al., 2013), exhumed lateral margins of basal shear surfaces have not previously been documented, and the evolution of flow confinement over multiple submarine landslides has not been investigated.

This study aims to document a unique example of three exhumed, stacked submarine landslides including the lateral margins of two superimposed basal shear surfaces and their subsequent infills, using a seismic-scale outcrop of Permian, lower Ecca Group stratigraphy at the distal end of the Laingsburg deep-water system, Karoo Basin, South Africa. Specific objectives are: i) to investigate the evolution of three submarine landslides from basal shear surface erosion to infill and overspill; ii) to categorise the variations in confinement of remobilized and turbidite components that infill the basal shear surface; iii) to investigate variations in the basal shear surface across strike; and iv) to consider this example in terms of basin-scale sedimentation and degradation.

## **4.2 Geological background**

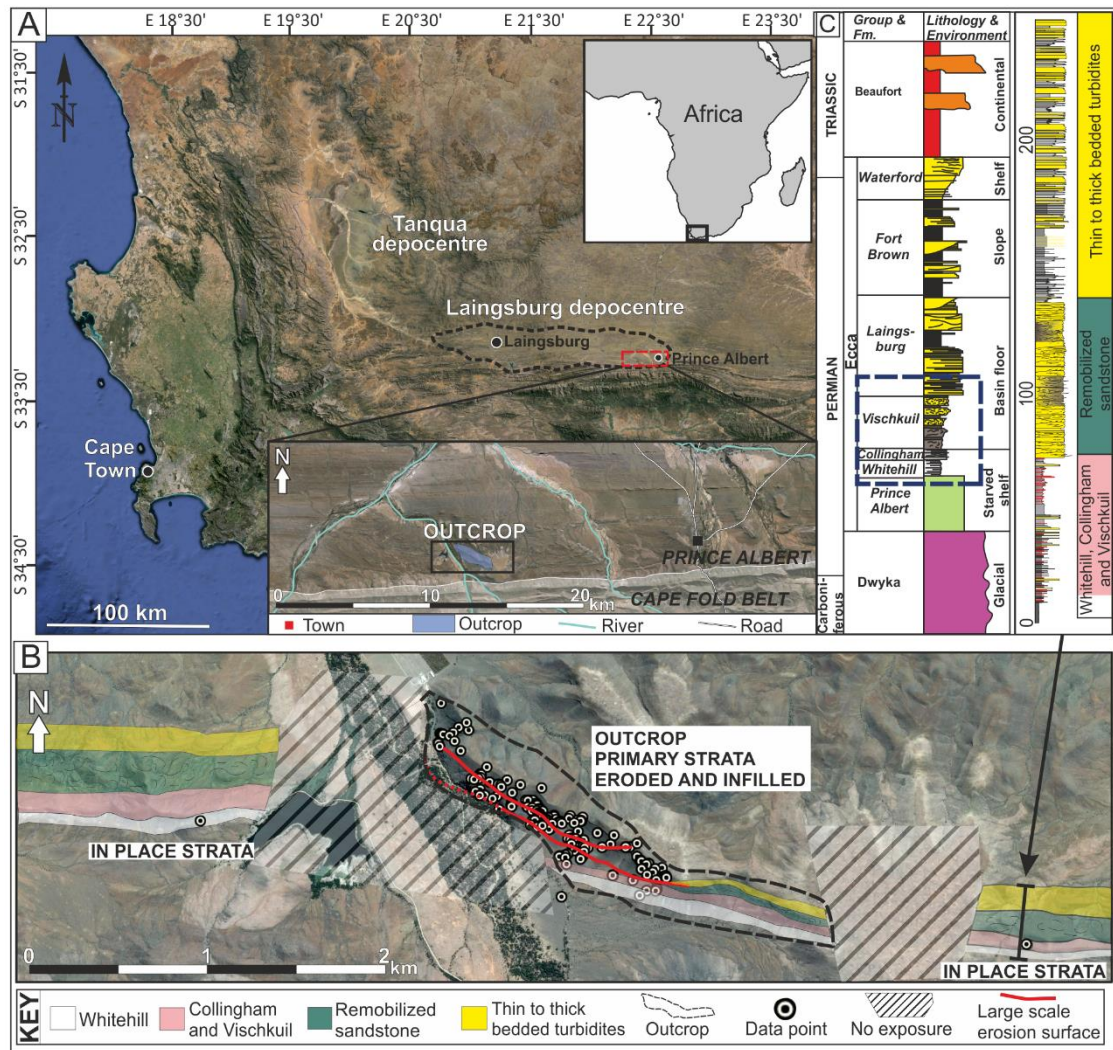
### *4.2.1 Karoo Basin and stratigraphy*

The Karoo Basin, South Africa (Fig. 4.2A), has been interpreted as a retroarc foreland basin (Visser and Prackelt, 1996; Visser, 1997; Catuneanu et al., 1998), and more recently as a thermal sag basin that subsequently evolved into a retroarc foreland basin in the Triassic (Tankard et al., 2009). The 8 km thick Karoo Supergroup (Fig. 4.2C) is subdivided into the Dwyka, Ecca and Beaufort Groups. The Dwyka Group comprises glacial deposits (Late



Carboniferous to Early Permian); the Eccca Group clastic marine deposits (Permian); and the Beaufort fluvial deposits (Permian to Triassic).

Basal deposits of the Lower Eccca Group (Fig. 4.2A) comprise mudstones, chert and shallow marine carbonates of the Prince Albert Formation, overlain by black carbonaceous mudstones of the Whitehill Formation and fine-grained turbidites, cherts and ashes of the Collingham Formation. These formations together average 250 m in thickness and are mapped for 800 km along the southern margin of the Karoo Basin (Viljoen, 1992, 1994; Visser, 1992; Johnson et al., 1997). In the Laingsburg depocentre, the Collingham Formation is overlain by the Vischkuil Formation, which forms the basal section of the 1800 m thick progradational succession through basin-floor deposits (Vischkuil and Laingsburg formations; Sixsmith et al., 2004; van der Merwe et al., 2010), channelized submarine slope (Fort Brown Fm.; Hodgson et al., 2011; Di Celma et al., 2011; Flint et al., 2011) to shelf-edge and shelf deltas (Waterford Fm.; Jones et al., 2015; Poyatos-Moré et al., 2016). Regional palaeoflow is towards the NE and E throughout the succession with the entry point to the SW (van der Merwe et al., 2014). The mapping of successive slope-to-basin-floor systems in the Laingsburg depocentre indicates the presence of a lateral, broadly E-W orientated basin margin to the south of the Laingsburg area (van der Merwe et al., 2014). In the east of the Laingsburg depocentre, the Vischkuil and Laingsburg formations thin and pinch out, along with the sand-rich component of the Fort Brown Formation. Around the town of Prince Albert (Fig. 4.1) the distal reaches of the Vischkuil and Laingsburg formations intercalate with the Ripon Formation, a deep-water system derived from the east (Kingsley, 1981; Visser, 1993). The Ripon Formation deposits are distinctive at outcrop due to their coarser (medium sandstone) grain size.



**Figure 4.2** (A) Image of southwestern Karoo Basin showing Tanqua and Laingsburg depocentres outlined and study area enlarged. (B) Enlargement of outcrop section showing data points and outcrop location. Sections east and west of the zones of no exposure/ tectonic deformation show in place strata unaffected by large-scale erosion surfaces. (C) (Left) Stratigraphic column of Late Carboniferous, Permian and Early Triassic deposits in the Laingsburg depocentre. Blue dashed box indicates units involved in this study. (Right) Logged section of strata outside of outcrop, showing in place deposit, unaffected by large-scale erosion. Lower logged units correspond to the Whitehill, Collingham and Vischkuil formations. Upper units of thick remobilized sandstone and bedded turbidites may correspond to the Vischkuil/ Laingsburg Formations or the equivalent formations to the East.

#### 4.2.2 Study location

This study focuses on a large outcrop at the distal end of the Laingsburg depocentre (Fig. 4.2A), located 95 km east of Laingsburg town and 14 km west of Prince Albert (Fig. 4.2A). The NW-SE orientated outcrop is 3 km in length and 150 m in height. The base of the outcrop is marked by in place strata of the Prince Albert, Collingham and Whitehill formations, which can be traced laterally across an area of 1.5-2 kilometres of either no exposure or intensely tectonically deformed strata, to more continuous outcrops to the east and west of the section (Fig. 4.2B).

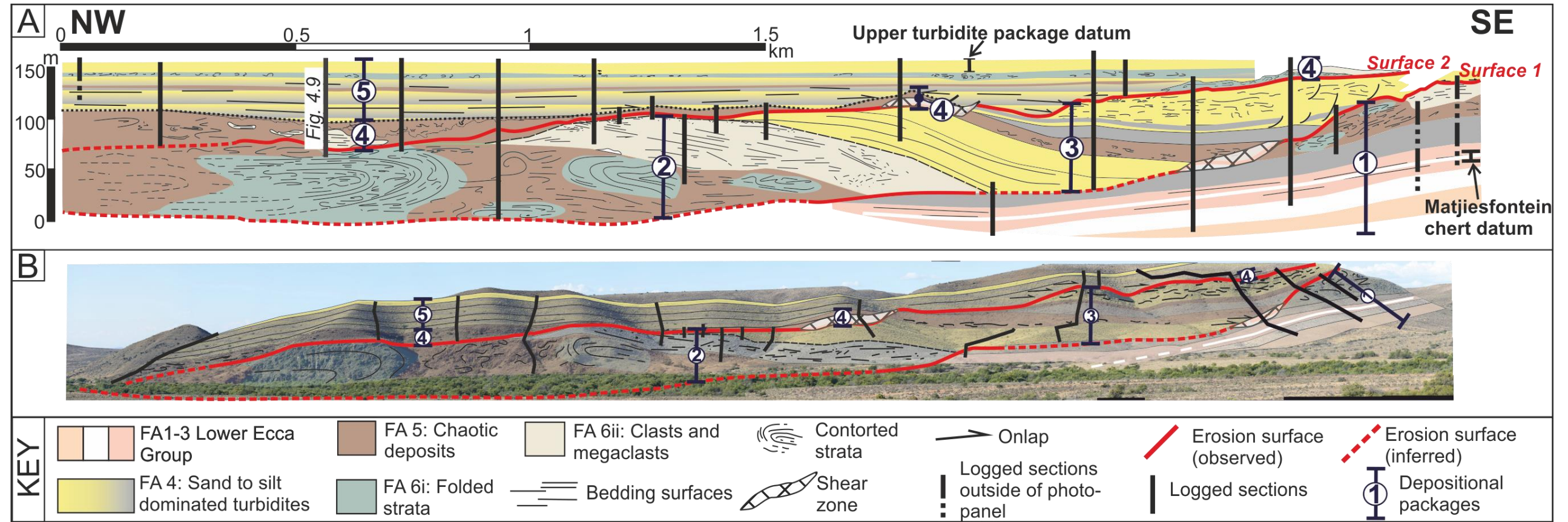
Uniquely at this location, both the Collingham and Whitehill formations are cut out over a >1.5 km long section, with highly contorted overlying deposits (Fig. 4.2B). The overall tectonic shortening direction in the southern Karoo Basin is to the north, with west-east trending and north verging thrust faults and folds that are closely associated with quartz on slip planes. In the study area, the amount of shortening is ~38% (Spikings et al., 2015). The structural dip varies from 10° to 40° and the dip direction from NW to NE, and shows minor displacement in the form of a thrust fault in the northeast of the section. Syn-sedimentary deformation is readily identifiable as being bound by undeformed units, and the faults and folds not following the regional tectonic trends outlined above.

### **4.3 Methodology**

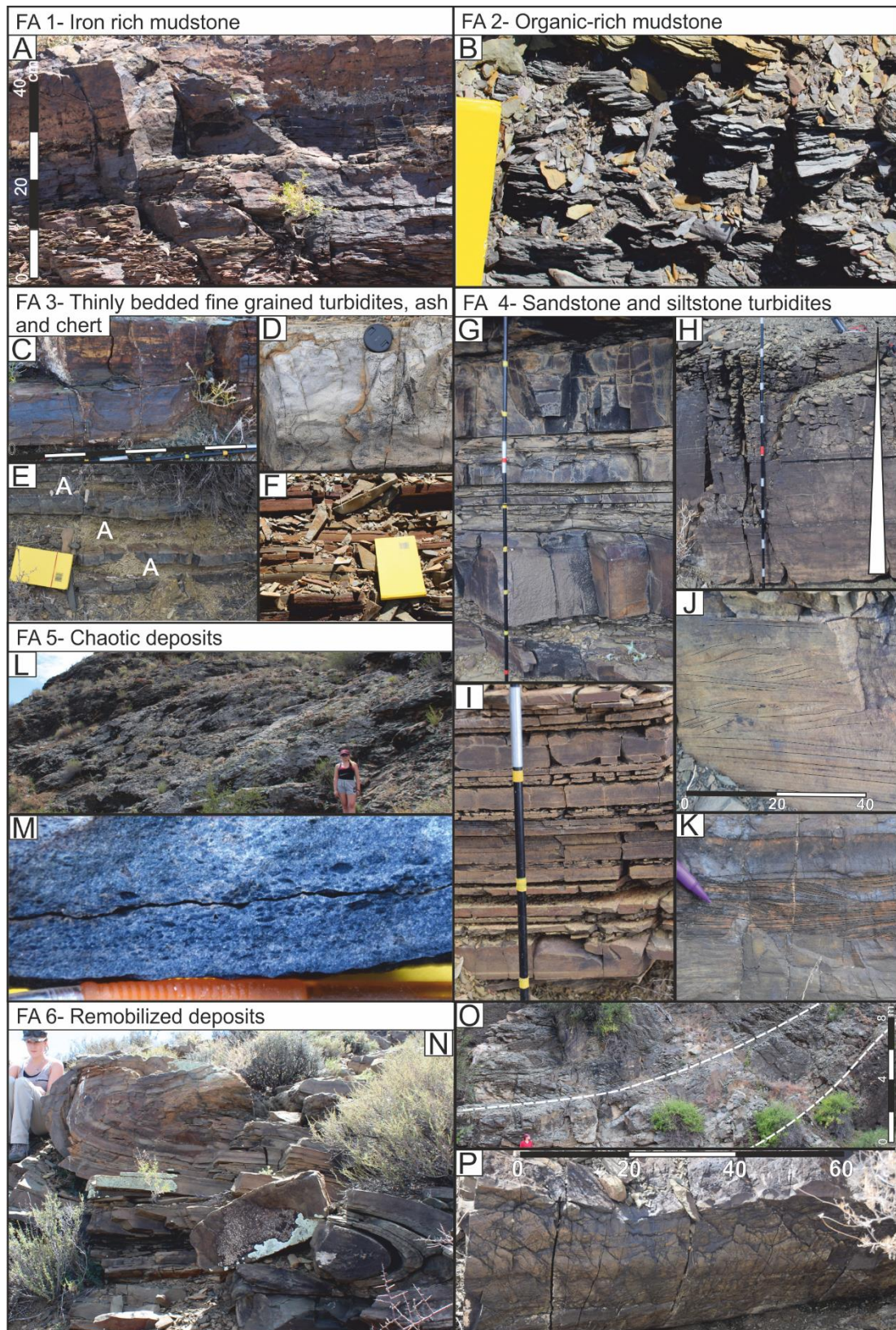
Twenty long measured sections (up to 150 m), and numerous shorter sections, totalling 1500 m, were logged at cm-scale to document lithology, grain size, sedimentary structures and key stratal boundaries (Figs 4.2B and 4.3). The correlation framework is constrained by walking stratigraphic surfaces between sections (Fig. 4.3) augmented with photopanel compilations using Unmanned Aerial Vehicle photography (Fig. 4.3B). A laterally continuous sandstone package, a distinctive 10 m thick package of sharp topped, thin-bedded sandstone and siltstone turbidites, which can be traced laterally across 2.5 km of the outcrop, is used as an upper correlation datum (Fig. 4.3). In addition, a distinctive and uniform bed present throughout the basin-fill known as the Matjiesfontein chert, a laterally extensive 40-50 cm thick white chert bed in the Collingham Formation identified across the SW Karoo Basin (Fig. 4.3) was used as a basal datum. Palaeocurrent data were collected from ripple cross laminations, flutes and grooves, with fold hinges and bedding plane measurements providing kinematic data within contorted units. Regional-scale measured sections were collected several kilometres either side of the outcrop to constrain the large-scale architecture with general facies associations shown in Figure 4.2B.

### **4.4 Facies associations**

Six facies associations have been classified based on sedimentary facies and interpreted processes.



**Figure 4.3** (A) Logs and correlation of units across outcrop. Colours indicate facies associations, red lines show observed and interpreted surfaces. Numbers indicate package divisions. Log of Surface 2 infill (Packages 4 and 5) shown in figure 4.9. (B) Photopanel of outcrop with overlay of logged sections, facies associations and erosional surfaces. Panel and logs shown in more detail in Appendix B.1.



**Figure 4.4** Representative photographs depicting facies associations present throughout the outcrop. (A) Iron-rich mudstone, Prince Albert Formation. (B) Organic rich mudstone, Whitehill Formation, notebook shown 20 cm long. (C) Iron cemented sandstone turbidite beds. (D) Matjiesfontein chert, marker bed, lens cap 7 cm in diameter. (E) Interbedded sandstone/siltstone turbidites and ash deposits (marked as A), notebook 20 cm long. (F) Interbedded turbidites and chert layers, notebook 20 cm long. (G) Sharp

*topped sandstone and siltstone beds, upper turbidite marker package. (H) Sandstone to siltstone graded turbidite beds. (I) Thin-bedded turbidites. (J) Planar and climbing ripple laminated turbidite. (K) Iron-rich ripple laminated turbidite. (L) Thick debrite. (M) Section of debrite with mm- cm scale mudstone clast in distinctive blue mud-rich matrix, pencil for scale. (N) Folded interbedded sandstone and siltstone turbidites, geologist for scale. (O) Folded and slumped sandstone beds, white dashed lines indicates fold of beds, geologist for scale. (P) Base of folded sandstone bed.*

#### FA 1: Iron-rich mudstone

This facies association comprises dark-grey, carbonaceous, iron-rich mudstone with common chert nodules, carbonate concretions and large petrified wood clasts. Remobilized mudstone beds are also present within a dark mudstone matrix, usually well cemented and iron rich (Fig. 4.4A), <50 cm in thickness, folded and/or disaggregated. Packages are >30 m thick with a sharp upper contact with organic-rich mudstone.

#### Interpretation

FA 1 is the Prince Albert Formation, which was deposited either in a marine basin as shelf deposits (Strydom, 1950; Buhmann et al., 1989; Visser, 1991, 1994), or in a freshwater lake environment (Herbert and Compton, 2007). Prince Albert Formation sediments accumulated from syn- to post-glacial suspension fall-out and flocculation of fines from large inflows of sediment-laden water (Domack, 1983; Smith and Ashley, 1985), with some input by turbidity currents and mud flows of semi-consolidated sediments (Tankard et al., 1982; Visser, 1991).

#### FA 2: Organic-rich mudstone

This facies association comprises a uniform, laterally continuous, 30 m thick package of organic-rich, black coloured, thinly laminated mudstone (Fig. 4.4B), which weathers white. The unit has a sharp upper and lower contact with bounding lithostratigraphic units.

#### Interpretation

FA 2 is the Whitehill Formation, a carbonaceous mudstone (Visser 1979; Tankard, 2009), which formed in anoxic conditions across the Karoo Basin (Oelofsen, 1987), indicating little seabed topography at the time of deposition. The sedimentation rate for the Whitehill Formation is thought to be very low with almost no coarse clastic input in relatively shallow water (Flint et al., 2011).

#### FA 3: Thinly bedded fine grained turbidites, ash and chert

This facies association consists of interbedded siltstone (<1-30 cm), organic rich/iron cemented beds (Fig. 4.4C), chert (<40 cm), iron-rich splinter weathered mudstone, sandstone beds (<20 cm) and sandy ash deposits (<1-40 cm) (Fig. 4.4E). Beds are planar and laterally continuous

(Fig. 4.4F), including the distinctive 45 cm thick Matjiesfontein chert bed, traceable across the outcrop belt (Fig. 4.4D). Sandstone and coarse siltstone beds with normally graded bed tops contain planar, ripple and climbing ripple lamination. These deposits gradually transition upward into sandstone beds. Packages are up to 30-35 m thick.

#### Interpretation

The Collingham Formation comprises suspension and turbidity current deposits (Johnson et al., 2006) in a brackish-marine setting (Scheffler et al., 2006; Tankard et al., 2009). Interlayered ashfall tuffs may have derived from volcanoes located in what is now northern Patagonia, where Permian silicic-andesitic volcanic and plutonic rocks crop out (McKay et al., 2015).

#### FA 4: Sandstone and siltstone turbidites

Interbedded, sharp based and topped siltstone and sandstone beds varying in thickness (<0.01-3 m) with grading ranging from, no grading (Figs 4.4G and 4.4I), through weak normal grading, to well graded with siltstone caps (Fig. 4.4H). Beds are structureless (Fig. 4.4G) or contain a variety of sedimentary structures including planar (Fig. 4.4J), ripple and climbing ripple lamination (Figs 4.4J and 4.4K), flutes and grooves on bed bases, and a range of dewatering structures including pipes, ball-and-pillow and flame structures. Beds range from laterally continuous to discontinuous with thickening and thinning to pinchout over 10s of metres. Commonly, the more discontinuous beds onlap underlying packages and have widely dispersed palaeocurrent directions. Packages range from 5-50 m thick. Locally, this facies association forms tightly folded and contorted units (transitioning to FA 6) with highly variable fold axis orientations.

#### Interpretation

Structureless and normally graded sandstones are interpreted as sand-rich high-density turbidity current deposits (Bouma, 1962; Lowe, 1982; Mutti, 1992; Kneller and Branney, 1995). The absence of sedimentary structures indicates rapid deposition and limited development of depositional bedforms. Planar- and ripple-lamination are a product of reworking of the bed beneath low-density turbidity currents (Allen, 1984; Southard, 1991; Best and Bridge, 1992). Dewatering structures are a result of sediment liquefaction (Mulder and Alexander, 2001; Stow and Johansson, 2002). Abrupt thickness changes, onlap and widely dispersed palaeocurrent directions indicate interaction of flows with underlying topography (Kneller et al., 1991). Normally graded beds with siltstone caps indicate 3D topographical confinement of turbidites (e.g. Pickering and Hiscott, 1985; Houghton, 1994; Sinclair and Tomasso, 2002; Sinclair and

Cowie, 2003). Sharp bed tops and lack of grading suggest deposition in an unconfined setting. Generally, these beds are more laterally consistent in thickness suggesting that depositional processes were not strongly affected by seabed topography. Localised folded and contorted units indicate remobilization.

#### FA 5: Chaotic deposits

Poorly sorted conglomerate that comprises sub-angular to sub-rounded intrabasinal mudstone clasts (mm – 10s of cm in diameter), mm-scale terrestrial organic material and other remobilized deposits (FA 6; cm's – 100s m in diameter) supported by a matrix of claystone, siltstone and/or sandstone (Fig. 4.4M). Thicknesses of chaotic packages can vary from 0.5-50 m, and vary laterally and stratigraphically, along with clast size and lithology, forming undulating top surfaces (Fig. 4.4L).

#### Interpretation

The poor sorting and matrix-supported fabric indicate cohesive debris flow deposits. Variations in thickness, lithology, and clast size result from changes in lithology of the primary sediment, transport distance and seabed topography. Cohesive freezing of material (Middleton and Hampton, 1976) creates irregular top surfaces.

#### FA 6: Remobilized deposits

This FA comprises two broad types:

Folded strata: Small scale (0.4-5 m) (Figs 4.4N and 4.4P) and large scale (up to 80 m amplitude; Fig. 4.4O) folded sandstone and siltstone beds, exhibiting a variety of shapes, sizes and orientations. Fold attitude varies from upright to recumbent, with interlimb angles from isoclinal to open. Beds are sheared and faulted, and vary in their degree of preservation of primary sedimentary structures. Commonly, small-scale folds are detached and randomly orientated. Large-scale folded strata can show stronger vergence directions.

and

Clasts and megaclasts: Blocks of remobilized strata, varying in size, degree of disaggregation, and preservation of primary sedimentary structures. Clasts vary in scale from 10 cm diameter to 60 m thick and 750 m in length. Clasts are fractured and disaggregated at their edges with brittle deformation features. Smaller clasts are present within a matrix. Commonly, clasts comprise FA3 (Collingham Fm.) with minor amounts of FA2 (Whitehill Fm.).

#### Interpretation

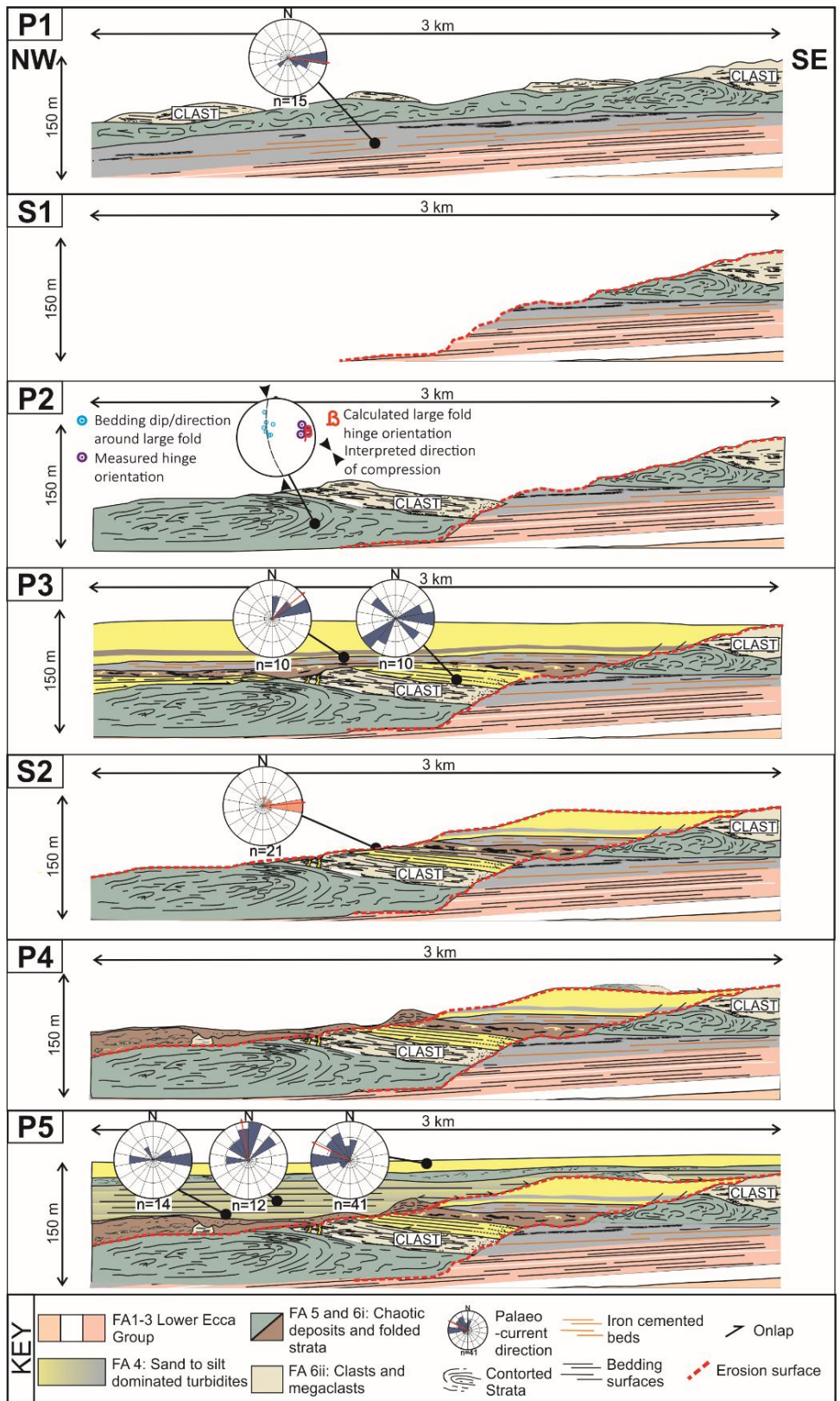


Folded strata are interpreted to form through ductile deformation during remobilization of primary bedding and transport in slumps and slides. The variety of fold sizes, attitudes, interlimb angles and primary bedding preservation is a result of the lithology, amount of consolidation prior to remobilization, and transport distance.

Clasts and megaclasts are interpreted to be entrained at the headwall of the primary flow, or entrained from the substrate during transport. Large clasts are transported as slide blocks. Disaggregation at edges of clasts is interpreted to form during collision with other debris during transport.

#### **4.5 Stratigraphic subdivision and correlation**

The stratigraphic architecture is constrained using the two marker units described in the Methodology section (Fig. 4.3). The physical stratigraphy is also sub-divided by two large-scale erosion surfaces 1 and 2 (Fig. 4.3), which were walked out and identified by abrupt facies changes where underlying strata are truncated and overlying strata thin, fine and onlap the surface. The depositional architecture can be constrained by the dip of the strata below, outside, and above the interval of interest. Mean lithology, and in particular the proportion of clay, inside and outside the two main basal shear surfaces, Surface 1 and 2, are similar, and therefore the surface morphology and architecture of infilling stratal packages is unlikely to have been substantially altered by differential compaction.



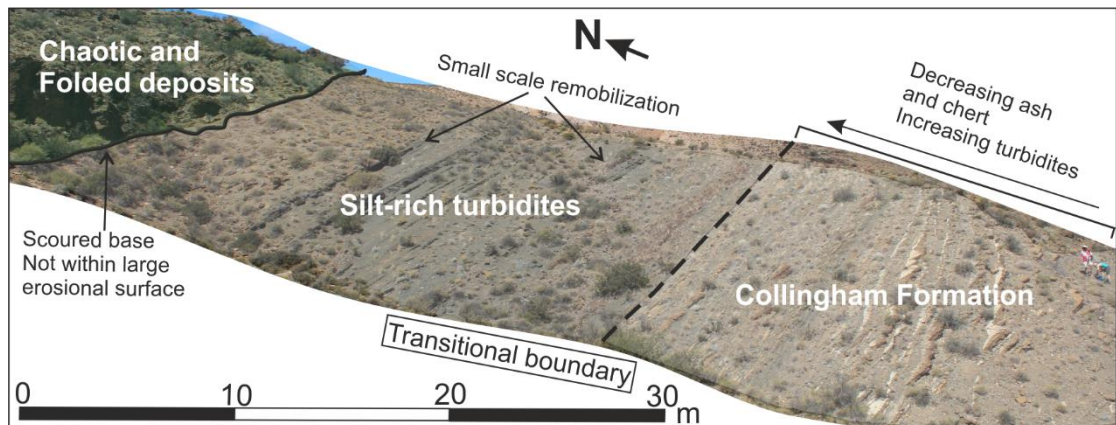
**Figure 4.5** Sketches illustrating stratigraphic evolution, divided into 7 key stages. (P1) Deposition of lower Ecca group, folded and chaotic strata and megaclasts. (S1) Formation of surface 1, (P2) overlain by folded, chaotic deposits and clasts. (P3) Deposition of onlapping and infilling turbidites and chaotic strata. (S2) Formation of surface 2. (P4) Infill of surface by chaotic deposits. (P5) Deposition of onlapping and infilling turbidites and folded strata. Palaeocurrents from ripple, groove, flute and scout marks. Note formation and filling of surfaces may have been instantaneous.

#### 4.5.1 Sequence of erosion and deposition

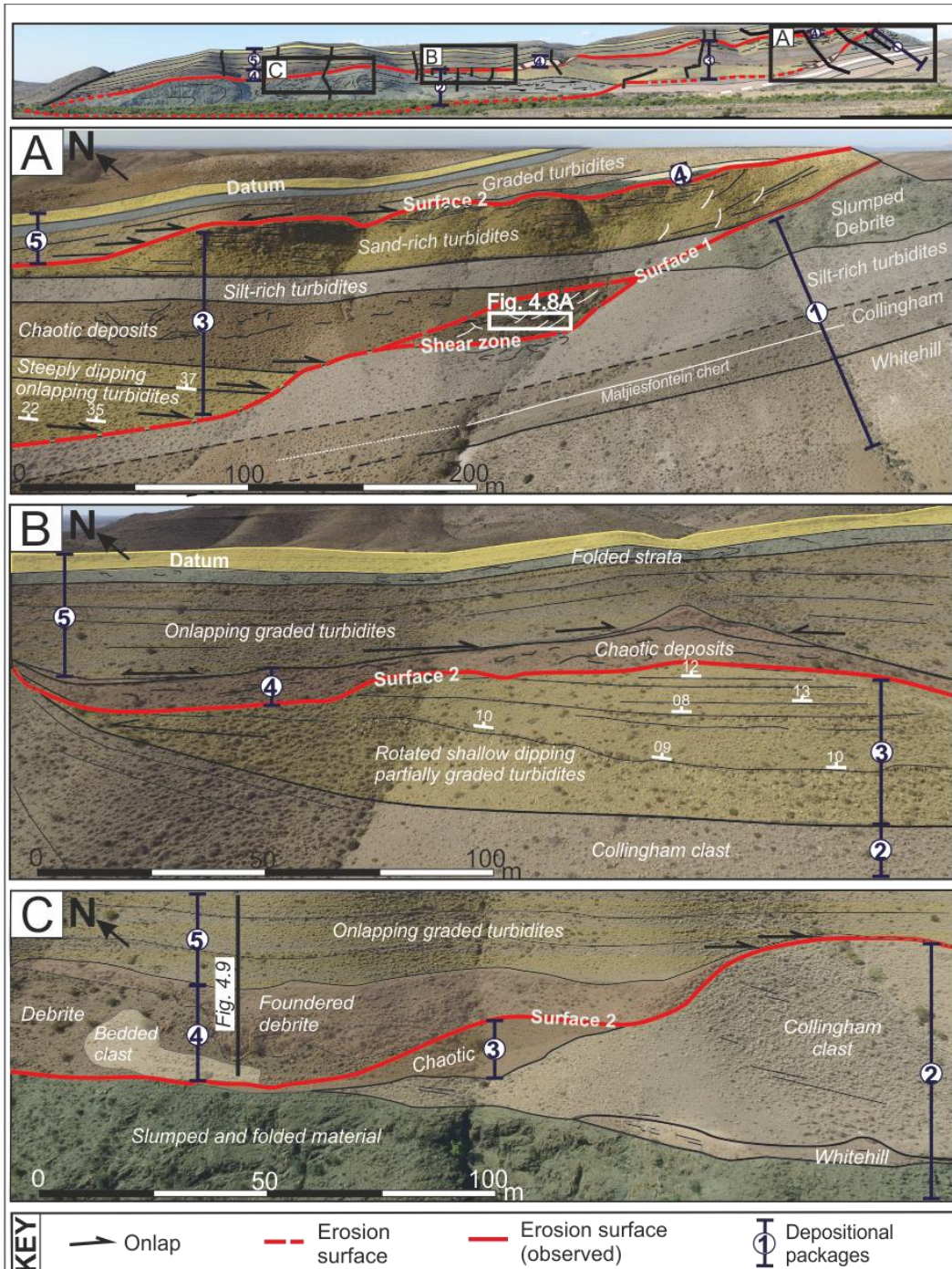
The stratigraphy of the outcrop has been subdivided into 5 depositional packages (Figs 4.3 and 4.5).

##### 4.5.1.1 Package 1

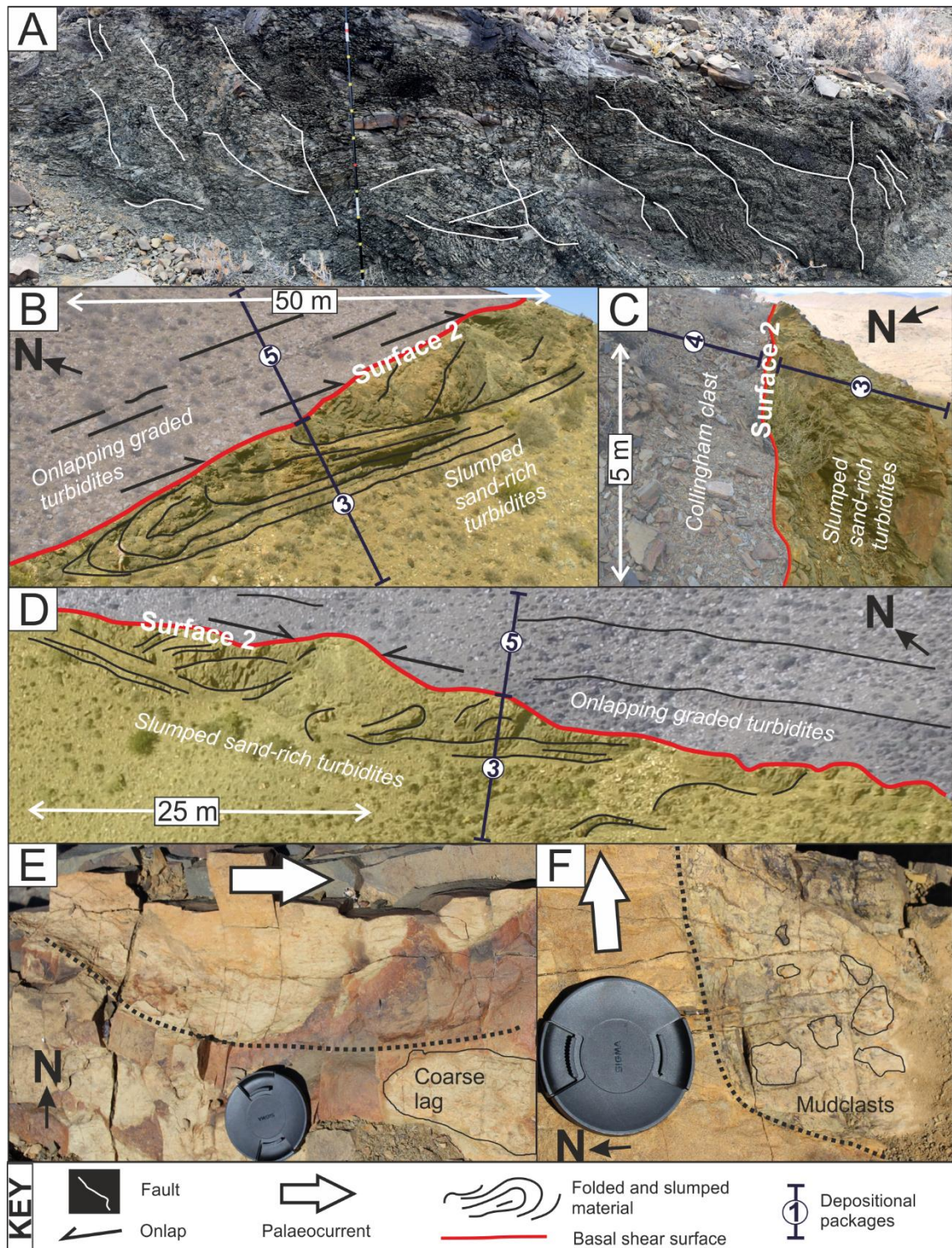
The base of Package 1 (P1, Fig. 4.5) comprises >50 m of Lower Ecca Group stratigraphy, including the upper Prince Albert Fm. (FA1; Fig. 4.4A), the Whitehill Fm. (FA2; Fig. 4.4B), and the Collingham Fm. (FA 3; Figs 4.4C, 4.4D, 4.4E and 4.4F). Palaeocurrent measurements from ripple lamination indicate eastward palaeoflow (Fig. 4.5). This basal section is overlain by a 25-30 m thick unit of thin siltstone turbidites with subordinate sandstone beds (FA 4), and intercalated small-scale (1-2 m) slumps that comprise siltstone beds (FA 6i; Fig. 4.6). The overlying 15-30 m thick unit comprises slumps (FA 6i) with a debrite matrix (FA 5) with minor basal incision (a few metres deep) that marks an uneven basal contact, although no large-scale erosional confinement is observed (Figs 4.6 and 4.7A). A 20 m thick and >100 m exposed outcrop length megaclast (FA 6ii) of Collingham Fm. (FA 3) (Fig. 4.5) is present at the top of this unit. Package 1 is in place east and west of the outcrop (Fig. 4.2B and 4.2C), but is locally cut-out by Surface 1 (Figs 4.5 and 4.7A).



**Figure 4.6** Photograph of lower stratigraphy, Collingham Fm. with Matjiesfontein chert bed, decreasing upwards in ash and chert with a transitional boundary to overlying silt-rich turbidites. A sharp, slightly erosive boundary marks the deposition of chaotic and remobilized strata.



**Figure 4.7** Key architectural characteristics across outcrop. (A) Lower stratigraphy (Package 1) cut by Surface 1, which passes from a sharp, stepped surface to intense zone of sheared mudrock laterally (detailed photo shown in figure 4.8A), overlain by onlapping turbidites and chaotic deposits (Package 3), cut by Surface 2, overlain by chaotic deposits and megaclast (Package 4) and further overlain by onlapping graded turbidites, chaotic packages and upper turbidite package datum (Package 5). (B) Collingham clast (Package 2) overlain by onlapping but rotated turbidites (Package 3), cut by Surface 2 and overlain by debrites and further onlapping turbidites (Package 4). (C) Debrite and slumps (Package 2) overlain by megaclasts (Package 2) and debrites (Package 3), cut by Surface 2 overlain by debrites (Package 4) and onlapping, graded turbidites (Package 5). Facies association colour key shown on figure 4.3.



**Figure 4.8** Photos basal shear zone (Surface 1) and slumped sandstone-rich turbidites and surface 2. (A) Section of basal shear zone with foiled fabric, contorted strata, sheath folds and white lines showing numerous small scale faults. (B) Stepped section of surface 2 cutting folded and dewatered sandstone turbidites (Package 3). Overlying turbidites onlap surface (Package 5). (C) Erosional surface eroding slumped sandstone (Package 3) overlain by Collingham clast (Package 4). (D) Stepped surface 2 with onlapping turbidites (Package 5) from opposing sides of topography. (E) Scour present on top of erosional surface with coarse lag of medium sandstone and mudclasts. (F) Scour on top of erosional surface mantled with mudstone clasts.

#### 4.5.1.2 Surface 1

Surface 1 (S1, Fig. 4.5) cuts down from the SE to the NW of the outcrop (Figs 4.5 and 4.7A) with an averaged compacted gradient of 8°. The width of this surface is 2.0-4.5 km with a depth of >90 m. In the SE, the surface initially incises the sand-rich folded strata in the upper part of Package 1, forming a sharp and smooth erosional contact (Fig. 4.7A). The surface is less distinct where it incises the underlying siltstone-rich sediment. Instead, a zone with an intense shear fabric up to 10 m thick is present that comprises small-scale (2-3 m thick/2-10 m long) sheath folds and low angle faults with varied orientations and displacement of 0.01-1 m (Fig. 4.8A). Shear zone sediments consist of lenticular packages of highly deformed and foliated siltstone and sandstone with no internal sedimentary structures (Fig. 4.8A). The lower part of this surface is inferred by thinning of the overlying deposits and truncation of underlying beds. To the NW, this surface passes into the subcrop, such that the deepest point of erosion is not exposed (Fig. 4.3).

#### 4.5.1.3 Package 2

The base of Package 2 (P2, Fig. 4.5) is confined by Surface 1. In the NW of the outcrop, at its deepest exposed point, Surface 1 is overlain by a >60 m thick section of folded sandstone (FA 6i) with a debrite matrix (FA 7) (Figs 4.4O and 4.7C), exposed for >1.5 km, and dipping into the subcrop (Fig. 4.3). Metre-scale folds are present throughout the unit with intense shearing and thrusts along steep planes. Fold attitude varies from upright to recumbent, with interlimb angles from isoclinal to open. Hinge line and bedding plane measurement of smaller folds appear to be distributed randomly with most detached and supported by a debritic matrix. The fold axis of a 50 m high isoclinal fold is orientated roughly E-W, with the pole to best fit girdle of bedding measurements also indicating an E-W orientation of the fold hinge line (Fig. 4.5). Sharply overlying this unit is a megaclast of Whitehill and Collingham formations (FA 6ii), 750 m in outcrop length and up to 60 m thick (Fig. 4.7C). Bedding plane measurements within the clast are at higher angles (10-20°) and different orientations to the surrounding in-place strata and the clast shows deformed edges. In the SE, Package 2 comprises fine and medium sandstone packages 0.5-2 m thick, interbedded with thin bedded siltstone packages <0.5 m thick, which onlap Surface 1 (Fig. 4.3A).

#### 4.5.1.4 Package 3

The lowermost strata of Package 3 (P3, Fig. 4.5) onlaps Surface 1, and comprises thick turbidite beds (FA 4) (Fig. 4.7A). Basal beds thicken and thin (0-2 m thick) over 10s of metres, and onlap

the underlying megaclast at high angles (Figs 4.7A and 4.7B). Bedding orientations vary across the package, with an increase in dip from an average of 0-5°N centrally over the megaclast (Fig. 4.7B) to 20°-30° NNE towards the SE of the outcrop where the package onlaps Surface 1 (Fig. 4.7A). Ripple palaeocurrents show a large variation in direction (Fig. 4.5). An overlying 16-18 m thick package of thin bedded (1-10 cm thick) planar and rare ripple laminated sandstone turbidites (FA 4) (Fig. 4.3), interbedded with thin siltstone beds (<1 cm-2 cm) contains rare small-scale slumps (0.2-4 m thick). These lower two packages are cut out by Surface 2 to the NW. Overlying these thin bedded sandstones is a discontinuous 18-20 m package of small scale slumps (FA 6i; 0.2-4 m thick) interbedded with laminated siltstone (FA 4) and a further 10-12 m package of thin bedded siltstone with rare, thin (< 10 cm) sandstone beds (FA 4). Both packages onlap Surface 1 to the SE (Fig. 4.7A) and are eroded by Surface 2 to the NW (Fig. 4.5).

In the SE, the overlying 2-4 m thick package comprises thickly bedded fine- and medium-grained sandstone turbidites (FA 4) with NW and NE flute and groove palaeocurrents (Fig. 4.5). This is overlain by 3-5 metres of laterally continuous thin bedded (<1-3 cm) coarse siltstones and fine sandstones (FA 4). Beds have sigmoidal shapes and are moderately bioturbated. Overlying this is a package (up to 40 m thick) of fine and medium sandstone beds, which comprises structureless amalgamated beds with dewatering structures and some intercalated debrites and folded strata (FA 5 and 6i). The unit becomes more slump and debrite dominated as it thickens to the SE of the outcrop (Figs 4.8B, 4.8C and 4.8D), and dissected by numerous extensional faults with throws of cm to 10 m and displacement to the N and E (Fig. 4.7A).

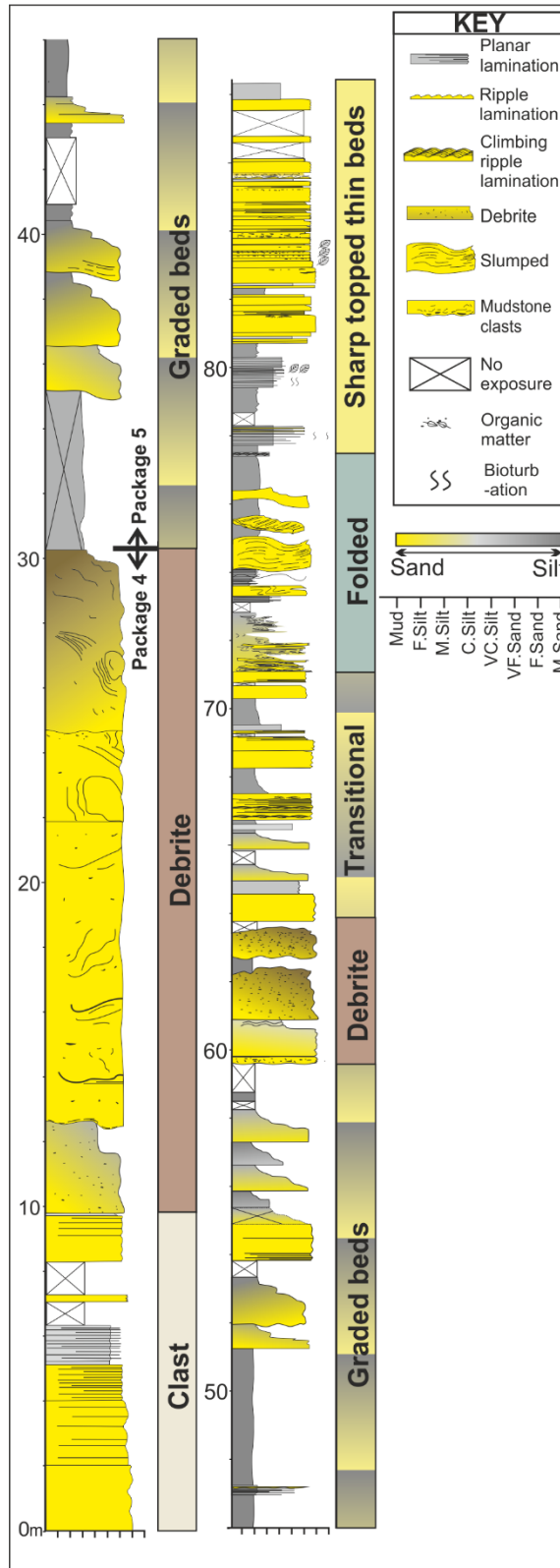
#### 4.5.1.5 Surface 2

Surface 2 (S2, Fig. 4.5) cuts down from the SE to the NW across the outcrop (Fig. 4.7) with an estimated compacted gradient of 4°. The surface is 2.0-4.5 km wide and >60 m deep. In the SE of the outcrop, where the surface cuts the sandstone-rich strata of upper Package 3, the surface is sharp with a stepped character (Figs 4.7A, 4.8B, 4.8C and 4.8D). Here, the surface is cut by numerous small scours that are 10s of cm wide and long and up to 15 cm deep (Figs 4.8E and 4.8F), with palaeocurrents to the E (Fig. 4.5). The scours are draped with mudstone clasts and coarser grained sand (medium sandstone) lag deposits (Figs 4.8E and 4.8F). Towards the centre of the outcrop where Surface 2 cuts through Package 3 fine grained chaotic facies, the surface becomes less distinct and forms a shear zone up to 6 m in thickness (Fig. 4.3). In the shear zone, beds are tightly folded and displaced (0.01-10 m) by faults. Further NW, the location of Surface 2 is expressed as a sharp, locally erosive contact between underlying and overlying debrites (Figs 4.7B and 4.7C).

#### 4.5.1.6 Package 4

Package 4 (P4; Fig. 4.5) consists of debrites with highly disaggregated Collingham Fm. clasts (FA 6ii), from m to 10s of m in length and 1-10 m in thickness (FA 6ii) supported by a fine siltstone matrix, onlapping Surface 1 and locally thickening in lows (FA 5; Figs 4.3, 4.5, 4.6 and 4.8D). In the central area and NW of the outcrop, the lower package comprises debrites. Individual debrites comprise mm to cm diameter angular mudstone clasts and metre-scale folded sandstone beds (FA 6i) supported by a poorly sorted siltstone to fine sandstone matrix (FA 5) with clasts of bedded sandstone and coarse siltstone up to 20 m thick and 100 m in outcrop length (Figs 4.3, 4.7B, 4.7C and 4.9). This package of debrites thins and onlaps onto Surface 2 to the southwest. Overlying this is a unit of slumped and folded strata (FA 6i) (1-13 m in thickness), with some preservation of primary sedimentary structures (originally <1-2 cm thin bedded sandstones and siltstones, similar to Package 3 strata) in the central section of the outcrop (Fig. 4.7B) and small-scale extensional faulting (mm-20 cm throw) prevalent throughout with material down-stepping towards the SE. This passes into poorly sorted sandstone (FA 5) in the NW of the outcrop, which founders up to 5 m into the debrite below (Figs 4.7C and 4.9) and onlaps onto Surface 2.





**Figure 4.9** Logged section through Package 4 and Package 5. Base of log is Surface 2. Location of log shown on figure 4.3 and 4.7C. Chaotic deposits of Package 4 are overlain by thick graded turbidite beds which transition upwards into thinner sharp topped beds with intervening layers of chaotic and folded deposits that are laterally extensive over the outcrop. Top 12 m of log are used as upper datum for figure 4.3. Key for facies association on figure 4.3.

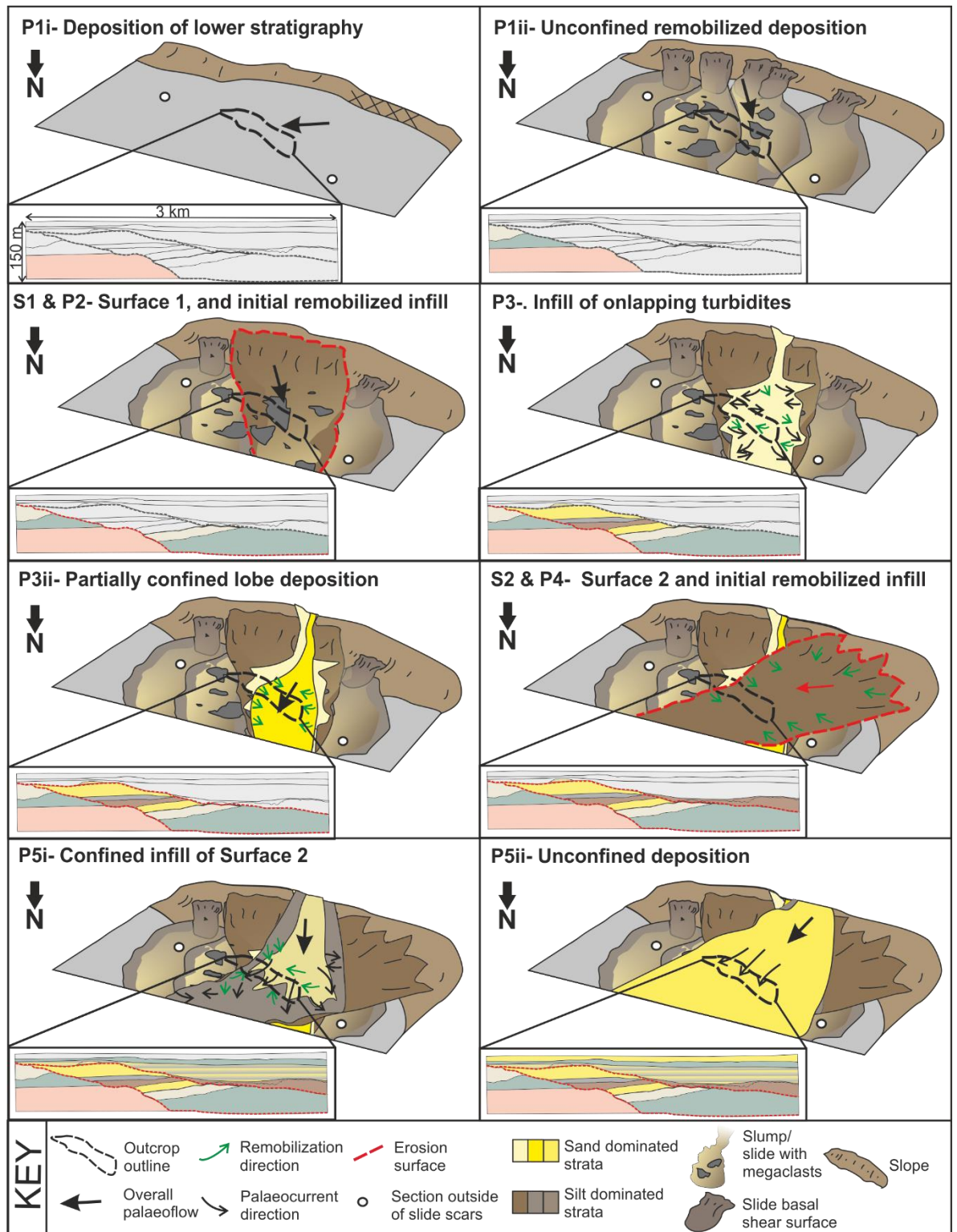
#### 4.5.1.7 Package 5

The basal section (22-32 m thick) of Package 5 consists of 0.3-2 m thick normally graded turbidite beds with thick siltstone caps (FA 4), interbedded with thinly laminated fine siltstone (FA 4) (0.1-4 m thick) (Fig. 4.9). Commonly, sandstone beds are planar laminated, with rare ripple laminations. Ripple palaeocurrents throughout this basal section are towards the E or W (Fig. 4.5). Package 5 thins to the SE (6-10 m thick) and onlaps Surface 2 (Fig. 4.7A). The basal section of Package 5 is overlain by a 2-4 m thick, laterally extensive debrite (FA 5) that comprises siltstone and fine sandstone, with extensive mm to cm diameter mudstone clasts throughout (Fig. 4.9). The debrite is overlain by another turbidite unit consisting of interbedded sandstone and siltstone beds with mudstone caps decreasing stratigraphically (FA 4) (Fig. 4.9). Beds contain mudstone clasts and organic matter at bed tops. Rare ripple and climbing ripple laminations are present, with a laterally traceable 0.5-1 m thick climbing ripple laminated bed with palaeocurrents generally towards the N but with a wide dispersal pattern (Fig. 4.5). This unit thins from 12 to 4 m from NW to SE, and onlaps Surface 2 to the SE (Figs 4.5 and 4.7A). Overlying this is a 3-5 m thick unit that comprises folded and dewatered sandstone beds (FA 6i) in a siltstone matrix (FA 5; Figs 4.4N, 4.7A, 4.7B and 4.9) that thins over thicker Package 3 deposits in the SE (Fig. 4.5). Overlying this is a laterally continuous turbidite unit (15 m thick) that is uniform across the section and is used as an upper datum, with flute and groove palaeocurrents to the NW, and ripple palaeocurrents N-W (Figs 4.3, 4.4i, 4.4G, 4.7A, 4.7B and 4.9).

## 4.6 Discussion

### 4.6.1 *Evolutionary model*

Palaeocurrent measurements and the wider stratigraphic context of the outcrop, in combination with the sedimentary architecture and facies, have enabled the formation of an evolutionary model (Figs 4.5 and 4.10).



**Figure 4.10** Sketches illustrating depositional and erosional evolution over the outcrop and the surrounding area, with sequential panels simplified from figure 4.3. (P1i) Deposition of lower *Ecca* Group stratigraphy towards the east. (P1ii) Unconfined remobilized deposition. (S1 and P2) Erosion by basal shear surface 1 and remobilized infill towards the north. (P3i) partially confined turbidite infill, with overlying chaotic deposits. (P3ii) Partially remobilized intraslope lobe complex. (S2 and P4) Erosion by basal shear surface 2 and chaotic infill. (P4i) Fully confined turbidite and chaotic infill of surface 2. (P5ii) Overspill of confining topography and unconfined turbidite deposition.

#### 4.6.1.1 Package 1

Lower Ecca Group deposits present throughout the Karoo Basin are interpreted as basin floor deposits (e.g. Visser 1979; Oelofsen, 1987), with their uniform nature suggesting little to no seabed topography (P1i, Fig. 4.10). The large-scale debrite overlying the Lower Ecca Group strata with no confining erosion surface (Fig. 4.6) suggest that they were unconfined in a downslope area, having outrun their basal shear surface onto the lower slope/basin-floor (e.g. Frey-Martinez et al., 2006; Posamentier and Martinsen, 2011) (P1ii; Fig. 4.10). The megaclast is interpreted as a rafted block, and the origin from basin floor strata indicates a period of uplift/tilting of the southern basin margin to allow up-dip entrainment (P1ii; Fig. 4.10). Megaclasts carried within the debrite may have moved to the top due to kinetic sieving (Middleton and Hampton, 1976) or moved as slide blocks (Gee et al., 2006).

#### 4.6.1.2 Surface 1

Surface 1 (S1, Fig. 4.10) is interpreted as a basal shear surface/zone, overlain by a thick debrite that was either involved in the formation of the surface or emplaced later. The depth of erosion indicates a location on the submarine slope. The change noted in the nature of the surface, from a sharp erosional surface to a zone of intense shearing, coincides with the change in material from thickly bedded sandstone to thin-bedded siltstone (Figs 4.3 and 4.7A). The shear zone indicates that in the finer deposits strain was accommodated along multiple failure planes. The deformation along the basal shear surface/zone may have formed in the initial emplacement event, or been a protracted record of deformation (e.g. Alves and Lourenço, 2010). The overall thickness of the succession, and therefore the original depth of Surface 1 incision and the gradient of the basal shear surface/zone will have been reduced by burial and compaction.

#### 4.6.1.3 Package 2

The axis of folds in slumps is thought to originate parallel to sub-parallel to the strike of the slope (Bradley and Hansen, 1998) therefore indicating the gross transport direction (Woodcock, 1979; Farrell, 1984; Farrell and Eaton, 1987). Bedding and hinge line measurements taken from large-scale fold structures in the lower slumped unit suggest a N or S movement direction if this is an attached structure and not a clast (Fig. 4.5). The range of sediments, types of deformation and presence of shear surfaces/ thrusts indicate several sources and methods of transport of the debrite and slump deposits. The presence of megaclasts of the Collingham and Whitehill formations suggest that updip these strata had

been tilted sufficiently to be entrained in the headwall or from the substrate by overriding mass flows (S1 and P2, Fig. 4.10). These infilling strata may represent: i) the failed material that was involved in the initial mass flow that formed the basal shear surface, ii) later infilling deposits (e.g. Laberg et al., 2014), or iii) a combination of both (Ogiesoba and Hammes, 2012).

#### 4.6.1.4 Package 3

Deposition of Package 3 marks the change to turbiditic strata (P3i, Fig. 4.10). Beds onlap topography created by the megaclast in the NW and Surface 1 in the SE. The widely dispersed palaeocurrents in the lower section of Package 3 (Fig. 4.5) indicate turbidity current deflection and reflection off erosional and depositional relief (e.g. Baines, 1984; Edwards et al., 1994; Haughton, 1994; Kneller and McCaffrey, 1999; Jackson and Johnson, 2009). The thin normal grading of lower Package 3 turbidites suggests that the flows were weakly confined down-dip. The thick, tabular sand-rich strata in the SE are interpreted as a lobe complex (*sensu* Deptuck et al., 2008; Prélat et al., 2009) that onlaps Surface 1 in the SE of the outcrop (P3ii, Fig. 4.10). Palaeocurrents at the base of the lobe complex have a more consistent direction to the NE, indicating less topographic influence than deposits below (Fig. 4.5). The consistent thick bedded sandstone packages suggest axial lobe deposits with a highly aggradational stacking pattern. The aggradational stacking and the absence of graded bed tops and lack of fines suggest downstream flow-stripping (Sinclair and Tomasso, 2002) within a 3D confining topography, similar to intraslope lobe complexes (Spychala et al., 2015). Higher-density and coarser portions of flows are confined by a downstream topographical barrier, while low-density and finer portions of flows are able to breach this barrier and continue down-dip. The lobe complex is highly deformed with extensive soft-sediment deformation and shear failure surfaces in the SE of the outcrop, likely a result of instability after deposition above the lateral margin slope. Post-depositional tilting of this entire package is evident from the increased angle of bed dips (on average 20°) towards the basal shear surface/zone (Fig. 4.7A and 4.7B).

#### 4.6.1.5 Surface 2

Surface 2 is interpreted as a second basal shear surface (S2, Fig. 4.10). Variation in the character of the shear surface/zone is coincident with lithological variation in the eroded material. The surface is sharp and stepped where eroded into the lobe complex sandstones. The presence of numerous scour features as well as overlying mudstone clasts and coarse sediment lags indicate that, at least over the lobe deposits, the surface was exposed and formed a sediment bypass zone (*sensu* Stevenson et al., 2015) prior to infill. In the central area, a zone of intense shear formed indicating that in the finer deposits strain was accommodated

along multiple failure planes. This deformation may have formed in the initial emplacement event, or be a protracted record of deformation during infill (e.g. Alves and Lourenço, 2010).

#### 4.6.1.6 Package 4

The debritic units represent the initial remobilized infill of Surface 2, onlapping and infilling in topographic lows. The direction of transport is unknown due to the degree of disaggregation, but may represent shedding of material from unstable margins or from an unstable headwall area (P4, Fig. 4.10). The recognition of thin bedded strata in the central area similar to that in the underlying Package 3 turbidites, and syn-sedimentary faulting, suggests the source of this material was from the substrate at the margin.

#### 4.6.1.7 Package 5

Beds initially onlap topography created by underlying debrites (Package 4) and Surface 2 with palaeocurrents indicating reflection and deflection of turbidity currents (e.g. Edwards et al., 1994) (P5i, Fig. 4.10). The thick, normal graded nature of turbidites suggests down-dip flow confinement that formed transient ponded accommodation. Laterally extensive debrites indicate continued slope instability and failure sourced from the headwall and/or lateral margins (P5i, Fig. 4.10). The transitional package (Fig. 4.9) marks the change from thick, normally graded beds to thinner, sharp topped beds with climbing ripple laminated beds, suggesting rapid decrease in flow confinement (e.g. Jobe et al., 2012; Morris et al., 2014). The thinning of the upper slumped layer over the lobe complex may indicate remnant Surface 2 topography, or may be a product of differential compaction during early burial (e.g. Alves, 2010). Deposition of the sharp-topped sandstone and siltstone beds of the uniform datum package is interpreted to represent the healing of the basal shear surface (P5ii, Fig. 4.10) when the flows were unconfined, with more consistent NE palaeocurrents.

### 4.6.2 *Evolution of surfaces*

The large scale, concave shape and gradient of basal shear surfaces documented indicates locations at the margins of the submarine landslides, with extensional structures signifying either the headwall or lateral margin. Indicators of transport direction include: bedding and hinge line measurements taken from large-scale fold structures in Package 1 suggesting N or S movement; Package 3 flute and groove measurements indicating NE palaeoflow; Surface 2 scours indicating E palaeoflow; and, Package 5 flute and groove measurements indicating NW to NE palaeoflow. In addition, the presence of an uplifting lateral basin margin to the south of the outcrop, and regional palaeocurrent and thickness trends (van der Merwe et al., 2014),

support failure directions towards the north. Therefore, these basal shear surfaces are orientated sub-parallel to the direction of palaeoflow and are interpreted as lateral margins (Bull et al., 2009; Alves, 2015) rather than headwalls.

Basal shear surfaces have been shown to be highly variable in their degree of substrate entrained, depth of incision, and changes in flow dynamics (e.g. Frey-Martinez et al., 2006; Bull et al., 2009; Alves and Lourenço, 2010; Laberg et al., 2016; Ortiz-Karpf et al., 2017a). The primary morphology of a basal shear surface/zone is further complicated by post depositional remobilization, occurring directly after deposition on unstable gradients and/or due to differential compaction, especially over variably lithified substrate (Alves and Lourenço, 2010). Outcrop observations help to constrain where the character of the basal shear surface/zone can be attributed to shearing at the time of emplacement or secondary failure and compaction.

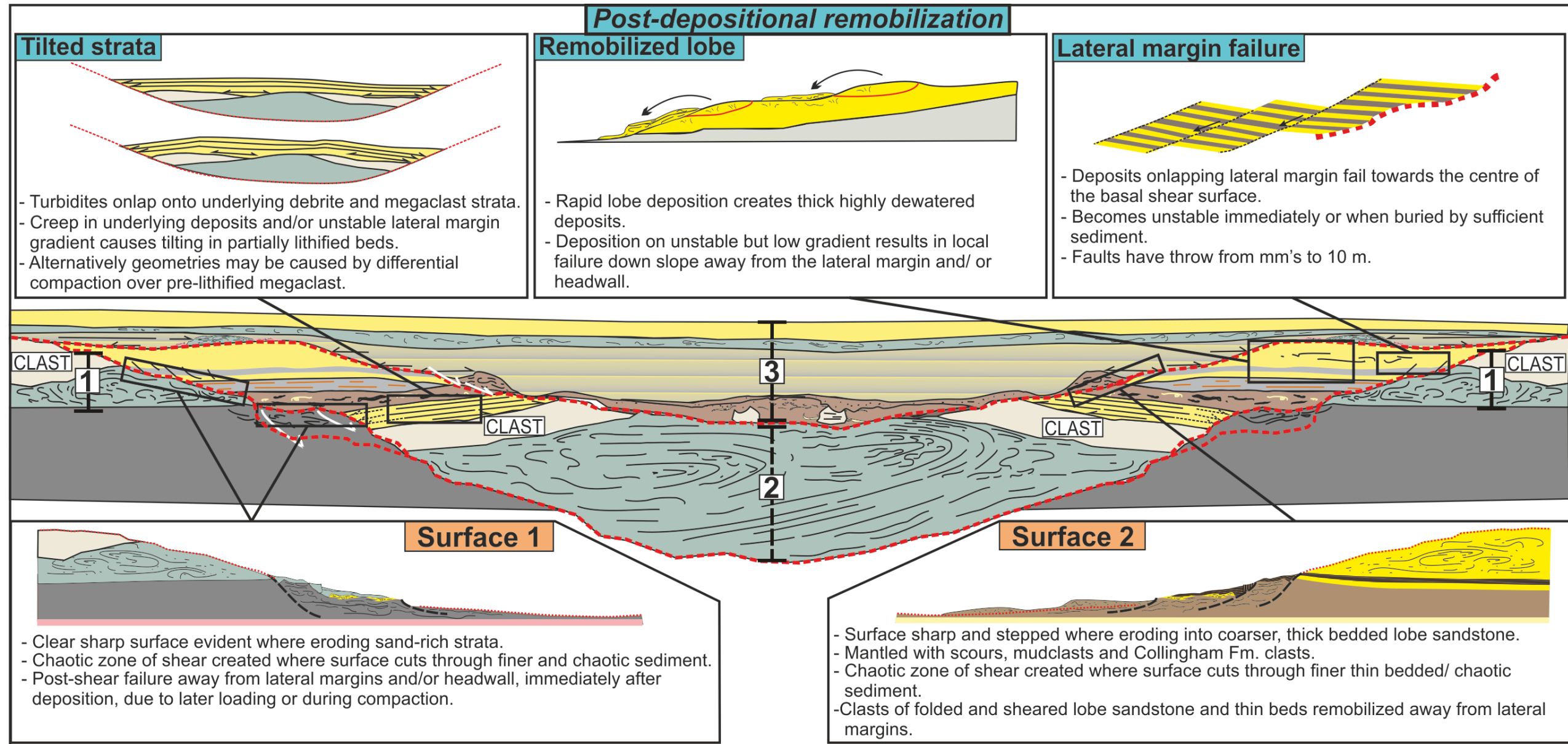


Figure 4.11 Post deposition failure of surfaces. Including tilting of onlapping strata and failure away from lateral margins and headwall. Both Surface 1 and 2 basal shear surfaces display a variation when eroding into coarser sediment (sharp/stepped) or finer material (chaotic zone of shear). Dashed brackets numbered 1-3 refer to slide complex subdivisions (Stage 1, 2 and 3), discussed in text and shown in figure 4.12.



The thickness of a basal shear zone is in part controlled by the character of the sheared strata, the relative density/ thickness of the flow, the mode of transport (Alves and Lourenço, 2010), and the longevity of the movement. This study documents a clear association between the lithology of eroded material and the nature of the basal shear surface/ zone (Fig. 4.11). Sharp, stepped surfaces occur when eroding into thickly bedded sandstone (Figs 4.8 and 4.11) and several-metre thick shear zones form where eroding into chaotic deposits/thinly bedded siltstone (Figs 4.7A and 4.11). The characteristics of the flow(s) that formed the initial basal shear surface are unknown, and may be responsible for some of the spatial variations in basal shear zone thickness and morphology.

Secondary failures are documented in the form of debrite packages overlying basal shear surfaces (Package 4), extensional faulting towards the SW in the central area (Package 3) and towards the N and E at the lateral margin (Package 4), and remobilization of the lobe complex (Package 3) (Fig. 4.7A). Downthrow was away from lateral margins and formed due to later deposition on an unstable gradient (Fig. 4.11). The unusual geometries and variation in dip across Package 3 (Figs 4.7A, 4.7B and 4.11) may be a factor of post deposition movement: i) directly after deposition, ii) later due to loading and/or differential compaction prior to erosion by Surface 2, or iii) later after the deposition of the entire succession. Differential compaction can be shown to have had an impact over the megaclast, which was lithified prior to deposition, therefore forming a topographic high (e.g. Alves, 2010). This causes the increased tilting in the overlying strata due to greater compaction than the megaclast. The increased angle of bedding dip (on average 20°) towards the lateral margins of the basal shear surface (Figs 4.7A, 4.7B and 4.11), and stratigraphic decrease suggests that there was incremental post-depositional movement of strata above the basal shear surface (Fig. 4.11).

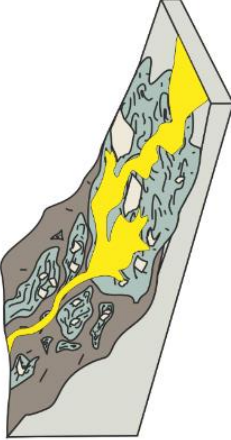
Palaeocurrent indicators from deposits directly overlying Surfaces 1 and 2, suggest different failure directions (Fig. 4.5). These two surfaces may represent two unrelated events, or represent different slip planes within a single slide complex. Infill of Surface 1 prior to erosion by Surface 2 indicates several depositional episodes rather than different phases of the same event, similar to the Hinlopen slide (Vanneste et al., 2006) or the Sahara Slide Complex (Li et al., 2017). If Surface 1 and 2 represent the basal shear surfaces that coalesce updip into the headwall of a larger slide this could be characteristic of retrogressive erosional events (Piper et al., 2012). If distinctly separate events, the initial failure event that formed Surface 1 may have removed deposits at the toe-of-slope, subsequently rendering the slope gradient unstable updip.

The sizes and dimensions of the basal shear surfaces are similar to large-scale confining surfaces within entrenched slope valley systems (e.g. Posamentier and Kolla, 2003; Beaubouef, 2004; Hubbard et al., 2009; Hodgson et al., 2011). Channel systems can be partially infilled with debrites (e.g. Posamentier and Kolla, 2003), but do not contain the ponded turbidites noted in this study. Erosional channel complexes are usually characterised by large scale, composite stepped surfaces formed by several stages of erosion (Campion et al., 2000; Sprague et al., 2002) and the stacking of component channels, and channel complexes (e.g. Macauley and Hubbard, 2013) and internal levee successions (Kane and Hodgson, 2011). These components are not present in this example.

#### *4.6.3 Confinement styles*

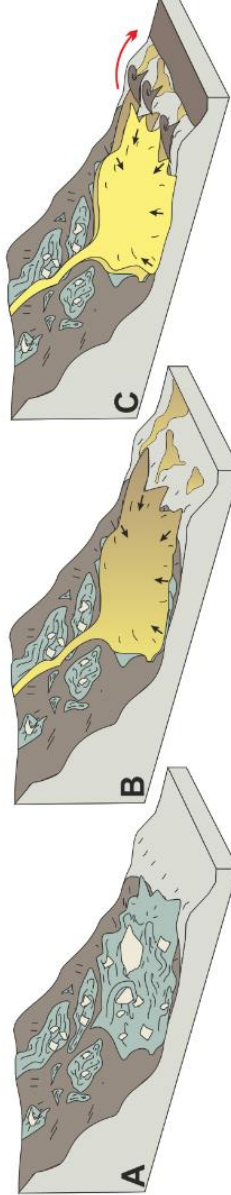
In this example, it is evident that >100 m of slope accommodation was formed as a result of substrate entrainment and emplacement of three large submarine landslides. Variations in flow confinement can occur at m-to 10s of metres scale above relief on upper surfaces of remobilized units (Armitage et al., 2009; Jackson and Johnson, 2009; Kneller et al., 2016). Flow confinement can also occur at a larger scale (10s-100 m), above basal shear surfaces when a large frontal ramp is formed during the erosion and/or as a result of remobilized deposits forming a topographical barrier down-dip (Frey-Martinez et al., 2006; Moernaut and De Batist, 2011; van der Merwe et al., 2011; Alves, 2015). Here, both the confinement of initial remobilized deposits (formed during failure or deposited immediately after) within the basal shear surface, as well as the confinement of later turbidites/remobilized deposits is considered (Figs 4.12 and 4.13).

### 1 Slide 1- Unconfined onlap



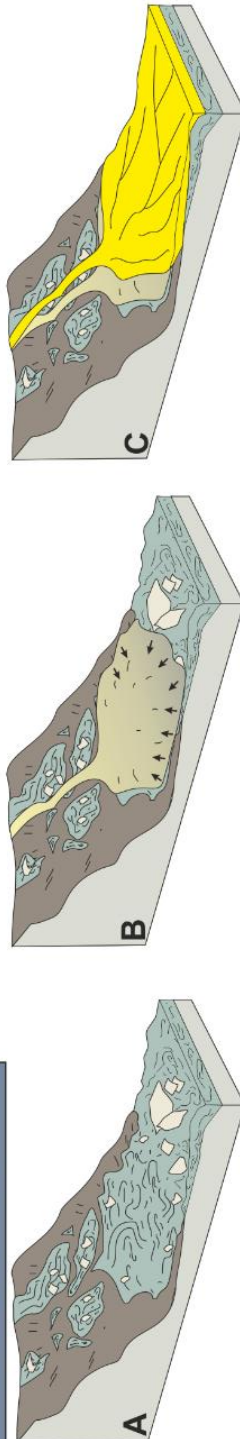
- Unconfined remobilized deposits, which have outrun their basal shear surface, onto an area of relatively low gradient.
- Turbidity currents can onlap and become ponded within rugose surface topography, resulting in reflection and deflection of flows.

### 2 Slide 2- Partially confined infill



A) Slide basal shear surface creates concave shape and possible frontal ramp creating topography down-dip. Initial remobilized deposits partially confined within basal shear surface can further increase down-dip topography.  
 B) Partially confined turbidites onlap and infill topography, with some grading of beds, reflection and deflection of flows.  
 C) Thick sand rich flows undergo flow-stripping forming a sand-rich intraslope lobe complex and bypass finer sediment down-dip. Rugose MTD topography healed, onlap present on steep lateral margin

### 3 Slide 3- Confined infill



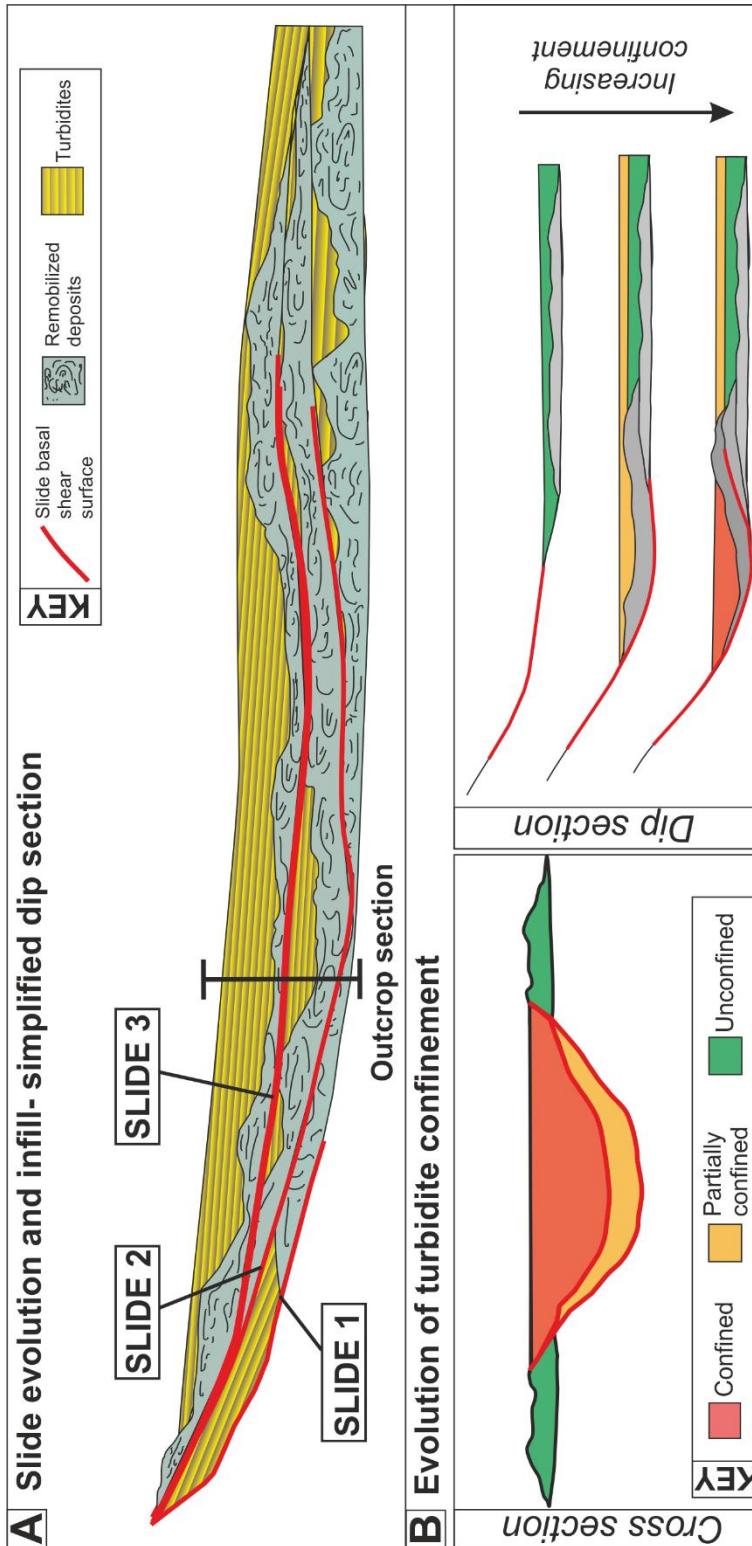
A) Slide scar basal shear surface creates concave shape and possible frontal ramp creating topography down-dip. Initial remobilized deposits partially confined within basal shear surface can further increase down-dip topography.  
 B) Turbidites are confined by lateral margins and down-dip topography, forming fully graded, ponded beds.  
 C) Gradually topography is healed by infilling turbidites, transitioning to unconfined flows, which breach topographical barrier and form a laterally continuous package.

### KEY

Sand dominated strata	Silt dominated strata	Slide basal shear surface
		Slide/slump deposit with clasts
		Reflected/ deflected palaeocurrent direction

**Figure 4.12** *Three key stages of outcrop evolution. Stage 1- deposition of frontally emergent remobilized deposits with onlapping turbidity currents, with basal shear surface located up-dip of the outcrop exposure in this study. Stage 2- Formation of basal shear surface 1, with initial remobilized deposits either frontally confined with frontal ramp creating down-dip topography or frontally emergent and creating a mounded topographic barrier down-dip. Subsequent infilling turbidites are partially confined. Stage 3- Formation of basal shear surface 2 with initial remobilized deposits either frontally confined with frontal ramp creating down-dip topography or frontally emergent and creating a mounded topographic barrier down-dip. Subsequent turbidite and remobilized infill transitions stratigraphically from fully confined to unconfined.*

Three discrete stages of topography-controlled evolution are recognised. Stage 1 (Fig. 4.12) involves the deposition of large-scale unconfined slumps, slides and debrites, sourced from an uplifting tilted southern basin margin, but not contained by a basal shear surface. Stage 2 (Fig. 4.12) includes the formation of Surface 1 with steep lateral margins and initial infill of 60 m of thick, sand rich remobilized deposits. This package is overlain by onlapping turbidites and a lobe complex, with a stacking pattern and sand-rich nature that suggests weak down-dip confinement. Stage 3 (Fig. 4.12) includes the formation of a less steep lateral margin to the basal shear surface that is overlain by thinner debritic deposits and a turbiditic infill with a distinct change from thick well graded and onlapping beds to sharp topped laterally continuous beds, which supports a transition from confined (ponded) to unconfined deposition. Previous models have classified the remobilized infill above a basal shear surface into two end member scenarios: frontally emergent where deposits have outrun the basal shear surface onto the seabed, or frontally confined where topography downslope results in the ponding of remobilized deposits within basal shear surface accommodation, restricting outflow onto the seabed (Frey-Martinez et al., 2006; Moernaut and De Batist, 2011). Factors determining the confinement style of slides are the shape of the slope profile (controlling the headwall height, depth of incision and location of frontal ramp), the gradient of the slope (controlling the length of the slope section and the height drop of the basal shear surface) and the geotechnical properties of the substrate (e.g. Moernaut and De Batist, 2011).



**Figure 4.13** (A) Simplified dip section of Stage 1, 2 and 3 basal shear surfaces and subsequent deposits, showing possible scenario to create strike section documented in this study. (B) Evolution of turbidite confinement from Stages 1-3 showing transition from unconfined turbidites, to partially confined and fully confined with each subsequent failure. Dip section shows how increasing slope gradient and mounding of deposits down-dip could create increased turbidite confinement whilst initial remobilized deposits remain frontally emergent with decreasing run-out distance.

Stage 1 (Fig. 4.12) deposits can be classified as part of a frontally emergent slide (*sensu* Frey-Martinez et al., 2006) with its corresponding basal shear surface located up-dip of the outcrop (Figs 4.12 and 4.13A). Stage 2 (Fig. 4.12) shows evidence of partially graded turbidites overlying thick remobilized deposits, suggesting weak down-dip confinement. This supports deposition behind a frontally confined slide (*sensu* Frey-Martinez et al., 2006) (Figs 4.12 and 4.13A). Similarly, in Stage 3 (Fig. 4.12) thick graded turbidites indicate either a section of a frontally confined slide with down-dip confinement formed by a frontal ramp on the basal shear surface, or a frontally emergent slide with the MTC infill forming a topographical barrier. The latter may be more likely as the remobilized infill of Surface 2 is relatively thin at the outcrop location and therefore a large proportion may have bypassed down-dip (Figs 4.12 and 4.13A). Moreover it is not possible to resolve whether the remobilized deposits infilling the surface were those involved in the original slide, although this relationship is commonly invoked from stratal relationships in 3D reflection seismic data (e.g. Posamentier and Kolla, 2003; Posamentier and Martinsen, 2011; Ortiz-Karpf et al., 2017a).

The formation of a slide as frontally emergent or frontally confined will greatly affect the amount and location of onlapping and ponded infill. Frontally emergent slides will likely leave larger evacuated depressions with down-dip confining topography, within which thick packages of turbidites and remobilized deposits can aggrade (e.g. Stage 3). In addition, surface ponding of flow will occur on top of the rugose surface of the emergent remobilized deposit when up-dip accommodation is healed (e.g. Stage 1). Frontally confined slides will have a complex rugose top surface, with localised depressions infilled with turbidites and remobilized deposits, but likely contain comparatively thinner infilling packages. Therefore, it is more likely that Stage 2 and 3 deposits also represent frontally emergent slides and subsequent infill but with increasing amounts of seabed topography, resulting in increased flow confinement.

Moernaut and De Bastist (2011) suggested that an increase in slope gradient, such as that documented by uplift/tilting of the basin margin in this study, may result in more frontally emergent (unconfined) slides forming due to reduced static and kinetic friction along the basal shear surface and therefore more efficient potential energy transfer. Although this may only be the case when considering individual slides, due to the multiphase nature of the succession, the stacking of multiple remobilized deposits downslope will result in a higher down-dip topographic barrier forming through time, which would require more gravitational potential energy to overcome. The increase in slope gradient will create a progressively more out-of-phase slope profile, possibly resulting in increased basal shear surface depths within subsequent slides, leading to more frontal confinement (Frey-Martinez et al., 2006; Moernaut

and De Batist, 2011). The properties of the material in which the failure occurred is thought to influence slope stability, with failures within rheologically stronger material being smaller and more deep-seated than those in weaker material, typically resulting in a steeper post-failure slope (McAdoo et al., 2000). Therefore, successive failures progressively evacuating deeper and more consolidated material may create smaller, more confined slides. Although slides likely remained 'unconfined' within this study due to the factors discussed above, initial remobilized infill may have become relatively more 'confined' with shorter run-out distances, and therefore creating more 3D topographic closure, resulting in increased confinement of later turbidite and remobilized infill (Figs 4.13A and 4.13B).

Regardless of whether down-dip confining topography was created by a frontal ramp in the basal shear surface or mounded mass flow deposits, there is a clear signature of increasing confinement within the turbiditic infill from Stage 1 to Stage 3 (Figs 4.12, 4.13A and 4.13B). This may be a natural evolution for multiphase failures on steepening/lengthening slopes (Fig. 4.13B), which occur globally and have been widely documented, including in ancient tectonically controlled settings (Alves and Lourenço, 2010), related to salt withdrawal (Ogiesoba and Hammes, 2012) and modern volcanic islands (Carracedo et al., 1999; Urgeles et al., 2001). Therefore, this model is applicable to both modern and ancient multiphase submarine landslides in many geographical locations.

#### 4.6.4 *Source slope*

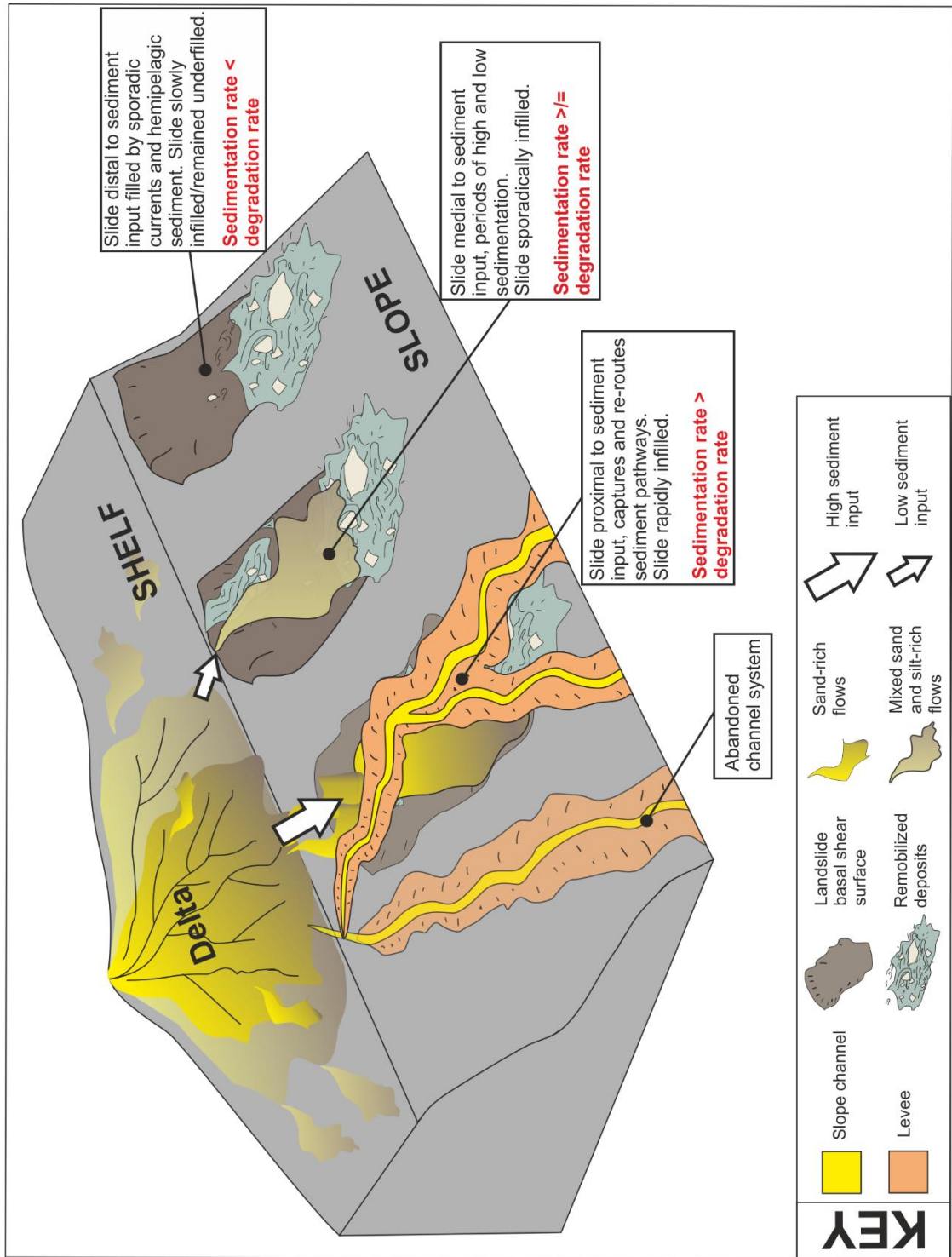
The large scale and deeply erosional basal shear surfaces with infilling deposits recognised in this study are located in the distal, easternmost area of the Laingsburg depocentre (Fig. 4.2A). Palaeocurrent and sedimentological evidence suggests that they were not fed through the depocentre from the westerly dominant sediment transport direction (Flint et al., 2011; van der Merwe et al., 2014; Fig. 4.5). The material present within the slides includes a large range of grain sizes, including medium-grained sandstone, which is unusually coarse for deposits in the Laingsburg system (Grecula et al., 2003; Sixsmith et al., 2004; Hodgson et al., 2006; Hofstra et al., 2015). This larger grain size and more northward trending palaeocurrents in the study area (Fig. 4.5) suggests that many of the infilling packages are more genetically related to the Ripon Fm. deposits present to the east around the Prince Albert area. Coupled with the interpreted north-facing basin margin that controlled later Fort Brown Fm. deposition (van der Merwe et al., 2014), this suggests that the failure surfaces and much of the infilling strata originated from a lateral basin margin to the south. Although ponded deposits infilled the accommodation created by basal shear surfaces (Fig. 4.10), no long-term southerly sediment

conduit has been documented. This suggests that the source slope of these failures was not a major supply margin to the basin at this point, rather an actively uplifting lateral confining slope.

#### 4.6.5 *Sedimentation rates vs. degradation rates*

Many studies have shown how submarine slides can capture/reroute sediment pathways (e.g. Loncke et al., 2009; Ortiz-Karpf et al., 2015) and pond deposits (e.g. Alves and Cartwright, 2010; Kneller et al., 2016). These studies are examples of slope failures in locations with high sediment input, such as directly down-dip of delta fronts (Fig. 4.14). The loading caused by high sediment input may be a controlling factor in causing failure in these locations. These features can be healed quickly where sedimentation rates are greater than degradation rates. Conversely slope failure can also occur in areas of little sediment input, with only passive, hemipelagic infill or infill by sporadic flows/bottom currents, such as on non-supply margins or salt/mud diapir controlled topography (e.g. McAdoo et al., 2000). In these locations, the degradation rate of the slope greatly outpaces the sedimentation rate. The stacked slide complex outlined in this study clearly has episodic coarse sediment infill but also shows evidence of periods with low rates of sedimentation. There is no evidence of large-scale, long-term sediment bypass in the form of channel complexes. It is also unknown if Surface 1 became completely filled and overspilled prior to the erosion of Surface 2.





**Figure 4.14** Sketch of shelf and slope systems indicating how interplay of sediment supply rate and rate of slope degradation can vary the infill of submarine slide basal shear surfaces. Slides in areas of high sediment supply can cause the capture and rerouting of sediment pathways, and become quickly infilled and overspilled. In locations distal to sediment supply, slides can remain underfilled with degradation rate outpacing sedimentation. In intermediary areas periods of high and low sediment supply mean that on average sediment supply is roughly equal to degradation rate.

Overall, the sedimentation rate was in balance with the degradation rate throughout most of the system evolution. It is possible that these failures occurred in the periphery of an area of sediment input to create these changing conditions, for example capturing flows transported across the shelf/upper slope feeding the Ripon system to the east but unable to re-route entire slope systems (Fig. 4.14). The model presented in Figure 4.14 demonstrates how wider scale knowledge of the basin, which is often lacking in outcrop studies, can be gained from general characterisation of slide infill.

## 4.7 Conclusions

This study documents an exceptionally well-exposed example of the formation, evolution and infill of a multiple seismic-scale, submarine landslides. Two 2.0-4.5 km wide basal shear surfaces/zones, Surface 1 and 2, are interpreted as rare examples of lateral margins commonly identified in subsurface data. Surface 1 and 2 document minimum evacuation depths of 90 m and 60 m, with compacted gradients of 8° and 4°, respectively. The basal shear surfaces/zones display variation across strike, coincident with changes in lithology of eroded deposits. Sharp, distinct, commonly stepped surfaces formed where thick sand-rich deposits are eroded and are sometimes mantled with scours and bypass lags. Where these surfaces cut mud-rich deposits, shear zones up to 10 m thick developed, with evidence of protracted development likely due to oversteepening and weakening of material during erosion or after loading. The evolution of this submarine landslide complex can be divided into three stages: 1) unconfined deposition of slumps and slides that outran their basal shear surface; 2) erosion by basal shear surface 1, overlain by thick debritic/chaotic strata and infilled by weakly confined turbidites and a lobe complex; 3) erosion by basal shear surface 2, overlain by thin debritic deposits and infilled by confined turbidites that transition stratigraphically into unconfined turbidites. All three stages of failure are likely 'frontally emergent' slides, with stacking of failed deposits down-dip. The progressive increase in down-dip topography caused a stratigraphic increase in confinement of turbidity currents. The failure source slope was likely a non-supply lateral basin margin that was actively tilting/uplifting, as evidenced by the entrainment of megaclasts from underlying basin-floor successions. Periods of high and low energy deposition are apparent, with only minor sediment bypass and no development of channels. Therefore, this slide complex likely formed in a location with fluctuating sediment input, which over the timescale of the slide complex, was comparable to the degradation rate.

The increase in initial remobilized deposit and turbidite infill confinement, with stacking of slides, may represent a model applicable to other failures on steepening/lengthening slopes. Moreover, the recognition of these submarine landslides in an area peripheral to the main

sediment input highlights the necessity to consider wider basin sedimentation/degradation rates when assessing impact of slope failures on sediment routing, hydrocarbon reservoir connectivity, and seal potential.



## 5 Deepwater channel-lobe transition zone dynamics

### 5.1 Introduction

Deepwater channel-lobe transition zones (CLTZs) separate well-defined channels from well-defined lobes, and are areas within turbidite systems where sediment gravity flows undergo rapid expansion due to abrupt decrease in confinement and/or gradient change (Mutti and Normark, 1987; 1991). The understanding of CLTZ formation and dynamics is therefore pertinent in discerning and predicting facies distributions and the depositional architecture of submarine fans. Studies of systems on the present-day seabed, hereafter referred to as 'modern', show that CLTZs comprise a distinctive assemblage of erosional bedforms including isolated and coalesced scours, and depositional bedforms including sediment waves and lag deposits (e.g. Kenyon and Millington, 1995; Kenyon et al., 1995; Palanques et al., 1995; Wynn et al., 2002a; Fildani and Normark, 2004). CLTZs are dominated by sediment bypass processes, with a relatively thin record of erosion and deposition (Mutti and Normark, 1987; 1991; Normark and Piper, 1991; Stevenson et al., 2015). Models of CLTZs developed from modern seabed studies convey the distribution of erosional and depositional bedforms at a point in time (e.g. Kenyon et al., 1995; Palanques et al., 1995; Wynn et al., 2002a, 2002b; Dorrell et al., 2016), with potential to look at short periods via repeat surveys (e.g., Hughes Clarke et al., 2012), but do not allow the capture of long term (hundreds to thousands of years) changes in the dimensions and character of CLTZs. To do this requires stratigraphic control.

Although CLTZs have been shown to be common features in modern settings, they are not reported in detail from ancient subsurface systems, this is likely due to the limited vertical resolution (typically 10-20 m) of reflection seismic data. However, several exhumed sections of CLTZs have been studied (e.g. Mutti and Normark, 1987; Vicente Bravo and Robles, 1995; Ito, 2008; van der Merwe et al., 2014; Hofstra et al., 2015; Pemberton et al., 2016; Postma et al., 2016). Within the stratigraphic record CLTZs are recorded either as a single surface separating lobes and channel fills (e.g. Elliott, 2000; Gardner et al., 2003) or expressed as a rock volume (e.g. Hofstra et al., 2015; Pemberton et al., 2016) displaying similar scour features shown in modern seabed datasets. However, limitations in palaeogeographic constraint, and dip and strike control on depositional architecture have precluded the development of more advanced evolutionary models. As CLTZs are dominated by erosion and sediment bypass processes their preservation in the rock record requires them to later aggrade (e.g. Pemberton et al., 2016) or for feeder channels to be abandoned or to avulse before they cannibalise the zone (e.g.

Hofstra et al., 2015). Furthermore, sediment bypass criteria, which may be used to recognise ancient CLTZs, have been synthesised from a wide range of systems and settings (e.g. Stevenson et al., 2015), but never constrained from an entire exhumed sediment bypass dominated zone.

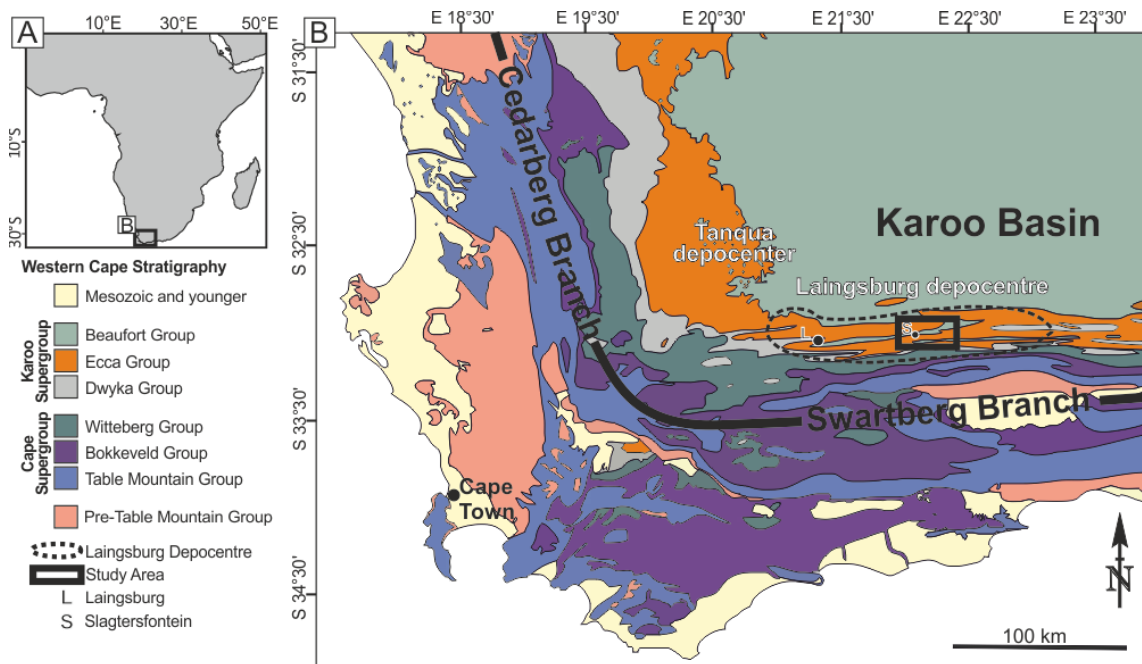
Here, four sub-parallel dip-oriented >20 km long correlation panels from continuous outcrops are presented, that capture the transition down-dip from slope to basin-floor deposits in Units D/E and E of the Permian Fort Brown Formation, Karoo Basin, South Africa. These data are used to understand the dynamic evolution of a base of slope environment, including a uniquely well-exposed CLTZ, within subunit E3, with excellent palaeogeographic constraint to genetically related up- and down-dip deposits. Specific objectives are: i) to identify recognition criteria for a CLTZ in the ancient record; ii) to constrain the three-dimensional depositional architecture of an exhumed CLTZ; iii) to examine the spatial extent and temporal changes of a CLTZ; and iv) to discuss the transfer of CLTZs into the stratigraphic record and to present the first dynamic model of their evolution.

## 5.2 Terminology

Here, the definition of Mutti and Normark (1987, 1991) and Wynn et al. (2002a) for CLTZs is used, as ‘the region that, within any turbidite system, separates well-defined channels or channel-fill from well-defined lobes or lobe facies’, and thus CLTZs form in sand-detached geographic areas (*sensu* Mutti, 1985). CLTZs are examples of sediment bypass-dominated zones (*sensu* Stevenson et al., 2015).

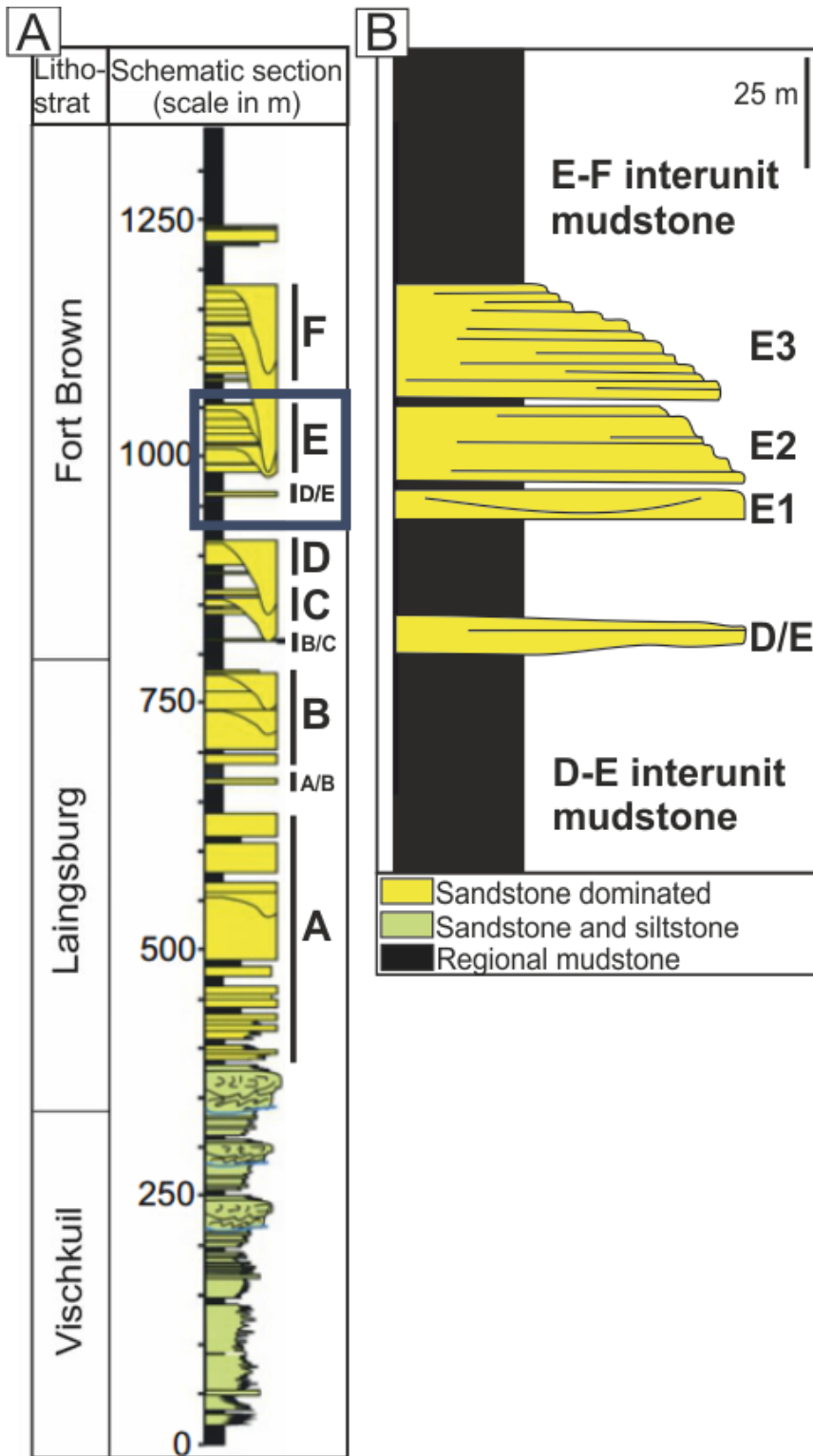
## 5.3 Geological background and location of study

The Karoo Basin has been traditionally interpreted as a retroarc foreland basin (Visser and Prackelt, 1996; Visser, 1997; Catuneanu et al., 1998). More recent studies (Tankard et al., 2009, 2012) suggest that subsidence during the deepwater phase of the basin was controlled by mantle flow over a complex arrangement of basement blocks. The late Carboniferous to Jurassic Karoo Supergroup comprises approximately 8000 m of sediments divided into the Dwyka, Ecca and Beaufort Groups (Fig. 5.1).



**Figure 5.1** (A) Location of the study area within southwestern Africa. Black box indicates location of map B. (B) Regional geological map of the Western Cape. The study area is located in the Laingsburg depocentre, where Ecca Group stratigraphy is exposed, north of the Swartberg branch of the Cape Fold Belt (Modified from Flint et al., 2011).

The Permian Ecca Group in the Laingsburg depocentre records the eastward progradation of the basin margin with a stratigraphic succession from basin-floor deposits (Vischkuil and Laingsburg formations; van der Merwe et al., 2010) through channelized submarine slope (Fort Brown Formation; Hodgson et al., 2011; Di Celma et al., 2011) to shelf-edge and shelf deltas (Waterford Formation; Jones et al., 2015) (Fig. 5.2). Units C-F of the Fort Brown Formation have been mapped in detail over 2500 km<sup>2</sup> from slope valleys, down-dip through channel-levee systems, to basin-floor lobe complexes (van der Merwe et al., 2014), and are separated by regional mudstone (claystone and siltstone) units (Fig. 5.2).

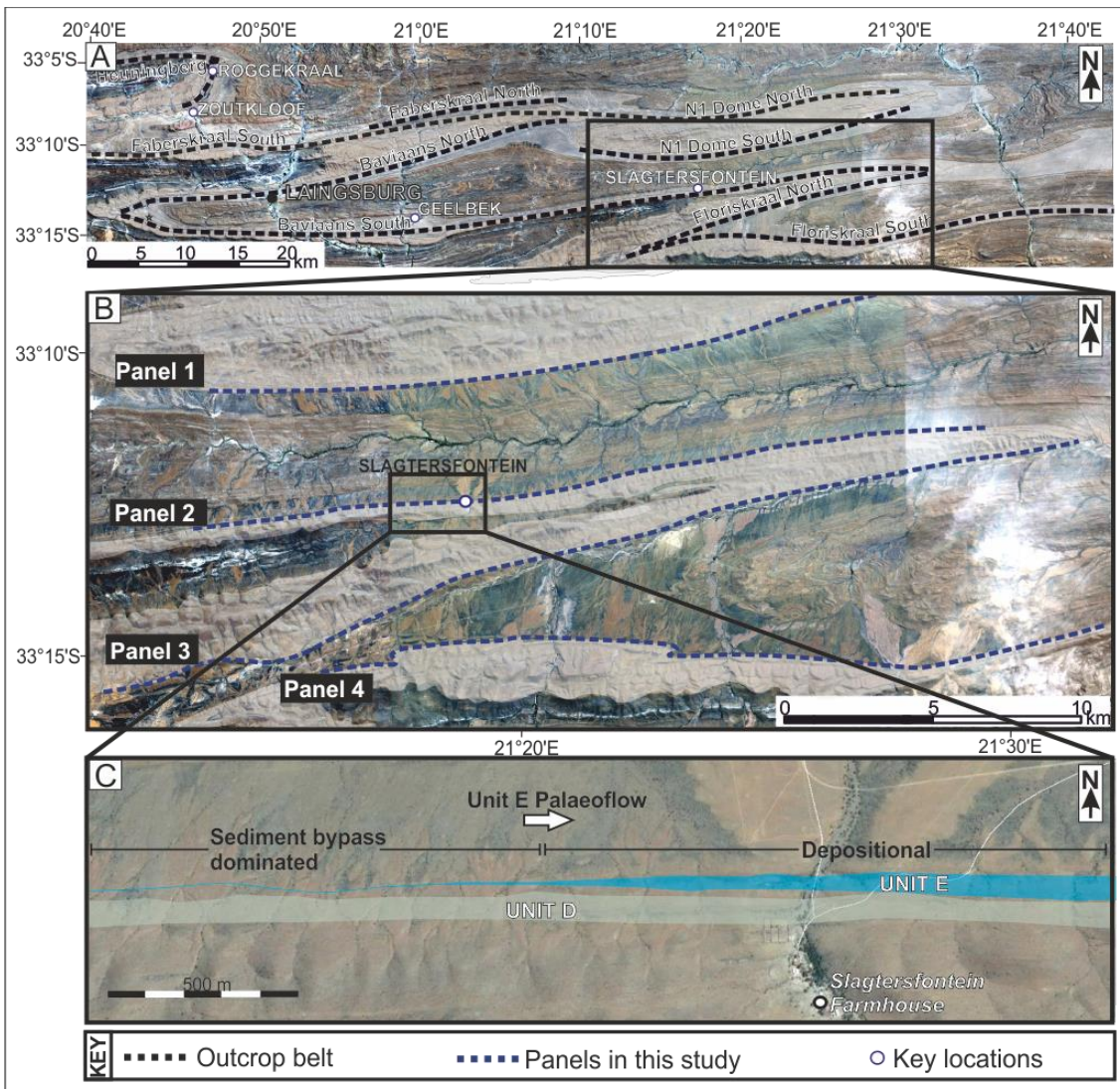


**Figure 5.2** (A) Stratigraphic column showing the Permian Ecca Group deposits in the Laingsburg depocentre, southwestern Karoo Basin. This stratigraphy represents margin progradation from deepwater basin plain deposits (Vischkuil and Laingsburg formations), through submarine slope (Fort Brown Formation) and continues to shallow water (Waterford Formation). Blue box indicates detailed section shown in B. (B) Submarine slope system Unit D/E and Unit E of the Fort Brown Fm., the focus of this study (modified from van der Merwe et al., 2014).

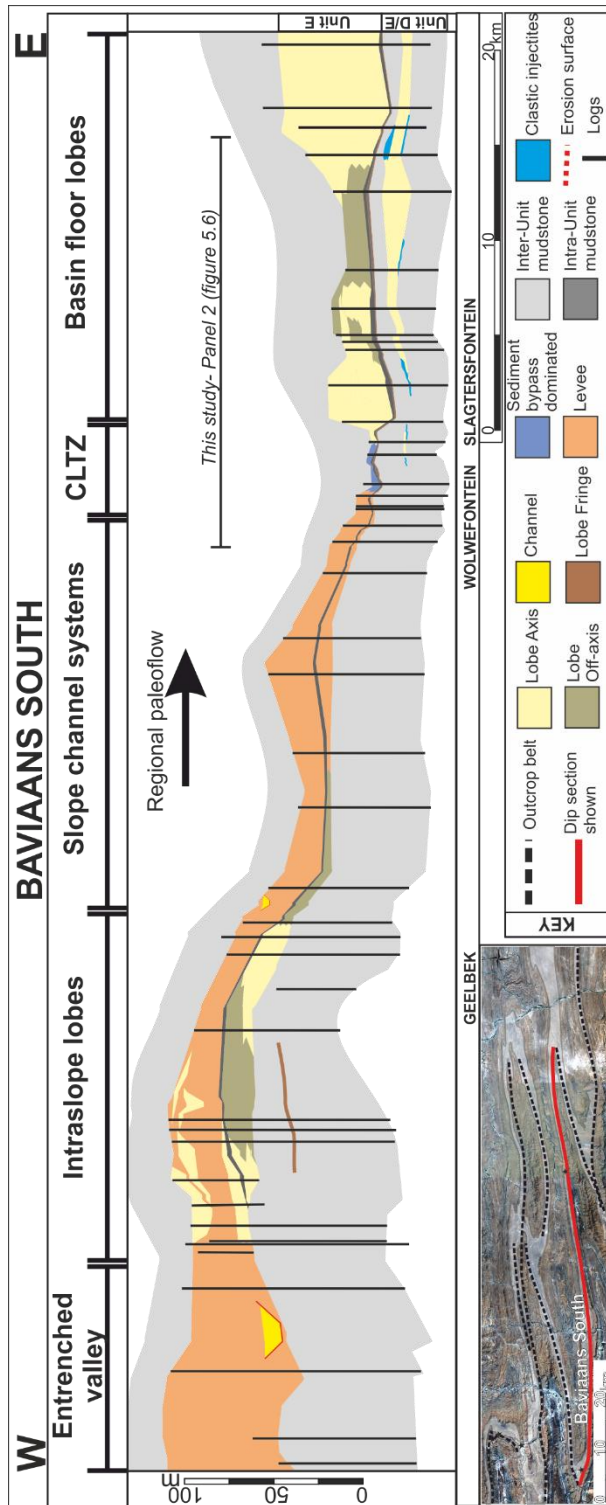


The Fort Brown Formation comprises Units B/C, C, D, D/E, E, and F respectively (Fig. 5.2) and regional studies have led to the interpretation of each unit as a lowstand sequence set (Flint et al., 2011). There is also a Unit G, which is not discussed here. This study focuses on Units D/E and E (Fig. 5.2B), which are exposed along a series of sub-parallel post-depositional fold limbs (Fig. 5.3). Detailed mapping and correlation of Unit E in this study utilises regional correlation work undertaken in previous studies in this area (Figueiredo et al., 2010, 2013; Flint et al., 2011; van der Merwe et al., 2014; Sychala et al., 2015). Unit E comprises three depositional sequences, each including a sand-rich lowstand systems tract (LST; subunits E1, E2, and E3) and a related transgressive/highstand systems tract mudstone, which is approximately 1-8 m thick between each LST (Figueiredo et al., 2010, 2013).

Regional mapping and correlation of Units C to F have demonstrated an architectural change from sand-attached (Units C and D) to sand-detached CLTZs (Units E and F) (*sensu* Mutti, 1985; van der Merwe et al., 2014). The recognition of intraslope lobes in Units D/E and E (Fig. 5.4) (Figueiredo et al., 2010; Sychala et al., 2015) supports the presence of a stepped slope profile at the time of deposition (van der Merwe et al., 2014; Fig. 5.4). This paper focuses on the sedimentology and stratigraphic expression of Unit D/E and subunits E2 and E3, over an area with channel-levee systems mapped up-dip and lobe complexes down-dip, supporting deposition on the lower slope to basin-floor (van der Merwe et al., 2014). This also characterises the sediment bypass-dominated zone recognised in subunit E3 (van der Merwe et al., 2014), as a CLTZ.



**Figure 5.3.** (A) Location of the study area relative to Laingsburg town. Dashed lines indicate the location of outcrop belts. White shading indicates the exposure of Fort Brown and Laingsburg formations. Locations marked Roggekraal, Zoutkloof and Geelbek are the study areas related to the corresponding up-dip deposits of Unit E (Spychala et al., 2015). (B) Enlarged area shows the four sections of regional panels involved in this study and the key Slagtersfontein location. The northern panel 1, contains 64 logs, the central northern panel 2, contains 67 logs, the central southern panel 3, contains 39 logs, and the southern panel 4 contains 30 logs. The highest concentration of data is in the Slagtersfontein study area on panel 2. Locally the top of Unit E3 along panel 3 is lost to modern erosion by a tributary of the Gamka River. Aerial photographs are from NASA Visible Earth (National Aeronautics and Space Administration, <http://visibleearth.nasa.gov/>; regional scale) and Chief Directorate: National Geo-spatial Information, South Africa (<http://www.ngi.gov.za/>; Laingsburg depocentre). (C) Google Earth image of Slagtersfontein study area showing laterally continuous Unit D and abrupt thickening of Unit E down-dip. Tops and bases of units are mapped by walking surfaces and tracking with GPS.



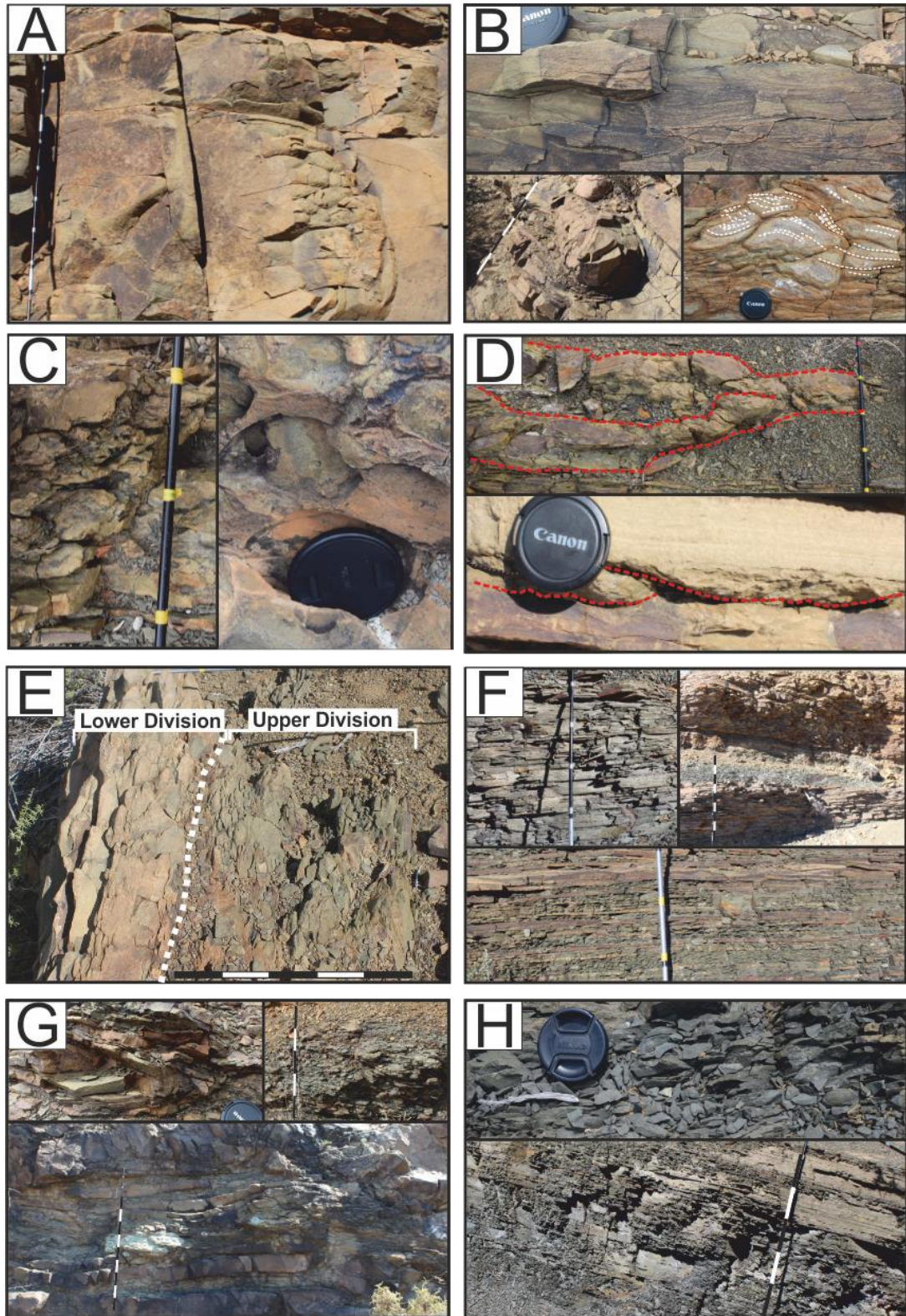
**Figure 5.4** Regional dip correlation panel along the Baviaans South outcrop belt with data from previous studies (van der Merwe et al., 2014; Sychala et al., 2015), showing the D-E interunit mudstone, Unit D/E, Unit E, and the E-F interunit mudstone. Interpretations of architectural elements show the down-dip transition in Unit E from slope channels, through intraslope lobes, channel-levee systems and channel-lobe transition zone, to basin-floor fans. Datum used is top Unit B, an underlying basin-floor fan (shown in Fig. 5.2A). Map highlights the location of outcrop belt within Figure 5.3, with the red line denoting the location of this dip section and black dashed lines showing other exposed sections.

## 5.4 Methodology

Collection of over two hundred measured sections permitted construction of four sub-parallel >20 km long correlation panels oriented along depositional dip (Fig. 5.3), with this area of interest between channel-levee and lobe systems, recognised from previous regional studies (van der Merwe et al., 2014; Fig. 5.4). Logged sections document the lithology, grain size, sedimentary structures and stratal boundaries at cm scale resolution. The correlation framework was established by walking stratigraphic surfaces between sections and using regional mudstones (Fig. 5.4; van der Merwe et al. 2014). The top of underlying sand-rich Unit D is used as a datum as it is a basin-floor fan over the study area (van der Merwe et al., 2014; Hodgson et al., 2016) with minor thickness changes healed partially by the D-E mudstone. Structurally restored palaeocurrent data were collected from ripple laminations, flutes and grooves. Spatial data are presented in palinspastically restored positions according to calculated post-depositional south to north shortening of 17.2% (Spikings et al., 2015). The Slagtersfontein detailed panel was constructed by closely spaced logged sections, with photopanel and detailed sketches aiding interpretation of erosional and depositional bedforms.

## 5.5 Facies groups

Eight distinct groups of lithofacies are described and interpreted in terms of sedimentary processes (Table 1; Fig. 5.5).



**Figure 5.5** Representative photographs of sedimentary facies. (A) Structureless sandstone; (B) Structured sandstone, dashed white lines indicate sheared climbing ripple laminations; (C) Mudstone clast conglomerate; (D) Scoured siltstone and sandstone, dashed red lines indicate erosional surfaces; (E) Hybrid beds, dashed white line indicates division between lower sandstone turbidite and upper debris; (F) Interbedded sandstone and siltstone; (G) Remobilised deposits; (H) Hemipelagic mudstone. Scales: logging pole with 10 cm divisions, camera lens 7 cm in diameter.

Table 5.1 Table of facies groups for Chapter 5.

Facies	Lithology and sedimentary structures	Bed and package thickness and geometry	Interpretation	Architectural element
<b>Amalgamated structureless sandstone</b>  <b>(Fig. 5.5A)</b>	Fine-grained sandstone, commonly amalgamated. Weak-normal grading at bed tops. Erosional bases and rare flutes and grooves. Dewatering structures (e.g. pipes) and deformation structures (e.g. ball and pillow structures) at bed contacts. Rare, discontinuous mudstone clast layers (clasts <3 cm a-axis, sub-angular and elongate, <5% volume) dispersed within beds and present at amalgamation surfaces.	Beds 0.1-1 m thick. Packages up to 30 m thick. Beds and packages tabular.	Structureless and weak normal grading suggests deposition from sand-rich high-density turbidity currents (Bouma, 1962; Lowe, 1982; Mutti, 1992; Kneller and Branney, 1995). Lack of structures indicates rapid deposition. Dispersed rip-up clasts and clast-rich amalgamated contacts suggest progressive aggradation from depletive steady high-density flow (Kneller and Branney, 1995). Dewatering structures form post-deposition, due to sediment liquefaction (Mulder and Alexander, 2001; Stow and Johansson, 2002).	Lobe axis
<b>Structured sandstone (Fig. 5.5B)</b>	Fine-grained sandstone with planar, current ripple and climbing ripple lamination; dewatering structures (e.g. pipes) and deformation structures (e.g. ball and pillow structures). Climbing ripple lamination can exhibit a high angle of climb (15-30°) and stoss-side preservation of laminae. Sheared and overturned climbing ripple laminations present in localised areas at bed tops.	Beds 0.05-1m thick. Packages up to 5 m thick. Beds and packages tabular to lenticular	Planar lamination indicate upper stage plane bed conditions (Allen, 1984; Talling et al., 2012); or traction carpet deposition (spaced stratification) (Hiscott and Middleton, 1980; Lowe, 1982; Sumner et al., 2008; Cartigny et al., 2013). High angle climbing ripples form from continuous bedload traction under high aggradation rates (Allen, 1970; Jobe et al., 2012; Morris et al., 2014). Sheared and overturned climbing ripple laminations, are soft-sediment deformation structures (Allen and Banks, 1972; Allen, 1985).	Lobe axis
				Lobe off-axis
				External levee

<p><b>Lenticular mudstone clast conglomerate and sandstones (Fig. 5.5C)</b></p>	<p>Poorly sorted fine- and medium-grained sandstone and siltstone with well- to sub-round mudstone clasts (mm up to 15 cm, a-axis). Beds can be matrix- or clast-supported comprising 10-80% clasts by volume. Commonly, overlies erosion surfaces at the bases of sandstone packages or interstratified with siltstone.</p>	<p>Beds 0.5-1.5 m packages up to 2 m thick. Beds and packages often lenticular with sharp undulating base and top surfaces. Highly discontinuous</p>	<p>Deposition in high energy environment, fluctuating between erosion, bypass and deposition. Accumulation of a residual lag from bypassing energetic sediment gravity flows (Mutti and Normark, 1987; Gardner et al., 2003; Beaubouef, 2004; Brunt et al., 2013b; Stevenson et al., 2015). Intraformational mudstone clasts collect in areas of reduced bed shear stress including scours or down-dip of gradient change induced hydraulic jumps (Johnson et al., 2001).</p>	<p>Sediment bypass-dominated zone</p>
<p><b>Scoured siltstone and sandstone (Fig. 5.5D)</b></p>	<p>Thin-bedded siltstone with thin, lenticular and poorly sorted silty sandstone beds; both overlie and are cut by erosion surfaces. Several erosion surfaces can coalesce to form composite surfaces. Scour dimensions are typically &lt;3-15 m long, 1-3 m wide and &lt;1 m deep, locally displaying asymmetry with steeper headwalls, in planform exposures.</p>	<p>Beds and packages 0.02- 1 m thick. Lenticular, sharp and undulating bases and tops. Highly discontinuous.</p>	<p>Multiple isolated and composite scour surfaces indicate protracted periods of erosion and sediment bypass down-dip (Beaubouef et al., 1999; Chapin et al., 1994; Kane et al., 2009b; Macdonald et al., 2011a, 2011b; Macauley and Hubbard, 2013; Hofstra et al., 2015; Stevenson et al., 2015). Megaflutes interpreted from planform scour geometries.</p>	<p>Sediment bypass-dominated zone</p>
<p><b>Hybrid beds (Fig. 5.5E)</b></p>	<p>Bipartite bed. Lower division comprising weakly normally graded fine-grained sandstone, dewatering structures, rare planar lamination, and mudstone clast layers (clasts 1-10 cm a-axis, sub-angular, elongated, &lt;5% volume). Upper division comprising poorly sorted silt sandstone with dispersed mudstone clasts (mm-cm scale, sub-angular, elongate, &gt;50% volume) and plant fragments. Two types: i) thick sand-rich lower division with rare mudstone clast layers, poorly sorted, coarse-grained upper division; or ii) thin silty lower division, poorly sorted upper division, with a minor coarse-grained component.</p>	<p>Beds 0.2-2 m thick. i) Lower division 0.2-1 m thick. Upper division 0.05-0.5 m thick. ii) Lower division &lt;0.2 m thick. Upper division 0.05-0.5 m thick. Beds generally tabular. Packages up to 20 m thick and generally tabular.</p>	<p>Deposition of the lower division from a sand-rich turbidity current with the 'linked' poorly sorted upper division. Hybrid event beds (Haughton et al., 2003, 2009) form preferentially towards the base and fringes of lobe deposits (e.g. Hodgson, 2009; Talling, 2013), but can form in any environment where mud and mudstone clasts are entrained into the turbulent flow, increasing sediment volume, damping turbulence, and developing high-concentration to pseudo-laminar flow conditions (e.g. Ito, 2008; Haughton et al., 2003, 2009; Baas et al., 2011).</p>	<p>Lobe axis  Lobe off-axis  Lobe fringe</p>

<p><b>Interbedded sandstone and siltstone (Fig. 5.5F)</b></p>	<p>Three types documented based on bed thickness and sandstone proportion:</p> <p>i) interbedded siltstone and very fine-grained sandstone. Current, and low angle (&lt;5°) climbing, ripple laminated. 'Pinch and swell' bed geometry common in cross-section where ripple sets are draped by siltstone;</p> <p>ii) thin-bedded siltstone with minor sandstone beds and silt rich hybrid beds. Ripples are 1-2 cm in height and &lt;4 cm wavelength;</p> <p>iii) Thin (&lt;2 cm) siltstone beds with rare normally graded very fine-grained sandstone at bed bases. Bioturbation fabric (<i>Planolites</i>) is common throughout (ii) and (iii).</p>	<p>i) Beds 2-30 cm thick, packages 0.5-6 m thick. Beds tabular or show thickness change with ripple geometries.</p> <p>ii) Beds mm-20 cm thick, packages 0.5-7 m thick. Beds and packages tabular.</p> <p>iii) mm-5 cm thick. Packages 0.1-3 m thick and laterally extensive for 10's kms.</p>	<p>Deposition from dilute turbidity currents, with the finer sediment residual within the flow after deposition of the coarser fraction of sediment load. Climbing ripples form through late stage tractional modification of waning or low-density flows, with high sediment fall out rates (Lowe, 1988). Thin beds and low angle of climb suggests lower rates of suspended load fallout. Starved ripples indicate deposition from sediment-limited weak traction currents (Jobe et al., 2012). Very thin-bedded, laterally extensive, silt-dominated deposits are interpreted as derived from numerous dilute turbidity currents.</p>	<p>Lobe off-axis</p> <p>Lobe fringe</p> <p>Spill-over fringe</p> <p>External levee</p>
<p><b>Contorted and chaotic deposits (Fig. 5.5G)</b></p>	<p>Sandstone and siltstone, coherently folded to highly disaggregated. Contorted clasts supported by a poorly sorted silt-prone matrix. Chaotic deposits have a poorly sorted matrix of very fine-grained sandstone to coarse-grained siltstone beds, lack internal structure and contain dispersed sub-angular, elongate, mm-cm scale mudstone clasts and plant fragments.</p>	<p>Beds cms-2 m thick. Packages up to 10 m thick, extending laterally for 10's of metres.</p>	<p>These facies are interpreted as mass flow deposits derived from remobilization processes to form slides and slumps. Highly disaggregated examples are interpreted as debrites.</p>	<p>Not characteristic of any specific environment, can occur in association with all architectural elements.</p>
<p><b>Hemipelagic mudstone (Fig. 5.5H)</b></p>	<p>Claystone and fine-grained siltstone, with mm scale laminations or structureless.</p>	<p>Beds mm-3 cm. Packages up to 70 m thick. Packages highly regionally extensive for 10's of kms up-dip, down-dip and laterally.</p>	<p>Background hemipelagic deposition, with occasional distal dilute turbidity currents. Regional drapes during shutdown of sand and coarse coarse-grained silt supply.</p>	<p>Regional mudstone</p>



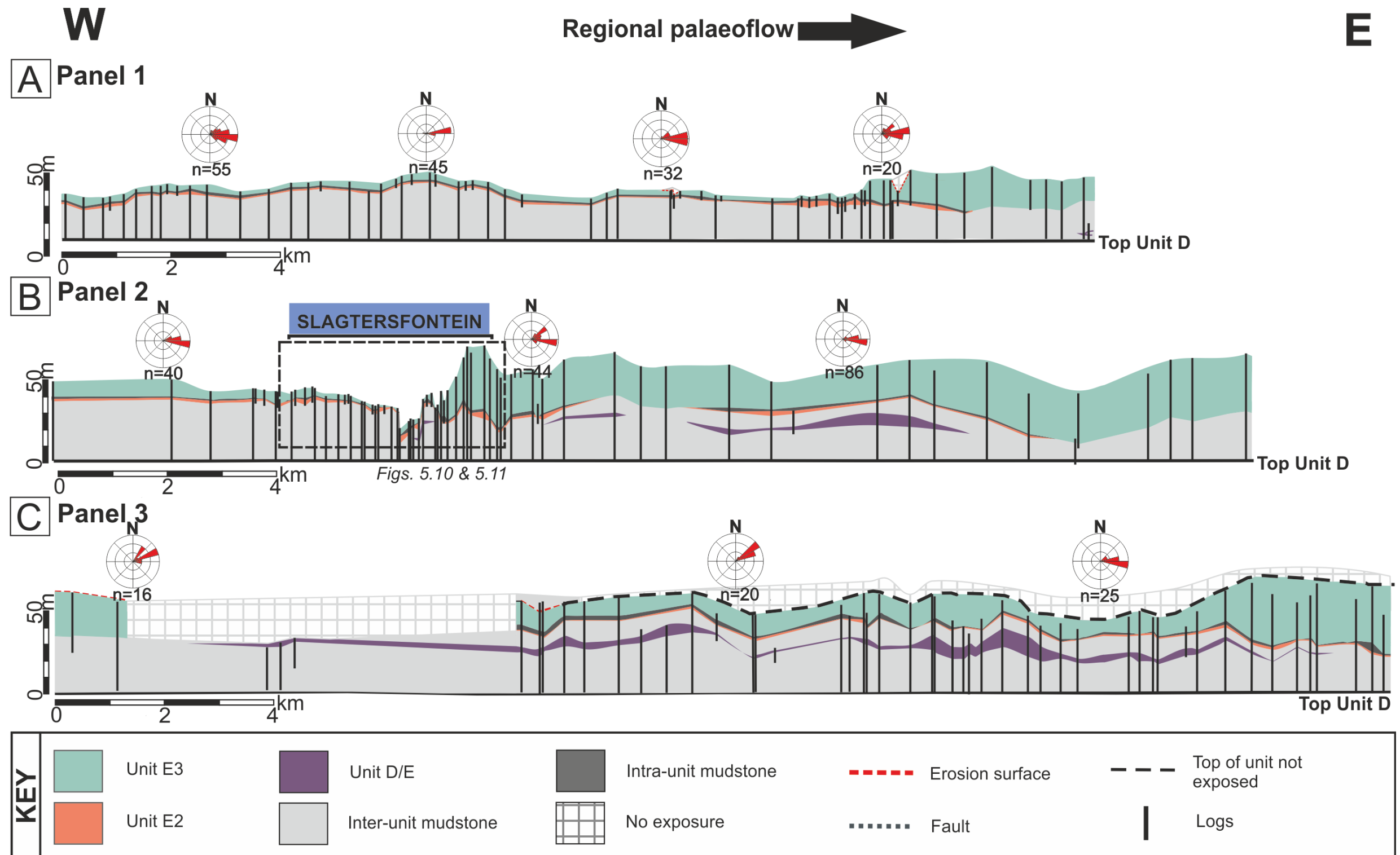
## 5.6 Architectural elements

The stratigraphic context of Units D/E and E has been well established (Figueiredo et al., 2010; Flint et al., 2011; van der Merwe et al., 2014; Spsychala et al., 2015). Five broad environments of deposition are identified based on the occurrence of constituent facies and facies groups, mapped geometries, palaeogeographic context, and utilizing the depositional environment interpretations of previous studies in the Fort Brown Formation (Hodgson, 2009; Pr lat et al., 2009; Hodgson et al., 2011; Kane and Hodgson, 2011; Brunt et al., 2013a, 2013b; Morris et al., 2014; Spsychala et al., 2015):

- 1) External levees (Piper and Deptuck, 1997; Piper et al., 1999; Deptuck et al., 2007; Kane et al., 2007, 2009a, 2010; Kane and Hodgson 2011; Morris et al., 2014): These deposits are dominated by thin-bedded siltstone and sandstone, and structured sandstone, with high proportions of current ripple and climbing ripple laminated beds with consistent palaeocurrent directions (Fig. 5.5F). Locally, chaotic deposits form where levees have collapsed. External levees have been mapped for up to 10 km away from their genetically-related channels, which are not identified within this study. Down-dip, packages can be laterally continuous for several kilometres and change in thickness and facies. Typically, successions fine- and thin-upwards due to decreasing overspill during levee construction (e.g., Hiscott et al., 1997; Peakall et al., 2000; Kane and Hodgson, 2011). The tabular geometry, lateral continuity and consistent palaeocurrent direction, characterise these successions as external levees (cf. Kane and Hodgson, 2011).
- 2) Lobe deposits: Lobes are subdivided into transitional sub-environments, lobe axis, lobe off-axis and lobe fringe, based on decreasing sand content and decreasing degree of bed amalgamation (Pr lat et al., 2009; Pr lat and Hodgson, 2013). Lobe axis deposits primarily comprise thick-bedded, amalgamated structureless sandstone (Fig. 5.5A), and represent deposition of high-energy sediment-laden turbidity currents. Lobe off-axis deposits comprise stratified successions of medium-bedded, structured sandstones with more tractional structures (Fig. 5.5B) formed by deposition from comparatively lower energy currents. Lobe fringe deposits comprise thin-bedded, sandstone and siltstone (Figs 5.5E and 5.5F), deposited from dilute currents and/or silt-rich hybrid beds, resulting from entrainment of fine-grained sediment and mudstone clasts. At kilometre-scale this architectural element is lobate in planform and lens shaped in cross-section (e.g. Pr lat et al., 2009).

- 3) Sediment bypass-dominated zones (van der Merwe et al., 2014; Stevenson et al., 2015): These are characterised by thin deposits of discontinuous structureless and structured sandstone beds (Fig. 5.5B) commonly highly dewatered due to rapid deposition. Composite erosion surfaces and scours are draped by lag deposits of coarser grained material (medium-grained sandstone and mudstone clasts (Fig. 5.5C)), but without major (more than several metres) incision. The large scale geometry of this architectural element is thin and highly discontinuous.
- 4) Spill-over fringes: These tabular, thin-bedded siltstone deposits are extensive over the study area and represent a subdivision of the interbedded sandstone and siltstone facies (type iii). Their distinctive tabular geometry and lateral continuity and monotonous facies over 10s of kilometres distinguishes these deposits from lobe fringes which can be traced laterally over kilometre scale to genetically related sand-rich lobe deposits. The stratigraphic and geographic position of this facies, down-dip of intraslope lobes, supports an interpretation that it represents flows that partially breached up-dip confining topography, causing the flow to be stripped as the fine-grained, upper, low-density portion of flows continued down-dip (into the study area) (Sinclair and Tomasso, 2002). Coarser grained portions of flows are ponded up-dip in intraslope accommodation, as demonstrated by Sychala et al. (2015). This facies is similar in appearance to lobe fringe deposits, but is spatially disconnected from its genetically-related lobe axis deposits.
- 5) Regional mudstone (siltstone and claystone) drapes (Fig. 5.5H): These are extensive and laterally continuous (10s to 100 km) hemipelagic mudstones, present between all units and subunits, aiding correlation.

## 5.7 Correlation panels



**Figure 5.6** Regional correlation panels of Unit D/E and subunits E2 and E3. Panels positioned north (top) to south (base). Southern panel (panel 4) shown on Figure 5.7 with facies associations, consisting of E3 with two small outcrops of Unit E2, in the up-dip area. Relative spatial positions shown in fence diagram (Fig. 5.8). More detailed panel of Slagtersfontein CLTZ shown in detailed panels (Figs 5.10 and 5.11). Rose diagrams show palaeocurrent directions from ripples, grooves and flutes throughout all units.

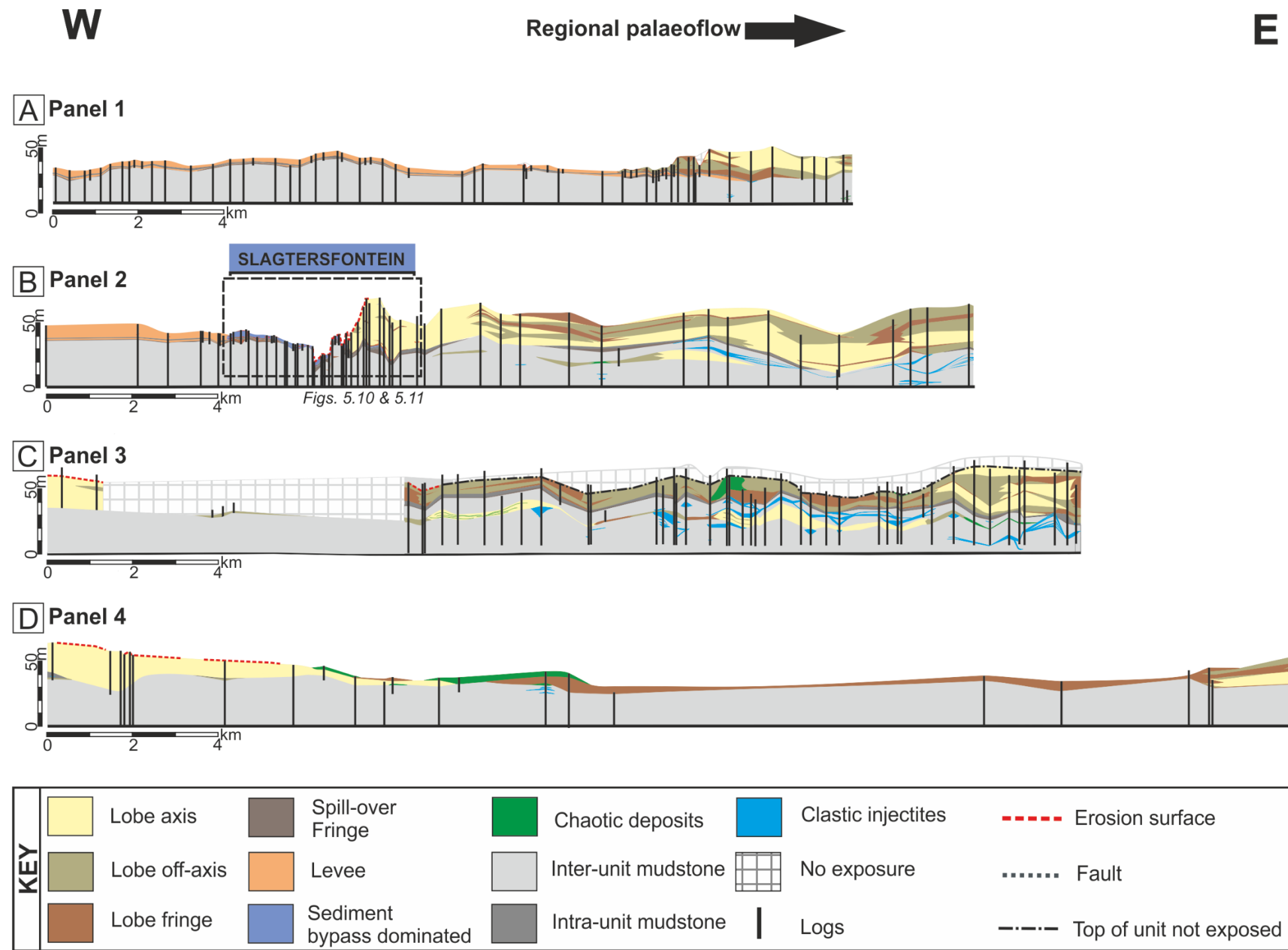
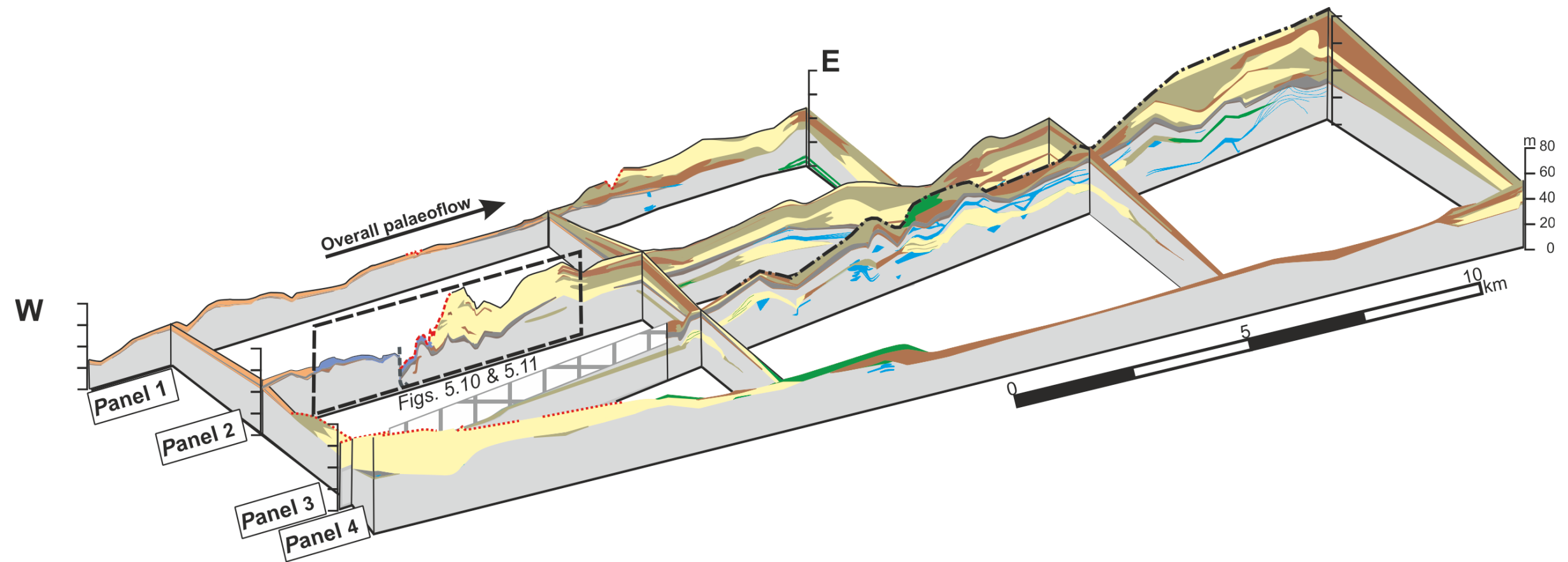
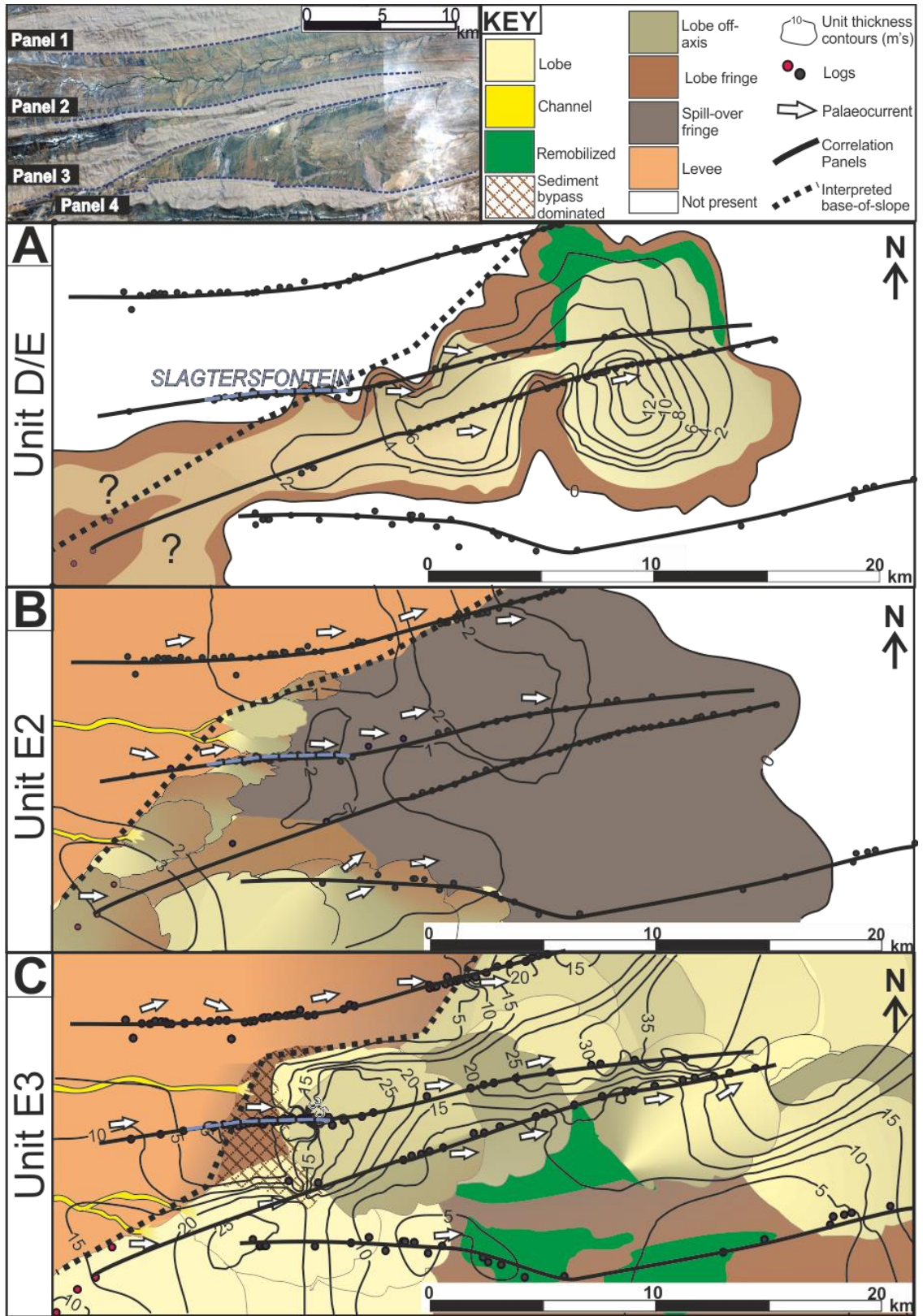


Figure 5.7 Regional correlation panels showing facies associations of Unit D/E and subunits E2 and E3. For Unit divisions of panels A, B and C see Figure 5.6. For logs and more detailed panels, see Appendix B.2-5.



**Figure 5.8** Fence diagram showing 3D architecture and facies associations of Units D/E, E2 and E3. For geographic positions of outcrop belts see Figure 5.3B. For unit divisions see Figure 5.6. For key see Figure 5.7.



**Figure 5.9** Combined thickness isopach maps and gross depositional environment reconstructions for (A) Unit D/E, (B) Subunit E2 and (C) Subunit E3. Contours indicate thickness of unit in metres, contour spacing at 2 m for D/E, 1 m for E2 and 5 m for E3. Black circles indicate locations of data from logged sections shown on panels (Figs 5.6 and 5.7), red circles indicate data from logs presented in Appendix A

and B2-5. White arrows indicate average palaeocurrent direction. Geographic area covered is the same as that shown in Figure 5.3B, presented in palinspastically restored positions. Mapped thickness distributions were created by fitting a surface to thickness values extracted from the logged sections. The surfacing operation was conducted in ArcGIS using the simple kriging tool within the Geostatistical Wizard (<http://resources.arcgis.com/en/home/>). Output maps are extended to the extremities of the input data by the surfacing algorithm, which creates rectangular maps that may extend beyond the edge of the input data. Additional modifications were made to subunit E3 surfaces to account for minimum values of the down-dip logged sections along panel 3. Channel and lobe boundaries are not precise locations and are interpreted from thickness trends and palaeocurrent directions. Palaeogeographic maps are based on the distribution of sedimentary facies and architectural elements.

### 5.7.1 Unit D/E

Unit D/E is a discontinuous unit, up to 12 m thick and present within the regional D-E mudstone which varies in thickness (10-50 m) (Fig. 5.6). Throughout the study area, Unit D/E has a sharp base and top, and palaeocurrents towards the E/ENE (Fig. 5.9A). In the north of the study area (panel 1; Figs 5.7A, 5.8 and 5.9A), the unit consists of a single <1 m thick debrite. In the central area (panel 2; Figs 5.7B, 5.7C, 5.8 and 5.9A), Unit D/E is discontinuous around Slagtersfontein, and then thickens south (panel 3) and east from a few cm to 12 m, transitioning from lobe fringe and off-axis to lobe axis. In an intervening area along panel 3 (Figs 5.7C, 5.8 and 5.9), the Unit abruptly thins and fines to <1 m of siltstone. In this interval, and where Unit D/E thins and pinches out eastward it is associated with numerous clastic injectites (cf. Cobain et al., 2015) (Figs 5.7B, 5.7C and 5.8). Unit D/E also thins and fines abruptly southward (panel 4; Figs 5.7D, 5.8 and 5.9A).

The sharp base and top, with no evidence of erosion, indicate abrupt initiation and cessation of sand supply. The comparatively abrupt southward transition over 3 km from sandstone through thin-bedded siltstone to pinchout (Fig. 5.9A) suggests topographic confinement (Smith, 2004a; Sychala et al., 2017). The northward transition is more gradual (Fig. 5.9A) and is interpreted as unconfined. The facies distribution, elongate geometry and palaeogeographic context are consistent with weakly confined lobes that intercalate with subtle ( $< 1^\circ$ ) topography (Smith, 2004a; Sychala et al., 2017). The abrupt changes in thickness suggest deposition over irregular seabed topography. The location of the feeder channel is poorly constrained due to exposure limitations but is interpreted to be out of the study area towards the southwest based on the palaeocurrent and thickness trends (Fig. 5.9A).

### 5.7.2 *Subunit E1*

The pinch out of E1 (Fig. 5.2) occurs up-dip to the west of the study area (Figueiredo et al., 2010), and does not feature as part of this work.

### 5.7.3 *Subunit E2*

In the north (panel 1; Figs 5.6A and 5.7A), E2 comprises 0.5-1 m of spill-over fringe deposits overlain by 2-3 m of external levee deposits for 14 km down-dip. Over the following 2 km down-dip, the unit thickens to 5-6 m, with localised contorted strata (Figs 5.6A, 5.7A and 5.8). Down-dip, E2 pinches out or is incised by E3. In the up-dip part of panel 2 (Fig. 5.6B and 5.7B), E2 similarly comprises spill-over fringe deposits overlain by external levee deposits. Down-dip in the Slagtersfontein area, E2 coarsens and consists of structured and structureless sandstone, which thicken and thin abruptly (0-3 m) over metre-scale distances due to basal scouring and onlap on to underlying topography, and is overlain by thin (<15 cm) silt-rich hybrid beds, interpreted as lobe fringe deposits (Figs 5.7B, 5.8 and 5.9). Two kilometres farther down-dip, in an area where the underlying D-E mudstone is thinner (Figs 5.6B, 5.7B, 5.8 and 5.9), E2 abruptly fines to thin-bedded, spill-over fringe deposits. Continuing down-dip, E2 thins from 5 to 1 m and maintains this thickness for a further 12 kilometres until it thins or is eroded out in the east. For 4 kilometres up-dip in the southerly panels (Fig. 5.6C, 5.7C and 5.7D), E2 comprises a single 1-2 m bed of structureless sandstone with rip-up clasts, that abruptly pinches out down-dip, with numerous associated clastic injectites.

The external levee deposits in the northwest of the study area (Figs 5.7A, 5.7B and 5.8) are likely related to confined channels in the subcrop to the north (Fig. 5.9B). The deposits at Slagtersfontein (panel 2), and to the south (panels 3 and 4), are interpreted as lobe fringes. The abrupt sand-prone pinch outs of E2 in the south (Figs 5.6C, 5.7C and 5.7D) follow a similar pattern to the underlying Unit D/E suggesting topographic confinement (Fig. 5.9B). The sand-prone pinch out and observed basal scouring and thickness changes in the Slagtersfontein study area are discussed further in the detailed section below (Figs 5.10 and 5.11).

### 5.7.4 *Subunit E3*

A thin package (<0.5 m) of spill-over fringe deposits is present at the base of E3 where there is limited overlying erosion. In the north this package is overlain by external levee deposits (2-5



m thick) for 14 km down-dip. These transition in to 2-3 m of thin-bedded and silt-rich hybrid bed, lobe fringe deposits, and medium-bedded structured and structureless sandstone lobe off-axis deposits. E3 then abruptly thickens into 20 m of thickly-bedded sand-rich lobe axis and off-axis deposits and maintains a similar thickness and facies down-dip (Figs 5.6A, 5.7A, 5.8 and 5.9C).

The up-dip 4 kilometres of E3 of panel 2 (Figs 5.6B and 5.7B) consists of external levee facies that thin basinward from 10 to 4 m. Down-dip at Slagtersfontein (Figs 5.3, 5.6B and 5.7B), the external levee is truncated by a composite erosion surface overlain by bypass-dominated facies. Further down-dip, E3 thickens abruptly (20 cm to >4 m) over 40 m, and for a further 700 m down-dip comprises 1-5 m of lobe axis sandstone with a scoured base and top and common internal soft-sediment deformation. Here, the base of E3 cuts down several metres through the E2-E3 intra-unit mudstone, and locally removes E2 over outcrop lengths of metres to 10s of metres (Figs 5.6B, 5.7B and 5.9C). The top surface of E3 is cut by a bypass assemblage of 1-3 m long scours, mantled by mudstone clasts and/or draped with thin siltstone beds. Farther down-dip, E3 thickens abruptly to 19 m over 200 m (a rate of 9 cm/m), and is dominated by lobe axis deposits and sand-rich hybrid beds. Two hundred metres farther down-dip the unit reaches 40 m thick, with truncation of basal beds (Fig. 5.7B). E3 remains 37-39 m thick, and then thins to 18 m over 1 kilometre with thick axial lobe deposits and few hybrid beds (Figs 5.7B and 5.9C). E3 continues to thicken and thin (between 16 and 37 m) farther basinward, with an overall transition from lobe axis to lobe off-axis and lobe fringe deposits (Figs 5.6B, 5.7B, 5.8 and 5.9C).

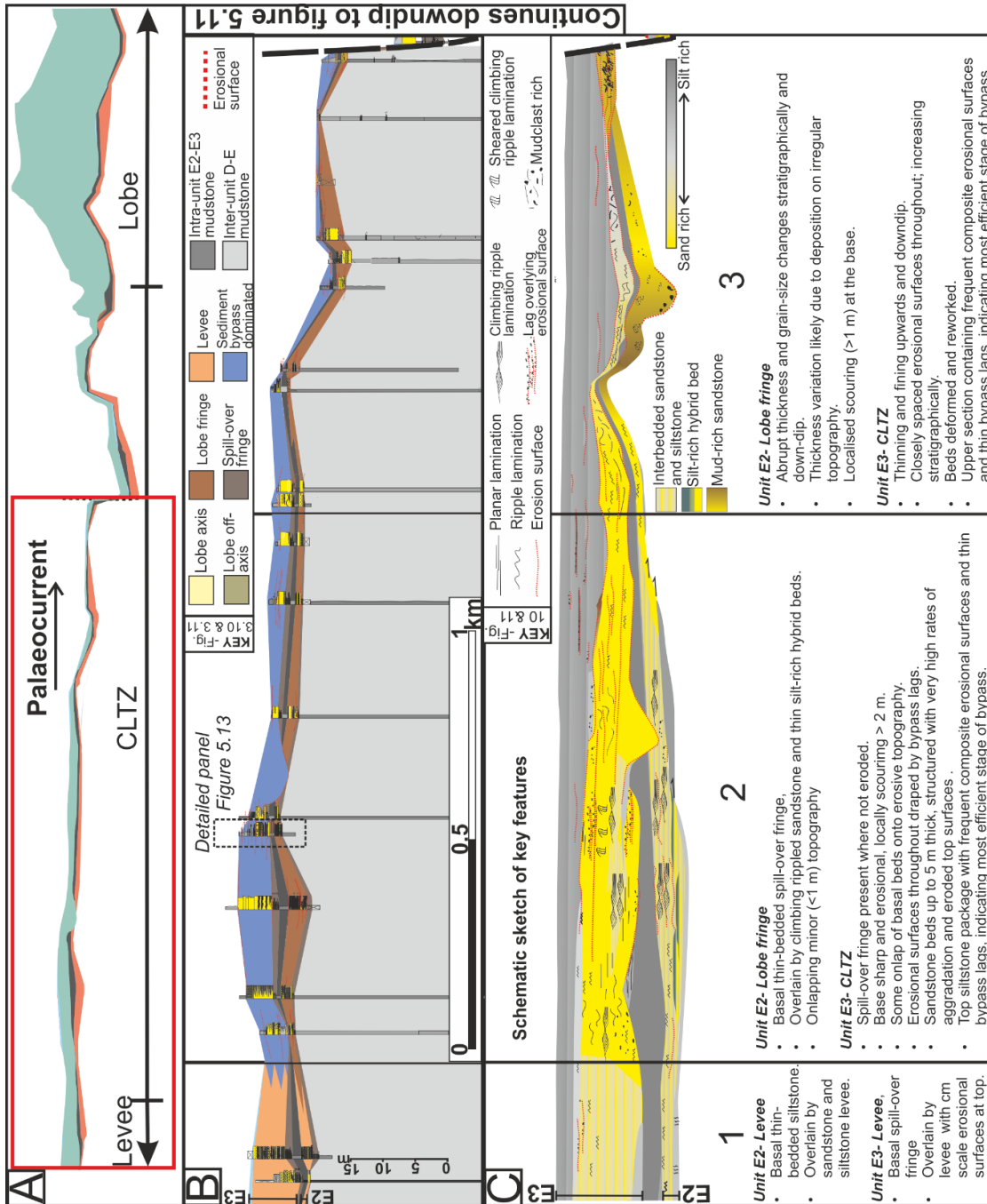
Across strike to the south (panels 3 and 4; Figs 5.6C, 5.7C and 5.7D) up-dip E3 comprises 22-35 m of thick-bedded amalgamated lobe axis sandstones with a sharp base and top to the unit. Locally, a scoured top surface is marked by >10 m long and >4 m wide megafutes with superimposed ripple lamination (Figs 5.6C and 5.7C). Down-dip, beyond 7 kilometres of no exposure, E3 thins from 15 to 6.5 m over 1 kilometre, comprising lobe off-axis sandstones and silt-rich hybrid bed prone lobe fringe deposits. Here, the top surface is scoured, with erosion surfaces mantled by mudstone clasts. Down-dip of this area, the upper part of E3 is not preserved due to present day fluvial erosion. Thicknesses are therefore minimum values (Figs 5.6C and 5.7C). For 11.5 kilometres, E3 is at least 7-14 m thick, comprising lobe off-axis and fringe deposits, with localised contorted, chaotic and disaggregated bedding (Figs 5.7C and 5.8). For the remaining 5.5 kilometres of exposure, E3 thickens to 37 m, dominated by lobe

axis amalgamated sandstone (Figs 5.7C and 5.8) with minor off-axis and fringe deposits. In the far south (panel 4), after initial thick axial deposits, E3 thins to 4 m over 9 kilometres down-dip (Figs 5.7D, 5.8 and 5.9) followed by an abrupt change to chaotic deposits and lobe fringe siltstone for 18 kilometres. Distally, deposits thicken and coarsen abruptly into 15 m of lobe off-axis, lobe axis and minor thin-bedded fringe material (Figs 5.7D, 5.8 and 5.9).

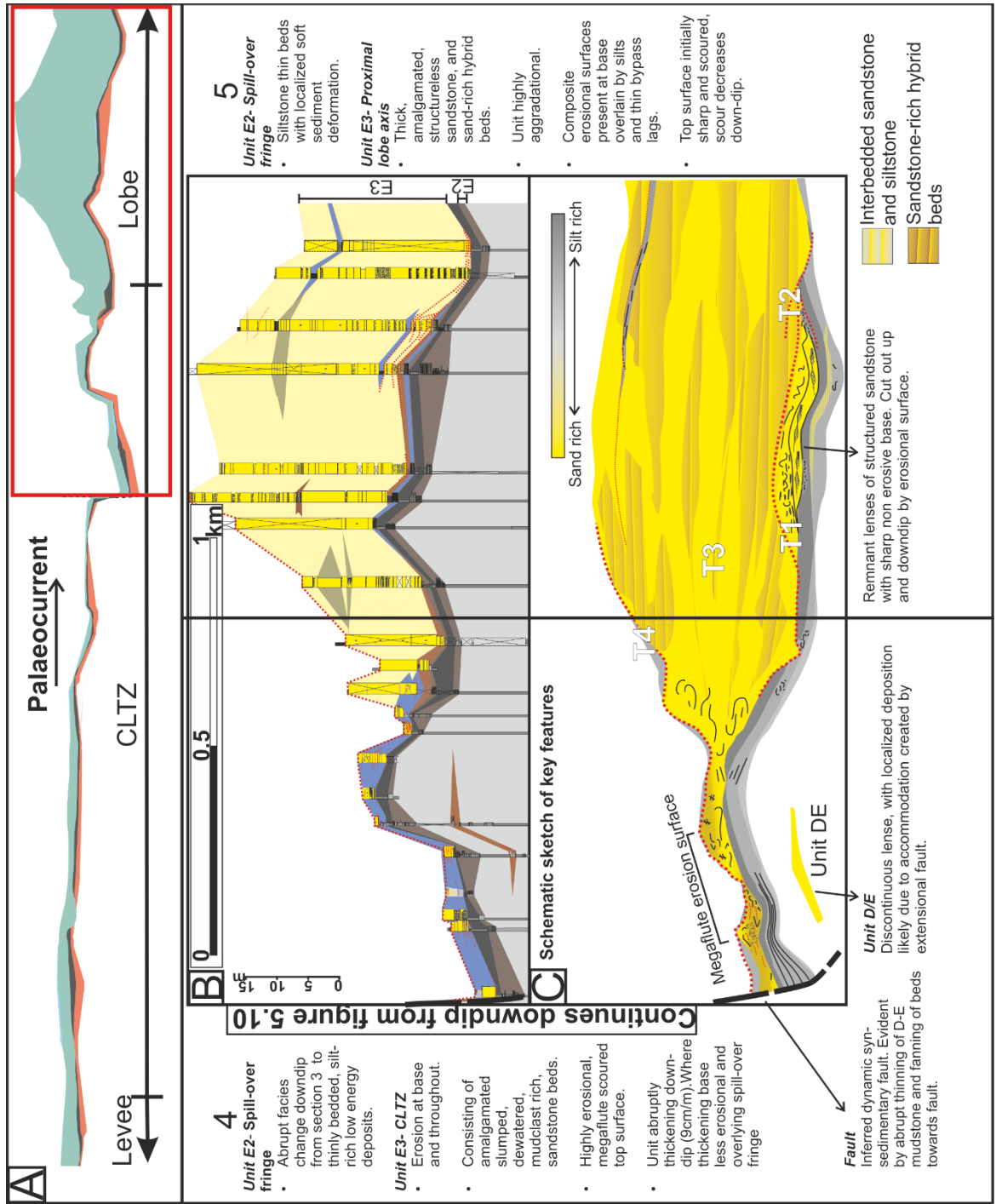
External levee deposits in the northwest of the study area likely confine channels in the subcrop. The sediment bypass-dominated zone is restricted to the Slagtersfontein study area (Figs 5.7B, 5.8 and 5.9) with a minor component in up-dip panels 3 and 4. Slagtersfontein is discussed in more detail below (Figs 5.10, 5.11 and 5.12). In the south, the thinning and pinch out of E3 down-dip suggests a similar pattern of intrabasinal confinement recognised in the underlying units D/E and E2 (Figs 5.8 and 5.9) indicating the presence of a broadly north-facing intrabasinal slope. Lobe fringe deposits are silt-rich hybrid bed prone lateral to the interpreted lobe axis (panel 1, proximal lobe deposits, panel 3, down-dip of an area of no exposure). In more distal areas these become more thin-bed dominated (eastern areas of panels 2, 3, and 4).

## **5.8 Slagtersfontein detailed section**

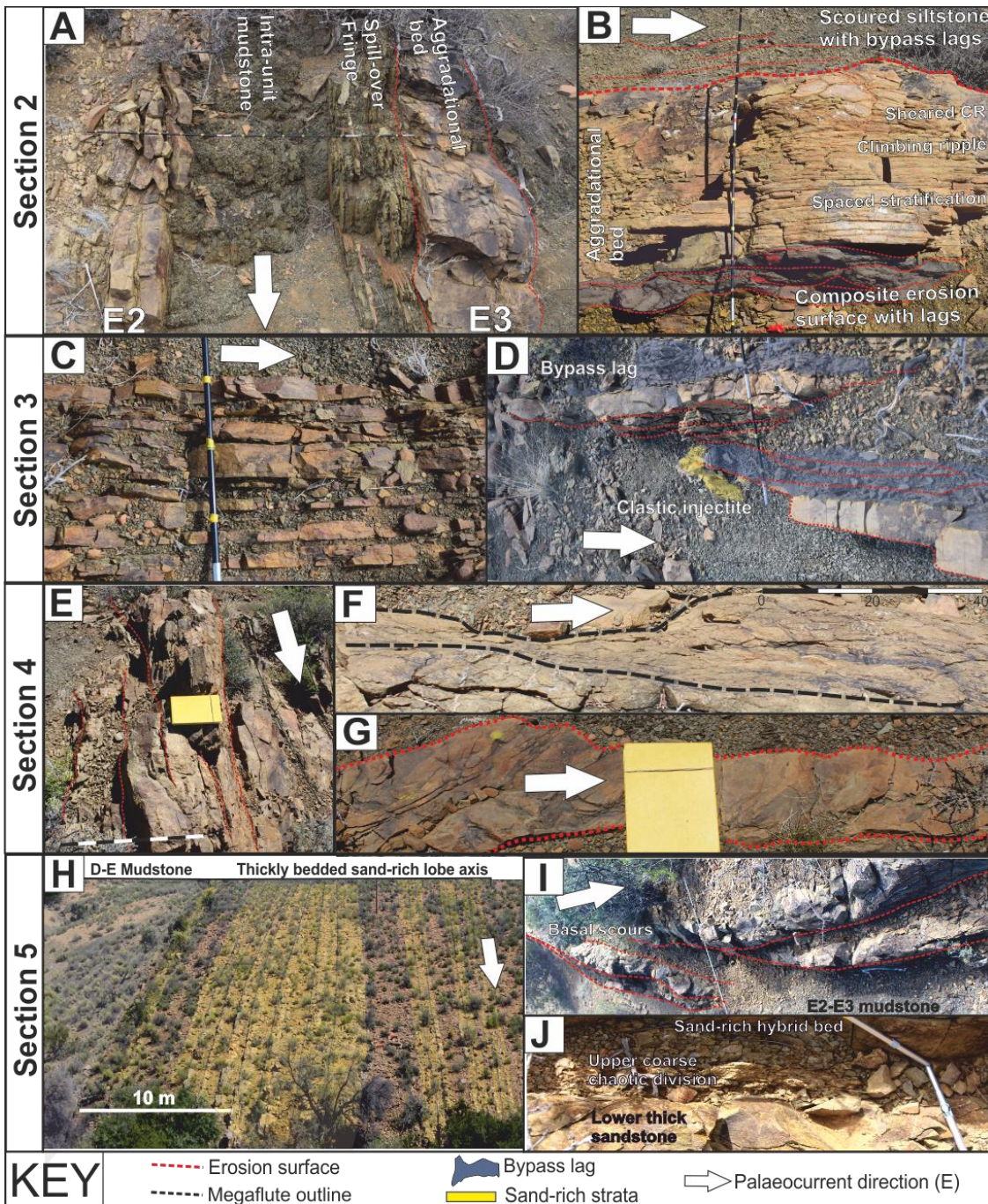
The sedimentology and depositional architecture of subunits E2 and E3 are considered in more detail in the Slagtersfontein area as they change abruptly in facies and character down-dip. The Slagtersfontein area is split into 5 sections (Section 1 up-dip to Section 5 down-dip) for description purposes (Figs 5.10, 5.11 and 5.12), which are supported by closely spaced logged sections measured at mm resolution (Fig. 5.13). The near-continuous presence of the underlying E2 and the E2-E3 mudstone in this area (Figs 5.10 and 5.11) suggests there are no deep scour- or channel-fills of E3 age.



**Figure 5.10** Slagtersfontein detailed section, location shown on figure 5.6, 5.7 and 5.8. Up-dip area of Slagtersfontein panel, divided into sections 1-3 for description purposes. Deposits transition from levee (section 1) to sediment bypass dominated zone (sections 2 and 3), figure 5.11 continues down-dip showing sections 4 and 5. (A) Simplified panel section across whole Slagtersfontein study area, highlighting the focus of this figure. Colours indicate subunits E2 and E3 separated by the E2-E3 intra-unit mudstone. (B) Panel showing logged sections of E2 and E3, datumed on Top Unit D. For larger regional panel 2, see figures 5.7 and 5.8. Logs and log key are in Appendix B2-5. (C) Schematic sketch of key features in subunits E2 and E3 across section, showing down-dip changes in thickness, facies and sedimentary structures.



**Figure 5.11** Down-dip area of Slagtersfontein panel, continuing from Figure 5.10, divided into sections 4-5 for description purposes. Deposits transition from thin, dewatered, scoured and reworked sandstone (section 4) to abruptly thickening lobe deposits (section 5). (A) Simplified panel section across whole Slagtersfontein study area, highlighting the focus of this figure. Colours indicate sub-units E2 and E3 separated by the E2-E3 intra-unit mudstone. (B) Panel showing logged sections of E2 and E3, and localised deposition of Unit D/E. Datum for panel is Top Unit D. (C) Schematic sketch of key features in subunits E2 and E3 showing down-dip changes in thickness, facies and sedimentary structures. T1- T4 refer to sequence of deposition shown in Figure 5.15. For key see Figure 5.10.



**Figure 5.12** Representative photographs of Unit E3 over sections 2 to 5 of the Slagtersfontein CLTZ. (A) Basal spill-over fringe deposits and aggradational sandstone bed. (B) Composite erosional surfaces, aggradational sandstone bed with scoured top and overlying siltstone and lag deposits. (C) Rippled thin sandstone beds. (D) Discontinuous lenticular sandstone beds cut by erosional surfaces and draped by lags. (E) Highly dewatered sandstone beds with erosional surfaces throughout. (F) Megafault scour at top of unit, eroding dewatered sandstone. (G) Thin eroded sandstone bed, constituting the entire coarse component of E3. (H) Thick amalgamated sandstone beds and sand-rich hybrid beds of E3 proximal lobes. (I) Discontinuous lenticular sandstone beds, cut by erosional surfaces and draped by lags, at the base of E3 lobe deposits. (J) Sand-rich hybrid bed. Scales: logging pole with 10 cm divisions, notebook 15 cm in length.

### 5.8.1 Section 1

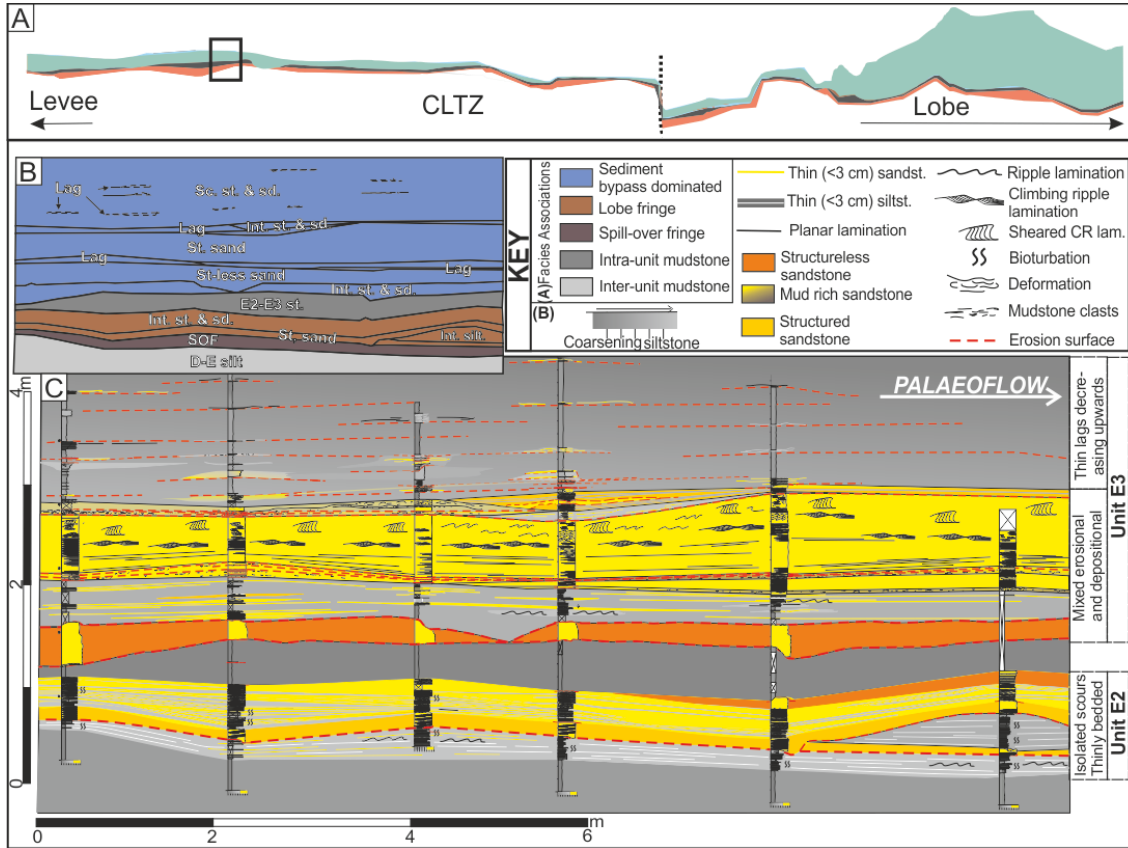
Subunit E2 comprises spill-over fringe (0.5 m) overlain by external levee deposits (<3 m). E3 comprises similar facies with thicker external levee deposits (<5 m) overlain by a thin-bedded siltstone package (up to 0.5 m) containing subtle erosion surfaces and thin (cm-scale) mudstone clast conglomerate lags (bypass-dominated facies) (Fig. 5.10).

### 5.8.2 Section 2

E2 comprises spill-over fringe deposits (0.4 m thick) overlain by lobe fringe deposits 2 m thick (Figs 5.10 and 5.11). Onlap of basal beds onto underlying mudstones suggests minor (10s of cm to a few metres) seabed topography. E3 includes a basal package of thin-bedded spill-over fringe, abruptly overlain by lenticular, laminated sandstone cut by numerous erosion surfaces that are mantled by cm-scale mudstone clast conglomerates (bypass-dominated facies) (Figs 5.10, 5.12A and 5.12B). Structured sandstone beds include planar lamination, ripple and climbing ripple lamination, and dewatering structures. Locally, E3 erodes into E2 (Fig. 5.10).

Figure 5.13 presents a 20 m long section, which demonstrates detailed bed-scale variations within Section 2. E2 spill-over fringe beds are overlain erosionally by a <0.3 m thick climbing ripple laminated sandstone bed. These are subsequently overlain by thin-bedded siltstones containing multiple erosion surfaces and climbing ripple laminated sandstone beds. The E2 to E3 intra-unit mudstone (0.8 m thick) is removed by irregular erosion surfaces, infilled by structureless medium-grained sandstone, cut by a further erosion surface overlain by thin-bedded siltstones and climbing ripple laminated sandstones. These beds are incised by numerous small (1-20 cm) erosion surfaces that coalesce to form a larger composite surface, draped by thin sandstone beds and mudstone clast conglomerate. A distinctive overlying 1-2 m thick sandstone bed passes from structureless through spaced stratification (following Hiscott, 1994) to steepening upward stoss-side preserved climbing ripple lamination. Climbing ripples are progressively sheared and overturned towards the bed top. Basal structureless and stratified sandstone (spaced stratification) (Fig. 5.12) are interpreted to form under traction carpet conditions (laminar sheared layers; Vrolijk and Southard, 1997) of a rapidly depositing voluminous flow. As flow wanes, sedimentation rates decreases, reducing laminae spacing (Cartigny et al., 2013) and transitioning to climbing ripple laminations (Fig. 5.10) (Sumner et al., 2008). The increasing angle of climb suggests further waning and increasing suspension fall out rate (Jobe et al., 2012). Sheared and overturned ripples indicate rapid aggradation. These

structured sandstone beds, therefore, represent highly aggradational deposits, which are cut by further erosional surfaces, obscuring their depositional morphology and draped by thin lags decreasing in occurrence upwards within laminated siltstone.



**Figure 5.13** (A) Location of section shown in B and C within the CLTZ. Colours indicate subunits E2 and E3 separated by the E2-E3 intra-unit mudstone. (B) Outline of beds over outcrop and coloured with facies association scheme. Abbreviations: Sc. st. and sd.- Scoured siltstone and sandstone, Int. st. & sd.- Interbedded siltstone and sandstone, Lag- Bypass lag, St-less sand- Structureless sandstone, Int. st. & sd.- Interbedded siltstone and sandstone, E2-E3 st.- E2- E3 intra-unit mudstone, Int. silt.- Interbedded siltstone, SOF- Spill-over fringe, D-E silt- Unit D-E inter-unit mudstone. (C) Sections logged at mm scale over 20 m outcrop distance, showing bed scale changes in subunits E2 and E3 within the CLTZ. This key area shows features consistent with a fluctuation of high and low energy deposits throughout E3, with a layering of medium sandstone, low energy thin-beds, composite erosional surface with mudclast lags, thick aggradational beds, and further erosional surface and lag deposits which decrease upwards. For whole Slagtersfontein section see Figures 5.10 and 5.11.

### 5.8.3 Section 3

E2 has an erosional base that removes spill-over fringe deposits (Fig. 5.10). Localised basal scouring is up to 1 m and draped by a fine-grained sandstone, with large (>15 cm long) rounded mudstone clasts. Overlying the erosion surface, E2 thickens and coarsens upward then thins and fines (Fig. 5.10). Down-dip, beds thin and fine and become mudstone clast-rich,

and E2 and E3 amalgamate (Fig. 5.10). E3 is thinner than in the up-dip area (Sections 1 and 2), and gradually thins down-dip through Section 3 from 2.0 to 0.1 m (Fig. 5.10). Beds are <15 cm thick, planar laminated, interbedded sandstone and siltstone (Fig. 5.12C) or slumped and discontinuous with mm-scale mudclasts throughout (Fig. 5.12D). Numerous erosion surfaces lead to highly irregular tops and bases to beds that thicken and thin abruptly (10s of cm) over metre scale outcrop distances. Discontinuity at the base (Fig. 5.10) is due to the infilling of erosional topography and truncation. The absence of significant deposition (>2 m) and more evidence of erosion suggests increased sediment bypass compared to Section 2. Overall, there is a fining- and thinning-upward trend, with sandstone beds at the base of E3, and the number of erosion surfaces increasing upwards, suggesting increased sand bypass through the unit (Fig. 5.10).

#### 5.8.4 Section 4

The D-E mudstone decreases abruptly in thickness from 30 to 11 m over a 60 m outcrop distance (Figs 5.10 and 5.11), and subunits E2 and E3 are offset. Neither the top surface of Unit D nor the overlying Unit F is offset. Where the D-E mudstone thickness decreases Unit D/E is locally present, thinning out down-dip. E2 is locally thicker, with beds thickening and fanning up-dip and deformed in areas. E3 is also locally thicker and deformed. Both E2 and E3 gradually thin down-dip of this area, where the D-E mudstone thickness returns to its up-dip thickness. This area represents the pinch out of sand-prone E2 lobe deposition, comprising only spill-over fringe down-dip (Fig. 5.11). The thickness and dip changes support the presence of a down-dip facing dynamic syn-sedimentary growth fault that soles out within the D-E mudstone. That there is stratigraphic continuity, but thickness changes in all units, suggests that at any one time there was only a minor expression of the fault on the seabed.

Down-dip of this area, E3 comprises medium- to thick-bedded lobe deposits with a scoured base and top surface (Figs 5.12E, 5.12F and 5.12G). The scours on the top surface (1-5 m in length and 0.5-2 m in width), are mantled by cm-scale mudstone clasts and laminated siltstone (Figs 5.11 and 5.12F), interpreted as a lag, and deposits of fine-grained tails of turbidity currents, respectively. The amount of strata removed is unknown, but the bypass assemblage is overlain by fine-grained siltstone that is similar to the background sedimentation (Fig. 5.12G). Sandstone beds are mudstone clast-rich and moderately deformed, with numerous erosion surfaces throughout (Fig. 5.12E), suggesting dewatering during deposition and



reworking by bypassing flows. Down-dip, the sand-prone part of E3 thickens abruptly (9 cm/m) (Fig. 5.11).

#### 5.8.5 Section 5

E2 comprises spill-over fringe. E3 continues to thicken basinward at a rate of 7 cm/m, attaining a maximum thickness of 40 metres (Figs 5.11 and 5.12H). Up-dip in Section 5, basal beds of E3 are erosive, overlain by thin mudstone clast lags (Figs 5.11 and 5.12I). Down-dip, basal erosion decreases, and a package of tabular climbing ripple laminated sandstone beds is preserved (Fig. 5.11). These are removed 700 m basinward, and overlain by discontinuous lenticular mud-rich (matrix and clast) sandstone beds (Fig. 5.11). Overlying this basal package are stratified packages of amalgamated sandstone and sand-rich hybrid beds (Figs 5.11, 5.12H and 5.12J). Sand-rich hybrid bed packages make up a significant proportion (>50%) of these proximal lobe deposits, but are not present down-dip. The abrupt basinward thickening and high sand content is suggestive of rapidly decelerating flows. The erosive features over- and underlying the lobe deposits (Figs 5.11 and 5.12I) are suggestive of deposition in an area of high energy but with temporally fluctuating flow conditions.

### 5.9 Architecture of an exhumed CLTZ

In the Slagtersfontein area, the palaeogeographic context between levee and lobe systems (van der Merwe et al., 2014), and the change from up-dip areas dominated by erosion with widespread evidence for sediment bypass (sections 1-4) to down-dip areas dominated by thick sand-prone lobe deposits (Section 5), support the interpretation of a CLTZ in this area during the evolution of E3. Therefore, this area permits a unique opportunity to document a CLTZ and to assess the criteria for their recognition in the rock record. The base of subunit E3 comprises spill-over fringe deposits (Figs 5.7, 5.9 and 5.10), where not eroded out, which are considered time-equivalent to the sand-rich deposits in the up-dip intraslope lobe complex (Spsychala et al., 2015). This zone is interpreted as sediment bypass-dominated due to minimal amounts of erosion compared to channel systems and limited deposition compared to lobe systems. Subsequently, erosional and depositional elements (*sensu* Mutti and Normark, 1991) in the stratigraphic record are limited in thickness and spatial extent reflecting the dominance of sediment bypass. The assemblage of erosional and depositional elements in Sections 2-4 in subunit E3 are synthesised here.

### 5.9.1 *Erosional elements*

Isolated and composite erosional features are numerous in the form of relatively flat surfaces and concave scours. Scours throughout the Slagtersfontein CLTZ are generally composite >2 m deep features. Larger scale features cut through the E2-E3 intra-unit mudstone and into Unit E2 and are rarely >3 m deep (Figs 5.10 and 5.11). The irregular shaped scours are draped by a combination of lag deposits and thin-bedded siltstone. The amalgamation and 2D view of these features means their morphology cannot be constrained accurately. Scours on top of sandstone beds are 1-5 m in length and up to several m in width (van der Merwe et al., 2014), often display asymmetry with steeper headwalls, and are interpreted as megafutes. They form individual and composite features on large-scale deflation surfaces (Fig. 5.11), interpreted to represent prolonged periods of weakly confined sediment bypass, which extend many kilometres (Fig. 5.7C). The lack of significant incision (>3 m deep) suggests widespread scouring rather than channel development, although the presence of shallow high aspect ratio channels is possible, where flows locally became more confined. The lack of deeper scour features (e.g. Hofstra et al., 2015) suggests flows were not sufficiently concentrated in a single location and temporally fluctuated between deposition, bypass and erosion. The Slagtersfontein CLTZ, although evidently in a fairly axial environment (indicated by the high energy nature of deposits, erosion and scours), is likely lateral to the main position of channel propagation given the presence of external levees and absence of main channel-fills, therefore mega-scours (e.g. Hofstra et al., 2015) may be present out of section.

### 5.9.2 *Depositional elements*

Mudstone clast conglomerates, interpreted as lag deposits, are common throughout the Slagtersfontein CLTZ (Figs 5.10, 5.11 and 5.13). The clasts are likely sourced from the widespread E2-E3 mudstone, with a large range of clast sizes and roundness suggesting different transport distances and/or rheology. Poorly sorted lenses of mudstone and medium-grained sandstones are also interpreted as 'coarse-grained' lag deposits as this grain-size is otherwise exceptionally rare in the Fort Brown Fm. Aggradational beds are recognised in the proximal areas of the CLTZ, with spaced, climbing ripple and sheared climbing ripple lamination. These aggradational beds are present stratigraphically and spatially between coalesced scours and bypass lags (Fig. 5.12), for outcrop lengths up to 20 m, with their original depositional morphology and extent unknown. These beds therefore may represent rapidly depositing sheets from unconfined flows, and/or long wavelength aggradational bedforms

with the latter similar to sediment waves (e.g. Wynn and Stow, 2002; Wynn et al., 2002a, 2002b; Cartigny et al., 2011; Symons et al., 2016). Small-scale slumping and dewatering structures, especially in thick amalgamated sandstone beds, are common throughout the CLTZ (sections 2-5, Figs 5.10 and 5.11), suggesting rapid deposition due to flow deceleration followed by liquefaction whilst flows continued.

Hybrid beds are not generally associated with proximal lobe settings (Haughton et al., 2003, 2009; Hodgson, 2009), but are common immediately down-dip of the CLTZ in the proximal lobe (Section 5). Sand-rich hybrid bed occurrence solely in this location may be a direct result of the CLTZ. As sand-rich, high energy, flows traverse the scoured, mud-rich zone, the down-dip transformation from non-cohesive to more cohesive flow may be driven by incorporation of mud and mudstone clasts via erosion, damping turbulence (Baas and Best, 2002; Amy and Talling, 2006), and producing high-concentration to pseudo-laminar flow conditions (Talling et al., 2004; Ito, 2008; Baas et al., 2011). The sharp contact between the upper and lower division of the hybrid beds suggests the flow had partitioned into cohesive and non-cohesive components. Mudstone clasts present in the tops of the lower division, are aligned with flow, suggesting transport by turbulent mechanisms, with clasts likely supported in the rear of the flow (Hodgson, 2009). The lack of mud suggests finer portions of turbidity currents and less-cohesive, mud-rich debris flows, may have bypassed this axial area and continued onwards to form the silt-rich hybrid beds recognised in lateral lobe fringes. Although not typically associated with proximal lobes in other studies, hybrid bed rich strata have been noted as occurring in highly aggradational phases of fan development, and phases of channel propagation (Haughton et al., 2009).

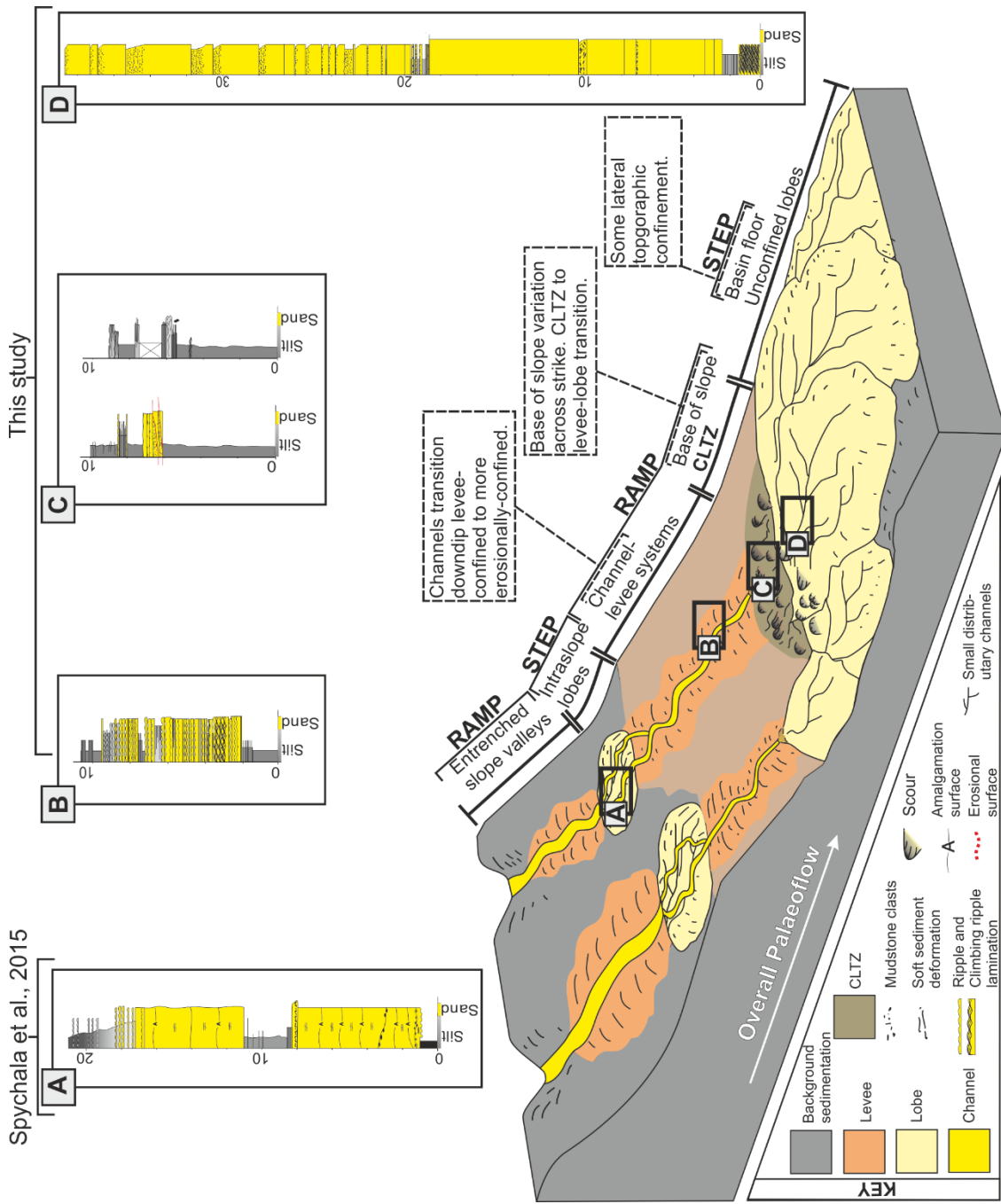
## 5.10 Discussion

### 5.10.1 Evolution of slope profile

Evidence for intraslope lobe complexes (Spychala et al., 2015) and widespread spill-over fringe deposits, shows that E2 and E3 deposition in the study area commenced when flows had healed up-dip slope accommodation and were able to bypass down-dip. The Slagtersfontein CLTZ is therefore interpreted as forming in a base of slope area between a higher gradient 'ramp' (*sensu* Prather, 2003; Prather et al., 2017) and a lower gradient basin-floor 'step' (*sensu* O'Byrne et al., 2004) (Fig. 5.14), with no evidence of further topographic influence to the east, with lobe deposits gradually thinning and pinching out over a further 40 kms (van der Merwe

et al., 2014). The presence of syn-sedimentary faulting supports deposition above an unstable ramp in a base of slope area. Growth faulting due to sediment instability is common in submarine slope settings (Galloway, 1986), and possibly nucleated in this location as a result of differential compaction over the margin of a Unit D sandstone-filled channel complex immediately below. The rate of change in facies and thickness in Slagtersfontein, and presence of the fault, suggests that the change from slope to basin-floor was sharp, and may have formed an abrupt break-in-slope.

Key areas of basinward thickening and abrupt change in facies in Unit D/E, and subunits E2 and E3 is identified in multiple correlation panels in similar locations (Fig. 5.9), suggesting a long lived break-in-slope position. The 10 km distance between panels 2 and 1 marks a key change in facies and architecture across-strike in subunit E3. The facies and thickness changes in the north are gradual with some interfingering of levee and lobe deposits, followed by a gentle thickening of lobes, marking a levee-lobe transition zone. This compares with steeper and/or more incised morphology in the Slagtersfontein area, suggesting a highly variable base of slope physiography across strike (Fig. 5.14).

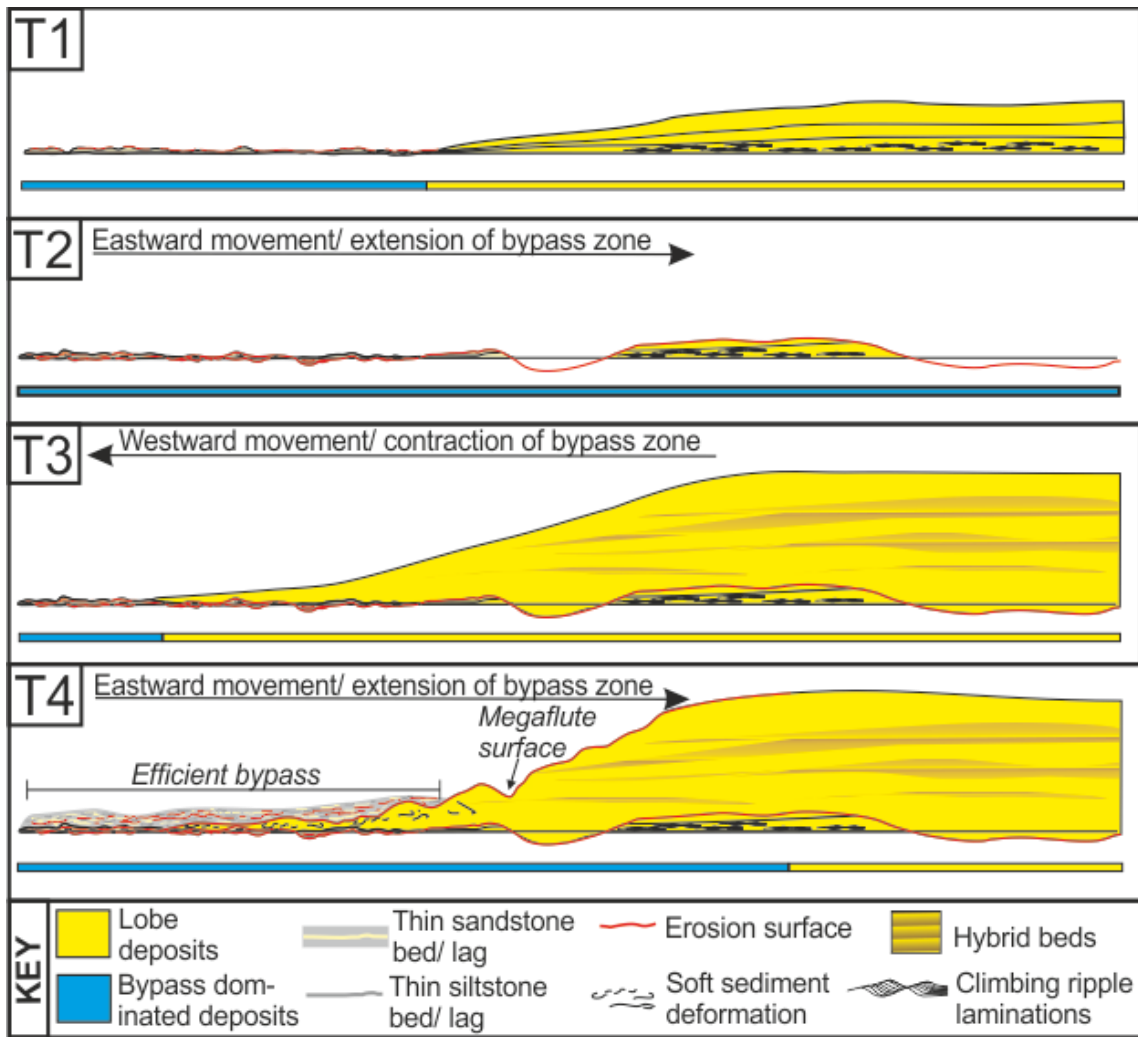


**Figure 5.14** Summary figure of overall stepped-slope profile architecture and related deposits of Unit E. Flows were fed through entrenched slope channels to intraslope lobes, and channel levee systems, to the CLTZ and basin-floor lobes. Logs show typical section through key areas. Logs from outside of the study area modified from van der Merwe et al., 2014.

### *5.10.2 Spatial variability and evolution of the CLTZ*

Across-strike and down-dip variations have been noted throughout the E3 CLTZ. The maximum strike width of the CLTZ measured as the distance between panels 1 and 3, is 11 kilometres (restored). This extends to a maximum of around 14 km in width where the CLTZ scour surfaces extend laterally and are present across the top surface of E3 to the South (panels 3 and 4, Figs 5.7C, 5.7D, 5.8 and 5.9C).

More variation in the character and extent of the CLTZ has been recorded in dip section, illustrated in four time slices (Fig. 5.15). At T1 the CLTZ was approximately 3 km in dip length with a minimum 2 m thick lobe deposit down-dip (Fig. 5.11). Subsequently (T2), the CLTZ lengthened to approximately 4 km, with T1 deposits partially eroded and the area of deposition moving basinward (Fig. 5.11). During T3, the CLTZ shortened to approximately 2 km, with lobe deposition above the composite T2 erosion surface (Fig. 5.11). A final lengthening of the CLTZ (T4) to approximately 5.5 km along this 2D section, but expanding to at least 6 km across strike to the south, resulted in the formation of the youngest scoured surface that accentuates the rate of basinward thickening of the proximal lobe deposits (Fig. 5.11), and creates the most widespread scour surface (Fig. 5.7). The absence of levee deposits under- or overlain by bypass indicators (Fig. 5.10), suggests this is the most up-dip expression of the CLTZ. The CLTZ migration evident at Slagtersfontein reflects the minimum amount of migration in the zone, with evidence of additional fluctuations likely lost due to later erosion, and observations restricted by outcrop constraints across strike.



**Figure 5.15** Sketch of interpreted variations in the CLTZ over the Slagtersfontein section shown in Figures 5.10 and 5.11. T1-T4 show the minimum extent of progressive expansions and contractions of the CLTZ. T1 shows the initial location of bypass and deposition dominated areas with initial deposition of structured sandstone with a minimum thickness of a few metres. T2 shows the eastward movement or extension of the bypass dominated channel-lobe transition zone, with erosion of initial lobe deposits and focus of deposition shifted down-dip. T3 shows the westward movement or contraction of the bypass zone and backfilling of the system, with build-up of sand-rich proximal lobe deposits over bypass surfaces. T4 shows the final stage of CLTZ extension or easterly movement, indicated by efficient sediment bypass in the up-dip area, a large erosional surface cutting into the lobes and a widespread megafault surface which expands down-dip of this area.

#### 5.10.2.1 Allogenic and autogenic control

This study documents a depositional strike variability in the down-dip transition from channel-levee systems to lobe complexes. The dominant controls on the lateral variation within the system are considered to be physiographic changes along the base of slope and variations in flow dynamics through time. The formation of features such as scour fields have been associated with the occurrence of hydraulic jumps, commonly occurring within base of slope areas where changes in gradient and flow confinement lead to flows changing from

supercritical to subcritical (Mutti and Normark, 1987, 1991; Weirich, 1989; Kostic and Parker, 2006; Sumner et al., 2013). Down-dip reacceleration of flows suggests that flows can repeatedly become supercritical across the CLTZ, resulting in multiple hydraulic jumps (Sumner et al., 2013; Dorrell et al., 2016). Incoming flows are more likely to be supercritical where they have traversed areas of steeper gradient. This suggests a higher gradient slope up-dip of Slagtersfontein may have resulted in incoming flows being supercritical, and more likely to undergo hydraulic jump when they reached the base of slope.

Experimental studies have shown that increasing the slope angle up-dip of a break in slope can lengthen the geographical zone in which hydraulic jumps occur (Kostic and Parker, 2006). A larger magnitude break-in-slope will result in greater changes in the level of turbulence at the initial hydraulic jump, creating a greater reduction in flow velocity and increasing scouring (Lee et al., 2002). The slope gradient will vary temporally, for example shallowing through erosion, thus changing these conditions. Flows are more likely to be supercritical in axial locations (e.g. Slagtersfontein) in close proximity to the feeder channel, where they are subject to higher concentrations and velocities. Therefore, the criticality of the incoming flow at a single location will vary temporally with migrations or avulsions in the feeder system. Changes in flow magnitude may also be expected to affect the dip extent of the CLTZ (Fig. 5.15). Flows with larger amounts of suspended sediment will be able to reach greater velocities, shifting the position of the hydraulic jump zone farther down-dip (Kostic and Parker, 2006). Larger amounts of suspended sediment will also increase flow stratification, which has been shown to cause flows to undergo hydraulic jumps at depth averaged Froude numbers lower than 1 (Waltham, 2004; Huang et al., 2009; Sumner et al., 2013; Dorrell et al., 2016). Variations in flow and sediment input may therefore control the locations and spread of hydraulic fluctuations and ultimately the CLTZ location and dimensions.

Temporal evolution within the system (e.g. modifications of slope gradient, flow/deposit interactions) will also influence the size and location of the CLTZ, affecting the flow pathways and sediment routing, leading to different stages of development such as those noted in this study. If system input is stable, channel-levee systems will eventually adjust to the equilibrium profile (Pirmez et al., 2000; Kneller, 2003; Covault et al., 2016). As the system matures and becomes more efficient, a higher proportion of flows with a larger amount of their initial sediment load will reach the base of slope (Hodgson et al., 2016). This may result in a basinward migration of the CLTZ or increase in CLTZ length with deposition tending to occur



further down-dip of the feeder channel-mouth in efficient systems compared to more inefficient systems (Mutti and Normark, 1987). Conversely, periods of channel aggradation (e.g. Covault et al., 2016), may restrict sediment supply down-dip reducing the size of the CLTZ. Therefore, the spatial extent of the CLTZ may relate to phases of higher and lower efficiency in the channel system. Accommodation changes across the slope will also affect the size of flows and the amount of material reaching the base of slope (e.g. Meckel et al., 2002; Smith, 2004b; Hay, 2012; Marini et al., 2015). Up-dip intraslope lobe accommodation (Spychala et al., 2015) restricted the supply of sediment down-dip. The initial coarse-grained deposits (T1) represent the first flows that were able to bypass their coarser component over healed accommodation, down the ramp, and onto the basin-floor. As intraslope accommodation was healed, higher energy flows bypassed down-dip to form thicker and coarser deposits (T3).

#### 5.10.2.2 Flow scale variability within the CLTZ

As well as the large-scale changes in the spatial extent of the CLTZ, variability at the scale of individual flows may contribute to the distribution of features. Overall, the exhumed CLTZ records the interplay of erosional and depositional processes and bedform / sheet-deposit development laterally over metre-scale distances. There are no discrete areas within the stratigraphic expression of the CLTZ of dominantly large-scale erosion (e.g. composite scouring) or deposition (e.g. sediment waves), as suggested in previous models (e.g. Wynn et al., 2002a). Studies of the modern seabed have shown that processes are dynamic, with adjacent scours simultaneously eroding and being filled due to density currents undergoing hydraulic jumps at different spatial locations (Macdonald et al., 2011a; Sumner et al., 2013). As noted previously, submarine density currents can form a region of scattered hydraulic jumps as they undergo the transition from supercritical to subcritical at different points (Sumner et al., 2013; Dorrell et al., 2016) through spatially variable flow-relief interactions (e.g. Groenenberg et al., 2010) and/or through waxing and waning of individual flows (Dorrell et al., 2016). This region of scattered hydraulic jumps would create strong vertical uplift, keeping sediment in suspension (over the CLTZ), delaying abrupt sediment deposition, and creating a field of scours (Wynn et al., 2002a; Dorrell et al., 2016). For flows with low Froude numbers the flow dynamics of successive hydraulic jumps have been shown to maintain basal shear stress and sediment transport across a CLTZ. This enables large-scale deposition to occur immediately downstream of the CLTZ, forming sediment waves and thick, dewatered proximal lobe deposits (Dorrell et al., 2016). However, localised erosion and deposition at individual jumps will lead to small-scale topographic variations on the seabed with subsequent turbidity

currents encountering a more marked change or reversal in slope aspect (Lee et al., 2002). This will result in spatial variations of bed shear stress related to flow-topography interactions (e.g. Agadir basin, Macdonald et al., 2011a). Therefore, over short timescales without the need of CLTZ migration, both erosional and depositional processes are likely to occur within the same zone (Fig. 5.16A), due to fluctuations in flow conditions and interaction with a dynamic seabed topography.

### 5.10.3 Comparison to other CLTZs

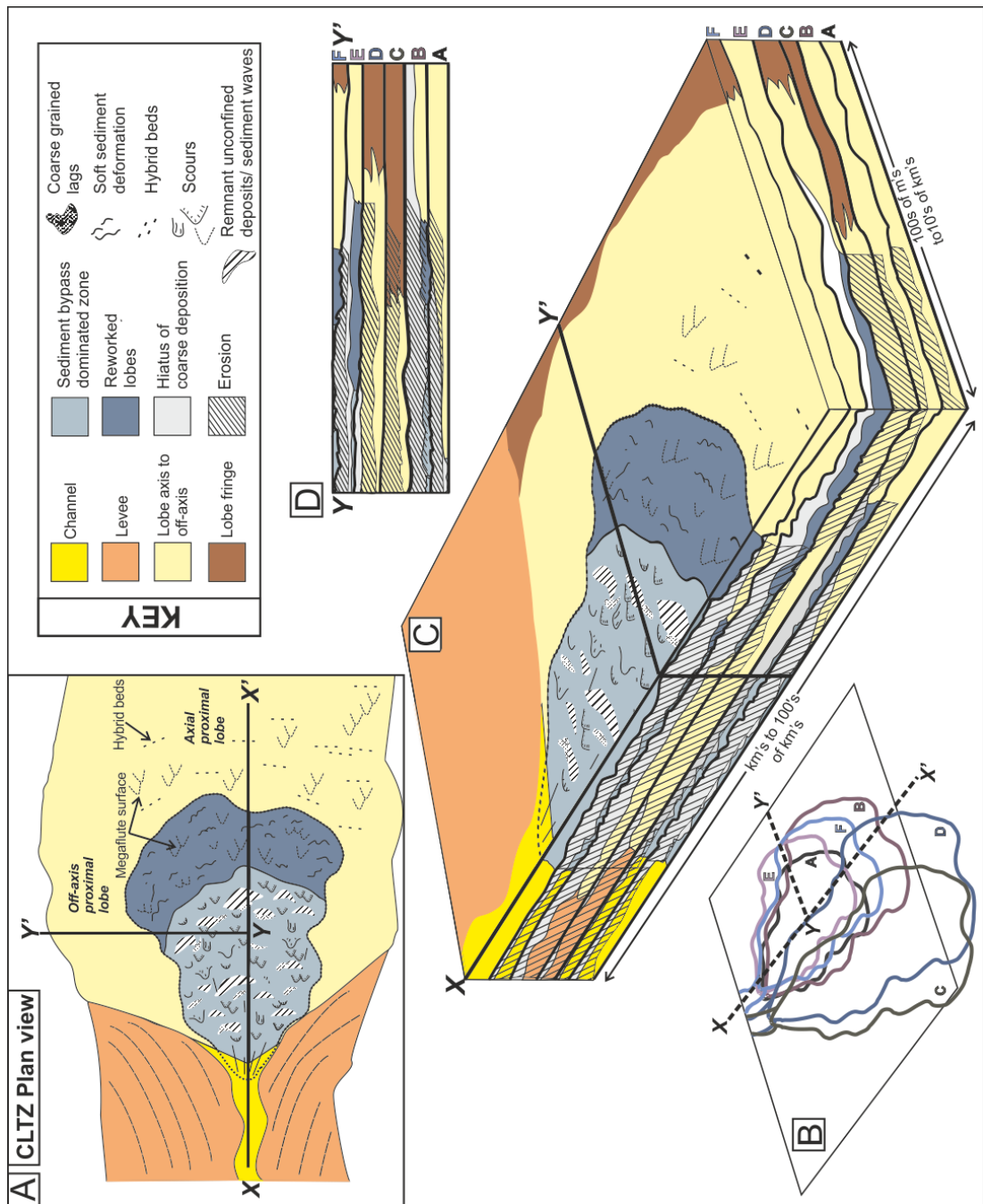
**Table 5.2** CLTZ lengths from modern sea-floor datasets (modified from Wynn et al., 2002).

Location	CLTZ Length (km)	Basin/Fan Area (km <sup>2</sup> )	Reference
<b>Agadir Channel mouth</b>	30-60	>40,000	Wynn et al. (2002a)
<b>Umnak Channel mouth</b>	100–120	48,000	Kenyon and Millington (1995)
<b>Lisbon Canyon mouth</b>	40	25,000	Wynn et al. (2002a)
<b>Rhone Fan</b>	30-40	>60,000	Wynn et al. (2002a) Kenyon et al. (1995)
<b>Valencia Fan</b>	>100	>10,000	Morris et al. (1998) Palanques et al. (1995)
<b>Navy Fan</b>	3-4	560	Normark et al. (1979)
<b>Unit E, Fort Brown Fm. Karoo basin</b>	6	680	This study

Key variables in determining formation of a CLTZ (e.g. the magnitude of slope break and the mud content within the flows) have been considered by other studies (Mutti and Normark, 1987; Wynn et al., 2002a). As demonstrated in this study, these factors can vary spatially from axial to margin flow positions and temporally due to changes in flow dynamics and topographical controls within a single system. Systems on continental margins show CLTZ

lengths of 30-120 kilometres (Kenyon and Millington, 1995; Kenyon et al., 1995; Palanques et al., 1995; Morris et al., 1998; Wynn et al., 2002a). Wynn et al. (2002a) documented a relationship between the length of the CLTZ and the size and type of the turbidite system.

Table 2 (modified from Wynn et al. (2002a) to include this study) indicates that the E3 CLTZ has a length and basin/fan area comparable to the Navy Fan (Normark et al., 1979; Wynn et al., 2002a) but are an order of magnitude smaller than all others (Kenyon and Millington, 1995; Kenyon et al., 1995; Palanques et al., 1995; Morris et al., 1998; Wynn et al., 2002a). A key similarity between E3 and the Navy Fan is their sand-rich nature with all other CLTZs interpreted to have formed in comparatively more silt-rich systems (Wynn et al., 2002a). Flows in mud-rich systems will be more efficient (Mutti, 1992; Gladstone et al., 1998), promoting sediment bypass and the formation of more longitudinally extensive CLTZs (Mutti and Normark, 1987). The greater flow thickness and enhanced stratification of mud-rich flows may also lead to hydraulic jumps only occurring in the lower part of the flow, with the upper flow bypassing the jumps, again enhancing the degree of sediment bypass (Dorrell et al., 2016) and aiding the development of more extensive CLTZs. As well as the sand to mud ratio, the scale of the feeder system is considered to influence the size of CLTZs (Mutti and Normark, 1987), with larger feeder channels associated with larger amounts of suspended sediment and greater flow velocities extending the zone of hydraulic jumps (Kostic and Parker, 2006) to form larger CLTZs (Mutti and Normark, 1987; Wynn et al., 2002a). Another key variable is the gradient change at the base of slope. The magnitude, incoming gradient and length of the slope break will influence flow conditions, and therefore the size of the CLTZ. Although an absolute slope angle cannot be measured from this study, slope breaks from other systems with CLTZ indicate only a small magnitude ( $<1^\circ$ ) change is needed (e.g. Kenyon et al. (1995)  $0.6^\circ$ -  $0.3^\circ$ ).



**Figure 5.16** (A) Plan view of a CLTZ, highlighting the key depositional features and their spatial distribution modified from Wynn et al. (2002). Note area of mixed depositional and erosional features, area of reworked and scoured lobe and axial- and off-axis proximal lobe deposits. Diagram in Wheeler space illustrates movement of a CLTZ over 6 time periods A-F, with (B) showing a plan view outline for each time period and (C) illustrating resultant build-up of deposits and potential erosion over a dip-section (X-X') and a distal strike-section. (D) A further strike-section through a more proximal area of the CLTZ, illustrating deposition and potential erosion. This diagram highlights the composite nature of deposits and erosional surfaces throughout CLTZs and the dynamic expansions, contractions and shifting of the zone that they represent. Overall preservation potential is variable but low, with shifting of the zone often decimating evidence of previous positions. The dark black lines represent periods of migration of the CLTZ. Grey draping units represent a hiatus in sand deposition and may include silt-rich lateral or frontal lobe fringe.

#### 5.10.4 *A generic model for CLTZ stratigraphic architecture*

This outcrop study expands upon the findings of previous studies of exhumed CLTZs (Mutti and Normark, 1987; Wynn et al., 2002a; Pemberton et al., 2016). Most significantly, that CLTZs are not fixed and can expand or contract, and migrate several kilometres. Datasets from modern and active systems are unable to capture this variability through time, and previous outcrop datasets have been limited in palaeogeographic constraint. Moreover, this study demonstrates a juxtaposition of depositional and erosional elements within the CLTZ, rather than separation into discrete zones. This may partially be a factor of the migration of the zone due to allogenic and autogenic controls described above as well as preservation potential, but recent observations of the modern seabed (Macdonald et al., 2011a; Dorrell et al., 2016) and monitoring of active systems (e.g. Hughes Clark et al., 2012) suggest zones of mixed erosional and depositional bedforms may be forming instantaneously.

The areas of most intense reworking (numerous erosional surfaces, scours and bypass lags) across Slagtersfontein are in the up-dip area of the CLTZ, in closest proximity to the mouth of the feeder channel (Figs 5.10 and 5.11). Figure 5.16 demonstrates how stratigraphic surfaces form within a CLTZ, and how minimal deposition and composite erosion surfaces can represent several stages of migration, expansion and contraction of a CLTZ. Distally and laterally away from the axial areas, deposits show less reworking and preserve primary features. The unique preservation of the Slagtersfontein CLTZ, unaffected by later stage progradation and incision of the channel system, suggests this section is either: (i) a sufficiently off-axis transect through the CLTZ and was not cannibalised as the channel propagated (Hodgson et al., 2016); or (ii) underdeveloped and the channel never fully propagated through the zone (Hofstra et al., 2015). Given the evidence for high-energy erosion and deposition, the spatial control on system position, and the absence of overlying external levee deposits, the partially developed model is favoured. An abrupt system shutdown may have been caused by channel avulsion or an abrupt decrease in regional sediment supply, as the upper surface is draped by a system-wide hemipelagic mudstone.

The stratigraphic expression of CLTZs has been poorly constrained to date, with models consisting of composite surfaces separating underlying lobes from overlying channels (Gardner et al., 2003; Pyles et al., 2014), the identification of individual features (Mutti and Normark,

1987), or lenticular bodies infilling scours (Pemberton et al., 2016). This study demonstrates how CLTZs can migrate and change their planform geometry in response to spatially and temporally variable flow dynamics and topographic controls. This results in highly variable and composite stratigraphic surfaces and the juxtaposition of distinctive erosional and depositional elements to form complicated stratigraphic successions. The dynamic nature of a CLTZ documented here, within a tightly constrained regional stratigraphic framework, enables a generic model of CLTZ transfer into the stratigraphic record to be constructed for the first time (Fig. 5.16).

Key characteristics of the model are outlined in Table 5.3. Many of these features have been documented previously in outcrop and modern seabed datasets, indicating that the model can be widely applied, although the specific characteristics will be expressed differently. For example, the Fort Brown Formation has a limited grain-size range (silt to upper fine sand), with lag deposits identified by the presence of lower medium sand. In systems with a wider grain-size, lag deposits would be represented by a wider grain-size range, and be less well sorted. The depths of scours in this study are significantly smaller than others documented in modern CLTZs, this may reflect an off-axis exposure of the CLTZ, or be related to the size of the feeder system. In modern seabed datasets, coarse grained sediment waves orientated perpendicular to flow direction have been identified (e.g. Morris et al. 1998; Wynn et al., 2002b), but these depositional bedforms remain elusive in outcrop record.

This range of features forms a characteristic assemblage, enabling recognition of CLTZ zones at outcrop and possibly sub-surface. It is important to recognize that end-member models are possible, for instance that presented by Pemberton et al. (2016) where sandstones infill a zone of complex scours producing lenticular sand bodies. In comparison, the model presented herein represents a dynamic CLTZ producing a far more spatially variable and heterogeneous sedimentary infill. This model may represent the norm for many CLTZs with lack of spatial variability recognized in other studies likely a factor of outcrop constraints.

Table 5. 3 Key characteristics of CLTZ model with examples from other outcrop and modern seafloor studies.

Characteristic	Description	Further examples
<b>Thin stratigraphic expression</b>	Entire thickness varies from a surface separating lobes from channel-levee to a 5 m stratigraphic expression.	Mutti and Normark, 1987; Gardner et al., 2003; van der Merwe et al., 2014; Hodgson et al., 2016
<b>Amalgamated erosional features</b>	Intense vertical concentration of erosive surfaces, both sub-horizontal, and as discrete scour forms.	Mutti and Normark, 1987; Wynn et al., 2002a; Macdonald et al., 2011a; Ito et al., 2014; Hofstra et al., 2015; Pemberton et al., 2016.
<b>Coarse grained lag deposits</b>	Mudclast horizons and relatively coarse-grained sediment (equating to medium sand in the Fort Brown Fm.) overlying erosive surfaces	Mutti and Normark, 1987; Wynn et al., 2002a; Ito et al., 2014; Stevenson et al., 2015?
<b>Aggradational bedforms including sediment waves</b>	Abundance of structureless sandstone, spaced stratification, climbing ripple and sheared ripple laminations suggesting rapid deposition in the Karoo. Elsewhere cross stratified gravels.	Mutti and Normark, 1987; Vincente Bravo and Robles, 1995; Morris et al., 1998; Wynn et al., 2002; Ito et al., 2014
<b>Soft sediment deformation</b>	Small scale localized slumping and overturned bedding reflecting rapid deposition	Mutti and Normark, 1987; Wynn et al., 2002a.
<b>Thin bedded siltstone packages</b>	Preservation of thin-bedded siltstones representing low-energy flows demonstrate that aggradation was sufficiently rapid to preserve fine-grained deposits.	-
<b>Interfingering with down-dip proximal lobes</b>	Reflecting rapid migration of the CLTZ system in response to controls external to the CLTZ.	Gardner et al., 2003.
<b>Interfingering with up-dip and lateral levee deposits</b>	Reflecting growth and decay of CLTZ and migration of feeder systems	-
<b>Sand-rich hybrid beds within proximal lobes</b>	Significant erosion causes evolution of flows over CLTZ.	-

## 5.11 Conclusions

This study reports the first detailed stratigraphic expression of a long-lived and well-preserved CLTZ at outcrop. Exceptional palaeogeographic context of the system uniquely allows dip and lateral constraints on dimensions through time. With previous studies primarily focused on modern seabed data, the temporal variability in CLTZ evolution documented here allows development of the first dynamic CLTZ model. This model encompasses: lateral variability; sedimentological recognition criteria; expansion, contraction and migrations of the zone; and transfer into the stratigraphic record. Lateral variations across the base of slope include transition from, inter-fingering levee to lobe deposits off-axis in the system, to a bypass-dominated CLTZ in a more proximal area. This variation is considered to be the result of physiographic changes and variations in flow dynamics across the base of slope. Key recognition criteria for CLTZs have been established including: scours, composite erosional surfaces, bypass lags, and remnant rapidly unconfined sheets/ sediment waves. In addition, previously undocumented, abundant sand-rich hybrid beds are recognised in proximal lobe deposits down-dip of the CLTZ. Overall the CLTZ is a dynamic area, with interactions of different parameters including physiography (both in slope gradient and shape), flow magnitude and character, and the position and extent of channel confinement. This results in changes in the dip and strike extent (maximum 14 km in strike and 6 km in dip), and geometry of the CLTZ and creates a distinct area of juxtaposed remnant erosional and depositional features. The consequence of this dynamic character is a complicated and composite transfer of the CLTZ into the stratigraphic record.





## 6 Disconnected submarine lobes, and their role in the evolution of a stepped slope over multiple sea-level cycles

### 6.1 Introduction

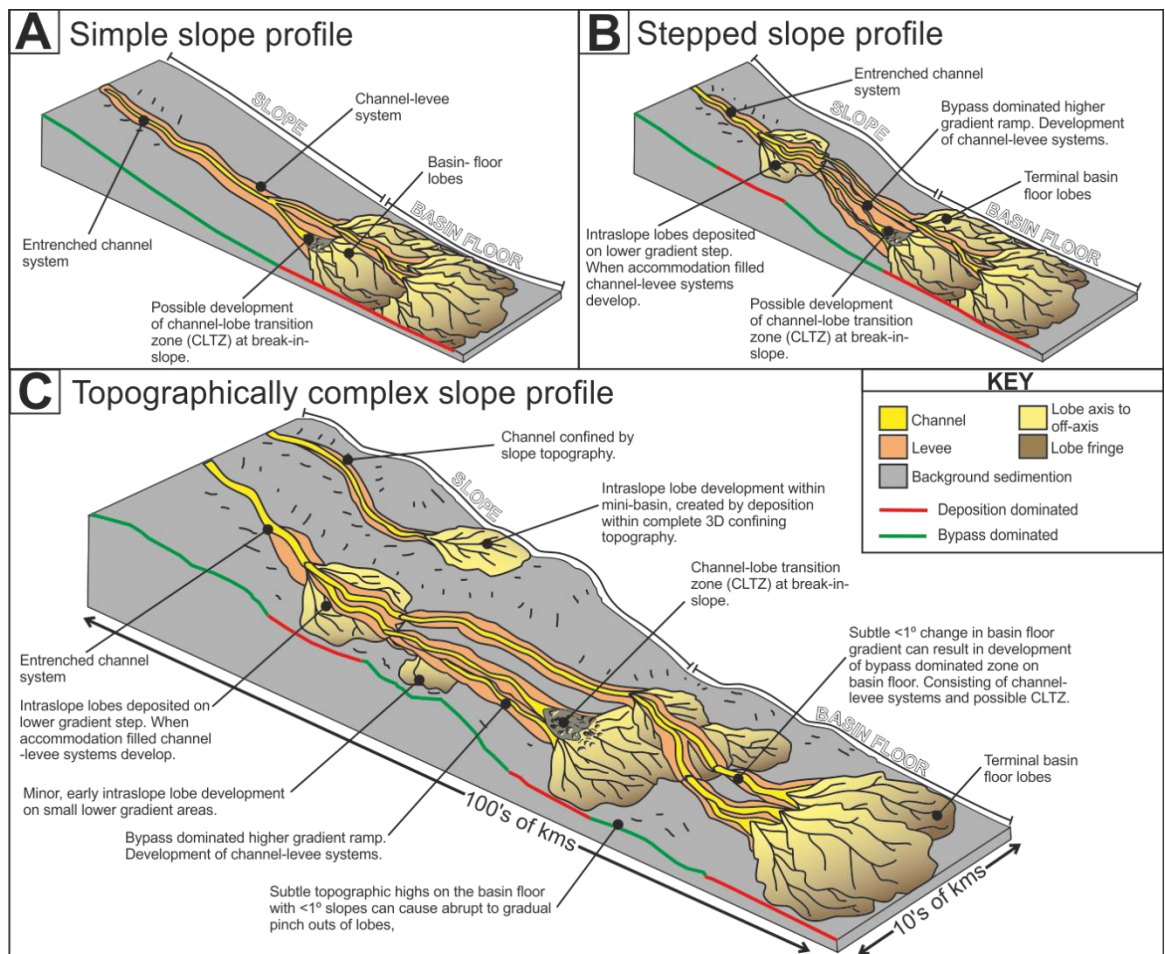
Topographically complex submarine slope types range from ponded mini-basins, which form when 3D confining topography is present and flows are initially almost completely confined to an updip area (e.g. Prather et al., 1998; Badalini et al., 2000; Winkle and Booth, 2000; Sinclair and Tomasso, 2000; Shultz and Hubbard, 2005; Prather et al., 2012a,b, 2017; Sylvester et al., 2015); through tortuous corridors, whereby sediment distribution pathways are rerouted by topographical barriers (e.g. Smith, 2004a; Hay, 2012); to stepped slope profiles, which are more subtle, comprise a series of higher gradient ramps linking lower gradient steps that lack the 3D closure of mini-basins (e.g. O'Byrne et al., 2004; Smith, 2004a; Hay, 2012). Slopes can rarely be fully characterised into topographical end members, and vary spatially and temporally (Fig. 6.1). Distinctive end members with high amplitude seabed morphology and associated major gradient changes have been well documented in seismic datasets (e.g. Prather et al., 1998, 2017; Jackson et al., 2008; Deptuck et al., 2012; Hay, 2012) and in outcrop studies (e.g. Castagnola Fm. (4-12°; Felletti, 2002; Southern et al., 2015; Marini et al., 2016); the Laga Fm. (6-8°; Marini et al., 2015); and the Grès d'Annot Fm. (4-10°; Amy et al., 2007; Salles et al., 2014)).

Whilst the effects of high-gradient stepped slopes on deposition have been examined, it is less clear what impact subtle gradient changes ( $< 1^\circ$ ) have on sediment distribution and flow pathways. Subtle gradient changes have been shown by experimental studies (e.g. Baines, 1984; Edwards et al., 1994; Kneller and Buckee, 2000), exhumed (e.g. Patacci et al., 2014), and modern datasets (e.g. Stevenson et al., 2014) to have a profound impact on flow processes and therefore the configuration of deep-water systems. Despite this, previous outcrop studies on the effects of subtle fixed and dynamic topography on depositional processes are limited in their spatial and temporal extent (e.g. Smith, 2004b; Spychala et al., 2017a), and their influence over multiple deposition cycles remains unknown. Studies using reflection seismic datasets can show evolution over multiple stages of deposition (e.g. Beaubouef and Abreu, 2006; Mayall et al., 2010; Hay et al., 2012), but generally focus on highly complex topographic templates, such as tortuous corridors (Smith, 2004a; Hay et al., 2012), minibasins (Booth et al., 2003; Beaubouef and Abreu, 2006; Madof et al., 2009), and piggy-back basins/ foredeep margin slopes (Covault et al., 2009) and/or do not span multiple large scale sea-level cycles

(e.g. Beaubouef and Abreu, 2006; Barton, 2012). Moreover, these studies lack the resolution to characterize sedimentary facies and architecture.

Changes in slope gradient and orientation have been documented to have an important impact on gravity flow behavior, with consequent effect on sedimentary facies (e.g. Baines, 1984; Kneller and McCaffrey, 1991; Edwards et al., 1994; Haughton, 1994; Smith, 2004a; Hodgson and Haughton, 2004; Stevenson et al., 2013; Spychala et al., 2017a) and depositional architecture (e.g. Prather, 2003; Deptuck et al., 2012; Hay, 2012; Prather et al., 2012a; b; Moody et al., 2012; Wynn et al., 2012). Flows can respond to gradient variation in a number of ways; acceleration, deceleration, reflection, deflection, which affects erosional and depositional patterns (e.g. Baines et al., 1984; Edwards et al., 1994; Haughton, 1994; Kneller and Buckee, 2000; Jackson and Johnson, 2009; Nasr-Azadani et al., 2014). Turbulent flows often leave a complex stratigraphic record due to substantial modification of the slope/ basin floor through erosion during formation (Normark and Piper, 1991). Therefore, it is often unclear whether slope topography or spatial changes in flow dynamics were responsible for patterns left in the sedimentary record (Kneller, 1995; Baines, 1998; Kneller and McCaffrey, 1999; Kneller and Buckee, 2000).

This study aims to characterise three thin sandstone bodies (units A/B, B/C and D/E) from the Laingsburg and Fort Brown formations, Karoo Basin, South Africa. These units differ greatly in sedimentology and architecture from the larger slope to basin floor units A, B, C, D, E and F, did not significantly modify the slope to basin floor profile during formation and are therefore utilized as topography indicators. Building on previous studies of the larger units this study aims to document the evolution of a stepped slope profile over multiple sea-level cycles. Specific objectives are: i) to document the spatial variability in thickness and facies trends within units A/B, B/C and D/E to assess influence of fixed and/or dynamic seabed topography; ii) to understand the depositional processes and environments of units A/B, B/C and D/E; iii) to investigate when seabed topography formed, how it evolved over time, and whether it influenced deposition of larger units C, D, E and F; and iv) to develop a model for stepped slope profile evolution over a series of sea-level cycles.

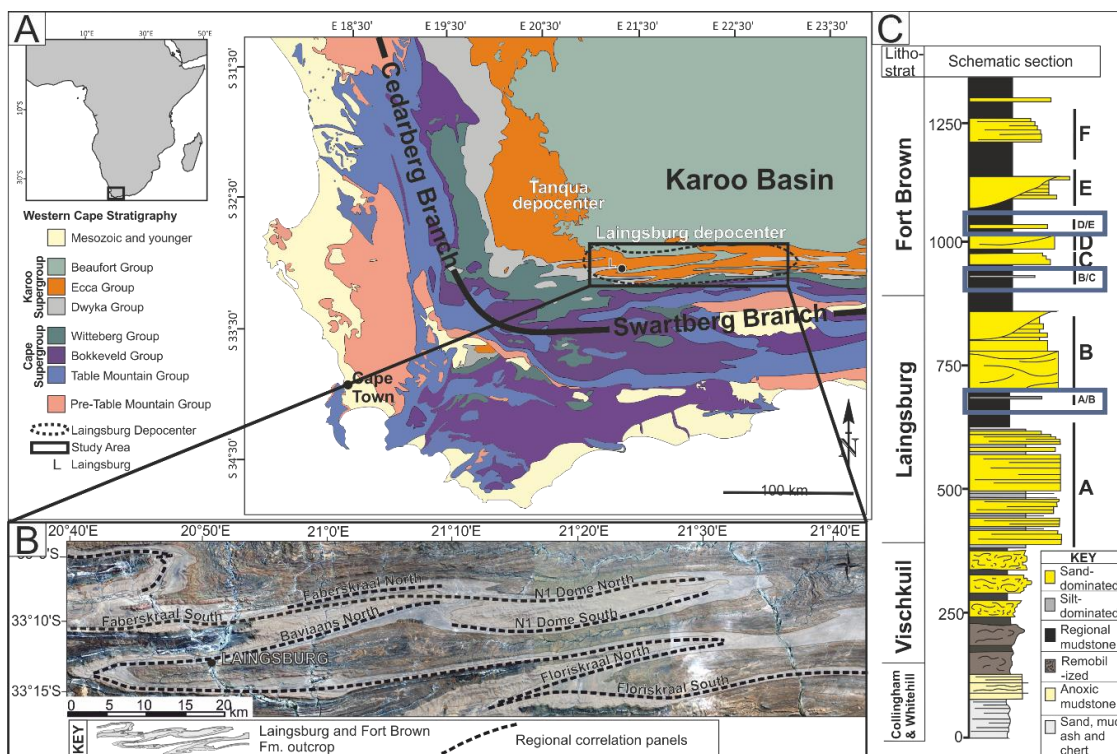


**Figure 6.1** Examples of slope and basin floor topography and resultant deposits. (A) Simple slope profile with single break-in-slope changing from bypass dominated channel-levee system to depositional dominated basin floor lobes, with potential for channel-lobe transition zone (CLTZ) development at base-of-slope. (B) Stepped-slope profile with higher gradient ramps linking lower gradient steps. Formation of entrenched channel/channel levee systems on ramps and intraslope/ basin floor lobes on steps, with potential for CLTZ development at breaks-of-slope. (C) Topographically complex slope, encompassing varying magnitudes of topography. Development of several ramps within entrenched channel/channel levee systems, including a step on the basin floor. Intraslope and basin-floor lobe development on lower gradient steps. Formation of tortuous corridor controlled by slope topography, and minibasin where 3D closure occurs. Topography on slopes is generally of much greater magnitude than on the basin floor.

## 6.2 Geology of the Karoo Basin

The Karoo Basin, South Africa (Fig. 6.2), has been interpreted as a retroarc foreland basin (Visser and Prackelt, 1996; Visser, 1997; Catuneanu et al., 1998), and more recently as a thermal sag basin that subsequently evolved into a retroarc foreland basin in the Triassic (Tankard et al., 2009). The 8 km thick Karoo Supergroup (Fig. 6.2C) is subdivided into the Dwyka, Ecca, and Beaufort Groups. The Dwyka Group comprises glacial deposits (Late Carboniferous to Early Permian); the Ecca Group clastic marine deposits (Permian); and the Beaufort fluvial deposits (Permian to Triassic). Basal deposits of the Lower Ecca Group (Fig.

6.2C) comprise mudstones, chert and shallow marine carbonates of the Prince Albert Formation, overlain by black carbonaceous mudstones of the Whitehill Formation and fine-grained turbidites, cherts and ashes of the Collingham Formation. These formations are mapped for 800 km along the southern margin of the Karoo Basin (Viljoen, 1992, 1994; Visser, 1992; Johnson et al., 1997). In the Laingsburg depocentre, the Collingham Formation is overlain by the Vischkuil Formation, which forms the basal section of the 1800 m thick progradational succession through basin-floor deposits (Vischkuil and Laingsburg formations; Sixsmith et al., 2004; van der Merwe et al., 2010), channelized submarine slope (Fort Brown Formation; Hodgson et al., 2011; Di Celma et al., 2011; Flint et al., 2011) to shelf-edge and shelf deltas (Waterford Formation; Jones et al., 2015; Poyatos-Moré et al., 2016). Regional palaeoflow is towards the northeast and east throughout the succession with the entry point to the southwest (van der Merwe et al., 2014). The mapping of successive slope-to-basin-floor systems in the Laingsburg depocentre indicates the presence of a lateral, east-to-west oriented basin margin to the south of the Laingsburg area (van der Merwe et al., 2014).



**Figure 6.2** (A) Map of Africa and geological map of SW Africa with location of Laingsburg depocentre. (B) Enlarged section of Laingsburg depocentre showing location of outcrop belts along post depositional fold limbs. Black dashed lines highlight the regional scale correlation panels. (C) Stratigraphic column of Ecca group stratigraphy, highlighting Laingsburg and Fort Brown submarine fan Units A, B, C, D, E and F as well as discontinuous smaller fan units A/B, B/C and D/E.

### 6.2.1 *The Laingsburg and Fort Brown Formations*

The Laingsburg Formation consists of units A, A/B and B, and the Fort Brown Formation includes units B/C, C, D, D/E, E, and F respectively (Fig. 6.2C; Flint et al., 2011). This study examines all units in the Laingsburg and Fort Brown formations, and represents the first detailed study on the less extensive, thinner units A/B, B/C and D/E (Fig. 6.2C), which are exposed along a series of sub-parallel post-depositional fold limbs (Fig. 6.2B), and intersected in a number of cored research boreholes. Detailed mapping and correlation of all units utilizes regional correlation work undertaken in previous studies (Grecula et al., 2003; Figueiredo et al., 2010; Di Celma et al., 2011; Flint et al., 2011; Hodgson et al., 2011; Kane and Hodgson, 2011; Brunt et al., 2013a; b; Figueiredo et al., 2013; Morris et al., 2014a; b; van der Merwe et al., 2014; Spychala et al., 2015; Morris et al., 2016; Spychala et al., 2017a). The Laingsburg and Fort Brown formations have been divided into four composite sequence sets, the first comprising Unit A, and the second units A/B and B, the third units B/C, C and D; and the fourth units D/E, E and F (Flint et al., 2011). Each of units C, D, E and F represents a lowstand sequence set, with an overlying 10-30 m thick regional hemipelagic mudstone representing the corresponding transgressive/highstand sequence set (Flint et al., 2011), both components together forming a composite sequence. Lowstand sequence sets can be subdivided into separate depositional sequences, including a sand-rich lowstand systems tract (LST; e.g. E1, E2, and E3) and an overlying transgressive/highstand systems tract mudstone (~1-5 m thick) (Figueiredo et al., 2010; 2013; Di Celma et al., 2011; Hodgson et al., 2011).

Regional mapping and correlation of units C to F have demonstrated an architectural change from sand-attached (units C and D) to sand-detached channel-lobe transition zones (units E and F) (*sensu* Mutti, 1985) (van der Merwe et al., 2014). The recognition of intraslope lobes in units D/E, E and F (Figueiredo et al., 2010; Spychala et al., 2015), and sand bypass-dominated zones, including thin channel-levee deposits and a channel lobe transition zone (van der Merwe et al., 2014) supports the presence of a stepped slope profile at the time of E and F deposition. This paper focuses on the sedimentology and stratigraphic expression of the thinner units and the implications these have for fixed and evolving slope topography throughout the Laingsburg and Fort Brown Formations, resulting in the formation of a stepped slope profile.

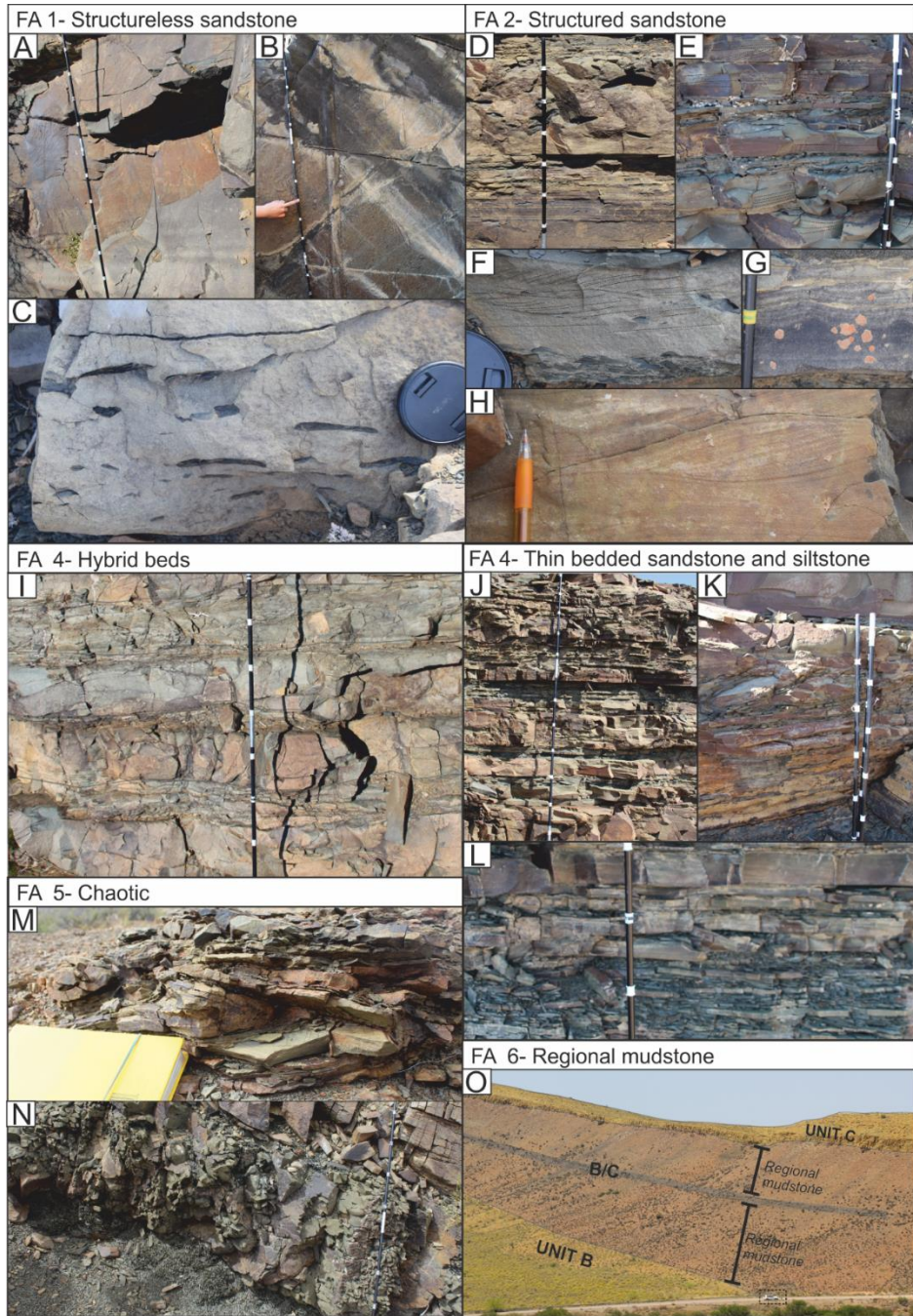
### 6.3 Methodology

Over 100 measured sections, logged at mm-cm scale, have been used to build thickness and facies maps of Units A/B, B/C and D/E over 10s of kilometres in dip and strike directions. Logged sections document the lithology, grain size, sedimentary structures and stratal boundaries. The correlation framework was established by walking out stratigraphic surfaces between sections. Thickness distributions were created by fitting a surface to values obtained from logged sections using the kriging tool within ArcGIS's Geostatistical Wizard. Maps are extended beyond the extremities of the input data by the surfacing algorithm, with unrealistic values removed and observed trends applied. Facies association maps that represent the gross depositional environments for each study interval were constructed using data from previous studies in the Karoo (Grecula et al., 2003; Figueiredo et al., 2010, 2013; Di Celma et al., 2011; Flint et al., 2011; van der Merwe et al., 2014; Spsychala et al., 2015, 2017a;b). Unit C, D, E and F palaeogeographic maps are modified from van der Merwe et al. (2014) incorporating data from Spsychala et al. (2015). Trends within the palaeoenvironmental maps are based on restored palaeocurrent data collected from ripple laminations, flutes and grooves.

A 3D datacube was constructed in Petrel by importing 100 composite logs and 6 well logs consisting of the complete Whitehill Fm. to Waterford Fm. stratigraphy, with the Whitehill Fm. used as a basal datum. Tops and bases of key lithostratigraphic units were selected using the well top function, and additional data were used to interpret polylines to add datapoints between outcrop logs. Depth structure maps were constructed for each key surface using the 'make a surface' function and thickness maps were created between key surfaces. Post depositional tectonic shortening was corrected by stretching 13% in the Y direction, according to a mean value for palinspastic restoration derived by Spikings et al. (2015).

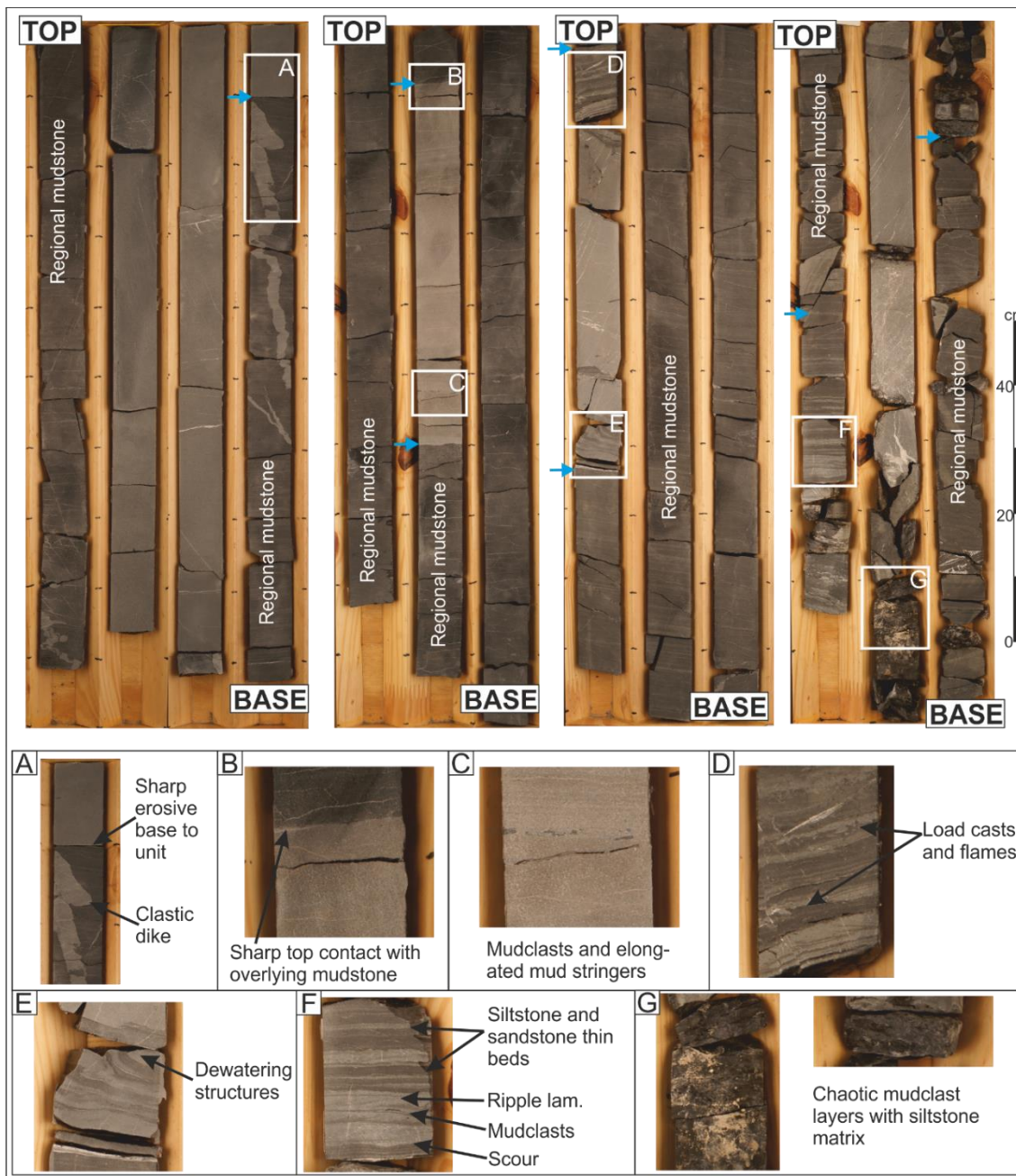
### 6.4 Results

Six distinct groups of lithofacies are described and interpreted in terms of sedimentary processes for Units A/B, B/C and D/E (Fig. 6.3).

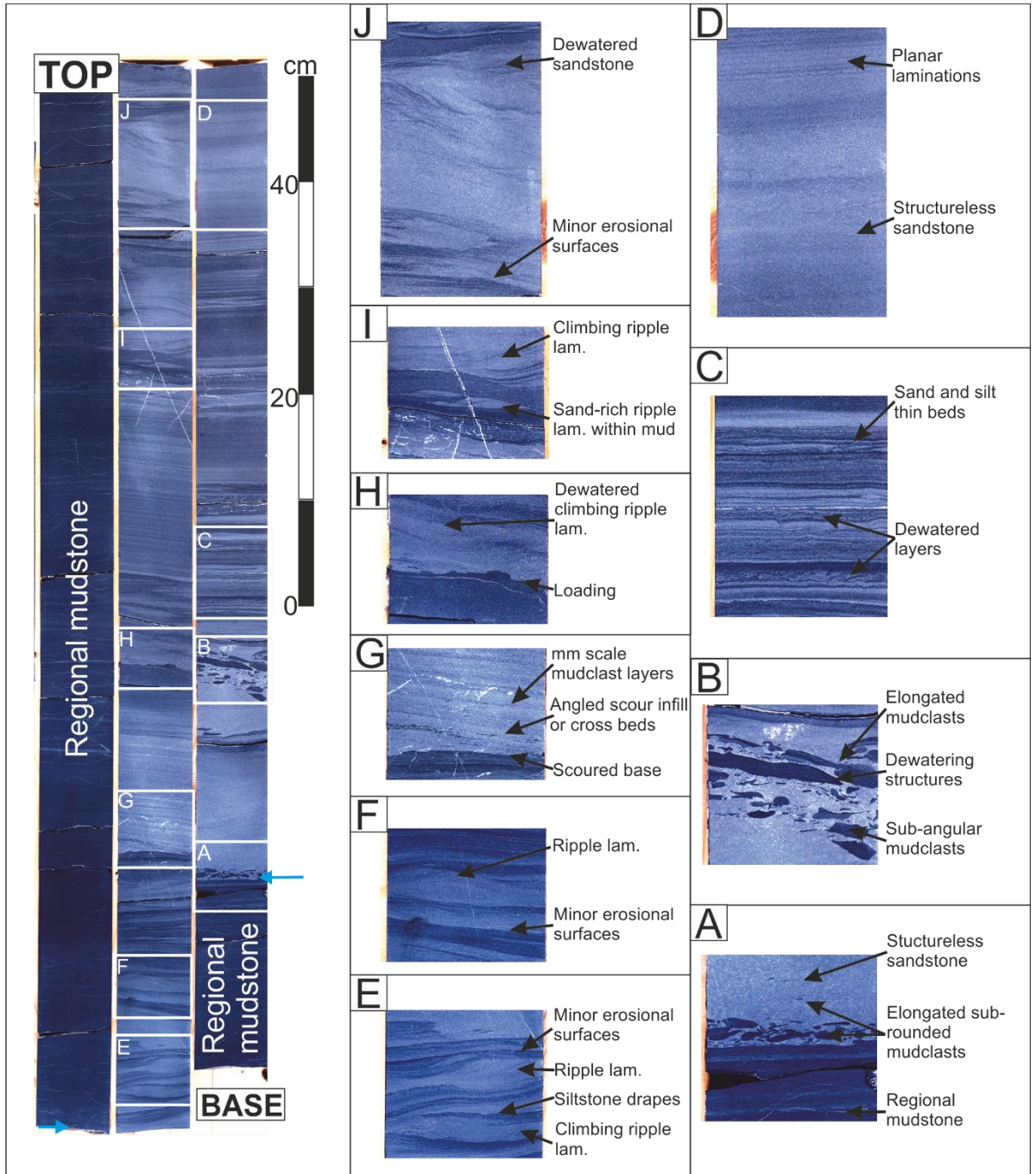


**Figure 6.3** Representative photographs depicting facies associations present throughout the outcrop. (A) Thick structureless amalgamated sandstone. (B) Base of structureless sandstone bed showing grooves and tool marks. (C) Elongated mudstone clasts present near the base of a structureless sandstone bed, lens cap 7 cm in diameter. (D) Laminated and graded tops of structured sandstone beds. (E) Planar/ripple laminated very fine sandstone- siltstone beds. (F) Climbing ripple laminated sandstone bed, with mudclasts draping laminations and forming a layer at the base of the bed, lens cap 7 cm in diameter. (G) Dewatered banded sandstone. (H) Ripple laminated sandstone, pencil 7 cm in length. (I) 10-30 cm beds with bi-partite bed structure, lower division of fine sandstone and thinner upper division of poorly sorted sandstone and siltstone with mm-cm mudstone clasts and organic matter. (j) Interbedded 10-15 cm sandstone beds and thinner siltstone beds. (K) Interbedded sandstone and siltstone with deformation. (L) Interbedded cm thick siltstone beds, overlain by thicker structured sandstone beds. (L) Tightly folded sandstone and siltstone thin beds, notebook 15 cm in length. (N) Debrite with mm-cm scale mudclasts and organic fragments. (O) 10s of m thick regional mudstone packages separating larger and smaller fan units, car for scale marked by dashed box.

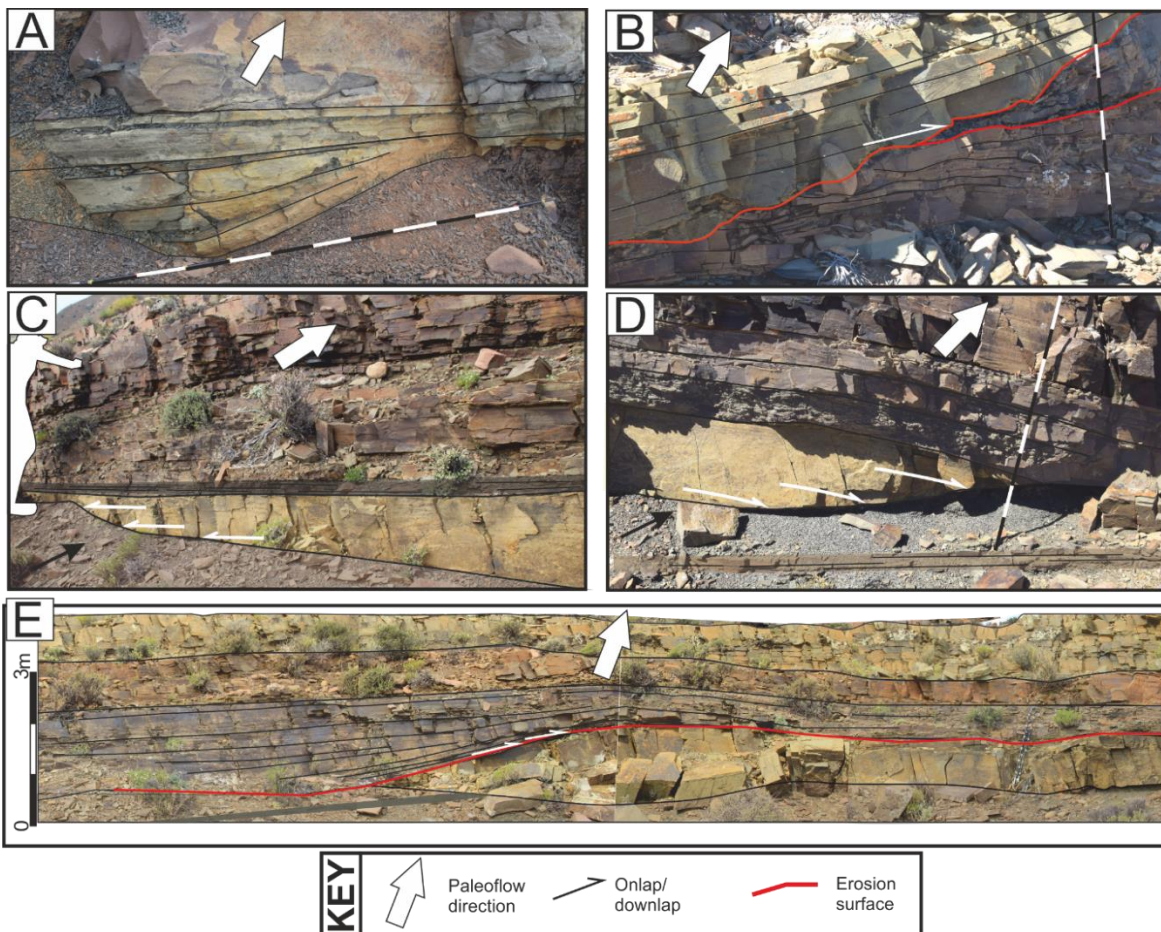




**Figure 6.4** Core examples of Unit B/C demonstrating key features and range of structures recognised, including: sharp base and top of units; clastic injectites surrounding unit; mudclast layers throughout unit and mudclast conglomerates; ripple laminated sandstone and siltstone; planar laminated sandstone and siltstone; dewatering structures and small scale scouring. Blue arrows indicate top and base of units.



**Figure 6.5** Core examples of Unit A/B demonstrating key features and range of structures recognised, including: sharp base and top of units; mudclast layers throughout unit; ripple laminated sandstone and siltstone; planar laminated sandstone and siltstone; dewatering structures and small scale scouring. Colour and hue modified from original to accentuate structures.



**Figure 6.6** Range of discontinuous beds within A/B, B/C and D/E. (A) Basal scour with draped infilling sandstone and siltstone. (B) Erosional surface cutting 1-2 m within unit truncating strata, with onlap of overlying beds. (C) Onlap of basal beds onto topography created by regional mudstone. (D) Downlap of basal beds onto regional mudstone. (E) Erosion surface within unit cutting down to base. Infilling beds onlap, and then drape over surface.

#### 6.4.1 Structureless sandstone

##### Description

Structureless sandstone beds are fine-grained, thin to thick-bedded (0.1-1 m thick) with common dish and pillar structures, and weak normal grading at bed tops (Figs 6.3A and 6.4A). Typically, beds are tabular with erosional bases with common flutes, grooves and other tool marks (Fig. 6.3B). Discontinuous mudstone clast layers are common at bed amalgamation surfaces, bed bases, and dispersed within beds, with clasts sub-angular to sub-rounded (< 15% clasts by volume, 0.1-10 cm A-axis; Figs 6.3C and 6.4C). Loading and flame structures are also common at amalgamated bed contacts. Basal beds commonly thicken and thin over metres to 100s of metres, pinching out, infilling scoured sections, onlapping or downlapping onto

underlying mudstone (Fig. 6.6). Beds occur in packages up to 14 m in thickness (generally < 5 m).

#### Interpretation

Structureless and weakly normal graded sandstone beds suggest deposition from sand-rich high-density turbidity currents (Bouma, 1962; Lowe, 1982; Mutti, 1992; Kneller and Branney, 1995). Lack of sedimentary structures suggests rapid deposition and no bedform development. The presence of dispersed rip-up clasts and clast-rich amalgamated contacts suggest progressive aggradation of deposits formed by depletive steady high-density flows (Kneller and Branney, 1995). Loading and dewatering structures form syn- and post-depositionally, as a result of sediment liquefaction (Mulder and Alexander, 2001; Stow and Johansson, 2002).

#### 6.4.2 *Structured sandstone*

##### Description

Fine-grained sandstone beds (0.05-1 m thick) primarily consist of ripple and climbing ripple lamination (Figs 6.3F, 6.3H, 6.5E and 6.5F) but also include planar lamination (Figs 6.3D, 6.3E and 6.5D) and dewatering structures (load cast and flames, and dish and pillar) (Figs 6.3G and 6.5H). Climbing ripple lamination can exhibit a high angle of climb (15-30°) with stoss-side preservation of laminae. Locally, sheared climbing ripple laminations are present. Ripple cross-laminae can be heterolithic comprised of both sandstone and siltstone laminae, and mm-cm scale mud clasts (Figs 6.3F and 6.5E). Beds occur in packages up to several metres thick (Fig. 6.3E). Bed geometries range from tabular to lenticular, draping surfaces as depositional features, or as remnant erosional features. In packages, the basal beds thicken and thin over 10s to 100s of metres, pinching out and onlapping/ downlapping on to underlying mudstones (Fig. 6.6).

##### Interpretation

Climbing ripples form from continuous bedload traction under highly depositional flows. The high angle of climb, with stoss-side preservation, indicates high rates of aggradation (e.g. Allen, 1970; Jobe et al., 2012; Morris et al., 2014a; b). Commonly, this is associated with non-uniformity in flows and accompanying decrease in velocity and/or flow height, possibly linked to an abrupt decrease in gradient or loss of confinement (e.g. Jobe et al., 2012; Morris et al., 2014a; b), driving deposition through reduced flow capacity (e.g. Kneller and Branney, 1995). The presence of heterolithic siltstone and sandstone foresets likely indicates deposition from fines-rich flows (Baas et al., 2016). Millimetric to centimetric mud clasts may travel as bedload

if overpassing, where larger particles skip over a bed of smaller particles (Raudkivi, 1976; García, 2008), however they might be expected to accumulate in ripple troughs. Alternatively, they may be deposited by capacity driven deposition from a flow containing both sand, and a wide range of suspended mud-chips. Planar lamination forms under upper stage plane bed conditions (Allen, 1984; Talling et al., 2012). Abrupt changes in basal bed thickness and onlap onto underlying mudstone are interpreted to result from interaction with minor seabed topography with downlap representing the pinch out of beds where flows waned sufficiently to deposit the coarser grained portion of flow.

### 6.4.3 *Hybrid beds*

#### Description

This facies consist of a bipartite bed structure with a lower division comprising weakly normally graded fine-grained sandstone (0.1 – 1 m thick), with some dewatering structures and rare planar lamination, and occasional mudstone clast layers (clasts 1- 10 cm a-axis). The upper division comprises poorly sorted very fine-grained sandstone and siltstone (0.1 – 1 m thick) with dispersed sub-angular, elongate, mm-cm scale mudstone clasts and plant fragments (Fig. 6.3I).

#### Interpretation

The bipartite beds form through deposition of the lower division from a sand-rich turbidity current with the 'linked' poorly sorted upper division interpreted as deposition from a co-genetic debris flow. Hybrid event beds (Haughton et al., 2003, 2009) are most commonly identified towards the bases and fringes of lobe deposits (e.g. Hodgson, 2009; Talling, 2013). However, hybrid beds can form in any environment where mud and mudstone clasts are entrained into the turbulent flow, damping turbulence, and developing high-concentration to pseudo-laminar flow conditions (e.g. Ito, 2002; Haughton et al., 2003, 2009; Talling et al., 2004; Baas et al., 2011).

### 6.4.4 *Thin bedded siltstone and sandstone*

#### Description

Siltstone and sandstone beds (<1 - 15 cm thick), form packages up to several metres thick (Fig. 6.3J). Beds can be planar (Fig. 6.5D), ripple (Fig. 6.5F), or climbing-ripple laminated. Packages can range from siltstone- to sandstone-dominated (Figs 6.3J and 6.3L), and locally can be folded and deformed (Fig. 6.3K). Beds can vary in thickness laterally from metres to cms over

10s to 100s of metre distances. Basal beds are sometimes discontinuous, with pinch out/onlap onto underlying mudstone (Fig. 6.6).

#### Interpretation

Thin-bedded siltstone-dominated packages indicate deposition from dilute turbidity currents, with the finer sediment residual within the flow after deposition of the coarser fraction of sediment load. Climbing ripple lamination forms through late stage tractional modification by flows, with high sediment fall out rates (Lowe, 1988). Low angle of climb suggests lower rates of suspended load fallout than in FA2. Localized deformation and folding indicates slumping of material and/or significant dewatering. Thickness variations, discontinuities and onlap of basal beds are interpreted to result from deposition on irregular topography.

#### 6.4.5 *Chaotic Facies*

##### Description

Units of contorted strata comprising thin- to thick-bedded sandstones and siltstones can be up to 4 m thick and extend laterally for 10s of metres. Chaotic units range from coherently folded (Fig. 6.3M) to highly disaggregated with contorted clasts supported by a poorly sorted silt-prone matrix. Disaggregated deposits include poorly sorted matrix-rich very fine-grained sandstone to coarse siltstone beds (0.1 – 2 m thick) that lack internal structure and contain dispersed sub-angular, elongate, mm-cm scale mudstone clasts and plant fragments (Figs 6.3N and 6.4G).

##### Interpretation

These units are interpreted as mass flow deposits derived from remobilization to form slide and slump deposits. Highly disaggregated and matrix-supported components are interpreted as debrites.

#### 6.4.6 *Regional mudstone*

##### Description

Claystone and fine siltstone may be laminated on a mm-scale or structureless (Figs 6.3, 6.4 and 6.5). This facies forms regionally extensive units that have been mapped for 10s of km and drape every sand-prone unit (Flint et al., 2011; van der Merwe et al., 2014).

##### Interpretation

These deposits are interpreted as background hemipelagic deposition, forming regional drapes during shutdown of sand and coarse silt supply.

## 6.5 Environments of deposition

The thin high aspect ratio sandstone units are interpreted as lobe deposits due to the lateral continuity of beds, the lack of major erosion surfaces, and their constituent facies. Four broad architectural elements have been characterized (Fig. 6.7) based on the occurrence of constituent facies, mapped geometries, and their palaeogeographic context, utilizing the depositional environment interpretations of previous studies (Prélat et al., 2009; Prélat and Hodgson, 2013; Brunt et al., 2013a; b; Morris et al., 2014a; b; Sychala et al., 2015).

**Lobe axis:** This association consists primarily of thick amalgamated sandstone beds, with mudstone clast horizons with minor structured sandstone (Fig. 6.7), up to 14 m thick. Typically, contacts with the underlying mudstone are sharp and sometimes scoured with numerous flutes, grooves and other tool marks. The proximal lobe axis comprises structureless and structured sandstone as well as thin-bedded sandstone and siltstone. Indicators of sediment bypass include multiple composite scours (cm – 1.5 m in depth, 0.5- 3 m in width) mantled with mud clasts lag horizons and high aspect ratio erosion surfaces (Figs 6.6E and 6.7),. Lenticular infilling packages over 100 m in width and up to 5 m thick onlap, drape and overtop surface topography (Fig. 6.6E).

**Lobe off-axis:** Consisting of stratified structureless and structured sandstone and sand-dominated thin beds (Fig. 6.7), packages are up to 5 m thick. Scouring can occur at the bases of beds and minor erosion may be present throughout. Packages can thicken and thin abruptly with bed thickness changes and onlap of the lower beds onto the regional mudstone.

**Lobe fringe:** Frontal and lateral lobe fringe deposits consist of thin structured/ structureless sandstone beds with common mud clast horizons, thin bedded sandstone and siltstone beds, hybrid beds and debrites (Fig. 6.7). Beds are mm to 50 cm thick with packages of thin beds up to 2.5 m and sandstone up to 70 cm. Sand-rich pinchouts are associated with significant clastic injectites (Cobain et al., 2015).

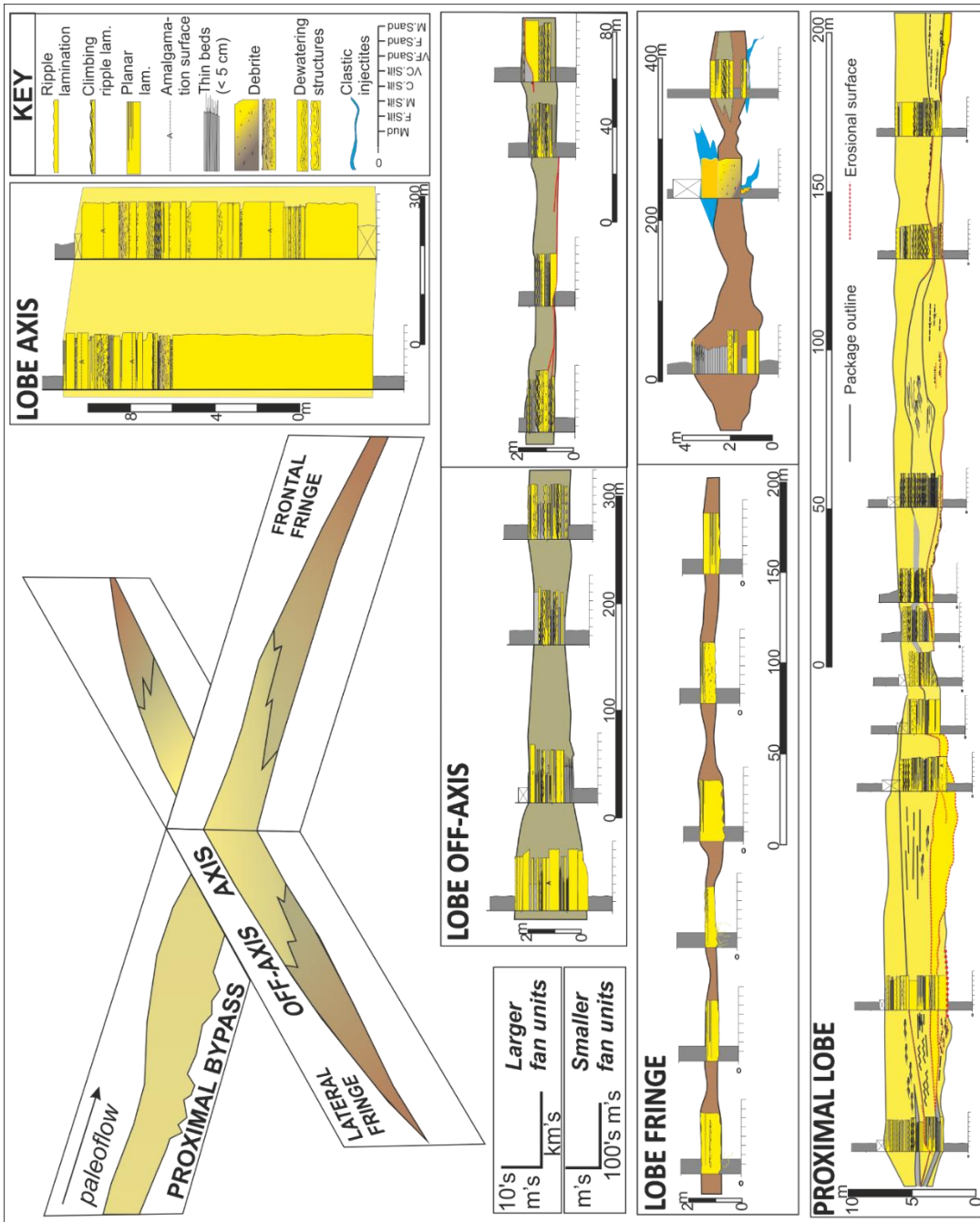
**Distal lobe fringe:** At distal pinchouts, deposits consist of thinly bedded siltstone with occasional starved ripples. These are distinguished from the regional mudstones as they are slightly coarser than the background sediments and have been walked out from more proximal

areas. It is therefore likely that other packages of distal lobe fringe facies are present but undocumented.

Hemipelagic mudstone: The regional mudstone represents periods of clastic shut off in the basin when hemipelagic material can accumulate to significant (2 to 10s of metres) thicknesses.

Syn-sedimentary deformation can be associated with all environments of deposition and may represent localized slumping of packages due to dewatering or remobilization due to instabilities caused by minor seafloor topography.





**Figure 6.7** Key architectural elements recognised in Units A/B, B/C and D/E. Sketch of 3D lobe shows divisions of sub-environments, with scale demonstrating general thickness of smaller and larger fan units. Lobe axis, lobe off-axis, lobe fringe and proximal lobe panels show representative section from Units A/B, B/C and D/E. Blue indicates interpretation as clastic injectite (Cobain et al., 2015).

### 6.6 Unit A/B, B/C and D/E thickness and facies distribution

The thin sandstone units are present discontinuously across the Laingsburg depocentre, but concentrated in the western, up-dip Baviaans and Heuningberg locations (Fig. 6.8). Typically, units A/B, B/C and D/E are an order of magnitude thinner than units A-to-F (Fig. 6.7), reaching a maximum of 14 m thick, and are generally < 5 m thick (Fig. 6.8). Overall, the thicker areas are

dominated by the axial lobe association, transitioning to off-axis and fringe deposits as the unit thins (Figs 6.7 and 6.8).

In the Baviaans area, Unit A/B shows palaeocurrents from flute and groove marks consistently towards the north-northeast, changing to eastward in the Heuningberg area (Fig. 6.8).

Palaeocurrents from current ripples are more dispersed and show a spread between north-northwest and east. The thickest A/B deposits (up to 14 m) follow a north to south trend, which coincides with the most axial lobe facies (Fig. 6.7). The unit thins and transitions to off-axis deposits abruptly towards Faberskraal and Geelbek to the east and more gradually to the west, with fringe deposits restricted to the peripheries of the system (Fig. 6.8). A localized area of increased thickness (up to 10 m) is present around Heuningberg, thinning abruptly in all directions (Fig. 6.8). Lateral pinch outs (Geelbek and Heuningberg) are a combination of highly laterally discontinuous sand-rich strata and silt-rich thin beds (Figs 6.7 and 6.8). In the most proximal Baviaans area, high aspect ratio erosional features (1- 5 m in depth and 10s of metres to 150 m in width) are present over a 10 kilometres strike oriented outcrop section (Figs 6.6, 6.7 and 6.8). The thick central areas of infill (> 3 m) comprise structureless, planar and climbing ripple laminated sandstone, which thin and fine laterally to interbedded siltstone and ripple laminated sandstone (> 1 m) (Fig. 6.6).

Unit B/C is also best developed in the regional up-dip areas of the depocentre (Baviaans, Heuningberg and Geelbek; Fig. 6.8) with the thickest and most axial deposits around Baviaans. The unit thins gradually towards Heuningberg and transitions into off-axis and fringe deposits (Fig. 6.8). Flute, groove and ripple palaeocurrents indicate a northeast direction of transport, with a northwest component in the Geelbek area (Fig. 6.8). Unit B/C is thinner overall than A/B (< 4 m thick) and less laterally extensive (Fig. 6.8). Towards Heuningberg and Faberskraal, deposits transition to off-axis and pinch out abruptly (Fig. 6.8). A discontinuous area of thicker (up to 4 m), sand-rich lobe fringe deposits is present around Geelbek, thinning abruptly in all directions (Fig. 6.8). Pinch-outs are sand-rich at the lateral (eastern) fringe (Fig. 6.7) and more silt-rich and thin-bedded (Fig. 6.7) towards the frontal (northern) fringe (Fig. 6.8).

Unit D/E is present in three discrete sites. Walking key regional markers including top Unit D, base Unit E and the D-E mudstone was necessary to establish that the three areas of deposition are at the same stratigraphic position. These depositional sites are the Heuningberg, Geelbek, and Floriskraal areas (Fig. 6.8). In Heuningberg, up to 14 m of axis and off-axis lobe deposits are present, which thin and transition to fringe deposits abruptly to the

west, south and east, and pinch out abruptly to the south/east and more gradually to the west (Fig. 6.8). In Geelbek, Unit D/E consists of a single debrite bed < 2 m thick (Fig. 6.8). In Floriskraal, a 14 m thick lobe-axis has a southwest to northeast orientation with palaeoflow to the east (Fig. 6.8). Unit D/E is highly discontinuous towards Slagtersfontein, transitions to off-axis and fringe deposits, and pinches out abruptly to the south and more gradually to the north (Fig. 6.8). Pinch outs are more sand-rich (Fig. 6.7) in the frontal (eastern) fringe and more silt-rich and thin-bedded (Fig. 6.7) in the lateral (southern) fringe with remobilized/ debritic deposits present in the northern lateral fringe (Fig. 6.8).

Each unit is bounded by regional mudstone. Locally, below the thin units silt-rich remobilized strata are present, cms to several metres in thickness, ranging from chaotic and highly disaggregated to laterally extensive (metres to 10s of metres).

### **Interpretation**

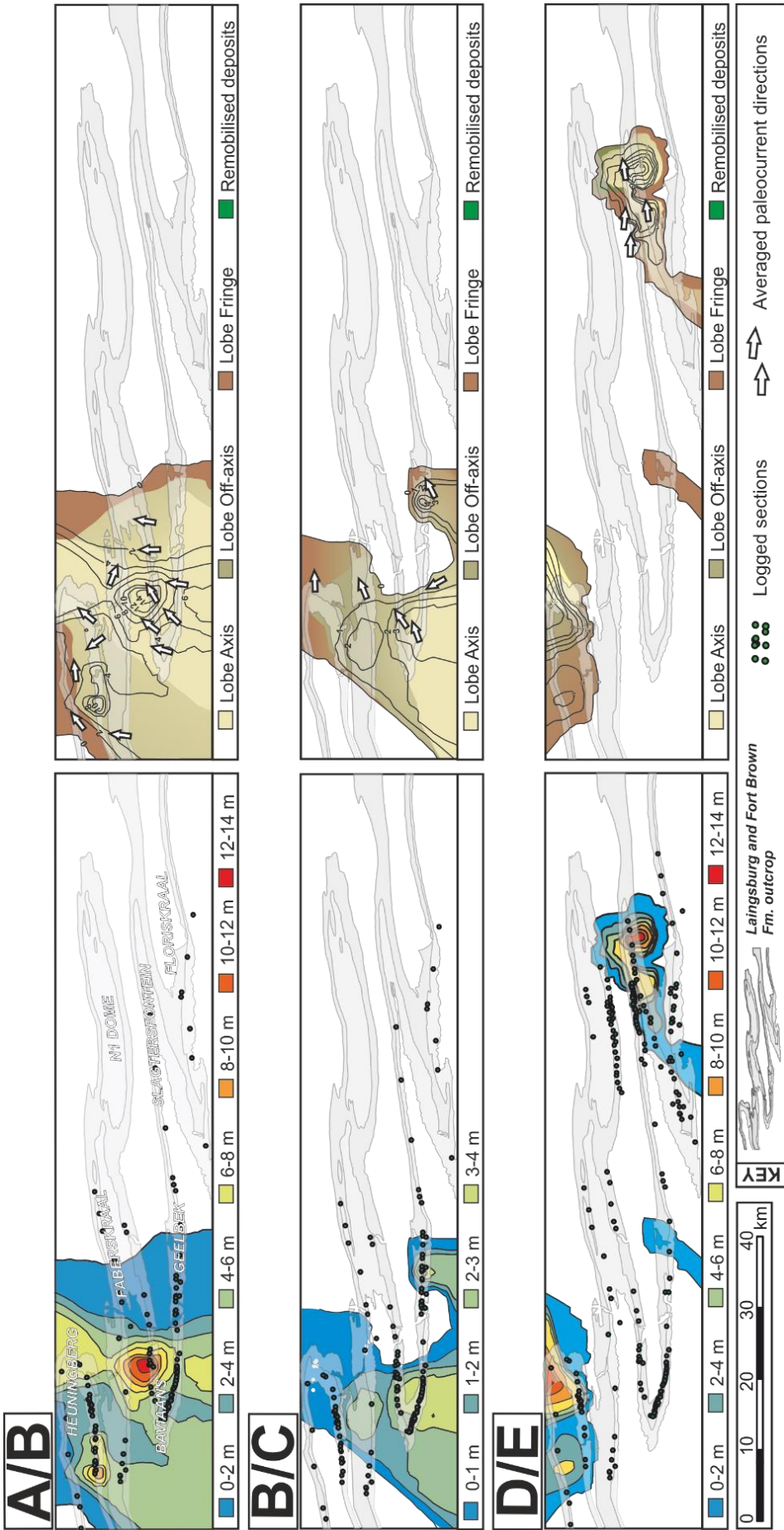
Facies and thickness distributions indicate that the A/B and B/C systems were fed from the southwest (Figs 6.8 and 6.9), with mean palaeoflow towards the northeast. Lenticular erosive features in the Baviaans area may represent either shallow scours, or weakly confined channels. In the case of channels, these features may represent small weakly confined distributive channels eroding into proximal lobes close to the base-of-slope, with distributive patterns likely, due to the lack of slope (e.g. van der Werff and Johnson, 2003). In the case of scours, this may also indicate a location close to the base-of-slope, with scouring commonly documented in channel-lobe transition zones (e.g. Wynn et al., 2002; Macdonald et al., 2011a,b; Hofstra et al., 2015; Pemberton et al., 2016) formed by hydraulic jumps where flows transition from super- to subcritical due to a reduction in slope gradient and/or flow confinement (Mutti and Normark, 1987, 1991; Weirich, 1989; Kostic and Parker, 2006; Sumner et al., 2013; Dorrell et al., 2016). The distribution of Unit D/E indicates at least two areas of sediment input, in the northeast and to the south (Figs 6.8 and 6.9). Similar geographical areas (Faberskraal and Geelbek) and directions of facies transition, thinning and pinch out are recognised in all three units (Figs 6.8 and 6.9). Thinning and pinch-out of A/B and B/C lobes is seen in Heuningberg, where a southeast facing intrabasinal slope has been recognised to have impacted flow behaviour in the underlying Unit A (Spsychala et al., 2017a). This intrabasinal slope is interpreted as present throughout A/B and B/C deposition (Figs 6.8 and 6.9), modifying facies, thickness and palaeocurrent trends by reflecting and deflecting flows. The influence of

this intrabasinal slope does not persist into Unit D/E deposition indicating that topography was healed by intervening units (Fig. 6.9).

Eastern pinch-outs in units A/B, B/C and of D/E consistently occur across the Faberkraal-Geelbek area (Figs 6.8 and 6.9), suggesting influence by some form of long-lived topographic feature. This change in the Faberkraal-Geelbek area indicates that deposition was at least partially controlled by long-lived slope/basin floor topography (Fig. 6.9). Lobe pinch outs indicate a decrease (or slight reversal) in slope gradient, confining deposition up-dip. This topography was fixed in location, but evidently subtle or dynamic, as the effect of large-scale topographic depression is not recognized in the intervening units (van der Merwe et al., 2014). Therefore, this topography formed progressively over time, with a subtle expression on the seafloor at any one time (e.g. Spsychala et al., 2017a).

The abrupt southward pinch out of Unit D/E in Heuningberg (Fig. 6.8) has been suggested by previous studies to be due to a north-facing slope, resulting from differential compaction over underlying stratigraphy (Figueiredo et al., 2010). The southwest to northeast oriented deposition of Unit D/E axis in Floriskraal (Fig. 6.8) and abrupt pinch out at Slagtersfontein may be the result of a southeast facing slope surface which would represent the regional base-of-slope (Fig. 6.9) (Chapter 5). The abrupt southward thinning and pinch out is likely the result of a north-facing lateral basin margin (Fig. 6.9) (van der Merwe et al., 2014; Chapter 5).

Remobilization within regional mudstones prior to A/B, B/C and D/E deposition is interpreted to indicate instability of locally steepened frontal and lateral slopes that subsequently control lobe deposits.



**Figure 6.8** Thickness (left) and facies (right) maps of Units A/B, B/C and D/E. Thickness maps show isopach thickness in metres. Facies maps represent gross depositional environment for the time interval. A/B and B/C deposits are restricted to up-dip of the Faberskraal-Geelbek area. A/B deposits are thickest, most sand-rich and axial in the Baviaans and Heuningberg areas, with bypass dominated proximal lobe scours/distributary channels present in the Baviaans area. Deposits decrease in thickness and sand content to off-axis facies to the east and west. Lobe fringe deposits and pinch-outs are a combination of sand- and silt-rich in Geelbek and Heuningberg. B/C deposits are thickest, most sand-rich and axial in the Baviaans area. Deposits decrease in thickness and sand content to off-axis and fringe facies to gradually to the north and more abruptly to the east and west. Pinchouts are sand-rich at the lateral east and west margins and silt rich to the north. Unit D/E is present discontinuously in (a) Heuningberg, with thick axial deposits abruptly thinning and pinching out west, south and east, (B) in Geelbek, present locally as a single debrite bed, and (c) in Floriskraal, present in a southeast-northwest transect decreasing in thickness abruptly to the east and west (Slagtersfontein) with sand-rich pinch out, to the south with a silt rich pinch out, and more gradually to the north (N1 Dome) with a silt and debrite-rich pinch out.

## 6.7 Discussion

### 6.7.1 Units A/B, B/C and D/E

The recognition of units A and B as basin-floor deposits (Sixsmith et al., 2004; Prélat and Hodgson, 2013; van der Merwe et al., 2014) implies that Unit A/B was also deposited in a basin-floor setting (Fig. 6.9). Units C, D and E are interpreted as slope to basin floor systems (Figueiredo et al., 2010; van der Merwe et al., 2014; Morris et al., 2014a; b; Sychala et al., 2015; Chapter 5), with the western, up-dip sections on the slope. The co-location of Unit B/C in this area indicates a slope setting. Unit D/E in Heuningburg and Geelbek likely represents intraslope lobes (Sychala et al., 2015); with the Floriskraal deposits on the basin floor (Chapter 5) (Fig. 6.9).

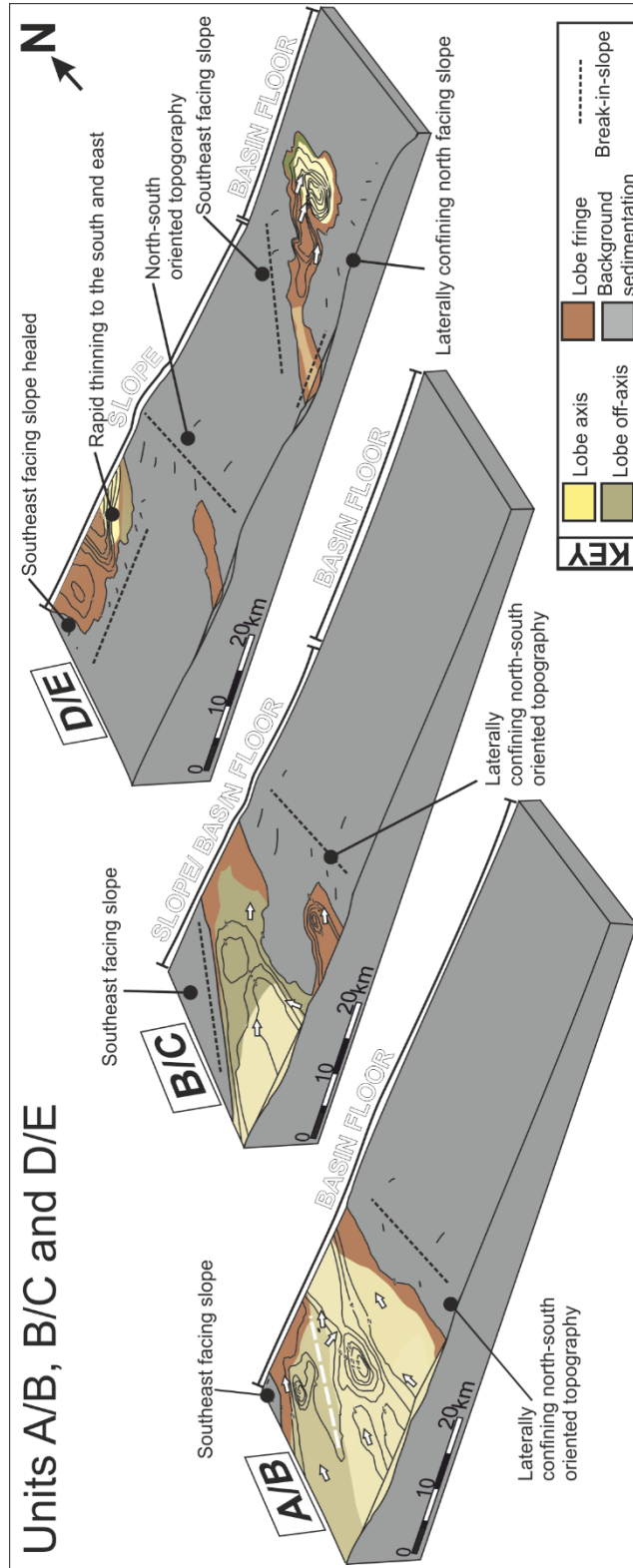
As presented above, Unit A/B, B/C, and D/E lobe deposits are sub-divided into axis, off-axis and lateral/frontal fringe (Fig. 6.7) with similar facies transitions to lobes in lobe complexes (*sensu* Prélat et al., 2009) recognised in the larger units. The thin sandstone units rarely record juxtaposition of multiple sub-environments (Fig. 6.7), indicating that deposition was not sustained long enough for lobes to stack compensationally to form a lobe complex, or for the propagation of channel-levee systems above lobes (e.g. Morris et al. 2014; Hodgson et al. 2016). In addition to the thickness differences, the thin units show key differences in facies and architecture to the larger units A-F (cf. Sixsmith et al., 2004; Prélat et al., 2009, 2010; Prélat and Hodgson, 2013). These include (a) a higher proportion of sand (Figs 6.4, 6.5 and 6.6) particularly in fringes (Fig. 6.7); (b) consistently sharp bases and tops (Figs 6.4, 6.5 and 6.7); (c) a higher proportion of mudstone clasts (Figs 6.4 and 6.5); (d) minor (< 1 m) basal scouring throughout, including at fringes (Figs 6.6 and 6.7); (e) abrupt thinning and pinch-out causing discontinuity (Figs 6.6 and 6.7); and (f) high aspect ratio erosion surfaces in proximal lobes.

Units A/B, B/C and D/E also exhibit aspects that are similar to the larger units A-F. In particular, they tend to display more silt-rich thin-bedded lateral fringes and more sand-rich and discontinuous frontal fringes (Figs 6.7 and 6.8). This variability has been documented by others in the Tanqua Karoo (Rozman, 2000; Pr elat et al., 2009; Groenenberg et al., 2010).

Units A/B, B/C and D/E stratigraphically overlie the thickest regional mudstone units in the Laingsburg and Fort Brown formations (Grecula et al., 2003; Di Celma et al., 2011; van der Merwe et al., 2014), and are interpreted as the initial deposits after the longest hiatuses in deepwater deposition. These are relative to the largest scale, and/or longest duration, relative sea-level rises (Flint et al., 2011). As these units represent the re-establishment of deepwater deposition, Flint et al. (2011) suggested they were distal expressions of larger scale lobe complexes similar to units C-F. However, the key differences in sedimentology and architecture presented here indicate these thin units are distinctly different, and therefore likely represent lobe deposition under different conditions. The absence of sustained supply to drive lobe stacking and propagating channel-levee systems suggests the thin units may not have been fully connected to upper slope and shelf feeder systems (Fig. 6.10). In this situation sediment input from the upper slope (e.g. through canyons) would be limited and additional sediment may have been sourced directly from the shelf and via slope failures (Fig. 6.10). With this range of source areas, flows may not have been restricted to long-lived conduits but instead were likely unconfined or weakly confined (e.g. Saller et al., 2004; Moody et al., 2012; Stevenson et al., 2013). Multiple sediment input locations would create widespread areas of lobe deposition that would not stack compensationally or aggradationally (Fig. 6.10). A lack of significant channelization could cause flows to traverse completely 'out-of-grade' areas (*sensu* Prather, 2003) that would erode the slope, causing significant entrainment of mud clasts. Unconfined flows would spread laterally and therefore be more susceptible to topographic perturbations than more channelized flows.

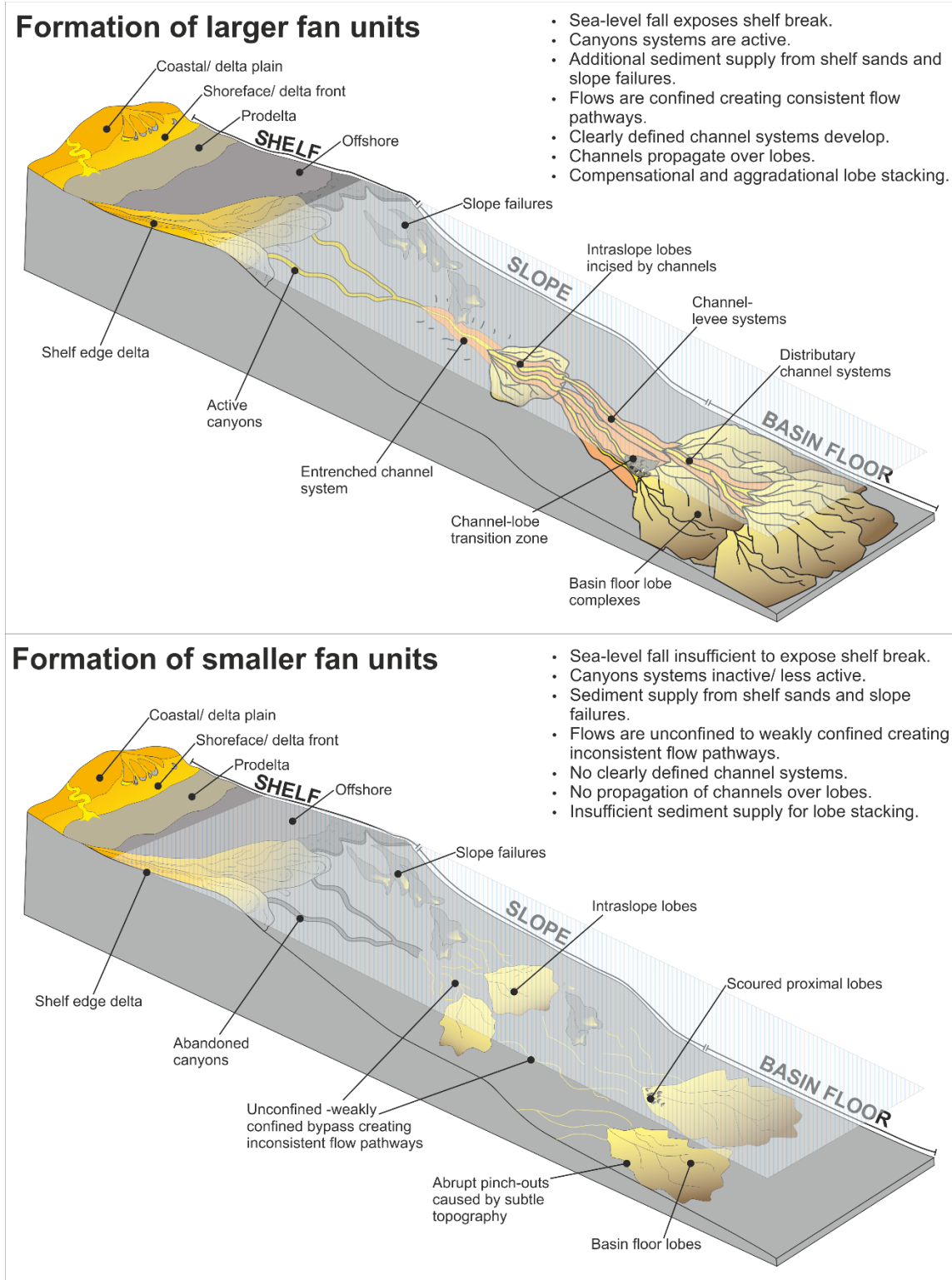
These disconnected feeder systems may indicate that relative sea-level falls that initiated Units A/B, B/C and D/E were not of sufficient magnitude to expose the shelf. Therefore, a relatively small scale rise in relative sea-level would be sufficient to cut off all sediment supply, creating an abrupt shut down of the deepwater system. Initiation and delivery of the larger scale Units A-F is interpreted as marking times when sea-level fell sufficiently to expose the shelf and activate upper slope feeder systems (Fig. 6.10). The lobe deposits of Units A/B, B/C and D/E are therefore interpreted as 'disconnected lobes', which are characterised by short-lived conduits, rather than continuous point-sourced flows through mature channel-levee systems. It may also be the case that the thin basal lowstand systems tract within each of the larger units (e.g. Sub-

units E1 and F1) also formed under similar conditions but the system became fully connected by the time of the second LST within each lowstand sequence set.



**Figure 6.9** Thickness and facies maps of smaller fan units overlain on 3D box models demonstrating controlling basin floor and slope topography.





**Figure 6.10** Shelf, slope and basin floor profile during deposition of larger and smaller fan units. Lower sea-level during deposition of larger units, exposes shelf and activates canyons in upper slope connecting sediment pathways down the slope. Comparatively lower sea-level during deposition of smaller units reduces/cuts off main sediment input.

## 6.7.2 *Thickness and facies distribution of Units C, D, E and F*

The pinch out trends in units A/B, B/C, and D/E indicate subtle seafloor topography, maintained over relatively long periods. Here, it is assessed whether the presence of seafloor topography affected the thicker, more laterally extensive units C, D, E and F, which have been mapped in detail in previous studies (Grecula et al., 2003; Figueiredo et al., 2010; Di Celma et al., 2011; Hodgson et al., 2011; Brunt et al., 2013a; van der Merwe et al., 2014; Spychala et al., 2015; Morris et al., 2016; Chapter 5).

### 6.7.2.1 Early phase slope topography: Units C and D

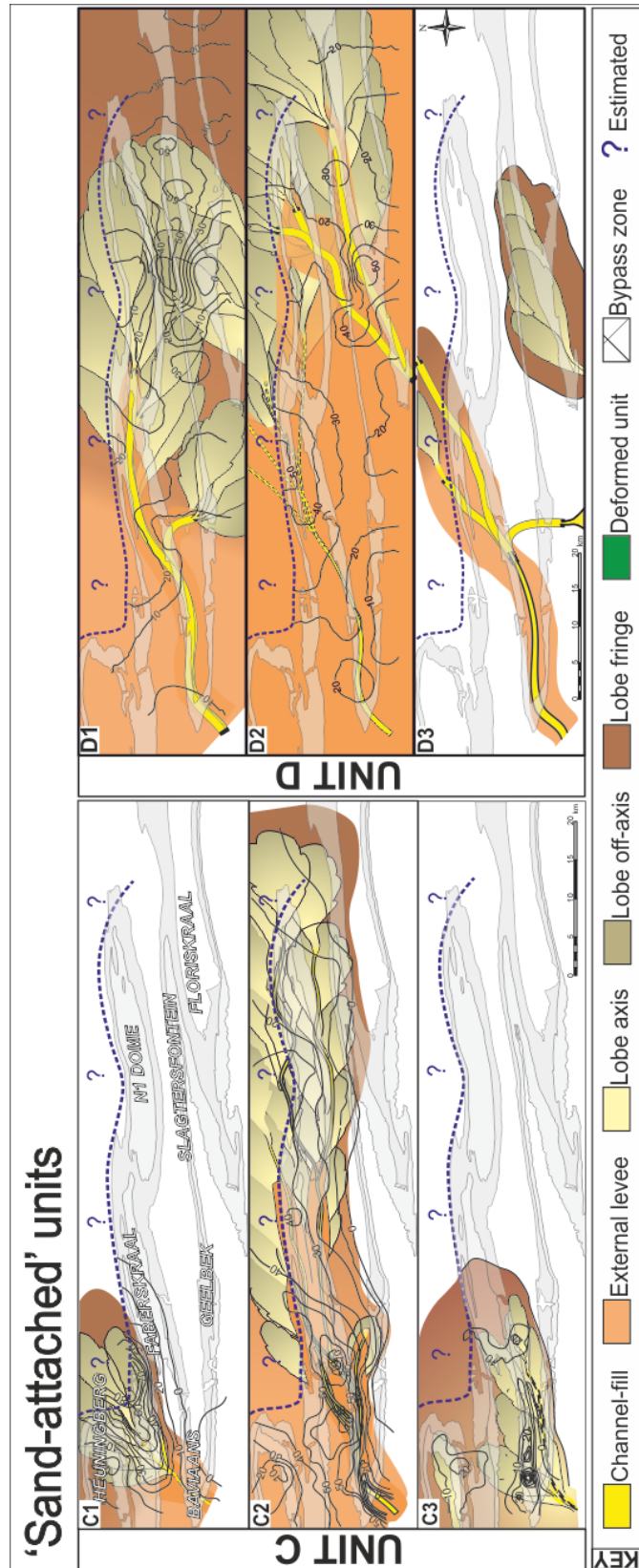
Sub-units C1 and C3 are both restricted to the up-dip, Heuningberg and Baviaans areas of the depocentre (Fig. 6.10) (Di Celma et al., 2011; Morris et al., 2014a; b), with lobe complex pinch-out around Faberskraal-Geelbek, a similar position to the underlying B/C Unit (Figs 6.8 and 6.11). The C3 lobe complex is < 20 m thick (Morris et al., 2014) and of comparable thickness to the thin Units A/B and D/E, whereas the C1 lobe complex reaches over 80 m thick. C2 is the thickest and most widespread of the C sub-units, consisting of channel-levee systems in the up-dip area around Heuningberg and Baviaans (Fig. 6.11) (Hodgson et al., 2011; Kane and Hodgson, 2011), dominated by erosion and bypass processes and with no lobe deposition (Morris et al., 2016). Down-dip of this location, coincident with the Faberskraal-Geelbek pinch outs of A/B, B/C and D/E (Fig. 6.8), channel-levee systems decrease in erosion depth, becoming less entrenched and more distributive (Fig. 6.11). Basin-floor lobe deposits are present down-dip in C3, confined to the N1 Dome area, with southern pinch out at Slagtersfontein.

The southern (lateral) pinch out of Unit C is likely related to topography formed through differential compaction of the underlying Units A and B (Fig. 6.12), which are thicker and more sand-rich in the south (Sixsmith et al., 2004; Di Celma et al., 2011; Flint et al., 2011; van der Merwe et al., 2014). The presence of lobes up-dip of the Faberskraal-Geelbek area similar to Units A/B and B/C (Figs 6.8 and 6.11) indicates the presence of a sustained area of local accommodation (Fig. 6.12). Other variations in spatial thickness are likely caused by compensational stacking (van der Merwe et al., 2014). The lack of channelized elements in C1 and C3 may indicate sediment input was insufficient to generate channel-levee systems. This is more likely the case in Unit C3, which is of a similar thickness to the thin units. Accommodation and topographic confinement likely decreased from C1 to C2, and possibly further from C2 to C3.

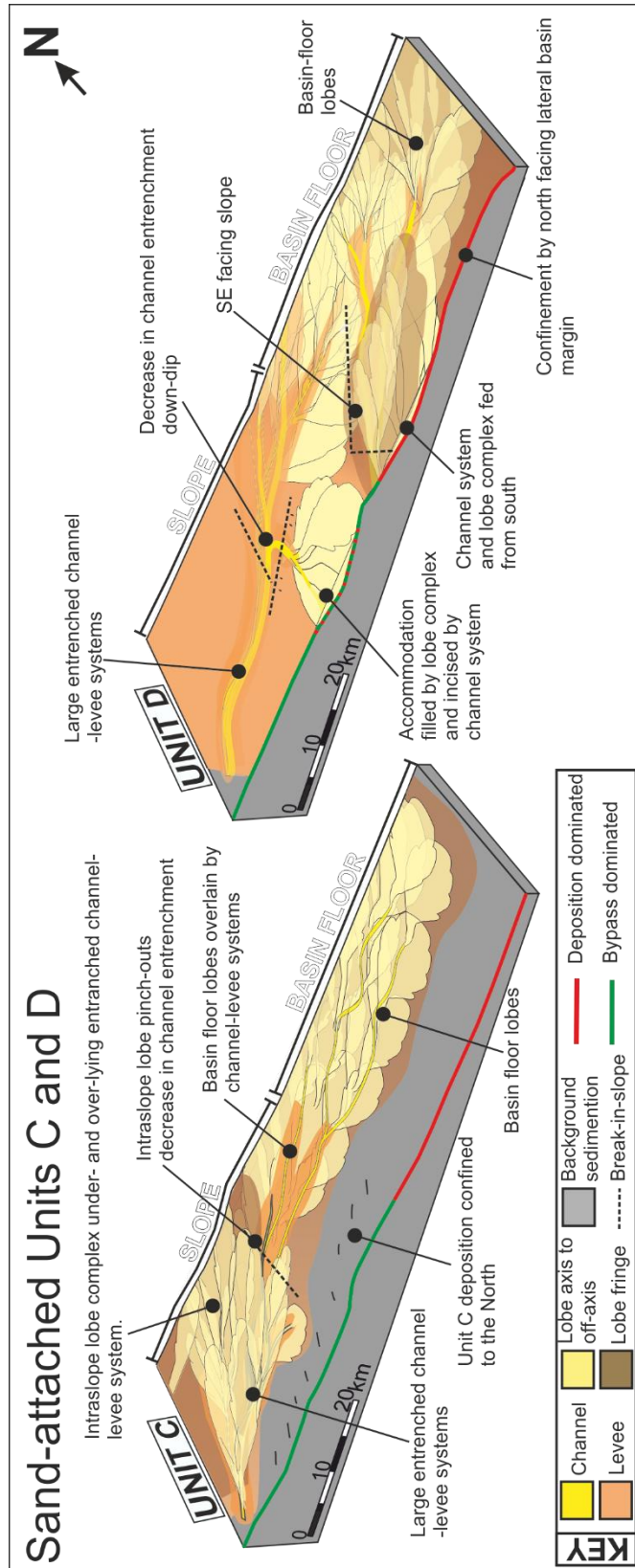
Sub-units D1, D2 and D3 comprise channel-levee systems in the up-dip Baviaans area (Fig. 6.11) with the development of channel-lobe (D1) and channel systems (D3) around Geelbek (Fig. 6.8). Channel-levee systems are highly entrenched in Baviaans (Fig. 11) (Hodgson et al., 2011; Kane and Hodgson, 2011; Brunt et al., 2013a; Morris et al., 2014a; b), decreasing in entrenchment down-dip at Faberskraal (Fig. 6.11) (Flint et al., 2011). Lobe complexes are present down-dip in the east (Slagtersfontein and Floriskraal), fed from two directions, the west and south-west (Brunt et al., 2013a) (Fig. 6.11). Lobe deposits thin (D1 and D2) or are absent (D3) around the N1 Dome, where Unit C lobes are thickest (Figs 6.8 and 6.11).

The increased up-dip accommodation noted throughout Unit C is not as clearly expressed in Unit D. The long-lived feeder system present in the southwest throughout Unit C and D time has been well documented (Figs 6.11 and 6.12) (Hodgson et al., 2011; Kane and Hodgson, 2011; Brunt et al., 2013a; Morris et al., 2014a). Although the area is dominated by sediment bypass processes the base of Unit D in Baviaans is sand-rich and interpreted as a frontal lobe (Kane and Hodgson, 2011; Morris et al., 2014b) (Fig. 6.12). The change from lobe (D1) to channel-levee systems (D2 and D3) down dip in Geelbek (Fig. 6.11) also indicates a stratigraphic transition from deposition to bypass dominated (Fig. 6.12). The less obvious impact of slope accommodation may be indicated by the absence of intra-unit mudstones in Unit D (van der Merwe et al., 2014) suggesting that sedimentation rate outpaced deformation rate.

An overall decrease in down-dip entrenchment of the eastward propagating Unit C2 and D channel systems at Faberskraal may be related to intrinsic factors such as flow deceleration. However, the coincidence with Faberskraal-Geelbek lobe pinch-outs, suggests that a change in slope gradient may have been the key control (Fig. 6.12). Throughout Unit D time, a second feeder system is present around Floriskraal (Figs 6.11 and 6.12), coincident with D/E deposition (Fig. 6.8) but this feeder channel is not present in underlying deposits (Figs 6.8 and 6.11). The formation of these lobes and channel-lobe systems in the same location and orientation throughout Unit D may indicate the presence of a southeast facing slope, like the underlying Unit D/E situation (Chapter 5) (Fig. 6.12).



**Figure 6.11** Thickness and facies maps of Units C and D. Thickness is shown as isopachs with units in metres. Facies maps represent gross depositional environments for the given time intervals. Based on studies by, Sixsmith et al., 2004; Di Celma et al., 2011; Hodgson et al., 2011; Brunt et al., 2013 a; Morris et al., 2014a, b; van der Merwe et al., 2014; Morris et al., 2016.



**Figure 6.12** Thickness and facies maps of 'sand-attached' units C and D overlain on 3D box models demonstrating controlling slope to basin floor topography. Based on studies by, Sixsmith et al., 2004; Di Celma et al., 2011; Hodgson et al., 2011; Brunt et al., 2013 a; Morris et al., 2014a, b; van der Merwe et al., 2014; Morris et al., 2016.

### 6.7.2.2 Later phase slope topography: Units E and F

Sub-units E1, E2 and E3 consist of up-dip channel-levee and lobe deposits that pinch-out in the Faberskraal-Geelbek area (Fig. 6.13) (Figueiredo et al., 2010; van der Merwe et al., 2014; Spychala et al., 2015). Down-dip E2 and E3 consist of thin channel-levee deposits, which transition to basin-floor lobes at the N1 Dome and Slagtersfontein, with initial deposits oriented southwest to northeast. E3 has an intervening sediment bypass dominated channel-lobe transition zone at Slagtersfontein (Chapter 5), characterized by scouring and sediment lags. E2 and E3 basin-floor lobes are underlain by widespread extensive siltstone (Fig. 6.13). E3 basin-floor lobes thin and pinch out abruptly south of Floriskraal (Fig. 6.13).

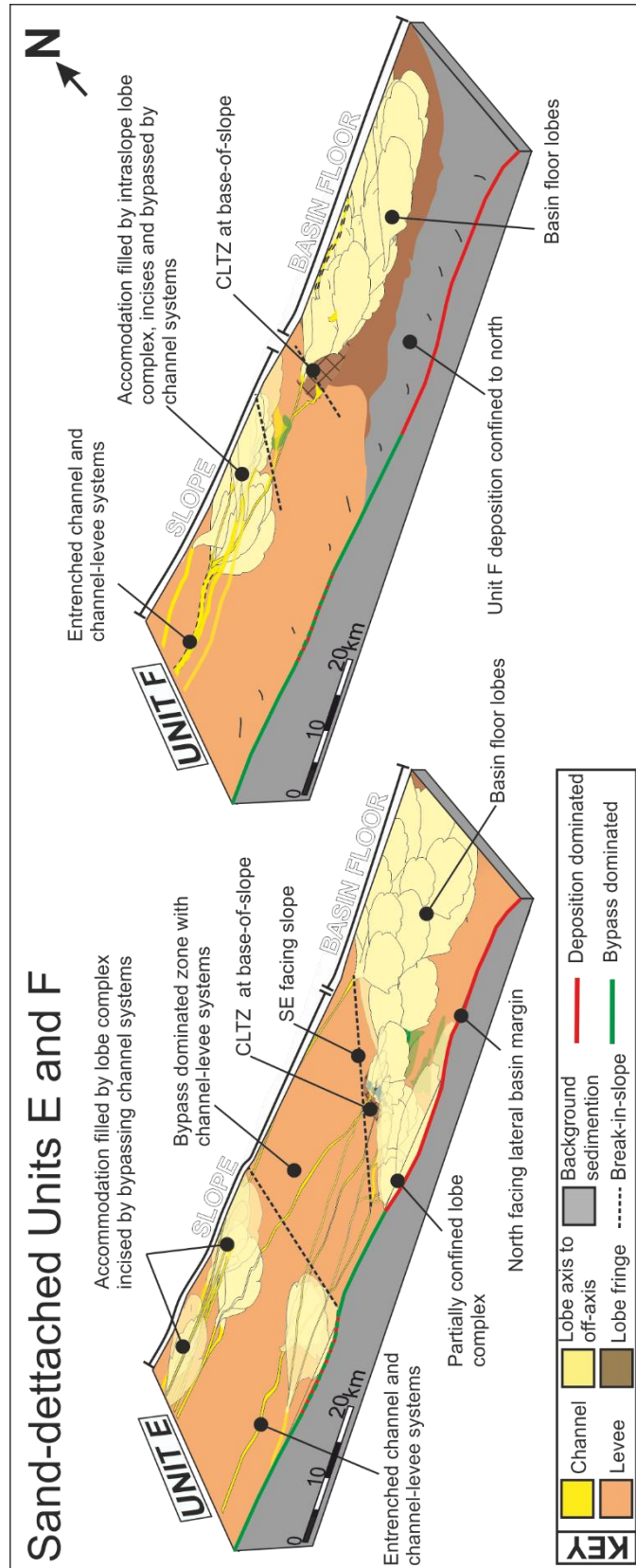
The formation of intraslope lobe deposits during Unit E (Figueiredo et al., 2010; van der Merwe et al., 2014; Spychala et al., 2015) indicates sustained accommodation on the slope (Fig. 6.14). The deposition of tabular, laterally continuous (kilometres in dip and strike), thin bedded siltstone packages (spill-over fringe deposits, *sensu* Chapter 5) beneath the basin floor lobes indicates that trapping of sand in intraslope lobes, and flow stripping of fines (Sinclair and Tomasso, 2002), occurred prior to any deposition down-dip (Fig. 6.14). Therefore, a fill and overspill model (e.g. Prather et al., 1998; Sinclair and Tomasso, 2002) can be inferred from the sediment grain-size distribution. This is supported by the occurrence of later channel incision into the intraslope lobes (Figs 6.13 and 6.14) (Spychala et al., 2015) which indicates accommodation was filled and the slope was at grade.

The zone of coarse sediment bypass present in E2 and E3 indicates a sustained area of decreased accommodation, close to equilibrium (Prather, 2003) (Figs 6.13 and 6.14). The development of a sediment bypass dominated channel-lobe transition zone, with scouring and rapid thickening of deposits down-dip may indicate that flows underwent hydraulic jumps, from supercritical to subcritical, due to an abrupt break-in-slope and/or decrease in flow confinement (Mutti and Normark, 1987; 1991; Weirich, 1989; Kostic and Parker, 2006; Sumner et al., 2013; Dorrell et al., 2016; Chapter 5). This represents the regional base-of-slope, likely southeast facing, indicated by facies transitions from channel-levee to lobe (Fig. 6.14). The abrupt southern pinch out of E3 lobes (Figs 6.13 and 6.14) indicates the influence of a southern lateral basin margin (Fig. 6.14) (van der Merwe et al., 2014; Chapter 5).

Unit F deposits are largely restricted to the north of the depocentre (Fig. 6.13). Sub-unit F1 consists of thin (< 5 m) lobe deposits, present in the Heuningburg area (Figueiredo et al., 2010) (Fig. 6.13). Sub-units F2 and F3 consist of thick, entrenched channel-levee systems in the

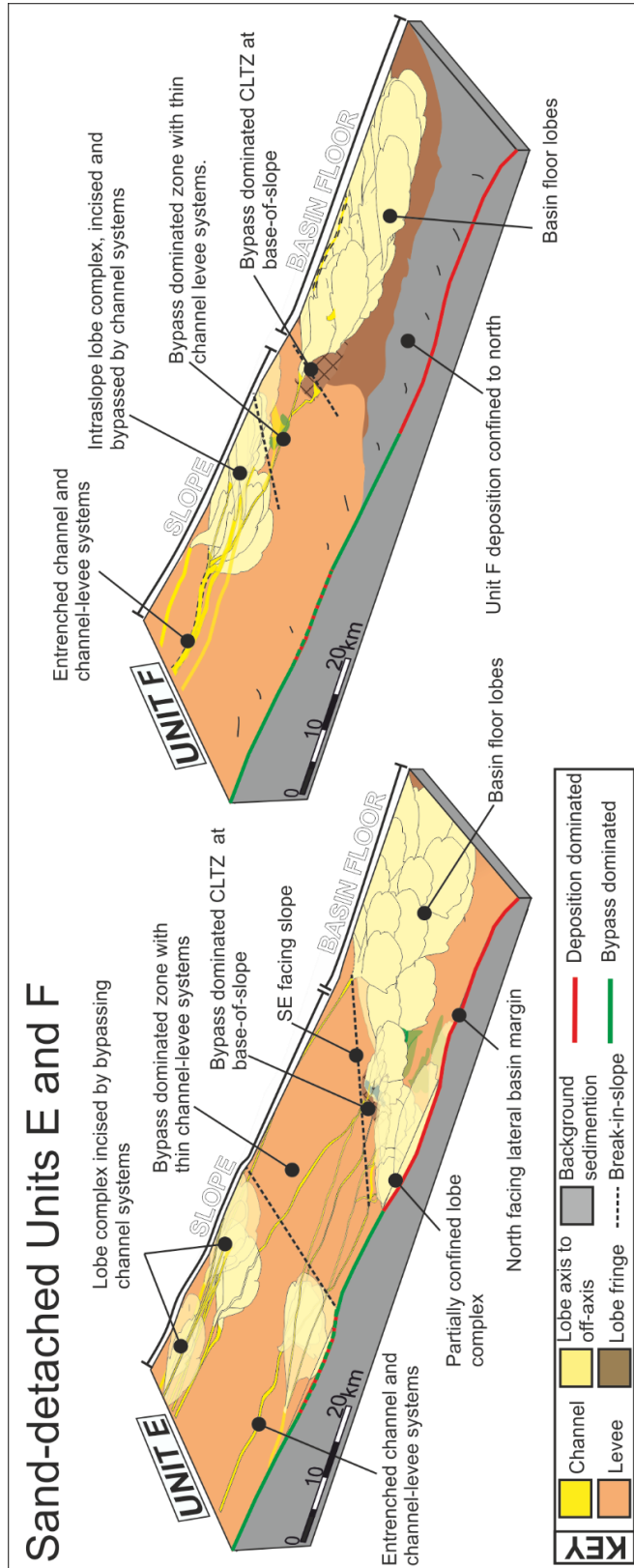
Heuningberg area passing down-dip into intraslope lobes around Faberskraal (Fig. 6.13) (Figueiredo et al., 2010; 2013). Down-dip F3 consists of thin channel-levee deposits that terminate in thick basin floor lobes around the N1 Dome, with an intervening sediment bypass dominated channel-lobe transition zone (Fig. 6.13), dominated by scours and bypass lags (van der Merwe et al., 2014).

Figueiredo et al. (2010) showed that the focus of Unit F to the north in the up-dip area, was likely related to a feeder channel in the northwest (Figs 6.13 and 6.14). The restriction of basin floor lobes also to the north may be a product of differential compaction of Unit E, with lesser compaction of axial lobe deposits to the south forming a topographic high and a lateral basin margin slope present further south (Fig. 6.14). The continued presence of a zone of coarse sediment bypass in the central area indicates a slope still close to equilibrium (Prather, 2003).



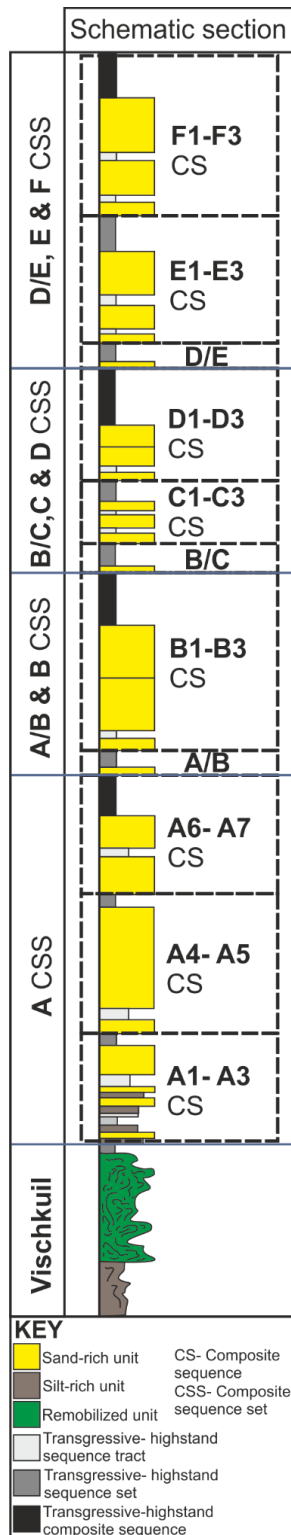
**Figure 6.13** Thickness and facies maps of Units E and F. Thickness is shown as isopachs with units in metres. Facies maps represent gross depositional environments for the given time intervals. Based on studies by, Figueiredo et al., 2010; 2013; van der Merwe et al., 2014; Spsychala et al., 2015; Chapter 5. .





**Figure 6.14** Thickness and facies maps of 'sand-detached' units E and F overlain on 3D box models demonstrating controlling slope to basin floor topography. Based on studies by, Figueiredo et al., 2010; 2013; van der Merwe et al., 2014; Spsychala et al., 2015; Chapter 5.

### 6.7.3 Slope to basin floor evolution: Units C-F



Throughout the deposition of Units C, D, E and F, several key areas have been recognised as having sustained usable deep-water accommodation (Figs 6.12 and 6.14). Although fixed in location, individual sub-units either completely or partially healed this accommodation. Therefore, this seabed topography must have been of low amplitude and formed progressively. The development of intraslope lobes in successive units in the same areas suggests that there were either several distinct episodes, or continuous slow generation of intraslope accommodation. At any one time confining topography/ gradient change allowing deposition of the thick, up-dip deposits would have been subtle, but long-term development in fixed locations led to a marked impact on the stratigraphic architecture (Fig. 6.15). Through the deposition of Units C and D the slope was sediment bypass-dominated (Fig. 6.12). Some up-dip accommodation formed during early and late Unit C time, with the pinch-out of these lobes coinciding with a change from highly entrenched to distributive channels in C2 and a reduction in entrenchment in Unit D (Fig. 6.12). The coincident location of these changes in successive units likely indicates overriding topographical control, such as a change in slope gradient. C1 and C3 lobe pinch outs indicate a decrease (or slight reversal) in slope gradient, confining deposition up-dip. The decrease in channel entrenchment in C2 and D in the Faberskraal-Geelbek area may have been the result of intrinsic processes, but the spatial coincidence with facies changes in other units, could indicate a topographic control, such as a reduction in slope gradient, which could cause flows to decelerate, decreasing their ability to erode. Conversely channels could be entrenched because the upper slope was 'above grade' (*sensu* Prather, 2003) and flows may have overtopped a topographic high

**Figure 6.15** Schematic section showing sequence stratigraphic division of Laingsburg and Fort Brown formations. Sand-rich Sub-unit sequence tract and overlying transgressive-highstand systems tract mudstones represent a sequence. Groups of these and the overlying inter-unit transgressive-highstand sequence set mudstones represent composite sequences. Groups of composite sequences and thicker interunit transgressive-highstand composite sequence mudstones represent composite sequence sets. A/B, B/C and D/E are deposited at the start of each composite sequence set (Flint et al., 2011).

and continued onto a higher gradient slope (past the Faberskraal-Geelbek area) forming a new, lower equilibrium level and causing knickpoints to migrate up-dip to develop entrenched channels (e.g. Prather et al., 1998; 2017).

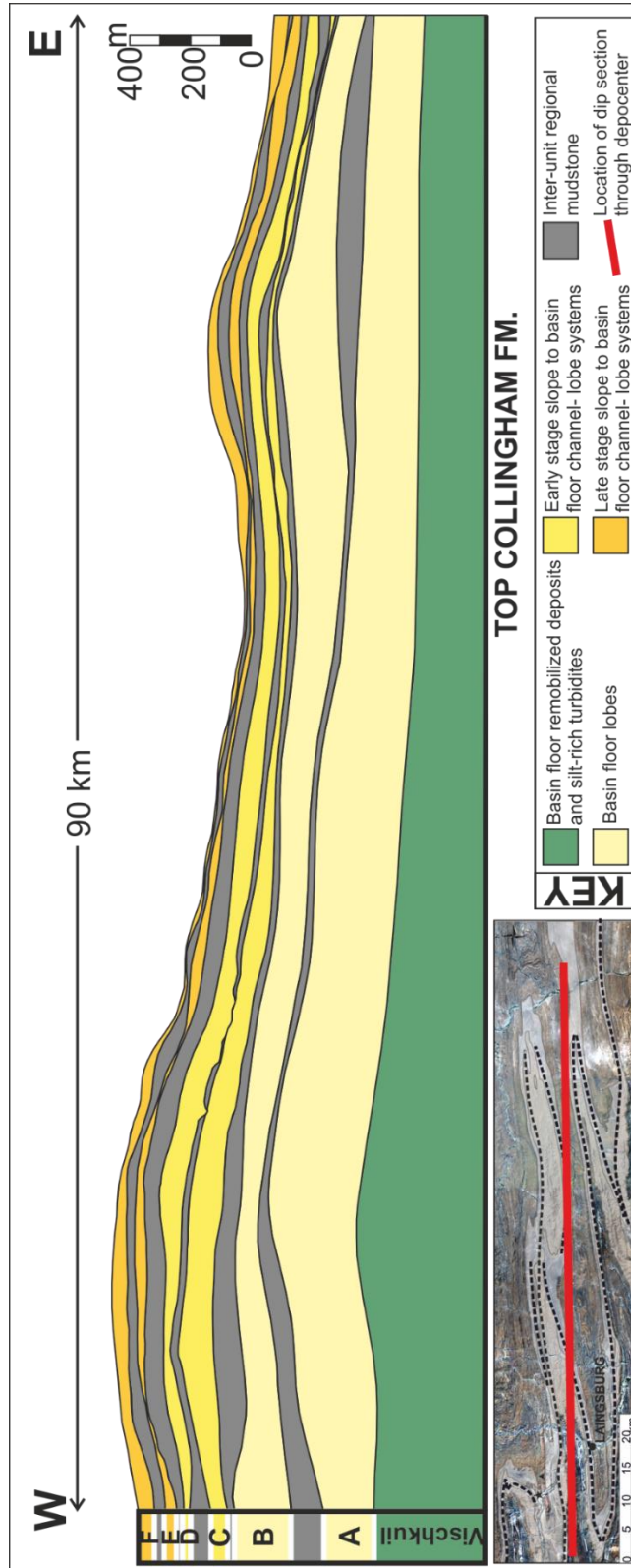
During deposition of Units E and F, accommodation was present up-dip of the Faberskraal-Geelbek area (Fig. 6.14), in similar locations to C1 and C3 (Fig. 6.12 and 6.15) (van der Merwe et al., 2014). Distinct phases of infill and overspill of this up-dip accommodation are interpreted throughout Units E and F on the basis of incised intraslope lobes (Figueiredo et al., 2010; Spychala et al., 2015) and 'spill-over fringe' deposits underlying basin-floor lobes (Chapter 5) (Fig. 6.14). These data support phases of intraslope topography generation during each period of sand shut off. Zones of coarse sediment bypass in Units E and F likely indicate an increase in slope gradient in this location in order for flows to bypass efficiently. Absence of Units D/E and D3, as well as the thinning of D2 in the central area, may be indicators of this gradient increase.

#### *6.7.4 Early basin floor topography development and evolution*

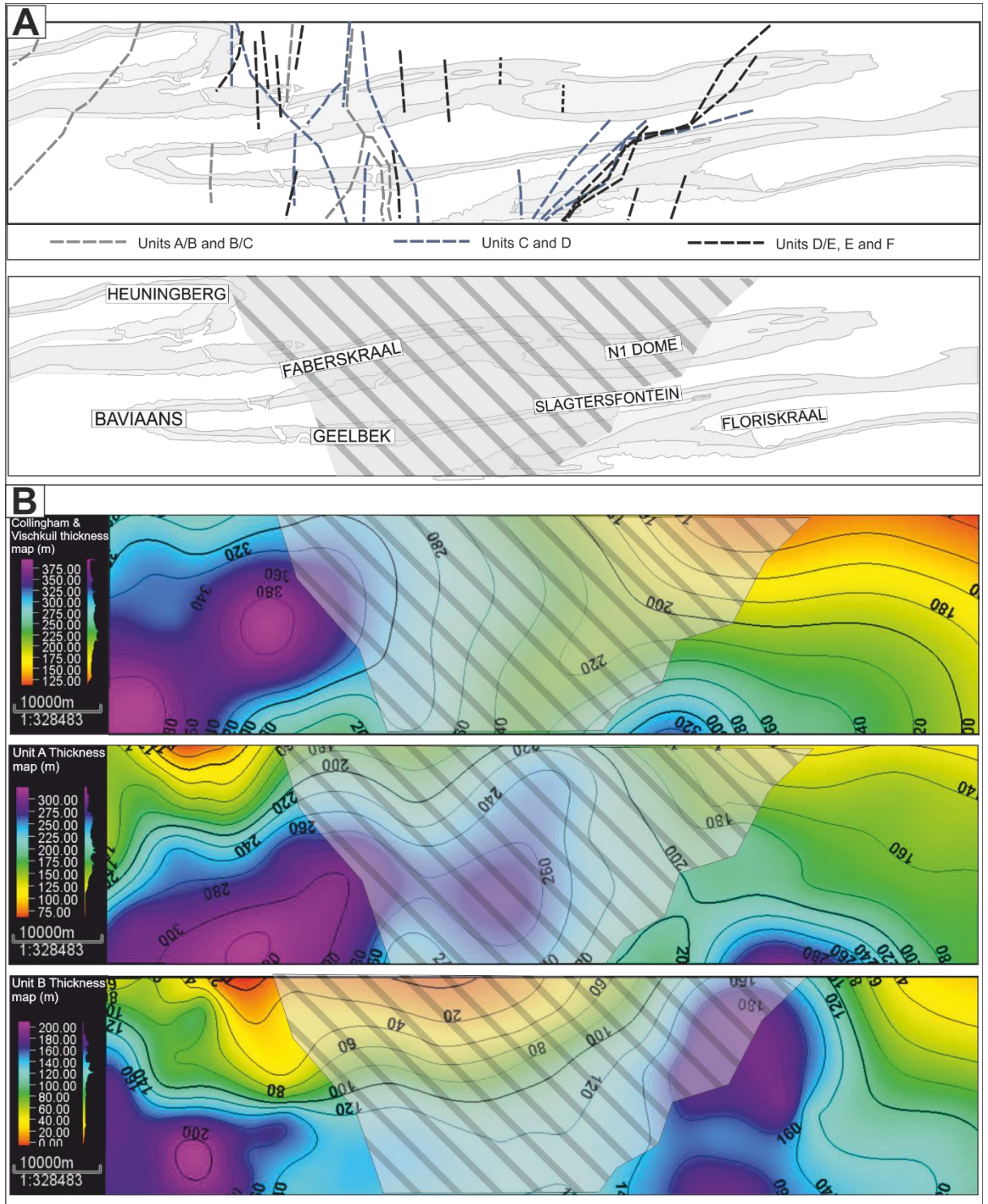
Seabed topography impacted the distribution of sediment across the slope and on the basin floor throughout the deposition of Units A/B, B/C, C, D, D/E, E and F (Figs 6.9, 6.12 and 6.14), and areas of more pronounced sedimentation remained fixed through the deposition of all of these units (Fig. 6.16). In order to understand when this long-term development of topography initiated, a 3D datacube was constructed in Petrel using the laterally persistent Collingham Formation as a basal datum and regional mudstones to correlate units throughout the entire basin. Figure 6.16 shows a dip section of the Vischkuil, Laingsburg and Fort Brown formations through the centre of the basin, demonstrating the two areas of increased thickness separated by a zone of thinning in all units. Thickness maps have also been constructed using this datacube, from the early stage starved basin plain deposits and mass transport deposits of the Collingham and Vischkuil formations through the overlying basin-floor lobes of Units A and B in the Laingsburg Formation (Fig. 6.17).

The Collingham, Vischkuil, and Laingsburg formations (Fig. 6.17) have the same general thickness patterns documented in the overlying units. In particular, thicker deposits in the west, thinning in the central area and thickening to the east and southeast. The northward thinning in Unit A is related to distance from the feeder system (Sixsmith et al., 2004) as well as the lateral intrabasinal slope documented by Spychala et al. (2017a). The easterly thinning in Unit A occurs in the Faberskraal-Geelbek area, and is consistent with the pinch-out of Units

A1, A2, A4, and A7 (Sixsmith et al., 2004), indicating increased accommodation up-dip of Faberskraal-Geelbek. The thickening of deposits around Floriskraal may indicate a second feeder system to the south, such as that recorded in Units D and D/E. The northward thinning of Unit B coincides with an axial to distal transition of facies, but is also related to a topographic high interpreted in the Heuningberg area (Grecula et al., 2003). The eastward thinning of Unit B (Fig. 6.17) coincides with a transition from channel-levee to lobe systems, with the thickening down-dip (Fig. 6.17) associated with renewed channelization (Grecula et al., 2003), and may indicate a second feeder system south of Floriskraal.



**Figure 6.16** Dip-section through central line of Laingsburg depocentre showing thickness of Vischkuil, Laingsburg and Fort Brown formations. The section demonstrates system scale compensational stacking between units as well as the prevalence of two separate areas of increased deposition with an intervening area of thinning, exacerbated by differential compaction.



**Figure 6.17** (A) Lobe updip, downdip and lateral pinchouts of smaller and larger units colour coded into stratigraphic packages. Grey shaded area indicates the region of sustained topographic influence throughout deposition of all units. (B) Thickness maps of the combined Collingham and Vischkuil formations, Unit A and Unit B. Overlay shows area of sustained topographic influence.

### 6.7.5 Topographic evolution of a stepped slope profile

The thickness and facies distributions for all deep-water units discussed above show, to varying extents, fixed locations of sustained topographic influence. Thickness and facies trends show that the systems were not 'at grade' (*sensu* Prather, 2003) at the initiation of deposition. Intra-slope accommodation was evident and therefore an 'out of grade' slope was generated during deposition of the thick regional mudstones of the transgressive and highstand sequence sets within each composite sequence. The mechanism by which accommodation was being created during deposition of each mudstone-dominated highstand sequence set (see Fig. 6.15) remained consistent in location, but was outpaced by sedimentation during deposition of lowstand clastic units. Therefore, longer hiatuses in clastic input inferred from mudstone thicknesses (see Fig. 6.15) would have led to higher amplitude intra-slope accommodation, with Units A/B, B/C and D/E deposited during these times. These units therefore likely represent deposition at times of maximum seabed topography.

The thinning of the Vischkuil Fm., Units A and B (Fig. 6.17), the absence of A/B, B/C and D/E (Fig. 6.9), the thinning of Units C and D (Fig. 6.11), and the formation of sediment bypass dominated zones in Units E and F (Fig. 6.13) all occur in the central area (Figs 6.16 and 6.17). This indicates a long-lived area of reduced accommodation, which is interpreted as a long-lived higher gradient 'ramp' above a stepped slope profile. This stepped profile had a more evident effect in the later Units E and F (van der Merwe et al., 2014), but was present to some extent from the onset of deep-water sand supply to the depocentre (Figs 6.16 and 6.17).

The cause of the protracted deformation of the slope is unknown, but it is clear that it was active prior to the onset of sand deposition (Unit A) in the basin (Fig. 6.17). Influence of inherited bathymetry alone (e.g. Adeogba et al., 2005; Gamberi and Rovere, 2011; Olafiranye et al., 2013) therefore cannot be the cause as it would be healed over time. Although differential compaction over an inherited structure is a possible contribution, it would have to be significant to cause continued stacking of thick, sand-rich elements throughout the basin-fill. Dynamic mechanisms have the potential to create significant and reoccurring accommodation. Salt and shale diapirism have been recognised as mechanisms that create slope deformation in many basins (e.g. Barton, 2012; Deptuck et al., 2012; Hay, 2012; Prather et al., 2012a, b), especially in the Gulf of Mexico (Prather et al., 1998; Prather, 2000; Meckel et al., 2002) but neither salt nor mobile shale have been recognised in the Laingsburg depocentre. Active tectonic structures can also create topographically complex slopes (e.g.

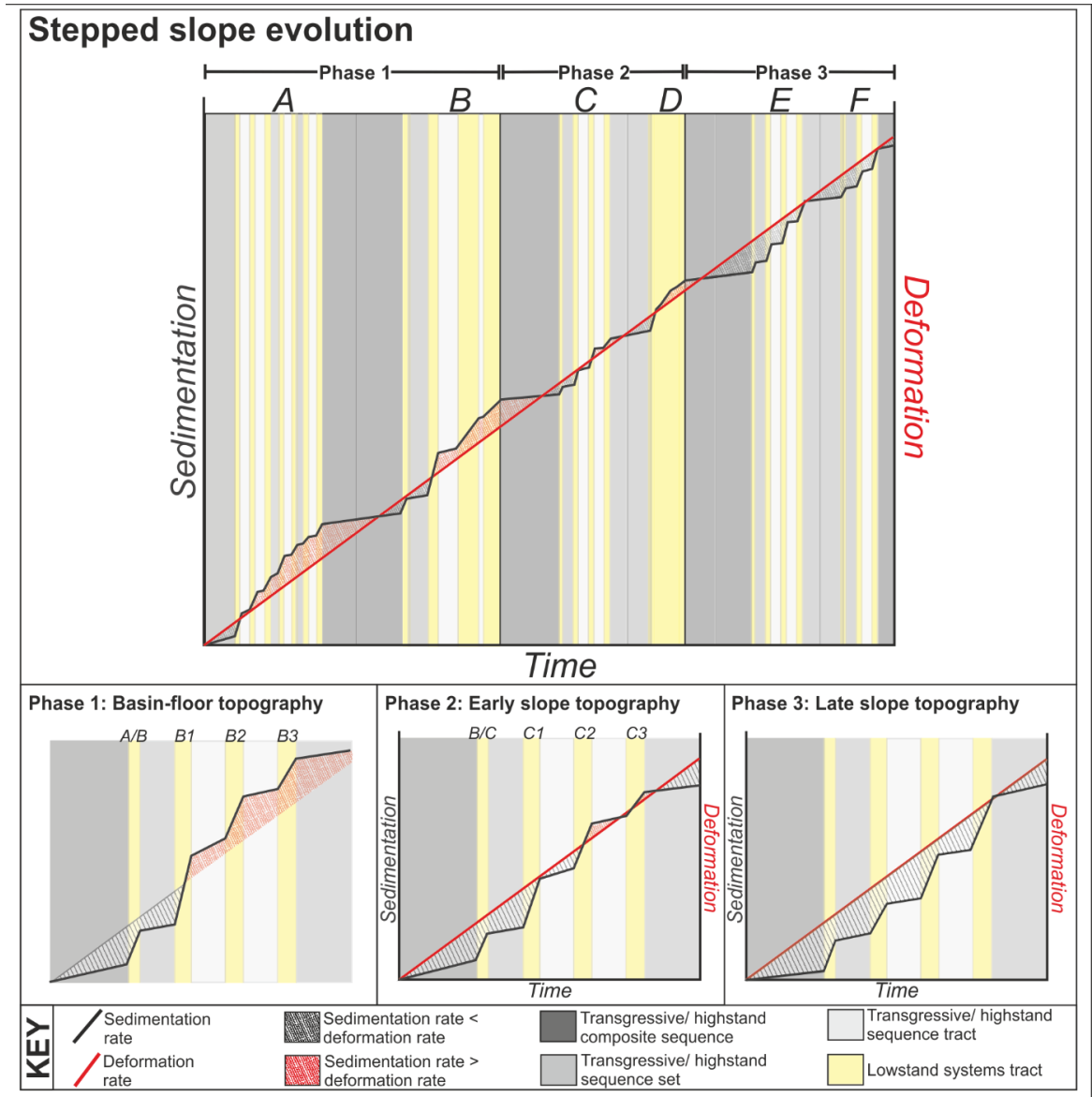
Hodgson and Haughton, 2004; Burgeen and Graham, 2014). However, no large-scale syn-sedimentary tectonic structures are documented in the Karoo Basin, although it is possible structures could be present at high angles to the post-depositional fold structures associated with the deformation front of the Cape Fold Belt. The characterization of the Karoo Basin as a thermal sag basin related to subduction dynamic topography (Tankard et al., 2009) suggests that differential subsidence or localized uplift could be possible mechanisms for generating this deformation. The repeated accommodation created west of the Faberskraal-Geelbek area indicates this area was undergoing subsidence at an increased rate compared to east of the area. This could indicate increased subsidence relative to the overall subsiding basin, or a stationary/uplifting basement block east of Faberskraal-Heuningberg which may have resulted in a steeper slope, leading to the formation of the E and F bypass dominated zones. Thermal subsidence can vary with upper crustal heterogeneity or thickness of basement, which are variable across the Karoo Basin (Binks and Fairhead, 1992; Bumby and Guirard, 2005) or with spatial variations in mantle downwelling and crustal heterogeneity (Tankard et al., 2009), with magnetic anomalies in the underlying basement (Weckmann et al., 2007; Tankard et al., 2009; Lindeque et al., 2011 indicating a highly complex upper crust.



**Table 6. 1** Example mechanisms for creating topography on the slope to basin floor and applicability to the Laingsburg depocentre stepped slope formation.

<b>Mechanism for creating topography</b>	<b>Description</b>	<b>Timescale over which stratigraphy is affected*</b>	<b>Height of topography created</b>	<b>Local/regional</b>	<b>Static/dynamic</b>	<b>Example</b>	<b>Applicable to Laingsburg depocentre stepped slope formation?</b>
Erosional and depositional relief	Erosion or deposition by single or multiple flows, e.g. scours and canyons or lobes and MTCs	Short to mid	cm to 100s of m	Local	Static	Prélat et al., 2009; Gamberi and Rovere, 2011; Kneller et al. 2016	<b>No</b> -Not forming topography over long enough time period -Not continuously active -Topography would heal and become less apparent over time.
Mobile substrate	Salt and shale diapirs and walls and associated withdrawal mini-basins	Mid to long	m to 100s of m	Local/regional	Dynamic	Prather et al., 1998; Mayall et al., 2006; Clark and Cartwright, 2009; Barton, 2012; Deptuck et al., 2012; Hay, 2012; Prather et al., 2012a, b; Doughty-Jones et al., 2017.	<b>No</b> -No mobile shale or salt has been recognised in the Laingsburg depocentre.
Tectonic structures	Small scale to regional scale faulting and folding, including gravity-driven structures	Short to long	cm to 100s of m	Local/regional	Static/dynamic	Hodgson and Haughton, 2004; Jackson et al., 2008; Mayall et al., 2010; Burgeen and Graham, 2014	<b>No</b> - No large scale faulting or folding is apparent in the depocentre. - Local evidence of growth fault -If present, faulting/ folding would be very gradual and at high angles to the later Cape Fold Belt-related fold structures
Inherited relief	Residual topography from underlying basement or stratigraphy	Short to mid	m to 100s of m	Local/regional	Static	Adeogba et al., 2005; Olafiranye et al., 2013	<b>Partial</b> - Basement heterogeneities have been recognised in magnetic surveys (Tankard, 2009) suggesting underlying basement was not uniform. - Thickness changes are not apparent in early deposits (Whitehill and Collingham formations) and therefore relief developed during Laingsburg and Fort Brown formation deposition.
Differential compaction	Accentuation of underlying topography through variably compacting substrate	Short to long	m to 10s of m	Local	Dynamic	Posamentier, 2003; Koša, 2007	<b>Partial</b> - Differential compaction over basement structures may have exacerbated formation of topography. - Compaction differences between sand-rich intraslope deposits (e.g. intraslope lobes) and silt-rich lower slope deposits (e.g. sediment bypass-dominated zones) may have exacerbated continued formation of stepped slope profile.
Regional uplift and subduction	Uniform or differential uplift or subduction over sub-basins or basins	Mid to long	10s of m to 100s of m	Regional	Static/dynamic	Barton and Wood, 1984; Leeder and Gawthorpe, 1987	<b>Partial</b> -Increased accommodation in the upper slope indicates basin subsidence may have been variable, possibly due to underlying basement blocks or variations in mantle down-welling. - The formation of a lateral basin margin to the south indicates either decreased subsidence or uplift to the south of depocentre.

\* Short= Instantaneous to < my, mid= millions of years to 10s of million years, long= 10s of million years to 100s of million years.



**Figure 6.18** Graph showing comparison of sedimentation and deformation rates throughout the deposition of the Laingsburg and Fort Brown formations. Phase 1 includes Units A, A/B and B; overall sedimentation rate outpaces deformation rate, with units A/B deposited onto a more deformed slope. Phase 2 includes Units B/C, C and D; overall sedimentation rate was roughly equal to deformation rate, periodically healing and overspilling slope topography in time of increased sedimentation. Phase 3 includes Units D/E, E and F; overall sedimentation rate was outpaced by deformation rate. Sedimentation rate was only sufficiently high during the later stage Sub-units E3 and F3 to equal deformation rate.

Overall, three key stages of stepped slope evolution can be documented in the Laingsburg depocentre (Fig. 6.18). In this model, in the absence of a strong chronostratigraphic framework, the rate of slope deformation is assumed to be constant, with variations in sediment input and the stacking of systems resulting in varying stages of topographic influence.

- Phase 1 (Fig. 6.18) is represented by the basin-floor units (A, A/B and B). These units were deposited at a time of high sediment supply, which outpaced the rate of deformation and therefore healed any accommodation created during times of sand shut off (Fig. 6.18). During early stages of Unit A sedimentation, healed slope accommodation (*sensu* Prather, 2000, 2003) would dominate. Due to the longer term sand shut off between the Unit A and B composite sequence sets, it is likely that Unit A/B and initial Unit B flows were deposited in partially confined healed slope accommodation. During Unit A and B deposition, once sedimentation rate outpaced deformation rate, depositional and erosional patterns (relatively minor during A and B deposition) could compensate to modify the basin floor profile and reach equilibrium.
- Phase 2 (Fig. 6.18) is represented by Units B/C, C and D. These units were deposited at a time of moderate sediment supply, in balance with deformation rate, with phases of healing and degradation of the slope evident within the Unit C and D lowstand sequence sets (Figs 6.12 and 6.13). The B-B/C transgressive and highstand sequence set sand shut-off caused B/C to commence deposition on a deformed slope (Fig. 6.18). Therefore, Unit B/C and initial Unit C sedimentation likely occurred in partially confined slope accommodation with continued C and D deposits filling healed slope accommodation (*sensu* Prather, 2003). The entrenched channel systems show that slope profile was above grade and eroding to establish a graded profile (e.g. Pirmez et al., 2000; Deptuck et al., 2012; Hay, 2012).
- Phase 3 (Fig. 6.18) is represented by Units D/E, E and F. These units were deposited at a time of lower sediment supply, with deposition commencing on a more deformed slope after the D-D/E transgressive and highstand sequence set sand shut-off. Units D/E, E1, F1 and F2 were deposited in perched slope accommodation, with E2, E3 and F3 deposited in healed slope accommodation (*sensu* Prather, 2003) where they proceeded to 'fill and overspill' accommodation to bypass sediment down-dip (e.g. Prather et al., 1998; Pirmez et al., 2000; Beaubouef and Friedmann, 2000; Booth et al., 2003; Barton, 2012; Bohn et al., 2012).

Overall this evolution demonstrates the transition from a relatively 'simple' slope to basin floor profile (Fig. 6.1) to a stepped slope profile (Fig. 6.1) with development of significant healed, but not ponded accommodation (*sensu* Prather, 2003), throughout. Previous studies have demonstrated that stepped slopes evolve temporally, with formation mechanisms generally inferred as either forming through mobile substrates or later stage tectonics (Prather, 2003; Hay, 2012) or through healing of minibasins (Satter et al., 1993; Prather et al., 1998; Prather,

2003). This study demonstrates that stepped slope profiles can evolve from relatively 'simple' slope profiles without mobile substrate or significant tectonic deformation, through subtle slope deformation, stacking of multiple systems and significant periods of coarse clastic shut off, which allow deformation to outpace healing of the profile. This highlights a key consideration suggested by previous seismic studies (e.g. Prather, 2003; Jackson et al., 2008) that the size and scale of deformation compared to sedimentation rate is critical, and that systems with episodic sediment flux form more slope accommodation (Prather, 2000, 2003). This study shows that subtle and slow but persistent deformation over a significant area of slope (many kilometres) with significant periods of sand shut off can modify sediment delivery pathways and consequently sand distribution to an extent comparable to that generated by more obvious mobile substrate and tectonics. This has implications for hydrocarbon reservoir prediction within slope systems which have become increasingly significant as exploration targets in many basins worldwide (e.g. Weimer and Link, 1991; Mayall et al., 2006).

This example of an evolving slope could therefore aid interpretation in lower resolution seismic and modern seafloor datasets, in systems where i) sedimentation rate outpaces deformation rate, ii) deformation rate is similar to sedimentation rate and iii) deformation rate outpaces sedimentation rate. Moreover, the evolution of the Laingsburg depocentre can be used as a tool for predicting the architecture of slope to basin floor deposition in basins with more subtle topographic complexities.

## **6.8 Conclusions**

The thickness and facies distribution of Units A/B, B/C and D/E indicate that they were strongly influenced by the presence of seabed topography on the slope and basin floor. Both dynamic and fixed seabed topography influenced unit distribution with influence of central, north to south trending, topography apparent throughout. The thin sand-rich nature of the units, with evidence of increased erosion, lack of lobe stacking and channel propagation, indicates significant differences from lobes in the larger units of the Laingsburg and Fort Brown formations. In a sequence stratigraphic context, these thin units represent the first sand deposition following major rises in sea-level which disrupted the previous lowstand sand supply to the system. The characteristics of the thin units are interpreted as marking only partial re-establishment of sand delivery pathways, expressed as a previously unrecognised type of intraslope lobe, here termed disconnected lobes that are not sourced from major feeder channel-levee systems, but rather accumulate from flows sourced from periodic

failures on the shelf and upper slope. Such disconnected lobes, are sedimentologically distinctive from other types of intraslope lobe, and restricted both in their stratigraphic position and deposit thickness, as a result of their formation within the initial stages of long-term relative sea-level fall. In contrast, larger units generally formed in periods of lower sea-level that were likely sufficient to expose the shelf break and develop and reuse mature upper slope sediment distribution pathways, with the possible exception of with initial deposition of units E and F.

The intraslope lobes of Units A/B, C, D/E, E and F indicate continued creation of slope accommodation in the up-dip area. The absence of units A/B, B/C and D/E, increased channel entrenchment in Units C and D, as well as the development of bypass-dominated zones in Units E and F all indicate the sustained presence of a ramp farther down dip in the central area.

Similar areas of increased and decreased thickness in the underlying Collingham, Vischkuil, and Laingsburg formations suggests that the stepped slope topography was well-developed before the onset of major sand input to the basin. This topography had an increasing influence on sediment routing upward through the deep-water stratigraphy, suggesting that the mechanisms for creating the topography were active in fixed geographical positions throughout sedimentation.

Overall, three key stages of stepped slope profile evolution in the same spatial position can be recognised, with an increasing impact on slope to basin floor systems. Phase 1 sedimentation rate outpaced deformation rate, healing slope topography. Phase 2 sedimentation rate was roughly equal to deformation rate, with intermittent phases of healing of slope topography. Phase 3 sedimentation rate was outpaced by deformation rate, with the stepped slope topography showing a dominant control on system architecture. Slope deformation initiated prior to clastic deposition in the basin and was likely constant throughout deposition of the Laingsburg and Fort Brown formations. The cause of this deformation is unknown but may have been differential subsidence across basement heterogeneities. The model presented here can be applied to predict accommodation change and deep-water system architecture across evolving stepped slope profiles, and shows that subtle but persistent deformation paired with significant periods of clastic shut off, can have a comparable impact on sediment routing systems to mobile substrate and active tectonics. The key to understanding this slope evolution was established from topographical indicators given by the distribution of

'disconnected lobes'. This suggests that thin sandstone units can be a better indicator of seabed topography over multiple sea-level cycles than thicker and more extensive systems that can overwhelm, but still be influenced by, perturbations in gradient.



## 7 Discussion and Conclusions

Here, the research questions posed in Chapter 1 are addressed, with reference to the results presented in Chapters 3-6. This chapter concludes with recommendations for potential future research arising from this PhD thesis.

### 7.1 Introduction

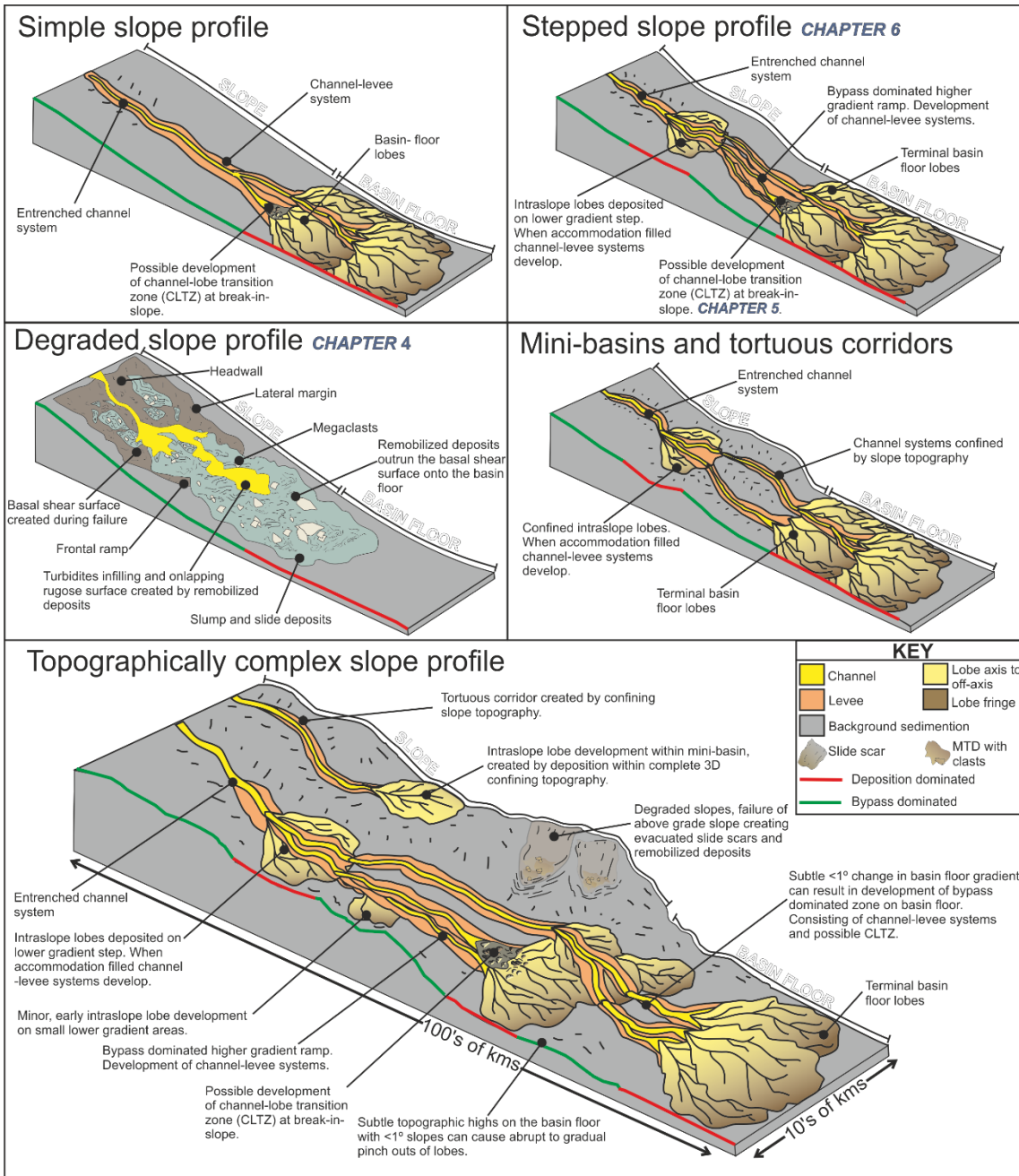
Understanding the effects of spatially and temporally variable topography on turbidity current processes and stratigraphic architecture is becoming ever more important as slope to basin flow profiles are increasingly recognised as topographically complex (e.g. Prather, 2000, 2003; Prather et al., 2012; Stevenson et al., 2013; Doughty-Jones et al., 2017). Topography can take the form of obstacles and slopes, which are frontal, lateral or oblique, and increase or decrease in gradient (Section 7.2), all of which impact flow processes and stratigraphic architecture on bed to system scale. The effect of topography on flow processes also varies temporally, with changes in flow dynamics, healing of topography and deformation of the slope and basin floor (Section 7.3). The variation in flow processes and complex evolution means these areas have variable degrees of preservation in the stratigraphic record (Section 7.4). These issues have significant implications for understanding and predicting hydrocarbon reservoir potential and sand connectivity in topographically complex slope to basin floor systems (Section 7.5).

### 7.2 How does orientation and gradient of slope to basin floor topography influence sediment gravity flow processes and resultant stratigraphic architecture?

The gradient changes of orientation of slope with respect to flow, impact erosional and depositional processes at a range of scales (e.g. Baines, 1984; Kneller and McCaffrey, 1999; Haughton, 1994; Kneller and Buckee, 2000; Smith, 2004a; Hodgson and Haughton, 2004; Jackson and Johnson, 2009; Deptuck et al., 2012; Prather et al., 2012a, b; Stevenson et al., 2013; Spychala et al., 2017a; Doughty-Jones et al., 2017). The field-based research presented here, tied to case studies from the literature, has led to three distinct configurations being identified based on the resultant stratigraphic architecture: i) frontal decreases in slope gradient (intraslope flats and base of slope) and reversals (intraslope); ii) frontal increases in slope gradient (intraslope ramps); and iii) lateral and oblique-lateral slopes. The various effects



of frontal and lateral slope perturbations on a range of slope to basin floor systems have been studied to characterise the resultant changes in facies and architecture (Chapters 4, 5 and 6). Together these changes in gradient and orientation can lead to the development of topographically complex slope to basin floor profiles (Fig. 7.1).



**Figure 7.1** Models of a simple slope profile, a stepped slope profile, a degraded slope profile and slope profile with mini-basin and tortuous corridors and a combined model showing a topographically complex slope.

## 7.2.1 *Frontal slope- gradient decrease and reversal*

### 7.2.1.1 Intraslope

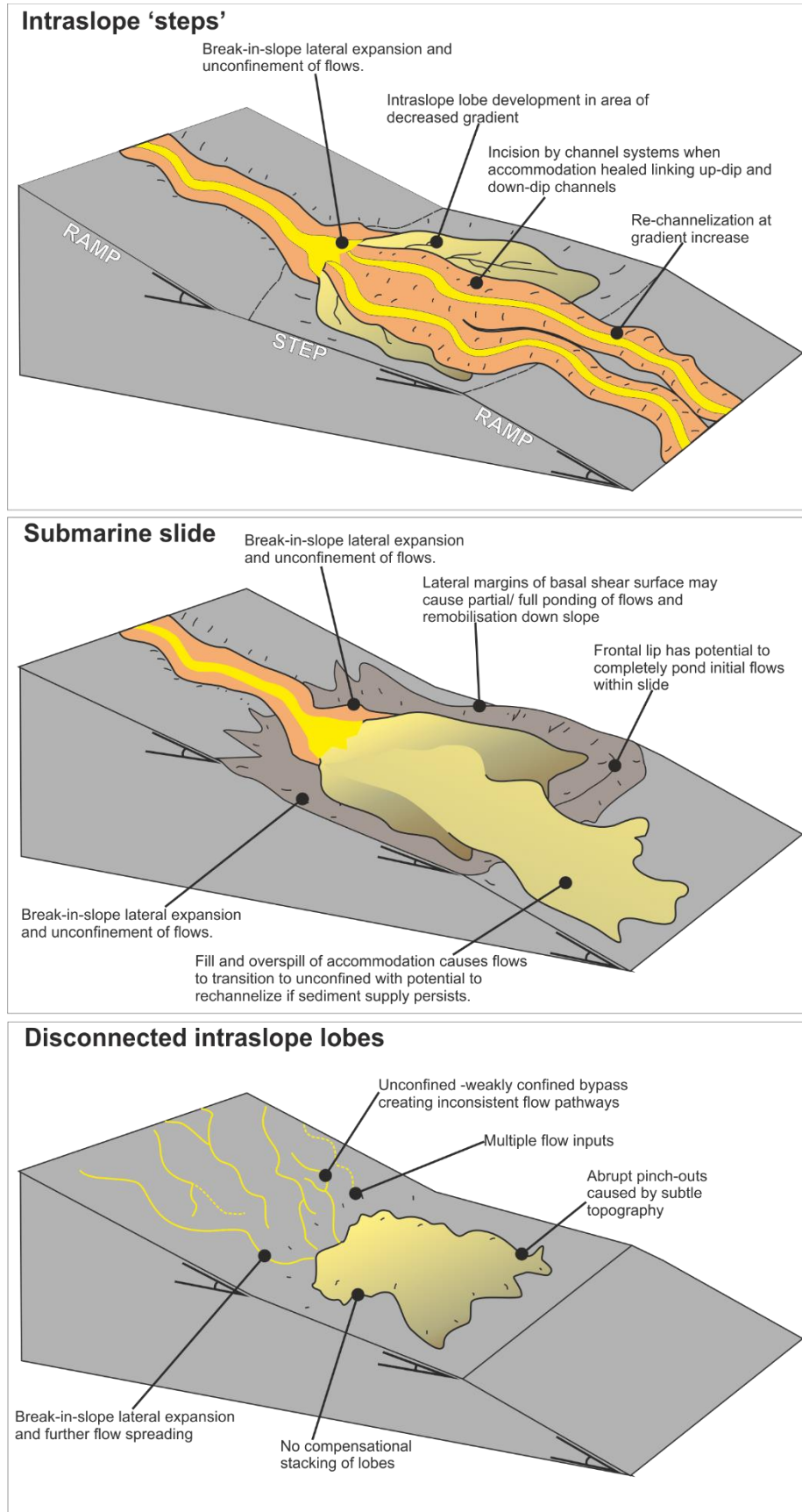
Downslope decreases and possible reversals in slope gradient have been interpreted to be the cause of intraslope accommodation and lobe development within Units B/C, C, D/E, E and F of the Fort Brown Formation (Chapters 5 and 6) as well as within the submarine slide basal shear surfaces at Vrisgewaagd farm (Chapter 4). These intraslope lobes are primarily recognised due to palaeogeographic context (van der Merwe et al., 2014) and are interpreted to form on a lower gradient step, within a stepped slope profile (Fig. 7.1) (Chapter 6). Key sedimentological criteria for recognition of intraslope lobes include: lobe dimensions, which are often an order of magnitude smaller than basin floor lobes due to restricted accommodation; lobe stacking patterns, which are often more aggradational than basin floor lobes; distinctive facies, including highly dispersed or opposing palaeocurrent directions, increased proportion of ripple and climbing ripple laminations, increased amount of erosional surfaces, and facies transitions over shorter distances; sand percentage, which is higher in intraslope lobes due to flow stripping of finer-grained materials; and incision by channels, indicating slope accommodation was transient (Spychala et al., 2015).

The degree of intraslope lobe confinement is a key consideration in characterising intraslope lobes. Intraslope steps (Fig. 7.2) are weakly confined to unconfined areas (Prather, 2003), with lobe deposition occurring due to a decrease in gradient and flow confinement. Weak down-dip confinement can cause flow stripping (Sinclair and Tomasso, 2002), whereby the upper, finer portions of flows are bypassed down-dip, leading to the development of sand-rich lobes (e.g. Chapter 6). This grain-size segregation has also been noted in Late Pleistocene intraslope systems offshore Nigeria (Jobe et al., 2017), and numerical simulations (Wang et al., 2017). Slide scars (e.g. Chapter 4) and intraslope minibasins (e.g. Prather et al., 1998; Badalini et al., 2000; Winkle and Booth, 2000; Sinclair and Tomasso, 2000; Shultz and Hubbard, 2005; Prather et al., 2012a, b, 2017; Sylvester et al., 2015; Doughty-Jones et al., 2017) can create 3D enclosing topography, within which confined intraslope lobes can form (Figs 7.1 and 7.2). Initial flows in confined intraslope lobes are fully ponded within topography, with similar characteristic to small confined basins (e.g. the Castagnola Formation, Felletti, 2002; Southern et al., 2015; Marini et al., 2016), including the formation of thick siltstone caps (e.g. Marini et al., 2016), as upper, finer grained portions of flows are unable to surmount downdip topography. As accommodation is healed flows gradually transition to weakly confined

(undergoing flow stripping) and unconfined, eventually infilling and overflowing confining topography (e.g. fill and over spill model; Sinclair and Tomasso, 2002).

Another consideration in intraslope lobe development is the magnitude and distribution of sediment input. Where concentrated channelized flows reach an area of lower gradient they can form intraslope lobes such as those discussed above and shown in Figure 7.2. Conversely, where sediment input is not concentrated in a single channel system and is widespread 'disconnected' intraslope lobes can form (Fig. 7.2) (Chapter 6).

These 'disconnected' lobes (Fig. 7.2) are characterised by thin lobe deposits that are widespread due to multiple sediment inputs and do not stack aggradationally or compensationally as a result. As no focused conduit (channel system) is constantly eroding a single area in order to grade the slope, the flows are likely traversing 'out-of-grade' areas (*sensu* Prather, 2003), and are therefore constantly eroding the slope. This is evident from the scoured bases of beds and high proportions of mudclasts within (Chapter 6). This widespread erosion may cause loss of energy in flows as well as forming subtle erosional topography throughout the slope, with the weak confinement allowing flows to be widespread as they reach a reduced gradient. Therefore, flows may react more to topography, due to: (a) increased subtle topography; and (b) lower energy and thinner flows unable to erode as they reach the low gradient area. These factors would cause more deflection of flows resulting in more numerous, widespread and complex pinch-outs and thinning of deposits.



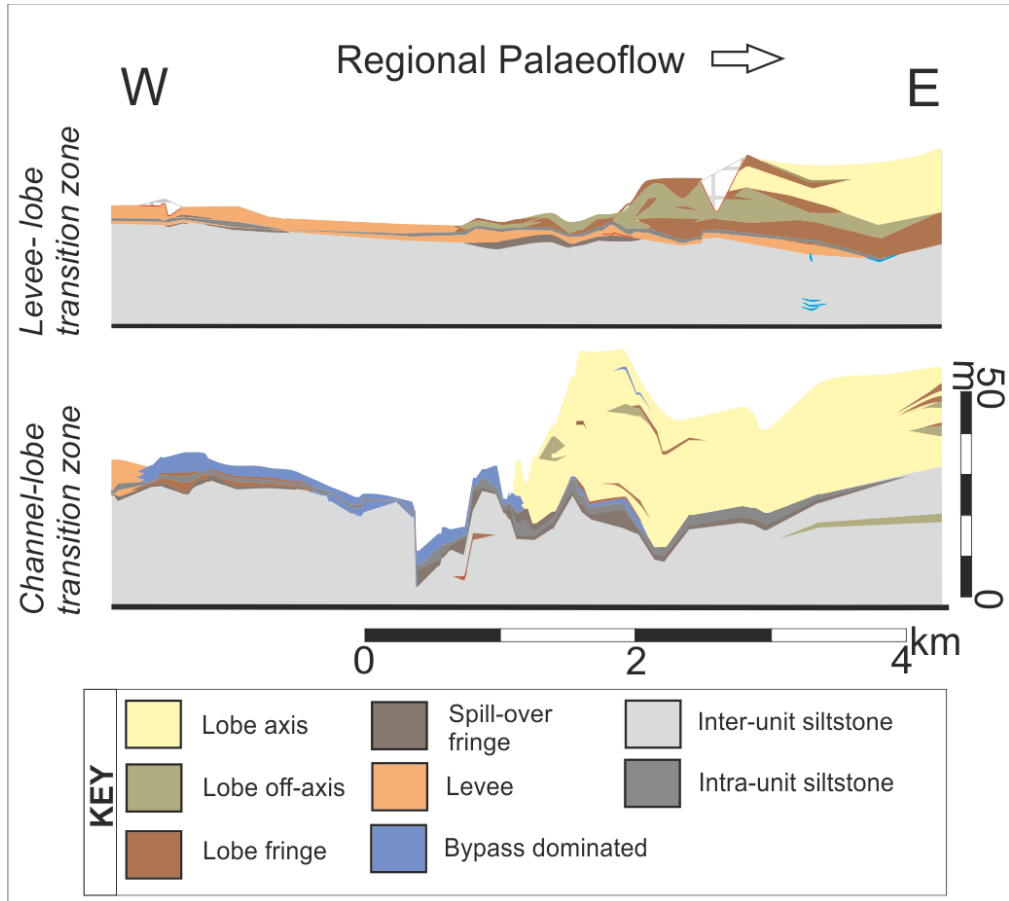
**Figure 7.2** Types of intraslope lobe. Partially confined lobes in intraslope steps. Confined to unconfined lobes in submarine slides and 'disconnected' intraslope lobes with multiple input points.

### 7.2.1.2 Base of slope

The most marked decrease in gradient is generally associated with the transition from slope to basin floor, at the base of slope. Unconfined basin-floor environments are dominated by lobe deposition (e.g. Shanmugam and Muiola, 1991; Shanmugam et al., 1995; Bouma, 2000; Johnson et al., 2001; Hodgson et al., 2006; Pr lat et al., 2009) and lower slope settings are characterised by channel-levee systems (e.g. Peakall et al., 2000; Babonneau et al., 2002; Posamentier, 2003; Posamentier and Kolla, 2003; Kane et al., 2007; Wynn et al., 2007; Di Celma et al., 2011; Hodgson et al., 2011). Therefore, the area in between the slope and basin-floor (the base-of-slope) commonly coincides with the development of channel lobe transition zones (e.g. Mutti and Normark, 1987; Gardner et al., 2003; Brunt et al., 2013a; Van der Merwe et al., 2014; Hofstra et al., 2015; Pemberton et al., 2016).

Changes in the character of this slope break (e.g. up-dip gradient, down-dip gradient, ratio and length of gradient decrease) can lead to variability in the sedimentological and stratigraphic expression of the base-of-slope area, between successive systems (e.g. Unit D to E, Chapters 5 and 6) or within a single system (e.g. Unit E3, Chapter 5). This variability from connected channel-levees and lobes to a spatially distinct sediment bypass dominated CLTZ that can be transferred into the rock record (Fig. 7.3) is considered to relate to: i) the relative decrease in slope gradient; ii) the distance over which gradient changes; and/or iii) the properties of incoming flows, associated with proximity to feeder system (Chapter 5).

The Sub-unit E3 CLTZ can be characterised spatially into distinct zones (Fig. 7.4): (a) a proximal area of mixed erosional and depositional features, including composite scour forms, sediment waves and bypass lags; (b) a zone of more efficient sediment bypass, characterised by shallow (cm scale) composite erosional surfaces and drapes; and (c) a zone of reworked lobe deposits, with thick slumped sandstone beds, numerous erosional surfaces throughout, a significant mudclast and silt component, and a scoured top surface.



**Figure 7.3** Variations across the base of slope in Sub-unit E3 (Chapter 5) from a levee-lobe transition zone (top) to a channel-lobe transition zone.

A CLTZ has also been noted within the younger Sub-Unit F3, which contains a similar array of features in a bypass dominated zone (Chapter 6), comprising of an area of minor deposition with composite scours mantled by lag deposits (Appendix B.2), with thick basin floor lobes down-dip (Chapter 6; Appendix B.2). CLTZs with scours and lags are restricted to these later units suggesting that the flows had a greater tendency to produce a hydraulic jumps (Weirich, 1989; Kostic and Parker, 2006; Sumner et al., 2013) possibly due to the lower slope being of higher gradient, producing a more pronounced gradient change at the base-of-slope. This increased gradient may be associated with ongoing deformation and formation of the stepped slope profile (Chapter 6). Although not bypass dominated throughout, Unit A5 does show evidence of significant erosion at the base-of-slope where a comparatively larger scour (10s metres deep, hundred metres in length) has been documented (Hofstra et al., 2015).

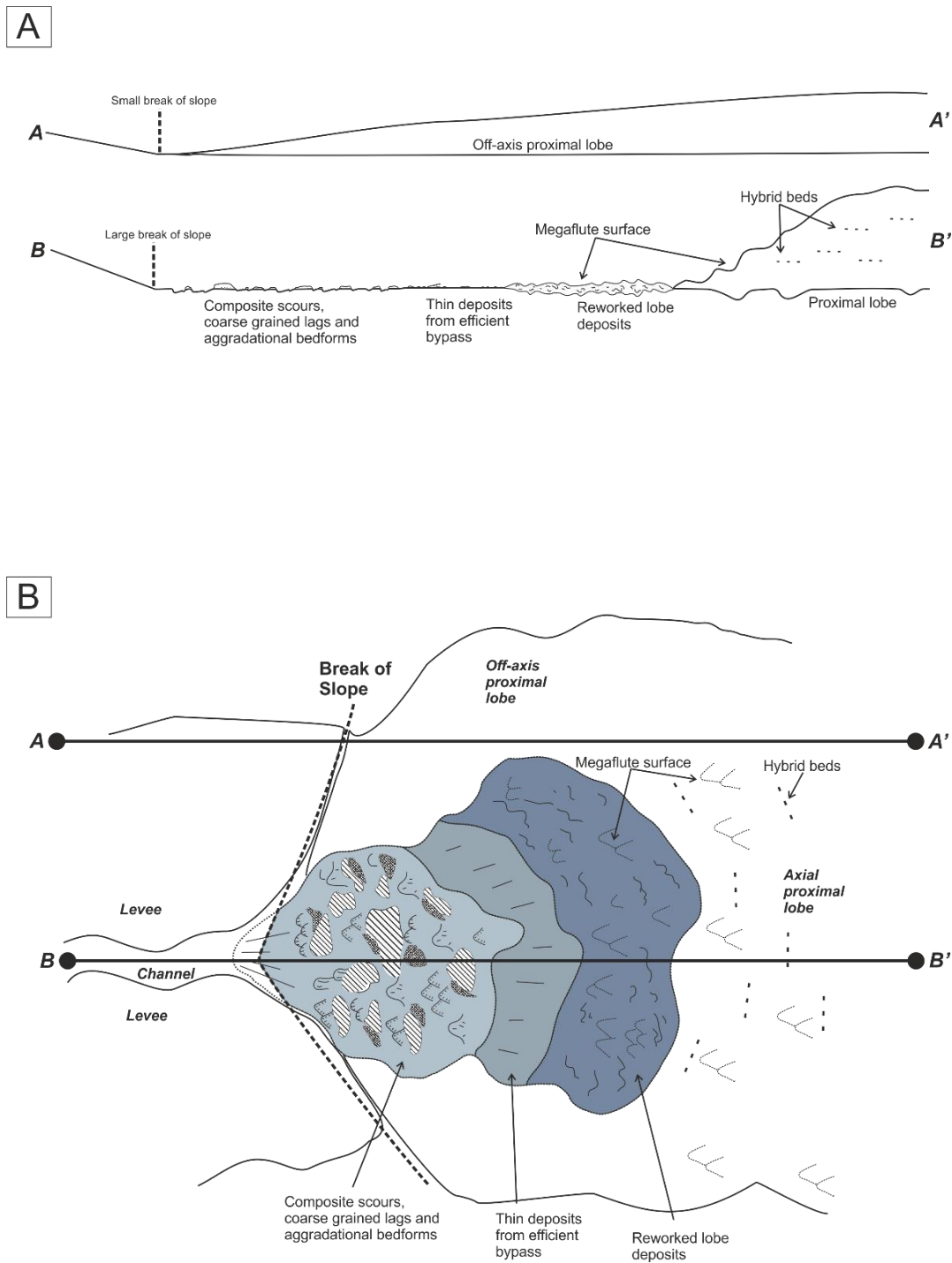


Figure 7.4 (A) cross sections and (B) plan view of CLTZ, modified from Wynn et al. (2002a).

### 7.2.2 Frontal slope- gradient increase

Downdip of intraslope lobe deposits in stepped slope profiles, intraslope minibasins and slide scars (as discussed above), slope profiles can increase in gradient (i.e. ramps in stepped slope profiles, Prather, 2000, 2003; O'Byrne et al., 2004; Smith, 2004a; Hay, 2012). This increase can

cause a similarly dramatic change (Section 7.1.1), which is associated with an increase in sediment bypass and the initiation of channelized flows (e.g. Hay, 2012; Stevenson et al., 2013, 2014). Sediment bypass has been shown to initiate with small gradient increases (fraction of a degree); for example, in the Agadir Basin Stevenson et al. (2013) show acceleration of turbidity currents with an increase in slope gradient from  $<0.02^\circ$  to  $>0.06^\circ$ , therefore intensifying ambient mixing at the head and reducing mixing in the body of the flow.

Whilst traversing step flats or slide scars, even when mostly healed, it is likely that flows will decrease in velocity and capacity due to spatial variations in gradient and topography, with some flows still becoming partially confined within these areas. Flows initially overspilling this area, may accelerate due to the increase in gradient, but will initially be unconfined to weakly confined with no pre-existing conduits, and depending on the number of entry locations onto this higher gradient area and the concentrations of flows, may remain relatively unconfined for significant periods (e.g. Sub-units E2 and E3, Chapter 5). In some cases, flows may remain unchannelized throughout unit deposition (e.g. Units A/B, B/C and D/E, Chapter 6). These unconfined to weakly confined flows are bypass dominated, leaving relatively thin depositional records (e.g. Sub-units E2 and E3, Chapter 5), and may show similar characteristics to unconfined channel bypass, described by Stevenson et al. (2013) in the Madeira channel system. Conversely, complete downdip re-channelization of flows may occur (i) when the volume and duration of flows bypassing the area is sufficient to create through going conduits, or (ii) when the gradient decrease/ reduction in confinement is insufficient for lobe formation and instead creates weakly confined channel complexes (e.g. Moody et al., 2012).

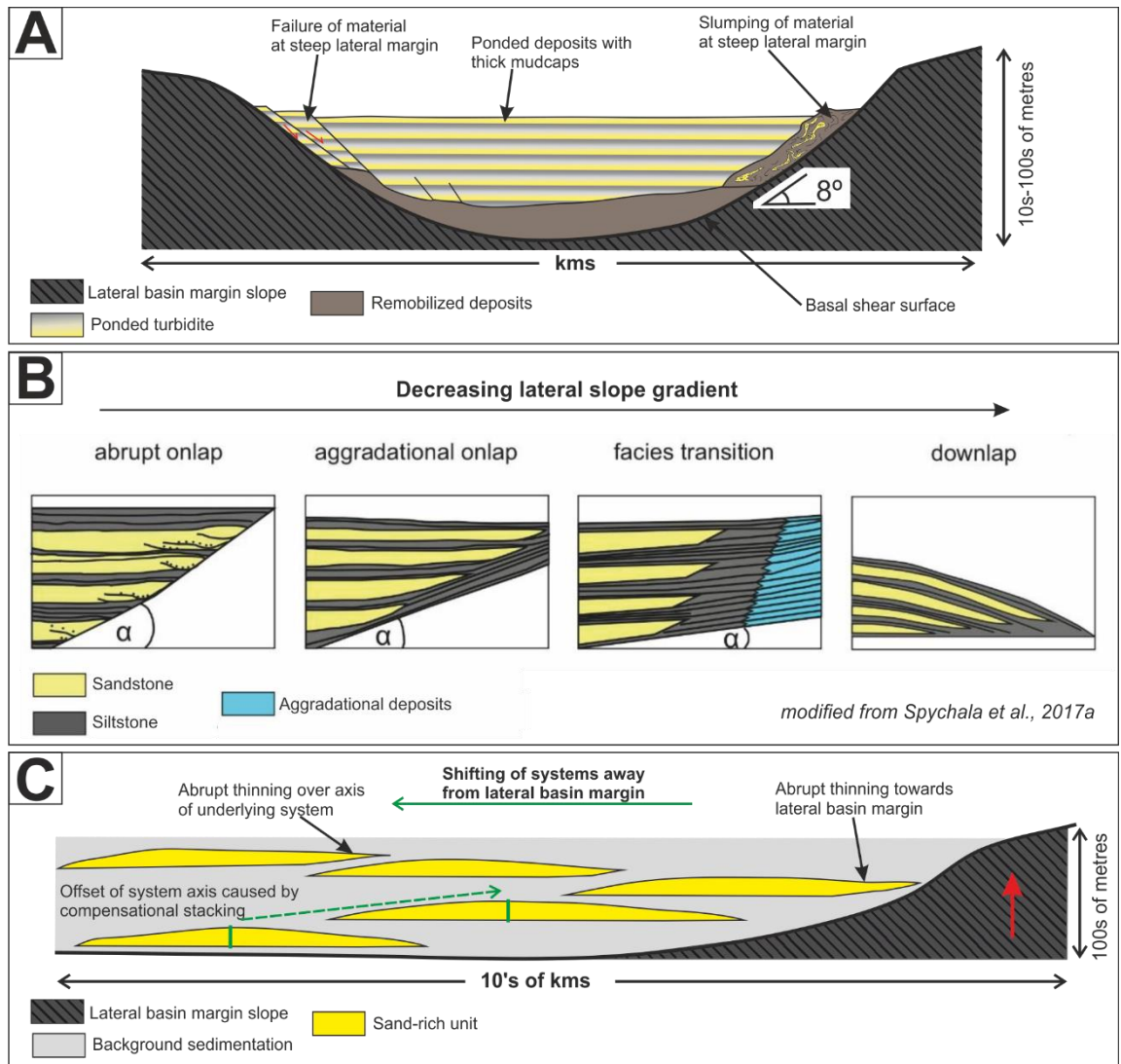
### *7.2.3 Lateral and oblique-lateral slopes*

The effects of lateral and oblique-lateral slopes on flows vary greatly with flow properties as well as the height, gradient and orientation of the slope (Kneller et al., 1991; Kneller, 1995; McCaffrey and Kneller, 2001; Amy et al., 2004). Lateral slopes of several magnitudes and scales have been interpreted to affect sedimentology and stratigraphic architecture of slope to basin floor deposits in the Laingsburg depocentre. High gradient lateral margins have been shown to contribute to confinement of flows and can be dynamic and drive instability and failure (Fig. 7.5A) (Chapter 4). Low gradient lateral/oblique slopes can cause varying onlap styles and pinch outs in lobes and lobe complexes (Fig. 7.5B) (Chapter 6). Regional-scale lateral slopes have been demonstrated to control depositional architecture of multiple systems (Fig. 7.5C) (Chapters 5 and 6).



High gradient lateral margins can cause the abrupt pinch out of turbidites; and drive instabilities. The infill of a submarine slide basal shear surface documented in the Laingsburg depocentre (Chapter 4) has shown that lateral margins of an  $8^\circ$  (compacted) gradient are sufficient to cause post-depositional slumping of infilling strata in the form of more cohesively faulted sediments and chaotic slumps, away from the lateral margin towards the deepest eroded point (Fig. 7.5A) (Chapter 4). Similar abrupt onlap, sometimes associated with remobilization, has been documented from small confined basins (Fig. 7.5B) with slope gradients of  $5^\circ$  - $12^\circ$  (e.g. Pickering and Hilton, 1998; Sinclair, 2000; Haughton, 2000; Sinclair and Tomasso, 2002; Amy et al., 2004; Hodgson and Haughton, 2004; Smith and Joseph, 2004; Amy et al., 2007; Aas et al., 2010; Etienne, 2012; Etienne et al., 2012; Yang and Kim, 2014; Marini et al., 2015). In areas of lower lateral slope gradient (e.g.  $<0.3^\circ$ ) lobes can show aggradational onlap and facies transitions (Fig. 7.5B) (Spsychala et al., 2017a) (Chapter 6).

Lateral slopes can also have an impact at regional scale. The relatively abrupt pinch out of several basin floor systems of the Fort Brown Formation (D/E and E3; Chapters 5 and 6) indicate the uplift of a lateral basin margin, that affected both the architecture of the units and possibly the stacking of multiple systems (Chapter 6). The stacking of several of the slope to basin floor systems in the Laingsburg depocentre has been interpreted to be influenced by differential compaction over the sand-rich axes compared to the silt-rich margins of systems, and related compensational stacking (Grecula et al., 2003; Pr elat et al., 2009; van der Merwe et al., 2014). When the basin margin began to uplift in the south it caused the systems to stack towards the north (Fig. 7.5C) (Chapter 6).



**Figure 7.5** Outcrop examples of the effect of lateral slopes on sedimentology and stratigraphic architecture of slope to basin floor systems at varying scales. (A) High gradient lateral margins of submarine slide basal shear surfaces can contribute to complete ponding of later flows as well as cause remobilization down-slope into the centre of the basal shear surface. (B) The style of onlap of intraslope and basin floor lobes can be controlled by lateral slopes, varying from abrupt onlap against high gradient slopes to downlap in unconfined settings (from Spychala et al., 2017a). (C) The stacking of multiple lobe complexes through successive depositional systems can be influenced by active uplift of a lateral basin margin.

### 7.3 How does topographic influence on turbidity currents vary and evolve?

The topographic influence on flows can vary significantly over different timescales by varying the properties of individual flows or changes in the gradient/size/distribution of topography (Kneller and Buckee, 2000).

#### 7.3.1 *Topography evolution over deposition of a single system*

Throughout the deposition of a single system, flows vary according to their physical properties as well as changes along the flow pathway. Therefore, each flow reaching a specific point is subtly different. Moreover, topography can vary in location and relative magnitude. As flows erode and deposit they modify the shape of the seabed with which subsequent flows will interact. For example, with topographic height increase relative to flow height, flow stratification increases and a hydraulic jump is more likely to occur downstream of topographic change (Kneller and Buckee, 2000). If topography is decreased through depositional healing or erosion of slope/ obstacles, subsequent flows will interact with lower magnitude topography.

Examples of the varying response of flows to topography over a single system have been recognised throughout the Laingsburg depocentre and include the following.

##### 7.3.1.1 CLTZ migration and evolution

Detailed documentation of the Sub-unit E3 channel-lobe transition zone has shown that this sediment bypass dominated zone did not remain fixed through time and expanded, contracted and migrated throughout the formation of down-dip basin floor lobes (Chapter 5). This is interpreted to relate to (a) changes in flow dynamics, i.e. affecting the location where flows undergo a hydraulic jump (Waltham, 2004; Huang et al., 2009; Sumner et al., 2013; Dorrell et al., 2016); (b) the evolution of the feeder system, with flows travelling further into the basin through a more efficient channel system that is closer to equilibrium (Pirmez et al., 2000; Kneller, 2003; Covault et al., 2016; Hodgson et al. 2016); and (c) spatial variations of bed shear stress related to flow-topography interactions (e.g. Agadir basin, Macdonald et al., 2011a).

##### 7.3.1.2 Slope accommodation infill and overspill

The various types and formation of intraslope lobes has been discussed in section 7.1.1.1. When slope accommodation is being infilled flows can be partially or fully confined up-dip. As the accommodation is healed by continuous sedimentation, later flows interact with subdued topography. This phenomenon has been documented in other systems and termed the 'fill and

spill' model (e.g. Winker, 1996; Prather et al., 1998; Sinclair and Tomasso, 2002). The stratigraphic record of Sub-units E2, E3 and F3 of the Fort Brown Formation documents this process fully on an exhumed stepped slope for the first time (Chapters 5 and 6). Initially lobes form in an area of reduced gradient (section 7.1.1). Sand-rich deposits are contained within this up-dip area, whilst the finer upper portions of flow are able to continue down-dip, through flow stripping (Sinclair and Tomasso, 2002). These fines create widespread draping of siltstone thin-beds down-dip, as more sand is retained in the up-dip area. These deposits are present for 10s of kilometres in dip length and several kilometres in strike, and are termed 'spill-over fringe' (Chapter 5). As the first sand-rich flows breach up-dip confinement they are initially unconfined to weakly confined with no pre-existing conduits (section 7.1.2) therefore initial base-of-slope lobes are similar to 'disconnected intraslope lobes' (section 7.1.1), e.g. Sub-unit E2 (Chapters 5 and 6). As up-dip accommodation continues to heal, channel-levee systems can propagate over lobes e.g. Sub-unit E2 (Spychala et al., 2015).

This fill and spill evolution can also be documented in the infill of submarine slide basal shear surfaces (Chapter 4). Due to the lateral (Section 7.1.3) and frontal confinement (section 7.1.1) initial flows are fully ponded with thick siltstone caps (section 7.1.3) (Fig. 7.5A); these transition to unconfined flows stratigraphically as they break topography (Chapter 4). As the location of the slide scar is in a peripheral area to the main sediment input (Chapter 4), there is no later incision by channels. When accommodation was filled in this area, an up-dip area of sediment input likely switched and possibly filled other slope accommodation or continued down the main conduit out of section (Chapter 4).

### *7.3.2 Topography evolution over deposition of multiple systems*

Over longer timescales the effects of topography on entire systems can vary significantly, by varying the slope to basin floor profile through long acting processes such as deformation and uplift. Long term changes in the effect of topography can be seen in the evolution of the submarine slide scar complex (Chapter 4) as well as the evolution of the entire stepped slope profile (Chapters 5 and 6).

#### *7.3.2.1 Stacking of basal shear surfaces and evolving infill confinement*

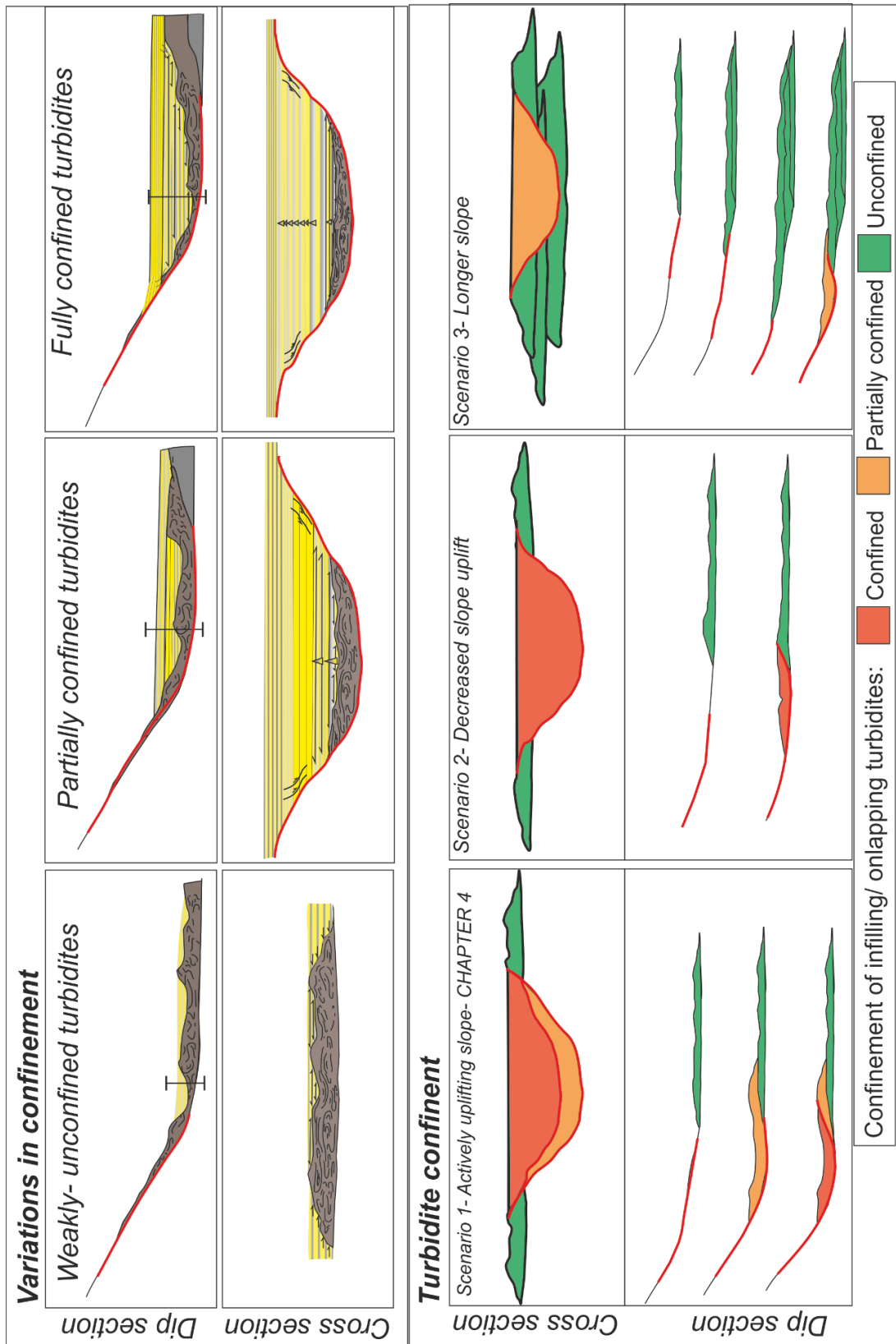
Chapter 4 documents the evolving confinement of submarine slide infill, forming on an actively tilting lateral basin margin. The submarine slide complex forms in three distinct stages: (1) deposition of unconfined remobilized deposits that have outrun their basal shear surface onto the lower slope or basin floor, with the rugose top surface causing the partial ponding and

confinement of flows; (2) erosion of a basal shear surface and infill with thick remobilized deposits and partially confined turbidity currents; and (3) erosion of a second basal shear surface and infill of thinner remobilized deposits and fully confined flows that stratigraphically transition to unconfined as accommodation is healed (Fig. 7.6).

The increase in turbidity current confinement is likely related to the down-dip stacking of the initial remobilized infill of slide scars, therefore forming larger down-dip topographic barriers (Fig. 7.6). Moreover, the increase in slope gradient will create a progressively more out-of-phase slope profile, which may result in increased basal shear surface depths within subsequent slides, leading to more frontal confinement (Fig. 7.6) (Frey-Martinez et al., 2006; Moernaut and De Batist, 2011).

Using this outcrop example as a model for actively uplifting slopes it is possible to speculate on the changes in flow confinement that may occur in other scenarios. For example, if a slope was uplifting more gradually or to a lesser degree it is possible that remobilized deposits would have insufficient gravitational potential energy to overcome the down-dip topographic barrier and would more quickly become confined (Fig. 7.6). Arguably, an increase in slope gradient could also cause more rapid confinement with a more out of phase slope profile resulting in increased basal shear surface depths within subsequent slides, also leading to more frontal confinement (Frey-Martinez et al., 2006; Moernaut and De Batist, 2011). If the slope was longer remobilized deposits would have greater gravitational potential energy and run out over longer distances, therefore numerous remobilized deposits would have to stack to create the down-dip confinement necessary to partially confine turbidity currents (Fig. 7.6).

Using this outcrop to speculate on stacking patterns in these situations may allow for improved prediction of reservoirs within the infill of submarine slides. Partially confined turbidity current deposits have the greatest reservoir potential due to the stripping of finer portions of flows leaving them sand-rich. Therefore, predicting where and when these situations can occur will aid hydrocarbon exploration.

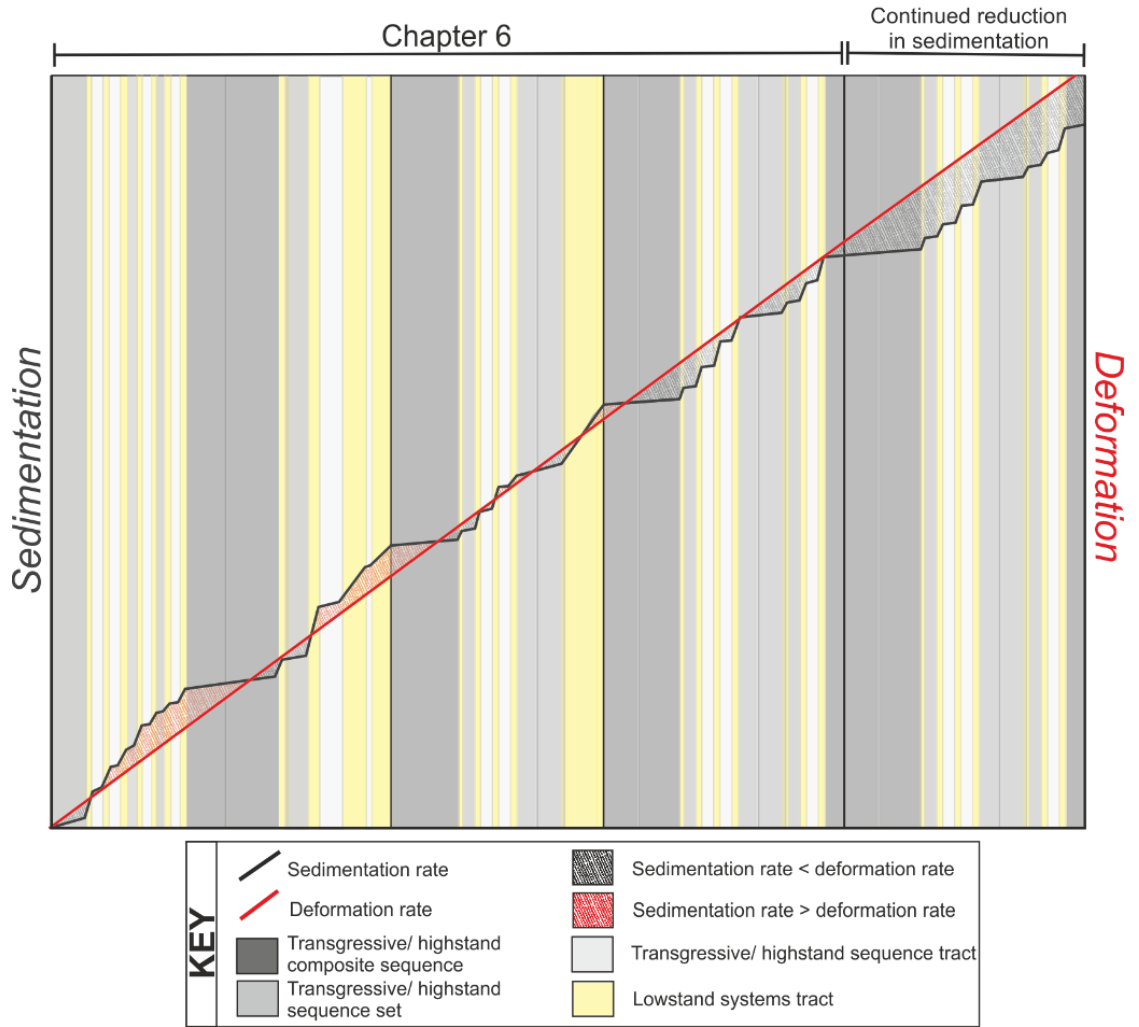


**Figure 7.6** Variation in turbidity current confinement overlying varying morphologies of basal shear surface and initial remobilized infill, with stacking example from Chapter 4 and two other scenarios of decreased slope uplift and a longer slope.

### 7.3.2.2 Evolution of slope to basin floor topography

The formation of stepped slope profile occurs when sedimentation rate exceeds the rate of subsidence, with slope accommodation considered to be 'healed' when depositional packages show evidence of late stage bypass e.g. E3 and F3 (Prather, 2000; Pirmez et al., 2000; Meckel et al., 2002; Hay, 2012). Higher subsidence rate in relation to sedimentation rate would be required to largely confine sand-rich portions of flows to the slope e.g. E1, E2, F1 and F2. Therefore, in a scenario similar to that of the Laingsburg depocentre, if the sedimentation rate was to continue decreasing in the pattern discussed in Chapter 6 then it is likely deformation rate would further outpace sedimentation rate (Fig. 7.7). In this scenario, the relative confinement of slope accommodation would increase, with the possibility that it would not fill and overspill, thus acting as a 'true mini-basin' with deposit fully ponded on the slope (Prather, 2000; Prather et al., 2012a) – a sill-and-fill model. The relatively subtle topography and low rate of deformation compared to many slopes with mobile substrates (e.g. Prather, 2003; Hay, 2012) is likely the cause of the relatively long duration and intermediate phases of stepped slope formation. It is evident that given sufficient time, slope accommodation and therefore slope deposits with sufficient reservoir potential can form in 'passive' basins with relatively subtle topography.

Continued slope development



**Figure 7.7** Graph showing comparison of sedimentation and deformation rates throughout the deposition of the Laingsburg and Fort Brown formation (more detail given in figure 6.18), further extended to show a scenario where deformation continues to outpace sedimentation.



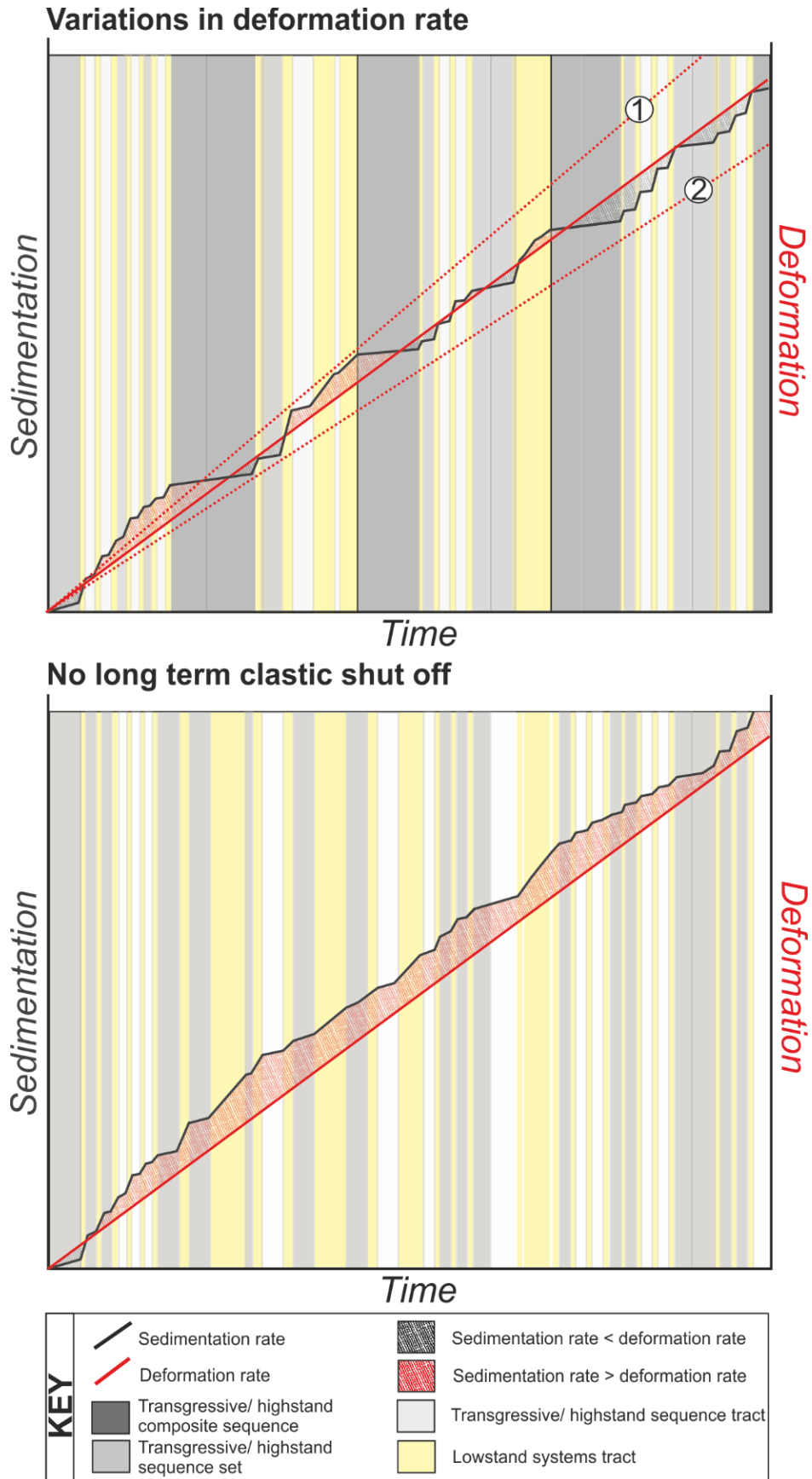


Figure 7.8 (Top) Variations in sedimentation vs. deformation rate if deformation were to increase/decrease in magnitude, and (bottom) if no long-term clastic shut off were to occur.

The graphical representation of sedimentation and deformation rate for the formation of the stepped slope profile can be modified to predict slope accommodation in other scenarios (Fig. 7.8). If deformation rate were higher than that in the Laingsburg depocentre (top graph, Fig. 7.8) then it would significantly outpace sedimentation rate earlier on in system development, possibly accelerating the development of the stepped slope profile, and leading to the development of fully ponded accommodation in the latter stages of evolution, similar to systems deformed by mobile substrate (e.g. Deptuck et al., 2003; Prather, 2003; Adeogba et al., 2005; Hay, 2012). Conversely, if deformation rate was less than in the Laingsburg depocentre (Fig. 7.8), sedimentation rate would outpace deformation rate throughout deposition of the Laingsburg and Fort Brown formations and therefore erosional and depositional processes could heal topography created by deformation and keep the profile closer to equilibrium (Pirmez et al., 2000).

Another likely contribution to the formation of the stepped slope profile was the long-term periods of clastic shut off between the lowstand sequence sets (Chapter 6). This also meant that the impact of the topography was more pronounced at the initiation of each lowstand sequence set (Chapter 6). Without high frequency or long duration clastic shut off there was not sufficient time for slope deformation to build and restore topographic flats or lows within the slope (e.g. Prather, 2000, 2003). In this scenario sedimentation rate will significantly outpace deformation rate (bottom graph, Fig. 7.8) and a stepped slope profiles will not evolve.

#### **7.4 How are topographically complex components transferred into the stratigraphic record?**

Through the examination of modern seafloor datasets it is evident that the stratigraphic record does not directly reflect the seafloor processes at the time of formation. This is due to: (a) a bias towards depositional processes, which leave a greater stratigraphic signature, with bypass processes leaving little or no record; (b) strata only recording flow properties as they were during a depositional phase; (c) later erosion of material creating an incomplete record; and (d) the later modification of deposits by dewatering, slumping, faulting and failure during early compaction, and later structural deformation.

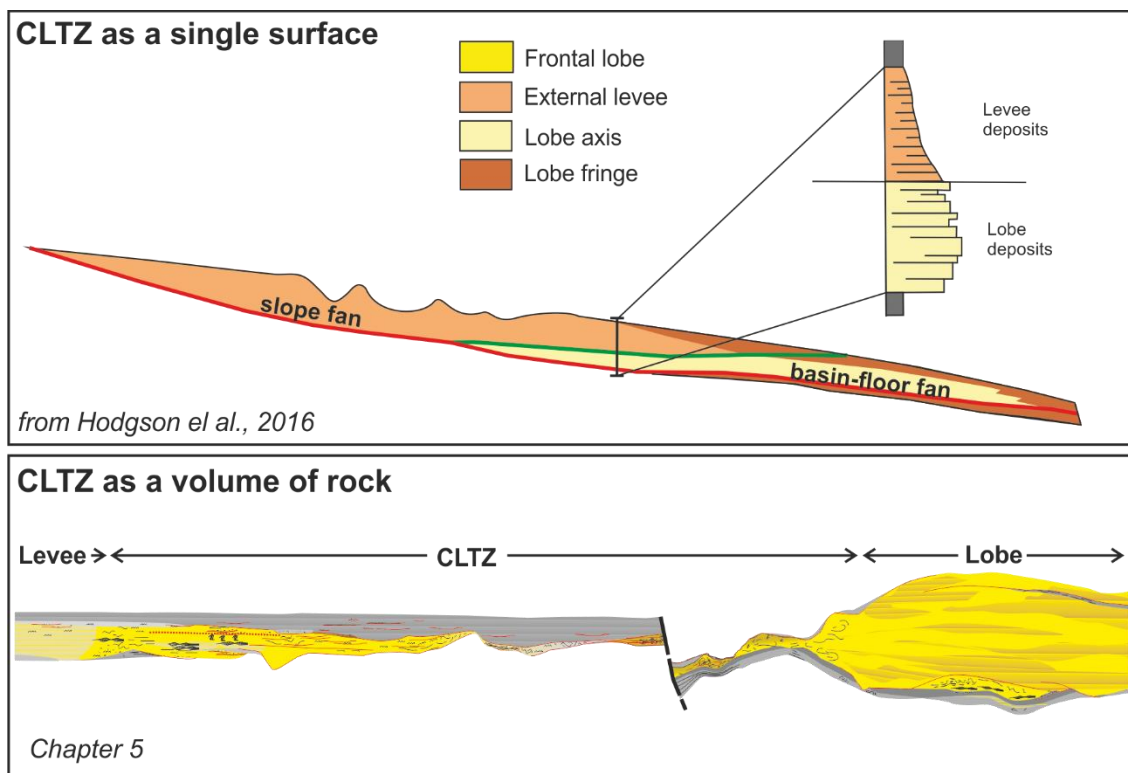
Preservation potential of features varies in response to system evolution (e.g. Hodgson et al., 2016). Therefore, when interpreting environments and evolution of deep-water systems from the stratigraphic record these issues need to be evaluated. Several examples of the complexity of transfer into the stratigraphic record have been noted in the Laingsburg depocentre, with

more issues arising where flows undergo significant changes, such as in topographically complex areas and where surfaces are time transgressive.

#### 7.4.1 Bypass dominated zones

By definition bypassing flows should neither erode nor deposit and therefore leave no stratigraphic record. Despite this, fully bypassing flows are likely rare in the 'real world' with small-scale erosion or deposition occurring as flows traverse 'bypass dominated' areas. The description 'bypass dominated' (*sensu* Stevenson et al., 2015) is used to imply that flows with large sediment loads are traversing an area with minimal (mm- cm scale) erosion or deposition, and that for a specific stratigraphic interval, flows are leaving a negligible stratigraphic record. Due to this negligible record, sediment bypass dominated zones can be challenging to identify at outcrop, and are deciphered through features consistent with subtle erosional and depositional signatures from bypassing flows (Chapter 5) and recognition of down-dip sediments (Chapter 5 and 6).

##### 7.4.1.1 Channel-lobe transition zones



**Figure 7.9** Example of CLTZ preservation as a single surface (from Hodgson et al., 2016) and as a volume of rock (Chapter 5).

Overall, there is both temporal and spatial control on preservation potential of CLTZs. The CLTZ can be preserved as a surface (Fig. 7.9) (e.g. Chapter 6; Elliott, 2000; Gardner et al., 2003) or a net-depositional volume of rock (Fig. 7.9) (e.g. Chapter, 5; Hofstra et al., 2015; Pemberton et al., 2016). The preservation potential and style is a result of when the CLTZ is evolving within a system. In order to preserve the bypass-dominated area, the feeder channel must not later propagate through the system and erode the CLTZ; this is characteristic of progradational phases in system evolution (Hofstra et al., 2015; Hodgson et al. 2016). In retrogradational phases CLTZs are preserved, with development most substantial between these two phases at the maximum extent of channel propagation (Hofstra, 2016). Within CLTZs minimal deposition and composite erosion surfaces can represent several stages of migration, expansion and contraction (Chapter 5). Due to constant erosion and bypass of sediment, parts of the CLTZ can be significantly reworked and have low preservation potential. Distally and laterally away from the axial areas, deposits show less reworking and preserve primary features. The unique preservation of the Slagtersfontein CLTZ, unaffected by later stage progradation and incision of the channel system, suggests this section is either: (i) a sufficiently off-axis transect through the CLTZ and was not cannibalised as the channel propagated (Hodgson et al., 2016); or (ii) the channel never fully propagated through the zone (Hofstra et al., 2015). The unique preservation of the E3 CLTZ and the draping of regional mudstone may suggest an abrupt shut-off of the system, or a significant avulsion of the feeder system out of the study area to the north.

#### *7.4.2 Basal shear surfaces*

Submarine slide basal shear surfaces can have a complex transference into the stratigraphic record as they are time transgressive (Chapter 4). After the initial erosion of the basal shear surface the primary morphology of a basal shear surface/zone is further complicated by post depositional remobilization, occurring directly after deposition on unstable gradients (e.g. section 7.1.3) and/or due to differential compaction (section 7.3.3), especially over variably lithified substrate (Alves and Lourenço, 2010). Moreover, as the shear can commonly form a zone of significant thickness (up to 10 m; Chapter 4), there is potential for reactivation of many of the numerous slip planes due to dewatering, or loading by later infilling deposits. These surfaces therefore remain unstable long after initial erosion and can cause faulting in overlying material and creep.

### 7.4.3 *Differential compaction*

Compaction is important to consider when comparing ancient systems in the subsurface with modern equivalent. Differential compaction can result in significant alterations in primary morphology especially over spatially heterogeneous substrate such as within and outside of submarine slide basal shear surfaces, and over variably lithified substrate, such as megaclasts (e.g. Alves, 2010). Differential compaction can consequently cause the tilting, faulting or slumping of material in both early (soon after deposition) and late (during lithification) stages of burial.

Differential compaction can also affect areas where sand-rich units significantly thin, by compacting sand-prone units to a lesser degree than the draping mudstone. This is highlighted in the stacking of Units A-F in the Laingsburg depocentre. The overall down-dip thinning and then thickening recognised in most units to some degree (Chapter 6), creates a more significant signature in the stacking of all units. Therefore, differential compaction can highlight areas of fixed topography influencing several stacked units by creating a greater signature in the stratigraphic record, compared to a single system.

## **7.5 Subsurface applications and implication of study**

The use of outcrop analogues is a key tool to augment seismic datasets by documenting and quantifying sedimentary architecture, hierarchy, and sedimentary facies relationships that are below seismic resolution (e.g. Dreyer et al., 1993; Howell et al., 2014). Over 75% of global Cenozoic reservoir discoveries are associated with stepped slope profiles (O'Byrne et al., 2004), meaning they have had significant focus in recent reflection seismic-based research (Prather 2000, 2003; Steffens et al., 2003; Hay, 2012; Prather et al., 2012; Doughty-Jones et al., 2017), but the Laingsburg depocentre is the only exhumed example documented at seismic scale (van der Merwe et al., 2014). Topographic complexity can lead to unusual configurations of deep-water systems, with evolving flow-relief interactions, and therefore improved understanding of these can lead to reduction in uncertainty and improving prediction of reservoirs and seals during hydrocarbon exploration and production (e.g. Prather, 2003; Smith, 2004a; Jackson et al., 2009; Deptuck et al., 2012).

### 7.5.1 *Bypass dominated zones and up-dip pinch outs*

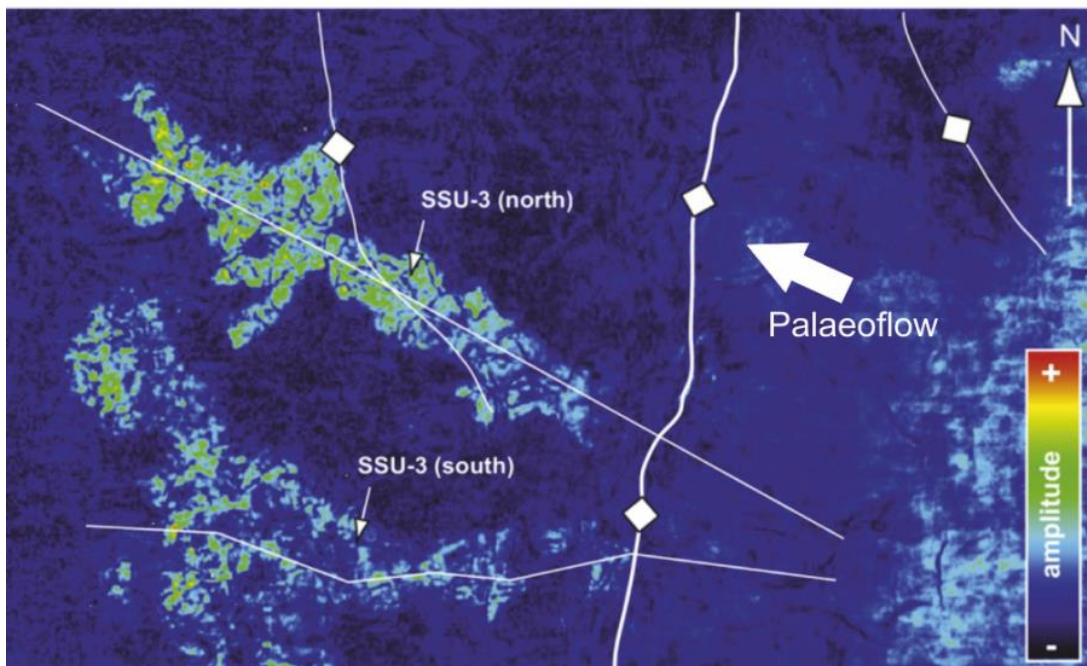
Areas of coarse sediment bypass are challenging to recognise in outcrop and are usually below seismic resolution (Fig. 7.10). However, they have been identified as key areas in the search for

updip stratigraphic trap targets (e.g. the Jubilee Field, offshore Ghana; Dailly et al., 2012). Therefore, there is significant uncertainty when predicting connectivity of sands up- and down-dip of sediment bypass dominated zones, and the likelihood of fluid leakage from lobes to channels. Sediment bypass-dominated zones that developed in channel-lobe transition zones in ramp to step settings have been investigated in detail (Chapters 5 and 6). Better understanding of the sedimentology and stratigraphy of these zones helps improve prediction of the degree of connectivity between up-dip channel-fills and down-dip lobes. Several factors need to be considered when assessing sand connectivity including: reservoir potential of sand, lateral variation across strike and temporal changes to the system.

Across the CLTZ, the sand component of Sub-unit E3 is thin (< 1 m and below conventional reflection seismic detection), has significant mud component, both in matrix and clast form, is highly dewatered and partially slumped, and is highly complicated due to numerous scours. Along the 2D exposed section at Slagtersfontein it is possible that the thin, 'dirty' and highly disconnected sandstone would prevent migration of hydrocarbons and therefore create an up-dip stratigraphic trap for the down-dip thick, sand-rich lobes which thicken abruptly at a rate of 9 m/100 m, to a maximum of 40 m in thickness. Examination of the same unit across strike complicates this assessment (Fig. 7.3 and 7.4), with the section to the north showing a direct connection between sand-rich levee and lobe deposits. The recognition of several stages of migration further complicates the 3D architecture of the CLTZ, which shortened and lengthened during deposition of Unit E from 2 km to 6 km indicating that CLTZs are dynamic features that build a complicated and composite stratigraphy. Therefore, any prediction of connectivity in 3D is highly challenging and presents significant risks for hydrocarbons. In the case of Slagtersfontein as an analogue for an updip stratigraphic trap, this may have worked as a combination trap due to the presence of a small extensional growth fault that may have effectively disconnected the lobes from the CLTZ.

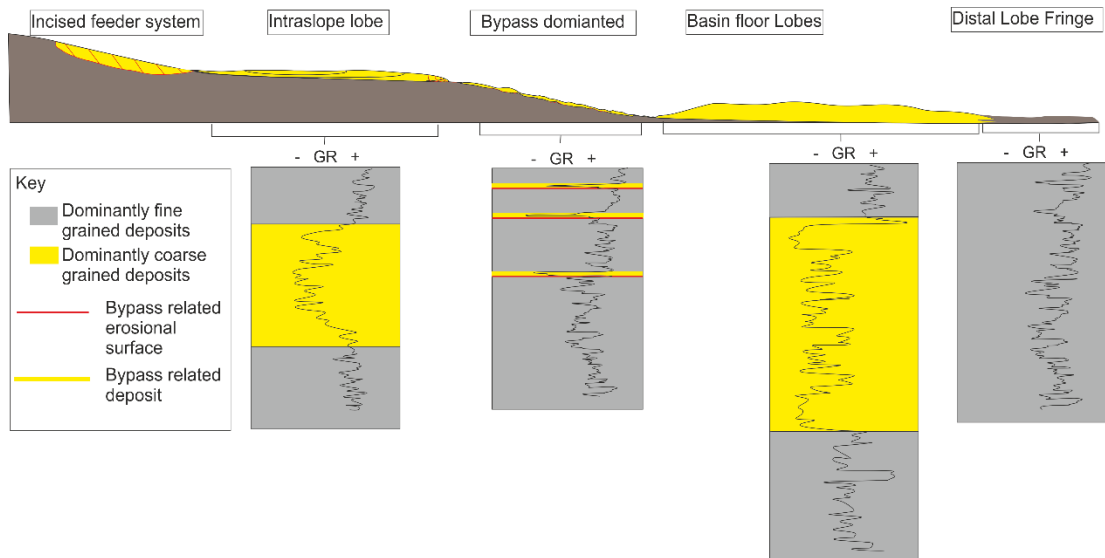
Reflection seismic datasets can be used to interpret areas of coarse sediment bypass as distinct areas of low amplitude separating areas of high amplitude (e.g. Fig. 7.10). These sand bodies may appear to be isolated and potential reservoirs. As discussed above, connectivity of sands below seismic resolution is possible. Figure 7.10 shows an example of 'disconnected' sand-rich channel systems from the Måløy Slope, offshore Norway, with an area of sediment bypass created by a localised steepening in slope gradient (Jackson et al., 2008). Examples from the Laingsburg depocentre have shown the possible development of weakly confined bypass dominated channels in high gradient 'ramps', feeding significant down-dip lobes (Chapters 5 and 6), which would leave a stratigraphic record several metres in thickness, (i.e.

below seismic resolution). Therefore, systems such as that shown in Figure 7.10 may have significant risks for up-dip leaking of hydrocarbons.



**Figure 7.10** Kyrre Formation, Måløy Slope, Norway- In this seismic section an area of high amplitude reflectors has been recognised, which well data has shown to be sand rich, lying down-dip of a fold structure with no apparent sand, suggesting that sand was bypassed over the structure (from Jackson et al., 2008).

Seismic reflection datasets are often augmented with well log and core data. These can be used to interpret the presence of bypass surfaces. Within core the presence of erosion surfaces can be used to interpret channel incision and bypass-dominated intervals. These surfaces may be overlain by lag deposits of intraformational or extrabasinal clast-rich conglomerate (Beaubouef et al., 1999; Pickering et al., 2001; Pickering and Corregidor, 2005; Luthi et al., 2006; Mayall et al., 2006; Hubbard et al., 2009; Grundvåg et al., 2014), or draped by fine-grained sandstone and mudstone. Where draped by sandstone or sand-rich lags, these surfaces can be recognised on gamma ray logs (Fig. 7.11). In gamma rays logs of CLTZs, these surfaces are represented as small negative spikes in sections that are otherwise similar to those of distal lobe fringes (Fig. 7.11) (Stevenson et al., 2015), therefore caution is needed when these apparently minor sand bodies are recognised up-dip of reservoir sands that have been interpreted as isolated. Conversely, if recognised down-dip of lobe complexes and considered terminal, they may actually indicate that the system continues down-dip with more distal reservoir targets.



**Figure 7. 11** Bypass related erosional surfaces and deposits can be visible as sharp negative spikes in gamma ray logs. Recognition of these spikes can distinguish between bypass surfaces and distal lobe fringe fines. In a basinal context these bypass surfaces are key conduits between up-dip and down-dip coarse deposits. Logs modified from Stevenson et al. (2015).

### 7.5.2 Stepped slope evolution

This study has shown that through the understanding of sedimentation rate and deformation rate it is possible to demonstrate the evolution from a 'simple' slope to a stepped slope profile, and to predict the development of ponded or perched accommodation (Section 7.3.2.2). Through the understanding and prediction of stacking patterns and sediment partitioning of systems at composite sequence scale, areas of long-term preferential sand volume can be predicted, with secondary control from differential compaction influencing compensational stacking patterns (Section 7.4.3).

Thin sand units, interpreted as disconnected lobe complexes (Chapter 6), have been shown to be key indicators for showing areas of long-term increased accommodation during slope evolution. The thickness of these units (<14 m) means they may not be discernible on most seismic datasets but are recognisable in core and well logs (Fig. 7.12). These units are represented as anomalous negative sections in gamma ray and neutron porosity logs in otherwise thick positive sections representing regional mudstone units (Fig. 7.12).



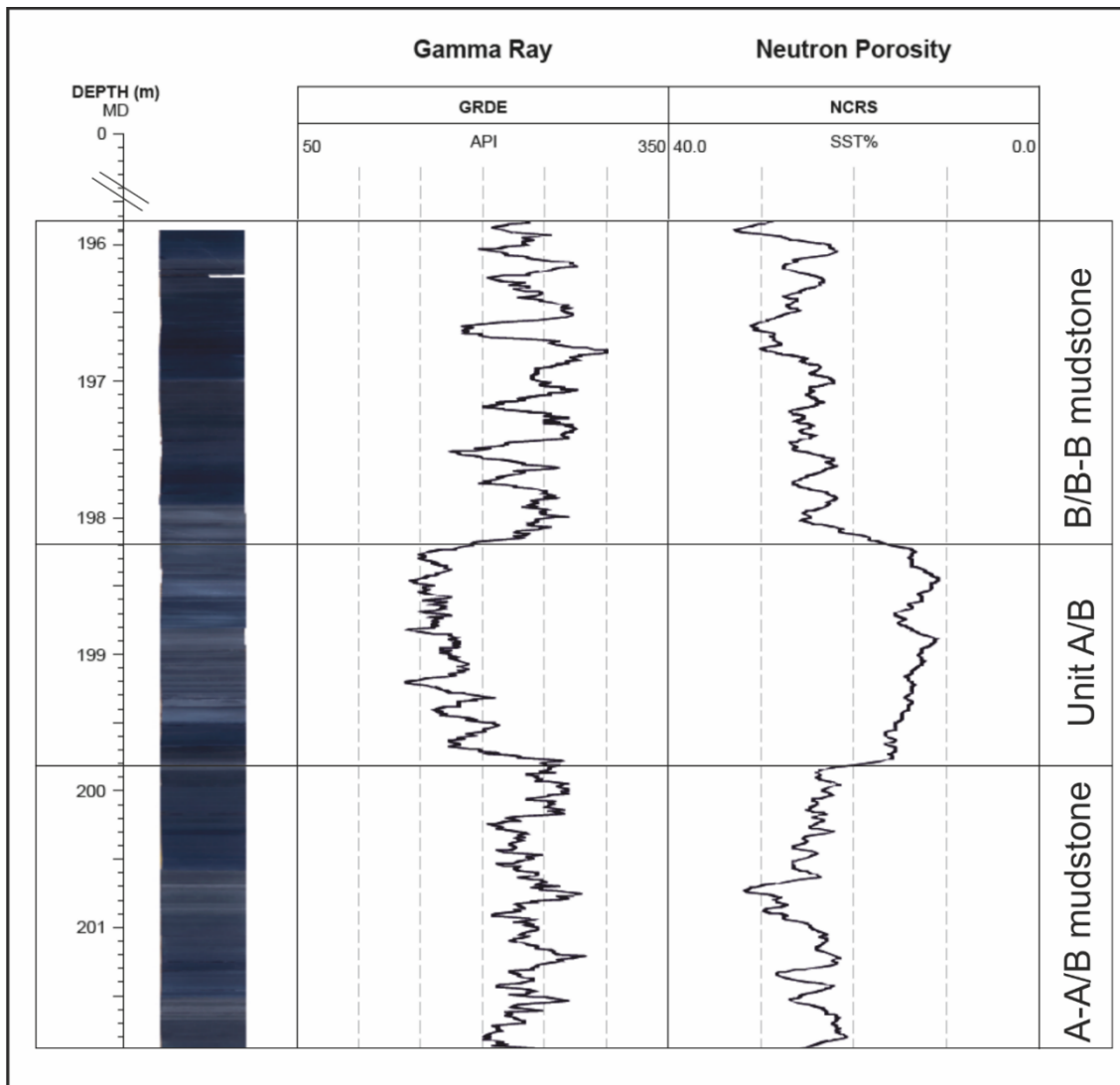


Figure 7.12 Core, Gamma Ray and Neutron Porosity logs of Unit A/B.

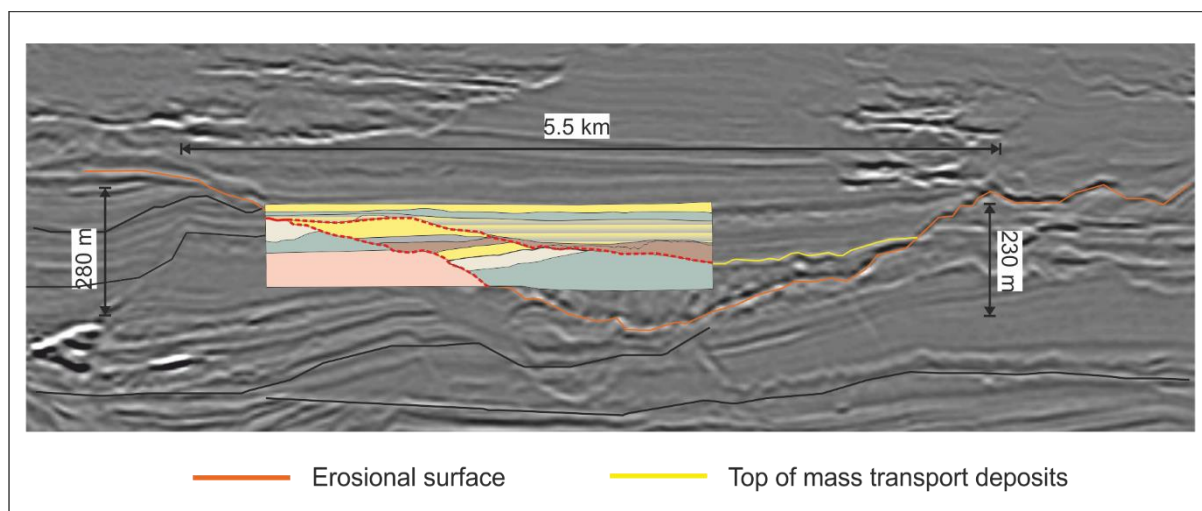
These units may only represent secondary reservoir targets due to their simple geometry and sand-rich nature with thin waste zones. However, their thin discontinuous nature, sharp-base and tops, and abrupt sand-rich pinchout mean that are prone to clastic injection (Cobain et al. 2017). Nonetheless, they may aid in the prediction of the geometry and architecture of bounding thicker sand-rich systems below and above (Chapter 6).

### 7.5.3 Submarine slide complexes

Mass-transport complexes can act as seals to hydrocarbon reservoirs or, less commonly, as reservoirs in their own right (e.g. Gamboa et al., 2010; Omosanya and Alves, 2013; Alves et al., 2014). Application of the results of this work to subsurface data sets will provide better understanding of transport and depositional process within stacked submarine slides (Chapter 4), which is currently lacking in seismic and modern datasets. The erosive nature of the mass

flow and subsequent infill influences sand distribution pathways and connectivity across continental slope successions, which can impact the distribution of hydrocarbon reservoirs and seals (Prior et al., 1984; Masson et al., 1997; Gee et al., 2006; Heniö and Davies, 2006; Alves and Cartwright, 2009; Morley, 2009; Joanne et al., 2013).

Infill of submarine slide basal shear surfaces can be highly variable (Chapter 4), with infill successions further complicated by truncation by subsequent basal shear surfaces (Chapter 4). Figure 7.13 shows a simplified stratigraphic panel of the outcrop presented in Chapter 4 overlying a similar sized slide scar from offshore Colombia (Ortiz-Karpf, 2016; Ortiz-Karpf et al., 2017). The complexity shown by the simplified panel is not discernible on seismic datasets and would likely not be predicted even if several well logs were drilled through this submarine slide. The sand-rich turbidity currents and mass flows captured within the slide scar surfaces deposited thick sand beds which represent potential for hydrocarbon reservoirs and seals respectively (Kneller et al., 2016). However, this study highlights the discontinuous and truncated nature of many packages that infill the basal shear surfaces, which may create reservoir and seal pairs, but have potential for leaking in 3D and may be highly compartmentalized.



**Figure 7.13** Overlay of simplified panel from Chapter 4 onto example of submarine slide from Magdalena fan, offshore Colombia (from Ortiz-Karpf, 2016).

Where turbidite systems are confined within slides, they show many similarities with deposits in partially ponded transient minibasins (e.g. Booth et al., 2003; Beaubouef and Abreu, 2006; Madof et al., 2009) with the potential to form sand-rich systems isolated within the slope. These may represent significant reservoir potential where failure has occurred in a silt-rich

slope systems. However, completely ponded turbidites have thick mudstone caps which may create highly compartmentalized reservoirs that are uneconomic. Partially confined turbidite systems tend to be overall more sand-rich due to flow-stripping and therefore may represent more economic reservoirs. If these systems transition upwards to unconfined, filling and overspilling accommodation, there may be potential for leaking of hydrocarbons in 3D. Conversely, if these systems are truncated by further basal shear surfaces and overlain by mud-rich and debritic remobilized deposits, they may become completely isolated bodies of sand in 3D. Therefore submarine slide complexes forming through multiple failures can represent significant reservoir and seal potential (e.g. Meckel et al., 2002), and applying models to predict confinement of remobilized and turbidite infill in various slope scenarios (Section 7.3.2.1) can aid discovery and more accurate interpretations of reservoirs within submarine slides

## 7.6 Conclusions

The effect of changes in topographic relief, gradient, orientation, and amplitude, in slope to basin floor settings, even where relatively subtle ( $<1^\circ$  changes in gradient), have a profound impact on flow behaviour, patterns of erosion and deposition, and resultant stratigraphic architecture from individual bed to system scale. Slope profiles cannot be simply classified by types, such as simple or stepped or ponded profiles, because of the range of obstacles and flow types which vary in time and space.

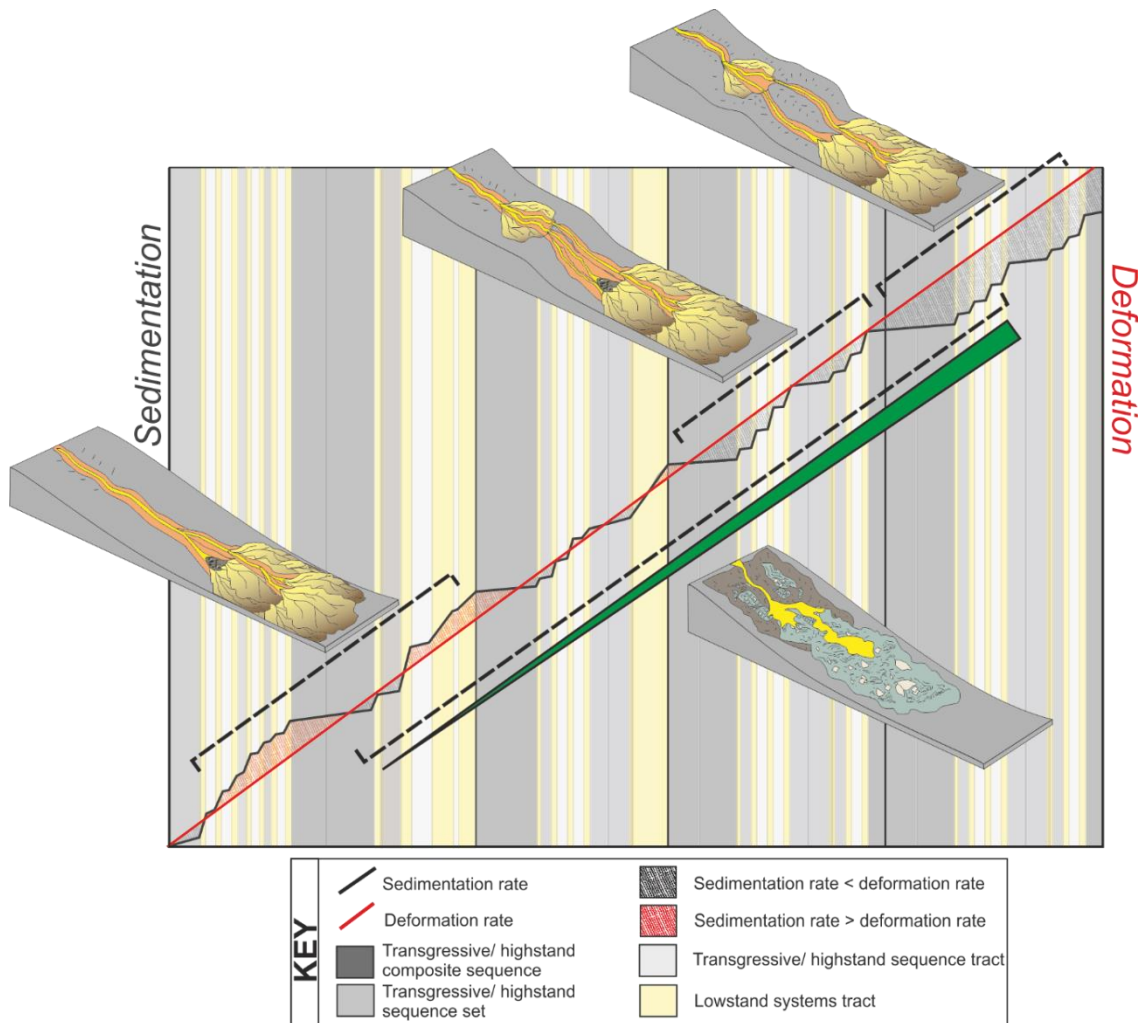
Downslope decrease and reversals in gradient, resulting from the formation of intraslope steps and minibasins by deformation, or evacuation by submarine slides, can result in the formation of intraslope lobe deposits. Intraslope lobes can vary from fully to partially or weakly confined, and can be fed by a single or multiple sources. Reduction in gradient at the base-of-slope can lead to the formation of areas of coarse sediment bypass, with intense scouring and lag deposition, known as channel-lobe transition zones (CLTZs). CLTZs vary in length spatially and temporally due to changes in flow dynamics and length and gradient change of slope break, resulting in a thin but composite and complicated stratigraphic expression. Increases in gradient downslope can accelerate flows. Initially, numerous weakly confined conduits can form which can evolve into channel-levee complexes with sustained flow input.

Lateral slopes can have varying effects on sedimentary processes and depositional architecture, from bed to system scale, primarily depending on slope gradient and orientation. High gradient lateral slopes are unstable, and can cause remobilization downslope as well as

onlap and abrupt pinch out of beds. Lower gradient lateral slopes can cause aggradational onlap and facies transitions over longer length scales. Large scale lateral slopes, such as lateral basin margins, aided by differential compaction can control the stacking of multiple systems.

Topographic influence can evolve during the life of a single system through variations in flow-relief (erosional and depositional) interactions, and healing of topography. This evolution is shown in the contraction/expansion and migration of a CLTZ and the infill and overspill of slope accommodation. Over multiple depositional systems changes in topography are more pronounced. The stacking of submarine slides and their basal shear surfaces can drive variations in the style of subsequent flow confinement.

Over the timescale of multiple systems, spanning several sea-level cycles of varying magnitude, the balance between sedimentation and deformation rate of the slope is crucial in understanding and predicting the formation of stepped slopes, and the distribution of sands and shales (Fig. 7.14). When sedimentation rate outpaces deformation rate, the system can work towards reaching equilibrium through erosional and depositional processes. However, when the deformation rate is just greater than sedimentation rate, stepped slopes can form. At higher relative rates of deformation minibasins may form. Even if the deformation rate is constant, the sedimentation rate is highly variable over different periodicities related to sea level/climate cycles, meaning that the slope physiography will continually change through time. For example, slope systems with significant periods of coarse clastic starvation are more susceptible to the development of stepped or ponded slope accommodation.



**Figure 7.14** When deformation rate is constant and sedimentation rate gradually decreases simple slope profiles can evolve into stepped slope profiles and then slopes with minibasins and tortuous corridors. Slope degradation can occur associated with all slope types but slope failures may increase in frequency and magnitude as relative slope deformation increases.

Topographically complex areas can have complicated transference into the stratigraphic record. Areas that are bypass dominated, such as CLTZs, can be represented by a single surface that is time transgressive or a relatively thin but composite body of sediment. Preservation potential of CLTZs varies according to the time in which the zone formed (during progradation or retrogradation), the lateral confinement, and the distance from the feeder system. Basal shear zones of submarine slides are also time transgressive, with primary erosional morphology further complicated by post depositional remobilization and differential compaction.

Topographic complexity can lead to unusual and dynamic configurations of deep-water systems and therefore difficulty in identifying potential hydrocarbon reservoirs and their seals. Bypass dominated zones can cause the formation of up-dip stratigraphic pinch out in lobes, with outcrop studies showing across strike and sub-seismic scale connectivity, indicating

significant risk of fluid loss. Bypass zones can be identified in core and gamma ray logs using recognition criteria which can support interpretation in subsurface datasets. The prediction of stepped slope evolution, and therefore the stacking patterns, and sediment partitioning of slopes can aid identification of areas of consistently increased sand volume. The identification of thin 'disconnected' lobes can indicate areas of fixed and dynamic topography and therefore increased sand volume in under- and over-lying units. Understanding the varying infill and truncation of submarine slide complexes can aid recognition of potential reservoirs and seals.

The transition zone from submarine slope to basin-floor, or from ramp to step, are important sites of gradient change, and therefore flow process change. This leads to complicated interactions between flow behaviour and evolving seabed relief over different length scales and time scales. This research has analysed several sites where these interactions can be investigated at multiple scales and in different configurations within a well constrained palaeogeographic setting. Although the resulting stratigraphic records in these settings is complicated, there are predictable process responses that are recorded in the depositional architecture than can be used to reduced uncertainty in subsurface settings with sparse datasets.

## **7.7 Recommendations for further research**

### *7.7.1 What is the detailed sedimentological expression of the stepped slope topography in early basin floor Units A and B?*

The subtle expression of changing topography has been noted in the small Units A/B, B/C, and D/E along with thickness and facies changes within the larger Units C, D, E and F (Chapter 6). Although thickness and some facies variation have been noted in Units A and B in similar locations (Chapter 6), due to regional scale mapping/different foci of previous research, it is unclear if more detailed indicators of early expression of the stepped slope profile can be seen within the areas of fixed topographic influence. Using the key areas of topographic change recognised in this study (Chapters 5 and 6), and the creation of A and B thickness maps using the Datacube it is now possible to distinguish specific areas of focus that may show subtle topographic indicators in these thick regional basin floor systems. Understanding the early indicators of stepped slope evolution may aid in the prediction of their formation.

### 7.7.2 *How does the sedimentological expression of slope to basin floor topography differ in passive vs active margins?*

The sedimentological expression of subtle topographic variability within slope and basin floor profiles has been examined within this study based on a passive continental margin setting. Slopes forming in active continental margin settings are generally subject to significant structural influence at higher magnitudes of topographic control. Comparing the outcrop examples in this study to similar environments in active settings such as the CLTZ and submarine slides exposed in the lower Pleistocene, Kazusa Group exposed on the Boso Peninsula, central Japan (Ito, 1992, 1994, 2008; Ito et al., 2014) would help to decipher the key differences that passive and active continental margins have on sediment distribution and creation of topography. Moreover integrating these outcrop studies with seismic datasets of active settings, for example the Magdalena Fan, offshore Colombia located at a junction between the Nazca, South American, Cocos and Caribbean plates (Ortiz-Karppf, 2016), would further allow basin scale comparison of submarine slide formation in active vs. passive settings. Key differences to investigate between active and passive settings include: (a) how the magnitude of topography varies; (b) how the rates of slope deformation vary; and (c) the relative timing of deformation, when is the onset, does it continue throughout deposition?

### 7.7.3 *Integration with modern seafloor datasets, numerical and physical experiments*

Commonly, studies on submarine slopes are conducted from outcrop and modern data sets. While outcrop data sets can provide detailed insights into sedimentary facies and geometries, modern seafloor studies enable the examination of topographic variability at basin scale without the bias of preservation.

Experimental datasets including both numerical process modelling (e.g. Wang et al., 2017) and physical process modelling (e.g. flume tank experiments) allow reconstruction and investigation of various topographic configurations, to test interpretations made at outcrop, and observations of the modern seafloor (e.g. Pohl et al., 2016). Flume tank experiments allow only relatively simple topographic changes to be investigated (e.g. changes in slope gradient), but allow for direct observations of multiple flows and their resultant deposits. This aids knowledge of flow processes and preservation potential at points of gradient change as well as small scale evolution of a system over multiple flows. Numerical process modelling allows investigation of far more complex bathymetric profiles. Models are run over different configurations (gradient and slope) to work towards quantifying and constraining the full range

of flow-topography interactions. Various profiles can be tested, which can be idealised or modelled directly on modern seafloor datasets (e.g. Wang et al., 2017). Accurately interpreted palaeobathymetry from the ancient record is critical, but hard to constrain with confidence; through integration with experimental datasets it will be possible to automatically test scenarios to better constrain interpretation.





## 8 References

- Aas, T.E., Howell, J.A., Janocko, M. and Jackson, C.A.L.** (2010) Control of Aptian palaeobathymetry on turbidite distribution in the Buchan Graben, Outer Moray Firth, Central North Sea. *Marine and Petroleum Geology*, **27**, 412-434.
- Adeogba, A.A., McHargue, T.R. and Graham, S.A.** (2005) Transient fan architecture and depositional controls from near-surface 3-D seismic data, Niger Delta continental slope. *AAPG Bulletin*, **89**, 627-643.
- Alexander, J. and Morris, S.** (1994) Observations on experimental, nonchannelized, high-concentration turbidity currents and variations in deposits around obstacles. *Journal of Sedimentary Research*, **64**, 899-909.
- Alexander, J., Bridge, J.S., Cheel, R.J. and Leclair, S.F.** (2001) Bedforms and associated sedimentary structures formed under supercritical water flows over aggrading sand beds. *Sedimentology*, **48**, 133-152.
- Alfaro, E. and Holz, M.** (2014) Seismic geomorphological analysis of deepwater gravity-driven deposits on a slope system of the southern Colombian Caribbean margin. *Marine and Petroleum Geology*, **57**, 294-311.
- Allen, J.R.L.** (1970) A quantitative model of climbing ripples and their cross-laminated deposits: *Sedimentology*, **14**, 5-26.
- Allen, J.R.L.** (1984) Parallel lamination developed from upper-stage plane beds: a model based on the larger coherent structures of the turbulent boundary layer. *Sedimentary Geology*, **39**, 227-242.
- Allen, J.R.L.** (1985) *Principles of Physical Sedimentology*: London, Allen and Unwin, p.196.
- Allen, J.R.L., and Banks, N.L.** (1972) An interpretation and analysis of recumbent folded deformed cross-bedding. *Sedimentology*, **19**, 257-283.

- Alves, T.M.** (2010) 3D Seismic examples of differential compaction in mass-transport deposits and their effect on post-failure strata. *Marine Geology*, **271**, 212-224.
- Alves, T.M.** (2015) Submarine slide blocks and associated soft-sediment deformation in deep-water basins: A review. *Marine and Petroleum Geology*, **67**, 262-285.
- Alves, T.M.** and **Cartwright, J.A.** (2010) The effect of mass-transport deposits on the younger slope morphology, offshore Brazil. *Marine and Petroleum Geology*, **27**, 2027-2036.
- Alves, T.M.** and **Lourenço, S.D.N.** (2010) Geomorphic features related to gravitational collapse: Submarine landsliding to lateral spreading on a Late Miocene- Quaternary slope (SE Crete, eastern Mediterranean). *Geomorphology*, **123**, 13-33.
- Alves, T.M., Kurtev, K., Moore, G.F.** and **Strasser, M.** (2014) Assessing the internal character, reservoir potential, and seal competence of mass-transport deposits using seismic texture: A geophysical and petrophysical approach. *AAPG Bulletin*, **98**, 793-824.
- Amerman, R., Nelson, E.P., Gardner, M.H.** and **Trudgill, B.** (2011) Submarine mass transport deposits of the Permian Cutoff Formation, West Texas, USA: internal architecture and controls on overlying reservoir sand deposition, in Craig Ship, R. et al. (eds.), Mass-Transport Deposits in Deepwater Settings. *SEPM, Special Publication*, **96**, 235-267.
- Amy, L.A.** and **Talling, P.J.** (2006) Anatomy of turbidites and linked debrites based on long distance (120× 30 km) bed correlation, Marnoso Arenacea Formation, Northern Apennines, Italy. *Sedimentology*, **53**, 161-212.
- Amy, L.A., McCaffrey, W.D.** and **Kneller, B.C.** (2004) The influence of a lateral basin-slope on the depositional patterns of natural and experimental turbidity currents, in Joseph, P., Lomas, S.A (eds.), Deep-Water Sedimentation in the Alpine Basin of Se France: New Perspectives on the Grès d'Annot and related systems. *Geological Society London Special Publication*, **221**, 311-330.
- Amy, L.A., Hogg, A.J., Peakall, J.** and **Talling, P.J.** (2005) Abrupt transitions in gravity currents. *Journal of Geophysical Research*, **110**, F03001.

- Amy, L.A., Kneller, B.C. and McCaffrey, W.D.** (2007) Facies architecture of the Gres de Peira Cava, SE France: landward stacking patterns in ponded turbiditic basins. *Journal of the Geological Society*, **164**, 143-162.
- Anderson, A.M.** (1974) Arthropod trackways and other trace fossil from the Early Permian lower Karoo beds of South Africa. *Unpublished Ph.D. Thesis*, University of Witwandsrand, Johannesburg, South Africa.
- Andersson, P.O.D., Worden, R.H., Hodgson, D.M. and Flint, S.** (2004) Provenance evolution and chemostratigraphy of a Palaeozoic submarine fan-complex: Tanqua Karoo Basin, South Africa: *Marine and Petroleum Geology*, **21**, 555–577.
- Antobreh, A.A. and Krastel, S.** (2007) Mauritania Slide Complex: morphology, seismic characterisation and processes of formation. *International Journal of Earth Sciences*, **96**, 451-472.
- Armi, L. and Farmer, D.M.** (1986) Maximal two-layer exchange through a contraction with barotropic net flow. *Journal of Fluid Mechanics*, **164**, 27-51.
- Apps, G.G., Peel, F.J., Travis, C.J. and Yeilding, C.A.** (1994) Structural controls on the Tertiary deep water deposition in the northern Gulf of Mexico, in Weimer, P., et al., (eds.) Submarine fans and turbidite systems – sequence stratigraphy, reservoir architecture, and production characteristics, Gulf of Mexico and international: Gulf Coast section SEPM Foundation 15<sup>th</sup> Annual Research Conference, 1-7.
- Armitage, D.A., Romans, B.W., Covault, J.A. and Graham, S.A.** (2009) The influence of mass-transport-deposit surface topography on the evolution of turbidite architecture: the Sierra Contreras, Tres Pasos Formation (Cretaceous), southern Chile. *Journal of Sedimentary Research*, **79**, 287-301.
- Baas, J.H. and Best, J.L.** (2002) Turbulence modulation in clay-rich sediment-laden flows and some implications for sediment deposition. *Journal of Sedimentary Research*, **72**, 336-340.

- Baas, J.H., Best, J.L. and Peakall, J.** (2011) Depositional processes, bedform development and hybrid bed formation in rapidly decelerated cohesive (mud–sand) sediment flows. *Sedimentology*, **58**, 1953-1987.
- Baas, J.H., Best, J.L. and Peakall, J.** (2016) Predicting bedforms and primary current stratification in cohesive mixtures of mud and sand. *Journal of the Geological Society*, **173**, 12-45.
- Babonneau, N., Savoye, B., Cremer, M. and Klein, B.** (2002) Morphology and architecture of the present canyon and channel system of the Zaire deep-sea fan. *Marine and Petroleum Geology*, **19**, 445-467.
- Babonneau, N., Savoye, B., Cremer, M. and Bez, M.** (2004) Multiple terraces within the deep incised Zaire canyon: are they confined levees?, in Lomas, S.A., and Joseph, P. (eds.), Turbidite Sedimentation in Confined Systems. *Geological Society of London, Special Publication*, v. 222, 91–114
- Badalini, G., Kneller, B. and Winker, C.D.** (2000) Architecture and processes in the late Pleistocene Brazos-Trinity turbidite system, Gulf of Mexico continental slope, in Weimer, P., et al. (eds.), Deep-Water Reservoirs of the World: SEPM, Gulf Coast Section, 20th Annual Research Conference, p. 16-34.
- Baeten, N.J., Laberg, J.S., Forwick, M., Vorren, T.O., Vanneste, M., Forsberg, C.F., Kvalstad, T.J. and Ivanov, M.** (2013) Morphology and origin of smaller-scale mass movements on the continental slope off northern Norway. *Geomorphology*, **187**, 122-134.
- Baeten, N.J., Laberg, J.S., Vanneste, M., Forsberg, C.F., Kvalstad, T.J., Forwick, M., Vorren, T.O. and Hafliðason, H.** (2014) Origin of shallow submarine mass movements and their glide planes—Sedimentological and geotechnical analyses from the continental slope off northern Norway. *Journal of Geophysical Research: Earth Surface*, **119**, 2335-2360.
- Baines, P.G.** (1984) A unified description of two-layer flow over topography. *Journal of Fluid Mechanics*, **146**, 127-167.

**Baines, P.G.** (1995) *Topographic Effects in Stratified Flows*, Cambridge Univ. Press, New York,

Baines, P.G. and Davies, P.A. (1980) Laboratory studies of topographic effects in rotating and/or stratified fluids, *in Orographic Effects in Planetary Flows*, chap. 8, GARP Global Atmospheric Research Programme, Garp Publication Series, **23**, 233-299.

**Bailleul, J., Robin, C., Chanier, F., Guillocheau, F., Field, B. and Ferrière, J.** (2007) Turbidite systems in the inner forearc domain of the Hikurangi convergent margin (New Zealand): New constraints on the development of trench-slope basins. *Journal of Sedimentary Research*, **77**, 263-283.

**Barley, B.** (1999) Deepwater problems around the world. *The Leading Edge*, **18**, 488-493.

**Barton, M.D.** (2012) Evolution of an intra-slope apron, offshore Niger Delta Slope: Impact of step geometry on apron architecture, *in* Prather, B.E., et al. (eds.), *Application of the Principles of Seismic Geomorphology to Continental-slope and Base-of-slope systems: Case Studies from Seafloor and Near-seafloor Analogues: SEPM (Society for Sedimentary Geology) Special Publication 99*, p. 181- 197.

**Barton, P. and Wood, R.** (1984) Tectonic evolution of North Sea basin: crustal stretching and subsidence. *Geophysical Journal, Royal Astronomical Society*, **79**, 987-1022.

**Beaubouef, R.T.** (2004) Deep-water leveed-channel complexes of the Cerro Toro Formation, Upper Cretaceous, southern Chile. *AAPG Bulletin*, **88**, 1471-1500.

**Beaubouef, R.T. and Friedmann, S.J.** (2000) High resolution seismic/sequence stratigraphic framework for the evolution of Pleistocene intra slope basins, western Gulf of Mexico: depositional models and reservoir analogs, *in* Weimer, P., et al., (eds.), *Deep-water Reservoirs of the World: Gulf Coast Section SEPM 20th Annual Research Conference*, p. 40-60.

**Beaubouef R.T. and Abreu V.** (2006) Basin 4 of the Brazos–Trinity slope system: anatomy of the terminal portion of an intra-slope lowstand systems tract. *Gulf Coast Section*

*Association of Geological Societies/SEPM, 56th Annual Convention, Transactions:*  
Lafayette, Louisiana, p. 39–48.

**Beaubouef, R.T. and Abreu, V.** (2010) MTCs of the Brazos-Trinity slope system; thoughts on the sequence stratigraphy of MTCs and their possible roles in shaping hydrocarbon traps, *in* Mosher, D.C., et al., eds., *Submarine Mass Movements and Their Consequences*. Springer Netherlands, p. 475-490.

**Beaubouef, R.T., Rossen, C., Zelt, L.B., Sullivan, M.D., Mohrig, D.C. and Jennette, D.C.** (1999) Deep-water sandstones, Brushy Canyon Formation, West Texas: AAPG Continuing Education Course Note Series no. 40, The American Association of Petroleum Geologists, p. 48.

**Beaubouef, R.T., Rossen, C. and Lovell, R.W.W.** (2007) The Beacon Channel: A newly Recognized Architectural Type in the Brushy Canyon Formation, Texas, USA, *in* Nielsen, T.H. et al., (eds.). *Atlas of Deep-Water Outcrops*. AAPG Studies in Geology 56. AAPG and Shell Exploration & Production, p. 432-444.

**Bellaiche, G., Coutellier, V. and Droz, L.** (1986) Seismic evidence of widespread mass transport deposits in the Rhône deep-sea fan: their role in the fan construction. *Marine Geology*, **71**, 327-340.

**Bernhardt, A., Jobe, Z.R., Grove, M. and Lowe, D.R.** (2012) Palaeogeography and diachronous infill of an ancient deep-marine foreland basin, Upper Cretaceous Cerro Toro Formation, Magallanes Basin, Chile. *Basin Research*, **24**, 269-294.

**Bersezio, R., Felletti, F., Riva, S. and Micucci, L.** (2009) Trends in bed thickness and facies of the turbiditic sandstone bodies: unravelling the effects of basin confinement, depositional processes, and modes of sediment supply, *in* Kneller, B., et al., (eds.), *External Controls on the Deep-water Depositional Systems*. SEPM Special Publication 92, 303-321.

**Best, J. and Bridge, J.** (1992) The morphology and dynamics of low amplitude bedwaves upon upper stage plane beds and the preservation of planar laminae. *Sedimentology*, **39**, 737-752.

- Binks, R.M. and Fairhead, J.D.** (1992) A plate tectonic setting for Mesozoic rifts of West and Central Africa. *Tectonophysics*, **213**, 141-151.
- Blum, M., Martin, J., Milliken, K. and Garvin, M.** (2013) Paleovalley systems: insights from Quaternary analogs and experiments. *Earth-Science Reviews*, **116**, 128-169.
- Bohn, C.W., Flemings, P.B. and Slingerland, R.L.** (2012) Accommodation change during bypass across a latestage fan in the shallow Auger basin, *in* Prather, B.E., et al. (eds.), Application of the Principles of Seismic Geomorphology to Continental-slope and Base-of-slope Systems: Case Studies from Seafloor and Near-seafloor Analogues: SEPM (Society for Sedimentary Geology) Special Publication 99, p. 225–242, doi: 10.2110 /pec.12.99.0225 .
- Bonnel, C., Dennielou, B., Droz, L., Mulder, T. and Berné, S.** (2005) Architecture and depositional pattern of the Rhône Neofan and recent gravity activity in the Gulf of Lions (western Mediterranean). *Marine and Petroleum Geology*, **22**, 827-843.
- Booth, J.R., Dean, M.C., DuVernay, A.E. and Styzen, M.J.** (2003) Paleo-bathymetric controls on the stratigraphic architecture and reservoir development of confined fans in the Auger Basin: central Gulf of Mexico slope. *Marine and Petroleum Geology*, **20**, 563-586.
- Bouma, A.** (1962) Sedimentology of some flysch deposits. A graphic approach to facies interpretation. Elsevier, Amsterdam, 168 pp.
- Bouma, A.H.** (2000) Fine-Grained, Mud-Rich Turbidite Systems: Model and Comparison with Coarse-Grained, Sand-Rich Systems, *in* Bouma, A.H. and Stone, C.G. (eds.), Fine-grained Turbidite Systems. *AAPG Memoir 72/SEPM Special Publication*, **68**, 9-19.
- Bradley, D. and Hanson, L.** (1998) Paleoslope analysis of slump folds in the Devonian flysch of Maine. *The Journal of Geology*, **106**, 305-318.
- Brunt, R.L., Di Celma, C.N., Hodgson, D.M., Flint, S.S., Kavanagh, J.P. and van der Merwe, W.C.** (2013a) Driving a channel through a levee when the levee is high: An outcrop example of submarine downdip entrenchment. *Marine and Petroleum Geology*, **41**, 134-145.



- Brunt, R.L., Hodgson, D.M., Flint, S.S., Pringle, J.K., Di Celma, C., Prélat, A. and Grecula, M.** (2013b) Confined to unconfined: Anatomy of a base of slope succession, Karoo Basin, South Africa. *Marine and Petroleum Geology*, **41**, 206-221.
- Buhmann, D., Buhmann, C. and von Brunn, V.** (1989) Glaciogenic banded phosphorites from Permian sedimentary rocks. *Bulletin of the Society of Economic Geologists*, **48**, 741–750.
- Bull, S., Cartwright, J. and Huse, M.,** (2009) A review of kinematic indicators from mass-transport complexes using 3D seismic data. *Marine and Petroleum Geology*, **26**, 1132-1151.
- Bumby, A.J. and Guiraud, R.** (2005) The geodynamic setting of the Phanerozoic basins of Africa. *Journal of African Earth Sciences*, **43**, 1-12.
- Burgess, P.M., Flint, S. and Johnson, S.** (2000) Sequence stratigraphic interpretation of turbiditic strata: an example from Jurassic strata of the Neuquén basin, Argentina. *Geological Society of America Bulletin*, **112**, 1650-1666.
- Burgreen, B. and Graham, S.** (2014) Evolution of a deep-water lobe system in the Neogene trench-slope setting of the East Coast Basin, New Zealand: lobe stratigraphy and architecture in a weakly confined basin configuration. *Marine and Petroleum Geology*, **54**, 1-22.
- Callot, P., Sempere, T., Odonne, F. and Robert, E.** (2008) Giant submarine collapse of a carbonate platform at the Turonian-Coniacian transition: The Ayabacas Formation, southern Peru. *Basin Research*, **20**, 333-357.
- Campion, K.M., Sprague, A.R., Mohrig, D., Lovell, R.W., Drzewiecki, P.A., Sullivan, M.D., Ardill, J.A., Jensen, G.N. and Sickafoose, D.K.** (2000) Outcrop expression of confined channel complexes, in Weimar, R.M. et al., (eds.) *Gulf Coast Section Society of Economic Palaeontologists and Mineralogists*, 127-150.
- Canals, M., Lastras, G., Urgeles, R., Casamor, J.L., Mienert, J., Cattaneo, A., De Batist, M., Hafliadon, H., Imbo, Y., Laberg, J.S. and Locat, J.** (2004) Slope failure dynamics and

impacts from seafloor and shallow sub-seafloor geophysical data: case studies from the COSTA project. *Marine Geology*, **213**, 9-72.

**Cartigny, M.J., Postma, G., van den Berg, J.H. and Mastbergen, D.R.** (2011) A comparative study of sediment waves and cyclic steps based on geometries, internal structures and numerical modeling. *Marine Geology*. **280**, 40-56.

**Cartigny, M.J.B., Eggenhuisen, J.T., Hansen, E.W.M. and Postma, G.** (2013) Concentration-dependant flow stratification in experimental high-density turbidity currents and their relevance to turbidite facies model. *Journal of Sedimentary Research*, **83**, 1046-1064.

**Cartigny, M.J., Ventra, D., Postma, G. and Den Berg, J.H.** (2014) Morphodynamics and sedimentary structures of bedforms under supercritical-flow conditions: New insight from flume experiments. *Sedimentology*, **61**, 712-748.

**Catuneanu, O.** (2004) Basement control on flexural profiles and the distribution of foreland facies: The Dwyka Group of the Karoo Basin, South Africa. *Geology*, **32**, 517-520.

**Catuneanu, O., Hancox, P.J. and Rubidge, B.S.** (1998) Reciprocal flexural behaviour and contrasting stratigraphies: a new basin development model for the Karoo retroarc foreland system, South Africa. *Basin Research*, **10**, 417-439.

**Chapin, M.A., Davis, V.P., Gibson, J.L. and Pettinghill, H.S.** (1994) Reservoir architecture of turbidite sheet sandstones in laterally extensive outcrops, Ross Formation, western Ireland, in Weimer, P., Bouma, A.H., and Perkins, B.F. (eds.), *Submarine Fans and Turbidite Systems: Gulf Coast Section SEPM 15<sup>th</sup> Annual Research Conference*, 15<sup>th</sup>, 53-68.

**Christie, A.D.M.** (1990) Origin, classification and utilization of oil shales in South Africa. *South African Journal of Science*, **86**, 9-15

**Clark, I.R. and Cartwright, J.A.** (2009) Interactions between submarine channel systems and deformation in deepwater fold belts: Examples from the Levant Basin, Eastern Mediterranean sea. *Marine and Petroleum Geology*, **26**, 1465-1482.

- Cobain, S., Peakall, J. and Hodgson, D.M.** (2015) Indicators of propagation direction and relative depth in clastic injectites: Implications for laminar versus turbulent flow processes. *Geological Society of America Bulletin*, **127**, 1816-1830.
- Cobain, S.L., Hodgson, D.M., Peakall, J. and Shiers, M.N.** (2017) An integrated model of clastic injectites and basin floor lobe complexes: implications for stratigraphic trap plays. *Basin Research*, doi: 10.1111/bre.12229.
- Cole, D.** (1992) Evolution and development of the Karoo Basin, in De Wit, M.J. and Ransome, I.G.D. (eds.) *Inversion Tectonics of the Cape Fold Belt, Karoo and Cretaceous Basins of Southern Africa*. Balkema, Rotterdam, p. 87-99.
- Cole, D.I. and McLachlan, I.R.** (1991) Oil potential of the Permian Whitehill Shale Formation in the main Karoo Basin, South Africa. *Proceedings, Gondwana Seven: Sao Paulo, Instituto de Geociencias, Universidade de Sao Paulo*, 379-390.
- Covault, J.A. and Romans, B.W.** (2009) Growth patterns of deep-sea fans revisited: Turbidite-system morphology in confined basins, examples from the California Borderland. *Marine Geology*, **265**, 51-66.
- Covault, J.A., Hubbard, S.M., Graham, S.A., Hinsch, R. and Linzer, H.G.** (2009) Turbidite-reservoir architecture in complex foredeep-margin and wedge-top depocenters, Tertiary Molasse foreland basin system, Austria. *Marine and Petroleum Geology*, **26**, 379-396.
- Covault, J.A., Sylvester, Z., Hubbard, S.M., Jobe, Z.R. and Sech, R.P.** (2016) The stratigraphic record of submarine-channel evolution. *The Sedimentary Record*, **14**, 4-11.
- Dakin, N., Pickering, K.T., Mohrig, D. and Bayliss, N.J.** (2013) Channel-like features created by erosive submarine debris flows: Field evidence from the Middle Eocene Ainsa Basin, Spanish Pyrenees. *Marine and Petroleum Geology*, **41**, 62-71.
- Dailly, P., Henderson, T., Hudgens, E., Kanschak, K. and Lowry, P.** (2013) Exploration for Cretaceous stratigraphic traps in the Gulf of Guinea, West Africa and the discovery of the Jubilee Field: a play opening discovery in the Tano Basin, Offshore Ghana, in Mohriak,

W.U. et al., (eds.), *Conjugate Divergent Margins: an introduction*. Geological Society, London, Special Publications, **369**, 235-248.

- Diegel, F.A., Karlo, J.F., Schuster, D.C., Shoup, R.C. and Tauvers, P.R.** (1995) Cenozoic structural evolution and tectono-stratigraphic framework of the northern Gulf coast continental margin, *in* Jackson, M.P.A., et al., (eds.), *Salt tectonics: A global perspective: American Association of Petroleum Geologists Memoir*, **65**, 109–151.
- Demyttenaere, R., Tromp, J.P., Ibrahim, A., Allman-Ward, P. and Meckel, T.** (2000) Brunei deep water exploration: from sea floor images and shallow seismic analogues to depositional models in a slope turbidite setting, *in* Weimer, P. et al., (eds.), *Deepwater reservoirs of the world, GCSSEPM Foundation 20th Annual Research Conference*, 304-317
- Deptuck, M.E., Sylvester, Z., Pirmez, C. and O’Byrne, C.** (2007) Migration-aggradation history and 3-D seismic geomorphology of submarine channels in the Pleistocene Benin-major Canyon, western Niger Delta slope. *Marine and Petroleum Geology*, **24**, 406-433.
- Deptuck, M.E., Piper, D.J., Savoye, B. and Gervais, A.** (2008) Dimensions and architecture of late Pleistocene submarine lobes off the northern margin of East Corsica. *Sedimentology*, **55**, 869-898.
- Deptuck, M.E., Sylvester, Z. and O’Byrne, C.** (2012) Pleistocene seascape evolution above a “simple” stepped slope profile- Western Niger Delta, *in* Prather B.E., et al., (eds.), *Application of the Principles of Seismic Geomorphology to Continental-Slope and Base-of-Slope Systems: Case Studies from Seafloor and Near-Seafloor Analogues SEPM Special Publication 99*, p. 199- 224.
- De Wit, M.J. and Ransome, I.G.** (1992) Regional inversion tectonics along the southern margin of Gondwana, *in* De Wit, M.J. and Ransome, I.G.D. (eds.), *Inversion Tectonics of the Cape Fold Belt, Karoo and Cretaceous Basins of Southern Africa*. Amsterdam, Balkema, p. 15-22.
- Di Celma, C., Brunt, R.L., Hodgson, D.M., Flint, S.S. and Kavanagh, J.P.** (2011) Spatial and temporal evolution of a Permian submarine slope channel-levee system, Karoo Basin, South Africa. *Journal of Sedimentary Research*, **81**, 579-599.

- Domack, E.W.** (1983) Facies of late Pleistocene glacial-marine sediments on Whidbey Island, Washington, in B.F. Molnia (ed.) *Glacial-marine Sedimentation*, 535-570. Plenum Press, New York.
- Dorrell, R.M., Peakall, J., Sumner, E.J., Parsons, D.R., Darby, S.E., Wynn, R.B., Özsoy, E. and Tezcan, D.** (2016) Flow dynamics and mixing processes in hydraulic jump arrays: Implications for channel-lobe transition zones. *Marine Geology*, **381**, 181-193.
- Doughty-Jones, G., Mayall, M. and Lonergan, L.** (2017) Stratigraphy, facies and evolution of deep-water lobe complexes within a salt-controlled intra-slope minibasin. *AAPG Bulletin*.
- Dreyer, T., Fält, L.-M., Høy, T., Knarud, R., Steel, R. and Cuevas, J. L.** (1993) Sedimentary architecture of field analogs for reservoir information (SAFARI): a case study of the fluvial Escanilla Formation, Spanish Pyrenees, in Flint, S.S. and Bryant, I.D. (eds.), *The Geologic Modeling of Hydrocarbon Reservoirs and Outcrop Analogs. International Association of Sedimentologists, Special Publications*, **15**, 57–80
- Driscoll, N.W., Weissel, J.K. and Goff, J.A.** (2000) Potential for large-scale submarine slope failure and tsunami generation along the US mid-Atlantic coast. *Geology*, **28**, 407-410.
- Dykstra, M., Kneller, B. and Milana, J.-P.** (2006) Deglacial and postglacial sedimentary architecture in a deeply incised paleovalley-paleofjord – The Pennsylvanian (late Carboniferous) Jejenes Formation, San Juan, Argentina. *GSA Bulletin*, **118**, 913–937.
- Dykstra, M., Garyfalou, K., Kertznus V., Kneller, B., Milana, J.P., Molinaro, M., Szuman, M., and Thompson, P.** (2011) Mass-transport deposits: combining outcrop studies and seismic forward modeling to understand lithofacies distributions, deformation, and their seismic stratigraphic expression, in Shipp, P. Weimer and Posamentier, H. (eds.) *Mass Transport Deposits in Deepwater Settings. SEPM, Special Publication* **96**, 293–310.
- Edwards, D.A.** (1993) *Turbidity Currents: Dynamics, Deposits and Reversals, Lecture Notes in Earth Sciences*, **44**. Springer-Verlag. Berlin.

- Edwards, D.A., Leeder, M.R., Best, J.L. and Pantin, H.M.** (1994) On experimental reflected density currents and the interpretation of certain turbidites. *Sedimentology*, **41**, 437-461.
- Eggenhuisen, J.T., McCaffrey, W.D., Houghton, P.D. and Butler, R.W.** (2010) Small-scale spatial variability in turbidity-current flow controlled by roughness resulting from substrate erosion: field evidence for a feedback mechanism. *Journal of Sedimentary Research*, **80**, 129-136.
- Elliott, T.** (2000) Megaflute erosion surfaces and the initiation of turbidite channels. *Geology*, **28**, 119–122.
- Ercilla, G., Casas, D., Estrada, F., Vázquez, J.T., Iglesias, J., García, M., Gómez, M., Acosta, J., Gallart, J., Maestro-González, A. and Team, M.** (2008) Morphosedimentary features and recent depositional architectural model of the Cantabrian continental margin. *Marine Geology*, **247**, 61-83.
- Etienne, S.** (2012) Caractérisation architecturale haute-résolution des lobes turbiditiques sableux confinés. Exemple de la Formation des Grès d'Annot (Eocène-Oligocène, SE-France). *Unpublished Ph.D. Thesis*, Université Bordeaux.
- Etienne, S., Mulder, T., Bez, M., Desaubliaux, G., Kwasniewski, A., Parize, O., Dujoncquoy, E. and Salles, T.** (2012) Multiple scale characterization of sand-rich distal lobe deposit variability: Examples from the Annot Sandstones Formation, Eocene–Oligocene, SE France. *Sedimentary Geology*. **273-274**, 1-18.
- Færseth, R.B. and Lien, T.** (2002) Cretaceous evolution in the Norwegian Sea—a period characterized by tectonic quiescence. *Marine and Petroleum Geology*, **19**, 1005-1027.
- Fallgatter, C., Kneller, B., Paim, P.S.G. and Milana, J.P.** (2017) Transformation, partitioning and flow–deposit interactions during the run-out of megaflows. *Sedimentology*, **64**, 359–387.  
Doi: 10.1111/sed.12307
- Farrell, S.G.** (1984) A dislocation model applied to slump structures, Ainsa Basin, South Central Pyrenees. *Journal of Structural Geology*, **6**, 727-736.

- Farrell, S.G. and Eaton, S.** (1987) Slump strain in the Tertiary of Cyprus and the Spanish Pyrenees. Definition of palaeoslopes and models of soft-sediment deformation, *in* (Jones, M.F. and Preston, R.M.F. (eds.) *Deformation of Sediments and Sedimentary Rocks, Special Publication of the Geological Society of London*, **29**, 181-196.
- Faure, K. and Cole, D.** (1999) Geochemical evidence for lacustrine microbial blooms in the vast Permian Main Karoo, Paraná, Falkland Islands and Huab basins of southwestern Gondwana. *Palaeogeography, Palaeoclimatology, Palaeoecology*, **152**, 189-213.
- Felletti, F.** (2002) Complex bedding geometries and facies associations of the turbiditic fill of a confined basin in a transpressive setting (Castagnola Fm., Tertiary Piedmont Basin, NW Italy). *Sedimentology*, **49**, 645-667.
- Felletti, F. and Bersezio, R.** (2010) Quantification of the degree of confinement of a turbidite-filled basin: A statistical approach based on bed thickness distribution. *Marine and Petroleum Geology*, **27**, 515-532.
- Figueiredo, J., Hodgson, D.M. and Flint, S.S.** (2010) Depositional environments and sequence stratigraphy of an exhumed Permian mud-dominated submarine slope succession, Karoo basin, South Africa. *Journal of Sedimentary Research*, **80**, 97-118.
- Figueiredo, J.P., Hodgson, D.M., Flint, S.S. and Kavanagh, J.P.** (2013) Architecture of a channel complex formed and filled during long-term degradation and entrenchment on the upper submarine slope, Unit F, Fort Brown Fm., SW Karoo Basin, South Africa. *Marine and Petroleum Geology*, **41**, 104-116.
- Fildani, A. and Normark, W.R.** (2004) Late Quaternary evolution of channel and lobe complexes of Monterey Fan. *Marine Geology*, **206**, 199-223.
- Fildani, A., Normark, W.R., Kostic, S. and Parker, G.** (2006) Channel formation by flow stripping: Large-scale scour features along the Monterey East Channel and their relation to sediment waves. *Sedimentology*, **53**, 1265-1287.

- Flint, S.S., Hodgson, D.M., Sprague, A.R., Brunt, R.L., van der Merwe, W.C., Figueiredo, J., Prélat, A., Box, D., Di Celma, C. and Kavanagh, J.P.** (2011) Depositional architecture and sequence stratigraphy of the Karoo basin floor to shelf edge succession, Laingsburg depocentre, South Africa. *Marine and Petroleum Geology*, **28**, 658–674. doi: 10.1016/j.marpetgeo.2010.06.008.
- Frey-Martinez, J., Cartwright, J. and Hall, B.** (2005) 3D seismic interpretation of slump complexes: examples from the continental margin of Israel. *Basin Research*, **17**, 83-108.
- Frey-Martínez, J., Cartwright, J. and James, D.** (2006) Frontally confined versus frontally emergent submarine landslides: a 3D seismic characterisation. *Marine and Petroleum Geology*, **23**, 585-604.
- Galloway, W.E.** (1986) Growth faults and fault-related structures of prograding terrigenous clastic continental margins. *Gulf Coast Association of Geological Societies Transactions*, **36**, 121-128.
- Gamberi, F. and Rovere, M.** (2011) Architecture of a modern transient fan (Villafranca fan, Gioia basin-Southeastern Tyrrhenian Sea). *Sedimentary Geology*, **236**, 211-225.
- Gamberi, F., Rovere, M. and Marani, M.** (2011) Mass-transport complex evolution in a tectonically active margin (Gioia Basin, Southeastern Tyrrhenian Sea). *Marine Geology*, **279**, 98-110.
- Gamberi, F., Rovere, M., Mercorella, A. and Leidi, E.** (2014) The influence of a lateral slope on turbidite lobe development on a modern deep-sea slope fan (Villafranca deep-sea fan, Tyrrhenian Sea). *Journal of Sedimentary Research*, **84**, 475-486.
- Gamboa, D., Alves, T., Cartwright, J. and Terrinha, P.** (2010) MTD distribution on a 'passive' continental margin: the Espírito Santo Basin (SE Brazil) during the Palaeogene. *Marine and Petroleum Geology*, **27**, 1311-1324.
- Gardner, M.H., Borer, J.A., Melick, J.J., Mavilla, N., Dechesne, M. and Wagerle, R.N.** (2003) Stratigraphic process–response model for submarine channels and related features from



studies of Permian Brushy Canyon outcrops, West Texas. *Marine and Petroleum Geology*, **20**, 757–787.

**Gee, M.J., Watts, A.B., Masson, D.G. and Mitchell, N.C.** (2001) Landslides and the evolution of El Hierro in the Canary Islands. *Marine Geology*, **177**, 271-293

**Gee, M.J.R., Gawthorpe, R.L. and Friedmann, S.J.** (2006) Triggering and evolution of a Giant Submarine Landslide, Offshore Angola, revealed by 3D seismic stratigraphy and geomorphology. *Journal of Sedimentary Research*, **76**, 9-19.

**Gervais, A., Savoye, B., Mulder, T. and Gonthier, E.** (2006) Sandy modern turbidite lobes: A new insight from high resolution seismic data. *Marine and Petroleum Geology*, **23**, 485-502.

**Gladstone, C., Phillips, J.C. and Sparks, R.S.J.** (1998) Experiments on bidisperse, constant-volume gravity currents; propagation and sediment deposition. *Sedimentology*, **45**, 833-843.

**Grecula, M.** (2000) Stratigraphy and architecture of tectonically controlled turbidite systems, Laingsburg Formation, Karoo Basin, South Africa. *Unpublished Ph.D. Thesis. University of Liverpool*, 184 pp.

**Grecula, M., Flint, S.S., Wickens, H.D.V. and Johnson, S.D.** (2003a) Upward-thickening patterns and lateral continuity of Permian sand-rich turbidite channel fills, Laingsburg Karoo, South Africa. *Sedimentology*, **50**, 831-853.

**Grecula, M., Flint, S., Potts, G., Wickens, D. and Johnson, S.** (2003b) Partial ponding of turbidite systems in a basin with subtle growth-fold topography: Laingsburg-Karoo, South Africa. *Journal of Sedimentary Research*, **73**, 603-620.

**Groenenberg, R.M., Hodgson, D.M., Pr lat, A., Luthi, S.M. and Flint, S.S.** (2010) Flow–deposit interaction in submarine lobes: insights from outcrop observations and realizations of a process-based numerical model. *Journal of Sedimentary Research*, **80**, 252-267.

- Grundvåg, S.A., Johannessen, E.P., Helland-Hansen, W. and Plink-Björklund, P.** (2014) Depositional architecture and evolution of progradationally stacked lobe complexes in the Eocene Central Basin of Spitsbergen. *Sedimentology*, **61**, 535-569.
- Habgood, E.L., Kenyon, N.H., Masson, D.G., Akhmetzhanov, A., Weaver, P.P., Gardner, J. and Mulder, T.** (2003) Deep-water sediment wave fields, bottom current sand channels and gravity flow channel-lobe systems: Gulf of Cadiz, NE Atlantic. *Sedimentology*, **50**, 483-510
- Hafliðason, H., Sejrup, H.P., Nygård, A., Mienert, J., Bryn, P., Lien, R., Forsberg, C.F., Berg, K. and Masson, D.** (2004) The Storegga Slide: architecture, geometry and slide development. *Marine Geology*, **213**, 201-234.
- Hälbich, I.W.** (1992) The Cape Fold Belt – Agulhas Bank Transect across the Gondwana Suture in Southern Africa. Global Geotransect 9. American Geophysical Union and Interunion Committee on the Lithosphere, Washington D.C.
- Hand, B.M.** (1969) Antidunes as trochoidal waves. *Journal of Sedimentary Research*, **39**, 1302-1309.
- Hand, B.M.** (1974) Supercritical flow in density currents. *Journal of Sedimentary Research*, **44**, 637-648.
- Hanquiez, V., Mulder, T., Toucanne, S., Lecroart, P., Bonnel, C., Marchès, E. and Gonthier, E.** (2010) The sandy channel-lobe depositional system in the Gulf of Cadiz: Gravity processes forced by contour current processes. *Sedimentary Geology*, **229**, 110-123.
- Hampton, M.A., Lee, H.J. and Locat, J.** (1996) Submarine landslides. *Reviews of Geophysics*, **34**, 33–59.
- Haughton, P.D.** (1994) Deposits of deflected and ponded turbidity currents, Sorbas Basin, southeast Spain. *Journal of Sedimentary Research*, **64**, 233-246.
- Haughton, P.D.W.** (2000) Evolving turbidite systems on a deforming basin floor, Tabernas, SE Spain. *Sedimentology*, **47**, 497-518.

- Haughton, P.D., Barker, S.P. and McCaffrey, W.D.** (2003) 'Linked' debrites in sand-rich turbidite systems—origin and significance. *Sedimentology*, **50**, 459-482.
- Haughton, P., Davis, C., McCaffrey, W. and Barker, S.** (2009) Hybrid sediment gravity flow deposits classification, origin and significance. *Marine and Petroleum Geology*, **26**, 1900-1918.
- Hay, D.** (2012) Stratigraphic evolution of a tortuous corridor from the stepped slope of Angola, in Prather, B.E., et al., (eds.), Application of the Principles of Seismic Geomorphology to Continental-Slope and Base-of-Slope Systems: Case Studies from Seafloor and Near-Seafloor Analogues, SEPM Special Publication, v. 99, p. 163-180.
- Heiniö, P. and Davies, R.J.** (2007) Knickpoint migration in submarine channels in response to fold growth, western Niger Delta. *Marine and Petroleum Geology*, **24**, 434-449.
- Herbert, C.T. and Compton, J.S.** (2007) Depositional environments of the lower Permian Dwyka diamictite and Prince Albert shale inferred from the geochemistry of early diagenetic concretions, southwest Karoo Basin, South Africa. *Sedimentary Geology*, **194**, 263-277.
- Hiscott, R.N.** (1994) Traction-carpet stratification in turbidites- Fact or Fiction?: *Journal of Sedimentary Research*, v. A64, 204-208.
- Hiscott, R.N. and Middleton, G.V.** (1980) Fabric of coarse deep-water sandstones, Tourelle Formation, Quebec, Canada. *Journal of Sedimentary Petrology*, **50**, 703-722.
- Hiscott, R.N. and Pickering, K.T.** (1984) Reflected turbidity currents on an Ordovician basin floor, Canadian Appalachians. *Nature*, **311**, 143-145.
- Hiscott, R.N., Hall, F.R. and Pirmez, C.** (1997) Turbidity-current overspill from the Amazon channel: texture of the silt/sand load, paleoflow from anisotropy of magnetic susceptibility and implications for flow processes, in Flood, R.D et al., (eds.), Proceedings of the Ocean Drilling Program, Scientific Results 155, Ocean Drilling Program, College Station, Texas, p. 53–78.

- Hodgson, D.M.** (2009) Origin and distribution of bipartite beds in sand-rich submarine fans: Constraints from the Tanqua depocentre, Karoo Basin, South Africa. *Marine and Petroleum Geology*, **26**, 1940–1956.
- Hodgson, D.M.** and **Haughton, P.D.W.** (2004) Impact of syn-depositional faulting on gravity current behaviour and deep-water stratigraphy: Tabernas–Sorbas Basin, SE Spain, in Lomas, S., Joseph, P., (eds.), *Confined Turbidites Systems*. Geological Society, London, Special Publications, v. 222, p. 135–158.
- Hodgson, D.M., Flint, S.S., Hodgetts, D., Drinkwater, N.J., Johannessen, E.P. and Luthi, S.M.** (2006) Stratigraphic evolution of fine-grained submarine fan systems, Tanqua depocenter, Karoo Basin, South Africa. *Journal of Sedimentary Research*, **76**, 20–40.
- Hodgson, D.M., Di Celma, C., Brunt, R.L. and Flint, S.S.** (2011) Submarine slope degradation and aggradation and the stratigraphic evolution of channel-levee systems. *Journal of the Geological Society*, **168**, 625–628. doi: 10.1144/0016-76492010-177.
- Hodgson, D.M., Kane, I.A., Flint, S.S., Brunt, R.L. and Ortiz-Karpf, A.** (2016) Time-transgressive confinement on the slope and the progradation of basin-floor fans: Implications for the sequence stratigraphy of deep-water deposits. *Journal of Sedimentary Research*, **86**, 73–86.
- Hoffman, J.S., Kaluza, M.J., Griffiths, R., McCullough, G., Hall, J. and Nguyen, T.** (2004) Addressing the Challenges in the Placement of Seafloor Infrastructure on the East Breaks Slide-A Case Study: The Falcon Field (EB 579/623), northwestern Gulf of Mexico. *Offshore Technology Conference, Contribution 16748*, pp. 18.
- Hofstra, M.**, (2016) The stratigraphic record of submarine channel-lobe transition zones. *Unpublished Ph.D. Thesis. University of Leeds*.
- Hofstra, M., Hodgson, D.M., Peakall, J. and Flint, S.S.** (2015) Giant scour-fills in ancient channel-lobe transition zones: Formative processes and depositional architecture. *Sedimentary Geology*, **329**, 98–114.

- Holbrook, J.M. and Bhattacharya, J.P.** (2012) Reappraisal of the sequence boundary in time and space: Case and considerations for an SU (subaerial unconformity) that is not a sediment bypass surface, a time barrier, or an unconformity. *Earth-Science Reviews*, **113**, 271-302.
- Howell, J.A., Martinius, A.W. and Good, T.R., 2014.** The application of outcrop analogues in geological modelling: A review, present status and future outlook, *in* Martinius, A. W. et al., (eds) *Sediment-Body Geometry and Heterogeneity: Analogue Studies for Modelling the Subsurface*. Geological Society, London, Special Publications, **387**, 1-25.
- Hsu, S.K., Kuo, J., Lo, C.L., Tsai, C.H., Doo, W.B., Ku, C.Y. and Sibuet, J.C.** (2008) Turbidity Currents, Submarine Landslides and the 2006 Pingtung Earthquake off SW Taiwan. *Terrestrial, Atmospheric and Oceanic Sciences*, **19**, 767–772.
- Huang, H., Imran, J., Pirmez, C., Zhang, Q. and Chen, G.** (2009) The critical densimetric Froude number of subaqueous gravity currents can be non-unity or non-existent. *Journal of Sedimentary Research*, **79**, 479-485.
- Hubbard, S.M., de Ruig, M.J. and Graham, S.A.** (2009) Confined channel-levee complex development in an elongate depo-center: deep-water Tertiary strata of the Austrian Molasse basin. *Marine and Petroleum Geology*, **26**, 85-112.
- Hughes Clarke, J.E., Brucker, S., Muggah, J., Hamilton, T., Cartwright, D., Church, I, and Kuus, P.** (2012) Temporal progression and spatial extent of mass wasting events on the Squamish prodelta slope, *in* Eberhardt, E. et al., (eds.), *Landslides and Engineered Slopes: Protecting Society through Improved Understanding*, p. 1091-1096.
- Hunt, J.E., Wynn, R.B., Talling, P.J. and Masson, D.G.** (2013) Turbidite record of frequency and source of large volume (> 100 km<sup>3</sup>) Canary Island landslides in the last 1.5 Ma: Implications for landslide triggers and geohazards. *Geochemistry, Geophysics, Geosystems*, **14**, 2100-2123.

- Hürlmann, M., Martí, J. and Ledesma, A.** (2004). Morphological and geological aspects related to large slope failures on oceanic islands: The huge La Orotava landslides on Tenerife, Canary Islands. *Geomorphology*, **62**, 143-158.
- Huyghe, P., Foata, M., Deville, E. and Mascle, G.** (2004) Channel profiles through the active thrust front of the southern Barbados prism. *Geology*, **32**, 429-432.
- Ito, M.** (1992) High-frequency depositional sequences of the upper part of the Kazusa Group, a middle Pleistocene forearc basin fill in Boso Peninsula, Japan. *Sedimentary Geology*, **76**, 155-175.
- Ito, M.** (1994) Compositional variation in depositional sequences of the upper part of the Kazusa Group, a middle Pleistocene forearc basin fill in the Boso Peninsula, Japan. *Sedimentary Geology*, **88**, 219-230.
- Ito, M.** (1998) Contemporaneity of component units of the lowstand systems tract: An example from the Pleistocene Kazusa forearc basin, Boso Peninsula, Japan. *Geology*, **26**, 939-942.
- Ito, M.** (2002) Downflow transformation from turbidity currents to debris flows at a channel-to-lobe transitional zone: The Lower Pleistocene Otadai Formation Boso Peninsula, Japan. *Journal of Sedimentary Research*, **78**, 668-682.
- Ito, M.** (2008) Downfan transformation from turbidity currents to debris flows at a channel-to-lobe transitional zone: the lower Pleistocene Otadai Formation. *Journal of Sedimentary Research*, **78**, 668-682.
- Ito, M., Ishikawa, K. and Nishida, N.** (2014) Distinctive erosional and depositional structures formed at a canyon mouth: A lower Pleistocene deep-water succession in the Kasuza forearc basin on the Boso Peninsula, Japan. *Sedimentology*, **61**, 2042-2062.
- Jackson, C.A-L.** (2011) Three-dimensional seismic analysis of megaclast deformation within a mass transport deposit; implications for debris flow kinematics. *Geology*, **39**, 203-206.

- Jackson, C.A. and Johnson, H.D.** (2009) Sustained turbidity currents and their interaction with debrite-related topography; Labuan Island, offshore NW Borneo, Malaysia. *Sedimentary Geology*, **219**, 77-96.
- Jackson, C.A-L, Barber, G.P., and Martinsen, O.J.** (2008) Submarine slope morphology as a control on the development of sand-rich turbidite depositional systems: 3D seismic analysis of the Kyrre Fm (Upper Cretaceous), Maloy Slope, offshore Norway. *Marine and Petroleum Geology*, **25**, 663-680.
- Joanne, C., Lamarche, C., and Collot, J.-Y.** (2013) Dynamics of giant mass transport in deep submarine environments: the Matakaoa Debris Flow, New Zealand. *Basin Research*, **25**, 471–488
- Jobe, Z.R., Lowe, D.R. and Morris, W.R.** (2012) Climbing-ripple successions in turbidite systems: depositional environments, sedimentation rates and accumulation times. *Sedimentology*, **59**, 867-898.
- Jobe, Z.R., Sylvester, Z., Howes, N., Pirmez, C., Parker, A., Cantelli, A., Smith, R., Wolinsky, M.A., O'Byrne, C., Slowey, N. and Prather, B.** (2017) High-resolution, millennial-scale patterns of bed compensation on a sand-rich intraslope submarine fan, western Niger Delta slope. *Geological Society of America Bulletin*, **129**, 23-37.
- Johnson, M.** (1991) Sandstone petrography, provenance and plate tectonic setting in Gondwana context of the southeastern Cape-Karoo Basin. *South African Journal of Geology*, **94**, 137-154.
- Johnson, M.R., Van Vuuren, C.J., Visser, J.N.J., Cole, D.I., Wickens, H.D.V., Christie, A.D.M. and Roberts, D.L** (1997) The foreland Karoo Basin, South Africa, *in* Selly, R.C. (ed) African Basins: Sedimentary Basins of the World, **3**, p. 269–317. Elsevier Science, Amsterdam.
- Johnson, S.D., Flint, S.S., Hinds, D. and Wickens, H.de V.** (2001) Anatomy, geometry and sequence stratigraphy of basin floor to slope turbidite systems, Tanqua Karoo, South Africa. *Sedimentology*, **48**, 987-1023.

- Johnson, M.R., van Vuuren, C.J., Visser, J.N.J., Cole, D.I., Wickens, H.D., Christie, A.D.M., Roberts, D.L. and Brandl, G.** (2006) Sedimentary rocks of the Karoo Supergroup, In: *The Geology of South Africa* (Eds M.R. Johnson, C.R. Anhaeusser and R.J Thomas) *Geological Society of South Africa and Council for Geoscience*, 461–499.
- Johnson, S.D., Flint, S., Hinds, D. and De Ville Wickens, H.** (2001) Anatomy, geometry and sequence stratigraphy of basin floor to slope turbidite systems, Tanqua Karoo, South Africa. *Sedimentology*, **48**, 987-1023.
- Jolly, B.A., Whittaker, A.C. and Lonergan, L.** (2017) Quantifying the geomorphic response of modern submarine channels to actively growing folds and thrusts, deep-water Niger Delta. *Geological Society of America Bulletin*, doi: [10.1130/B31544.1](https://doi.org/10.1130/B31544.1).
- Jones, G.E.D., Hodgson, D.M. and Flint, S.S.** (2013) Contrast in the process response of stacked clinothems to shelf-slope rollover. *Geosphere*, **9**, 299-316.
- Jones, G.E.D., Hodgson, D.M. and Flint, S.S.** (2015) Lateral variability in clinoform trajectory, process regime, and sediment dispersal patterns beyond the shelf-edge rollover in exhumed basin margin-scale clinothems. *Basin Research*, **27**, 657-680. doi: [10.1111/bre.12092](https://doi.org/10.1111/bre.12092).
- Kane, I.A. and Hodgson, D.M.** (2011) Sedimentological criteria to differentiate submarine channel levee subenvironments: exhumed examples from the Rosario Fm. (Upper Cretaceous) of Baja California, Mexico, and the Fort Brown Fm. (Permian), Karoo basin, S. Africa. *Marine and Petroleum Geology*, **28**, 807-823.
- Kane, I.A., Kneller, B.C., Dykstra, M., Kassem, A. and McCaffrey, W.D.** (2007) Anatomy of a submarine channel-levee: an example from Upper Cretaceous slope sediments, Rosario Formation, Baja California, Mexico. *Marine and Petroleum Geology*, **24**, 540-563.
- Kane, I.A., Dykstra, M., Kneller, B.C., Tremblay, S. and McCaffrey, W.D.** (2009a) Architecture of a coarse grained channel-levee system: the Rosario Formation, Baja California, Mexico. *Sedimentology*, **56**, 2207-2234.



- Kane, I.A., McCaffrey, W.D. and Martinsen, O.J.** (2009b) Allogenic vs. autogenic controls on megaflute formation. *Journal of Sedimentary Research*, **79**, 643-651.
- Kane, I.A., McCaffrey, W.D. and Peakall, J.** (2010) On the origin of palaeocurrent complexity in deep marine channel-levees. *Journal of Sedimentary Research*, **80**, p. 54-66.
- Kennedy, J. F.** (1961) Stationary waves and antidunes in alluvial channels: Pasadena, California, W. M. Keck Lab, California Institute of Technology, Report KH-R-2, 146 p.
- Kensley, B.** (1975) Marine Isopoda from the continental shelf of South Africa. *Annals of the South African Museum*, **67**, 35-89.
- Kenyon, N.H., and Millington, J.** (1995) Contrasting deep-sea depositional systems in the Bering Sea, in Pickering, K. et al., (eds.), Atlas of Deep Water Environments: Architectural Style in Turbidite Systems: London, Chapman and Hall, p. 196-202.
- Kenyon, N.H., Millington, J., Droz, L. and Ivanov, M.K.** (1995) Scour holes in a channel-lobe transition zone on the Rhone cone, in Pickering, K.T. et al., (eds.), Atlas of Deep Water Environments: Architectural Style in Turbidite Systems: London, Chapman and Hall, 212-215.
- Kertzus, V.** (2009) Stratigraphic development of delta-fed slope systems: Offshore Ebro and Nile Deltas, *Unpublished Ph.D. Thesis*, University of Aberdeen, Aberdeen, United Kingdom.
- Kidd, R.B., Lucchi, R.G., Gee, M. and Woodside, J.M.** (1998) Sedimentary processes in the Stromboli Canyon and Marsili Basin, SE Tyrrhenian Sea: results from side-scan sonar surveys. *Geo-Marine Letters*, **18**, 146-154.
- King, P.R., Ilg, B.R., Arnot, M, Browne, G.H., Strachan, L.J., Crundwell, M. and Helle, K.** (2011) Outcrop and seismic examples of mass-transport deposits from a late Miocene deep-water succession, Taranaki Basin, New Zealand, in Shipp, R.G. et al., (eds) Mass-Transport Deposits in Deepwater Settings, *Society for Sedimentary Geology (SEPM) Special Publication*, **96**, 311-348.

- Kingsley, C.S.** (1981) A composite submarine fan-delta-fluvial model for the Ecca and lower Beaufort Groups of Permian age in the eastern Cape Province, South Africa. *Transactions of the Geological Society South Africa*, **84**, 27-40.
- Klaucke, I., Masson, D.G., Kenyon, N.H. and Gardner, J.V.** (2004) Sedimentary processes of the lower Monterey Fan channel and channel-mouth lobe. *Marine Geology*, **206**, 181-198.
- Kneller, B.** (1995) Beyond the turbidite paradigm: physical models for deposition of turbidites and their implications for reservoir prediction, in Hartley, A.J. and Prosser, D.J. (eds.), Characterization of deep marine clastic systems. *Geological Society of London, Special Publication*, **94**, 31- 49.
- Kneller, B.** (2003) The influence of flow parameters on turbidite slope channel architecture. *Marine and Petroleum Geology*, **20**, 901–910.
- Kneller, B.C. and Branney, M.J.** (1995) Sustained high-density turbidity currents and the deposition of thick massive sands. *Sedimentology*, **42**, 607-616.
- Kneller, B.C. and McCaffrey, W.D.** (1999) Depositional effects of flow non-uniformity and stratification within turbidity currents approaching a bounding slope: deflection, reflection and facies variation. *Journal of Sedimentary Research*, **69**, 980-991.
- Kneller, B. and Buckee, C.** (2000) The structure and fluid mechanics of turbidity currents: a review of some recent studies and their geological implications, *Sedimentology*, **47**, 62-94.
- Kneller, B., Edwards, D., McCaffrey, W. and Moore, R.** (1991) Oblique reflection of turbidity currents. *Geology*, **19**, 250-252.
- Kneller, B., Dykstra, M., Fairweather, L. and Milana, J.P.** (2016) Mass-transport and slope accommodation: Implications for turbidite sandstone reservoirs. *AAPG Bulletin*, **100**, 213-235.
- Komar, P.D.** (1971) Hydraulic Jumps in Turbidity Currents. *AAPG Bulletin*, **82**, 1477-1487.

- Koša, E.** (2007) Differential subsidence driving the formation of mounded stratigraphy in deep-water sediments; Palaeocene, central North Sea. *Marine and Petroleum Geology*, **24**, 632-652.
- Kostic, S.** (2011) Modeling of submarine cyclic steps: Controls on their formation, migration, and architecture. *Geosphere*, **7**, 294-304.
- Kostic, S. and Parker, G.** (2006) The response of turbidity currents to a canyon–fan transition: internal hydraulic jumps and depositional signatures. *Journal of Hydraulic Research*, **44**, 631-653.
- Kubo, Y.S.** (2004) Experimental and numerical study of topographic effects on deposition from two-dimensional, particle-driven density currents. *Sedimentary Geology*, **164**, 311-326.
- Laberg, J.S., Kawamura, K., Amundsen, H., Baeten, N., Forwick, M., Rydningen, T.A. and Vorren, T.O.** (2014) A submarine landslide complex affecting the Jan Mayen Ridge, Norwegian–Greenland Sea: slide-scar morphology and processes of sediment evacuation. *Geo-Marine Letters*, **34**, 51-58.
- Laberg, J.S., Strasser, M., Alves, T.M., Gao, S., Kawamura, K., Kopf, A. and Moore, G.F.** (2016) Internal deformation of a muddy gravity flow and its interaction with the seafloor (site C0018 of IODP Expedition 333, Nankai Trough, SE Japan). *Landslides*, **13**, 1-12.
- Lafuerza, S., Sultan, N., Canals, M., Lastras, G., Cattaneo, A., Frigola, J., Costa, S. and Berndt, C.** (2012) Failure mechanisms of Ana Slide from geotechnical evidence, Eivissa Channel, Western Mediterranean Sea. *Marine Geology*, **307**, 1-21.
- Lane-Serff, G.F., Beal, L.M. and Hadfield, T.D.** (1995) Gravity current flow over obstacles. *Journal of Fluid Mechanics*, **292**, 39-53.
- Lang, J. and Winsemann, J.** (2013) Lateral and vertical facies relationships of bedforms deposited by aggrading supercritical flows: from cyclic steps to humback dunes. *Sedimentary Geology*, **296**, 36-54.

- Lee, S.E., Talling, P.J., Ernst, G.G. and Hogg, A.J.** (2002) Occurrence and origin of submarine plunge pools at the base of the US continental slope. *Marine Geology*, **185**, 363-377.
- Leeder, M.R. and Gawthorpe, R.L.** (1987) Sedimentary models for extensional tilt-block/half-graben basins. *Geological Society, London, Special Publications*, **28**, 139-152.
- León, R., Somoza, L., Urgeles, R., Medialdea, T., Ferrer, M., Biain, A., García-Crespo, J., Mediato, J.F., Galindo, I., Yepes, J. and González, F.J.** (2017) Multi-event oceanic island landslides: New onshore-offshore insights from El Hierro Island, Canary Archipelago. *Marine Geology*, doi: 10.1016/j.margeo.2016.07.001.
- Li, W., Alves, T.M., Urlaub, M., Georgiopoulou, A., Klauke, I., Wynn, R.B., Gross, F., Meyer, M., Repschläger, J., Berndt, C. and Krastel, S.** (2017) Morphology, age and sediment dynamics of the upper headwall of the Sahara Slide Complex, Northwest Africa: Evidence for a large Late Holocene failure. *Marine Geology*, doi: 10.1016/j.margeo.2016.11.013.
- Linol, B. and De Wit, M.J.** eds. (2016) Origin and Evolution of the Cape Mountains and Karoo Basin. Springer.
- Lindeque, A., de Wit, M.J., Ryberg, T., Weber, M. and Chevallier, L.** (2011) Deep crustal profile across the southern Karoo Basin and Beattie Magnetic Anomaly, South Africa: an integrated interpretation with tectonic implications. *South African Journal of Geology*, **114**, 265-292.
- Liu, J.Y. and Bryant, W.R.** (2000) Seafloor Morphology and Sediment Paths of the Northern Gulf of Mexico Deep Water, in Bouma, A.H. and Stone, C.G., (eds) AAPG Memoir 72 / SEPM Special Publication No. 6845, 95-101.
- Locat, J. and Lee, H.J.** (2002) Submarine landslides: advances and challenges. *Canadian Geotechnical Journal*, **39**, 193-212.
- Loncke, L., Gaullier, V., Droz, L., Ducassou, E., Migeon, S. and Mascle, J.** (2009) Multi-scale slope instabilities along the Nile deep-sea fan, Egyptian margin: a general overview. *Marine and Petroleum Geology*, **26**, 633-646.

- Lopez-Mir, B., Muñoz, J.A. and Senz, J.G.** (2014) Restoration of basins driven by extension and salt tectonics: Example from the Cotiella Basin in the central Pyrenees. *Journal of Structural Geology*, **69**, 147-162.
- Løvholt, F., Harbitz, C.B. and Haugen, K.B.** (2005) A parametric study of tsunamis generated by submarine slides in the Ormen Lange/Storegga area off western Norway. *Marine and Petroleum Geology*, **22**, 219-231.
- Lowe, D.R.** (1982) Sediment gravity flows: II Depositional models with special reference to the deposits of high-density turbidity current. *Journal of Sedimentary Petrology*, **52**, 279–298.
- Lowe, D.R.** (1988) Suspended-load fallout rate as an independent variable in the analysis of current structures. *Sedimentology*, **35**, 765-776.
- Lucchi, R. and Camerlenghi, A.** (1993) Upslope turbiditic sedimentation on the southeastern flank of the Mediterranean Ridge. *Bollettino di oceanologia teorica ed applicata*, **11**, 3-25.
- Lucente, C.C. and Pini, G.A.** (2003) Anatomy and emplacement mechanism of a large submarine slide within a Miocene foredeep in the northern Apennines, Italy: A field perspective. *American Journal of Science*, **303**, 565-602.
- Luthi, S.M., Hodgson, D.M., Geel, C.R., Flint, S.S., Goedbloed, J.W., Drinkwater, N.J. and Johannessen, E.P.** (2006) Contribution of research borehole data to modelling fine-grained turbidite reservoir analogues, Permian Tanqua–Karoo basin-floor fans (South Africa). *Petroleum Geoscience*, **12**, 175-190.
- Macauley, R.V. and Hubbard, S.M.** (2013) Slope channel sedimentary processes and stratigraphic stacking, Cretaceous Tres Pasos Formation slope system, Chilean Patagonia. *Marine and Petroleum Geology*, **41**, 146-162.
- Macdonald, H.A., Wynn, R.B., Huvenne, V.A., Peakall, J., Masson, D.G., Weaver, P.P. and McPhail, S.D.** (2011a) New insights into the morphology, fill, and remarkable longevity (> 0.2 m.y.) of modern deep-water erosional scours along the northeast Atlantic margin. *Geosphere*, **7**, 845–867.

- Macdonald, H.A., Peakall, J., Wignall, P.B. and Best, J.** (2011b) Sedimentation in deep-sea lobe-elements: implications for the origin of thickening-upward sequences. *Journal of the Geological Society of London*, **168**, 319–331.
- Madof, A.S., Christie-Blick, N. and Anders, M.H.** (2009) Stratigraphic controls on a salt-withdrawal intraslope minibasin, north-central Green Canyon, Gulf of Mexico: implications for misinterpreting sea level change. *American Association of Petroleum Geologists Bulletin*, **93**, 535-561.
- Marini, M., Milli, S., Ravnås, R. and Moscatelli, M.** (2015) A comparative study of confined vs. semi-confined turbidite lobes from the Lower Messinian Laga Basin (Central Apennines, Italy): Implications for assessment of reservoir architecture. *Marine and Petroleum Geology*, **63**, 142-165.
- Marini, M., Patacci, M., Felletti, F. and McCaffrey, W.D.** (2016) Fill to spill stratigraphic evolution of a confined turbidite mini-basin succession, and its likely well bore expression: The Castagnola Fm, NW Italy. *Marine and Petroleum Geology*, **69**, 94-111.
- Martinsen, O.J.** (1989) Styles of soft-sediment deformation on a Namurian (Carboniferous) delta slope, Western Irish Namurian Basin, Ireland, in Whateley, M.H. and Pickering, K.T. (eds.) Deltas—Sites and Traps of Fossil Fuels, *Geological Society, London, Special Publications*, **41**, 167-177.
- Martinsen, O.J.** (1994) Mass movements, in Maltman, M., (ed) *The Geological Deformation of Sediments*. Chapman and Hall, London, pp. 127–165.
- Martinsen, O.J. and Bakken, B.** (1990) Extensional and compressional zones in slumps and slides in the Namurian of County Clare, Ireland. *Journal of the Geological Society of London*, **147**, 153-164.
- Marjanac, T.** (1987) Ponged megabeds and some characteristics of the Eocene Adriatic basin (Middle Dalmatia, Yugoslavia). *Mem. Soc. Geol. Ital*, **40**, 241-249.

- Marjanac, T.** (1990) Reflected sediment gravity flows and their deposits in flysch of Middle Dalmatia, Yugoslavia. *Sedimentology*, **37**, 921-929.
- Masson, D.G., Watts, A.B., Gee, M.J.R., Urgeles, R., Mitchell, N.C., Le Bas, T.P. and Canals, M.** (2002) Slope failures on the flanks of the western Canary Islands. *Earth-Science Reviews*, **57**, 1-35.
- Masson, D.G., Harbitz, C.B., Wynn, R.B., Pedersen, G. and Løvholt, F.** (2006) Submarine slides: processes, triggers and hazard prediction. *Philosophical Transactions of the Royal Society A*, **364**, 2009-2039. doi: 10.1098/rsta.2006.1810
- Masson, D.G., Wynn, R.B. and Talling, P.J.** (2010) Large landslides on passive continental margins: processes, hypotheses and outstanding questions, in Mosher, D.C., et al., (eds.) *Submarine Mass Movements and Their Consequences*, Springer, Netherlands, 153-165.
- Mayall, M., Jones, E. and Casey, M.** (2006) Turbidite channel reservoirs—Key elements in facies prediction and effective development. *Marine and Petroleum Geology*, **23**, 821-841.
- Mayall, M., Lonergan, L., Bowman, A., James, S., Mills, K., Primmer, T., Pope, D., Rogers, L. and Skeene, R.** (2010) The response of turbidite slope channels to growth-induced seabed topography. *AAPG Bulletin*, **94**, 1011-1030.
- McAdoo, B.G., Pratson, L.F. and Orange, D.L.** (2000) Submarine landslide geomorphology, US continental slope. *Marine Geology*, **169**, 103-136.
- McKay, M.P., Weislogel, A.L., Fildani, A., Brunt, R.L., Hodgson, D.M. and Flint, S.S.** (2015) U-PB zircon tuff geochronology from the Karoo Basin, South Africa: implications of zircon recycling on stratigraphic age controls. *International Geology Review*, **57**, 393-410.
- McLachlan, I.R. and Anderson, A.** (1973) A review of the evidence for marine conditions in southern Africa during Dwyka times. *Palaeontologia Africana*, **15**, 37-64.

- McLachlan, I.R. and Anderson, A.M.** (1975) The age and stratigraphic relationship of the glacial sediments in southern Africa. *Gondwana Geology. Australian Natl Univ Press, Canberra*, 415-422.
- McLachlan, I.R. and Jonker, J.P.** (1990) Tuff beds in the northwestern part of the Karoo Basin. *South African Journal of Geology*, **93**, 329-338.
- Meckel III, L.D., Ugueto, G.A., Lynch, D.H., Hewett, B.M., Bocage, E.J., Winker, C.D. and O'Neill, B.J.** (2002) Genetic stratigraphy, stratigraphic architecture, and reservoir stacking patterns of the upper Miocene–lower Pliocene greater Mars-Ursa intraslope basin, Mississippi Canyon, Gulf of Mexico, *in* Armentrout, J.M., and Rosen, N.C., (eds.), *Sequence Stratigraphic Models for Exploration and Production: Evolving Methodology, Emerging Models, and Application Histories: GCSSEPM (Gulf Coast Section, Society for Sedimentary Geology) Foundation 22nd Annual Bob F. Perkins Research Conference Proceedings*, p. 113-147.
- Meiburg, E. and Kneller, B.** (2010) Turbidity currents and their deposits. *Annual Review of Fluid Mechanics*, **42**, 135-156.
- Middleton, G.V.** (1965) Antidune cross-bedding in a large flume. *Journal of Sedimentary Research*, **35**. 922-927.
- Middleton, G.V. and Hampton, M.A.** (1976) Subaqueous sediment transport and deposition by sediment gravity flows, *in* Stanley, D.J., and Swift, D.J.P., (eds.) *Marine Sediment Transport and Environmental Management*, Wiley, New York, 197–218.
- Migeon, S., Savoye, B., Zanella, E., Mulder, T., Faugères, J.C. and Weber, O.** (2001) Detailed seismic-reflection and sedimentary study of turbidite waves on the Var Sedimentary Ridge (SE France): significance for sediment transport and deposition and for the mechanisms of sediment-wave construction. *Marine and Petroleum Geology*, **18**, 179-208.
- Mitchell, N.C.** (2006) Morphologies of knickpoints in submarine canyons. *Geological Society of America Bulletin*, **118**, 589-605.



- Moernaut, J. and De Batist, M.** (2011) Frontal emplacement and mobility of sublacustrine landslides: results from morphometric and seismostratigraphic analysis. *Marine Geology*, **285**, 29-45
- Moody, J.D., Pyles, D.R., Clark, J., and Bouroullec, R.** (2012) Quantitative outcrop characterization of an analog to weakly confined submarine channel systems: Morillo 1 member, Ainsa Basin, Spain. *AAPG Bulletin*, **96**, 1813-1841.
- Morley, C.K.** (2009) Growth of folds in a deep-water setting. *Geosphere*, **5**, 59-89.
- Morris, S.A., Kenyon, N.H., Limonov, A.F. and Alexander, J.** (1998) Downstream changes of large-scale bedforms in turbidites around the Valencia channel mouth, north-west Mediterranean: implications for palaeoflow reconstruction. *Sedimentology*, **42**, 365-377.
- Morris, E.A., Hodgson, D.M., Brunt, R.L. and Flint, S.S.** (2014a) Origin, evolution and anatomy of silt-prone submarine external levees. *Sedimentology*, **61**, 1734-1763.  
doi:10.1111/sed.12114.
- Morris, E.A., Hodgson, D.M., Flint, S.S., Brunt, R.L., Butterworth, P.J. and Verhaeghe, J.** (2014b) Sedimentology, stratigraphic architecture, and depositional context of submarine frontal-lobe complexes. *Journal of Sedimentary Research*, **84**, 763-780.
- Morris, E.A., Hodgson, D.M., Flint, S., Brunt, R.L., Luthi, S.M. and Kolenberg, Y.** (2016) Integrating outcrop and subsurface data to assess the temporal evolution of a submarine channel–levee system. *AAPG Bulletin*, **100**, 1663-1691.
- Moscardelli, L. and Wood, L.** (2008) New classification system for mass transport complexes in offshore Trinidad. *Basin Research*, **20**, 73-98.
- Moscardelli, L. and Wood, L.** (2015) Morphometry of mass-transport deposits as a predictive tool, *GSA Bulletin*, **128**, 47-80. doi: 10.1130/B31221.1
- Moscardelli, L., Wood, L. and Mann, P.** (2006) Mass-transport complexes and associated processes in the offshore area of Trinidad and Venezuela. *AAPG Bulletin*, **90**, 1059-1088.

- Mulder, T. and Alexander, J.** (2001) Abrupt change in slope causes variation in the deposit thickness of concentrated particle-driven density currents. *Marine Geology*, **175**, 221-235.
- Mutti, E.** (1977) Distinctive thin-bedded turbidite facies and related depositional environments in the Eocene Hecho Group (South-central Pyrenees, Spain). *Sedimentology*, **24**, 107-131.
- Mutti, E.** (1985) Systems and their relations to depositional sequences, in Zuffa, G.G., (ed.), Provenance of arenites: Interpreting provenance relations from detrital modes of sandstones: NATO-ASI Series 148: Dordrecht, D. Reidel, 65–93.
- Mutti, E.** (1992) Turbidite sandstones. Agip, Istituto di geologia, Università di Parma, Italy, 275 pp.
- Mutti, E. and Normark, W.R.** (1987) Comparing examples of modern and ancient turbidite systems: problems and concepts, in Leggett, J.K., and Zuffa, G.G., (eds.), Marine Clastic Sedimentology: Concepts and Case Studies: Oxford, UK, Graham & Trotman, 1-38.
- Mutti, E. and Normark, W.R.** (1991) An integrated approach to the study of turbidite systems, in Weimer, P., and Link, M.H., (eds.), Seismic facies and sedimentary processes of submarine fans and turbidite systems: New York, Springer-Verlag, 75–106.
- Nasr-Azadani, M.M. and Meiburg, E.** (2014) Turbidity currents interacting with three-dimensional seafloor topography. *Journal of Fluid Mechanics*, **745**, 409-443.
- Neal, J. and Abreu, V.** (2009) Sequence stratigraphy hierarchy and the accommodation succession method. *Geology*, **37**, 779-782.
- Normark, W.R.** (1970) Growth patterns of deep-sea fans. *AAPG Bulletin*, **54**, 2170-2195.
- Normark, W.R.** (1978) Fan valleys, channels, and depositional lobes on modern submarine fans: characters for recognition of sandy turbidite environments. *AAPG Bulletin*, **62**, 912-931.

- Normark, W.R.** (1990) Return to Ranger Submarine Slide, Baja California, Mexico. *Geo-Marine Letters*, **10**, 81-91
- Normark, W.R.** and **Gutmacher, C.E.** (1988) Sur submarine slide, Monterey fan, central California. *Sedimentology*, **35**, 629-647.
- Normark, W.R.**, and **Piper, D.J.W.** (1991) Initiation processes and flow evolution of turbidity currents: implications for the depositional record, *in* Osborne, R.H. (ed.), From Shoreline to Abyss: Contributions in Marine Geology in Honor of Francis Parker Shepard, Special publication- Society for Sedimentary Geology, **46**, 207-230.
- Normark, W.R.**, **Piper, D.J.W.** and **Hess, G.R.** (1979) Distributary channels, sand lobes, and mesotopography of Navy submarine fan, California Borderland, with applications to ancient fan sediments. *Sedimentology*, **26**, 749-774.
- Normark, W.R.**, **Mutti, E.** and **Bouma, A.H.** (1984) Submarine clastic systems: Deep sea fans and related turbidite facies. *Geo-Marine Letters*, **3**, 53-224.
- O'Byrne, C.J.**, **Prather, B.E.**, **Steffens, G.S.** and **Pirmez, C.** (2004) Reservoir architectural styles across stepped slope profiles: Implications for exploration, appraisal and development: American Association of Petroleum Geologists, International Conference and Exhibition, Cancún, Mexico, Abstracts CD.
- Oelofsen, B.W.** (1987) The biostratigraphy and fossils of the Whitehill and Irati Shale Formations of the Karoo and Paraná Basins, *in* McKenzie, G.D. (ed) Gondwana Six: Stratigraphy, Sedimentology and Palaeontology, Geophysical Monograph American Geophysical Union, **41**, 131-138.
- Oelofsen, B. W.** and **Araujo, D. C.** (1987) Mesosaurus tenuidens and Stereosternum tumidum from the Permian Gondwana of both Southern Africa and South America. *South African Journal of Science*, **83**, 370-372.
- Ogiesoba, O.** and **Hammes, U.** (2012) Seismic interpretation of mass-transport deposits within the upper Oligocene Frio Formation, south Texas Gulf Coast. *AAPG Bulletin*, **96**, 845-868.

- Olafiranye, K., Jackson, C.A.L. and Hodgson, D.M.** (2013) The role of tectonics and mass-transport complex emplacement on upper slope stratigraphic evolution: A 3D seismic case study from offshore Angola. *Marine and Petroleum Geology*, **44**, 196-216.
- Omosanya, K.O. and Alves, T.M.** (2013) A 3-dimensional seismic method to assess the provenance of Mass-Transport Deposits (MTDs) on salt-rich continental slopes (Espírito Santo Basin, SE Brazil). *Marine and Petroleum Geology*, **44**, 223-239.
- Ortiz-Karpf, A., Hodgson, D.M. and McCaffrey, W.D.** (2015) The role of mass-transport complexes in controlling channel avulsion and the subsequent sediment dispersal patterns on an active margin: the Magdalena Fan, offshore Colombia. *Marine and Petroleum Geology*, **64**, 58-75.
- Ortiz-Karpf, A., Hodgson, D.M., Jackson, C.A.L. and McCaffrey, W.D.** (2017a) Influence of seabed morphology and substrate composition on mass-transport flow processes and pathways: insights from the Magdalena fan, offshore Colombia. *Journal of Sedimentary Research*, **87**, 1-21.
- Ortiz-Karpf, A., Hodgson, D.M., Jackson, C.A.L. and McCaffrey, W.D.** (2017b) Mass-transport complexes as markers of deep-water fold-and-thrust belt evolution: insights from the southern Magdalena fan, offshore Colombia. *Basin Research*. DOI: 10.1111/bre.12208.
- Palanques, A., Kenyon, N.H., Alonso, B. and Limonov, A.F.** (1995) Erosional and depositional patterns in the Valencia Channel Mouth: an example of a modern channel-lobe transition zone. *Marine Geophysical Research*, **18**, 103-118.
- Pantin, H.M. and Leeder, M.R.** (1987) Reverse flow in turbidity currents: the role of internal solitons. *Sedimentology*, **34**, 1143-1155.
- Patacci, M., Houghton, P.D. and McCaffrey, W.D.** (2014) Rheological complexity in sediment gravity flows forced to decelerate against a confining slope, Braux, SE France. *Journal of Sedimentary Research*, **84**, 270-277.

- Peakall, J., McCaffrey, W.D. and Kneller, B.C.** (2000) A process model for the evolution, morphology, and architecture of sinuous submarine channels. *Journal of Sedimentary Research*, **70**, 434–448.
- Pelinovsky, E. and Poplavsky, A.** (1996) Simplified model of tsunami generation by submarine landslides. *Physics and Chemistry of the Earth*, **21**, 13-17.
- Pemberton, E.A.L., Hubbard, S.M., Fildani, A., Romans, B. and Stright, L.** (2016) The stratigraphic expression of decreasing confinement along a deep-water sediment routing system: Outcrop example from southern Chile. *Geosphere*, **12**, 114-134.
- Pickering, K.T. and Hiscott, R.N.** (1985) Contained (reflected) turbidity currents from the Middle Ordovician Cloridorme Formation, Quebec, Canada: an alternative to the antidune hypothesis. *Sedimentology*, **32**, 373-394.
- Pickering, K.T. and Hilton, V.C.** (1998) Turbidite systems of southeast France. *Vallis Press*, London, 229 pp.
- Pickering, K.T. and Corregidor, J.** (2005) Mass-transport complexes (MTCs) and tectonic control on basin-floor submarine fans, middle Eocene, south Spanish Pyrenees. *Journal of Sedimentary Research*, **75**, 761-783.
- Pickford, M.** (1995) Karoo Supergroup palaeontology of Namibia and brief description of a thecodont from Omingonde. *Palaeontologia Africana*, **32**, 51-66.
- Picot, M., Droz, L., Marsset, T., Dennielou, B. and Bez, M.** (2016) Controls on turbidite sedimentation: Insights from a quantitative approach of submarine channel and lobe architecture (Late Quaternary Congo Fan). *Marine and Petroleum Geology*, **72**, 423-446.
- Piper, D.J.W. and Deptuck, M.** (1997) Fine grained turbidites of the Amazon Fan: facies characterization and interpretation, in Flood, R.D., Piper, D.J.W., Klaus, A., Peterson, L.C. (eds.), *Proceedings of the Ocean Drilling Program: Scientific Results*, **155**, 79-108

- Piper, D.J. and Savoye, B.** (1993) Processes of late Quaternary turbidity current flow and deposition on the Var deep-sea fan, north-west Mediterranean Sea. *Sedimentology*, **40**, 557-582.
- Piper, D.J., Shor, A.N., Farre, J.A., O'Connell, S. and Jacobi, R.** (1985) Sediment slides and turbidity currents on the Laurentian Fan: Sidescan sonar investigations near the epicenter of the 1929 Grand Banks earthquake. *Geology*, **13**, 538-541.
- Piper, D.J.W., Hiscott, R.N. and Normark, W.R.** (1999) Outcrop-scale acoustic facies analysis and latest Quaternary development of Hueneme and Dume submarine fans, offshore California. *Sedimentology*, **46**, 47-78.
- Piper, D.J.W., Deptuck, M.E., Mosher, D.C., Hughes Clarke, J.E. and Migeon, S.** (2012) Erosional and depositional features of glacial meltwater discharges on the eastern Canadian continental margin, *in* Prather, B.E. et al., (eds.) Applications of the Principles of Seismic Geomorphology to Continental Slope and Base-of-slope Systems: Case Studies from Seafloor and Near-Seafloor Analogues, Society for Sedimentary Geology (SEPM), Special Publications, **99**, 61-80.
- Pirmez, C., Beaubouef, R.T., Friedmann, S.J. and Mohrig, D.C.** (2000) Equilibrium profile and base level in submarine channels: examples from Late Pleistocene systems and implications for the architecture of deep-water reservoirs, *in* Weimer, P., Slatt, R.M., et al. (eds.), Deep-water Reservoirs of the World: Gulf Coast Society of the Society of Economic Paleontologists and Mineralogists Foundation, 20<sup>th</sup> Annual Research Conference, 782–805.
- Plink-Björklund, P. and Steel, R.** (2002) Sea-level fall below the shelf edge, without basin-floor fans. *Geology*, **30**, 115-118.
- Pohl, F., Eggenhuisen, J., Cartigny, M and Hermidas, N.** (2016) Break-of-slope linked to unexpected downstream grain size coarsening in experimental and natural turbidites, *AGU Fall Meeting 2016 conference paper*.

- Posamentier, H.W.** (2003) Depositional elements associated with a basin floor channel-levee system: case study from the Gulf of Mexico. *Marine and Petroleum Geology*, **20**, 677-690.
- Posamentier, H.W.** and **Kolla, V.** (2003) Seismic geomorphology and stratigraphy of depositional elements in deep-water settings. *Journal of Sedimentary Research*, **73**, 367-388.
- Posamentier, H.W.** and **Walker, R.G.** (2006) Deep-water turbidites and submarine fans, *in* Posamentier, H.W and Walker R.G. (eds.) Facies models revisited, SEPM special publication, 399-521.
- Posamentier, H.W.** and **Martinsen, O.J.** (2011) The character and genesis of submarine mass-transport deposits: insights from outcrop and 3D seismic data, *in* Shipp, R.G., et al., (eds.) Mass-Transport Deposits in Deepwater Settings, Society for Sedimentary Geology (SEPM) Special Publication, **96**, 7-38.
- Postma, G.** and **Cartigny, M.J.** (2014) Supercritical and subcritical turbidity currents and their deposits – A synthesis. *Geology*, **42**, 987-990.
- Postma, G., Cartigny, M.** and **Kleverlaan, K.** (2009) Structurless, coarse-tail graded Bouma Ta formed by internal hydraulic jump of the turbidity current? *Sedimentary Geology*, **219**, 1-6.
- Postma, G., Hoyal, D.C., Abreu, V., Cartigny, M.J., Demko, T., Fedele, J.J., Kleverlaan, K.** and **Pederson, K.H.** (2016) Morphodynamics of supercritical turbidity currents in the channel-lobe transition zone, *in* Lamarche, G., Mountjoy, J., Bull, S., Hubble, T., Krastel, S., Lane, E., Micallef, A., Moscardelli, L., Mueller, C., Pecher, I., and Woelz, S. eds., Submarine Mass Movements and Their Consequences: 7th International Symposium, Springer International Publishing, 469-478.
- Poyatos-Moré, M., Jones, G.D., Brunt, R.L., Hodgson, D.M., Wild, R.J.** and **Flint, S.S.** (2016) Mud-dominated basin-margin progradation: processes and implications. *Journal of Sedimentary Research*, **86**, 863-878.

- Prather, B.E.** (2000) Calibration and visualization of depositional process models for above-grade slopes: a case study from the Gulf of Mexico. *Marine and Petroleum Geology*, **17**, 619-638.
- Prather, B.E.** (2003) Controls on reservoir distribution, architecture and stratigraphic trapping in slope settings. *Marine and Petroleum Geology*, **20**, 529-545.
- Prather, B. E., Booth, J. R, Steffens, G. S. and Craig, P. A.** (1998) Classification, lithologic calibration, and stratigraphic succession of seismic facies of intraslope basins, deep-water Gulf of Mexico: *AAPG Bulletin*, **82**, 701– 728.
- Prather, B.E., O’Byrne, C.J., Pirmex, C. and Sylvester, Z.** (2009) Sediment partitioning across tertiary continental slopes (abstract): American Association of Petroleum Geologists, Annual Convention, Denver, Colorado, Abstracts, CD.
- Prather, B.E., Pirmez, C., Sylvester, Z. and Prather, D.S.** (2012a) Stratigraphic response to evolving geomorphology in a submarine apron perched on the upper Niger Delta slope, *in* Prather, B.E., et al., (eds.), Application of the Principles of Seismic Geomorphology to Continental-slope and Base-of-slope Systems: Case Studies from Seafloor and Near-seafloor Analogues: SEPM (Society for Sedimentary Geology) Special Publication 99,p. 145–161, doi: 10 .2110 /pec .12 .99 .0145 .
- Prather, B.E., Pirmez, C. and Winker, C.D.** (2012b) Stratigraphy of linked intraslope basins: Brazos-Trinity system western Gulf of Mexico, *in* Prather, B.E., et al., (eds.), Application of the Principles of Seismic Geomorphology to Continental-Slope and Base-of-Slope Systems: Case Studies from Seafloor and Near-Seafloor Analogues: SEPM, Special Publication, v. 99, p. 83-110.
- Prather, B.E., O’Byrne, C., Pirmez, C. and Sylvester, Z.** (2017) Sediment partitioning, continental slopes and base-of-slope systems. *Basin Research*, **29**, 394-416.
- Prélat, A. and Hodgson, D.M.** (2013) The full range of turbidite bed thickness patterns in submarine lobes: controls and implications. *Journal of the Geological Society*, **170**, 209-214.



- Prélat, A., Hodgson, D.M. and Flint, S.S.** (2009) Evolution, architecture and hierarchy of distributary deep-water deposits: a high-resolution outcrop investigation from the Permian Karoo Basin, South Africa. *Sedimentology*, **56**, 2132-2154.
- Prior, D.B., Bornhold, B.D. and Johns, M.W.** (1984) Depositional characteristics of a submarine debris flow. *The Journal of Geology*, **92**, 707-727.
- Pyles, D.R.** (2008) Multiscale stratigraphic analysis of a structurally confined submarine fan: Carboniferous Ross Sandstone, Ireland. *AAPG Bulletin*, **92**, 557-587.
- Pyles, D.R. and Jennette, D.C.** (2009) Geometry and architectural associations of co-genetic debrite–turbidite beds in basin-margin strata, Carboniferous Ross Sandstone (Ireland): Applications to reservoirs located on the margins of structurally confined submarine fans. *Marine and Petroleum Geology*, **26**, 1974-1996.
- Qin, Y., Alves, T., Constantine, J.A. and Gamboa, D.** (2017) The role of mass wasting in the progressive development of submarine channels (Espírito Santo Basin, SE Brazil). *Journal of Sedimentary Research*, **87**, 500-516, DOI: 10.2110/jsr.2017.18
- Raudkivi, A.J.** (1976) *Loose Boundary Hydraulics*, Pergamon Press, Rotterdam.
- Reading, H.G. and Richards, M.** (1994) Turbidite systems in deep-water basin margins classified by grain size and feeder system. *AAPG Bulletin*, **78**, 792-822.
- Ricci-Lucchi, F.R. and Valmori, E.** (1980) Basin-wide turbidites in a Miocene, over-supplied deep-sea plain: a geometrical analysis. *Sedimentology*, **27**, 241-270.
- Romero Otero, G.A.** (2009) Deepwater sedimentary processes in an active margin, Magdalena submarine fan, offshore Colombia. *Unpublished Ph.D. Thesis*, The University of Oklahoma, USA.
- Rothwell, R.G., Pearce, T.J. and Weaver, P.P.E.** (1992) Late Quaternary evolution of the Madeira Abyssal Plain, Canary Basin, NE Atlantic. *Basin Research*, **4**, 103-131.

- Rothwell, R.G., Thomson, J. and Kähler, G.** (1998) Low sea-level emplacement of a very large late Pleistocene 'megaturbidite' in the western Mediterranean Sea. *Nature*, **392**, 377-380.
- Rottman, J.W. and Simpson, J.E.** (1989) The formation of internal bores in the atmosphere: A laboratory model. *Quarterly Journal of the Royal Meteorological Society*, **115**, 941-963.
- Rozman, D.J.** (2000) Characterization of a fine-grained outer submarine fan deposit, Tanqua-Karoo Basin, South Africa, in Bouma, A.H., and Stone, C.G. (eds.), *Fine-grained Turbidite Systems. AAPG Memoir 72/SEPM Special Publication*, **68**, 279-290.
- Rust, I.C.** (1973) The evolution of the Paleozoic Cape basin, southern margin of Africa, in A.E.M. Nairn, F.G. Stehli (eds.), *The Ocean Basins and Margins*, vol. 1. Plenum, New York, 247-276.
- Saller, A.H., Noah, J.T., Ruzuar, A.P. and Schneider, R.** (2004) Linked lowstand delta to basin-floor fan deposition, offshore Indonesia: An analog for deep-water reservoir systems. *AAPG Bulletin*, **88**, 21-46.
- Salles, L., Ford, M. and Joseph, P.** (2014) Characteristics of axially-sourced turbidite sedimentation on an active wedge-top basin (Annot Sandstone, SE France). *Marine and Petroleum Geology*, **56**, 305-323.
- Satterfield, W. M. and Behrens, E.W.** (1990) A Late Quaternary Canyon/Channel System, Northwest Gulf of Mexico Continental Slope. *Marine Geology*, **92**, 51-67.
- Scheffler, K., Hoernes, S. and Schwark, L.,** (2003) Global changes during Carboniferous–Permian glaciation of Gondwana: Linking polar and equatorial climate evolution by geochemical proxies. *Geology*, **31**, 605-608.
- Scheffler, K., Buehmann, D. and Schwark, L.** (2006) Analysis of late Palaeozoic glacial to postglacial sedimentary successions in South Africa by geochemical proxies—response to climate evolution and sedimentary environment. *Palaeogeography, Palaeoclimatology, Palaeoecology*, **240**, 184-203.

- Sequeiros, O.E., Naruse, H., Endo, N., Garcia, M.H. and Parker, G.,** (2009). Experimental study on self-accelerating turbidity currents. *Journal of Geophysical Research: Oceans*, **114**, C05025.
- Schminke, H.U., Fisher, R.V. and Waters, A.C.** (1973) Antidune and chute and pool structures in the base surge deposits of the Laacher See area, Germany. *Sedimentology*, **20**, 553-574.
- Shanmugam, G. and Moiola, R.J.** (1991) Types of Submarine Fan Lobes: Models and Implications (1). *AAPG Bulletin*, **75**, 156-179.
- Shanmugam, G., Bloch, R.B., Mitchell, S.M., Beamish, G.W., Hodgkinson, R.J., Damuth, J.E., Straume, T., Syvertsen, S.E. and Shields, K.E.** (1995) Basin-floor fans in the North Sea: sequence stratigraphic models vs. sedimentary facies. *AAPG Bulletin*, **79**, 477-511.
- Shipp, R.C., Nott, J.A. and Newlin, J.A.** (2004) Physical characteristics and impact of mass transport complexes on deepwater jetted conductors and suction anchor piles, in *OTC Paper 16751*, p. 11 Annual Offshore Technology Conference, Houston, Texas.
- Shultz, M.R. and Hubbard, S.M.** (2005) Sedimentology, stratigraphic architecture, and ichnology of gravity-flow deposits partially ponded in a growth-fault-controlled slope minibasin, Tres Pasos Formation (Cretaceous), southern Chile. *Journal of Sedimentary Research*, **75**, 440-453.
- Shultz, M.R., Fildani, A., Cope, T.D. and Graham, S.A.** (2005) Deposition and stratigraphic architecture of an outcropping ancient slope system: Tres Pasos Formation, Magallanes Basin, southern Chile, in Hodgson, D.M. and Flint, S.S., (eds) *Submarine Slope Systems: Processes and Products*, Geological Society, London, Special Publications, **244**, 27-50.
- Simpson, J.E.** (1997) *Gravity Currents in the Environment and the Laboratory*. 2nd Edition, Cambridge University Press. New York. 258 pp.
- Sinclair, H.D.** (1994) The influence of lateral basinal slopes on turbidite sedimentation in the Annot sandstones of SE France. *Journal of Sedimentary Research*, **64**, 42-54.

- Sinclair, H.D.** (2000) Delta-Fed Turbidites Infilling Topographically Complex Basins: A New Depositional Model for the Annot Sandstones, SE France. *Journal of Sedimentary Research*, **70**, 504-519.
- Sinclair, H.D.** and **Cowie, P.A.** (2003) Basin-floor topography and the scaling of turbidites. *The Journal of Geology*, **111**, 277-299.
- Sinclair, H.D.** and **Tomasso, M.** (2002) Depositional evolution of confined turbidite basins. *Journal of Sedimentary Research*, **72**, 451-456.
- Sixsmith, P.J., 2000.** Stratigraphic development of a Permian turbidite system on a deforming basin floor: Laingsburg Formation, Karoo basin, South Africa. *Unpublished Ph.D. Thesis*, University of Liverpool, Liverpool.
- Sixsmith, P.J., Flint, S.S., Wickens, H.D.** and **Johnson, S.D.** (2004) Anatomy and stratigraphic development of a basin floor turbidite system in the Laingsburg Formation, main Karoo Basin, South Africa. *Journal of Sedimentary Research*, **74**, 239-254. doi: 10.1306/082903740239.
- Smith, R.** (1987a) Structure and deformation history of the Central Wales Synclinorium, northeast Dyfed: evidence for a long-lived basement structure. *Geological Journal*, **22**, 183-198.
- Smith, R.** (1987b) The Griestoniensis Zone Turbidite System, Welsh Basin, in Leggett, J.K. and Zuffa, C.G. (eds.), *Marine Clastic Sedimentology: Concepts and Case Studies*. Graham & Trotman, London, 89-107.
- Smith, R.** (2004a) Silled sub-basins to connected tortuous corridors: Sediment distribution systems on topographically complex sub-aqueous slopes, in Lomas, S.A., and Joseph, P., eds., *Confined Turbidite Systems: Geological Society of London Special Publication 222*, 23-43.

- Smith, R.** (2004b) Turbidite systems influenced by structurally induced topography in the multi-sourced Welsh Basin, *in* Lomas, S.A., and Joseph, P., (eds.), *Confined Turbidite Systems: Geological Society of London Special Publication 222*, 209-228.
- Smith, N.D.** and **Ashley, G.** (1985) Proglacial lacustrine environment, *in* Ashley, G.M. et al., (eds.) *Glacial Sedimentary Environments, SEPM Short Course*, **16**, 135–216.
- Smith, R.** and **Joseph, P.** (2004) Onlap stratal architectures in the Grès d'Annot: geometric models and controlling factors, *in* Joseph, P., Lomas, S.A. (eds.), *Deep-Water Sedimentation in the Alpine Basin of Se France: New Perspectives on the Gres d'Annot and related systems. Geological Society London Special Publication*, **221**, 389-399.
- Smithard, T., Bordy, E.M.** and **Reid, D.** (2015) The effect of dolerite intrusions on the hydrocarbon potential of the Lower Permian Whitehill Formation (Karoo Supergroup) in South africa and Southern Namibia: A preliminary study. *South African Journal of Geology*, **118**, 489-510.
- Sobiesiak, M.S., Kneller, B., Alsop, G.I.** and **Milana, J.P.** (2016) Internal deformation and kinematic indicators within a tripartite mass transport deposit, NW Argentina. *Sedimentary Geology*, **344**, 364-381.
- Solheim, A., Berg, K., Forsberg, C.F.** and **Bryn, P.** (2005) The Storegga Slide Complex: repetitive large scale sliding with similar cause and development. *Marine and Petroleum Geology*, **22**, 97-107. doi:10.1016/j.marpetgeo.2004.10.013
- Southard, J.B.** (1991) Experimental determination of bed-form stability. *Annual Review of Earth and Planetary Sciences*, **19**, 423-55
- Southern, S.J., Patacci, M., Felletti, F.** and **McCaffrey, W.D.** (2015) Influence of flow containment and substrate entrainment upon sandy hybrid event beds containing a co-genetic mud-clast-rich division. *Sedimentary Geology*, **321**, 105-122.

- Spikings, A.L., Hodgson, D.M., Paton, D.A. and Spychala, Y.T.** (2015) Palinspastic restoration of an exhumed deepwater system: A workflow to improve paleogeographic reconstructions. *Interpretation*, **3**, SAA71-SAA87.
- Spörli, K.B. and Rowland, J.V.** (2007) Superposed deformation in turbidites and syn-sedimentary slides of the tectonically active Miocene Waitemata Basin, northern New Zealand. *Basin Research*, **19**, 199-216.
- Sprague, A.R., Sullivan, M.D., Campion, K.M., Jensen, G.N., Goulding, F.J., Garfield, T.R., Sickafoose, D.K., Rossen, C. and Jennette, D.C.** (2002). The physical stratigraphy of deep-water strata: A hierarchical approach to the analysis of genetically-related stratigraphic elements for improved reservoir prediction. *National AAPG/SEPM meeting abstracts, Houston, Texas*, 10–13.
- Spychala, Y.T.** (2016) Are all lobes made equal? Comparing the sedimentological processes and depositional architecture of submarine lobes in different palaeogeographic and sequence stratigraphic positions, *Unpublished Ph.D thesis*, University of Leeds, Leeds.
- Spychala, Y.T., Hodgson, D.M., Flint, S.S. and Mountney, N.P.** (2015) Constraining the sedimentology and stratigraphy of submarine intraslope lobe deposits using exhumed examples from the Karoo Basin, South Africa. *Sedimentary Geology*, **322**, 67-81.
- Spychala, Y.T., Hodgson, D.M., Stevenson, C.J. and Flint, S.S.** (2017a) Aggradational lobe fringes: The influence of subtle intrabasinal seabed topography on sediment gravity flow processes and lobe stacking patterns. *Sedimentology*, **64**, 582-608.
- Spychala, Y.T., Hodgson, D.M., Prélat, A., Kane, I.A., Flint, S.S. and Mountney, N.P.** (2017b) Frontal and lateral submarine lobe fringes: Comparing sedimentary facies, architecture and flow processes. *Journal of Sedimentary Research*, **87**, 75-96.
- Steffens, G.S., Biegert, E.K., Sumner, H.S. and Bird, D.** (2003) Quantitative bathymetric analyses of selected deepwater siliciclastic margins: receiving basin configurations for deepwater fan systems. *Marine and Petroleum Geology*, **20**, 547-561.

- Stevenson, C.J., Talling, P.J., Wynn, R.B., Masson, D.G., Hunt, J.E., Frenz, M., Akhmetzhanov, A. and Cronin, B.T.** (2013) The flows that left no trace: Very large-volume turbidity currents that bypassed sediment through submarine channels without eroding the sea floor. *Marine and Petroleum Geology*, **41**, 186-205.
- Stevenson, C.J., Talling, P.J., Masson, D.G., Sumner, E.J., Frenz, M. and Wynn, R.B.** (2014) The spatial and temporal distribution of grain-size breaks in turbidites. *Sedimentology*, **61**, 1120-1156.
- Stevenson, C.J., Jackson, C.A-L., Hodgson, D.M., Hubbard, S.M. and Eggenhuisen, J.** (2015) Sediment bypass in deep-water systems. *Journal of Sedimentary Research*, **85**, 1058-1081.
- Stewart, S.A. and Clark, J.A.** (1999) Impact of salt on the structure of the Central North Sea hydrocarbon fairways. *Petroleum Geology Conference series*, **5**, 179- 200.
- Stow, D.A., Howell, D.G. and Nelson, C.H.** (1985) Sedimentary, tectonic, and sea-level controls, in Bouma, A.H et al., (eds.) *Submarine fans and related turbidite systems*, 5-22.
- Stow, D.A. and Johansson, M.** (2002) Deep-water massive sands: nature, origin and hydrocarbon implications. *Marine and Petroleum Geology*, **17**, 145-174. doi: 10.1016/S0264-8172(99)00051-3.
- Straub, K.M., Paola, C., Mohrig, D., Wolinsky, M.A. and George, T.** (2009) Compensational Stacking of Channelized Sedimentary Deposits. *Journal of Sedimentary Research*, **79**, 673-688.
- Strong, N. and Paola, C.** (2008) Valleys that never were: time surfaces versus stratigraphic surfaces. *Journal of Sedimentary Research*, **78**, 579-593.
- Strydom, H.C.** (1950) The geology and chemistry of the Laingsburg phosphorites. *Annales of the University of Stellenbosch*, **26A**, 267–285.

- Sumner, E.J., Amy, L.A. and Talling, P.J.** (2008) Deposit structure and process of sand deposition from decelerating sediment suspensions. *Journal of Sedimentary Research*, **78**, 529-547.
- Sumner, E.J., Peakall, J., Parsons, D.R., Wynn, R.B., Darby, S.E., Dorrell, R.M., McPhail, S.D., Perrett, J., Webb, A. and White, D.** (2013) First direct measurements of hydraulic jumps in an active submarine density current. *Geophysical Research Letters*, **40**, 5904-5908.
- Sylvester, Z., Pirmez, C. and Cantelli, A.** (2011) A model of submarine channel-levee evolution based on channel trajectories: Implications for stratigraphic architecture. *Marine and Petroleum Geology*, **28**, 716-727.
- Sylvester, Z., Cantelli, A., Howes, N.C., Jobe, Z.R., Wolinsky, M.A., Pirmez, C. and Smith, R.** (2012) December. Topographic Surface-Based Modeling: Building Complex Stratigraphy with Geomorphic Surfaces. In *AGU Fall Meeting Abstracts*.
- Sylvester, Z., Cantelli, A. and Pirmez, C.** (2015) Stratigraphic evolution of intraslope minibasins: Insights from surface-based model. *AAPG Bulletin*, **99**, 1099-1129.
- Symons, W.O., Sumner, E.J., Talling, P.J., Cartigny, M.J. and Clare, M.A.** (2016) Large-scale sediment waves and scours on the modern seafloor and their implications for the prevalence of supercritical flows. *Marine Geology*, **371**, 130–148.
- Taki, K. and Parker, G.** (2005) Transportational cyclic steps created by flow over an erodible bed. Part 1. Experiments. *Journal of Hydraulic Research*, **43**, 488-501.
- Talling, P.J.** (2013) Hybrid submarine flows comprising turbidity current and cohesive debris flow: Deposits, theoretical and experimental analyses, and generalized models. *Geosphere*, **9**, 460-488.
- Talling, P.J.** (2014) On the triggers, resulting flow types and frequencies of subaqueous sediment density flows in different settings. *Marine Geology*, **352**, 155-182.



- Talling, P.J., Amy, L.A., Wynn, R.B., Peakall, J. and Robinson, M.** (2004) Beds comprising debrite sandwiched within co-genetic turbidite: origin and widespread occurrence in distal depositional environments. *Sedimentology*, **51**, 163-194.
- Talling, P.J., Masson, D.G., Sumner, E.J. and Malgesini, G.** (2012) Subaqueous sediment density flows: Depositional processes and deposit types. *Sedimentology*, **59**, 1937-2003
- Tankard, A., Welsink, H., Aukes, P., Newton, R. and Stettler, E.** (2009) Tectonic evolution of the Cape and Karoo basins of South Africa. *Marine and Petroleum Geology*, **26**, 1379-1412.
- Tankard, A., Welsink, H., Aukes, P., Newton, R., and Stettler, E.** (2012) Chapter 23: Geodynamic interpretation of the Cape and Karoo basins, South Africa, *in* Rioberts, D.G., and Bally, A.W., (eds.), *Phanerozoic Passive Margins, Cratonic Basins and Global Tectonic Maps*: Amsterdam, Elsevier, 869-94.
- Tankard, A.J., Jackson, M.P.A., Eriksson, K.A., Hobday, D.K., Hunter, D.R. and Minter, W.E.L.** (1982) *Crustal Evolution of Southern Africa*. Springer-Verlag, New York. 523 pp.
- Teiehart, C.** (1974) Marine sedimentary environments and their faunas in Gondwana area. *American Association of Petroleum Geologists Memoir*, **23**, 361-394
- Turner, B.R.** (1999) Tectonostratigraphical development of the Upper Karoo foreland basin: Orogenic unloading versus thermally-induced Gondwana rifting. *Journal of African Earth Sciences*, **28**, 215-238.
- Urgeles, R., Canals, M. and Masson, D.G.** (2001) Flank stability and processes off the western Canary Islands: a review from El Hierro and La Palma. *Scientia Marina*, **65** (Supplement 1), 21-31.
- van Andel, T.H. and KOMAR, P.D.** (1969) Ponged sediments of the Mid-Atlantic Ridge between 22 and 23 north latitude. *Geological Society of America Bulletin*, **80**, 1163-1190.

- van der Merwe, W.C.** (2010) Basing margin failure processes during the initiation of a deepwater system; the Vischkuil Formation, Laingsburg depocentre, SW Karoo Basin, South Africa, *Unpublished Ph.D. Thesis*, University of Liverpool, Liverpool.
- van der Merwe, W.C., Hodgson, D.M. and Flint, S.S.** (2009) Widespread syn-sedimentary deformation on a muddy deep-water basin-floor: the Vischkuil Formation (Permian), Karoo Basin, South Africa. *Basin Research*, **21**, 389-406. doi: 10.1111/j.1365-2117.2009.00396.x.
- van der Merwe, W., Flint, S. and Hodgson, D.** (2010) Sequence stratigraphy of an argillaceous, deepwater basin plain succession: Vischkuil Formation (Permian), Karoo Basin, South Africa. *Marine and Petroleum Geology*, **27**, 321-333.
- van der Merwe, W.C., Hodgson, D.M., Brunt, R.L. and Flint, S.S.** (2014) Depositional architecture of sand-attached and sand-detached channel-lobe transition zones on an exhumed stepped slope mapped over a 2500 km<sup>2</sup> area. *Geosphere*, **10**, 1076-1093.
- van der Merwe, W.C., Hodgson, D.M. and Flint, S.S.** (2011) Origin and terminal architecture of a submarine slide: a case study from the Permian Vischkuil Formation, Karoo Basin, South Africa. *Sedimentology*, **58**, 2012-2038.
- Van der Werff, W. and Johnson, S.** (2003) High resolution stratigraphic analysis of a turbidite system, Tanqua Karoo Basin, South Africa. *Marine and Petroleum Geology*, **20**, 45-69.
- Van Lente, B.** (2004) Chemostratigraphic Trends and Provenance of the Permian Tanqua and Laingsburg Depocentres, southwestern Karoo Basin, South Africa. *Unpublished PhD thesis*, University of Stellenbosch. 439 pp.
- Vanneste, M., Mienert, J. and Bünz, S.** (2006) The Hinlopen Slide: a giant, submarine slope failure on the northern Svalbard margin, Arctic Ocean. *Earth and Planetary Science Letters*, **245**, 373-388.
- Varnes, D.J.** (1958) Landslide types and processes, *in*, Eckel, E.B., (ed) Landslides and Engineering Practice, Highway research board special report, **29**, 20-47.

- Varnes, D.J.** (1978) Slope movement types and processes, *in* Schuster, R.L. and Krizek, R.J. (eds.) *Landslides, Analysis and Control, Special Report 176*, National Academy of Sciences, Washington, 11-33.
- Veevers, J.J., Cole, D.I. and Cowan, E.J.** (1994) Southern Africa: Karoo basin and Cape fold belt. *Geological Society of America Memoirs*, **184**, 223-280.
- Vicente Bravo, J.C. and Robles, S.** (1995) Large-scale mesotopographic bedforms from the Albion Black Flysch, northern Spain: characterization, setting and comparison with recent analogues, *in* Pickering, K.T et al., (eds.), *Atlas of Deep Water Environments: Architectural Style in Turbidite Systems*: London, Chapman and Hall, 216–226.
- Viljoen, J.H.A.** (1992) Lithostratigraphy of the Collingham Formation (Ecca Group), including the Zoutkloof, Buffels river and Wilgenhout river members and the Matjiesfontein chert bed. *Geological Survey, South African Committee for Stratigraphy, Lithostratigraphic Series*, **22**, 10 p.
- Viljoen, J.H.A.** (1994) Sedimentology of the Collingham Formation, Karoo Supergroup. *South African Journal of Geology*, **97**, 167-183.
- Visser, J.N.J.** (1979) Changes in sediment transport direction in the Cape Karoo Basin (Silurian-Triassic) in South Africa. *South African Journal of Science*, **75**, 72–75.
- Visser, J.N.J.** (1991) Self-destructive collapse of the Permo-Carboniferous marine ice sheet in the Karoo Basin: evidence from the southern Karoo. *South African Journal of Geology*, **94**, 255–262.
- Visser, J.N.J.** (1992) Basin tectonics in southwestern Gondwana during the Carboniferous and Permian, *in* de Wit, M.J. and Ransome, I.G.D. (eds.) *Inversion tectonics of the Cape fold belt, Karoo and Cretaceous basins of southern Africa*, Balkema, Rotterdam, 109-116.
- Visser, J.N.** (1993) Sea-level changes in a back-arc-foreland transition: the late Carboniferous-Permian Karoo Basin of South Africa. *Sedimentary Geology*, **83**, 115-131.

- Visser, J.N.J.** (1994) A Permian argillaceous syn- to post-glacial foreland sequence in the Karoo Basin, South Africa, *in* Deynoux, M. et al., (eds) *Earth's Glacial Record*, International Geological Correlation Project, **260**, Cambridge University Press, Cambridge, 193- 203.
- Visser, J.N.** (1996) Controls on Early Permian shelf deglaciation in the Karoo Basin of South Africa. *Palaeogeography, Palaeoclimatology, Palaeoecology*, **125**, 129-139.
- Visser, J.N.J.** (1997) Deglaciation sequences in the Permo-Carboniferous Karoo and Kalahari basins of the southern Africa: a tool in the analysis of cyclic glaciomarine basin fills. *Sedimentology*, **44**, 507–521. doi: 10.1046/j.1365-3091.1997.d01-35.x.
- Visser, J.N.J.** and **Loock, J. C.** (1978) Water depth in the main Karoo Basin, South Africa, during Ecca (Permian) sedimentation. *Geological Society of South Africa Transactions*, **81**, 185-191.
- Visser, J.N.J.** and **Prackelt, H.E.** (1996) Subduction, mega-shear systems and Late Palaeozoic basin development in the African segment of Gondwana. *Geologische Rundschau*, **85**, 632–646.
- Vrolijk, P.J.** and **Southard, J.B.** (1997) Experiments on rapid deposition of sand from high-velocity flows. *Geoscience Canada*, **24**, 45-54.
- Walker, R.G.** (1978) Deep-water sandstone facies and ancient submarine fans: models for exploration for stratigraphic traps. *AAPG Bulletin*, **62**, 932-966.
- Walker, D.** (2008) Topographic controls on deep-water sedimentation patterns—The Casaglia Monte della Colonna submarine slide, Marnoso-Arenacea Formation (Miocene), Northern Italian Apennines, M.S. thesis, Colorado School of Mines, Golden, Colorado, 184 p.
- Waltham, D.** (2004) Flow transformations in particulate gravity currents. *Journal of Sedimentary Research*, **74**, 129–134.

- Wang, X., Luthi, S.M., Hodgson, D.M., Sokoutis, D., Willingshofer, E. and Groenenberg, R.M.** (2017) Turbidite stacking patterns in salt-controlled minibasins: Insights from integrated analogue models and numerical fluid flow simulations, *Sedimentology*, **64**, 530-552.
- Weckmann, U., Jung, A., Branch, T. and Ritter, O.** (2007) Comparison of electrical conductivity structures and 2D magnetic modelling along two profiles crossing the Beattie Magnetic Anomaly, South Africa. *South African Journal of Geology*, **110**, 449-464.
- Weimer, P., and Link, M.H.** (1991) Global petroleum occurrences in submarine fans and turbidite systems, in Weimer et al., (eds.), *Seismic facies and sedimentary processes of submarine fans and turbidite systems*, Springer New York, 9-67.
- Weimer, P. and Pettingill, H.S.** (2007) Global overview of deep-water exploration and production. Atlas of deepwater outcrops, *AAPG Studies in Geology*, **56**, 7-11.
- Weirich, F.** (1989) The generation of turbidity currents by subaerial debris flows, California. *Geological Society of America Bulletin*, **101**, 278-291.
- Wickens, H.d.V.** (1994) Basin floor fan building turbidites of the southwestern Karoo Basin, Permian Ecca Group. *Unpublished PhD Thesis*, Port Elizabeth University, South Africa, 233pp.
- Wilson, D., Davies, J.R., Waters, R.A. and Zalasiewicz, J.A.** (1992) A fault-controlled depositional model for the Aberystwyth Grits turbiditic system. *Geological Magazine*, **129**, 595-607.
- Winker, C.D.** (1996) January. High-resolution seismic stratigraphy of a late Pleistocene submarine fan ponded by salt-withdrawal mini-basins on the Gulf of Mexico continental slope, in *Offshore Technology Conference*. Offshore Technology Conference.
- Winker, C.D. and Booth, J.R.** (2000) Sedimentary dynamics of the salt-dominated continental slope, Gulf of Mexico: Integration of observations from the seafloor, near-surface, and deep subsurface, in Weimer, P., et al., (eds.), *Deep-water Reservoirs of the World: The*

GCSSEPM Foundation 20th Annual Bob F. Perkins Research Conference Proceedings, 1059–1086.

**Winterwerp, J.C., Bakker, W.T., Mastbergen, D.R. and van Rossum, H. (1992)**

Hyperconcentrated sand-water mixture flows over erodible bed. *Journal of Hydraulic Engineering*, **118**, 1508-1525.

**Woodcock, N.H. (1979)** The use of slump structures as palaeoslope orientation estimators.

*Sedimentology*, **26**, 83-99.

**Wynn, R.B. and Stow, D.A. (2002)** Classification and characterisation of deep-water sediment

waves. *Marine Geology*, **192**, 7-22.

**Wynn, R.B., Kenyon, N.H., Masson, D.G., Stow, D.A. and Weaver, P.P. (2002a)**

Characterization and recognition of deep-water channel-lobe transition zones. *AAPG Bulletin*, **86**, 1441–1446.

**Wynn, R.B., Piper, D.J.W. and Gee, M.J.R. (2002b)** Generation and migration of coarse-grained

sediment waves in turbidity current channels and channel-lobe transition zones. *Marine Geology*, **192**, 59-78.

**Wynn, R.B., Cronin, B.T. and Peakall, J. (2007)** Sinuous deep-water channels: Genesis,

geometry and architecture. *Marine and Petroleum Geology*, **24**, 341-387.

**Wynn, R.B., Talling, P.J., Masson, D.G., Le Bas, T.P., Cronin, B.T. and Stevenson, C.J. (2012)**

The influence of subtle gradient changes on deep-water gravity flows: a case study from the Moroccan turbidite system, in Prather, B.E., et al., (eds.), Application of the Principles of Seismic Geomorphology to Continental-Slope and Base-of-Slope Systems: Case Studies from Seafloor and Near-Seafloor Analogues. Tulsa, OK, *SEPM Society for Sedimentary Geology Special Publication 99*, 371-383.

**Yang, S.-Y. and Kim, J.W. (2014)** Pliocene basin-floor fan sedimentation in the Bay of Bengal

(offshore northwest Myanmar). *Marine and Petroleum Geology*, **49**, 45-58



## Appendix A

### Appendix A.1

Table A.1 Total logs and thicknesses.

	Logged thickness (m)	Palaeocurrents	no. of logs
<b>Chapter 4</b>	1550	100	20
<b>Chapter 5</b>	11450	184	311
<b>Chapter 6</b>	959	100	341
<b>Total</b>	<b>13959</b>	<b>384</b>	<b>672</b>

### Appendix A.2

Table A.2 Log numbers, names, UTI grid reference and associated data chapter.

No.	Log name	X	Y	Function
1	VS20142	581114	6322969	<b>Chapter 4</b>
2	VRG20151	581112	6322877	
3	VS20141	581034	6322728	
4	VRG201510	581276	6322519	
5	VRG20159	581375	6322476	
6	VRG20155	581388	6322396	
7	COL20151	581608	6322420	
8	VRG20152	581582	6322386	
9	COL20152	581612	6322385	
10	VRG20157	581573	6322300	
11	COL20153	581636	6322346	
12	COL20154	581676	6322321	
13	VRG20153	581807	6322206	
14	VRG201511	581739	6322108	
15	VRG20154	581883	6322136	
16	VRG20156	582200	6321875	
17	VRG20158	582292	6321901	
18	VRG20158B	582293	6321902	
19	Bloukrans 1	578430	6324802	
20	Damascus	587871	6324552	
21	WFN201410	521025	6331025	<b>Chapter 5</b>
22	WFN20132	521359	6330383	
23	WFN20144	521730	6330901	
24	WFN20146	522090	6330877	
25	WFN20149	522313	6330984	
26	WFN20149	522571	6330965	
27	WFN20132	522767	6330960	



28	WFN20141	522858	6330882
29	WFN20142	523034	6330880
30	SLN20133	523282	6330996
31	SLN20132	523590	6330911
32	SLN201415	524180	6330983
33	SLN201415B	524713	6330965
34	SLN201414	525094	6331013
35	SLN201413	525419	6331015
36	SLN201412	525631	6330347
37	SLN201411	526236	6330960
38	SLN201410	526478	6330985
39	SLN20149	526644	6331009
40	SLN20148	526993	6331094
41	SLN20147	527085	6331125
42	SLN20146	527276	6331125
43	SLN20145	527623	6331185
44	SLN20144	527702	6331163
45	SLN20143	528031	6331186
46	SLN20142	528248	6331215
47	SLN20141	528388	6331223
48	SLN20131	528649	6331386
49	SLN201417	528963	6331183
50	SLN201418	529264	6331211
51	SLN201419	529536	6331234
52	SLN201420	530080	6331251
53	SLN201421	530534	6331417
54	SLN201422	530795	6331579
55	SLN201423	530999	6331540
56	SLN201424A	531941	6331770
57	SLN201424B	531938	6331687
58	SLN201424C	531931	6331699
59	SLN201426	532128	6331716
60	ALM20141A	534260	6332303
61	ALM20141B	534266	6332202
62	ALM20142	534461	6332240
63	ALM20143	534589	6332253
64	ALM20144	534975	6332332
65	ALM20144B	535055	6332591
66	ALM20145A	535191	6332403
67	ALM20145B	535226	6332405
68	ALM20147	535400	6332486
69	ALM20146B	535459	6332431
70	ALM20147	535563	6332515
71	ALM20148	535802	6332537
72	ALM20149	535922	6332553
73	ALM201410	536012	6332617
74	ALM201410B	536053	6332574
75	ALM201411	536279	6332604
76	ALM201413	536756	6332750
77	ALM201414	537250	6332974
78	ALM201415	537763	6333045
79	ALM201416	538464	6333165

80	ALM201417	538731	6333277
81	ALM201418	539021	6333363
82	ALM201419	539409	6333416
83	ALM201420	539494	6333443
84	WF20131	521261	6326709
85	SL201325	524843	6327122
86	SL201511	524912	6327179
87	SL20159	525067	6327201
88	SL201510	525310	6327229
89	SL201526	525973	6327183
90	SL201324	525621	6327212
91	SL20158	525800	6327271
92	SL20152	525951	6327281
93	SL201323B	525973	6327179
94	SL201425	526180	6327248
95	SL201322	526395	6327295
96	SL201424	526537	6327347
97	SL201512	526593	6327353
98	SL201423	526614	6327307
99	SL201320	526764	6327340
100	SL201422	526851	6327321
101	SL20137	527031	6327238
102	SL20138	527082	6327346
103	SL20139	527124	6327339
104	SL201427	527213	6327404
105	SL201310	527356	6327370
106	SL201412	527443	6327376
107	SL201410	527508	6327329
108	SL201313	527676	6327352
109	SL20145	527755	6327383
110	SL20148	527866	6327400
111	SL201411	527894	6327394
112	SL201315	527944	6327449
113	SL20144	528070	6327390
114	SL20142	528148	6327421
115	SL201316	528148	6327368
116	SL20141	528233	6327427
117	SL201317	528260	6327476
118	SL201413	528356	6327423
119	SL201318	526465	6327433
120	SL201414	528640	6327442
121	SL20143	528695	6327451
122	SL201415	528719	6327402
123	SL201416	528983	6327461
124	SL201417	529110	6327469
125	SL20131	529238	6327432
126	SL201419	529243	6327495
127	SL201418	529494	6327473
128	SL201420	529869	6327497
129	SL20133	530046	6327220
130	SL201319	530543	6327377
131	SL201326	531338	6327520

132	SL20134	531822	6327660
133	SL201327	532262	6327762
134	SL201328	533116	6327696
135	SL201428	534174	6328256
136	SL201429	534581	6328336
137	SL201430	536069	6328550
138	SL201431	536653	6328674
139	SL20132	537093	6328756
140	SL201434	538043	6328911
141	SL201433	538785	6329060
142	SL201435	539575	6329133
143	SL201436	541338	6329391
144	SL201437	541735	6329437
145	SL201438	543227	6329566
146	SL201440	545405	6329642
147	GRF20141	543163	6328467
148	GRF20142	543617	6328539
149	GRF20143	542869	6328437
150	GRF20144	542484	6328404
151	GRF20145	542257	6328347
152	GRF20176	541806	6328259
153	GRF20147	541438	6328157
154	GRF20148	541216	6328098
155	GRF20149	540911	6328022
156	GRF201410	540595	6327949
157	GRF201411	540159	6327872
158	GRF201412	539581	6327744
159	GRF201413	539316	6327652
160	GRF201414	538917	6327533
161	GRF201415	537721	6327239
162	GRF201416	537351	6327155
163	GRF201417	536657	6326936
164	GRF201418	536202	6326911
165	GRF201419	535758	6326758
166	GRF201420	535287	6326577
167	GRF201421	534885	6326399
168	LG20141	529030	6324666
169	LG20142	528778	6324735
170	LG20143	528522	6324488
171	SKW20141	533504	6326099
172	SKW20142	533127	6325950
173	SKW20143	533927	6326160
174	SKW20144	534277	6326260
175	STN20141	544086	6328636
176	STN20142	545841	6328930
177	STN20143	545320	6328848
178	STN20144	545125	6328789
179	STN20145	544528	6328687
180	STN20146	546674	6328978
181	STN20147	547360	6329112
182	STN20148	548486	6329272
183	GRF2013_3	536612	6322395

Revised logs

184	GRF2013_3	536612	6322395
185	Leu-Sku2014	533118	6322978
186	Leu-Sku2014	533118	6322978
187	S3FS1_	527008	6322755
188	S3FS1_	527008	6322755
189	S3FS1_02	516979	6326109
190	S3FS1_03	513059	6325247
191	S3FS1_04	521439	6326634
192	S3FS1_05	506291	6324305
193	S3FS1_06	529094	6327249
194	S3FS1_07	528989	6327389
195	S3FS1_08	529182	6327475
196	S3FS1_15	535172	6321830
197	S3FS1_17	510365	6324875
198	S3FS1_21	535106	6327983
199	S3FS1_22	525798	6324422
200	S3FS1_27	520446	6322764
201	S3FS1_29	519729	6321688
202	S3FS1_35	543548	6320986
203	S3FS1_35	543548	6320986
204	S3FS1_37B	521173	6321678
205	S3FS3	543148	6329568
206	S3FS3_00	526930	6322810
207	S3FS3_00	526930	6322810
208	S3FS3_01	527134	6322813
209	S3FS3_02	527178	6322822
210	S3FS3_08	542695	6329219
211	S3FS3_11	504567	6323836
212	S3FS3_12	524798	6326888
213	S3FS3_15	518162	6326046
214	S3FS3_16	542649	6328807
215	S3FS3_18	537394	6322135
216	S3FS3_19	531625	6323124
217	S3FS3_20	529283	6322805
218	S3FS3_21	529038	6325056
219	S3FS3_22	526881	6322807
220	S3FS3_23	546305	6329132
221	S3FS3_24	527086	6322812
222	S3FS3_28	538435	6321685
223	S3FS3_29	539360	6327953
224	S3FS3_30	534224	6322558
225	S3FS3_31	547130	6329311
226	S3FS3_32	547478	6329169
227	S3FS3_35	536839	6322239
228	S3FS3_36	532358	6322649
229	S3FS3_37	559282	6324537
230	S3FS3_38	540168	6321717
231	S3FS3_39	533516	6326389
232	S3FS3_40	537369	6327499
233	S3FS3_42	548189	6329374
234	S3FS3_43	548684	6329308
235	S3FS3_44	548339	6329635

236	S3FS3_47	547089	6322590
237	S3FS3_48	551755	6323585
238	S3FS3_49	555103	6324244
239	S3FS3_52	532721	6327818
240	S3FS3_53	533049	6328042
241	S3FS3_54	533410	6327992
242	S3FS3_56	544953	6329640
243	S3FS3_57	537000	6328382
244	S3FS3_58	540935	6329246
245	S3FS3_59	540555	6328124
246	S3FS3_63	527322	6322844
247	S3FS4_02	497819	6333757
248	S3FS4_03	501398	6334950
249	S3FS4_08	509142	6335039
250	S3FS4_24	548884	6323046
251	S3FS4_25	554367	6324266
252	S3FS4_26	557392	6324719
253	S3FS4_33	552361	6323952
254	S3FS4_34	552680	6324016
255	S3FS4_67	551878	6323889
256	S3FS6_01	498279	6333807
257	S3FS7_01	499705	6334595
258	S3FS7_02	503498	6335292
259	S3FS7_26	521387	6326547
260	S3FS7_35	503712	6323570
261	S3FS7_36	504384	6323714
262	S3FS7_37	531830	6327641
263	S3FS8	536773	6322298
264	S3FS8_010	496312	6333606
265	S3FS8_011	499816	6334753
266	S3FS8_019	500862	6334928
267	S3FS8_020	503915	6335314
268	S3FS8_022	502046	6335266
269	S3FS8_023	503185	6335524
270	S3FS8_025	507168	6335847
271	S3FS8_026	508964	6335964
272	S3FS8_027	505259	6335550
273	S3FS8_030	509514	6335966
274	S3FS8_031	510847	6336205
275	S3FS8_033	497357	6333809
276	S3FS8_034	513523	6336135
277	S3FS8_042	530153	6325461
278	S3FS8_078	518019	6320402
279	S3FS8_079	518920	6321231
280	S3FS8_080	526599	6322637
281	S3FS8_081	526575	6323054
282	S3FS8_082	524999	6322878
283	S3FS8_084	533153	6322801
284	S3FS8_085	533209	6322976
285	S3FS8_085	533209	6322976
286	S3FS8_086	530870	6322933
287	S3FS8_086	530870	6322933

288	S3FS8_087	528090	6322970
289	S3FS8_103	534834	6322820
290	S3FS8_103	534834	6322820
291	S3FS8_104	520385	6326615
292	S3FS8_115	525581	6327162
293	S3FS8_116	525978	6327185
294	S3FS8_117	527085	6327308
295	S3FS8_118	526926	6327293
296	S3FS8_119	527080	6327390
297	S3FS8_120	524381	6327050
298	S3FS8_122	525235	6327144
299	S3FS8_123	525366	6327152
300	S3FS8_124	522994	6326979
301	S3FS8_125	523394	6326938
302	S3FS8_130	522524	6326775
303	SKU2013_2	533599	6322946
304	SKU2013_2	533599	6322946
305	HBN01	479683	6340233
306	HBC02	480775	6339016
307	HBS13	471975	6334129
308	HBS12	472017	6334126
309	HBS11	471635	6334090
310	HBS10	473100	6334031
311	HBS09	473673	6334347
312	HBS08	476341	6334777
313	HBS07	476800	6335089
314	S3FS7_12	531408	6331602
315	S3FS4_20	531939	6331685
316	S3FS7_11	531941	6331687
317	S3FS4_17	532513	6331869
318	S3FS4_15	532772	6331918
319	S3FS4_44	533780	6332473
320	S3FS1_09	534781	6332380
321	S3FS4_21	534822	6333065
322	S3FS4_45	534866	6332610
323	S3FS7_09	535053	6332447
324	S3FS7_08	535191	6332401
325	S3FS7_07	535271	6332404
326	S3FS4_48	535626	6332520
327	S3FS4_46	536103	6333160
328	S3FS4_47	537529	6333023
329	S3FS4_49	539407	6333417
330	S3FS4_51	541624	6333903
331	S3FS4_50	548374	6336400
332	ALM201420	539494	6333443
333	SLN201422	530795	6331579
334	STN20146	546674	6328978
335	Gelbek DE	499132	6323610
336	Gelbek DE	498617	6323844
337	Gelbek DE	499027	6323610
338	SL201411	527894	6327394
339	S3FS3_06	535173	6326930

**Chapter 6**  
New and Revisited

340	STN20147	547360	6329112
341	ALM201419	539409	6333416
342	GRF201414	538917	6327533
343	HBN04	470892	6339787
344	SL20148	527866	6327400
345	S3FS3_31	547130	6329311
346	S3FS8_080	526599	6322637
347	S3FS3_39	533516	6326389
348	Dave_log 2.5B	473988	6326490
349	CAB_2	474227	6326567
350	GRF201417	536657	6326936
351	SL201319	530543	6327377
352	S3FS4_46	536103	6333160
353	S3FS4_48	535626	6332520
354	GRF2013_3	536612	6322395
355	SL201428	534174	6328256
356	S3FS3_32	547478	6329169
357	GRF201411	540159	6327872
358	S3FS3_23	546305	6329132
359	HBN05	468367	6339680
360	LG20142	528778	6324735
361	GRF201412	539581	6327744
362	LG20141	529030	6324666
363	SL201326	531338	6327520
364	S3FS3_56	544953	6329640
365	LG20143	528522	6324488
366	SL201429	534581	6328336
367	STN20145	544528	6328687
368	S3FS3_42	548189	6329374
369	STN20141	544086	6328636
370	S3FS6_08	468370	6339478
371	STN20143	545320	6328848
372	STN20142	545841	6328930
373	S3FS3_43	548684	6329308
374	SKW20142	533127	6325950
375	GRF201413	539316	6327652
376	S3FS3_40	537369	6327499
377	GRF201421	534885	6326399
378	GRF20153	542869	6328437
379	SKW20141	533504	6326099
380	SL201414	528640	6327442
381	SL20132	537093	6328756
382	GRF201418	536202	6323911
383	STN20144	545125	6328789
384	S3FS6_10	463733	6339329
385	S3FS3_44	548339	6329635
386	GRF201420	535287	6326577
387	S3FS3_29	539360	6327953
388	S3FS3_33	544607	6328899
389	GRF20141	543163	6328467
390	SKW20143	533927	6326160
391	GRF20157	541438	6328157

392	GRF201419	535758	6326758
393	S3FS3_41	544286	6328882
394	GRF20142	543617	6328539
395	SKW20144	534277	6326260
396	S3FS3_27	541331	6328129
397	GRF20158	541216	6328098
398	SL201431	536653	6328674
399	HBC02	480775	6339016
400	GRF20159	540911	6328022
401	SL201430	536069	6328550
402	S3FS3_34	541104	6328066
403	HBN01	479683	6340233
404	GRF201410	540595	6327949
405	GRF20154	542484	6328404
406	S3FS3_25	541856	6328719
407	GRF20156	541806	6328259
408	S3FS3_17	539056	6328293
409	HBN03	475800	6340522
410	S3FS3_59	540555	6328124
411	GRF20155	542257	6328347
412	HBN02	477565	6340120
413	S3FS3_16	542649	6328807
414	S3FS3	543148	6329568
415	Rog_2	480376	6340093
416	Rog_3	479799	6340238
417	Rog_5	476986	6340343
418	Rog_4	477749	6340350
419	Rog_6	476136	6340359
420	Rog_2011_2	480311	6338988
421	Rietkloof Rd_1	459620	6337805
422	Zout-N_M	479570	6337248
423	Zout-N_N	479611	6337291
424	Zout-N_O	479656	6337311
425	ALM201417	538731	6333277
426	ALM201418	539021	6333363
427	ALM20149	535922	6332553
428	ALM20144B	535055	6332591
429	ALM201410	536012	6332617
430	ALM201413	536756	6332750
431	ALM201414	537250	6332974
432	ALM201415	537763	6333045
433	ALM201413	536756	6332750
434	ALM201414	537250	6332974
435	ALM201415	537763	6333045
436	ALM20147	535400	6332486
437	ALM20147	535563	6332515
438	ALM20148	535802	6332537
439	ALM20149	535922	6332553
440	ALM201413	536756	6332750
441	ALM201414	537250	6332974
442	ALM201415	537763	6333045
443	STN20148	548486	6329272



444	SL201436	541338	6329391
445	SL201437	541735	6329437
446	SL201440	545405	6329642
447	WFN20132	521359	6330383
448	WFN20146	522090	6330877
449	WFN20144	521730	6330901
450	WFN20132	522767	6330960
451	WFN20149	522571	6330965
452	SLN201415B	524713	6330965
453	SLN201415	524180	6330983
454	WFN20149	522313	6330984
455	SLN201410	526478	6330985
456	SLN20133	523282	6330996
457	SLN20149	526644	6331009
458	SLN201414	525094	6331013
459	SLN201413	525419	6331015
460	WFN201410	521025	6331025
461	SLN20145	527623	6331185
462	SLN20143	528031	6331186
463	SLN201419	529536	6331234
464	SLN201420	530080	6331251
465	SLN20131	528649	6331386
466	SLN201421	530534	6331417
467	SLN201423	530999	6331540
468	Doorn_02	462548	6331586
469	Doorn_01	462602	6331590
470	Rietkloof Rd_3	454970	6337222
471	Rietkloof Rd_2	458051	6337400
472	Rietkloof Rd_1	459620	6337805
473	Faberskraal 1	493709	6332404
474	Faberskraal 2	497679	6330640
475	Faberskraal 3	497893	6334128
476	S3FS1_34	498709	6330968
477	Geelbek	498740	6322902
478	S3FS7_35	503712	6323570
479	S3FS3_11	504567	6323836
480	S3FS1_35	543548	6320986
481	Wilgerhout Rivier	485850	6327686
482	dan	488642	6328114
483	Rondekop	490495	6322892
484	Grootkloof	494383	6322942
485	N1 west	484345	6327389
486	Doornkfontein 2	465682	6331115
487	Skeid_2750	475402	6323740
488	Buffels Rivier	487600	6331350
489	Skeid_2350	475025	6323936
490	Doornkloof	462520	6331550
491	Amo_C	473586	6336221
492	Skeid_180	471866	6324968
493	STEG20152	473052	6335890
494	Doorn_10	461719	6331531
495	STEG20156	473515	6336125

496	JBR_01	488961	6331579
497	Skeid_280	471775	6325004
498	Skeid_200	471848	6324974
499	Skeid_160	471887	6324963
500	Skeid_3950	476572	6323451
501	Skeid_140	471907	6324958
502	Skeid_60	471985	6324955
503	ROJ20156	472066	6335668
504	Skeid_100	471946	6324954
505	Skeid_120	471926	6324956
506	Doornkloof 2	464325	6331300
507	Skeid_80	471966	6324954
508	Amo_B	472871	6335964
509	S3FS3_10	488482	6323511
510	Skeid_5850	478439	6323354
511	Skeid_-250	472250	6324910
512	Skeid_-270	472261	6324896
513	Middleplaas	488480	6323058
514	ROJ20151	472165	6335751
515	Krantz 3	483586	6323344
516	ROJ20155	471936	6335696
517	STEG20151	472913	6335828
518	STEG20155	473474	6336140
519	Doornkfontein	467629	6330828
520	BavAB201516	470617	6325244
521	Skeid_2550	475203	6323851
522	Amo_S	471197	6335602
523	ROJ20152	472006	6335777
524	Skeid_1750	474202	6324075
525	Skeid_3550	476169	6323540
526	Skeid_920	471171	6325108
527	Zoot_Dave	471905	6335844
528	Vischkuil_Ph 6	484105	6330068
529	BAVAB201510	470625	6325238
530	Skeid_840	471251	6325105
531	Skeid_0800	473035	6324613
532	Skeid_1020	473243	6324535
533	Skeid_1400	473696	6324181
534	Skeid_4350	476958	6323384
535	Skeid_1650	474177	6324200
536	ROJ20153	471826	6335723
537	Skeid_0200	472474	6324818
538	STEG20158	473708	6336007
539	STEG20159	474257	6335985
540	Skeid_6900	479331	6323343
541	Skeid_0080	472230	6324640
542	Skeid_0600	472848	6324684
543	BAVAB20157	470741	6325164
544	Bav_4	474428	6327012
545	Steekwekklaagte	472813	6335708
546	Bavab201518	470595	6325271
547	BAVAB20159	470653	6325210

548	BAVAB20158	470706	6325173
549	Skeid_720	471373	6325125
550	Amo_T	468898	6335220
551	Skeid_820	471271	6325106
552	Laura_2	480798	6327254
553	Joup_4	480174	6327359
554	Amo_M	464355	6335075
555	Klein Zoutkloof	482387	6331768
556	Skeid_4750	477351	6323351
557	Skeid_1200	473384	6324252
558	Skeid_4950	477521	6323325
559	Skeid_960	471131	6325110
560	Skeid_nose_1510	470579	6325330
561	Skeid_nose_Dave	470701	6325663
562	Skeid_940	471151	6325109
563	BAVAB20156	470875	6325140
564	BavAB201515	470582	6325337
565	Skeid_880	471211	6325104
566	STEG201510	475603	6336229
567	Skeid_900	471191	6325105
568	Skeid_0400	472525	6324559
569	Vischkuil_Ph 40	463373	6330777
570	Skeid_860	471230	6325102
571	Jakkalsfontein	467787	6335188
572	Skeid_2950	475563	6323686
573	Krantz 1B	480202	6323014
574	Zoutkloof 2	474633	6330765
575	Skeid_1040	471052	6325110
576	Skeid_980	471111	6325107
577	Zoutkloof	478591	6337431
578	BAVABE20151	476617	6323426
579	Amo_V	477600	6340027
580	Skeid_1000	471091	6325109
581	Skeid_4200	476787	6323440
582	Doorn_03	462502	6331582
583	Amo_H	478816	6337783
584	Amo_F	476781	6336408
585	Doorn_02	462548	6331586
586	Skeid_5350	477958	6323347
587	Poort_2b	473357	6326561
588	Skeid_1020	471072	6325108
589	Doorn_01	462602	6331590
590	Skeid_5650	478224	6323353
591	Skeid_3350	475955	6323589
592	Skeid_5750	478323	6323357
593	Skeid_3150	475767	6323629
594	Joup_2	479234	6327311
595	R354 Road	463356	6335062
596	Skeid_3700	476298	6323485
597	Poort_1B	475324	6327147
598	Laura_1	478748	6327281
599	OUPAB20152	478632	6327184

600	S3FS8_110	478278	6326783
601	Ouplaas_B	478534	6327391
602	OUPAB20151	478784	6327185
603	new heuningberg	465620	6339110
604	new heuningberg 2	470851	6339361
605	S3_FS4_Onion5	489069	6323327
606	Geel_10	499110	6323367
607	Geel_18	499252	6323305
608	Geel_9	499092	6323374
609	Geel_24	499372	6323311
610	Bav_0.5	473403	6326229
611	Rog_2	480376	6340093
612	CD_KC2	481873	6323533
613	Geel_8	499074	6323383
614	Geel_14	499179	6323381
615	Geel_17	499234	6323299
616	Geel_22	499333	6323301
617	Geel_26	499407	6323331
618	WD-Oup_04	479002	6326942
619	Geel_25	499381	6323317
620	Rog_2011_1	480612	6339924
621	Geel_15	499196	6323322
622	S3FS3_13	481880	6323485
623	WD_120	482252	6326944
624	Geel_13	499162	6323339
625	WD-Oup_03	479964	6326909
626	Rog_6	476136	6340359
627	CD_2380	475059	6324346
628	Rog_1	479803	6339767
629	CD_ERK2	483360	6323547
630	Geel_1	498616	6323413
631	Geel_21	499316	6323304
632	WD_80	482210	6326943
633	Geel_11	499124	6323354
634	WD_100	482230	6326944
635	CD_EKR3	482983	6323546
636	Geel_27	499428	6323337
637	CD_100	472799	6325321
638	CAB_2	474227	6326567
639	Rub_-1	484516	6327151
640	Bav_4c	473879	6326307
641	Bav_4b	473956	6326483
642	CD_KC1	480286	6323568
643	WD_60	482189	6326941
644	CD_0	472329	6325413
645	Rog_4	477749	6340350
646	CD_3570	476223	6323952
647	Ouplaas_B	478534	6327391
648	Bav_3b	473821	6326428
649	CD_3120	475805	6324100
650	CD_3220	475898	6324073

651	Rog_3	479799	6340238	
652	Bav-Oup_9	476228	6326797	
653	CD_3360	476028	6324029	
654	Bav_0	473351	6326214	
655	CD_460	473235	6325143	
656	B-OP_8	476829	6326825	
657	CD_880	473713	6324920	
658	(Bav_3)	475433	6326755	
659	CD_800	473664	6324955	
660	CD_820	473681	6324944	
661	CD_1080	473896	6324786	
662	CD_1400	474191	6324743	
663	CD_1740	474504	6324634	
664	CD_1900	474648	6324570	
665	CD_2400	475082	6324329	
666	CD_3770	476413	6323885	
667	S3FS3_04	493472	6323759	
668	S3FS3_05	494072	6323835	
669	RJ20143	522955	6321596	General strat
670	RJ20141	522857	6321602	General strat
671	S3FS8_083	522832	6321623	General strat
672	RJ20144	522998	6321629	General strat

## Appendix B- Additional correlation panels

B.1. Chapter 4- Vriesgwaadg Farm correlation panel with logs.

### Logs

<i>-VRG20151</i>	<i>-VRG201511</i>
<i>-VS20142</i>	<i>-VRG20156</i>
<i>-VS20141</i>	<i>-VRG20158</i>
<i>-VRG201510</i>	<i>-VRG20158B</i>
<i>-VRG20159</i>	<i>-COL20151</i>
<i>-VRG20155</i>	<i>-COL20152</i>
<i>-VRG20152</i>	<i>-COL20153</i>
<i>-VRG20157</i>	<i>-COL20154</i>
<i>-VRG20153</i>	

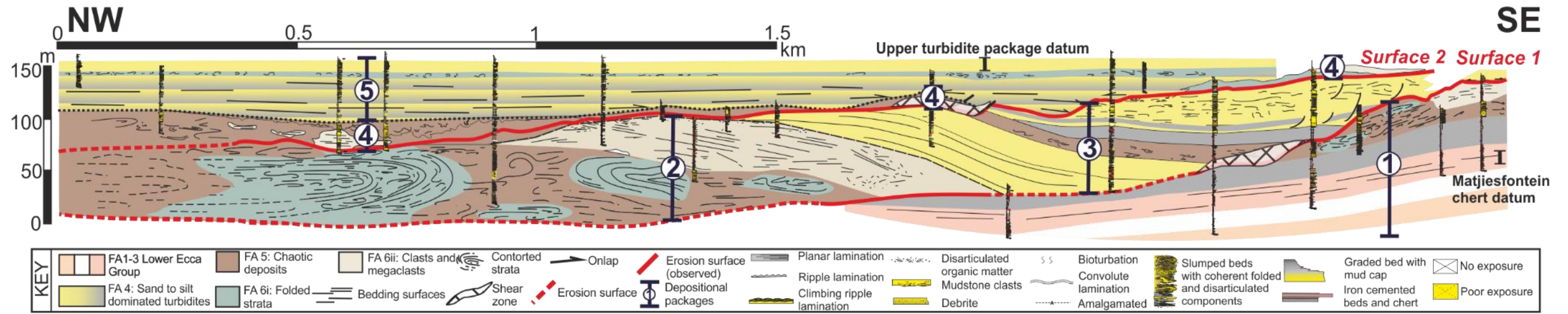
B.2. Chapter 5 and 6- Units D, D/E, E, F and G- N1 Dome South

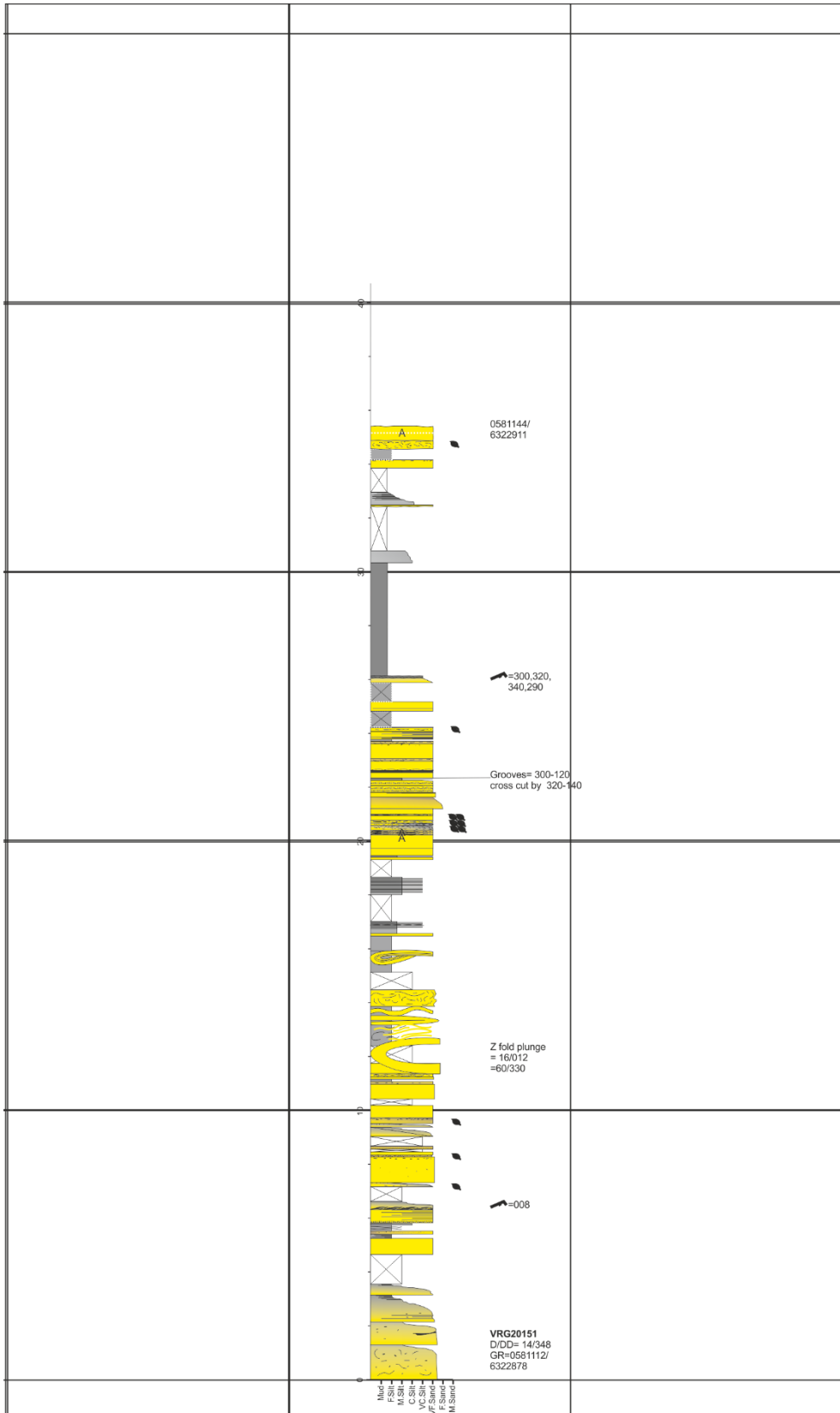
B.3. Chapter 5 and 6- Units Baviaans South panel

B.4. Chapter 5 and 6- Units D and E- Detailed Floriskraal North panel

B.5. Chapter 5 and 6- Units D and E- Detailed Floriskraal South panel

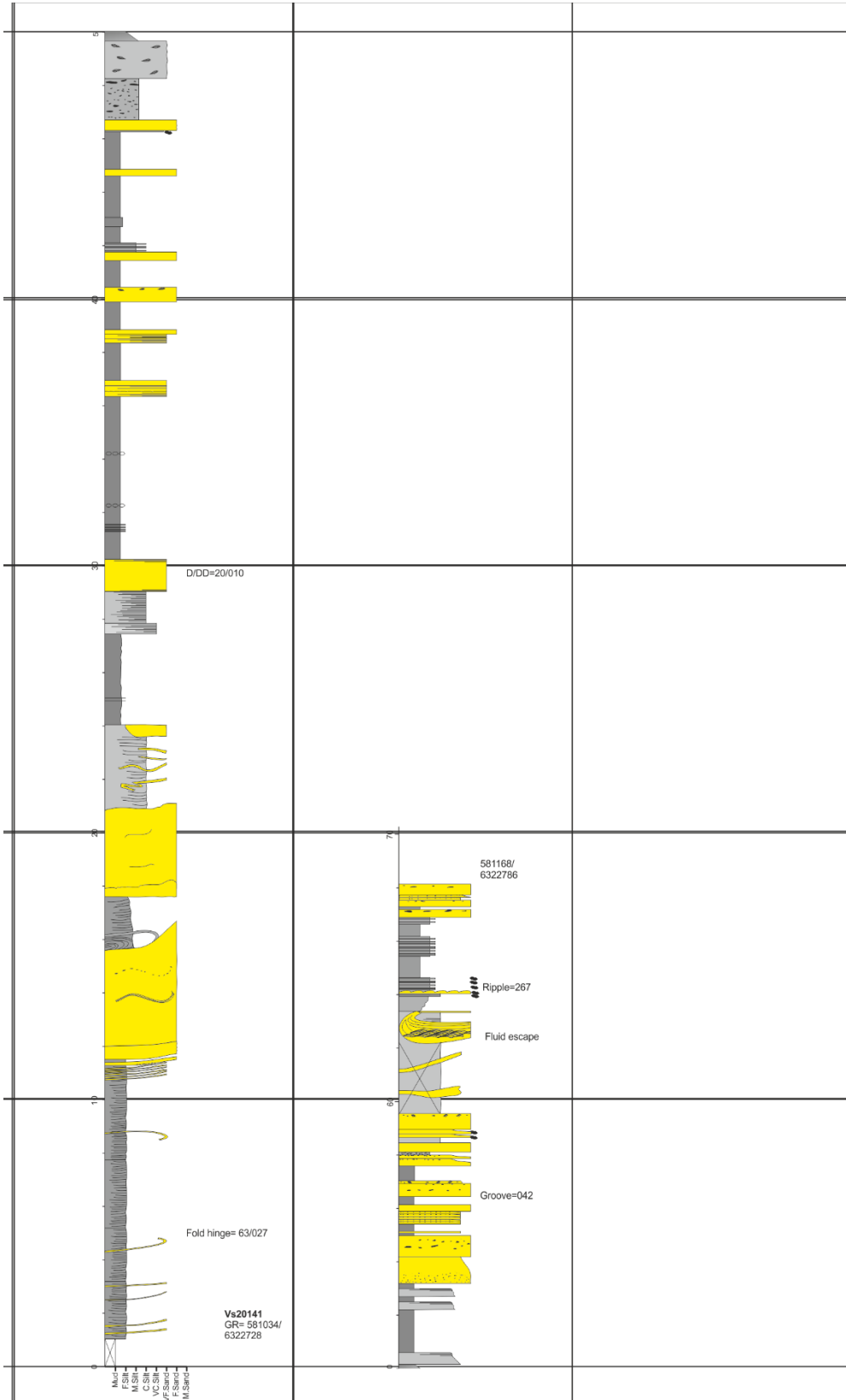
Appendix B.1- Vrisgewaagd



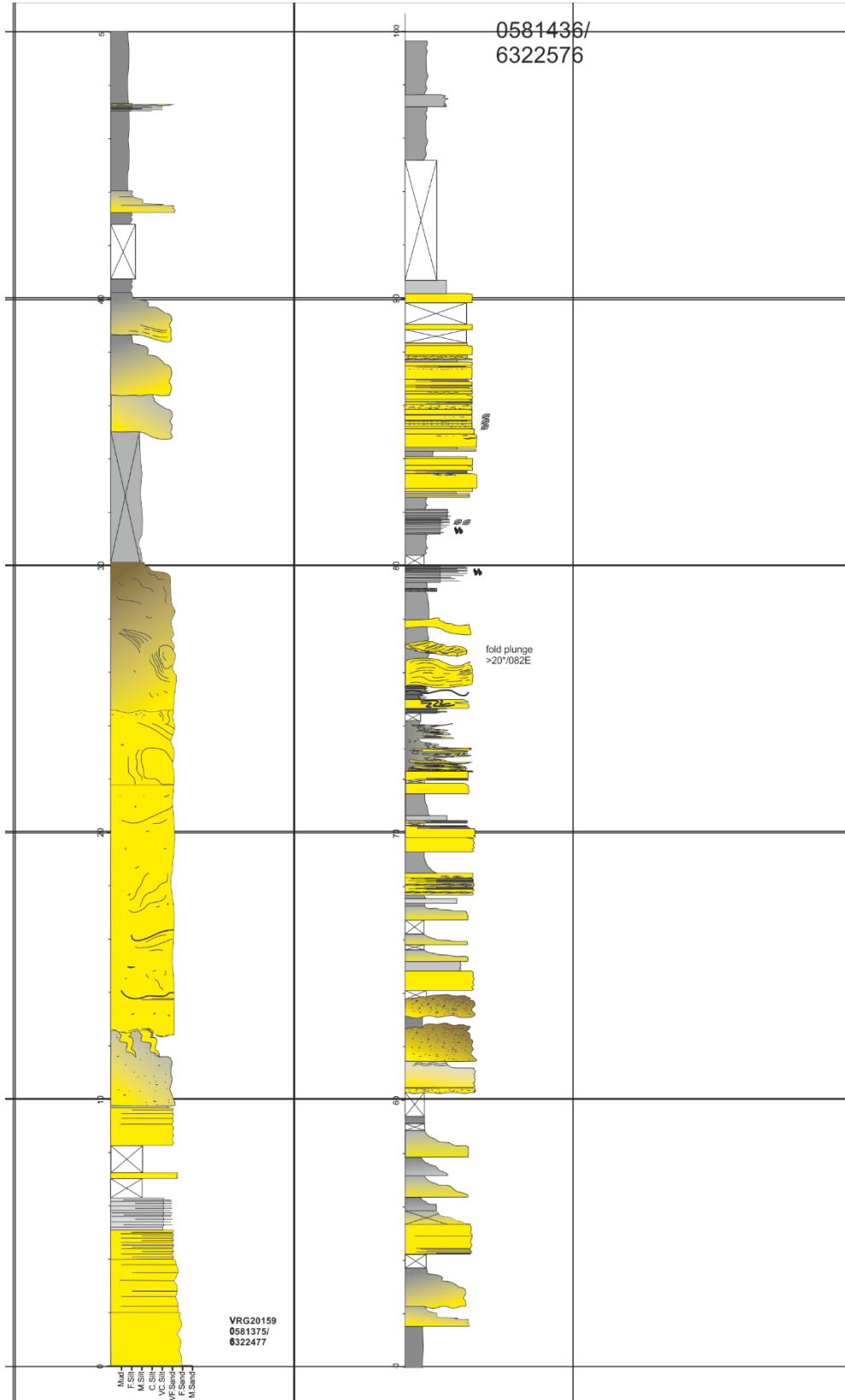


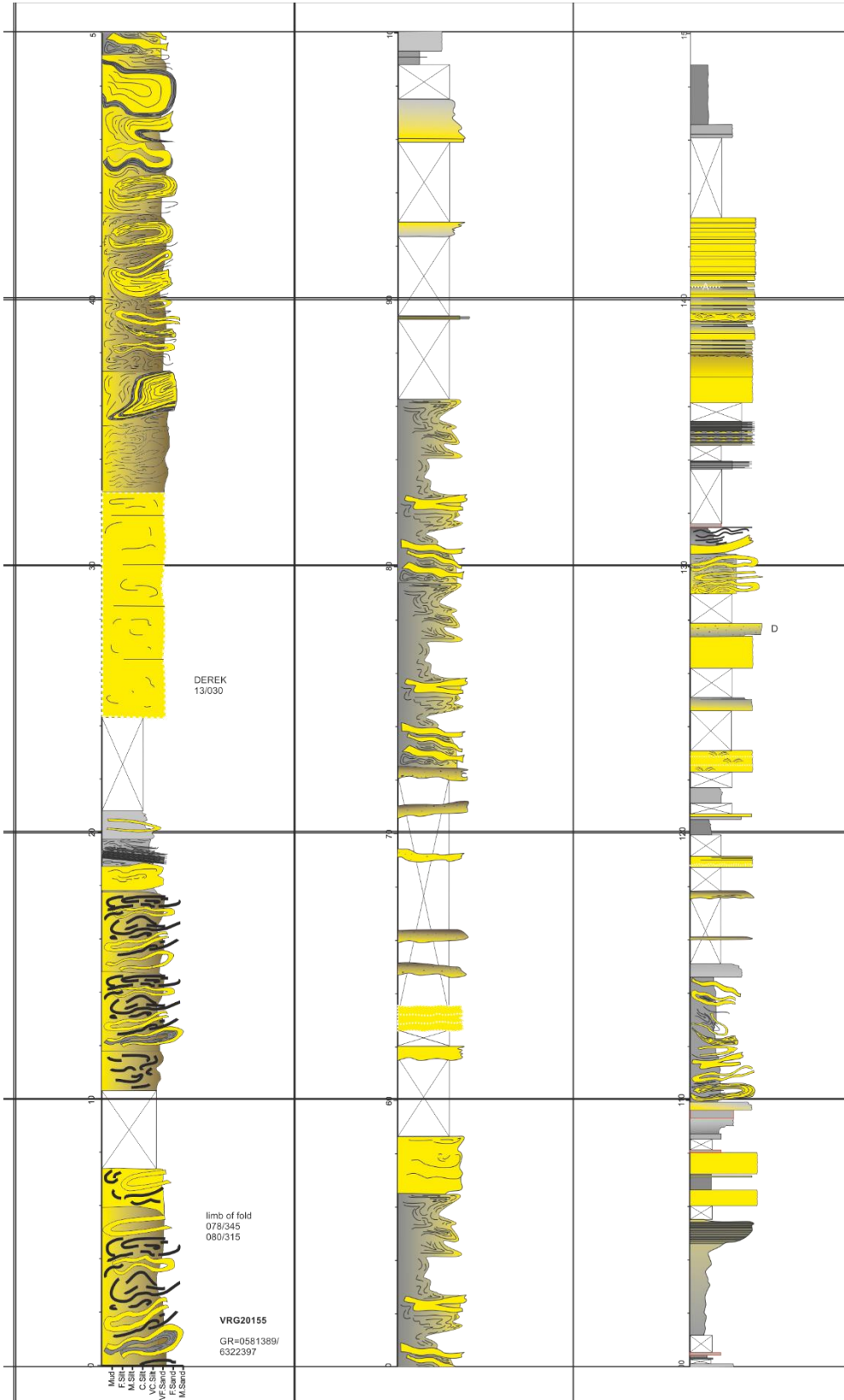




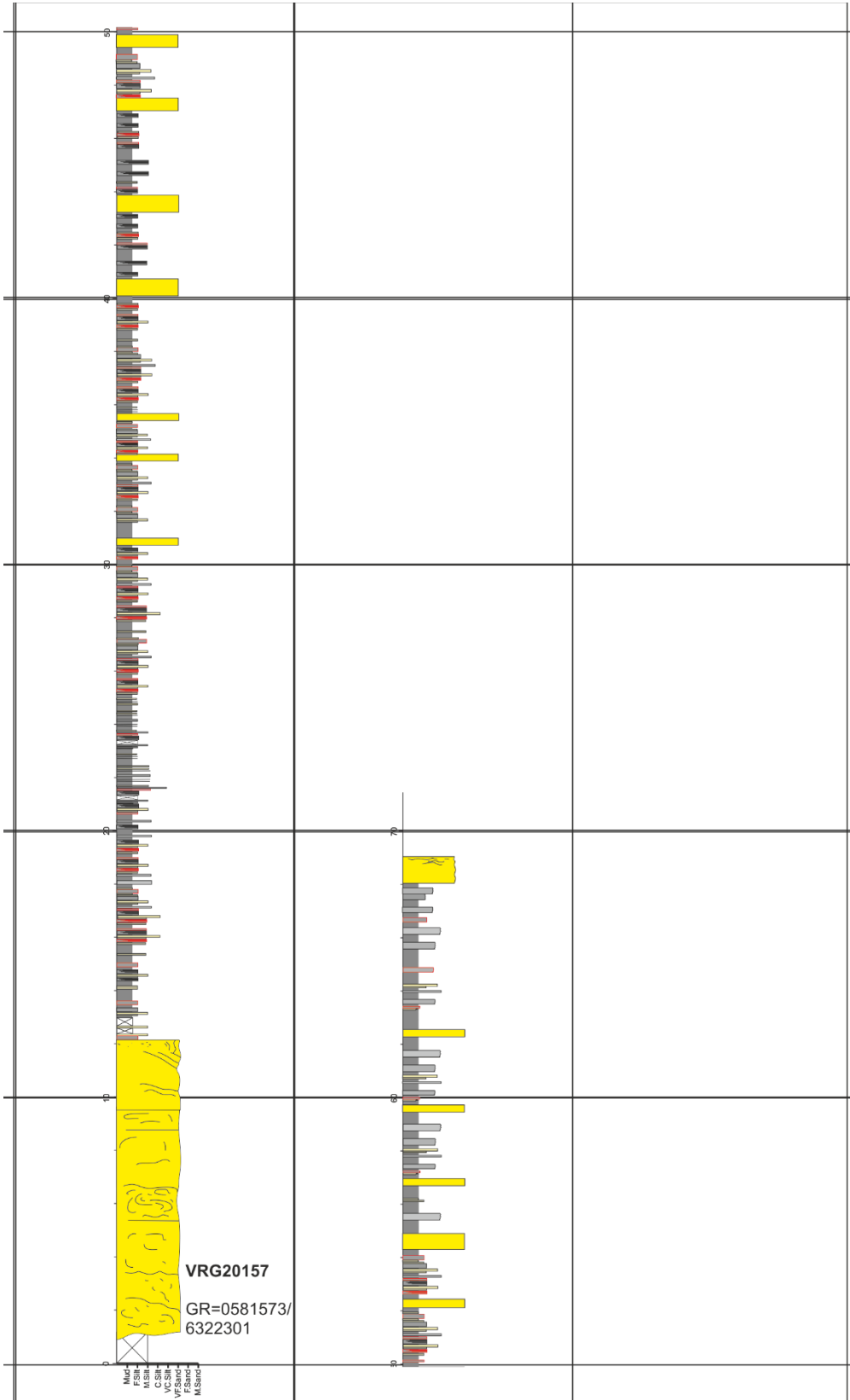


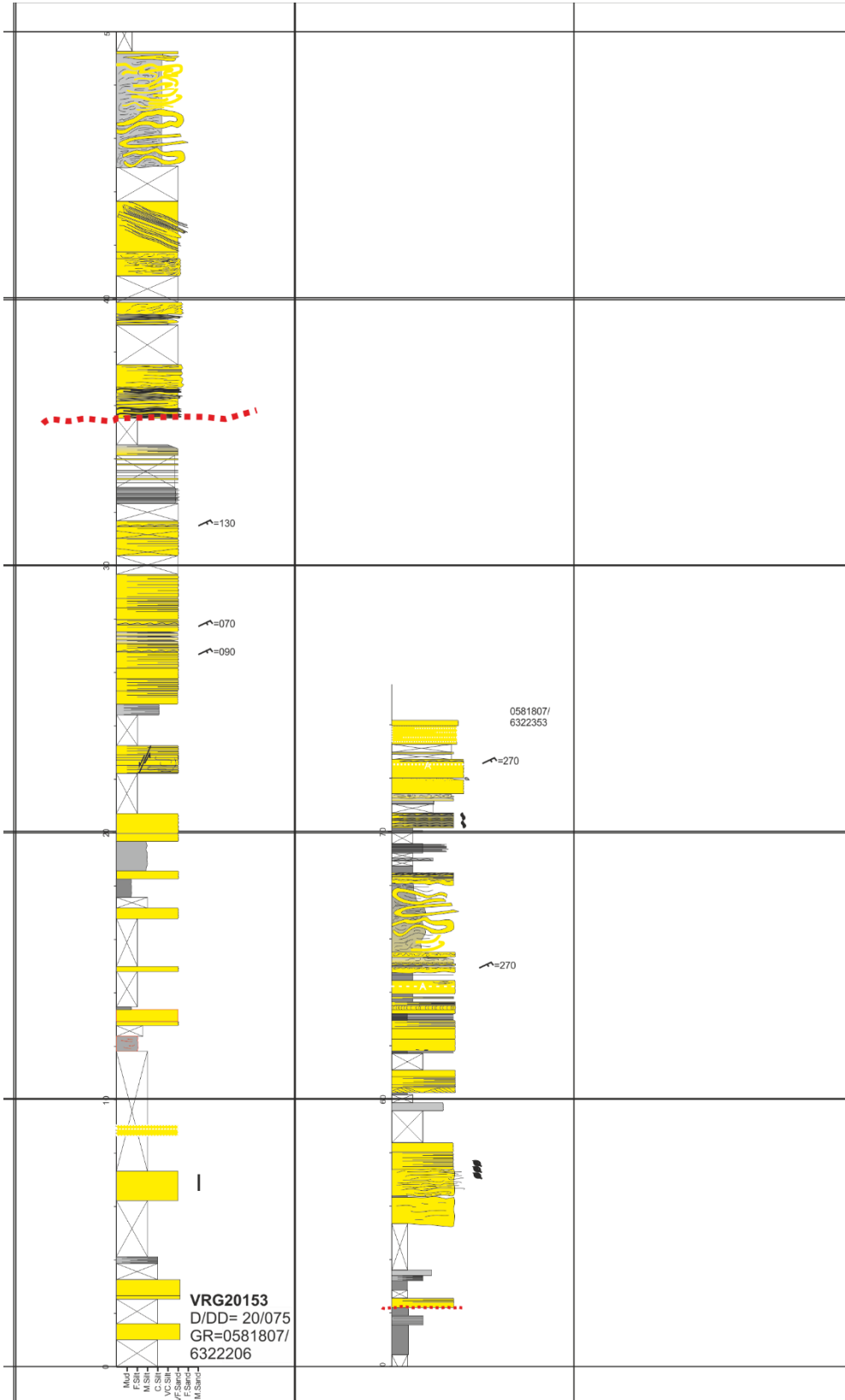






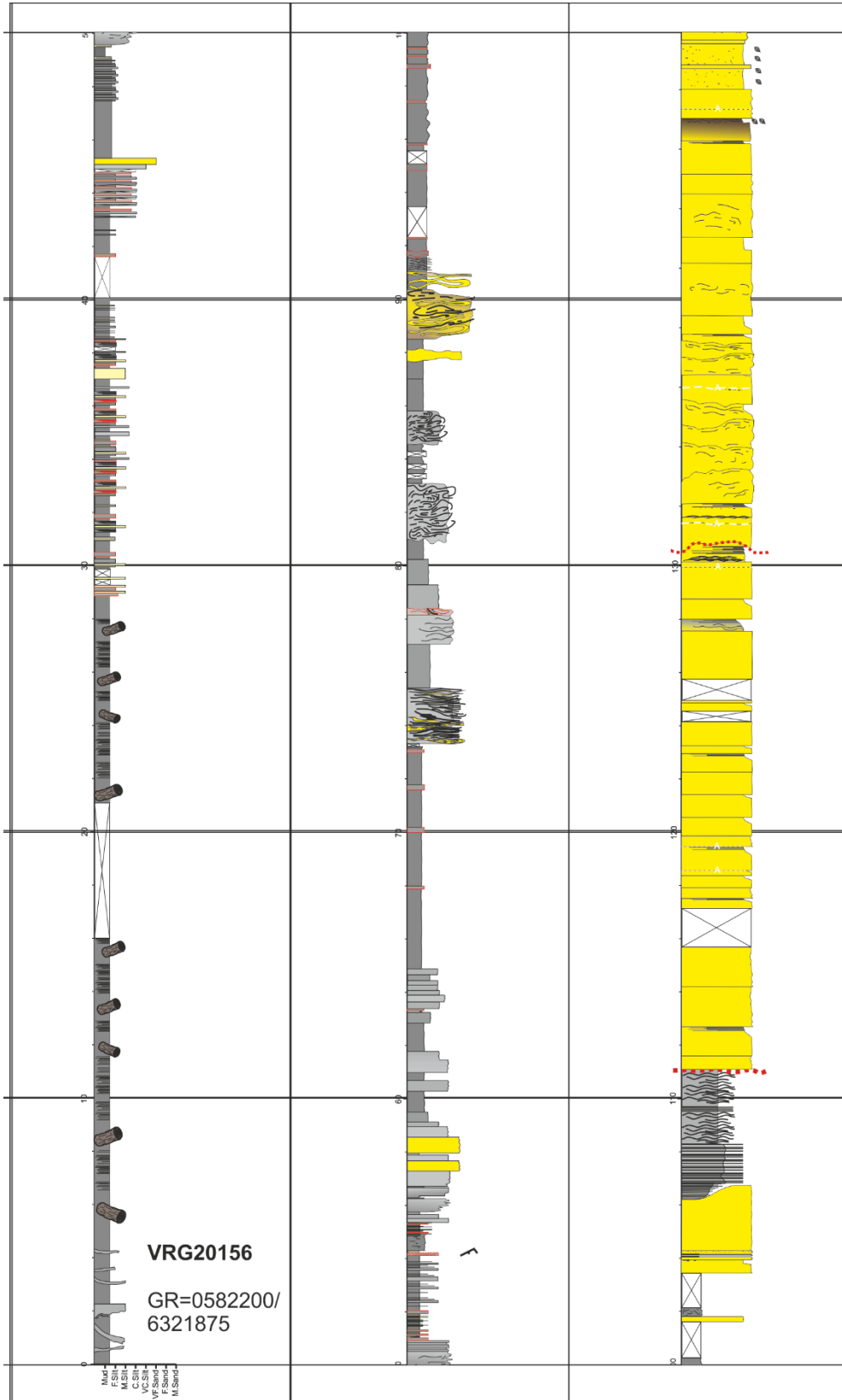


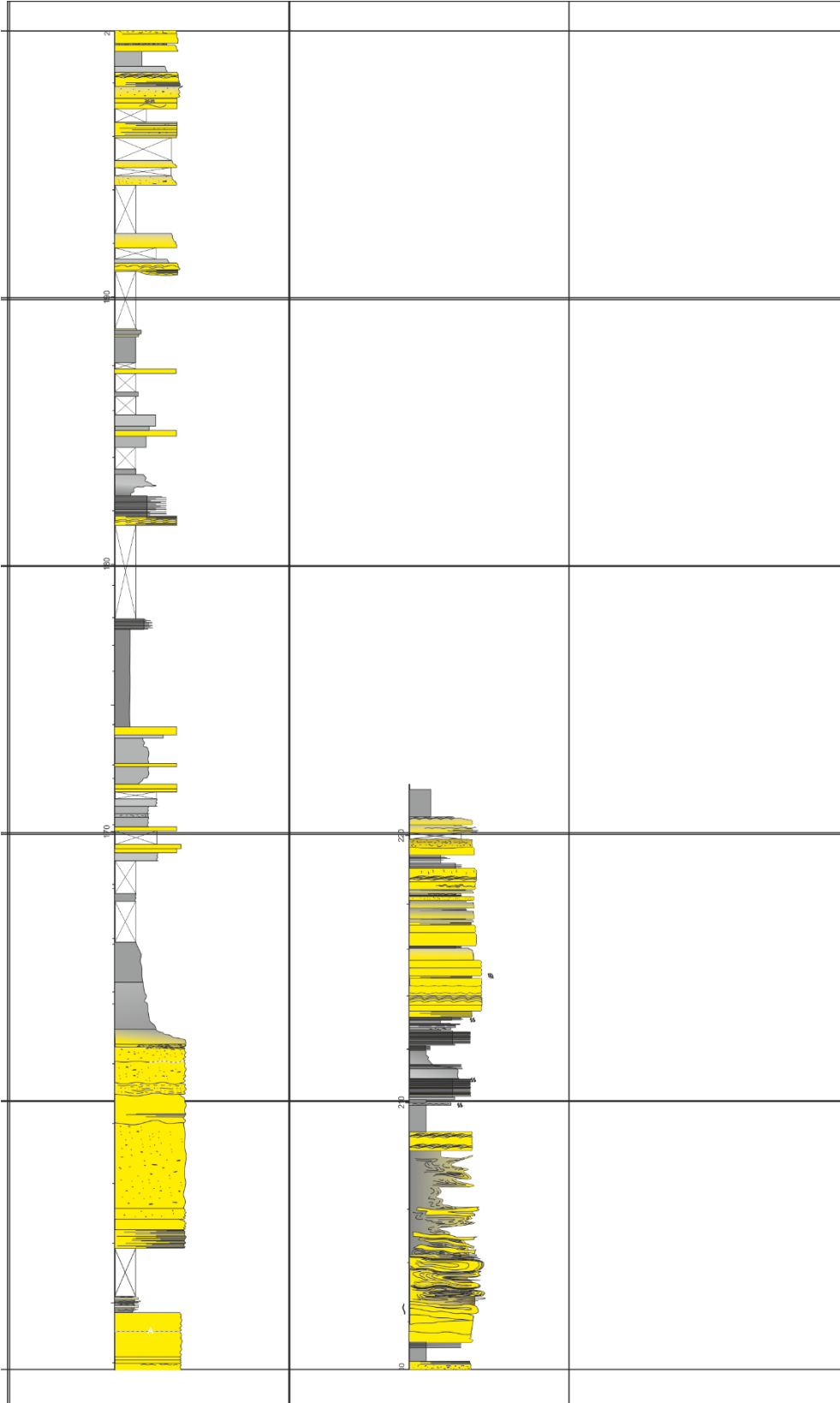


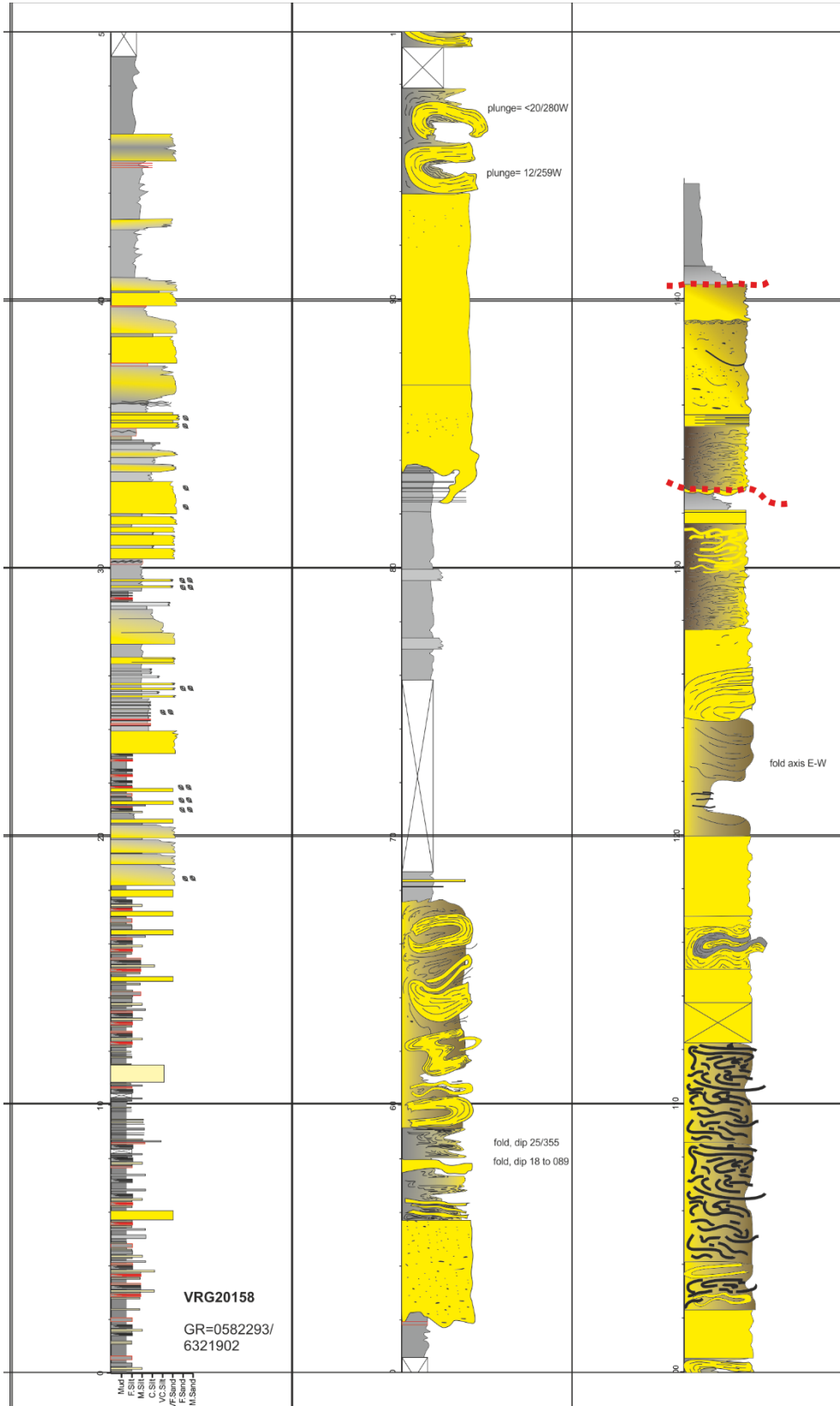


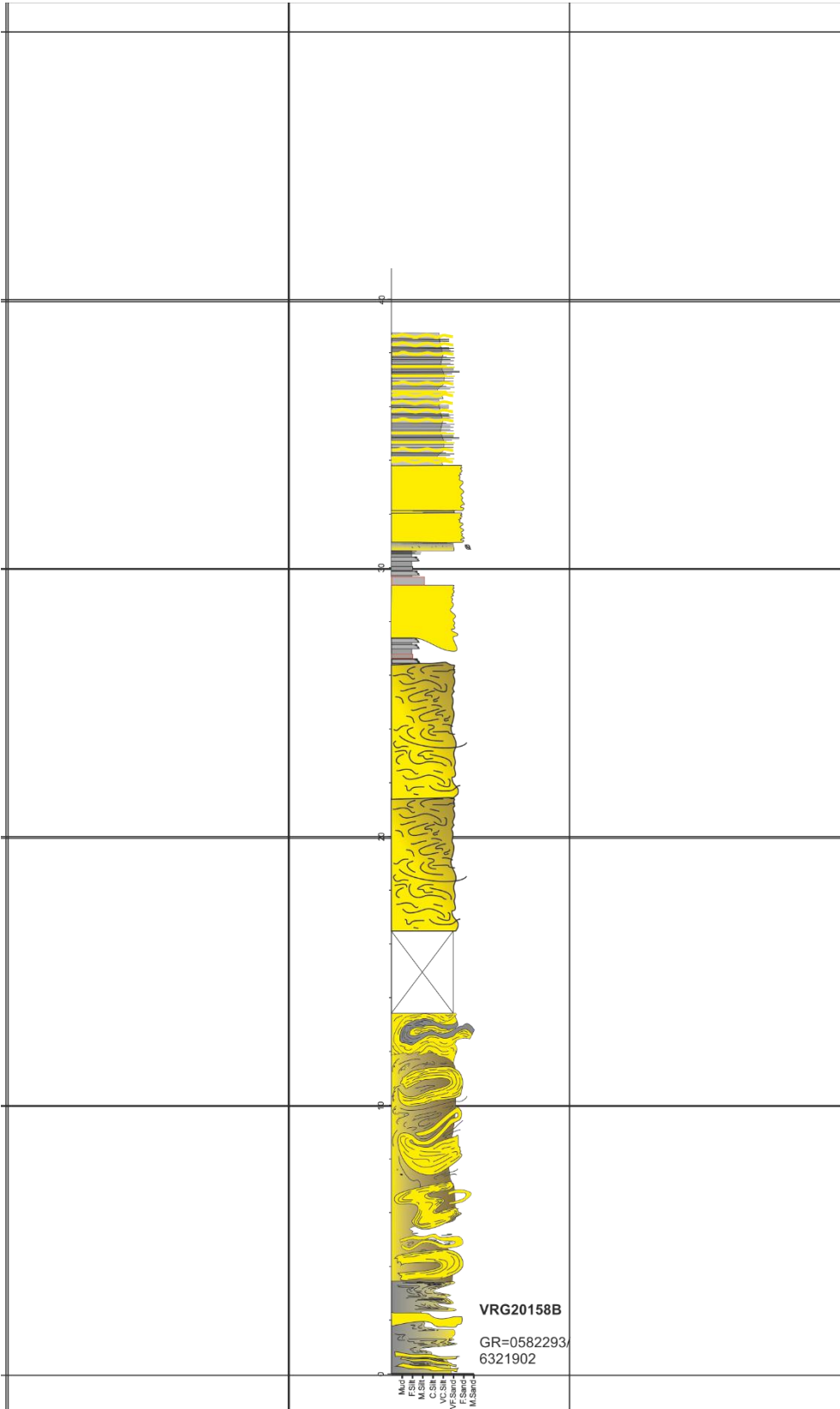


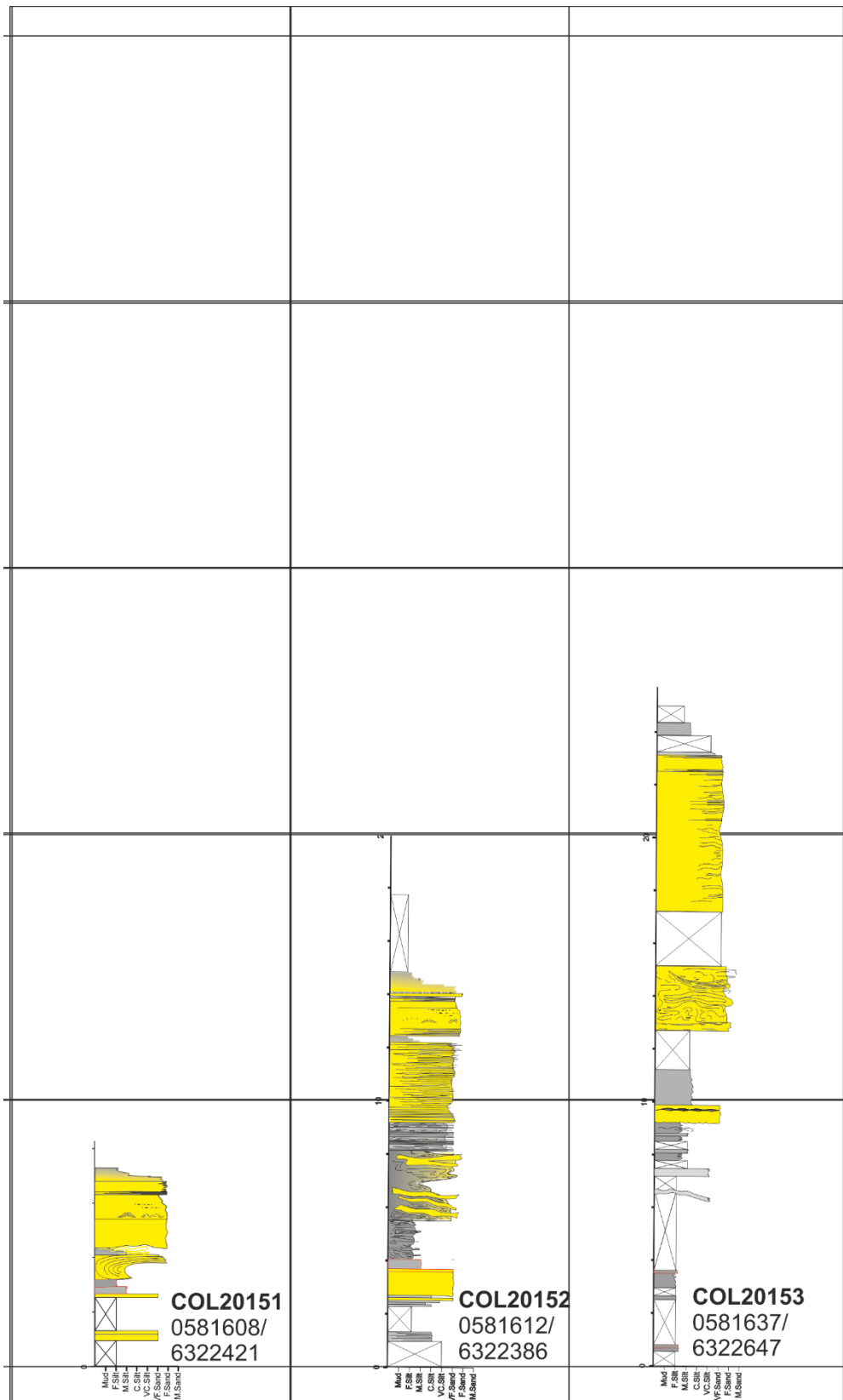


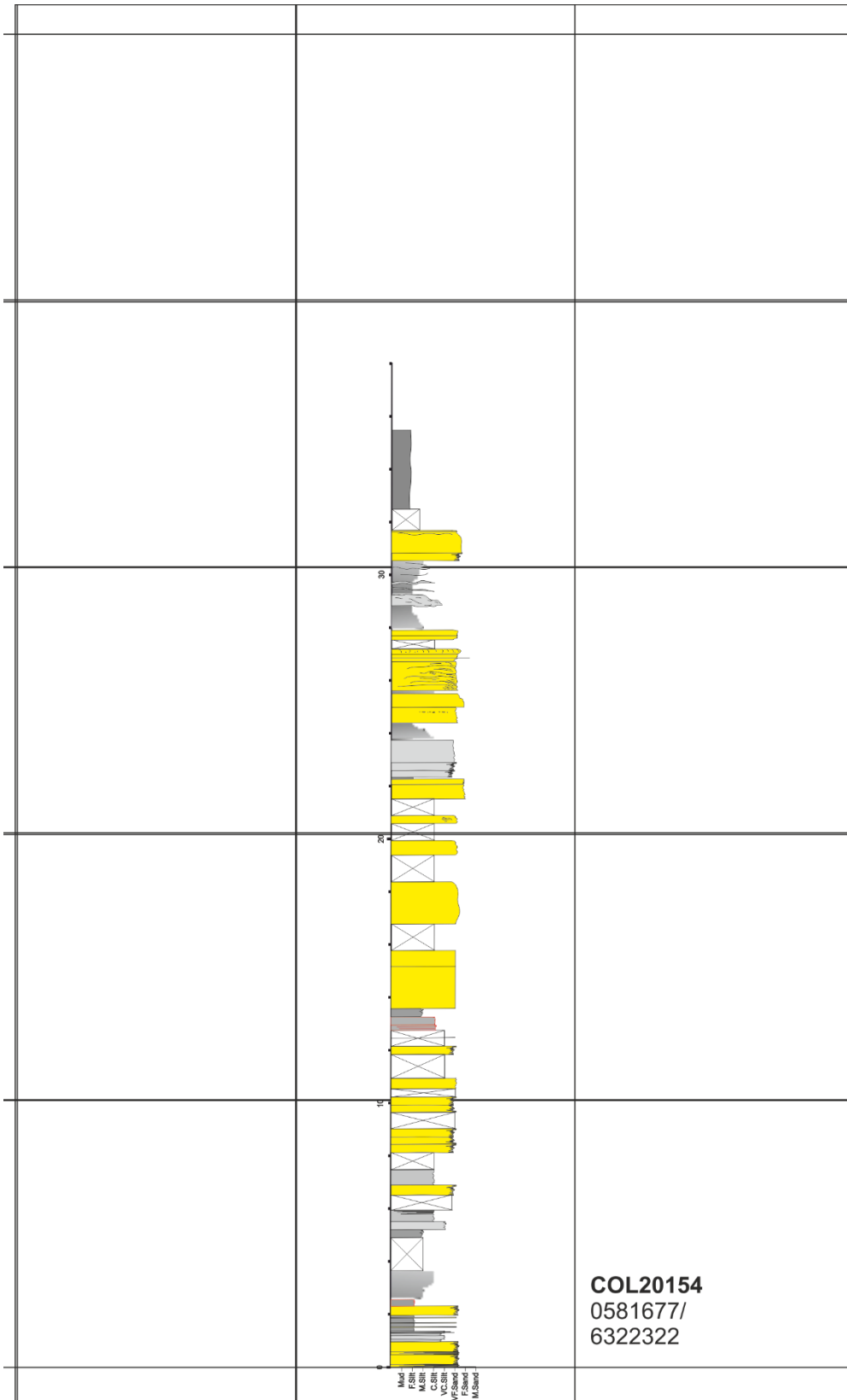







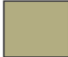
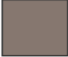

































# KEY

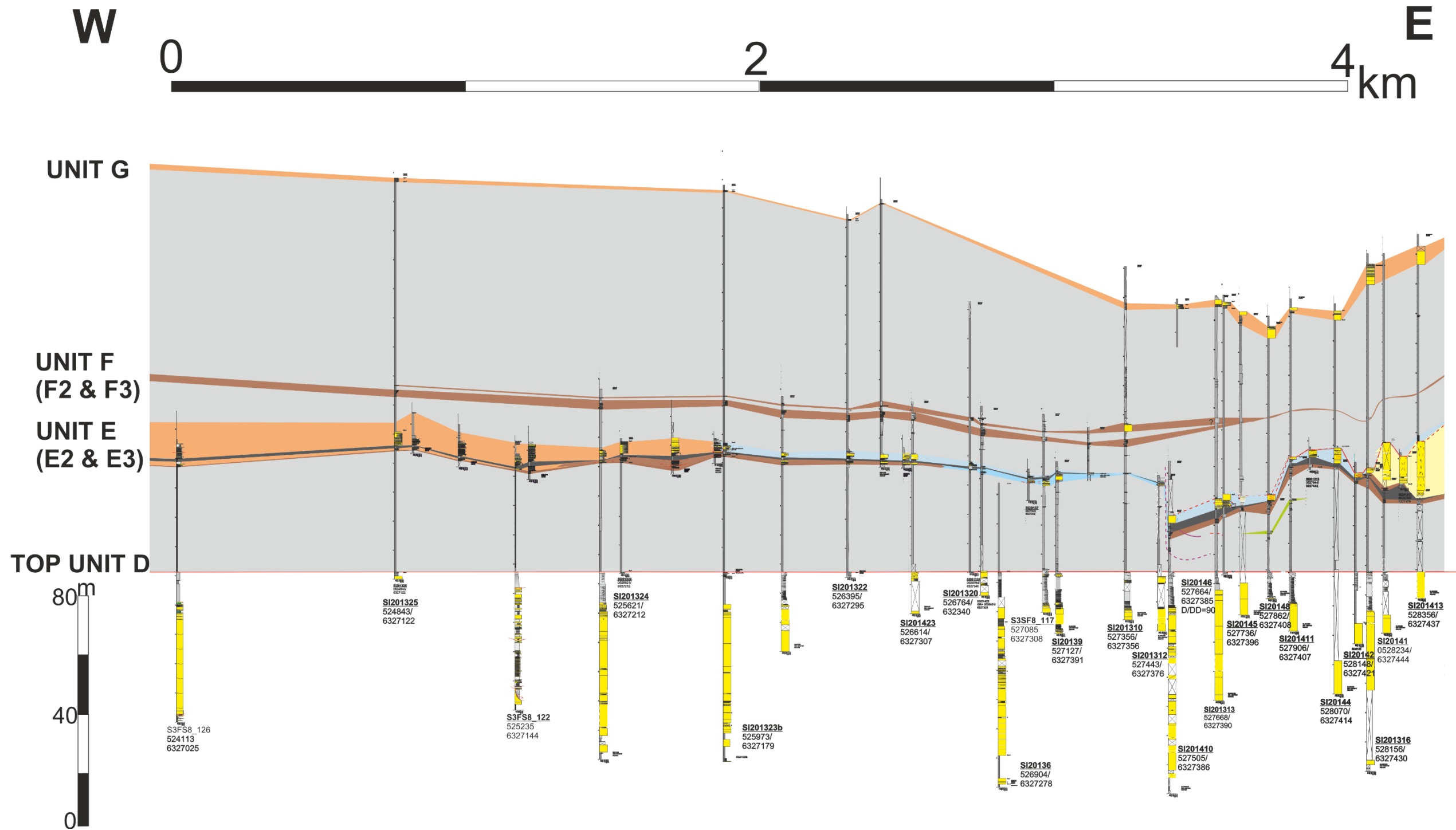
	Lobe axis		Sediment bypass dominated		Erosion surface
	Lobe off-axis		Spill-over fringe		Fault
	Lobe fringe		Inter-unit siltstone		Top of unit not exposed
	Sand rich hybrid beds		Intra-unit siltstone		No exposure
	Chaotic deposits		Clastic injectites		
	Levee				
	Planar lamination		Bioturbation		No exposure
	Ripple lamination		Convolute lamination		Slumped beds
	Climbing ripple lamination		Amalgamated bed contact		Clastic injectites
	Disarticulated organic matter		Hybrid bed		
	Mudstone clasts		Poor exposure		
	Debrite		Bypass lag		





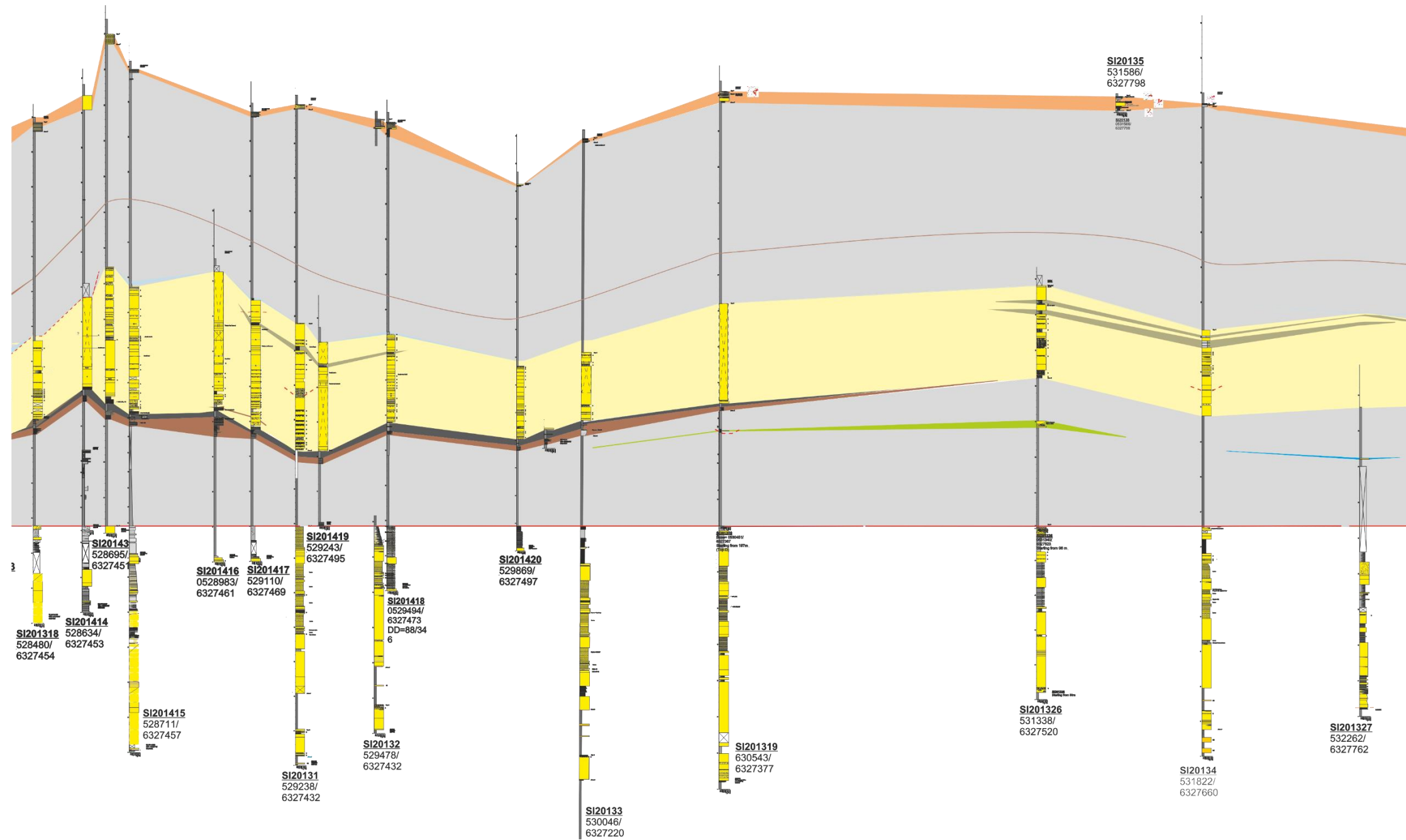


Appendix B.3- Baviaans South

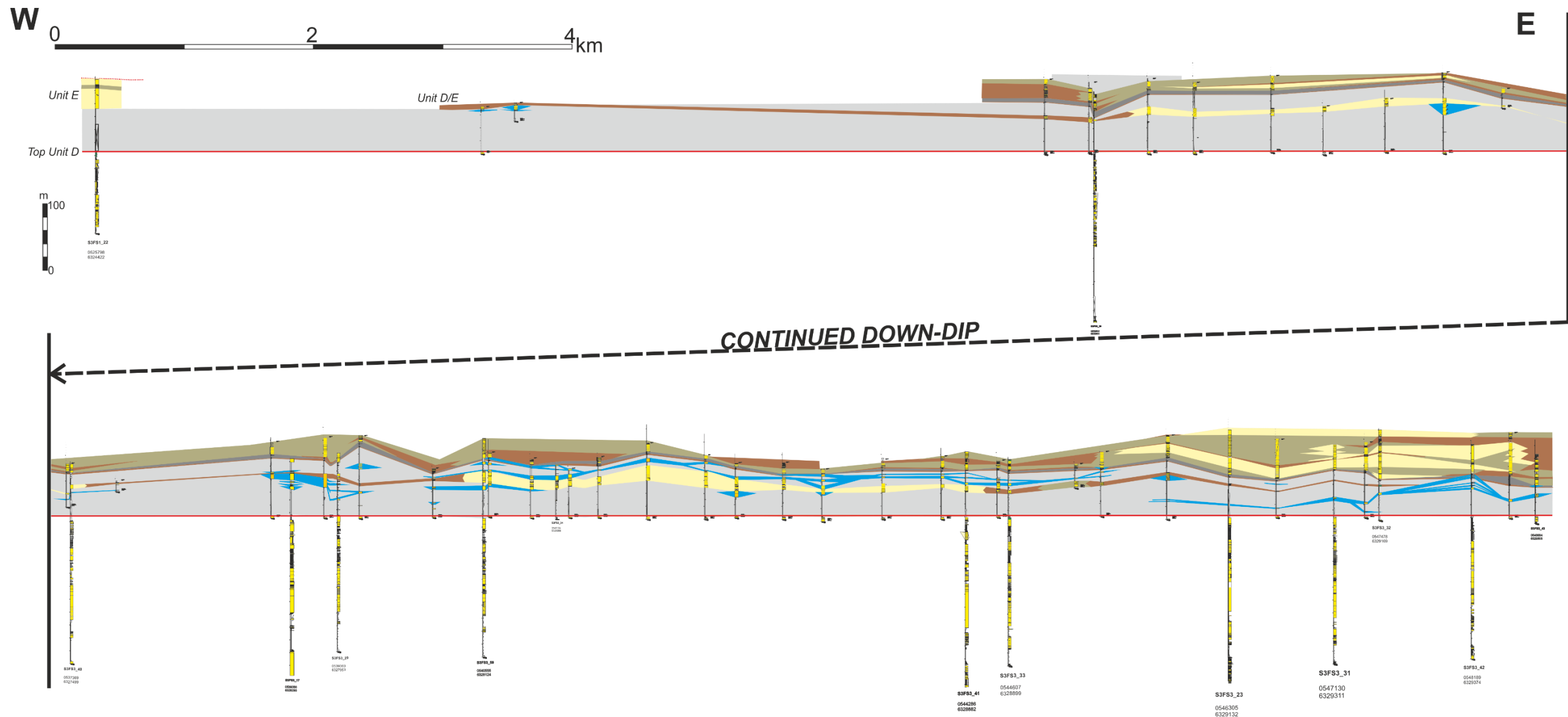


W

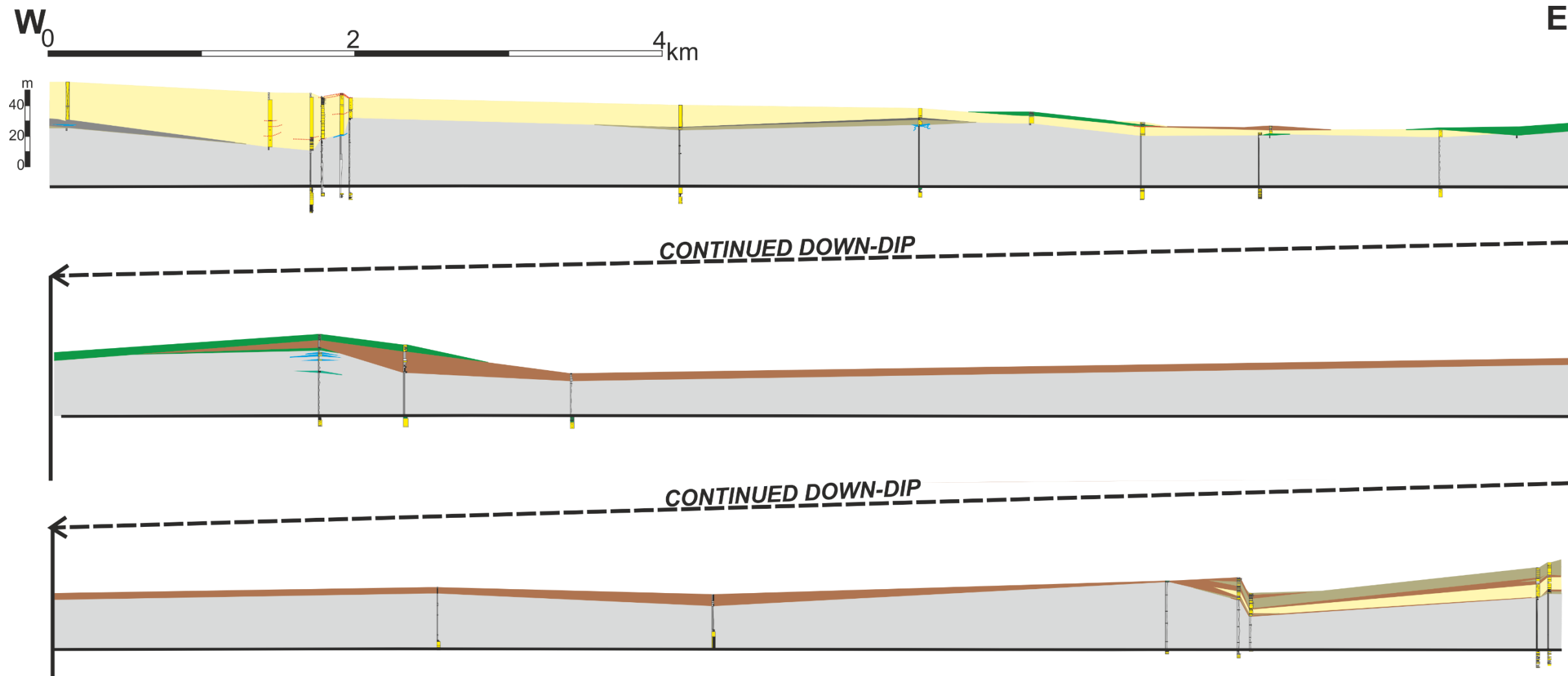
E



Appendix B.4- Floriskraal North



Appendix B.4- Floriskraal South



## Appendix C

### Appendix C.1

**Table C.1 Laingsburg Datacube Data imported. Datum is Top Whitehill Formation**

Composite logs	X	Y	Y 13% stretch	Correlation Panel	Section Covered
Rietkloof Rd Composite	461171	6337715	6339116	Heuinberg North	Top Whitehill to Unit E
Waterkloof Composite	467545	6338164	6339623	Heuinberg North	Top Whitehill to Base Unit C
Roggekraal Composite	478101	6339001	6340570	Heuinberg North	Top Whitehill to Base Unit C
Jakkalskraal W Composite	458288	6335711	6336851	Heuinberg South	Top Whitehill to Base Unit C
Steekwekklaagte Composite	472515	6337683	6339080	Heuinberg South	Top Whitehill to Base Unit C
Doornfontein Composite	466781	6330061	6330467	Faberskraal	Top Whitehill to Base Unit C
Vodacom Composite	474559	6329904	6330290	Faberskraal	Top Whitehill to Base Unit C
Buffels North Composite	487880	--	6330713	Faberskraal	Top Whitehill to Base Unit C
Ouplaas Composite	478278	6326783	6326763	Baviaans North	Top Whitehill to Top Unit F
Laingsburg Composite	487947	6328491	6328693	Baviaans North	Top Whitehill to Base Unit C
Blockhouse Composite	498422	6329961	6330354	Baviaans North	Top Whitehill to Top Unit E
N1 Dome Composite	534383	6334826	6335851	Baviaans North	Top Whitehill to Base Unit C
Skeiding Composite	472099	6323565	6323127	Baviaans South	Top Whitehill to Base Unit C
Ladismith Rd Composite	487534	6322211	6321596	Baviaans South	Top Whitehill to Base Unit C
Rondekop Composite	492488	6322197	6321581	Baviaans South	Top Whitehill to Base Unit C
Geelbek Composite	499650	6321893	6321237	Baviaans South	Top Whitehill to Deltas
Haartebeest Composite	510330	6324108	6323740	Baviaans South	Top Whitehill to Deltas
Wolfontein Composite	521757	6325867	6325728	Baviaans South	Top Whitehill to Deltas
Hunters Lodge Composite	525914	6320948	6320169	Baviaans South	Top Whitehill to Base Unit C
Vergenoeg Composite	543548	6320986	6320213	Baviaans South	Top Whitehill to Top Unit D
Dwyka Composite	559943	6324726	6324439	Baviaans South	Top Whitehill to Deltas

Table C.2 Laingsburg Datacube pseudo wells

Pseudo Wells	X	Y	Y 13% stretch	Correlation Panel	Section Covered
NW	450600	-	6362038	n/a	Top Whitehill to Base Unit C
N_side_1	483565	-	6362151	n/a	Top Whitehill to Base Unit C
N_side_2	516530	-	6362264	n/a	Top Whitehill to Base Unit C
N_side_3	549495	-	6362377	n/a	Top Whitehill to Base Unit C
NE	582460	-	6362490	n/a	Top Whitehill to Base Unit C
SW	451000	-	6303843	n/a	Top Whitehill to Base Unit C
S_side_1	483750	-	6303420	n/a	Top Whitehill to Base Unit C
S_side_2	516500	-	6302996	n/a	Top Whitehill to Base Unit C
S_side_3	549250	-	6302572	n/a	Top Whitehill to Base Unit C
SE	582000	-	6302148	n/a	Top Whitehill to Base Unit C
Estimation_1_Composite	488993	-	6340147	n/a	Top Whitehill to Base Unit C
Estimation_2_Composite	516467	-	6338084	n/a	Top Whitehill to Base Unit C
Estimation_3_Composite	554613	-	6338910	n/a	Top Whitehill to Base Unit C
Pseudo F	559401	-	6334466	n/a	Top Whitehill to Base Unit C



## **Appendix D**

Regional correlation panels from SLOPE database and previous work.

**D.1 Faberskraal North**

**D.2 Faberskraal South**

**D.3 Baviaans North**

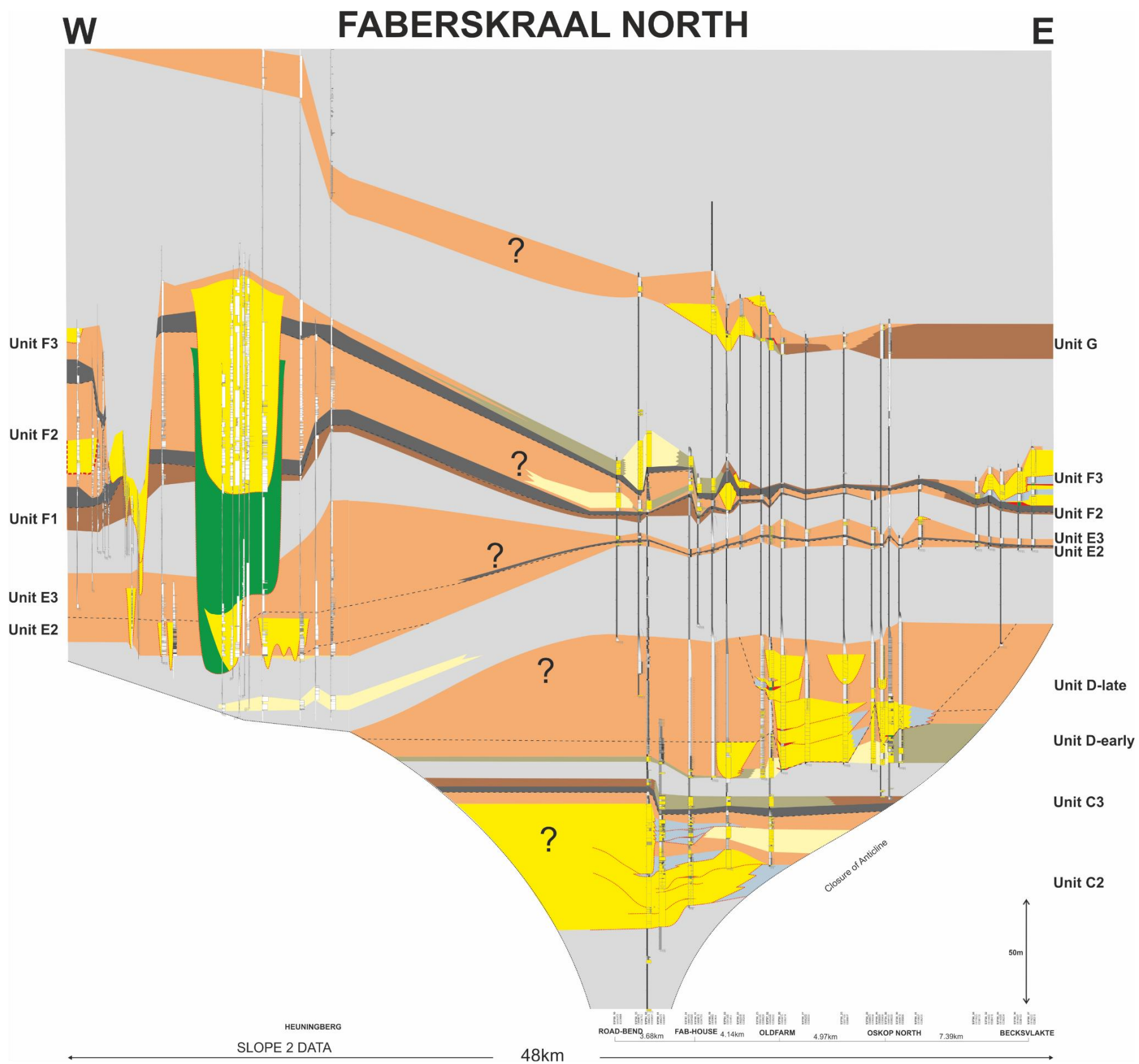
**D.4. N1 Dome South**

**D.5 Baviaans South**

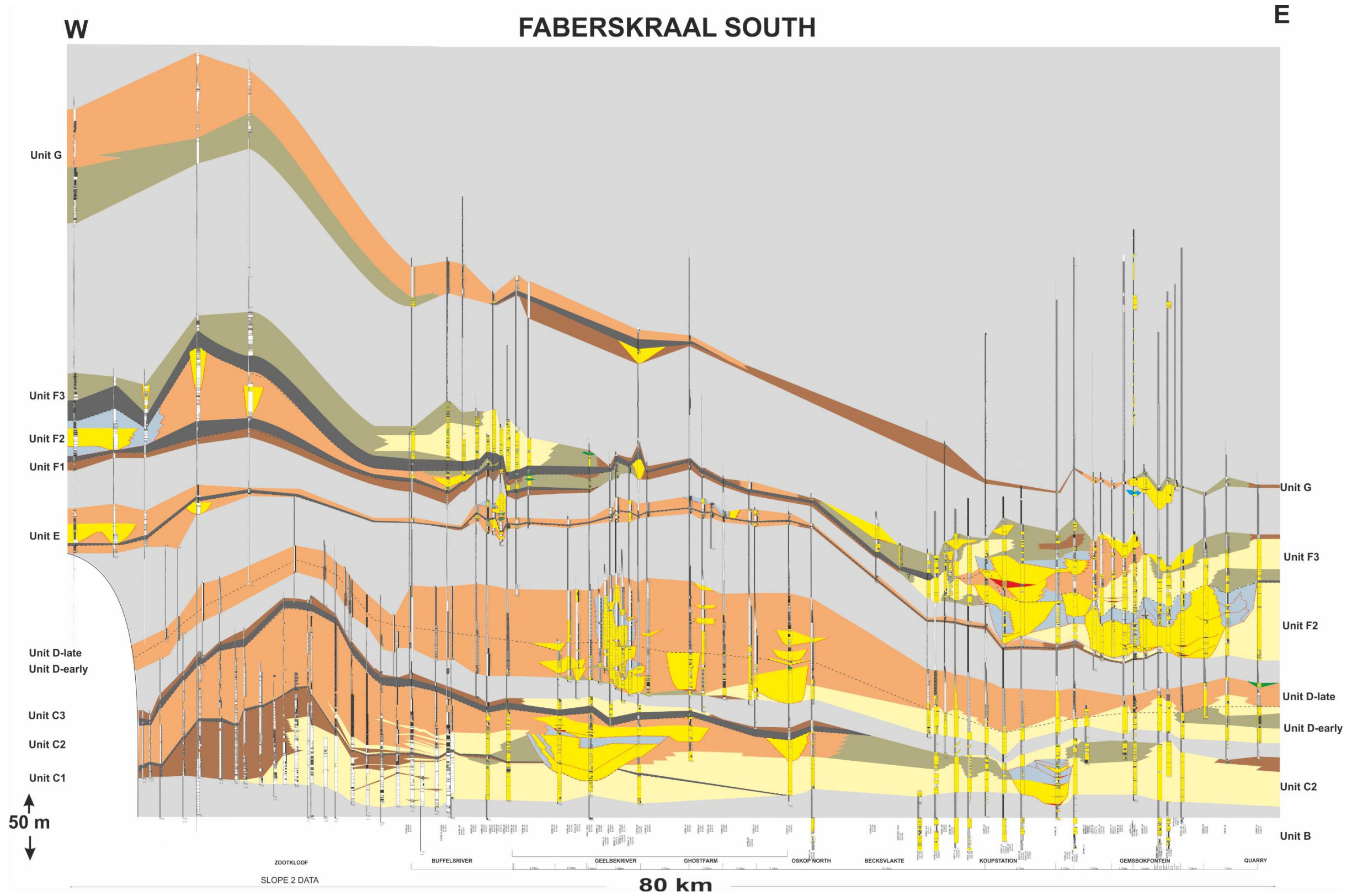
**D.6 Floriskraal North**

**D.7 Floriskraal South**

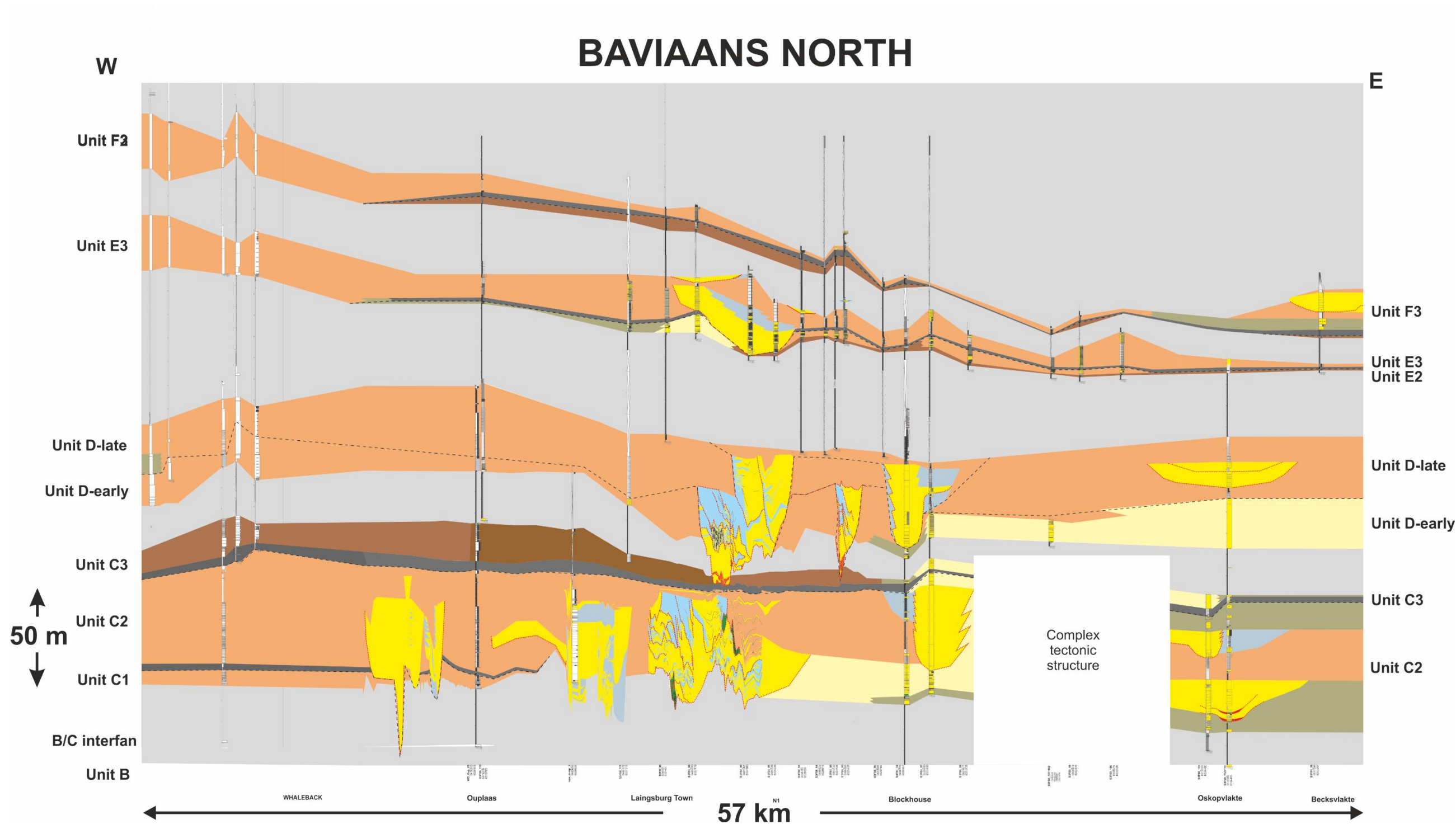
D.1 Faberskraal North



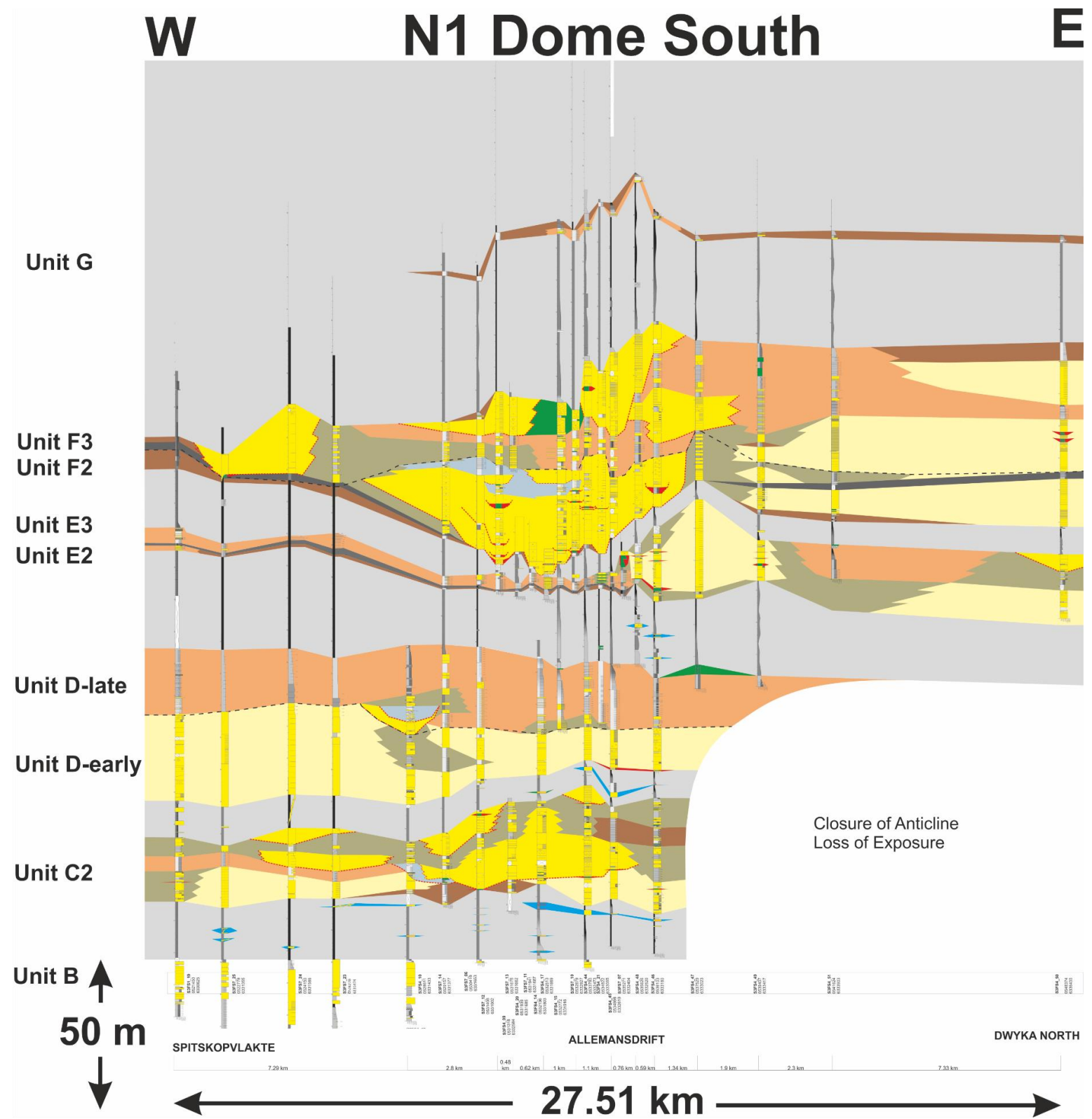
D.2 Faberskraal South



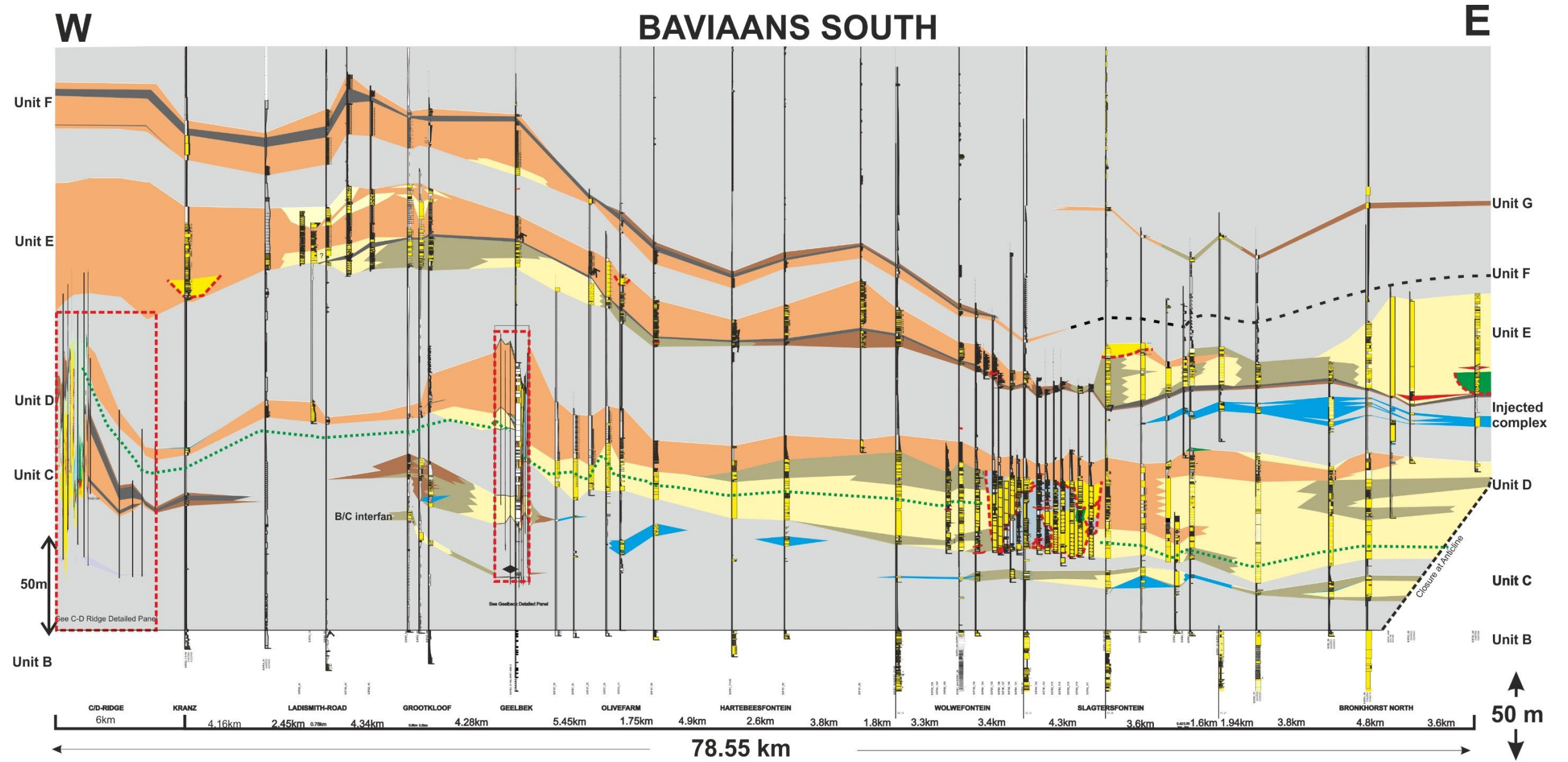
D.3. Baviaans North



D.4. N1 Dome South



D.5 Baviaans South





D.7 Floriskraal South

